Targeting Cerebral Oedema and Elevated Intracranial Pressure in a Preclinical Model of Ischaemic Stroke

A thesis submitted in fulfilment for the degree of

DOCTOR OF PHILOSOPHY

in

The Discipline of Anatomy and Pathology

Adelaide Medical School

The University of Adelaide

Annabel Sorby-Adams

May 2021

'Although neuroscience is my daily routine, I am still in awe every time I hold a human brain. After you take into account its substantial weight (an adult brain weighs in at three pounds), its strange consistency (like firm jelly), and its wrinkled appearance (deep valleys carving a puffy landscape) – what's striking is the brain's sheer physicality: this hunk of unremarkable stuff seems so at odds with the mental processes it creates.

Our thoughts and our dreams, our memories and experiences all arise from this strange neural material. Who we are is found within its intricate firing patterns of electrochemical pulses.

When that activity stops, so do you. When that activity changes character due to injury, you change character in lockstep. Unlike other parts of your body, if you damage a small piece of your brain, who you are is likely to change radically'

David Eagleman – The Brain: The Story of You

Copyright © 2021 - Annabel Sorby-Adams

All rights reserved

Table of Contents

Abstract

Stroke is a devastating condition, affecting over 17 million people worldwide annually. Interruption of cerebral arterial blood flow in ischaemic stroke initiates a cascade of deleterious events, leading to irreversible cell damage and secondary injury. Specifically, the development of cerebral oedema, whereby disruption to the blood–brain barrier (BBB) precipitates abnormal fluid accumulation within the brain parenchyma, leads to a consequent rise in intracranial pressure (ICP). Persistently elevated ICP results in loss of cerebral autoregulation and brain herniation, making it a leading cause of death and disability post-stroke. Despite this, current treatments fail to prevent the pathophysiological development of oedema, rather targeting the symptoms once established. As such, understanding the mechanisms underlying cerebral oedema and elevated ICP is essential in order to develop more targeted and effective treatments to prevent oedema genesis and improve patient outcomes.

Neurogenic inflammation, mediated by substance P (SP), has been linked to profound BBB disruption, oedema development and poor functional outcome post-stroke. SP binds to the neurokinin 1 tachykinin receptor (NK1-R), with administration of an NK1-R antagonist shown to ameliorate BBB dysfunction and cerebral oedema following stroke in rodent models. However, more clinically-relevant animal models are required to validate efficacy of novel stroke therapeutics to improve clinical translation. Thus, this thesis sought to determine the efficacy of NK1-R antagonist treatment in reducing cerebral oedema and ICP in a clinically-relevant ovine stroke model.

Merino sheep (*Ovis aries; n*=125) were used across the five thesis studies. For Aim 1 (*n*=34F), a non-survival permanent middle cerebral artery occlusion (MCAo) model was used to determine the efficacy of various NK1-R receptor antagonist regimens or decompressive craniectomy in reducing ICP post-stroke. Once an optimum dosage was determined, Aims 2 and 3 (*n*=23F;24M) involved development of a transient MCAo survival model and characterisation of the temporal profile of oedema and ICP. Finally, Aim 4 and 5 (*n*=9F;9M), sought to determine the ideal time-course of treatment, and investigate the efficacy of the NK1-R antagonist following transient stroke via assessment of neurological and functional outcomes. ICP was assessed via invasive monitoring, with arterial blood pressure, temperature and blood gases also measured. Magnetic resonance imaging (MRI) and immunohistochemistry (IHC) was also performed. Motion capture and a modified neuroscore was used to assess changes in motor function and demeanour.

This thesis identified that two doses of the NK1-R antagonist were efficacious in reducing ICP following permanent MCAo. A transient stroke model was successfully developed and characterised, with ICP peaking at 5-6 days post-stroke. NK1-R antagonist treatment, both acutely (1-3 days), and in a delayed fashion (5-day), significantly reduced ICP post-stroke. Finally, a motion capture tool was successfully established and validated as a quantitative method to assess motor function following transient ovine stroke, with animal gait significantly impaired post-stroke.

The work presented in this thesis encompasses a comprehensive evaluation of the efficacy of NK1-R antagonist treatment in a clinically-relevant ovine model, providing strong pre-clinical evidence for further investigation. Accordingly, Phase II trials are currently underway in Australia, the United Kingdom and the United States of America.

Declaration

I certify that this work contains no material which has been accepted for the award of any other degree or diploma in my name, in any university or other tertiary institution and, to the best of my knowledge and belief, contains no material previously published or written by another person, except where due reference has been made in the text. In addition, I certify that no part of this work will, in the future, be used in a submission in my name for any other degree or diploma in any university or other tertiary institution without the prior approval of the University of Adelaide and where applicable, any partner institution responsible for the joint award of this degree.

I also acknowledge that copyright of published works contained within this thesis resides with the copyright holder(s) of those works. I also give permission for the digital version of my thesis to be made available on the web, via the University's digital research repository, the Library Search and also through web search engines, unless permission has been granted by the University to restrict access for a period of time.

I acknowledge the support I have received for my research through the provision of an Australian Government Research Training Program Scholarship.

Annabel Sorby-Adams

Acknowledgements

This thesis would not have been possible without the immeasurable support of a number of people who have influenced not only my scientific career, but me as an individual.

Firstly, I would like to thank my doctoral supervisors. Emma Thornton, who was initially on my panel, Anna Leonard, Claire Jones and Renée Turner. Each of these incredible women shaped both the body of work in this thesis and ultimately the scientist I am today. Claire, thank you for your dedication and for teaching me to always extend myself. Anna, thank you for your love and unwavering belief in me. And Renée, thank you for your endless support and encouragement at every step of my PhD. I am so grateful for the relationship we have. You are my ultimate inspiration; always have, and always will be.

I would also like to thank all those who made the research feasible. In particular, the staff at the South Australian Health and Medical Research Institute (SAHMRI) Preclinical and Imaging Research Laboratories (PIRL). Loren, Robb, Dan, Caitlin, Sam, Paul, Kevin, Brett, Georgia – everyone played a vital role, overseen over the years by both the late (and great) Dr Tim Kuchel and more recently the fabulous Dr Chris Christou. The dedication to both the research and animals shown by each of these people was outstanding, and I am proud to have worked so closely with you all over the past 5 years. A huge thank you also to both past and present members of the Translational Neuropathology Laboratory, in particular Oana Marian, Bella Bilecki and Levi Elms; you kept me sane during 2018 and I am eternally grateful!

I would like to thank my inspirators and mentors. I was incredibly fortunate to receive funding for my PhD through the Peter Couche Foundation. Peter, the patron of the foundation who suffered a devastating pontine stroke in his early forties, and Stephen, his brother, provided me an opportunity for me to work closely with a family directly affected by the consequences of stroke, and I remain a proud ambassador for the foundation to this day. Peter, your dedication and resilience has been an inspiration throughout the entirety of my PhD, and I am so thankful to both you and Stephen for the opportunities you have awarded me. By way of mentors, I would like to thank Nawaf Yassi, who has nurtured my love of imaging, Kate Hayward, who kept me invigorated, and Jenny Morton, who gave me my first overseas and ultimately life-changing post.

I would like to thank my beautiful friends. I did not know the past 5 years of my life would so bring so many challenges but serendipitously, even greater happiness. Jess and B, honestly, I don't know where I would be without you! You have been my voice of reason, frustration, happiness, and undoubtedly the greatest gift of my PhD. Alice thank you for always keeping me sane and being the ultimate best friend and travel buddy during our year in the UK, and every year since. Kate, you have been there for me from day 1 and you have shaped who I am for the last 15 years; thank you for loving me unconditionally and always believing in me. Jess, Alex, Marie, Megs, Kels, Rubes, Sash, Kayla, Is and Souls; you are forever my soul sisters and I want to thank you for always being my biggest cheerleaders.

And finally, my family. In particular my parents and sister. I am so fortunate to have you. The countless hours you have spent encouraging and guiding me, from Dad providing anaesthetic, code and IT support, to Jen drafting countless applications, and Mum for endlessly loving and supporting me. I truly cannot ever thank you enough.

Publications arising from this thesis

SORBY-ADAMS, A. J., MARCOIONNI, A. M., DEMPSEY, E. R., WOENIG, J. A. & TURNER, R. J. 2017. The role of neurogenic inflammation in blood-brain barrier disruption and development of cerebral oedema following acute central nervous system (CNS) injury. *International Journal of Molecular Sciences,* 18.

SORBY-ADAMS, A. J., VINK, R. & TURNER, R. J. 2018. Large animal models of stroke and traumatic brain injury as translational tools. *American Journal of Physiology. Regulatory, Integrative and Comparative Physiology,* 315, R165.

SORBY-ADAMS, A. J., LEONARD, A. V., ELMS, L. E., MARIAN, O. C., HOVING, J. W., YASSI, N., VINK, R., THORNTON, E. & TURNER, R. J. 2019. Determining the temporal profile of intracranial pressure changes following transient stroke in an ovine model. *Frontiers in Neuroscience,* 13, 587.

SORBY-ADAMS, A. J., LEONARD, A. V., HOVING, J. W., YASSI, N., VINK, R., WELLS, A. J. & TURNER, R. J. 2019. NK1-R antagonist treatment comparable to decompressive craniectomy in reducing intracranial pressure following stroke. *Frontiers in Neuroscience,* 13, 681.

Contributions made by co-authors

The following people have contributed to authorship of the manuscripts enclosed in this thesis (in alphabetical order): Isabella M Bilecki, Jonathan Camargo Leyva, Robert Crowther, Eden R Dempsey, Levi E Elms, Jan W Hoving, Claire Jones, Anna V Leonard, Amanda M Marcoionni, Oana C Marian, Emma Thornton, Renée J Turner, Robert Vink, Adam J Wells, Joshua A Woenig, and Nawaf Yassi. The individual contributions of each author can be summarised as:

Conceptualisation of the work: ASA, RJT, AVL, CJ, RV, AJW, NY, RC.

Realisation of the work: ASA, RJT, AVL, CJ, ET, AJW, NY, OM, LE, IB, JH, JCL.

Documentation of the work: ASA, RJT, AVL, CJ, ET, AJW, NY, RV, OM, LE, IB, JH, AM, ED, JW, JCL.

Editing and review of the work: ASA, RJT, AVL, CJ.

Additional publications

SORBY-ADAMS, A. J., SCHNEIDER, W. T., GONCALVES, R. P., KNOLLE, F. & MORTON, A. J. 2020. Measuring executive function in sheep (Ovis aries) using visual stimuli in a semi-automated operant system. *Journal of Neuroscience Methods,* 351**,** 109009.

SORBY-ADAMS, A. J., LEAROYD, A. E., BATH, P. M., FARR, T. D., LEONARD, A. V., SCHIESSI, I., ALLAN, S. M., TURNER, R. J., AND TRUEMAN, R. C. 2021. Glyceryl trinitrate for the treatment of ischaemic stroke: determining efficacy in rodent and ovine species for enhanced clinical translation. *Journal of Cerebral Blood Flow and Metabolism, In Revision.*

Presentations arising from this thesis

Invited Presentations

1. Peter Couche Foundation Stroke Survivor Forum, Adelaide, Australia – *Contemporary collaboration in stroke research*, November 2020.

2. Neurosurgical Research Foundation Annual General Meeting, Adelaide, Australia – *Treating post-stroke brain swelling and elevated intracranial pressure*, September 2020.

3. Department of Neurology, The Royal Melbourne Hospital, University of Melbourne, Melbourne, Australia – *Bridging the gap: the importance of large animal models for improved clinical translation in stroke*, May 2020.

4. University of Manchester, Division of Neuroscience and Experimental Psychology, Manchester, United Kingdom – *Different strokes for different folks: the importance of large animal models for improved clinical translation in stroke*, December 2019.

5. Stroke Coalition of Preclinical Researchers (Stroke CORE) Meeting, Brisbane, Australia – *Overview, research and collaboration in the Translational Neuropathology Laboratory*, December 2018.

6. Vicon Motion Systems Headquarters, Oxford, United Kingdom – *Improving clinical translation in stroke: Using motion capture to determine functional recovery in an*

ovine stroke model, October 2018.

7. University of Oxford, Radcliffe Department of Medicine, Laboratory of Cerebral Ischaemia, Oxford, United Kingdom – *Large animal models of stroke as translational tools: targeting cerebral oedema and ICP in an ovine model*, October 2018.

8. Fraunhofer Institute for Cell Therapy and Immunology, Department of Cell Therapy, Leipzig, Germany – *Developing a biomechanical model to assess function in an ovine model of stroke*, October 2018.

9. The University of Nottingham, Division of Clinical Neurosciences, Nottingham, United Kingdom – *A novel approach to improving clinical translation in stroke: targeting cerebral oedema and ICP in a large animal model*, October 2018.

10. Stroke Society of Australasia STROKE 2018 Conference, Sydney, Australia – *From STAIRs to High Hurdles – developing a method of functional assessment in an ovine stroke model*- in Neurosciences Symposium, August 2018.

11. Neurosurgical Research Foundation Annual General Meeting, Adelaide, Australia – *Targeting brain swelling and pressure post-stroke*, September 2016.

Conference Presentations

1. **Sorby-Adams,** A., Leonard, A., Thornton, E., Vink, R., and Turner, R. *'Climbing the STAIRs for improved clinical translation: NK1 receptor antagonist treatment for the reduction of cerebral oedema and intracranial pressure following stroke in an ovine model*', Oral Presentation at the National Institutes of Health Stroke Research (NIHR) Workshop, Manchester, United Kingdom, September 2019.

2. **Sorby-Adams,** A., Leonard, A., Thornton, E., Vink, R., and Turner, R. *'Developing a method to assess functional recovery following stroke in a large animal model: a biomechanical and neurological outcome approach'*, Poster Presentation at BRAIN and PET, Yokohama, Japan, July 2019.

3. **Sorby-Adams**, A., Leonard, A., Thornton, E., Vink, R., and Turner, R. *'Targeting Cerebral Oedema and Intracranial Pressure in an ovine model: the NK1 receptor antagonist as a novel therapy'*, Poster Presentation at the Australasian Neuroscience Society Annual Scientific Meeting, Brisbane, December 2018.

4. **Sorby-Adams**, A., Leonard, A., Thornton, E., Vink, R., and Turner, R. *'Targeting Cerebral Oedema and Intracranial Pressure in an ovine model: the NK1 receptor antagonist as a novel therapy'*, Oral presentation at the 10th International Symposium on Neuroprotection and Neurorepair, Dresden, Germany, October 2018.

5. **Sorby-Adams,** A., Leonard, A., Thornton, E., Vink, R., and Turner, R. *'A novel agent for the treatment of cerebral oedema and elevated intracranial pressure*

following stroke in an ovine model', Poster presentation at the Australian Society of Medical Research SA Scientific Meeting, Adelaide, June 2018.

6. **Sorby-Adams**, A., Leonard, A., Thornton, E., Vink, R., and Turner, R. *'A novel agent for the treatment of cerebral oedema and elevated intracranial pressure following stroke in an ovine model'*, Poster Presentation at the Australasian Neuroscience Society Annual Scientific Meeting, Sydney, December 2017.

7. **Sorby-Adams**, A., Leonard, A., Thornton, E., Vink, R., and Turner, R. *'A novel agent for the treatment of cerebral oedema and elevated intracranial pressure following stroke in an ovine model'*, Poster Presentation at the Florey Postgraduate Research Conference, Adelaide, September 2017.

8. **Sorby-Adams**, A., Leonard, A., Thornton, E., Vink, R., and Turner, R. *'Take the pressure down: a novel agent for the treatment of cerebral oedema and elevated intracranial pressure following stroke'*, Oral presentation at the Australian Neurotrauma Forum, Hobart, October 2017.

9. **Sorby-Adams**, A., Leonard, A., Thornton, E., Vink, R., and Turner, R. *'Take the pressure down: a novel agent for the treatment of cerebral oedema and elevated intracranial pressure following stroke'*, Oral presentation at the Australian Society for Medical Research SA Scientific Meeting, Adelaide, June 2017.

10. **Sorby-Adams,** A., Leonard, A., Thornton, E., Hunter, D. and Turner, R. *'Delayed NK1 tachykinin receptor antagonist treatment reduces ICP following stroke in an*

ovine model', Poster Presentation at the Brain and PET Conference, Berlin, April 2017.

11. **Sorby-Adams,** A., Leonard, A., Thornton, E., Vink, R., and Turner, R. *'Characterising the temporal profile of cerebral oedema and intracranial pressure following stroke in an ovine model'*, Oral presentation at the Australasian Neuroscience Society Annual Scientific Meeting, Hobart, December 2016.

12. **Sorby-Adams**, A., Leonard, A., Thornton, E., Vink, R., and Turner, R. *'Determining the temporal profile of cerebral oedema and intracranial pressure following stroke in an ovine model'*, Oral presentation at the Australian and New Zealand Society for Neuropathology (ANZSNP) Scientific Meeting, Hobart, December 2016.

13. **Sorby-Adams**, A., Leonard, A., Thornton, E., Vink, R., and Turner, R. *'Characterising the temporal profile of cerebral oedema and intracranial pressure following stroke in an ovine model'*, Oral presentation at The Australian Society for Medical Research SA Scientific Meeting, Adelaide, June 2016.

14. **Sorby-Adams**, A., Leonard, A., Thornton, E., Vink, R., and Turner, R. *'Determining the temporal profile of cerebral oedema and elevated intracranial pressure following transient ovine MCA occlusion'*, Poster presentation at the Australian Neurotrauma Forum, Adelaide, October 2015.

Awards arising from this thesis

Brain Foundation Elizabeth Penfold Award, 2020.

Awarded for the best piece of original research in any of the neurosciences published in the last two years on the advice of three or more judges nominated by the Brain Foundation. Title of Paper: NK1-R antagonist treatment comparable to decompressive craniectomy in reducing intracranial pressure following stroke (2019) as published in *Frontiers in Neuroscience* 13: 681. Adelaide, South Australia.

National Institutes of Health Stroke Research Workshop Best Oral Presentation, 2019. Awarded for best oral presentation at the Annual Stroke Research Workshop. Manchester, United Kingdom.

South Australian Young Achiever of the Year Finalist, 2019. Finalist for the 2019 Young Achiever award in the STEM Category, recognising the innovation of young STEM learners and their contribution to the field. Adelaide, Australia.

Klaus Reymann Young Scientist Award, 2018. Awarded for an excellent contribution by a junior scientist to the field at the 10th International Symposium on Neuroprotection and Neurorepair. Dresden, Germany.

CSL Florey Next Generation Award Finalist, 2018. University finalist for the CSL Florey Next Generation award, recognising a PhD candidate who has demonstrated outstanding capability, creativity and potential in the biomedical sciences and/or health and medical research. Adelaide, Australia.

Hans-Jürgen and Marianne Ohff Grant, 2018. Research Grant awarded to support international travel to Germany for a conference (Dresden) and laboratory visit (Leipzig) to disseminate doctoral research findings. Adelaide, Australia.

Australian Society of Medical Research (ASMR) South Australian Scientific Meeting People's Choice Award, 2018. People's Choice Award for the best poster presentation at the annual ASMR Scientific Meeting. Adelaide, Australia.

Florey Postgraduate Research Conference CMAX Prize, 2017. Awarded for the best translational research poster presentation at the annual Florey Postgraduate Research Conference. Adelaide, Australia

Australasian Neuroscience Society, **Student Travel Award, 2016**. Awarded to support travel to present doctoral findings at the Australian Neuroscience Society Meeting. Hobart, Australia,

Thesis explanation

This thesis investigates the mechanisms underlying ischaemic stroke to subsequently determine the efficacy of a novel therapeutic agent targeting oedema and elevated intracranial pressure. Significant efforts were made throughout the course of candidature to publish research findings; therefore, this thesis contains 4 published papers, and 2 papers prepared in publication format. The overarching structure of the thesis is as follows; a general introduction, two review papers, a synopsis of the relevant background information, a methods chapter, four research papers, a general discussion, references, and appendices.

Due to the extensive background information underpinning this doctorate, the first 3 Chapters detail the ultimate purpose of this thesis. The first chapter is a general introduction to stroke, the second introduces the reader to the therapeutic target investigated, and the third highlights large animal models of stroke currently available to increase clinical translation. Introductory Chapters 2 and 3 comprise previously published works; however, these have been revised to avoid excessive repetition and to improve flow of concepts. Introductory chapters are then summarised in a brief synopsis including the overarching rationale for this thesis, choice of animal model used, and the doctoral aims (Chapter 4), following which project methods are discussed in detail (Chapter 5).

The experimental chapters provided include those that have already been published (Chapters 6 and 7, presented as accepted for publication) and those prepared in publication format (Chapters 8 and 9). The overall thesis is then summarised in a general discussion (Chapter 10). Chapters that have been published or prepared in publication format are prefaced by a signed statement of authorship.

Abbreviations

ABP	arterial blood pressure
ACA	anterior cerebral artery
ACoA	anterior communicating artery
ADC	apparent diffusion coefficient
AMPA	a-amino-3-hydroxy-5-methyl-4-isoxazolepropionic acid
ANOVA	analysis of variance
APA	ascending pharyngeal artery
AQP	aquaporin
ASIC	acid-sensing ion channel
ATP	adenosine triphosphate
BBB	blood-brain barrier
BCL-2	B-cell lymphoma
BCSF	blood-cerebrospinal fluid
Ca^{2+}	calcium ion
CAT	catalase
Cav-1	caveolin-1
CBF	cerebral blood flow
CBV	cerebral blood volume
CGRP	calcitonin gene-related peptide
CI	confidence interval
Cl^{-}	chloride ion
CLR	calcitonin receptor-like receptor
$CMRO_2$	cerebral oxygen metabolic rate
CNS	central nervous system
CO2	carbon dioxide
coW	circle of Willis
C_{max}	maximum concentration
CPP	cerebral perfusion pressure
CSF	cerebrospinal fluid
CT	computed tomography
DC	decompressive craniectomy
DCE	dynamic contrast enhancement
DNA	deoxyribonucleic acid
DSC	dynamic susceptibility contrast
DTI	diffusion tractography imaging
DWI	diffusion weighted imaging
EDTA	Ethylenediaminetetraacetic acid
ELISA	enzyme linked immunosorbent assay

FA	flip angle
FLAIR	fluid attenuated inversion recovery
fMRI	functional magnetic resonance imaging
GAD	Gadolinium-diethylene-triamine-pentaacetic acid
GFAP	glial fibrillary acidic protein
Glu	glutamate
gp60	60-kD glycoprotein
GPX	glutathione peroxidase
H+	hydrogen ion
H_2O_2	hydrogen peroxide
HTS	hypertonic saline
I/R	ischaemia reperfusion
ICA	internal carotid artery
ICAM	intracellular adhesion molecule 1
ICC	intraclass correlation coefficient
ICH	intracerebral haemorrhage
ICP	intracranial pressure
IFN-γ	interferon gamma
IHC	immunohistochemistry
IL	interleukin
IP^3	inositol-1,4,5-triphosphate
IT	inversion time
IV	intravenous
JAM's	junctional adhesion molecules
K^+	potassium ion
MABP	mean arterial blood pressure
MAC	minimum alveolar concentration
MAGUK	membrane-associated guanylate kinase
MCA	middle cerebral artery
MCAo	middle cerebral artery occlusion
MDCK	Madin-Darby Canine Kidney
mGlu	metabotropic glutamate
MLS	midline shift
MMCAI	malignant middle cerebral artery infarction
MMP	matrix metalloproteinase
MPRAGE	magnetisation-prepared rapid acquisition with gradient echo
MRA	magnetic resonance angiography
MRI	magnetic resonance imaging
mRS	modified Rankin Scale
NA	number of averages

Na^+	sodium ion
NAD^+	nicotinamide adenine dinucleotide
NF-κB	nuclear factor kappa-light-chain-enhancer of activated B cell
NF-AT	Nuclear factor of activated T-cells
NHMRC	National Health and Medical Research Council
NHP	non-human primate
NIHSS	National Institutes of Health Stroke Scale
NK	neurokinin
NK1-R	neurokinin 1 tachykinin receptor
NKCC1	Na + -K + -2Cl-cotransporter
NMDA	N-methyl-D-aspartate
nNOS	neuronal nitric oxide synthase
NO	nitric oxide
NO_3^-	peroxynitrite
NSAID	non-steroidal anti-inflammatory
NVU	neurovascular unit
O_2	oxygen
O_2^-	superoxide anion
OH•	hydroxyl radical
PARP-1	poly(ADP-ribose)polymerase-1
$PbtO_2$	brain tissue oxygenation
PCA	posterior cerebral artery
pCO_2	partial pressure of carbon dioxide
PCoA	posterior communicating artery
PET	positron emission tomography
PID	peri-infarct depolarisation
PIRL	Preclinical and Imaging Research Laboratories
PK	pharmacokinetic
PMCA	plasma membrane Ca^{2+}-ATPase
pMCAo	permanent middle cerebral artery occlusion
PNS	peripheral nervous system
pO_2	partial pressure of oxygen
PSD	post-stroke depression
PSD-95	post-synaptic density protein 95
RAMP	receptor activity modifying protein
RET	reverse electron transport
RCF	relative centrifugal force
ROI	region of interest
ROS	reactive oxygen species
SAH	subarachnoid haemorrhage

SAHMRI	South Australian Health and Medical Research Institute
SD	standard deviation
SEM	standard error of the mean
SOD	superoxide dismutase
SP	substance P
STAIR	Stroke Therapy Academic Industry Roundtable
SUR1	sulfonylurea receptor 1
TBI	traumatic brain injury
TE	echo time
TIA	transient ischaemic attack
TJ	tight junction
T_{max}	timing of the maximum
tMCAo	transient middle cerebral artery occlusion
TNF-α	tumour necrosis factor alpha
TOF	time-of-flight
tPA	tissue plasminogen activator
TRP	transient receptor potential
TRPV-1	transient receptor potential vanilloid receptor subtype 1
TR	repetition time
TSE	turbo spin echo
TTC	2,3,5-Triphenyltetrazolium chloride
US	United States
UK	United Kingdom
VA's	vertebral arteries
WHO	World Health Organization
ZO-1	zonula occluin-1

List of Figures

CHAPTER 1

CHAPTER 2

CHAPTER 3

CHAPTER 5

CHAPTER 6

CHAPTER 7

CHAPTER 8

CHAPTER 9

CHAPTER 10

List of Tables

Style Conventions

The abbreviations, punctuations and reference style used in this thesis conform with the *Oxford style manual* and *Harvard referencing style*. The spelling is British English and conforms with the *Oxford English Dictionary*.

Financial support

My doctoral studies were supported by funding from the Government of Australia (Research Training Scholarship) and the Peter Couche Foundation (doctoral top-up scholarship). The research carried out throughout the course of this thesis was supported by funding from the National Health and Medical Research Council (NHMRC; Project Grant 1082556), Brain Foundation (Australia) and the NeuroSurgical Research Foundation (Australia).

01

General Introduction

1.0 INTRODUCTION

Stroke is the second leading cause of mortality, and the principal cause of adult neurological disability, worldwide (Gorelick, 2019, Avan et al., 2019). Initially characterised by the World Health Organization (WHO) in 1970, stroke is defined as an acute onset of neurological deterioration, lasting more than 24 hours or leading to death, with no apparent cause other than that of presumed vascular origin (Muir, 2013, Markus, 2016). Since formulation of this definition, significant advances have been made in the fields of public health, medicine and basic science, which have dramatically increased our understanding of the pathophysiology and clinical manifestations of stroke (Sacco et al., 2013). The mechanisms underlying the disease are now recognised as a complex cascade of interrelated events leading to cell death and consequent patient deterioration. The purpose of this general introduction is to provide an overview of the molecular mechanisms underlying stroke, its complications and implications for treatment.

1.1 STROKE

1.1.1 Epidemiology

There are more than 80 million stroke survivors globally, and approximately 17 million people experiencing a new or recurrent event each year (Virani et al., 2020, Feigin et al., 2018, Gorelick, 2019). Despite improvements in stroke prevention and management, accumulating risk factors such as atherosclerosis and atrial fibrillation, together with a burgeoning elderly population, contribute to an increasing lifetime risk (Virani et al., 2020, Feigin et al., 2018), whereby a significant rise in the number of individuals living with stroke and its consequences is predicted to occur by the year 2030 (Ovbiagele et al., 2013). In Europe, the annual cost of stroke treatment and care is an estimated 27 billion euros, and in

2012, the cost of stroke in the United States (US) of America reached 71.5 billion US dollars (Rajsic et al., 2019). Given the increasing incidence of stroke, the American Heart Association has projected that by 2030, the total direct cost for stroke will reach up to 184.1 billion US dollars per annum (Ovbiagele et al., 2013). This has significant repercussions for the global economy and highlights the importance of stroke prevention and improved treatment through the development of novel therapies.

1.1.2 Aetiology

Disturbance of cerebral function in stroke is established to arise secondary to reduced perfusion of oxygen-and nutrient-providing arterial blood to neuronal tissue, compromising function and ultimately resulting in neuronal cell death. Neurovascular deficits can arise by two primary mechanisms: haemorrhage or ischaemia (Virani et al., 2020). Haemorrhagic stroke occurs when an arterial blood vessel within the brain bursts, resulting in leakage of blood into the surrounding tissue, and the development of either subarachnoid haemorrhage (SAH) or intracerebral haemorrhage (ICH). In comparison, ischaemic stroke arises as a result of arterial occlusion within the internal carotid or cerebral arteries, caused by thrombosis, embolism or systemic hypoperfusion, ultimately resulting in either permanent or temporary restriction of blood flow through the affected artery. In both stroke types, the symptoms observed post-ictus are largely associated with the anatomical location of the vessel affected and the respective distribution of blood flow. Given that the vast majority of strokes are ischaemic in nature, accounting for upwards of 87% of all stroke cases (Virani et al., 2020), ischaemic stroke will be the focus of this thesis.

1.1.3 Cerebrovascular Anatomy and Clinical Manifestations

The cerebrovasculature of humans is convoluted and highly complex, spanning a distance of approximately 700 kilometres (Greif and Eichmann, 2014). Blood is supplied to the brain via the circle of Willis (coW), a complex circulatory anastomosis at the base of the brain, which receives blood from the internal carotid arteries (ICAs) and vertebrobasilar system (Rosner et al., 2020). The coW, in turn, gives rise to three major paired arteries: the middle cerebral arteries (MCAs), anterior cerebral arteries (ACAs) and posterior cerebral arteries (PCAs) (Krishnaswamy et al., 2009). In cases of ischaemic stroke, these branches are considered end arteries, with occlusion markedly reducing blood supply to the brain territory supplied by the artery downstream. Clinically, the MCA is the most common site of occlusion, followed by the ACA and PCA, with resultant manifestations allowing for identification of the affected vessel (Nogles and Galuska, 2020).

1.1.3.1 Middle Cerebral Artery

The MCA supplies blood to 85% of the cerebral hemispheres (Figure 1.1). Considered a natural continuation of the ICA, it is subdivided into M1 sphenoidal/horizontal, M2 insular, M3 opercular and M4 cortical segments (Konan et al., 2020). The M1 segment, which horizontally traverses the sphenoidal sylvian fissure, gives rise to lateral lenticulostriate branches, which supply the caudate nucleus, internal capsule and basal ganglia (Navarro-Orozco and Sanchez-Manso, 2020). Upon reaching the junction of the operculo-insular cleft of the sylvian fissure, the M1 segment bifurcates into M2 branches, comprising superior and inferior trunks. The M2 branches run along the surface and subsequently supply blood to the insula, terminating at the central sulcus. Here, the M2 divides into M3 opercular branches, which traverse the superficial part of the sylvian fissure, ultimately branching into terminal cortical branches (M4). Branches of M4 comprise both superior and inferior divisions, which

supply almost the entire lateral surface of the brain including the motor and sensorimotor cortices, responsible for modulating motor and sensory functions of the face and upper extremities (Hui et al., 2020).

Occlusion of the MCA, clinically referred to as malignant middle cerebral artery infarction (MMCAI), often presents as hemiplegia and hemiparesis of the upper limbs, face and mouth, contralateral to the lesion, because of decussation of fibres at the level of the medulla oblongata (Navarro-Orozco and Sanchez-Manso, 2020). Additional impediments include dysarthria, aphasia and hemi-neglect (Acharya and Wroten, 2020). The superior division of M4 also gives rise to the artery of the precentral sulcus, which supplies the Broca's area, responsible for speech production. The middle temporal branches of M4 supply the primary auditory complex and Wernicke's area, which is responsible for speech comprehension (Acharya and Wroten, 2020). Accordingly, occlusion of the cortical M4 branches can result in Broca's aphasia and loss of verbal fluency, or Wernicke's aphasia, where the patient presents with impaired ability to comprehend spoken language (Acharya and Wroten, 2020, Ochfeld et al., 2010). This, however, is dependent on the individual and their respective dominant hemisphere for language.

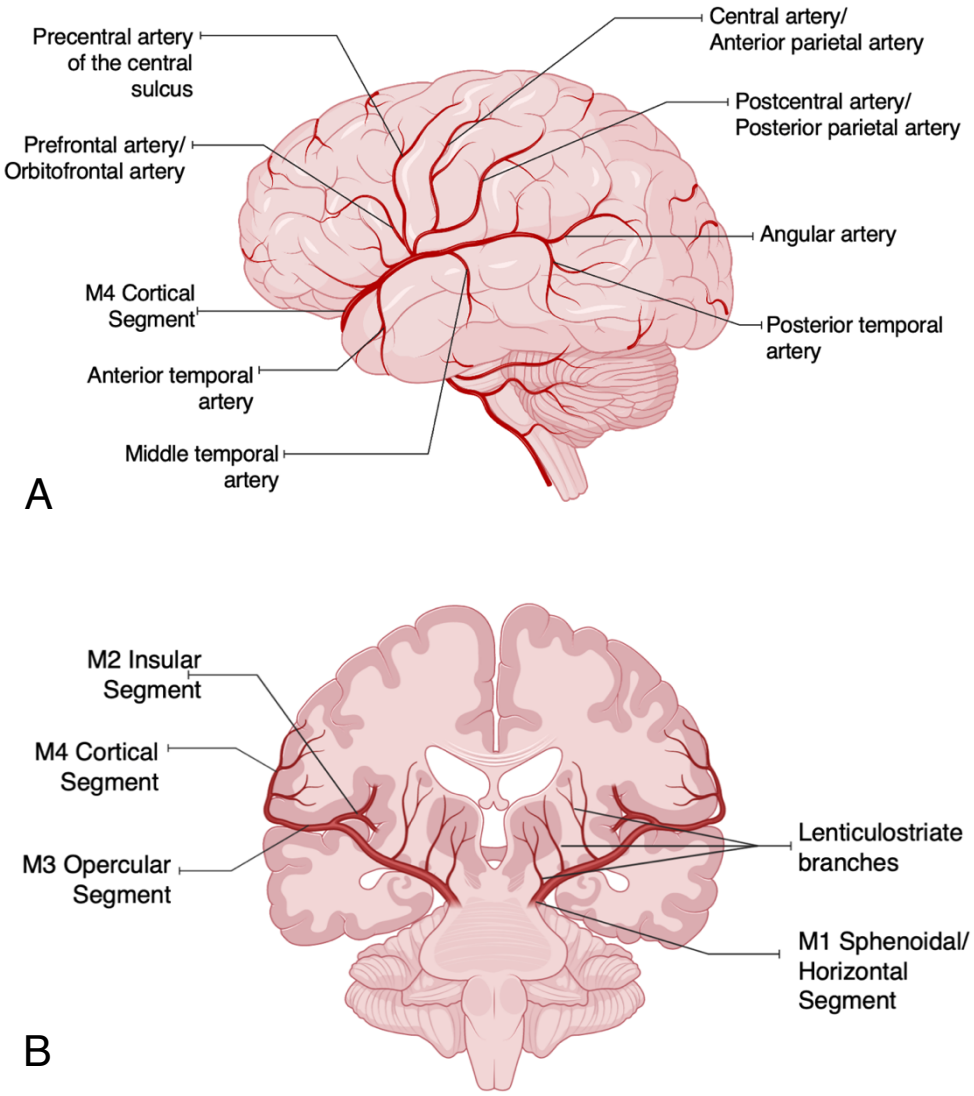

Figure 1.1. Cerebrovascular distribution of the middle cerebral artery and its branches. (A) Lateral view of the brain showing cortical M4 segment of the MCA and its branches. (B) Coronal view of the brain at the level of the thalamus showing M1 horizonal, M2 insular, M3 opercular and M4 cortical segments of the MCA, including lenticulostriate branches of M1 supplying sub-cortical structures. *Figure reprinted from 'Brain (lateral with arteries)' and 'Coronal brain with vessels (at caudal thalamus)', by BioRender.com (2021).*

1.1.3.2 Anterior Cerebral Artery

The ACA lies within the longitudinal fissure and comprises five segments, termed A1 to A5. These segments give rise to polar frontal, calossomarginal and pericallosal branches (Figure 1.2), which extend anteromedially to supply the midline portion of the frontal lobes and superior medial parietal lobes. Infarcts involving the ACA and its territories are uncommon

because of the rich anastomoses between cortical branches (Matos Casano et al., 2020). In individuals affected, however, deficits characteristically present as contralateral lower limb hemiparesis and hemiplegia. Other motor deficits can include bradykinesia, hypometria, akinesia, tremor, dystonia and motor neglect (Toyoda, 2012, Honig et al., 2017).

1.1.3.3 Posterior Cerebral Artery

The PCA is divided into four segments (Figure 1.2), P1 to P4, comprising anterior temporal, posterior temporal, medial occipital, posterior pericallosal, calcarine and parietooccipital branches, which largely supply the occipital lobe, in addition to the inferomedial portion of the temporal lobe, the midbrain and the upper brain stem (Konan et al., 2020). Interruption of blood supply through the PCA and its branches often presents as visual disturbances including hemianopia, quadrantanopia and visual agnosia. Patients may also present with cognitive and neuropsychological dysfunctions, including aphasia and memory impairment.

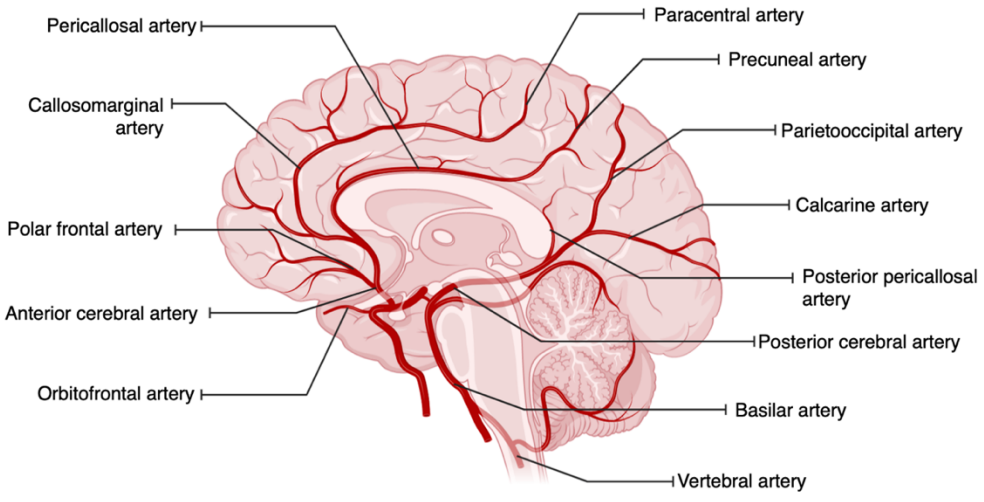

Figure 1.2. Cerebrovascular distribution of the anterior cerebral artery and posterior cerebral artery from a mid-sagittal view of the brain. *Figure reprinted from 'Brain (sagittal with arteries)', by BioRender.com (2020).*

1.1.4 Cerebral Collateralisation – Infarct Core and Penumbra

Each major branch of the MCA, ACA and PCA subsequently give rise to multiple small anastomoses to provide collateralisation of blood flow. Accordingly, if an artery supplying one region of the brain is occluded, neurons receiving direct blood supply will have almost complete cessation of cerebral blood flow (CBF), but neurons in the surrounding region will continue to receive blood, albeit reduced, from surrounding collateral vessels (Agarwal et al., 2013). Neurons receiving direct supply rapidly succumb to ischaemia, necrotising and becoming the infarct core. Cells surrounding the core become the penumbra, and although they too are receiving reduced blood and are electrically silent, supply via collateral vessels is sufficient to sustain survival (Doyle et al., 2008). By definition, regions of the brain receiving CBF below 20 mL/100 g/min define the penumbra; this is compared with regions of normal blood flow of ±50 mL/100 g/min. When blood flow is <10 mL/100 g/min, the tissue forms the infarct core (Hakim, 1998).

Despite receiving blood supply, although reduced, penumbral neurons remain at risk of conversion to permanent infarction if supply is not re-established in a timely manner, with every minute passing in which the vessel remains obstructed resulting in the death of 1.9 million neurons, loss of 14 billion synapses and destruction of 12 kilometres of myelinated axons (Saver, 2006). Therefore, the duration of ischaemia and overall CBF (as shown in Figure 1.3) play a crucial role in determining the fate of individual neurons (Doyle et al., 2008).

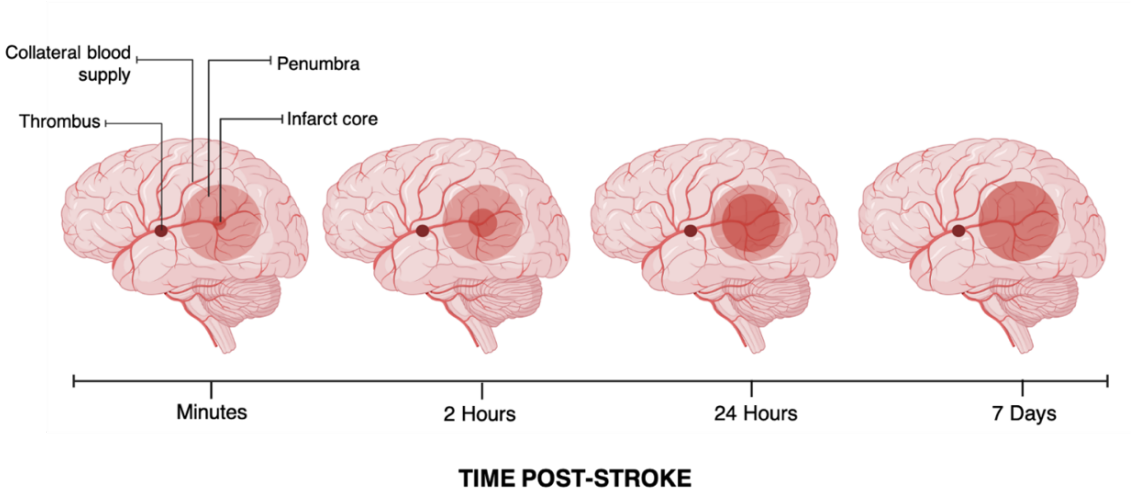

Figure 1.3. Evolution of the ischaemic penumbra. Vascular occlusion due to thrombosis or thromboembolism results in hypoperfusion to brain tissue within minutes of onset. The area of the brain receiving direct blood supply from the vessel rapidly succumbs to ischaemia and becomes the infarct core (dark pink). The area surrounding the core continues to receive blood supply, although diminished, from surrounding collateral vessels, thus becoming the ischaemic penumbra (light pink). If occlusion persists, the infarct core expands because of penumbral cells succumbing to persistent hypoperfusion. Infarct expansion continues to develop within the first 24 hours of stroke onset, whereby if blood flow is not re-established, the infarct eventually comprises all core and penumbral cells, which ultimately die because of persistent lack of blood supply, as seen at 7 days. *Figure created with BioRender.com (2021).*

1.2 STROKE PATHOPHYSIOLOGY

1.2.1 Mechanisms of Ischaemic Cell Death

At rest, the brain is responsible for up to 20% of the body's oxygen consumption (Özugur et al., 2020). Unlike other organ systems, neurons are reliant upon a constant supply of glucose to perform oxidative phosphorylation for the production of adenosine triphosphate (ATP) as the blood–brain barrier (BBB) restricts the movement of other energy sources, such as fatty acids, ketones and amino acids, into the brain (Robbins and Swanson, 2014). Consequently, immediately following cessation of blood supply, inhibition of mitochondrial aerobic respiration occurs. Under anaerobic conditions, mitochondria are forced to generate ATP via glycolysis, whereby lactate is produced, accumulating within cells and rapidly decreasing

intracellular pH (Kalogeris et al., 2012). Anaerobic respiration is significantly less efficient, with only two ATP molecules yielded per cycle compared with 36 under aerobic conditions (Sims and Anderson, 2002, Kalogeris et al., 2012). As a consequence, neuronal ATP stores are considerably diminished, resulting in impaired neuronal function.

1.2.2 Ionic Imbalances

The Na^+/K^+-ATPase pump is found in abundance in neuronal plasma membranes. Physiologically, Na^+/K^+-ATPase pumps consume in excess of 70% of the energy supplied to the brain as they are responsible for maintaining the ionic gradients of Na^+ and K^+ across the cell membranes, necessary for propagation of action potentials (Edvinsson et al., 1993). Immediately following onset of ischaemia, Na^+/K^+-ATPase pumps rapidly consume remaining ATP stores, such that within ±2 minutes, all remaining reserves are exhausted (Doyle et al., 2008). This leads to failure of energy-dependent processes, including the activity of the Na^+/K^+-ATPase pump itself and plasma membrane Ca^{2+}-ATPase (PMCA), a transport protein responsible for maintaining a physiologically low intracellular Ca^{2+} concentration (Edvinsson et al., 1993). Consequently, a rapid efflux of K^+ and influx of both Na^+ and Ca^{2+} ensues. Elevated extracellular K^+ and intracellular Na^+ and Ca^{2+} causes upregulation of Na^+-K^+-$2Cl^-$ co-transporter 1 (NKCC1), allowing for an influx of Cl^- into the cell (Martín-Aragón Baudel et al., 2017, Huang et al., 2019). The resultant ionic imbalances grossly increase intracellular hyperosmolarity and cause neuronal cell membrane depolarisation.

1.2.3 Excitotoxicity and Acidotoxicity

Neuronal depolarisation in cells that comprise the infarct core precipitates the abnormal and excessive release of neurotransmitters from axon terminals, with release of the excitatory

neurotransmitter glutamate playing a critical role in ischaemic pathophysiology. Elevated extracellular levels of glutamate and K^+ initiate peri-infarct depolarisation (PID) within minutes of ischaemic onset. Repeated PID leads to excessive accumulation of intracellular Ca^{2+}, expansion of compromised cells and resultant penumbral formation (Doyle et al., 2008, Hartings et al., 2003). Enhanced synaptic glutamate concentration also increases activation of N-methyl-D-aspartate (NMDA) and a-amino-3-hydroxy-5-methyl-4-isoxazolepropionic acid (AMPA) receptors (Doyle et al., 2008). NMDA receptors are permeable to Ca^{2+}, allowing for an additional influx upon activation, exacerbating the release of glutamate, termed excitotoxicity. Ischaemic injury further enhances the permeability of AMPA receptors to Ca^{2+}, leading to a prolonged and pathological intracellular influx. Glutamate also acts on G-protein coupled metabotropic glutamate (mGlu) receptors, which further contribute to excitotoxicity. Upon glutamate binding, mGlu G-protein subunit disassociation leads to increased production of secondary messenger inositol-1,4,5-triphosphate (IP^3), resulting in increased release of endoplasmic reticulum Ca^{2+} into the cytosol (Neumar, 2000). In concert with excitotoxicity, acidotoxicity due to intracellular acidosis initiates activation of acid-sensing ion channels (ASICs), with stimulation of glutamate-independent ASIC subtype 1a leading to a further influx of Ca^{2+} into the neuron (Simon, 2006).

Concurrent excitotoxicity and acidotoxicity enormously increase the intracellular Ca^{2+} concentration. Physiologically, intracellular levels of Ca^{2+} are around 0.1–1 μM but, under ischaemic conditions, rise to 50–100 μM (Doyle et al., 2008). Excessive Ca^{2+} accumulation initiates activation of many, if not all, deleterious Ca^{2+}-dependent enzymes, including proteases, phospholipases and deoxyribonucleic acid (DNA)-ases (Edvinsson et al., 1993). Catabolic enzymatic degradation of vital intracellular structures ensues, including lipolysis, proteolysis and endonuclease-mediated DNA destruction (Neumar, 2000). In the absence of

abundant ATP, cells are unable to undergo repair and resynthesis of vital structures, resulting in significant cellular damage, which grossly affects neuronal function. Such aberrant Ca^{2+} accumulation and excitatory neurotransmitter release can thus rapidly lead to acido- and excito- toxic cell death.

1.2.4 Reactive Oxygen Species

Intracellular overload of Ca^{2+} causes excessive mitochondrial production of deleterious reactive oxygen species (ROS), in particular superoxide anion (O_2^-), hydroxyl radical (OH•) and hydrogen peroxide (H_2O_2) (Neumar, 2000). As a consequence of excitotoxicity, NMDA receptors also recruit Ca^{2+}-dependent nitric oxide synthase (nNOS) via post-synaptic density protein 95 (PSD-95), resulting in the production of nitric oxide (NO) (Reis et al., 2017). NO subsequently combines with mitochondrial O_2^- to form the potent free radical, peroxynitrite (NO_3^-) (Reis et al., 2017). Neuronal tissue is particularly susceptible to free radicals because of low endogenous levels of antioxidants, including superoxide dismutase (SOD), glutathione peroxidase (GPX) and catalase (CAT) (Li and Yang, 2016). Overproduction of ROS under ischaemic conditions rapidly consumes remaining antioxidant stores, leading to oxidative stress. Here, unchecked abundant free radicals, in particular NO_3^-, cause destruction of cellular structures and key molecules including proteins, lipids and DNA (Sugawara and Chan, 2003).

There is evidence to suggest that early damage to DNA is able to undergo a degree of repair due to activation of poly(ADP-ribose)polymerase-1 (PARP-1) by NO. However, to perform its function, PARP-1 exhausts intracellular nicotinamide adenine dinucleotide (NAD^+), necessary for producing remaining ATP via glycolysis (Neumar, 2000). This results in complete ATP starvation within the cells, energy failure and resultant necrotic cell death.

ROS overproduction also leads to activation of resident brain microglia, which subsequently secrete ROS and additional cytotoxic factors such as the pro-inflammatory cytokines interleukin (IL)-1, IL-6 and tumour necrosis factor alpha (TNF-α) (Jiang et al., 2018). These cytokines enhance the expression of intercellular adhesion molecule-1 (ICAM-1), P-selectin and E-selectin, causing leukocyte migration, neuroinflammation and exacerbation of cell damage in a vicious cycle (Jiang et al., 2018).

1.2.5 Apoptosis

Ischaemic mitochondrial dysfunction also plays a critical role in mediating programmed cell death via apoptosis (Bakthavachalam and Shanmugam, 2017). Ca^{2+} overload leads to pore formation in the outer mitochondrial membrane (the mitochondrial permeability transition pore, mtPTP) facilitated by a group of pro-apoptotic proteins of the B-cell lymphoma (BCL-2) line, including Bax and/or Bak, facilitated by proteins Bad and Bid (Neumar, 2000). Pore formation subsequently initiates the intrinsic apoptotic pathway via cytochrome *c*; activation of downstream caspases ensues, with upregulation of caspase 3 causing DNA breakdown and initiation of programmed cell death via apoptosis.

The complex interplay of excitotoxicity, acidosis, oxidative stress and apoptosis (as summarised in Figure 1.4) thus contributes to cell death following ischaemic stroke.

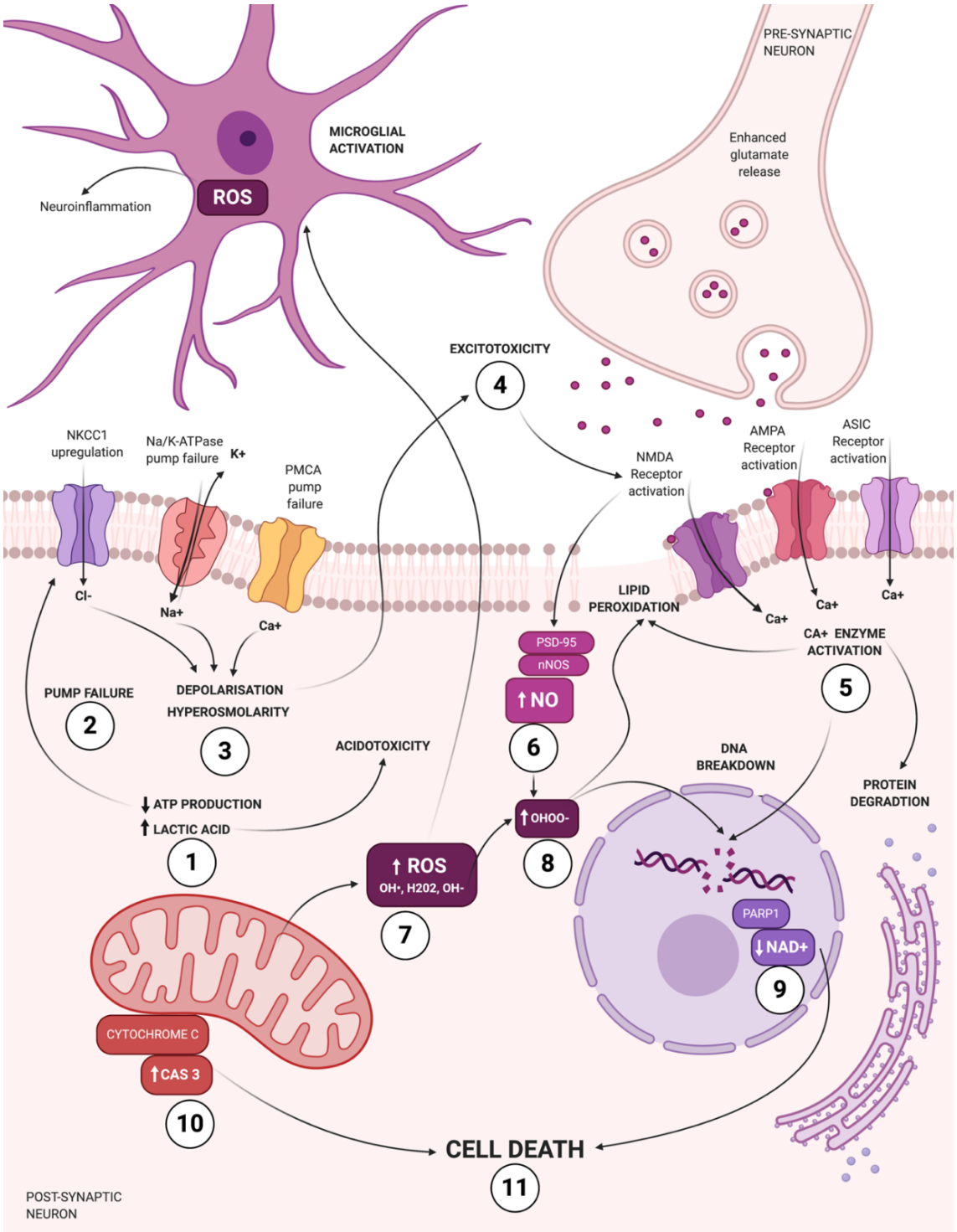

Figure 1.4. Mechanisms of ischaemic cell death following stroke. (1) Immediately following cessation of blood supply, inhibition of mitochondrial aerobic respiration occurs, resulting in depletion of ATP and accumulation of lactic acid as mitochondria switch to anaerobic respiration. (2) In the absence of sufficient ATP, energy-dependent pumps in the plasma membrane become dysfunctional. Notably, failure of Na^+/K^+-ATPase and PMCA pumps results in a rapid influx of Na^+ and Ca^{2+} and efflux of K^+. Intracellular accumulation of Na^+ and efflux of K^+ drives further influx of Cl^- via NKCC1. (3) Net intracellular accumulation of Na^+, Cl^- and Ca^{2+} results in neuronal depolarisation and significantly increases intracellular hyperosmolarity. (4) As a

result of plasma membrane depolarisation, aberrant release of neurotransmitters from axon terminals ensues, notably glutamate. Glutamate binds to AMPA and NMDA receptors in the post-synaptic cell membrane, leading to rapid influx of intracellular Ca^{2+} and resulting in a further release of glutamate from the post-synaptic cell (excitotoxicity). Intracellular lactic acid accumulation leads to activation of ASICs, which allow a further influx of Ca^{2+}. (5) Significant increases in intracellular Ca^{2+} via NMDA and AMPA receptor activation and ASICs lead to activation of Ca^{2+}-dependent enzymes, resulting in lipid peroxidation, protein degradation, ribosome disassociation and DNA breakdown. (6) NMDA receptor activation also leads to recruitment of nNOS via PSD-95, leading to synthesis of NO. (7) Mitochondrial Ca^{2+} overload increases synthesis of deleterious ROS including O_2^-, OH• and H_2O_2, causing damage to cellular structures and activation of microglia, with resultant glial ROS synthesis and secretion of cytotoxic factors initiating neuroinflammation. (8) NO subsequently binds O_2^- to form NO_3^- resulting in further damage to lipids, proteins and, in particular, DNA. (9) PARP-1 is synthesised in an attempt to repair damaged DNA; however, this consumes remaining NAD^+, necessary for producing ATP via glycolysis. This leads to complete energy starvation and necrotic cell death. (10) Mitochondrial dysfunction also results in the generation of caspase 3 via cytochrome *c*, initiating programmed cell death via apoptosis. (11) In concert, these processes cause complete ATP starvation, irreparable damage to cellular structures and, consequently, cell death. AMPA, a-amino-3-hydroxy-5-methyl-4-isoxazolepropionic acid; ASIC, acid-sensing ion channel; ATP, adenosine triphosphate; CAS 3, caspase 3; DNA, deoxyribonucleic acid; NAD^+, nicotinamide adenine dinucleotide; NKCC1, Na^+-K^+-$2Cl^-$ co-transporter 1; NMDA, N-methyl-D-aspartate; nNOS, nitric oxide synthase; PARP1, poly(ADP-ribose)polymerase-1; PMCA, plasma membrane Ca^{2+}-ATPase; PSD-95, post-synaptic density protein 95; ROS, reactive oxygen species. *Figure created with BioRender.com (2021).*

1.3 CEREBRAL OEDEMA

Irreparable cell damage arising in the minutes post-stroke precipitates numerous secondary injury processes, which continue to develop in the days to weeks post-ictus (Muir, 2013). Of these injury processes, cerebral oedema is the leading cause of patient deterioration in the week following stroke, accounting for significant morbidity and mortality (Hacke et al., 1996). Cerebral oedema is defined as the excess accumulation of water in the intracellular and/or extracellular spaces of the brain (Jha, 2003). Development commences shortly after cessation of blood flow and evolves in stages, which are broadly classified as cytotoxic, ionic and vasogenic oedema.

1.3.1 Cytotoxic Oedema

Cytotoxic oedema, characterised by the oncotic swelling of both neuronal and glial cells (Figure 1.5), is reported to occur as early as 30 minutes following the onset of ischaemia and persists for up to 24 hours (Liebeskind et al., 2019, Steiner et al., 2001b). Here, cellular swelling arises because of disrupted ion homeostasis and predominantly affects the cell bodies in the parenchymal grey matter (Ayata and Ropper, 2002, Battey et al., 2014). Driving this process is the aforementioned dysfunction of Na^+/K^+-ATPase pumps and amplified activation of NMDA receptors, both of which lead to an abnormal and excessive accumulation of intracellular Na^+ and Cl^- (Brogan and Manno, 2015). In addition, non-selective cation channels, upregulated as a result of ischaemia, provide an additional pathway for Na^+ influx. ATP depletion triggers calcium-activated, ATP-sensitive non-selective cation (NCCa-ATP) channel opening, whereby sulfonylurea receptor 1 (SUR-1), the pore-forming and regulatory subunit of the receptor, is transcriptionally upregulated within 2–3 hours of ischaemia (Simard et al., 2006), permitting the excessive influx of Na^+ into neurons (Liang et al., 2007). Transient receptor potential (TRP) channels and non-

selective K^+ channels enable a steady efflux of K^+; however, there remains a significantly greater influx of Na^+ to efflux of K^+, facilitating neuronal accumulation of Cl^- (Simard et al., 2007). As a result of these processes, there is a net intracellular accumulation of osmotically active molecules, predominantly Na^+ and Cl^-. This significantly increases intracellular osmotic pressure and drives water influx via aquaporin channels (AQP), in particular AQP4 (Lo et al., 2005). Although both neuronal and glial cells are affected, astrocytic cytotoxic swelling is more prominent than neuronal (Liang et al., 2007). Astrocytes are more prone because of their involvement in clearance of K^+ and glutamate, which ultimately results in cell overload and consequent water inflow. Because of extracellular K^+ accumulation, NKCC1 is upregulated in astrocytes, but not neurons, and AQP4 is shown to be overexpressed in astrocytic end-feet acutely post-stroke, facilitating water inflow (Clément et al., 2020). Together, this causes significant cellular swelling and ultimately precipitates bleb formation, in which morphological changes to the membrane architecture predispose the cell to rupture (Liang et al., 2007).

Given the significant energy crisis and ionic imbalances that ensue immediately following ischaemia, cytotoxic oedema is most prominent in the acute stages. Beyond 24 hours, the infarct is considered mature, having succumbed to ischaemic injury, and thus cytotoxic oedema development declines (Stokum et al., 2016, Michinaga and Koyama, 2015). Despite an increase in intracellular fluid and cell size, brain volume remains relatively constant in this setting (Simard et al., 2007). Loss of membrane integrity and inflow of water and solutes in cytotoxic oedema, however, comes at the expense of the extracellular space, with the volume markedly reduced (20% to 4–10%) (Liang et al., 2007). Extracellular depletion of Na^+ and Cl^- reserves thereby facilitates formation of transcapillary ionic oedema (Figure 1.5).

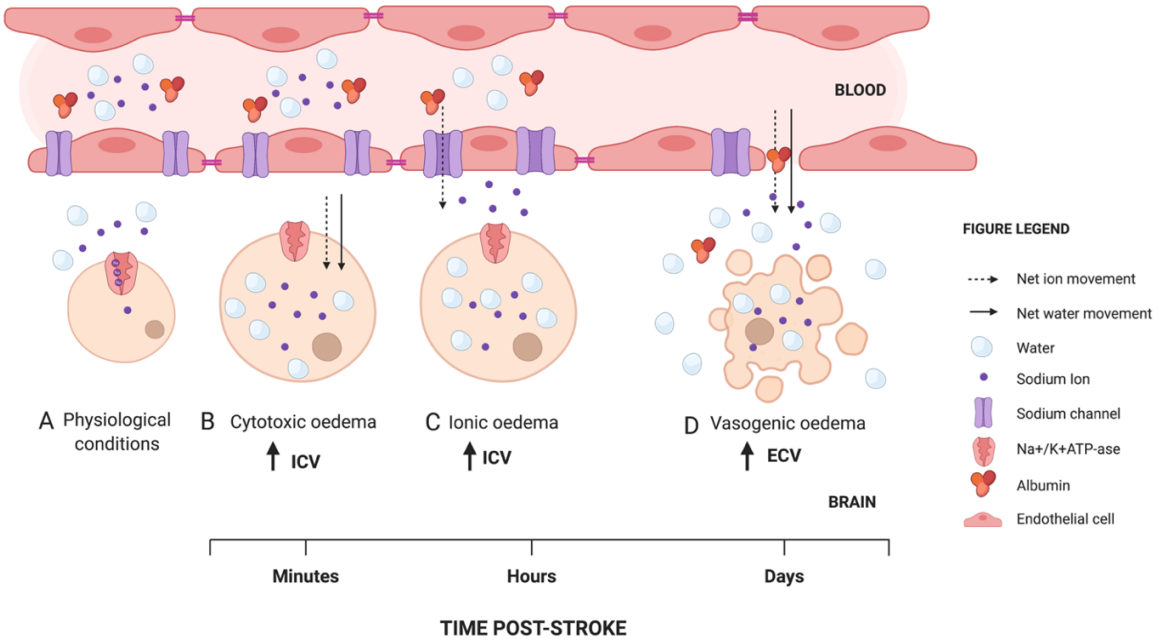

Figure 1.5. Development of cerebral oedema following stroke. (A) Physiological conditions: Na^+/K^+-ATPase pumps are active and maintain a greater net extracellular concentration of Na^+ than within neuroglial cells. (B) Cytotoxic oedema: In the minutes post-stroke, Na^+/K^+-ATPase pump failure permits the excessive intracellular accumulation of Na^+ and subsequent compartmental shift of water from the interstitial to the intracellular space, leading to an increase in intracellular volume and oncotic neuroglial cell swelling. (C) Ionic oedema: Depletion of extracellular ions due to cytotoxic oedema leads to the transcapillary formation of ionic oedema, in which Na^+ from the blood crosses the intact BBB to replenish reserves, leading to additional movement of water via osmosis. Here, intracellular volume remains elevated, but extracellular volume remains consistent. (D) Vasogenic oedema: Dissolution of barrier integrity permits uncontrolled extravasation of ions and large molecules into the parenchyma, leading to excessive accumulation of water, increase in extracellular volume and gross increase in total brain volume. Cells have undergone morphological changes to the cell membrane, predisposing them to rupture and further contributing to barrier dissolution and vasogenic oedema development. Dashed arrows indicate compartmental movement of Na^+, whereas continuous arrows indicate movement of water. Note the relative time course post-stroke for each of these processes. ICV, intracellular volume; ECV, extracellular volume. *Figure created with BioRender.com (2020).*

1.3.2 Ionic Oedema

Ionic oedema refers to the initial form of extracellular oedema in which ion depletion within the extracellular space creates a driving force for the movement of osmolytes across the intact capillary membrane to replenish interstitial concentrations (Stokum et al., 2016). Here, increased activity of barrier Na^+/H^+ exchangers, Na^+-K^+-Cl^- cotransporters or the calcium-activated potassium channel KCa3.1 enhances transcellular transport of Na^+ and Cl^- from the blood, into the brain, across the intact BBB (O'Donnell et al., 2004, O'Donnell et al., 2013). Ionic oedema precedes vasogenic oedema by approximately 6 hours and, unlike cytotoxic oedema, requires a minimal amount of CBF to deliver water and solutes to the endothelium (Liebeskind et al., 2019). Fluid is also hypothesised to be derived from the cerebrospinal fluid (CSF), with fluid movement facilitated by endothelial channels and transporters (Dobrivojevic et al., 2015). However, this gradient does not immediately manifest as mass fluid movement, and ultimately pathological brain swelling, until the permeability of the endothelial layer of the BBB is altered (O'Donnell et al., 2004).

1.3.3 Vasogenic Oedema

Vasogenic oedema occurs in the setting of BBB disruption and unlike cytotoxic and ionic oedema, which occur early following central nervous system (CNS) insult, begins to evolve as barrier disruption emerges, peaking at approximately 3–5 days post-stroke (Battey et al., 2014, Hacke et al., 1996). During vasogenic oedema, there is an abnormal movement of water from the intravascular compartment to the extracellular space within the brain parenchyma, evoking an increase in total brain volume (Treadwell and Thanvi, 2010) (Figure 1.5).

Under physiological circumstances, the BBB maintains a semi-permeable barrier between the brain and the circulating blood from the extracellular fluid (Simard et al., 2007). The neurovascular unit (NVU) is responsible for the integrity of the BBB and comprises a basement membrane, perivascular astrocytes, pericytes, neurons, microglia and endothelial cells, with each cellular and structural component playing an essential role in regulating movement of molecules across the barrier (Bell et al., 2020). Following stroke, cytotoxic oedema, neuroinflammation and ROS accumulation initiates BBB breakdown within 4–6 hours of stroke onset (Dostovic et al., 2016). If blood flow through the occluded vessel has been re-established, as is the goal of reperfusion therapy, flow of blood through damaged vessels where integrity has been lost enables the extravasation of large serum proteins such as albumin from the intravascular to the extracellular space. This alters osmolarity across the barrier and provides a driving force for fluid accumulation predominantly within the white matter of the brain (Simard et al., 2007). As these processes continue to develop over the days following stroke onset, so too does the abnormal and excessive accumulation of parenchymal fluid.

The pathological mechanisms by which BBB breakdown occurs following stroke is thought to be via two main routes. First, dissolution of endothelial tight junctions (TJs) following stroke enables abnormal paracellular movement of water and molecules between cells. Second, upregulated transcellular transport across endothelial cells may provide an alternative route for fluid entry. As vasogenic oedema is the focus of this thesis, these mechanisms are discussed in greater detail in Chapter 2. Recent evidence also suggests that compartmental movement of CSF may contribute to vasogenic oedema formation (Mestre et al., 2020). Indeed, disruptions to the glymphatic system (physiologically involved in cerebral waste regulation) have also been observed post-stroke, which may provide a route

for CSF to enter the infarcted hemisphere along perivascular spaces, thus contributing to oedema formation (Jessen et al., 2015). As a consequence of these cumulative processes, fluid accumulation in the extracellular space is markedly increased. Progressive vasogenic oedema within days of stroke onset leads to an increased parenchymal extracellular water content of more than 100% and, consequently, a significant increase in overall brain volume, which has implications for intracranial pressure (ICP) (Ayata and Ropper, 2002, Battey et al., 2014).

1.4 ELEVATED INTRACRANIAL PRESSURE

An increase in total brain volume within the closed cavity of the skull as a result of vasogenic oedema leads to a consequent rise in ICP (Battey et al., 2014, Brogan and Manno, 2015). Unfortunately, the development of cerebral oedema and concomitant rise in ICP are the leading cause of death in the first week following stroke, with the mortality rate of malignant cerebral oedema approaching 80% in the setting of large vessel occlusions, such as the MCA (Battey et al., 2014, Hacke et al., 1996, Zhang et al., 2014).

1.4.1 Cerebral Autoregulation

Normal ICP lies between 0 and 15 mmHg, with elevations in pressure greater than 25 mmHg associated with an increased risk of death and disability following stroke (Hewitt and Ellory, 2012). The skull and underlying inelastic dura mater restrict the expansion of the brain tissue; therefore, when the volume of one of the cerebral compartments is increased (brain tissue, arterial blood, venous blood or CSF), this must be compensated for by a decrease in one of the other compartments, a phenomenon explained by the Monro-Kellie doctrine (Ropper, 2014). Cerebral autoregulation is a complex, multifactorial process that permits

physiological regulation of the cerebral compartments to ensure constant CBF. CBF is dependent on cerebral perfusion pressure (CPP), which is defined as the net pressure gradient required to supply adequate oxygen and nutrients to neuronal cells (Mount and J, 2021). CPP is determined by the difference between ICP and mean arterial blood pressure (MABP), where: CPP = MABP – ICP.

In the initial stages of vasogenic oedema development, only small increases in ICP are observed as compensatory autoregulation is able to maintain ICP within normal limits. However, once compensatory mechanisms are exhausted, the increased volume of the cerebral parenchyma results in progressively larger increases in ICP, such that ICP opposes MABP. This leads to a marked reduction in CPP, which adversely restricts blood perfusion to the brain (Jha, 2003). Compromised cerebral tissue perfusion exacerbates cell injury, resulting in further global ischaemia and initiation of a vicious cycle in which progressive cytotoxic oedema ensues (Jha, 2003). As vasogenic oedema continues to develop, cerebral autoregulation is further impeded and ultimately fails, with ICP rising unabated, resulting in devastating neurological consequences, including herniation (Ropper, 2014).

1.4.2 Herniation Syndromes

The human brain is relatively compartmentalised because of the presence of the fibrous dura mater, which forms intracranial folds such as the falx cerebri and tentorium cerebelli (Figure 1.6). Pressure gradients exist between compartments, with development of hemispheric space-occupying oedema resulting in significant compartmental pressure increases (Dostovic et al., 2016, Shah and Kimberly, 2016). Persistently elevated ICP can force brain tissue to move between compartments in an attempt to relieve pressure, known as brain herniation (Shah and Kimberly, 2016). When brain tissue herniates, it can compress adjacent

structures, causing tissue deformation and additional constriction of blood vessels, further worsening tissue injury and causing neurological deficits and permanent tissue damage (Kim et al., 2015). There are several well-recognised anatomical herniation syndromes including central (transtentorial), transcalvarial, uncal and subfalcine herniation (Munakomi and J, 2020). Life-threatening herniation occurs when the cerebellar tonsils herniate downwards through the foramen magnum, as occurs in tonsillar herniation, leading to compression of vital cardiorespiratory centres within the medulla oblongata (Freeman, 2015). This can lead to intermittent or complete cessation of cardiorespiratory functions and subsequent death (Kim et al., 2015).

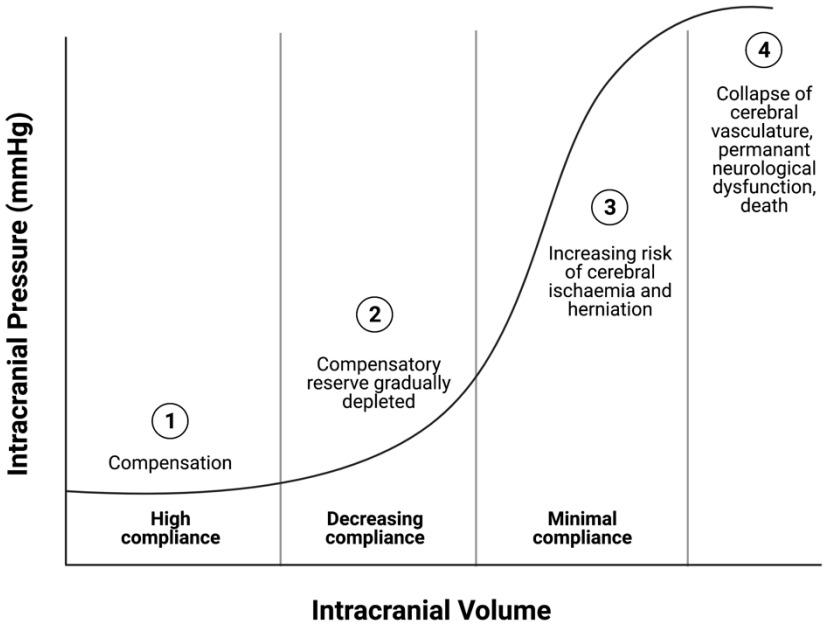

Figure 1.6. Evolution of intracranial pressure (ICP) following stroke. The pressure–volume curve for ICP has four zones. (1) Baseline intracranial volume under physiological conditions has good compensatory reserve and high compliance to minor volume fluctuations. (2) With evolving cerebral oedema and consequent increased brain and intracranial volume, gradual depletion of compensatory reserves occurs. (3) With persistent developing oedema and increasing brain volume, compensation is further reduced, with minimal compliance, leading to increased risk of cerebral ischaemia and herniation. (4) Critically high ICP causes collapse of the cerebrovasculature, increasing risk of permanent neurological dysfunction and death. *Figure adapted from Harary et al., 2018.*

Elevated ICP is thus commonly associated with devastating outcomes of death or persistent disability following ischaemic stroke (Pinto et al., 2020). It is largely accepted this is due to the effect of cerebral oedema and accumulation of fluid preceding vital tissue shifts (Steiner et al., 2001a). Nevertheless, one study has reported an elevation of ICP in the absence of cerebral oedema following ischaemic stroke in a rodent model, where it is proposed that increased CSF, as supported by the glymphatic theory, may be driving elevated ICP (Murtha et al., 2015). In the case of larger hemispheric strokes, however, such as occlusion of the MCA, there is a positive correlation between cerebral oedema and elevated ICP (Engelhorn et al., 2002). Effective management of oedema and elevated ICP thus remains crucial to reduce death and disability following stroke.

1.5 TREATMENTS FOR STROKE

1.5.1 Reperfusion Therapy

The main principle of treatment for ischaemic stroke involves timely recanalisation of the occluded vessel while improving collateralisation of blood flow (Rabinstein, 2020). The basis for early restoration of blood flow is to salvage penumbral cells, minimise permanent infarction and reverse neurological deficits.

Currently, recanalisation is achieved via thrombolysis with tissue plasminogen activator (tPA) or mechanical thrombectomy (Rabinstein, 2020). Both therapeutic approaches are predicated on targeting the penumbra, with more brain tissue and subsequent neurological function able to be salvaged if a stroke is detected and treatment is received expeditiously. Evidence suggests efficacy of tPA when administered up to 9 hours post-stroke, which has markedly extended its previous therapeutic window of 4.5 hours (Ma et al., 2019). Recent

advances in mechanical thrombectomy hold significant promise, with evidence of efficacious outcomes up to 16 hours post-ictus (Albers et al., 2018, Nogueira et al., 2018, Berkhemer et al., 2015, Smith and Yan, 2015, Goyal et al., 2016, Goyal et al., 2015). However, this procedure is reliant upon highly trained technicians and necessary imaging facilities, thereby limiting accessibility, especially for those located remotely and in low-income settings.

1.5.2 Complications of Treatment – Reperfusion Injury

While thrombolysis and reperfusion can prove beneficial, the restoration of blood flow can, in some instances, paradoxically worsen injury. Reperfusion at any time post-stroke where there is no viable penumbra to salvage can cause additional injury to neuronal tissue and associated vasculature, termed ischaemic reperfusion (I/R) injury (Mandalaneni et al., 2020). In such instances, restoration of oxygen can lead to aggravated production of ROS, where hypoxanthine, which has built up during ischaemia, is rapidly metabolised, leading to production of O^{-}, OH and hypochlorous acid. This is further exacerbated by overproduction of ROS by mitochondria due to reverse electron transport (RET) when oxygen availability is reinstated. In concert with aberrant ROS production, activation of platelets and neutrophils lead to exacerbation of neuroinflammation, amplifying BBB dysfunction (Woodruff et al., 2011). Accordingly, timely access to advanced brain imaging including specialist perfusion computed tomography (CT) or magnetic resonance imaging (MRI) is crucial to determine the volume of viable penumbra and the likelihood of benefit of reperfusion treatment.

1.5.3 Reperfusion Therapy – Secondary Injury

Finally, although reperfusion therapies have the potential to salvage the penumbra and improve neurological outcomes, unless received in a timely manner (ideally, within 6 hours

of stroke onset), treatment does not halt the progression of secondary injury processes and resultant development of cerebral oedema, and thus neurological dysfunction (Irvine et al., 2018). Given the heterogeneous nature of stroke, the pathogenesis of secondary injury can vary significantly between patients; however, in the setting of MMCAI (being the most prevalent), it is estimated that if the initial insult is not fatal, up to 80% of survivors will die in the week following stroke because of development of cerebral oedema and the associated rise in ICP (Battey et al., 2014, Hacke et al., 1996, Zhang et al., 2014). Such patients often exhibit a progressive and slow evolution of brain injury, with surmounting cerebral oedema and excessively elevated ICP presenting days following insult due to progressive cellular and molecular changes as previously detailed (Battey et al., 2014). Therefore, cerebral oedema remains a target for both surgical and pharmacological therapeutic intervention (Brogan and Manno, 2015).

1.6 TREATMENTS FOR CEREBRAL OEDEMA

A number of modalities exist for the treatment of cerebral oedema and elevated ICP, including general patient management, pharmacotherapies and surgical intervention (Freeman, 2015, Wijdicks et al., 2014). Determining the appropriate clinical approach, however, demands the need to first identify the evolving pathology. Assessment of oedema is indirect and involves imaging via either MRI or CT, in addition to application of clinical monitoring devices to measure ICP. Interventions are then typically approached in a stepwise manner (Table 1.1), with low-intervention strategies first exhausted before more invasive and/or surgical means considered if elevated ICP persists unabated.

1.6.1 General Management Approaches

Initial airway assessment is an important step in patient management, allowing for prompt intubation in comatose individuals (Jeon et al., 2014). Repositioning is undertaken to optimise venous drainage, with head elevation to 30 degrees proved to reduce ICP (Feldman et al., 1992, Shah and Kimberly, 2016, Schwarz et al., 2002). Such repositioning can, however, be associated with a concomitant decrease in CPP, which can offset any benefits to reduction of pressure (Kiening et al., 1997).

Mechanical hyperventilation is also initially considered to bring about a prompt reduction in ICP through the reduction of cerebral blood volume (CBV) (Cook et al., 2020, Christensen et al., 1973). Carbon dioxide (CO_2) is a potent cerebrovasodilator causing vasodilation of the cerebral arteries, increasing CBV and thus ICP (Simard et al., 2011). Accordingly, increasing respiration rate and decreasing the partial pressure of CO_2 (pCO_2) rapidly induces cerebral vasoconstriction, resulting in a reduction in CBV and ICP (Simard et al., 2011). Initially, modest hyperventilation is performed, with more aggressive pCO_2 thresholds set if ICP continues to rise. However, the immediate efficacy of treatment is often associated with unsustained clinical effects and worsening of infarct volume (Stocchetti et al., 2005, Marion et al., 2002). Rebound vasodilation following homeostatic regulation of pCO_2 and consequent return to baseline may also lead to worsening of cerebral oedema and subsequent elevation in ICP (Stocchetti et al., 2005, Marion et al., 2002, Simard et al., 2011). Further, to date, there is limited quality evidence regarding the efficacy of this approach and its ability to sustain meaningful reductions in ICP (Cook et al., 2020); thus, administration is contentious.

1.6.2 Pharmacological Intervention

1.6.2.1 Osmotherapy

Osmotherapeutic agents used for the management of cerebral oedema and elevated ICP include mannitol and hypertonic saline (HTS) (Burgess et al., 2016). Their predominant mechanism of action is believed to be via rheological effects, whereby creation of an osmolar gradient within the bloodstream draws water from the brain into the intravascular space, thereby reducing total brain volume (Brogan and Manno, 2015). An alternate hypothesis is that osmotherapies reduce viscosity and cerebrovascular resistance, initiating compensatory vasoconstriction and resultant decrease in CBV (Muizelaar et al., 1983). Neuroprotection at a cellular level by osmotic agents has also been proposed, largely because of their ability to reduce oxidative stress and inflammation via cytokine-mediated pathways; however, limited rigorous evidence for this exists (Mojtahedzadeh et al., 2014).

Mannitol has been used to treat acute stroke for more than 30 years (Bereczki et al., 2003). Early studies in large hemispheric infarction showed that mannitol administration reduced ICP (Schwarz et al., 1998) and increased CPP (Steiner et al., 2001a) when administered intravenously, although the effect on stroke outcome remained unclear. Investigations have since shown that administration does not have a favourable outcome on function and may be associated with heightened mortality independent of stroke severity (Bereczki et al., 2003, Papagianni et al., 2018). Further, use of mannitol is contraindicated where there is clear evidence of BBB breakdown (Witherspoon and Ashby, 2017) as repeated dosing may lead to mannitol accumulation within the brain parenchyma, paradoxically reversing the osmotic drive, leading to rebound oedema and resultant neurological deterioration (Brogan and Manno, 2015, Cho et al, 2007, Maioriello et al., 2002). Administration has also been shown

to cause adverse effects including activation of apoptotic cell death pathways, which can aggravate neuronal injury.

HTS is also used to manage elevated ICP in the setting of post-stroke oedema (Cook et al., 2020). Although its mechanisms of action are comparable to mannitol, it is able to cross the BBB less freely and thus may have a stronger osmotic effect (Jeon et al., 2014). Prior studies have shown a reversal of transtentorial herniation following HTS administration in a clinical setting, indicative of a reduction of cerebral oedema (Koenig et al., 2008). Reductions in ICP have also been shown, although such changes appear to be independent of dosing regimen (Harutjunyan et al., 2005), with dose frequency and strategy of administration varying significantly between studies (Harutjunyan et al., 2005, Schwarz et al., 1998). Despite its arguably greater efficacy compared with mannitol, it may still be of limited use if there is extensive barrier breakdown. Further, HTS administration is associated with a plethora of adverse effects including rebound cerebral oedema; hyperchloremic metabolic acidosis; phlebitis; congestive heart failure; transient hypotension; haemolysis; renal failure; osmotic demyelination; subdural haemorrhage; seizures; muscle twitching (Georgiadis and Suarez, 2003); and decreased platelet aggregation, prolonged coagulation and subsequent bleeding, in addition to ion imbalances including hypochloraemia and hyperkalaemia (Hauer et al., 2011, Surani et al., 2015).

Each of the osmolar agents has its own inherent risks and complications. HTS is associated with a reduced risk of ICP treatment failure (Burgess et al., 2016) and therefore may be used preferentially to mannitol in some patients, for example, those with SAH and vasospasm, where insufficient volume depletion and hypotension may further compromise cerebral perfusion (Freeman, 2015). Regardless, both osmotherapies require extensive monitoring of

electrolytes, osmolarity and volume throughout treatment. Thus, osmotic therapy may be used as a temporary measure to buy time and prevent acute brain stem compression until other measures such as surgery can be performed (Grande and Romner, 2012). Further, ongoing administration of HTS and mannitol for the management of post-stroke cerebral oedema and ICP remains controversial, given a lack of high-quality randomised trials supporting their efficacy (Wijdicks et al., 2014). This is an important consideration given neither treatment targets the mechanisms underlying abnormal fluid movement and accumulation within the brain parenchyma, as they simply aim to reverse the osmotic drive to reduce brain tissue water content.

1.6.2.2 Barbiturates

Barbiturates have been used to reduce ICP because of their ability to increase vascular tone, reduce cerebral metabolism and inhibit free radical-mediated lipid peroxidation (Demopoulos et al., 1980, Kassell et al., 1980). Typically administered agents include pentobarbital and thiopental, which are preferentially given to patients with refractory intracranial hypertension in titrated doses (Jeon et al., 2014). Initially used as a defence against oedema and evolving brain injury in traumatic brain injury (TBI) patients (Eisenberg et al., 1988), barbiturate coma is used less frequently for the management of oedema post-stroke given a lack of randomised control trials to support its efficacy (Wijdicks et al., 2014). Further, evidence suggests that barbiturate treatment can be associated with unsustained therapeutic properties and severe side effects, such as arterial hypotension and pulmonary failure (Bardutzky and Schwab, 2007, Schwab et al., 1997). Accordingly, barbiturate therapy is generally only used as a last-line therapy in extreme clinical situations (Mansour et al., 2013), as the hypotensive effect of therapy is likely to offset any reduction in ICP following treatment (Roberts and Sydenham, 2012).

1.6.2.3 Corticosteroids

Corticosteroid treatment for oedema management is predicated upon stabilising the BBB, thereby preventing its dissolution and the subsequent development of vasogenic oedema. While corticosteroid use has proved beneficial in the setting of intracranial tumours, there has been limited efficacy in the setting of ischaemic stroke (Ogun and Odusote, 2001). Further, there remains a significant discrepancy between clinical and experimental stroke studies, where efficacy of treatment is overwhelming in experimental stroke studies but evidence in clinical stroke is lacking (Davis and Donnan, 2004). A Cochrane review investigating the efficacy of corticosteroids in stroke deemed only 7 of 22 published trials acceptable for further analysis, with many studies reporting small patient cohorts, dosing discrepancies, incomparable assessment of outcomes and disparate conclusions (Qizilbash et al., 2002). Corticosteroid use for the treatment of cerebral oedema in stroke thus requires further assessment, with further inconclusive evidence regarding the benefit of steroid use on functional outcome and neurological impairment (Brogan and Manno, 2015, Sandercock and Soane, 2011).

1.6.3 Surgical Intervention

1.6.3.1 Ventriculostomy

Ventriculostomy is often considered early in the clinical course of management, as invasive methods to measure ICP involve insertion of transducers directly into the lateral ventricle (Steiner and Andrews, 2006). To bring about a reduction in pressure, this procedure involves insertion of an intraventricular catheter and drainage of the CSF, thus reducing the fluid compartment (Andrade et al., 2011). Patients submitted to continual CSF drainage present with lower ICP levels and favourable outcomes following TBI (Andrade et al., 2011, Chau et al., 2020). In the setting of stroke, patients with herniation or cerebellar infarction may

present with acute hydrocephalus, whereby placement of a ventriculostomy may be of significant benefit. This should, however, be followed by decompressive craniectomy (DC), as benefits of CSF drainage are, unfortunately, often short-lived (Wintermark et al., 2013).

1.6.3.2 Decompressive Craniectomy

DC aims to alleviate elevated ICP through removing part of the skull and opening the underlying dura, allowing the oedematous brain to swell freely without the confines of the skull, thereby bringing about a rapid, lifesaving reduction in ICP (Yang et al., 2005). The exact nature of the DC, including the location and amount of bone removed, is dependent on the underlying pathology (Beez et al., 2019). In cases of MMCAI, for example, DC of the parietal bone is typically performed, enabling free swelling of the affected parietal lobe (Gupta et al., 2004).

The clinical efficacy of DC in the setting of malignant cerebral infarction has been clearly established (DECIMAL, HAMLET, DESTINY and DESTINY II trials) (Vahedi et al., 2007a, Vahedi et al., 2007b, Geurts et al., 2013, Jüttler et al., 2007, Hofmeijer et al., 2009). Nevertheless, timing of the procedure is a crucial factor in determining patient outcome as evidence suggests that surgery performed later than 24 hours post-ictus is associated with a heightened mortality rate (Kurland et al., 2015, Vahedi et al., 2007a). Therefore, early identification of evolving cerebral oedema is crucial in maximising treatment efficacy (Chen et al., 2007), as when DC is used only as a last resort after conservative physiological management and pharmacotherapy have failed to produce meaningful reductions in ICP, outcomes are predictably poor (Grindlinger et al., 2016). Further, given that DC surgery is highly invasive, there is an increased risk of iatrogenic injury, in addition to a higher mortality rate in those older than 60 years and increased likelihood of moderate to severe

postoperative disability (Hofmeijer et al., 2009, Vahedi et al., 2007b). Accordingly, the correlation between age and functional outcome remains an extremely important pre-treatment prognostic factor in deciding if patients should undergo DC. Current clinical guidelines consequently recommended DC only be performed in patients younger than 60 in the first 24 hours of symptom onset and prior to any clinical signs of herniation (Chen et al., 2007). Finally, although surgical decompression enables the rapid reduction of ICP, it is a physical measure and does not influence the evolution of BBB dissolution, or the mechanisms underlying the genesis of cerebral oedema.

Table 1.1 Stepwise approach to the clinical management of elevated intracranial pressure

SIGNS OF INTRACRANIAL HYPERTENSION	Imaging – confirm presence of space-occupying oedema ICP monitoring – determine ICP If ICP is >20 mmHg, the following steps are taken
STEP 1: ELEVATED ICP	Head elevation and neutral neck position Ventriculostomy – CSF drainage Mechanical ventilation – light hyperventilation ($PaC0_2$ 30–35 mmHg) If ICP remains >20 mmHg, step 2
STEP 2: PERSISTENTLY ELEVATED ICP	Mannitol Mechanical ventilation – moderate hyperventilation ($PaC0_2$ 28–30 mmHg) If ICP remains >20mmHg, step 3
STEP 3: ICP CONTINUES TO RISE UNABATED	Barbiturate coma therapy Decompressive craniectomy

CSF, cerebrospinal fluid; ICP, intracranial pressure; $PaCO_2$, partial pressure carbon dioxide. *Table adapted from Jeon et al., 2014.*

1.7 IMPROVING TREATMENT OF CEREBRAL OEDEMA AND ELEVATED INTRACRANIAL PRESSURE

The burden of morbidity and mortality associated with cerebral oedema and elevated ICP, combined with the limitations of current treatments, emphasises the need for new treatment approaches. It is clear that existing treatments do not address the underlying injury mechanisms that lead to increased BBB permeability and subsequent development of cerebral oedema and elevated ICP. Indeed, there are currently no approved targeted treatments that interfere with key injury processes to reduce/reverse the evolution of BBB dysfunction and cerebral oedema following stroke. To develop more effective treatments, it is thus essential to elucidate the specific molecular mechanisms underlying post-stroke oedema genesis. Such an approach has the potential to markedly improve patient survival and outcome given it is directly targeting the injury mechanisms, and not simply treating the symptoms of cerebral oedema and elevated ICP once established.

To this end, a number of novel therapies targeting cation channels implicated in the formation of cytotoxic oedema have been developed in an effort to prevent subsequent development of vasogenic oedema, including therapies targeting ASICs, and SUR-1-regulated NCCa-ATP and TRP channels (Kimberly et al., 2014, Kimberly et al., 2018, Sheth et al., 2016a, Sheth et al., 2016b). However, given that cytotoxic oedema develops very early following stroke onset, it raises the question as to whether therapies targeting this aspect of cerebral oedema would alone be effective and provide clinical benefit beyond the acute phase following stroke.

Neurogenic inflammation, specifically the release of neuropeptides such as substance P (SP), has been shown to be critically involved in BBB permeability changes and development of cerebral oedema following stroke. These processes develop in a delayed fashion and directly contribute to the formation of vasogenic oedema. Thus, targeting neurogenic inflammation

following stroke may be a strategy to reduce BBB permeability and in turn reduce delayed development of vasogenic oedema and elevated ICP.

1.8 CONCLUSION

The increasing burden of stroke and concomitant development of cerebral oedema and elevated ICP is of significant clinical, and global, concern. This highlights the need for continued research and development of novel therapies targeting the mechanisms underlying ischaemic injury and oedema genesis. To this end, the following chapter will summarise the processes underlying neurogenic inflammation and its potential to be targeted therapeutically for the treatment of post-stroke cerebral oedema.

02

The Role of Neurogenic Inflammation in Blood–Brain Barrier Disruption and Development of Cerebral Oedema Following Stroke

Chapter revised from the original publication by **SORBY-ADAMS, A. J.,** MARCOIONNI, A. M., DEMPSEY, E. R., WOENIG, J. A., & TURNER, R. J. 2017. The role of neurogenic inflammation in blood–brain barrier disruption and development of cerebral oedema following acute central nervous system (CNS) injury. *International Journal of Molecular Sciences*, 18.

Statement of Authorship

Title of Paper	The Role of Neurogenic Inflammation in Blood-Brain Barrier Disruption and Development of Cerebral Oedema Following Acute Central Nervous System (CNS) Injury.
Publication Status	☑ Published ☐ Accepted for Publication ☐ Submitted for Publication ☐ Unpublished and Unsubmitted w ork w ritten in manuscript style
Publication Details	Sorby-Adams, A. J., Marcoionni, A. M., Dempsey, E. R., Woenig, J. A., & Turner, R. J. (2017). The Role of Neurogenic Inflammation in Blood-Brain Barrier Disruption and Development of Cerebral Oedema Following Acute Central Nervous System (CNS) Injury. *International Journal of Molecular Sciences, 18*(8). doi:10.3390/ijms18081788

Principal Author

Name of Principal Author (Candidate)	Annabel Sorby-Adams		
Contribution to the Paper	I was the first author and main contributor to the manuscript.		
Overall percentage (%)	60%		
Certification:	This paper reports on original research I conducted during the period of my Higher Degree by Research candidature and is not subject to any obligations or contractual agreements with a third party that would constrain its inclusion in this thesis. I am the primary author of this paper.		
Signature		Date	16.03.2021

Co-Author Contributions

By signing the Statement of Authorship, each author certifies that:

i. the candidate's stated contribution to the publication is accurate (as detailed above);

ii. permission is granted for the candidate in include the publication in the thesis; and

iii. the sum of all co-author contributions is equal to 100% less the candidate's stated contribution.

Name of Co-Author	Renee Turner		
Contribution to the Paper	Associate Professor Renee Turner is the head of the Translational Neuropathology Laboratory. She oversaw structure, drafting and final editing of the manuscript, and was the corresponding author.		
Signature		Date	16.03.2021

Name of Co-Author	Josh Woenig		
Contribution to the Paper	Mr Josh Woenig was a Research Assistant in the Translational Neuropathology Laboratory in 2017. He contributed to the preparation of the manuscript and editing.		
Signature		Date	16.03.2021

Name of Co-Author	Amanda Marcoionni		
Contribution to the Paper	Miss Amanda Marcoionni was an honours student in the Translational Neuropathology Laboratory in 2017. She contributed to the section on neuropeptides.		
Signature		Date	16.03.2021

Name of Co-Author	Eden Dempsey		
Contribution to the Paper	Miss Eden Dempsey was an honours student in the Translational Neuropathology Laboratory in 2017. She contributed to the section on the blood-brain barrier.		
Signature		Date	16.03.2021

2.0 INTRODUCTION

Originally characterised in peripheral tissues as a neurally elicited inflammatory process contributing to increased microvascular permeability and tissue swelling (Bayliss, 1901), neurogenic inflammation is now understood to occur following acute injury in the CNS. In the brain, neurogenic inflammation is characterised by the release of the neuropeptides SP and calcitonin gene-related peptide (CGRP). Increased SP expression is observed in perivascular tissue following stroke, with the magnitude of SP release being related to both the frequency and the degree of the insult. SP release is associated with profound BBB disruption and the subsequent development of vasogenic oedema, as well as neuronal injury and poor functional outcomes. Inhibition of SP through use of an NK1-R antagonist is highly beneficial following ischaemic stroke in preclinical models. In contrast, a beneficial role for CGRP has been delineated in stroke, given its potent vasodilatory effects (Omeis et al., 2008). Therefore, modulating neuropeptides represents a novel therapeutic approach for the treatment of cerebral oedema following acute CNS injury. This chapter will provide an overview of studies supporting a role for neurogenic inflammation in increased BBB permeability, cerebral oedema formation and development of functional deficits following stroke.

2.1 THE BLOOD–BRAIN BARRIER

The BBB is a highly specialised, semi-permeable barrier existing between the brain and blood, which serves to maintain homeostasis of the cerebral microenvironment by restricting the passage of compounds and toxins into the CNS (Ballabh et al., 2004). Structurally, the barrier comprises an array of components including endothelial cells with TJs, adherens junctions, astrocytes, pericytes and the basement membrane (Ballabh et al., 2004) (Figure

2.1). Together, these components provide the structural integrity required to enable the barrier to maintain fundamental roles including supplying the brain with essential nutrients such as oxygen and glucose, mediating the efflux of waste products, and facilitating the movement of nutrients and plasma proteins (Begley and Brightman, 2003).

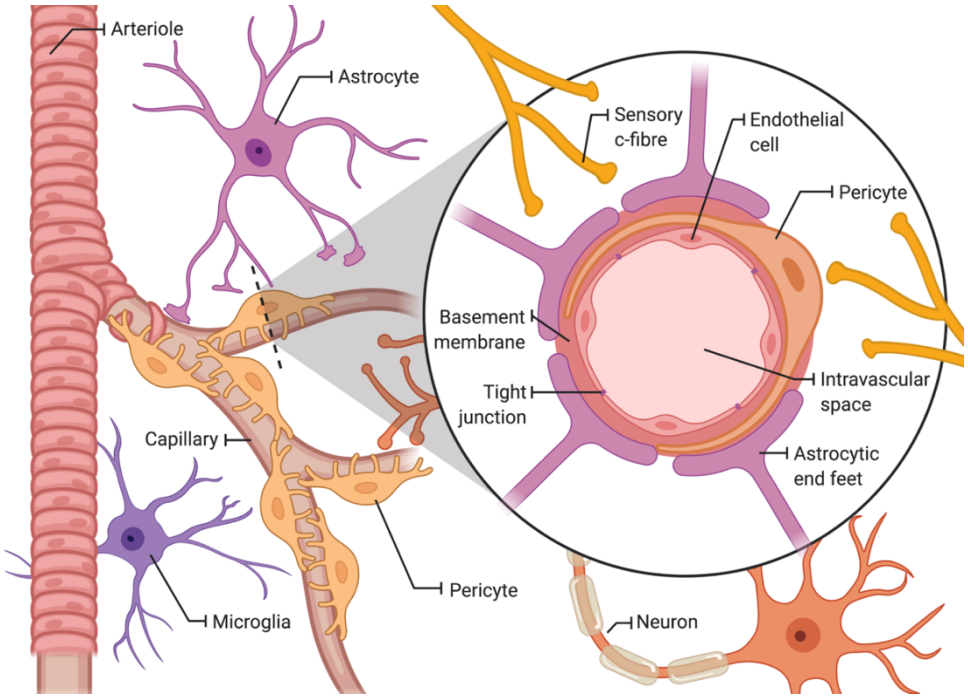

Figure 2.1. Cellular and structural components of the blood–brain barrier. *Figure adapted from 'Brain vascular system', by BioRender.com (2020).*

Under normal physiological conditions, nutrients and plasma proteins cross the BBB via two main transport mechanisms: paracellular and transcellular transport (Figure 2.2). Paracellular transport involves the passage of small solutes (<800 Da) between endothelial cells, as facilitated by TJs (Komarova and Malik, 2010). Conversely, transcellular transport is used by large plasma proteins, such as albumin, to cross the BBB via endocytosis. Vesicle-mediated transport of albumin occurs following budding of structures called caveolae into vesicles that migrate to the plasma membrane, where they fuse and release their contents (Komarova and Malik, 2010). These caveolae are flask-shaped plasma membrane

invaginations abundant in endothelial cells of the BBB, where cholesterol and caveolins are fundamental structural components (Parton and Simons, 2007). Caveolin-1 is the integral protein essential for caveolae formation, as mice with genetic ablation of caveolin-1 lack caveolae (Le Lay and Kurzchalia, 2005), and cannot endocytose albumin from the vasculature (Schubert et al., 2001). Each of these transport mechanisms are, in turn, central to the maintenance and function of the barrier.

2.1.1 Cellular Components of the Blood–Brain Barrier

The main cellular component of the BBB are mesodermally derived endothelial cells, supported by astrocytes and pericytes. Astrocytes are an important component of the BBB and have been shown to influence both its structure and its function. Astrocytic end-feet envelope the endothelial cells, providing structural support and enhancing the TJs in between (Persidsky et al., 2006). Astrocytes are able to rapidly respond to pathological stimuli in their surrounding environment and do so through conversion to a hypertrophic state with increased expression of intermediate filaments such as glial fibrillary acidic protein (GFAP) (Sofroniew, 2000). Pericytes are the other key cellular component, and have diverse functions including regulation of capillary haemodynamics (Joo, 1993), permeability of the BBB, clearance of toxic metabolites, angiogenesis and neuroinflammation (Yang et al., 2017).

2.1.2 Tight Junctions

Tight and adherens junctions form the junctional complexes that make up the BBB and comprise a complex network of transmembrane and cytosolic proteins, allowing these junctions to seal and mediate the gate function of the BBB (Lo et al., 2001). TJs are domains of occluded intercellular clefts, consisting of the integral membrane proteins occludin

(Furuse et al., 1993), claudins (Furuse et al., 2002), zonula occludin-1 (ZO-1) (Itoh et al., 1993) and junctional adhesion molecules (JAMs) (Martin-Padura et al., 1998).

Occludin was the first TJ protein identified and is one of the main junctional components (Chen et al., 1997). It consists of nine domains, with the second extracellular domain having a pivotal role in occludin assembly and localisation into TJs (Medina et al., 2000). This extracellular domain has also been implicated in altering TJ permeability when occludin levels decline (Wong and Gumbiner, 1997). It was initially suggested that occludin plays an important role in forming TJ-like structures (Furuse et al., 1996); however, TJ strands still develop in the absence of occludin (Saitou et al., 2000). Moreover, the morphology of TJs and trans-epithelial resistance in occludin-deficient mice do not differ from wild-type mice (Saitou et al., 2000), suggesting occludin is dispensable for TJ formation.

Claudins play a major role in both establishing and maintaining properties of the barrier (Furuse et al., 2002, Nitta et al., 2003). Upon the discovery of claudin-1 and claudin-2, it was revealed that they, not occludin as previously thought, are the major contributors to TJ strand formation (Furuse et al., 1998). Indeed, claudin-5-deficient mice demonstrate a size-selective loosening of the BBB, whereby the movement of small molecules across the barrier via paracellular transport is upregulated (Nitta et al., 2003). When Madin-Darby Canine Kidney Epithelial (MDCK) cells, a commonly used cell line to model the epithelium, were transfected with claudin-1, there was an increase in trans-epithelial resistance and a reduction in paracellular transport. This is in contrast to what has been demonstrated in occludin-deficient mice, where no changes in trans-epithelial resistance or paracellular transport were observed (Saitou et al., 2000).

ZO-1 belongs to the family of membrane-associated guanylate kinase (MAGUK) proteins (Gonzalez-Mariscal et al., 2000), and binds to the actin cytoskeleton, stabilising the TJs and contributing to their function. ZO-1 is also integral in mediating paracellular permeability (Fanning et al., 1998), with dissociation of ZO-1 leading to increased BBB permeability (Hawkins and Davis, 2005). *In vitro* studies have established roles for ZO-1 in endothelial cell–cell tension and recruitment of TJ proteins (Fanning et al., 1998, Jiao et al., 2011, Tornavaca et al., 2015).

JAMs are immunoglobulin G (IgG) type proteins consisting of A-, B- and C- subtypes (Stamatovic et al., 2016, Martin-Padura et al., 1998). Comprising a single transmembrane domain, the cytoplasmic C-terminus interacts directly with ZO-1 (Bazzoni and Dejana, 2004). JAMs are identified to play a key role in the formation of tubules and TJ complexes, as well as leukocyte adhesion and transmigration (Lamagna et al., 2005, Ebnet et al., 2003). Studies have observed reduced JAM expression and migration of JAMs from TJ complexes results in a loss of BBB integrity at the microvascular endothelium (Haarmann et al., 2010).

These various components comprising the BBB are tightly regulated to ensure that integrity and functionality is maintained. Nevertheless, following acute CNS injury, disruption to the structure and function of the barrier results in profound changes in BBB permeability.

2.2 MECHANISMS OF BLOOD–BRAIN BARRIER DISRUPTION POST-STROKE

Loss of structural integrity and heightened permeability of the BBB is a well-documented feature of ischaemic injury (Jiang et al., 2018, Yang and Rosenberg, 2011). The exact

mechanisms by which disruption ensues are debatable; however, acute hypertension, increased osmolality, classical inflammation, increased para/transcellular transport and enhanced activity of matrix metalloproteinases (MMPs) have all been implicated, among many others (Sifat et al., 2017). The timing and extent of such BBB permeability changes vary according to the severity and duration of the ischaemic insult. Nevertheless, it is accepted stroke is associated with both early and late alterations in permeability (Turner and Sharp, 2016), with the first alterations occurring within hours of stroke onset, and the second some 24–48 hours later (Rosenberg et al., 1998). For example, experimental stroke models have revealed that heightened barrier permeability observed at 4–12 hours post-stroke is attributable to elevations in caveolin-1 expression, driving changes in the transcellular pathway, followed by later disruption at 24–48 hours due to dysregulation of TJ proteins occludin, claudin-5 and ZO-1, which initiates changes in the paracellular pathway (Gu et al., 2012, Nag et al., 2007). Further, increased activity of the MMP system has been implicated in post-stroke BBB permeability changes (Turner and Sharp, 2016). Specifically, very early BBB permeability alterations have been attributed to the activity of MMP-2, which loosens the TJs (Lakhan et al., 2013), whereas delayed permeability changes at 4 hours to 4 days post-stroke are linked to profound MMP-9-mediated degradation of the basal lamina (Mun-Bryce and Rosenberg, 1998) and TJ components (Asahi et al., 2001, Clark et al., 1997). Such findings are in keeping with those of clinical stroke, with similar elevations in MMP levels observed in patients following ischaemic stroke (Anthony et al., 1997, Montaner et al., 2003, Ning et al., 2006, Rosell et al., 2008).

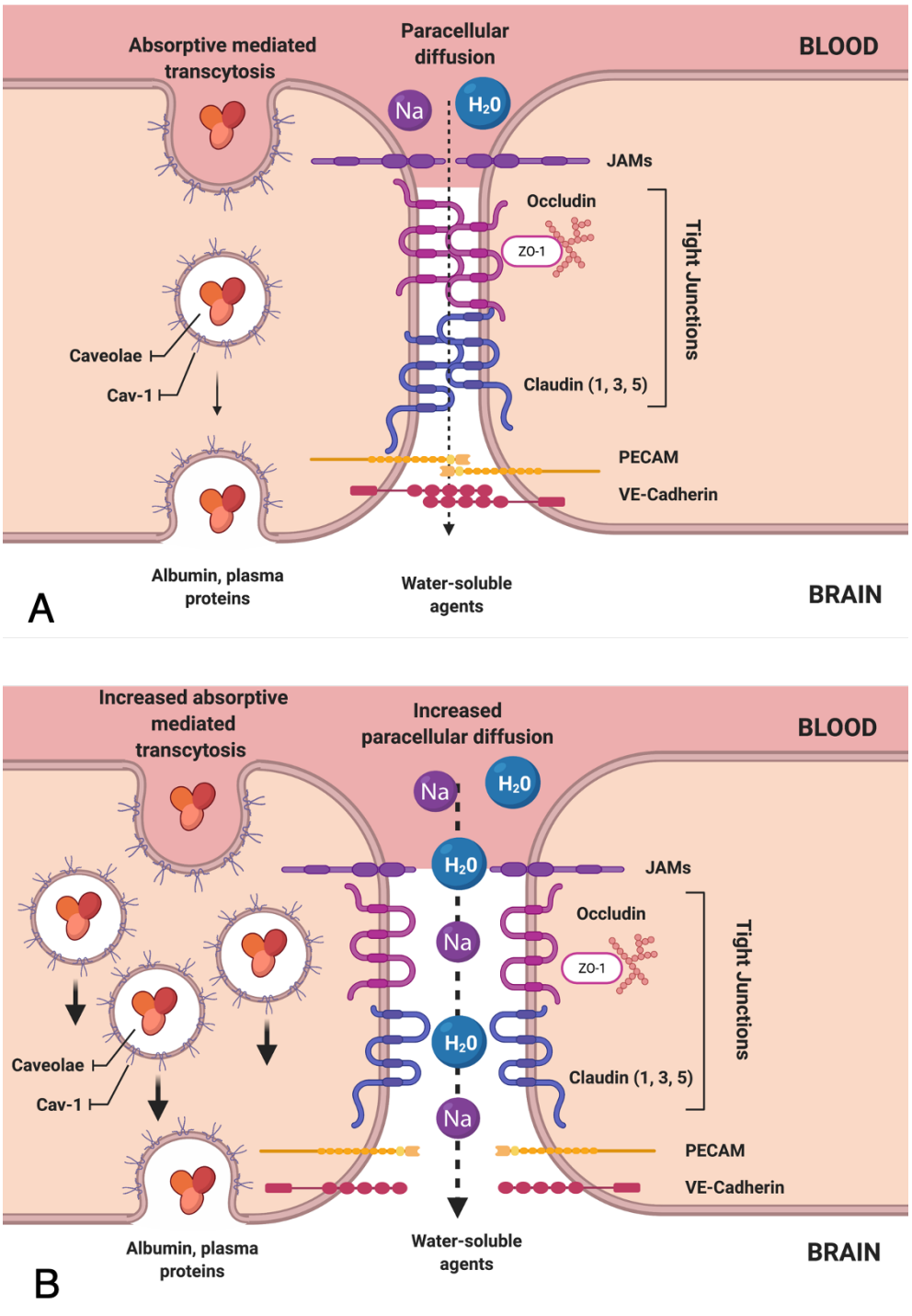

Figure 2.2. The blood–brain barrier under physiological conditions and following ischaemic stroke. (A) Under physiological conditions, transport across the barrier is regulated by TJs and absorptive mediated transcytosis via caveolae. (B) Following stroke, there is a loss of TJ integrity, leading to increased paracellular diffusion of water and ions. In addition, there is an upregulation of caveolae-mediated transcytosis, leading to an increased movement of albumin into the brain, with water following down its osmotic gradient. Cav-1, caveolin 1; ZO-1, zonula occludin 1; JAMs, junctional adhesion molecules; PECAM, platelet endothelial cell adhesion molecule; VE-cadherin, vascular endothelial cadherin; Na, sodium; H_20, water. *Figure created with BioRender.com (2020).*

2.3 NEUROGENIC INFLAMMATION

The concept of neurogenic inflammation was first described in the peripheral nervous system (PNS), where activated neurons of the dorsal root ganglia were observed to induce blood vessel vasodilation in the lower extremities (Bayliss, 1901). Following these early observations, the definition of neurogenic inflammation has evolved to encompass a painful local inflammatory response characterised by vasodilation, increased vascular permeability, tissue swelling and mast cell degranulation (Severini et al., 2002). In addition, there are tissue-specific responses such as smooth muscle contraction in the bladder, bronchoconstriction in the airways and ionotropic/chronotropic effects on the heart (Black, 2002).

Initiation of neurogenic inflammation occurs via activation of unmyelinated sensory c-fibres. C-fibres respond to a plethora of stimuli including mechanical stimulation, changes in the extracellular environment (such as increased osmolarity, pH and temperature changes), and a variety of agents including prostanoids, leukotrienes, histamine and serotonin (Harrison and Geppetti, 2001, Lewis et al., 2013). Activation initiates release of neuropeptides SP, CGRP, neurokinin A (NKA) and neurokinin B (NKB), among others (Severini et al., 2002). These neuropeptides act as neuromodulators and neurotransmitters in physiological and pathological processes where they are responsible for slow-onset, long-lasting modulation of synaptic transmission (Kleinman et al., 1985). In particular, SP is the most potent initiator of neurogenic inflammation, with CGRP able to further potentiate its effects (Harrison and Geppetti, 2001).

2.3.1 Substance P

SP is an 11 amino acid peptide member of the tachykinin peptide family (Figure 2.3), produced from alternative splicing of the preprotachykinin A gene (Hokfelt et al., 2000, Leeman and Ferguson, 2000, Maggi, 1995). SP is released from primary afferent neurons where it acts as a neurotransmitter. Under normal conditions, SP is synthesised and stored within both peripheral and central neurons (Hokfelt et al., 2000, Maggi, 1995, Otsuka and Yoshioka, 1993), with activation or damage of these neurons resulting in the rapid release of SP (Harrison and Geppetti, 2001, Hokfelt et al., 2000). SP may also be released from non-neuronal cells, including inflammatory and endothelial cells (Hokfelt et al., 2000).

SP is widely distributed throughout both the CNS and the PNS and released in response to Ca^{2+}-dependent depolarisation of neurons via various stimuli including changes in pH, electrical stimulation and ligand binding (Harrison and Geppetti, 2001). Within the CNS, the greatest SP immunoreactivity has been demonstrated in the amygdala, nucleus caudatus, putamen, globus pallidus, hypothalamus, substantia nigra, locus coeruleus and dorsal horn of the spinal cord (Severini et al., 2002, Sutoo et al., 1999, Ribeiro-da-Silva and Hokfelt, 2000). Within the PNS, SP is found throughout the enteric nervous system, respiratory tract, urinary system, lymphoid organs, blood vessels and cellular components of the blood (Severini et al., 2002). Indeed, SP-containing sensory nerves surround virtually all blood vessels in the body, with cerebral arteries having a particularly dense supply (Zacest et al., 2010, Edvinsson et al., 1983).

Following release, SP mediates its effects via high-affinity binding to the NK1-R, but it may also bind with varying affinity to the NK2 and NK3 tachykinin receptors depending upon receptor density/availability (Regoli et al., 1994). The NK receptors are members of the

rhodopsin family of 7-transmembrane G-protein coupled receptors, with the G-proteins associated with the intracellular domain of the NK receptor responsible for the transduction of the SP signal. Stimulation of intracellular G-proteins results in increased expression of cyclic adenosine monophosphate (cAMP) and a cascade of events leading to regulation of ion channels, enzyme activity and changes in gene expression (Kavelaars et al., 1994, Regoli et al., 1994).

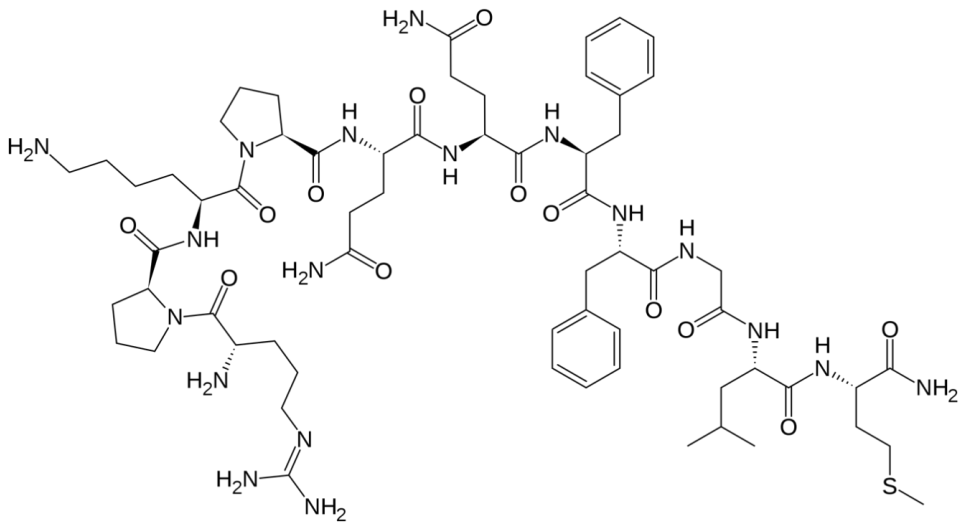

Figure 2.3. Two-dimensional molecular structure of substance P. The chemical formula for SP is $C_{23}H_{21}F_7N_4O_3$. The amino acid sequence is H-Arg-Pro-Lys-Pro-Gln-Gln-Phe-Phe-Gly-Leu-Met-NH. *Figure created using ADC ChemSketch 10.1 and Inkscape.*

The NK1-R is distributed throughout the CNS and is ubiquitously expressed throughout the brain (Sutoo et al., 1999, Sutoo et al., 2000). Stimulation of the NK1-R by SP initiates various biological processes including vasodilation, smooth muscle contraction and relaxation and plasma protein extravasation (Campos and Calixto, 2000). In addition, roles for SP have been documented in nociception (Wu et al., 2005), learning and memory (Hasenohrl et al., 2000), and anxiety and depression (Rupniak and Kramer, 1999). SP has also been implicated in a number of different pathologies including migraine (May and Goadsby, 2001a, May and Goadsby, 2001b), anxiety (Ebner et al., 2004, Ebner and

Singewald, 2006, Ebner et al., 2008), inflammatory bowel disease (Riegler et al., 1999, Goode et al., 2003), asthma (Bertrand and Geppetti, 1996), TBI (Donkin et al., 2011, Donkin et al., 2009, Nimmo et al., 2004, Vink et al., 2004) and stroke (Turner et al., 2006, Turner et al., 2011, Turner and Vink, 2012).

2.3.2 Calcitonin Gene-Related Peptide

CGRP is a 37 amino acid neuropeptide, co-expressed with SP in neuronal tissue (Ohtori et al., 2002). It has two isoforms, α-CGRP (Figure 2.4) and β-CGRP, with α-CGRP more abundant in both the CNS (Lange et al., 2009) and the PNS (Rosenfeld et al., 1983). α-CGRP is formed from the alternative splicing of the calcitonin/CGRP gene located on chromosome 11. CGRP is highly expressed in all vascular tissues, trigeminal ganglia and astrocytes (Moreno et al., 1999), and is particularly active in the cerebral circulation (Hanko et al., 1985), where it is stored and released from sensory neurons (Amara et al., 1982).

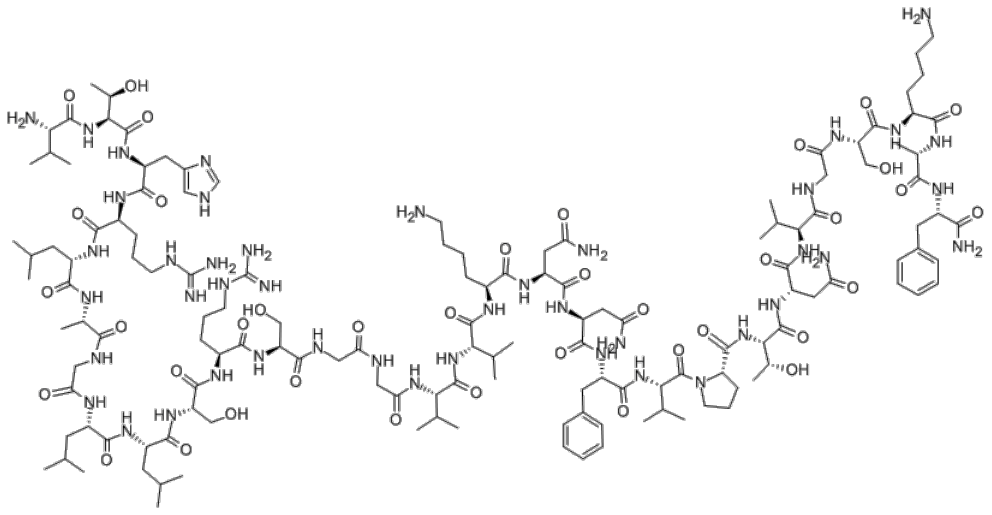

Figure 2.4. Two-dimensional molecular structure of α-calcitonin gene-related peptide. The chemical formula for α-CGRP is $C_{139}H_{230}N_{44}O_{38}$. *Figure created using ADC ChemSketch 10.1 and Inkscape.*

Calcitonin receptor-like receptor (CLR) is the receptor to which CGRP binds, and comprises two separate structures that come together, the G-protein coupled receptor CLR, and an accessory protein identified as receptor activity modifying protein (RAMP) (McLatchie et al., 1998). RAMP1 proteins are responsible for translocating CLRs to the plasma membrane so that CGRP molecules can bind to them. In the CNS, the CLR-RAMP1 receptor is primarily expressed along endothelial cells. CGRP release activates CLR-RAMP1, causing increases in cAMP, and resulting in potent vasodilation and increased blood flow (Bulloch et al., 1998, Zhang et al., 2010), with such CGRP-mediated vessel dilation located within the smooth muscle layer. CGRP has a particularly strong effect on cerebrovascular expansion (Omeis et al., 2008), and given it is co-stored and co-released with SP (Harrison and Geppetti, 2001), it is involved in neurogenic inflammation and potentiating the effects of SP (Legat et al., 2002). Beyond regulation of vascular tone, CGRP is also involved in angiogenesis, pain signalling, and the regulation of various behavioural processes including the stress response and fear-related behaviours (Legat et al., 2002, Oku et al., 1987).

2.4 NEUROGENIC INFLAMMATION POST-STROKE

Well documented in peripheral tissues (Severini et al., 2002), the concept of neurogenic inflammation as a response to tissue injury has more recently been extended to include the CNS (Nimmo et al., 2004, Turner et al., Stumm et al., 2001)(summarised in Figure 2.5). Intravenous SP administration induced a significant increase in plasma extravasation in the dura mater, an effect abolished by NK1-R antagonist pre-treatment (Cyrino et al., 2002). Further, activation of NK1-R on the vascular endothelium was shown to contribute to the development of cerebral oedema (Stumm et al., 2001). Similarly, treatment with capsaicin, which is known to bind to transient receptor potential vanilloid receptor subtype 1 (TRPV-

1) receptors initiating release of SP (Tang et al., 2006), elicited a neurogenic inflammatory response within the dura mater following administration (Markowitz et al., 1987). Capsaicin-induced neuropeptide depletion was shown to provide protection from neonatal hypoxia/ischaemic injury in rats, resulting in a reduction in infarct volume and apoptosis, and improved vascular dynamics, suggesting neuropeptides were mediating such effects (Khatibi et al., 2011). Indeed, initial studies in capsaicin pre-treated animals to deplete sensory neuropeptides have revealed that neuropeptide depletion prior to acute CNS injury is protective, with reductions in BBB permeability, cerebral oedema, and both motor and cognitive deficits (Nimmo et al., 2004, Turner and Vink, 2014). These studies clearly indicated a role for neuropeptides and neurogenic inflammation in such injury pathways. Subsequent studies have now clearly delineated a role for neurogenic inflammation in BBB dysfunction and genesis of cerebral oedema observed following acute CNS injury (Turner et al., Turner et al., 2011, Turner and Vink, 2012, Nimmo et al., 2004, Vink et al., 2004, Donkin et al., 2009).

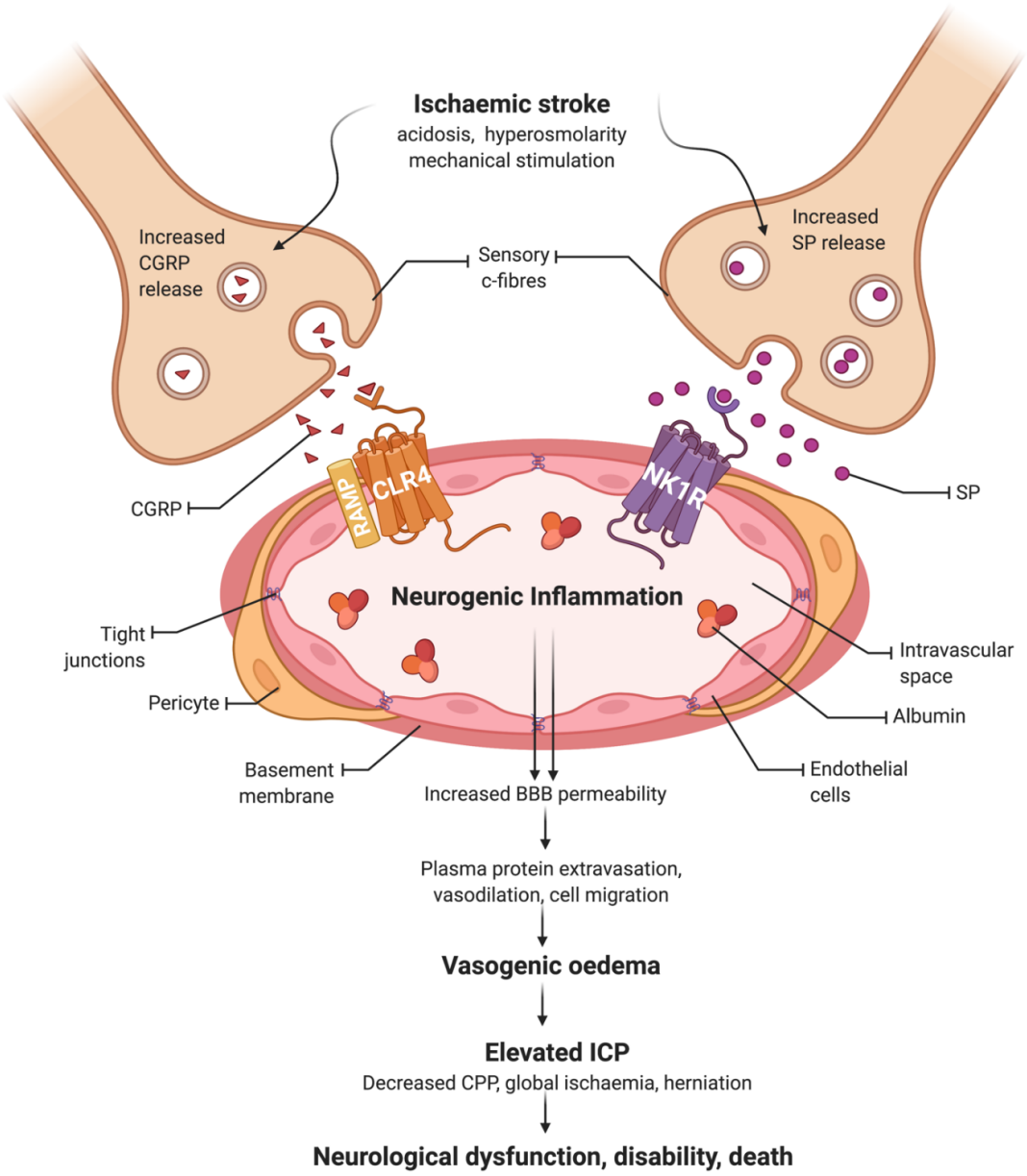

Figure 2.5. Neurogenic inflammation following ischaemic stroke. Ischaemic insult and initiation of downstream injury pathways stimulate development of neurogenic inflammation via co-release of the neuropeptide's SP and CGRP, which leads to vasodilation, increased BBB permeability and vasogenic oedema. This leads to a subsequent rise in ICP and decrease in CPP, and resultant global ischaemia, brain herniation, neurological dysfunction, disability and death. BBB, blood–brain barrier; CGRP, calcitonin gene-related peptide; CLR4, calcitonin receptor-like receptor 4; CPP, cerebral perfusion pressure; ICP, intracranial pressure; NK1-R, neurokinin 1 tachykinin receptor; RAMP, receptor activity modifying protein; SP, substance P. *Figure created with BioRender.com (2021).*

2.4.1 Substance P in Stroke

Following observations of SP release from the rabbit carotid body in response to hypoxia (Kim et al., 2001), such findings have been replicated in cerebral ischaemia (Turner et al., 2006, Turner et al., 2011, Turner and Vink, 2012, Turner and Vink, 2014, Yu et al., 1997). Overexpression of SP has been observed following stroke, where release is associated with an exacerbation of ischaemic tissue damage and poor neurological function (Yu et al., 1997). Our group has since further explored the role of neurogenic inflammation in cerebral ischaemia (Turner et al., 2006, Turner et al., 2011, Turner and Vink, 2012, Turner and Vink, 2014). We have shown that at 24 hours following stroke with reperfusion in a rodent model, SP immunoreactivity was increased in penumbral tissue, but not within core tissue, of the infarcted hemisphere (Turner et al., 2006). Such increases in SP immunoreactivity were observed in conjunction with significant disruption of the BBB, as measured by Evan's Blue extravasation, in addition to profound cerebral oedema and persistent functional deficits (Turner et al., 2006, Turner et al., 2011, Turner and Vink, 2012, Turner and Vink, 2014). A similar SP profile has been observed clinically, with elevated SP levels shown to be present in the serum of patients with complete stroke or transient ischaemic attack (TIA) at 12–24 hours following onset (Bruno et al., 2003). Serum SP levels were on average 4-fold higher in stroke/TIA patients compared with healthy controls at 12 hours and began to decline at 24 hours following injury. Taken together, these findings indicate that neurogenic inflammation, and in particular SP release, is a feature in ischaemic stroke that appears to be central to changes in BBB permeability and subsequent development of cerebral oedema.

2.4.2 Calcitonin Gene-Related Peptide in Stroke

Given its role as a potent vasodilator, it is not surprising that CGRP has also been investigated in the setting of cerebral ischaemia as a potential neuroprotectant. Indeed,

CGRP release is observed to increase under stressful conditions and following ischaemic tissue damage (Shao et al., 2015). This is in contrast to reports of reduced local CGRP levels following murine stroke with reperfusion, which is not conducive to the repair of damaged tissue (Zhang et al., 2011a). However, leptin treatment was shown to enhance CGRP expression and in turn reduce infarct volume and both neuronal apoptosis and necrosis, while also improving regional CBF. Further, CGRP has been proposed as a modulator of post-stroke depression (PSD), following observations that both CSF and hippocampal levels of CGRP were elevated in a rodent PSD model (Shao et al., 2015). Indeed, intracerebroventricular administration of CGRP enhanced PSD symptoms in a dose-dependent manner, suggesting PSD is mediated, at least in part, by CGRP. A similar pattern has been observed in clinical depression, with elevated CGRP levels recorded in the CSF of depressed patients (Mathe et al., 1994). Such findings indicate alterations in CGRP levels following stroke are more varied than those of SP and are highly dependent on the nature and severity of injury. Nevertheless, the increase in CGRP levels observed in some studies may represent a protective response to improve CBF and maintain tissue perfusion in the setting of cerebral ischaemia.

2.5 NEUROGENIC INFLAMMATION AND THE BLOOD–BRAIN BARRIER

It is well established that neurogenic inflammation increases BBB permeability; however, the exact mechanisms by which neurogenic inflammation, and specifically release of SP, precipitates such alterations following stroke remain unclear.

Some studies have reported SP/NK1-induced alterations in BBB integrity. Application of SP to cerebral capillary endothelial cell cultures has been shown to reduce the expression of

TJ components ZO-1 and caludin-5, although immediately following this, TJs were observed to be intact (Lu et al., 2008). In fact, it appears that SP may exert its initial effects on transcellular rather than paracellular transport across the BBB specifically by increasing transcytosis via the activation of caveolae-mediated transport. Indeed, the NK1-R is localised in caveolae within endothelial cells, and upon stimulation, can alter its expression or location, suggesting that it plays a dynamic role in this environment (Kubale et al., 2007, Monastyrskaya et al., 2005). In keeping with these findings, SP-induced stimulation of the NK1-R has been shown to stimulate the relocation of protein kinase C-α to caveolae, a process integral to the internalisation of caveolae and therefore transcellular transport across the barrier (Mineo et al., 1998).

However, the effects of SP on the BBB are not solely limited to alterations in permeability, with activation of the NK1-R by SP leading to increased migration of leukocytes, such as monocytes and neutrophils, across the barrier into the brain parenchyma via chemotactic effects (Cao et al., 2000, Souza et al., 2002, Schratzberger et al., 1997); increased endothelial cell expression of adhesion molecules (Annunziata et al., 2002, Toneatto et al., 1999, Li et al., 2008, Vishwanath and Mukherjee, 1996); and the exacerbation of local chemokine production (Ramnath and Bhatia, 2006). Indeed, SP applied to cultures of cerebral endothelial cells led to a dose-dependent increase in intracellular adhesion molecule-1 (ICAM-1), observed in conjunction with an increase in T cell adherence. Such findings suggest that increased SP levels in the setting of neurogenic inflammation have the capacity to increase the infiltration of inflammatory cells into the CNS tissue, in turn exacerbating the local neuroinflammatory response to acute CNS injury through the production of free radicals, pro-inflammatory cytokines and proteases targeting the extracellular matrix, such as MMPs (Corrigan et al., 2016a).

Taken together, it is evident neurogenic inflammation plays a role in altering BBB permeability, along with a capacity to perpetuate classical inflammation by enhancing immune cell trafficking into the brain, both of which lead to worsening of injury. Given the role of the SP/NK1 system in alterations to BBB permeability and transport following acute CNS injury, modulating neurogenic inflammation may represent a novel treatment target to interfere with this key injury cascade.

2.6 TARGETING NEUROGENIC INFLAMMATION POST-STROKE

Given the clear evidence that neurogenic inflammation is a feature of stroke associated with increased BBB permeability, genesis of cerebral oedema and the development of persistent functional deficits, it may represent a novel target for the treatment of cerebral oedema.

2.6.1 Neurokinin 1 Receptor Antagonists in Stroke

NK1-R antagonists are currently widely used clinically in patients undergoing chemotherapy to combat treatment nausea, with administration well tolerated by patients (Huskey et al., 2003, Inoue et al., 2017). NK1-R antagonists are also proposed to possess anxiolytic and antidepressant properties (Ibrahim and Preuss, 2020, Varty et al., 2003). Compounds currently approved for clinical use include aprepitant, casopitant, fosaprepitant, maropitant, netupitant and rolapitant (Figure 2.6). However, despite existing therapies, the potential utility of NK1-R antagonism for the treatment of cerebral oedema following stroke is yet to be realised clinically.

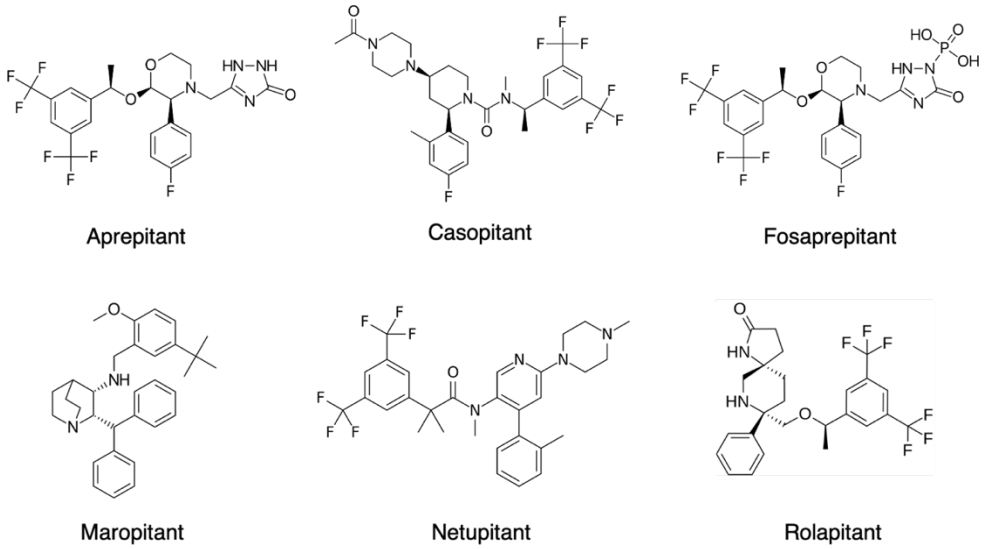

Figure 2.6. Two-dimensional molecular structures of currently in use neurokinin 1 receptor antagonists. The formulas for each of these agents are as follows: aprepitant, $C_{23}H_{21}F_7N_4O_3$; casopitant, $C_{30}H_{35}F_7N_4O_2$; fosaprepitant, $C_{23}H_{22}F_7N_4O_6P$; maropitant, $C_{32}H_{40}N_2O$; netupitant, $C_{30}H_{32}F_6N_4O$ and rolapitant, $C_{25}H_{26}F_6N_2O_2$. *Chemical structures created using ADC ChemSketch 10.1 and Inkscape.*

Yu and colleagues were the first to demonstrate preclinically that the NK1-R antagonist SR-14033 reduced infarct volume and improved neurological function when measured at 24 hours following focal cerebral ischaemia (Yu et al., 1997). Despite these initial positive results, no further studies were conducted. Our group has since extensively characterised the effect of NK1-R antagonist treatment following stroke. We have shown that NK1-R antagonist treatment at 4 hours post-stroke in a rodent model was associated with a significant reduction in BBB permeability and cerebral oedema, as measured at 24 hours (Turner et al., 2011). Further, this was associated with a recovery of behavioural function to baseline levels within 4 days of stroke onset. Despite this, no effect on infarct volume was observed. Nevertheless, function is a clinically useful measure of outcome and is often the endpoint in clinical trials. We have since demonstrated that NK1-R antagonist treatment is effective in mild to severe stroke, with a therapeutic window of up to 8 hours post-stroke for motor improvements and 12 hours post-stroke for sensory function improvements (Corrigan et al., 2016b). Further, we have demonstrated that NK1-R antagonist treatment can safely

and effectively be combined with tPA thrombolysis (Turner and Vink, 2012). Further, NK1-R antagonist treatment also limited the effects of reperfusion injury by reducing tPA-induced BBB permeability changes and complications such as haemorrhagic transformation.

2.6.2 Calcitonin Gene-Related Peptide Agonists in Stroke

Given its potent vasodilatory actions, CGRP has been shown to have neuroprotective actions in ischaemia (Bucinskaite et al., 1998, Cai et al., 2010, Kjartansson and Dalsgaard, 1987, Liu et al., 2011, Tam and Brain, 2004). Indeed, increased CGRP immunoreactivity showed a positive correlation with tissue flap survival following ischaemia (Bucinskaite et al., 1998). Despite this, investigations of CGRP treatment following stroke remain limited. Early CGRP intervention following brain injury can significantly reduce neuronal apoptosis and tissue damage while maintaining nerve regeneration (Macdonald et al., 2007). CGRP induces dose-dependent increases in vasodilation post-ischaemia, enhancing reperfusion and potentially contributing to penumbral rescue (Tam and Brain, 2004). Indeed, CGRP pre-treatment reduced infarct volume by 57% and significantly improved CBF in rodent stroke with reperfusion (Holland et al., 1994). Further, CGRP administered at the onset of reperfusion produced a significant reduction in infarct volume, BBB permeability and cerebral oedema following stroke in a rodent model (Liu et al., 2011). Such positive treatment effects were observed in concert with a reduction in AQP4 expression, ultrastructural damage to endothelial cells and TJ loss, suggesting that CGRP mediated stabilisation of the BBB. Indeed, exogenous CGRP significantly increased CBF and protected neurons following cerebral ischaemia (Zhang et al., 2010). CGRP has also proved beneficial in haemorrhagic stroke, given its ability to counteract vasoconstriction in human SAH (Juul et al., 1994).

CGRP is also central to the mechanisms underlying remote preconditioning, with intracerebroventricular morphine-induced remote preconditioning leading to increased

CGRP release in a dose-dependent manner. This suggests CGRP release is part of a protective response resulting in reduced lesion volume to protect ischaemic brain tissue from ischaemia/reperfusion injury (Zhang et al., 2011b). Such preconditioning effects were abolished when a CGRP release inhibitor was administered (Rehni et al., 2008). Further, delayed adrenomedullin (a member of the CGRP family) gene transfer 3 days following rodent stroke was associated with neuroprotection from the ischaemic insult, as evidenced by a reduction in infarct volume and apoptotic cell death combined with enhanced astrocyte migration (Xia et al., 2004).

2.7 CONCLUSIONS

It is clear that neurogenic inflammation is involved in enhanced permeability of the BBB following stroke and the subsequent development of cerebral oedema and poor functional outcome. In particular, SP is a key modulator of these processes, with NK1-R antagonist administration effective in reducing BBB permeability, cerebral oedema and functional deficits in preclinical rodent models of stroke. The role of CGRP following acute CNS injury is less clear; however, it has been clarified that CGRP-induced vasodilation improves outcomes in addition to stabilising the BBB. CGRP agonists should be further explored for their potential utility in improving CBF and stabilising the BBB following acute CNS injury.

Given the inability of current treatments to target the mechanisms of BBB alterations and genesis of cerebral oedema and concomitant rise in ICP post-stroke, modulation of neurogenic inflammation through the administration of an NK1-R antagonist represents a novel therapeutic approach to treat cerebral oedema to both reduce mortality and improve outcome. Thus, targeting neurogenic inflammation may provide an alternate treatment

strategy that is more specific and efficacious than current pharmacotherapies used, and without the risk of invasive surgery. However, this requires evaluation and screening in a more clinically relevant stroke model before clinical assessment is possible.

03

Large Animal Models of Stroke as Translational Tools

Chapter revised from the original publication by **SORBY-ADAMS, A. J**., VINK, R., & TURNER, R. J. 2018. Large animal models of stroke and traumatic brain injury as translational tools. *American Journal of Physiology. Regulatory, Integrative and Comparative Physiology*, 315, R165.

Statement of Authorship

Title of Paper	Large animal models of stroke and traumatic brain injury as translational tools
Publication Status	☑ Published ☐ Accepted for Publication ☐ Submitted for Publication ☐ Unpublished and Unsubmitted w ork w ritten in manuscript style
Publication Details	Sorby-Adams, A. J., Vink, R., & Turner, R. J. (2018). Large animal models of stroke and traumatic brain injury as translational tools. *American journal of physiology. Regulatory, integrative and comparative physiology, 315*(2), R165. doi:10.1152/ajpregu.00163.2017

Principal Author

Name of Principal Author (Candidate)	Annabel Sorby-Adams		
Contribution to the Paper	I was the first and corresponding author and main contributor to the manuscript.		
Overall percentage (%)	70%		
Certification:	This paper reports on original research I conducted during the period of my Higher Degree by Research candidature and is not subject to any obligations or contractual agreements with a third party that would constrain its inclusion in this thesis. I am the primary author of this paper.		
Signature		Date	16.03.2021

Co-Author Contributions

By signing the Statement of Authorship, each author certifies that:

i. the candidate's stated contribution to the publication is accurate (as detailed above);

ii. permission is granted for the candidate in include the publication in the thesis; and

iii. the sum of all co-author contributions is equal to 100% less the candidate's stated contribution.

Name of Co-Author	Renee Turner		
Contribution to the Paper	Associate Professor Renee Turner is the head of the Translational Neuropathology Laboratory. She oversaw drafting and structure of the manuscript.		
Signature		Date	16.03.2021

Name of Co-Author	Robert Vink		
Contribution to the Paper	At the time of publication Professor Robert Vink was the vice-chancellor of the University of South Australia and past head of the Translational Neuropathology Laboratory. He oversaw the section on traumatic brain injury (not included in this thesis) and drafting of the manuscript.		
Signature		Date	16.03.2021

3.0 INTRODUCTION

While there have been significant advances in understanding the pathophysiology of stroke, the translation of novel pharmacotherapies from bench to bedside has unfortunately been extremely poor. Over 1000 agents identified to be efficacious in experimental stroke models have yielded only one successful clinical therapy to date (O'Collins et al., 2006). This gap between theory and practice needs to be urgently addressed to improve patient outcomes and survival. Studies in animal models have greatly enhanced our understanding of the molecular mechanisms underlying stroke. To date, the majority of preclinical stroke work has been conducted in rodent models, which are well established; easy to handle and cost effective; comprise large physiological databases; permit extensive behavioural assessment; and provide the ease and ability to study transgenic animals. However, there are also a number of disadvantages of rodent models, including their small lissencephalic brain, small proportion of white matter compared with higher species and flimsy tentorium cerebelli, each of which is important when studying the response of the brain to injury. Nevertheless, information from rodent studies has greatly advanced our knowledge of the pathophysiology of stroke, and these models remain key research tools for initial discovery studies.

A potential strategy to improve clinical translation for stroke is the use of large animal models. Indeed, a set of preclinical guidelines has been established to improve the rigour of experimental stroke studies and increase their clinical predictive value (Fisher et al., 2009). These guidelines strongly recommend that after sufficient evidence of efficacy is obtained using rodent models, screening in large animal models should be conducted prior to commencement of clinical trials (Fisher et al., 2009). The use of such a large intermediate species may enhance successful translation to the clinic given the similarities in neuroanatomical structure to the human brain, and closer resemblance to the

pathophysiological and clinical manifestations of stroke. In light of these recommendations, the acute CNS injury field has moved towards incorporating more studies in large animal models as part of the preclinical assessment repertoire. To achieve this, however, the most suitable large animal species need to be identified, and both appropriate and reliable injury models developed and comprehensively characterised.

Rabbits were among the first larger animal species to be investigated using cerebral ischaemia models, and their extensive use was pivotal in preclinical studies determining the efficacy of tPA, which to this day remains the only approved pharmacological agent for the treatment of ischaemic stroke (Zivin et al., 1985). Many intermediate species have also been used to model stroke, including ferrets and gerbils; however, some of these species are lissencephalic, such that more researchers are now including larger species in their experimental design given their definitive gyrencephalic brain structure. Large animal models of stroke are available in a range of species including feline, canine, ovine, porcine and non-human primate (NHP) models. The appropriate selection of such experimental species for preclinical assessment is absolutely essential (Casals et al., 2011) and needs to fit the specific research requirements, as different models may be required to answer different stroke pathophysiology questions, and it is unlikely to be a one-size-fits-all approach.

This chapter summarises the available large animal models of ischaemic stroke, including discussion on the neuroanatomy, recommendations for large animal anaesthesia, surgical considerations, and key features and advantages/disadvantages of each species and model.

3.1 CEREBRAL STRUCTURE

A rich diversity of animal species have been used to model stroke to date (Figure 3.1), and inter-species differences in cerebral anatomy, brain size and complexity are important considerations that may influence experimental outcome. In terms of gross brain size, the encephalic weight of all mammalian species generally correlates with overall bodyweight (Hofman, 1983, Economos, 1980). Because of their relative brain mass and neuronal complexity, large mammals are generally considered more intelligent than their small mammal counterparts (Roth and Dicke, 2005). However, absolute brain size does not correlate with overall intelligence (Falk and Gibson, 2001, Gibson et al., 2001). NHP species possess brains significantly smaller than ungulates, yet express distinct cognitive and behavioural superiority, advantageous for neurobehavioural testing (Roth and Dicke, 2005, Cook and Tymianski, 2012). Further, humans and NHPs have relatively thick cortices compared with rodents, containing numerous high-velocity neurons, leading to enhanced processing capacity (Roth and Dicke, 2005).

Although lacking the neuronal complexity of the human brain, the use of small animal species, with small brain volumes, offers advantages in fixation procedures and relative strain heterogeneity (Fluri et al., 2015). Paradoxically, one of the main criticisms associated with past failures of neuroprotective agents and the use of rodent models is the vast differences in neuroanatomical structure compared with the human brain. Most notable is the lissencephalic (‘smooth brain’) structure of the rodent brain, lacking the cortical sulci and gyri of the human. Absence of a convoluted cerebral structure significantly decreases the cortical surface area to total brain mass ratio (Cook and Tymianski, 2011). Gyrification and enhanced surface area correlates with an increased number of neurons, which has implications for cortical functional organisation and development (Dubois et al., 2008).

The brains of larger animal species also lend themselves to superior quality MRI studies and offer the advantage of using the same instrumentation for physiological monitoring as is used in humans, with similar values observed, thus facilitating translation using clinically relevant variables.

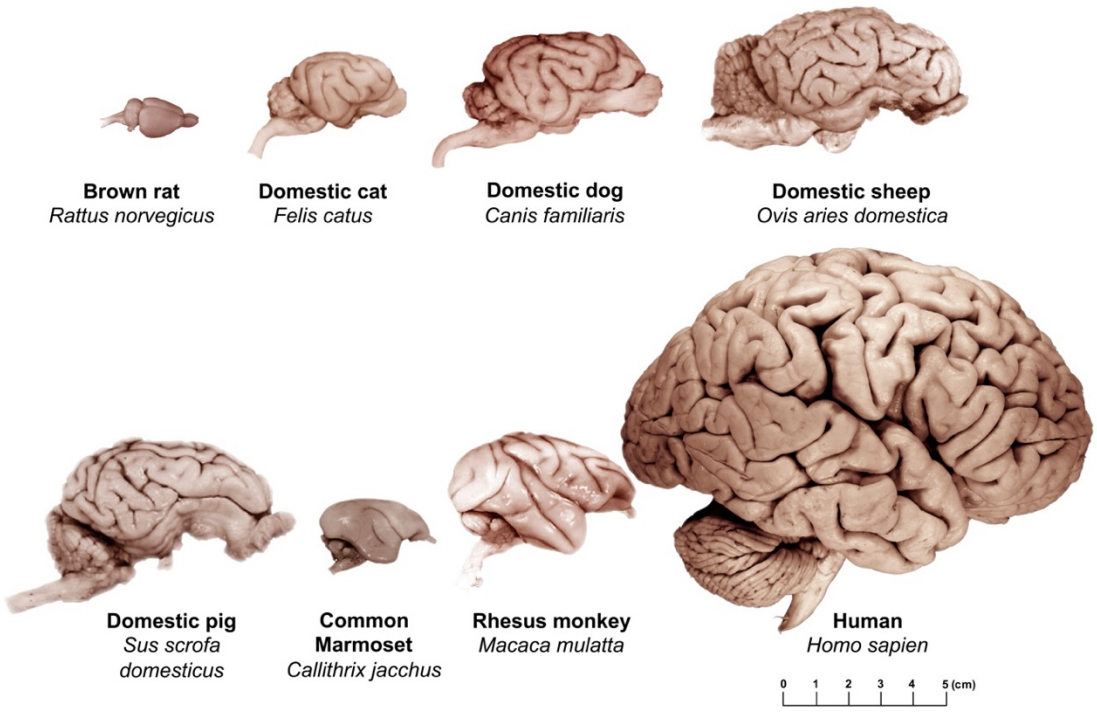

Figure 3.1. Gross comparative neuroanatomy of various large animal species used to model cerebral injury. Note the lissencephalic brain structure of the common marmoset and brown rat compared with the larger size and gyrencephalic structure of the dog, pig, sheep and rhesus monkey. *Images adapted with permission from the University of Wisconsin and Michigan State Comparative Mammalian Brain Collections and National Museum of Health and Medicine Collection. Preparation of images and specimens funded by the National Science Foundation and the National Institutes of Health*.

3.1.1 White Matter

Gyrencephalic brains have a higher proportion of sub-cortical white matter to grey matter compared with lissencephalic brains. White matter distribution correlates with absolute brain weight, and as large animal species generally have a greater brain mass they consequently

have a higher white to grey matter ratio (Philip et al., 2009). Clinically, the incidence of stroke involving regions of white matter is high, and thus using an experimental species that has a comparable white to grey matter distribution to that of humans is of particular relevance. Further, grey and white matter tissue have different thresholds for injury (Cai and Wang, 2016). The white matter, containing the myelinated axons of neurons, is extremely vulnerable to the effects of ischaemia and irreversible axonal injury (Petty and Wettstein, 1999). The neglect of white matter pathology has been exacerbated by ongoing use of rodents, which may be in part responsible for the plethora of neuroprotective agents, proven in their ability to successfully reduce grey matter damage, failing clinical trials (Dewar, 1999). In comparison, large animals such as porcine, canine, feline and ovine species have a relatively high proportion of white matter. NHPs used for investigation of cerebral injury are unique in that they include both lissencephalic and gyrencephalic species. The reduced volume of white matter in rodents also has implications in oedema development. This may partially account for the considerable inconsistency with respect to ICP increases reported in rodents after acute CNS injury (Gabrielian et al., 2011).

3.1.2 Meninges

In addition to the encephalic structure of large animals, the relative meningeal organisation is of importance when considering the progression of injury following stroke. Large animal species have well-developed meninges, with a strong and fibrous dura mater comparable to that of the human (Wells et al., 2012). This is of particular relevance to studies investigating the development of cerebral oedema and resultant rise in ICP as primary outcome measures. When pathological and excessive increases in ICP occur clinically, the brain may herniate onto adjacent structures or through the foramen magnum onto the brain stem, owing in part to the strong tentorium cerebelli that prevents displacement of the brain (Wells et al., 2015).

The comparatively flimsy tentorium of the rodent allows movement of the brain downwards to accommodate increased volume, leading to inconsistencies in ICP response (Gabrielian et al., 2013, Kotwica et al., 1991). Further, the measurable lack of compartmentalisation between the cerebrum and cerebellum of the rodent makes herniation unlikely following MCAo (Wells et al., 2015). In comparison, the strong fibrous tentorium cerebelli of large animals, including that of the sheep and pig, prevents pressure from diffusing downwards to accommodate the increased volume of the oedematous brain, leading to accumulation in the supra-tentorial compartment. The resultant effect is extensive elevations in ICP, midline shift and herniation of the brain, all of which are seen clinically (Wells et al., 2015). The ability to successfully measure ICP following transient stroke allows for investigation of autoregulation and changes in CPP, which is an important factor influencing reperfusion and subsequent evolution of the ischaemic penumbra (Markus, 2004). The choice of an appropriate experimental species must therefore take into consideration the ability to achieve an injury of clinical relevance.

3.2 CEREBROVASCULAR ANATOMY

Despite the variations in gross neuroanatomical structure, cerebrovascular anatomy is largely analogous across all mammalian species, and basic neural and vascular patterns are well conserved (Ashwini et al., 2008). In general, large animals have a greater cerebrovascular volume and vessel diameter than their small animal counterparts. Blood circulation and cerebral metabolism requirements in mammals are directly related to body weight, which has significant implications when choosing an appropriate experimental model (Dirnagl, 1999). Glucose and oxygen requirements in humans are three-fold greater than small animals, and thus the use of larger species with greater blood volume and energy

requirements is more clinically applicable, which is especially relevant when modelling stroke.

3.2.1 Circle of Willis

Blood is supplied to cerebral hemispheres by the circulus arteriosus cerebri, or coW. This circular anastomosis is located at the base of the skull and is composed of the ACAs, anterior communicating artery (ACoA), PCAs, posterior communicating cerebral artery (PCoA) and ICAs. The MCA is considered a natural continuation of the ICA, and although it is not part of the circle *per se*, occlusion of the MCA or its anastomoses is associated with the highest incidence of ischaemic stroke (Olsen, 1985, Nogles and Galuska, 2020). The basilar artery (BA) gives rise to the left and right PCAs and is formed by the vertebral arteries (VAs), which supply blood to the brain stem, cerebellum and upper spinal cord. Although the VAs and BA do not compose the coW, they are a common route of entry for endovascular approaches to stroke induction.

3.2.2 Inter-species Circle of Willis Variations

The coW is relatively well conserved in all mammalian species (Figure 3.2), and therefore, the relative reproducibility of stroke in both rodent and large animals has generally been high, enabling the generation of lesions comparable to those seen clinically (Ashwini, 2008). Despite similarities, however, there are several key differences between species that may influence experimental outcomes.

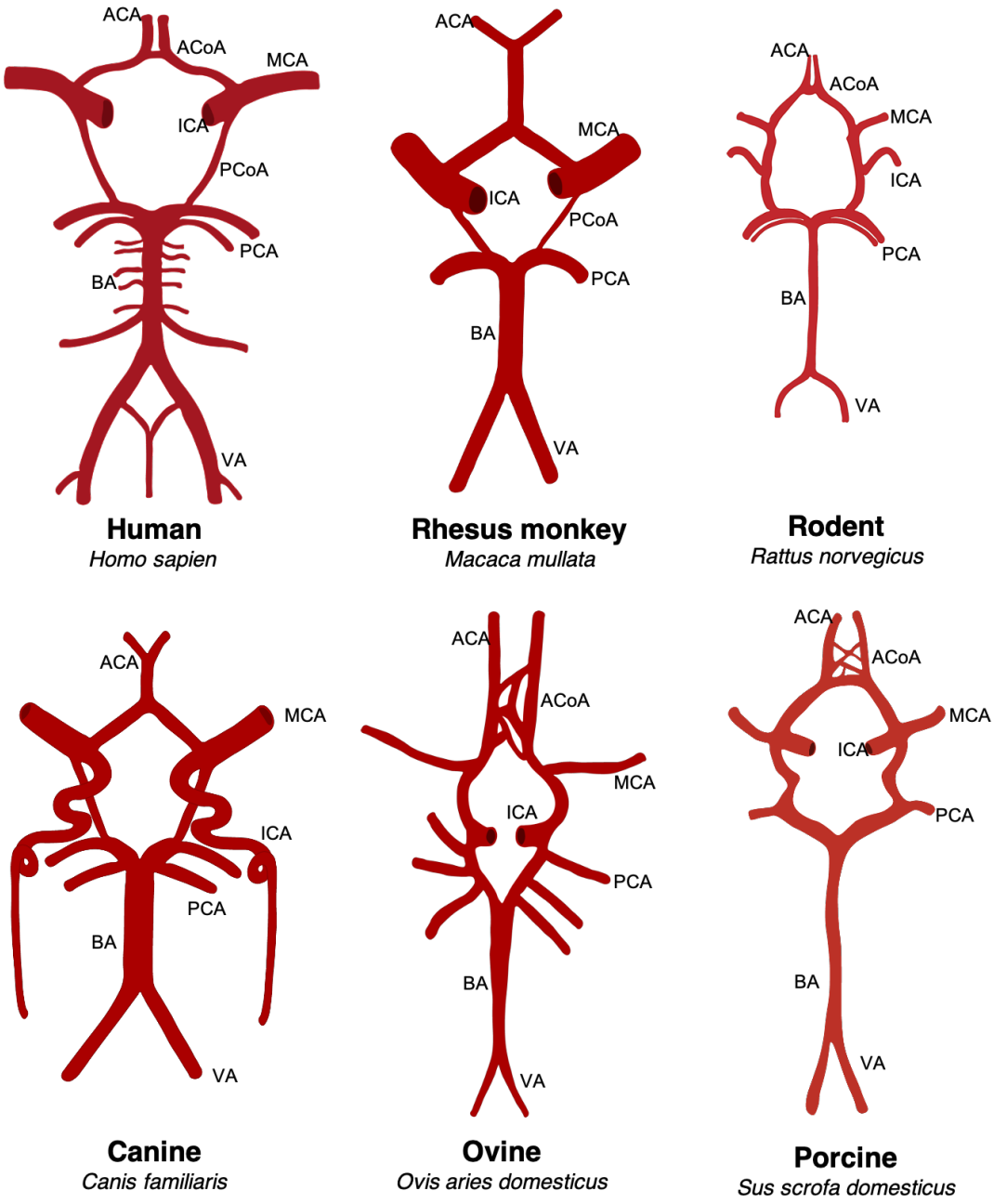

Figure 3.2. Comparative cerebrovascular anatomy of the circle of Willis. MCA, middle cerebral artery; ICA, internal carotid artery; ACoA, anterior communicating artery; ACA, anterior cerebral artery; PCoA, posterior communicating artery; PCA, posterior cerebral artery; BA, basilar artery; VA, vertebral artery. *Images adapted from Kapoor et al., 2003 and Ashwini et al., 2008.*

3.2.2.1 Ungulates

In ungulate species, the relative length and calibre of the PCoA is significantly greater than that of humans (Kapoor et al., 2003, Ashwini et al., 2008, Deepthi et al., 2016). In both porcine and ovine species, the PCA arises directly from the PCoA, rather than the BA, which may contraindicate their use in models of PCA stroke. Further, evidence of inter-species variation indicates that some animals have a network that comprises the ACoA, while others have total absence of the anastomosis (Kapoor et al., 2003). This presence of an ACoA network may compromise methods of occlusion involving the ACA because of collateralisation, whereas ACoA hypoblastia may lead to worsening of outcome because of poor hemispheric blood redistribution. Ruminants have a significantly longer ICA than any other species, continuing forward along the ventral aspect of the optic chiasm prior to bifurcation into the MCA. This may benefit transcranial approaches to MCAo, as the proximal MCA is more easily accessible than other large animal species, allowing for better visualisation and vessel access, in turn favouring reproducibility (Kapoor et al., 2003). Importantly, both sheep and pigs have a reticulated arterial anastomosis between the maxillary and internal carotid known as the rete mirabile (Figure 3.3), responsible for thermoregulation (Hoffmann et al., 2014). This complex arterial meshwork is located in the cavernous sinus (Deepthi et al., 2016) and is of particular anatomical significance when considering endovascular models of cerebral ischaemia, which are rendered virtually impossible because of the narrow diameter of arteries that comprise the rete.

3.2.2.2 Non-human Primates

Baboons have a network of arteries that join to form a communication between bilateral ACAs, rather than the single vessel found in humans. Some species, however, show a high

incidence of complete ACoA hypoplasia, which may, as with ungulates, have repercussions for ACA stroke models. Further, in NHP species, 60% of animals contain triplication/bifurcation of one or more arteries, and 44% of animals exhibit arterial hypoblastia (Langfitt et al., 1966). Such anomalies are seen considerably less in ruminants, with reports of variations in approximately 20% of animals and no reported anatomical abnormalities in the coW in pigs (Ashwini et al., 2008). Irrespective of species, variations in large animals are significantly less than seen in humans, where up to 70% of individuals have arterial anomalies in the coW (Ashwini et al., 2008).

3.2.2.3 Canines and Felines

Dogs and cats report arteria intercarotica caudalis, an intracavernous connection between the ICAs, which may have implications for catheter insertion and guidance in endovascular methods (Nanda and Getty, 1975). Canines also have extensive leptomeningeal anastomoses branching from the PCA, MCA and ACA, potentiating variation in lesion volume due to collateralisation (Symon, 1960). Further, as with sheep and pigs, cats have a rete mirabile, therefore limiting vascular occlusion by endovascular means.

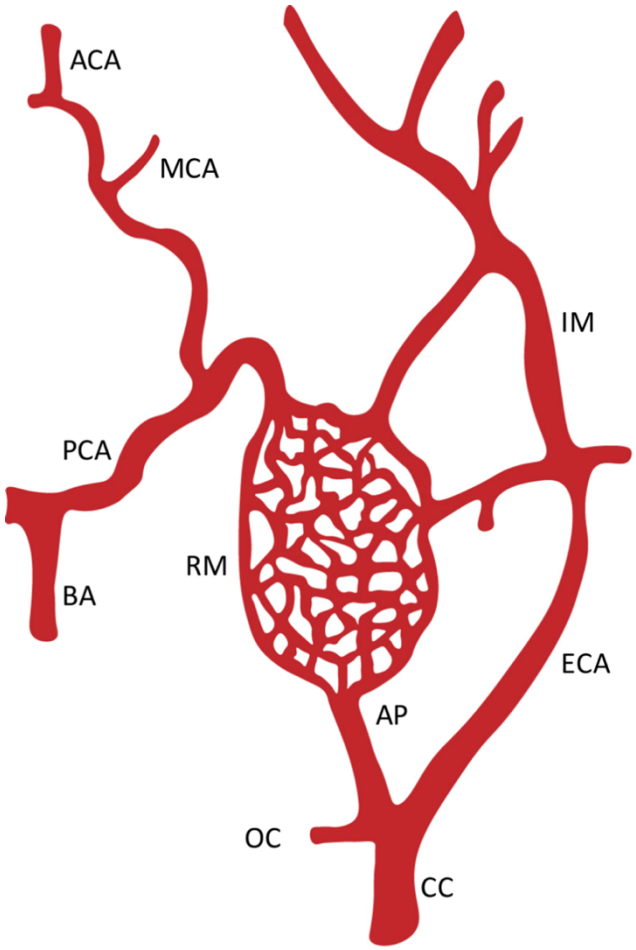

Figure 3.3. Diagrammatic representation of the extracranial rete mirabile present in porcine and ovine species. Note the mesh-like structure of the rete, contraindicating endovascular approaches of vascular occlusion in these species. CC, common carotid; ECA, external carotid artery; BA, basilar artery; RM, rete mirabile; AP, ascending pharyngeal artery; PCA, posterior cerebral artery; OC, occipital artery; MCA, middle cerebral artery; ACA, anterior cerebral artery; IM, internal maxillary artery.

Variations in cerebrovascular anatomy are an important consideration when choosing an experimental species as the choice of a particular genus can benefit model reproducibility due to anatomical homogeneity, whereas others may favour vascular/endovascular approaches. Despite individual variations, the choice of a species must always be made in concordance with the clinical condition to enhance translation, with both choice of animal and method of occlusion imperative.

3.3 SURGICAL CONSIDERATIONS FOR LARGE ANIMAL STROKE MODELS

Surgical procedures required for large animal models of stroke are often more technically demanding, time consuming and complex than equivalent approaches in small animals such as rodents. In addition to extensive aseptic surgical theatre set-up and equipment required, often comparable to the clinical theatre environment, there are a number of key considerations to be addressed prior to commencing an experiment. Recommended anaesthesia, physiological monitoring, antibiotics and analgesia will be discussed in detail in the following sections in relation to feline, canine, ovine, porcine and NHP species.

3.3.1 Anaesthesia

Because of the complexity of surgical procedures required to induce cerebral ischaemia in large animal species, anaesthesia is required, often for prolonged periods. Although anaesthetic agents are often administered during neurosurgical procedures, it must be recognised that human patients are rarely under their influence when suffering a stroke, and this should be acknowledged as a potential variable. Nevertheless, principles that apply to clinical anaesthesia are recognised as appropriate for large animal models. These conditions best preserve normal neurological function throughout and thereby facilitate the accurate determination of deficits applicable to the induced injury.

3.3.2 Pre-anaesthetic Considerations and Induction

It is recommended that all large animals requiring long-duration anaesthesia be fasted prior to surgery to reduce the risk of intraoperative regurgitation. Veterinary practice recommends food be withheld for a minimum of 12 hours in feline, canine, porcine and NHP species (Hall

et al., 2001). There is some speculation regarding optimum fasting duration in ruminant species, as abstinence from food has been shown to have little effect on rumen contents (Riebold, 2002). Fasting may, however, reduce ruminal tympany, in which gas accumulates in the rumen because of the bacterial fermentation process. It is therefore advised that food and water be withheld for 6 hours to reduce gaseous accretion.

For the purpose of all large animal surgery, it is highly recommended animals be induced with a sedative to ease handling and restraint, reduce distress and in turn decrease the required dose rate for maintenance anaesthesia by 30–50% (Flecknell, 2016a). Commonly reported induction agents and associated dosing regimens are detailed in Appendix 3.1. Anaesthetic induction and sedation also allows for ease of intubation and endotracheal tube insertion (Hendrickson and Baird, 2013). Intubation of the animal allows control of ventilation by mechanical means, thus facilitating regulation of the respiratory components of both pH and pCO_2. Although spontaneous breathing is reported, it is often accompanied by hypoventilation and consequent increase in lesion volume (Laletin and Bykov, 2015). Controlled ventilation in large animals offers significant advantage over rodents and other small animals, which can be difficult to intubate because of the small circumference of the larynx. Physical intubation in large animals is fairly uniform across species. However, the laryngeal anatomy of porcine species is unique because of the situation of the larynx within an airway sigmoid curve, which may lead to intubation difficulties (Greene and Benson, 2002). Consultation with an experienced veterinarian is therefore strongly advised prior to endotracheal tube insertion in these species.

It is recommended that mechanically ventilated animals are maintained on a combination of air/oxygen or pure oxygen to both preserve blood oxygenation levels and meet metabolic

demands. The latter is influenced by variables such as temperature, body weight and anaesthetic agent used, and thus oxygen delivery must be adjusted accordingly (Robertson, 2002). Maintaining animals on pure oxygen for durations of >12 hours is not recommended, however, because of the potential development of pulmonary oedema and oxygen toxicity (Greene, 2002). Further, the mechanical rate of ventilation for each species must be considered in relation to normal respiration rate and body mass to best maintain physiological pO_2 and pCO_2 levels (Pelosi et al., 1998). Species-specific physiological variables, including normal respiration rates and recommended ventilation, are summarised in Appendix 3.2.

3.3.3 Anaesthetic Maintenance

Following induction, intraoperative maintenance of anaesthesia can be achieved through the use of both intravenous and inhalational agents. The use of intravenous anaesthetic agents may be preferential for imaging purposes, where the use of equipment required for inhalational anaesthesia may be unfeasible, such as high-field MRI. However, inhalational agents are more frequently used, especially for longer-duration procedures. Inhalational anaesthetics agents used in rodent and large animal studies tend to be similar, with a preference for isoflurane commonly reported in canine, NHP, ovine and porcine models (Wells et al., 2015, Platt et al., 2014, Schwartz and Pile-Spellman, 2011, Christoforidis, 2011). However, respiratory depression and hypotension associated with isoflurane administration (Hudetz and Pagel, 2010, Lin et al., 1997) contraindicate prolonged surgical use, requiring close monitoring of respiratory and blood pressure parameters, in conjunction with depth of anaesthesia. Maintaining animals on a level of isoflurane that maintains the minimum alveolar concentration (MAC) below 1.5% is highly recommended as it reduces the likelihood of adverse events (Aranake et al., 2013). Intravenous and inhalational

anaesthetics may therefore be used in combination to eliminate the likelihood of adverse events if an appropriate depth of anaesthesia is not achievable under 1.5% MAC isoflurane alone. This can be achieved through continuous intravenous infusion using a pump and adjusting dose rates to achieve the desired level of anaesthesia. Intravenous anaesthetic agents such as propofol and ketamine have been used in NHP, porcine and ovine studies in conjunction with inhalational anaesthetics with reported success (Aranake et al., 2013, D'Ambrosio, 2004, Imai et al., 2006, Wells et al., 2015, Lin et al., 1997). Recommended MACs of various inhalational anaesthetic agents are detailed in Appendix 3.3.

Given the aforementioned length of anaesthesia required for many large animal models, the potential for neuroprotection brought about by anaesthetic regimen may contraindicate use of certain agents for extended durations. Valid animal modelling of acute CNS injury requires minimal interference from anaesthetic and analgesic agents to best preserve the natural course of brain injury, while minimising animal suffering (Rowe et al., 2013). Agents such as ketamine exhibit neuroprotective properties via inhibition of the NMDA receptor (Hudetz and Pagel, 2010, Orser et al., 1997), which has been shown to attenuate the deleterious neurochemical sequelae following brain injury (McIntosh et al., 1990). However, ketamine use has also been shown to increase cerebral oxygen metabolic rate ($CMRO_2$), which has implications for lesion volume and number of neuronal cells affected (Chang et al., 2002). Maintenance of animals on a combination of ketamine and isoflurane may offer a beneficial alternative in surgical procedures requiring prolonged duration (>4 hours) anaesthesia and has been reported in porcine, ovine and NHP models (Wells et al., 2012, Schwartz and Pile-Spellman, 2011, Platt et al., 2014). This anaesthetic combination produces a countering effect, eliminating the neuroprotective effect of pure ketamine and the respiratory distress associated with pure isoflurane, thus reducing confounding factors of

either anaesthetic agent administered alone (Wells et al., 2012, Wells et al., 2015). A comprehensive summary of commonly used intravenous, intramuscular and subcutaneous anaesthetic agents and recommended dosing regimens is detailed in Appendix 3.4 and inhalational agents in Appendix 3.5. These can be used in conjunction with recommended regimens from Appendix 3.3.

In addition to potential confounding effects of anaesthesia on outcome parameters, there are several species-specific complications that require consideration prior to study commencement. Pigs are especially prone to intraoperative development of malignant hypotension and hyperthermia, both of which can have fatal consequences (Wedel et al., 1991, Linkenhoker et al., 2010, Claxton-Gill et al., 1993). Peri-anaesthetic mortality is also common in feline and canine species, some 100 times that of humans, and thus animals must be carefully monitored for depth of anaesthesia (Carter and Story, 2013). As a result of the fermentation process in ruminating species, surgical positioning must be carefully considered to avoid excessive pressure on the rumen as up to 25% of anaesthetised animals will regurgitate intraoperatively (Riebold, 2002). Irrespective of preoperative fasting to reduce ruminal tympany, in some cases, appropriate degassing should be performed to avoid excessive pressure on the diaphragm, which can limit ventilation (Carroll and Hartsfield, 1996). Ruminants salivate excessively, such that for procedures requiring extended duration anaesthesia, it is highly recommended that the alkaline saliva is collected and returned to the animal via an orogastric tube to prevent the development of acidosis (Riebold, 2002). For other species, such as the cat and dog, pre-treatment with an anti-cholinergic agent such as atropine can significantly reduce intraoperative salivation.

Cumulative evidence calls for rigorous planning of anaesthetic regimens prior to study commencement, taking into consideration potential effects on depth and duration of anaesthesia, adverse events, and potential confounding effects of anaesthesia on secondary injury processes.

3.3.4 Physiological Monitoring

Physiological monitoring is not consistently reported in the rodent stroke literature as their small size makes the installation of monitoring devices technically challenging, and complications are often encountered. Large animal models offer significant advantages with the ability to assess and control physiological variables more easily given their size, and insertion of catheters, probes and other devices is more achievable compared with their rodent counterparts. Additionally, clinical monitoring equipment can often be used in these species, such as external blood pressure cuffs, pressure probes and electrocardiogram leads, increasing access to devices and improving clinical applicability. Physiological parameters such as MABP (Chileuitt et al., 1996, Patel et al., 1991), blood gases (Smrcka et al., 1998) and pH (Siesjo et al., 1996) have a substantial impact on outcome, and thus tight control is essential in surgical procedures inducing stroke to ensure consistency in lesion volume and injury severity.

3.3.4.1 Arterial Blood Monitoring

As a general rule, efforts should be made to ensure oxygen saturation is maintained at greater that 90% throughout surgical procedures, irrespective of species. Intraoperative control of pH and pCO_2 is vital to ensure acidosis or alkalosis is avoided. Control of pH is especially important in ruminating species, such as sheep, which are predisposed to developing acidosis following preoperative fasting and intraoperative loss of saliva (Riebold, 2002). Acidosis

can be corrected with modification of the ventilation parameters, as previously described, or intravenous infusion of bicarbonate when buffer levels are low within the blood. If acidosis persists, it may become irreversible and lead to premature mortality or necessitate animal euthanasia, and thus timely correction of metabolic and respiratory components of pH is paramount.

CO_2 is a potent cerebral vasodilator, and a relative increase of 1 mmHg pCO_2 equates to a 1.8 mL/100 g increase in CBF (Thomas et al., 2017). In humans, normocapnia is between 36 and 42 mmHg; therefore, it is recommended large animals are also maintained within these limits (Kitano et al., 2007). Hypercapnia in excess of 50 mmHg pCO_2 disrupts cerebral autoregulation and CBF, which can have significant implications for both ICP and CPP, and thus needs to be tightly controlled in studies examining ICP post-injury (Robertson, 2002). It is recommended that for procedures requiring craniotomy and micro-clip application, moderate hypocapnia is maintained at approximately 28–32 mmHg pCO_2 (Young and Stone, 1994) to promote brain relaxation and permit gentle retraction of the brain during surgery. If pCO_2 drops below 25 mmHg, however, vasoconstriction may occur to the point of inducing moderate hypoxia, leading to infarct expansion, and thus pCO_2 must be strictly monitored and maintained (Way and Hill, 2011, Wollman and Orkin, 1968).

3.3.4.2 Blood Pressure

Intraoperative maintenance of blood pressure is essential to ensure adequate tissue perfusion. In small animals, MABP lower than 60 mmHg is associated with compromised tissue perfusion and increases the risk of global hypoxia and resultant ischaemia (Zhu and Auer, 1995, Smith, 2002). However, in large animals, tissue perfusion is compromised with MABP lower than 70 mmHg (Greene, 2002). In survival models, long-duration hypotension with

MABP <70 mmHg can lead to skeletal muscle ischaemia and resultant post-anaesthetic myopathy (Smith, 2002). For short procedures, a non-invasive external blood pressure cuff applied to one of the limbs can provide periodical blood pressure measurements. However, for procedures of long duration (for example, non-survival experiments), intra-arterial measurement of blood pressure may be preferred and more accurate given it provides a continuous readout of blood pressure. This can be achieved via catheter insertion directly into the femoral artery, which can also be used for arterial blood sampling for blood gas analysis (Wells et al., 2012). Smaller arteries in the limbs tend to be used for arterial blood gas sampling in survival procedures via insertion of a small-gauge catheter, which can be removed at the end of the procedure without impeding the animal's movement or recovery.

3.3.4.3 Intraoperative Fluids

The large blood volume of large animal species, often comparable to humans, allows for ease of venepuncture and repeated collection of samples in a single animal, which is not always possible in rodent models, where terminal bleeds and/or anaesthesia may be required to yield a sufficient sample volume. Adequate fluid therapy is essential to ensure animal wellbeing and can be achieved via multiple routes including intraosseous, intraperitoneal and subcutaneous, with intravenous access being the preferred route of administration in large species (Mama, 2002). The large diameter of vessels in these species' benefits insertion of intravenous catheters, which would otherwise be challenging in rodents because of small-calibre vessels. In feline and canine species, the cephalic, and medial and lateral saphenous, veins are common sites of catheter insertion, whereas in species such as porcine and ovine, the femoral vein or vena cava are commonly used (Mama, 2002). The ability to deliver large fluid volumes significantly benefits models of acute CNS injury, allowing for rapid fluid replacement. Crystalloid and colloid fluids can be given, depending on whether fluids are

being administered for maintenance, replacement or ongoing loss. A minimum rate of 3 mL/hr is required to maintain venous access, with greater volumes required to replace volume lost intraoperatively (Pascoe, 2012). This is especially relevant as long-duration surgical procedures are associated with increased loss of saliva and urine, in addition to elevated vasopressin secretion and concomitant hypovolemia and hypotension (Pascoe, 2012). In these circumstances, significantly greater fluid volumes are required to ensure MABP is maintained. Fluid therapy must be planned accordingly, taking into account anaesthetic regimen, surgical duration and preoperative state.

3.3.5 Antibiotics

Models of stroke where animals are recovered following surgery necessitate appropriate postoperative care. Given the often extensive and highly invasive nature of surgical approaches required in large animal models, administration of antibiotics is deemed essential. This is especially evident given the facilities for postoperative housing, which are rarely an aseptic environment, and most animals inevitably soil wounds with faeces and urine. As per veterinary standards, parasitic prophylaxis is also highly recommended for all large species prior to commencement of experimentation. Appendix 3.5 details recommended antibiotic agents and dosing regimens.

3.3.6 Analgesics

Sufficient postoperative analgesia is required to ensure pain and distress experienced by the animal is minimised. Many methods are used to assess animal pain and guide appropriate administration of analgesics. Routine tests interpret particular clinical signs as suggesting the presence of pain, including general behaviour, activity, appearance, temperament, vocalisations, feeding, and changes in physiological variables such as respiratory and heart

rates (Flecknell, 2016b). Treatment is often based on the presence of the aforementioned clinical signs, and commonly used analgesics are broadly divided into opioids and non-steroidal anti-inflammatory (NSAID) medications. For procedures requiring craniotomy by either transorbital or pterional means, because of the sensitivity of the meninges it is recommended that a combination of analgesics is administered upon induction, such as buprenorphine (opioid) and carprofen (NSAID).

It must be acknowledged that in the setting of stroke, some analgesic agents can influence ischaemic tissue damage and thus reliability of results. Fentanyl is reported to increase ischaemic lesion size in rodent models, while opioids such as butorphanol have been shown to enhance ischaemic preconditioning thresholds in canines (Schwartz et al., 1997). Therefore, appropriate analgesic regimens should be planned well in advance to ensure animal distress is minimised and ischaemic pathophysiologies are not compromised. Commonly used analgesics and suggested dose rates are detailed in Appendix 3.6.

3.3.7 Drug Metabolism and Route of Administration

It is important to acknowledge that variations in digestion, detoxification and metabolism between herbivores and carnivores can result in significant differences in half-life, toxicity and administration of any given medication. This is especially evident in large animal species, as unlike rodents which have high metabolic rates, inter-species and strain variations can significantly influence drug interval and dosing regimens. For example, in some species which are so-called ‘poor’ biliary excreters (humans), versus ‘high’ biliary (dog) and ‘intermediate’ biliary (sheep, cats) excreting species, drug elimination may vary significantly, thus affecting optimum dosing (Toutain et al., 2010). In veterinary medicine, it is also assumed carnivores have a lower clearance of medications versus herbivores, owing

in part to extensive oxidative enzyme systems in herbivores providing rapid drug clearance via hepatic metabolism (Toutain et al., 2010).

In addition to discrepancies in metabolism, the preferred route of drug administration may vary between large animal species because of anatomical and physiological variations. In ruminant species, for example, oral application is contraindicated because of ruminal digestion. In cats, topical application is undesired because of grooming/licking behaviours (Toutain et al., 2010). The majority of large animal models thus require intravenous, subcutaneous or intramuscular administration to achieve maximum efficacy. In pigs, intramuscular injection must be deep because of the thick nature of the skin and significant layers of fat overlying the musculature (Greene and Benson, 2002), an issue not encountered in other large animal species. It is highly recommended that prior to commencement of all large animal studies, species-specific treatment regimens be devised, taking into account dose, metabolism and administration interval, and in consultation with a veterinary professional where required.

3.4 EXPERIMENTAL MODELS OF STROKE

Stroke models can be divided into three major subtypes: global ischaemia, focal ischaemia and haemorrhagic stroke. Given ischaemic stroke is the most common stroke type and the focus of this thesis, only large animal models of ischaemic stroke will be discussed in this chapter.

Experimental models of focal ischaemia rely on the permanent or transient disruption of blood flow to the desired cerebral area to produce a defined and reproducible lesion. To

determine the efficacy of novel pharmacotherapies in experimental animals, ensuring lesion size is consistent is essential, which can be directly influenced by the method of vessel occlusion. Experimental approaches to vessel occlusion in animal species include endovascular, transcranial and transorbital approaches. In rodents, the most commonly used endovascular method to induce focal ischaemia is via intraluminal thread/suture, in which a suture is inserted into the carotid artery and fed through the vasculature to occlude the origin of the MCA (Howells et al., 2010). In large animals, comparable endovascular occlusion is typically induced via autologous clot, or coil or balloon insertion, because of the large vascular diameter (Shaibani et al., 2006, Hill et al., 1955, Rink, 2008, Del Zoppo et al., 1986) (Figure 3.4).

Endovascular methods of occlusion allow for reproducibility and can be used to model both transient and permanent stroke, offering control of recanalisation timing (Howells et al., 2010). However, because of the complex vascular anatomy of large species, endovascular access to the coW is complicated and all but impossible in animals with a rete mirabile, and therefore not feasible in many large animal species (Hoffmann et al., 2014, Sakoh, 2000). Thus, access to the coW and anastomoses remains the biggest hurdle in many large animal stroke models, and direct access to the cerebrovasculature is often required via transcranial and transorbital means (Wells et al., 2012, Watson et al., 1997, Zauner et al., 1995). This method allows for permanent occlusion via electrocautery or ligation, or transient occlusion by microvascular techniques including aneurysm clip application (Wells et al., 2012, Wells et al., 2015) or photothrombosis (Kuluz et al., 2007, Maeda et al., 2005) (Figure 3.3). In particular, photothrombotic models have become increasingly used, where a photosensitive dye such as Rose Bengal is administered, followed by illumination under light to cause focal thrombosis and vessel occlusion. This approach has now been described for rodent (Labat-

gest and Tomasi, 2013) and large animal models alike (Kuluz et al., 2007, Maeda et al., 2005). However, the necessary volume of dye required for large animal species must be considered a potential variable.

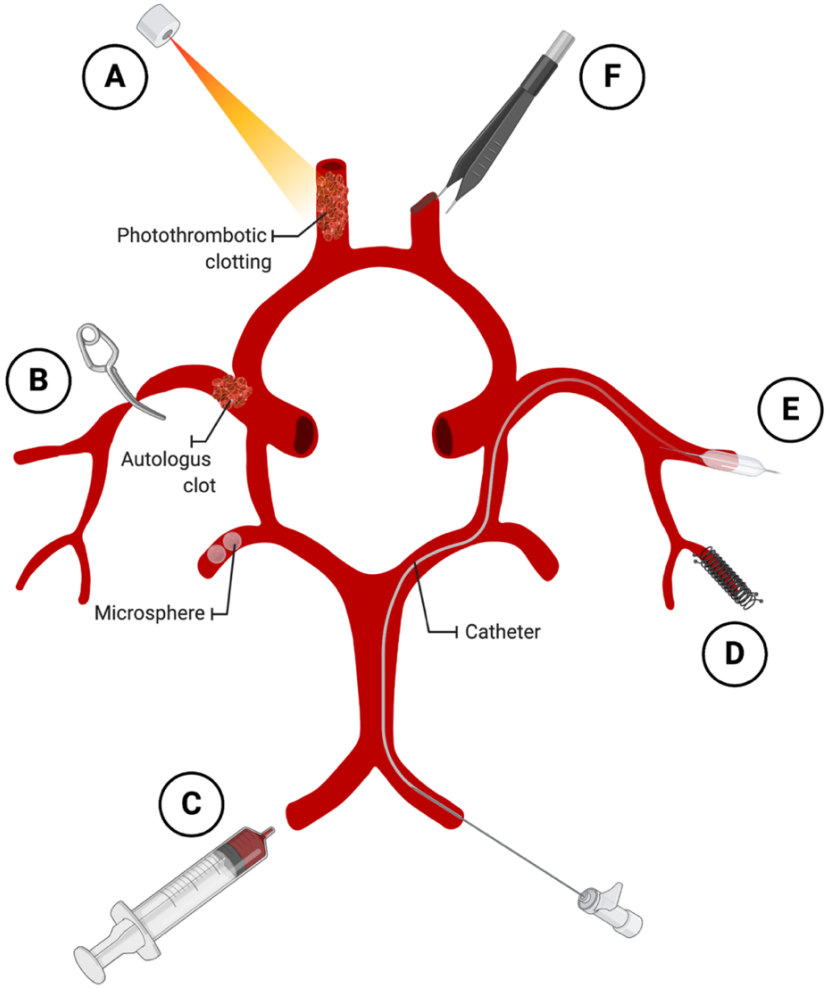

Figure 3.4. Schematic representation of different methods of vascular occlusion reported in large animal species. (A) Photothrombotic occlusion. (B) External aneurysm/micro-clip occlusion. (C) Autologous clot/microsphere occlusion. (D) Endovascular coil occlusion. (E) Endovascular balloon occlusion. (F) Direct ligation occlusion. A, B and F methods of occlusion require craniotomy to allow direct access to the vasculature. C, D and E can be achieved via endovascular approaches. *Figure created with BioRender.com (2021).*

The following sections will describe the various large animal species currently in use to model ischaemic stroke, approaches to vascular occlusion, outcome measures commonly assessed and species-specific considerations.

3.5 NON-HUMAN PRIMATE STROKE MODELS

NHP models offer distinct advantages when it comes to investigating cerebral ischaemia, providing a representation of key features of human behaviour, pathophysiology and neuroanatomy (Cook and Tymianski, 2012). A wide variety of NHP species have been used to model cerebral injury to date, including the squirrel monkey, owl monkey, marmoset, Senegal bush baby, baboon, rhesus and cynomolgus macaque, and African green and vervet monkey (Cook and Tymianski, 2012).

3.5.1 Lissencephalic versus Gyrencephalic Non-human Primate Species

The clinical applicability of several NHP species has been criticised because of their relative neuroanatomical structure, including the marmoset, squirrel monkey, owl monkey and Senegal bush baby, all of which are lissencephalic (Boulos et al., 2010). The relative size, lack of cortical sulci and gyri, and poor white to grey matter ratio in these species have been raised as potential limitations for their use (Cook and Tymianski, 2011). Indeed, a number of promising preclinical studies in the common marmoset have failed to produce desired outcomes clinically, with critics citing their lissencephalic brain, closer in resemblance to the rat than human, as a potential contributor (Philip et al., 2009, Diener et al., 2008). Despite noteworthy neuroanatomical variations, the relative reproducibility of stroke in lissencephalic NHP species is significantly more consistent than their gyrencephalic counterparts, allowing for precise functional mapping (Marshall and Ridley, 2003). It is suggested the lack of sulci and gyri favours visual representation of motor and sensory

cortices on the cerebral surface compared with gyrencephalic species, where representation may lie within the depth of a sulcus (Cook and Tymianski, 2011).

The use of gyrencephalic NHP species may better mimic the heterogeneity of human stroke and thus provide greater predictive value. Further, gyrencephalic NHP species exhibit additional anatomical features favouring them as models for cerebral ischaemia, including large brain mass, complex cortical organisation, dense white matter tracts, comparable vascular architecture and a relative grey to white matter ratio that more closely resembles the human brain (Cook and Tymianski, 2012). Irrespective of anatomical variations, the relatively unknown biological differences between lissencephalic and gyrencephalic NHP species add another dimension of uncertainty in choosing an appropriate species. Only one study to date has provided a direct comparison of biological differences between an NHP, namely the baboon, and the rat, although results of the study were inconclusive (Tagaya, 1997). Therefore, the relative biological benefit of using a particular NHP species remains elusive and requires further investigation, and an NHP *per se* may not always be the superior animal of choice when modelling stroke, with consideration of brain structure and specific research questions essential.

3.5.2 Approaches to Experimental Stroke Induction in Non-human Primates

Historically, the most common gyrencephalic NHP species used to investigate cerebral ischaemia is the baboon (Huang et al., 2000, Nehls et al., 1986, Tagaya et al., 1997). Transorbital access to the cerebral vasculature in this model requires enucleation (removal of the eye) with subsequent occlusion of the MCA and both ACAs required to produce a defined cortical lesion in the frontotemporal region, as the rich vascular collateralisation of the ACA may produce lesions of varying volumes, thereby complicating reproducibility (Del

Zoppo et al., 1986). Early studies in the baboon contributed to the discovery of the ischaemic penumbra and were pivotal for the preclinical evaluation of fibrinolytic therapies, including tPA (Astrup et al., 1981). Initially characterised as a model of permanent occlusion via either vascular suture ligation or aneurysm clip application, adaptations have been made for the development of a transient model (D'Ambrosio, 2004, Huang et al., 2000, Nehls, 1986). The transient model favours behavioural testing because of the high premature mortality rates and prolonged intensive care associated with the permanent occlusion model (Cui et al., 2013). However, the previously noted discrepancies in cerebrovascular anatomy of the baboon require occlusion of the MCA and bilateral A1 segments of the ACA, located between the ICA and ACoA, to produce a lesion in the MCA region. In relation to assessing functional outcome following stroke, the baboon is not an ideal candidate for neurobehavioural assessment because of its inherent aggressive nature and the surgical necessity for enucleation to induce cerebral ischaemia may inhibit the ability to perform detailed tasks requiring intact binocular vision (Mack et al., 2003).

Several studies have indicated the superiority of the cynomolgus and rhesus macaques as experimental NHP species (Hirouchi et al., 2007, Kito et al., 2001, Kuge et al., 2001) as there is less pronounced confounding vascular collateralisation in the cynomolgus macaque compared with the baboon (de Crespigny et al., 2005). Permanent MCAo (pMCAo) and transient MCAo (tMCAo) models have been described in the macaque via transorbital and pterional craniotomy approaches (Roitberg et al., 2003, West et al., 2009, Hirouchi et al., 2007), with both methods of cerebrovascular access producing defined lesions of high reproducibility, albeit with the need for extensive surgical skill to induce stroke and avoid iatrogenic injury. Further, the need for enucleation in this approach may confound assessments requiring binocular vision, and pterional craniotomy requires incision of the

temporalis muscle, adversely affecting mastication (Cook and Tymianski, 2011). Extensive surgical considerations and postoperative care associated with pterional/transorbital approaches to MCAo have prompted the development of a transfemoral endovascular model (Maeda et al., 2005). This model circumvents the need for complex surgery and reduces the risk of intraoperative trauma and intensive postoperative care. However, additional occlusion of the PCA is required to reduced collateral flow, and the endovascular route of access is associated with greater variability in lesion volume and higher mortality rate than open vessel methods (de Crespigny et al., 2005). Similarly, endovascular autologous clot models have been developed in the macaque to more closely approximate the thromboembolic stroke scenario (Wu et al., 2016). Although this method of occlusion has the advantage of more closely replicating the pathophysiology of human cerebral ischaemia, variability in lesion location and volume is a recurring complication (Wu et al., 2016). Despite contraindications, the macaque as a species is generally more docile than the baboon, offering the ability to perform more complex neurobehavioural tasks to assess cognitive, motor and sensory deficits (Cook and Tymianski, 2011).

Photothrombotic methods of vascular occlusion have also been described in NHP species, albeit infrequently (Maeda et al., 2005, Furuichi et al., 2007), with this method of occlusion benefiting studies investigating combined neuroprotection and thrombolysis treatment (Furuichi et al., 2007). However, the light source must be applied for a longer duration compared with smaller species to achieve complete vascular occlusion because of vessel diameter. Further, photothrombosis in NHPs is associated with variable lesion volume and location compared with other occlusion methods, and thus may be of limited clinical application (Maeda et al., 2005, Furuichi et al., 2007).

3.5.3 Outcome Measures in Non-human Primate Stroke Models

Irrespective of the specific species used to investigate cerebral ischaemia, the complexity of functional and behavioural assessment offered by NHP species is far superior to any other experimental model, large animal or otherwise (Mack et al., 2003). This is of particular relevance as human prognosis is largely determined by functional outcome, typically as a measure of disability or impairment in activities of daily living (Cook and Tymianski, 2011). Clinically, ischaemia in the region of the MCA affects sensory, motor and cognitive function (Gottesman and Hillis, 2010, Cook and Tymianski, 2011). Conversely, the vast majority of preclinical stroke research uses lesion volume as a predictor of poor outcome, yet the precise relationship between lesion volume and functional outcome has not been adequately assessed in humans because of inherent heterogeneity (Saver et al., 1999). Therefore, the ability to test behavioural outcomes in large animal species offers substantial benefit to improving clinical translation. There is no predefined disability index for NHPs, although a plethora of neurobehavioural approaches have been used to assess motor, sensory, balance, reflexive and cognitive behaviours (Mack et al., 2003, Roitberg et al., 2003, Marshall and Ridley, 2003). Specific NHP outcome scales have been developed to assess neurobehavioural deficits, which replicate clinical scoring systems (Roitberg et al., 2003, Mack et al., 2003). Activities such as the 'hill and valley staircase' task assess hemi-neglect as an indicator of hemiplegia, whereas the Kluver board can be used to test motor control (Marshall and Ridley, 2003). Further, the use of NHPs for evaluation of functions such as grip offers significant advantage over ungulate quadruped species, such as pigs and sheep, where such assessment is not possible. It must be acknowledged that despite the benefits of complex testing in primates, the inherent need to train animals to perform a particular behaviour, often for extended periods, creates another dimension of discordance in evaluating function and behaviour between human and NHP stroke.

3.5.4 Considerations in Non-human Primate Stroke Models

NHP species vary considerably in their relative cerebrovascular anatomy, physiology and behavioural characteristics (Cook and Tymianski, 2012). Therefore, the appropriate selection of NHP species must be made with due consideration of stroke syndrome (general/focal lesion), method of occlusion, route of vascular access and specific outcome measures of interest. All NHP models require access to sufficient housing facilities, specialised veterinary care, surgical expertise and established neurobehavioural apparatuses (Cook and Tymianski, 2011). Further, the ethical challenges inherent in all NHP research must be recognised. Primates develop more complex social relationships than many other large animal species, and the presence of neurological disease can significantly influence animal distress, anxiety and/or depression (Rossi, 2009, Wilkinson, 2009). Little is understood regarding how an injury of such severity can affect the social norms and general wellbeing for these species. Therefore, considerable effort must be made to eliminate distress and pain experienced by the animal, in addition to minimising alterations to environment and social structures. Clearly, the extensive limitations and constraints with the use of NHP species mean that alternate large animal species may be more appropriate and feasible for the modelling of acute CNS injury in many cases, and indeed may be more appropriate when considering neuroanatomical structure and neurobiology.

3.6 CANINE STROKE MODELS

The use of canines to model cerebral ischaemia offers advantage because of the relative size and gyrencephalic structure of brain, with high white to grey matter ratio, well-established white matter tracts and large cerebrovascular diameter (Traystman, 2003). The relative cerebrovascular architecture of the dog also offers distinct superiority when compared with

other large animal species, as canines lack a cerebrovascular rete mirabile, therefore favouring endovascular approaches of vessel occlusion (Gralla et al., 2006, Howells et al., 2010). Therefore, a plethora of studies have evaluated endovascular MCAo in canine models, with varying success reported (Shaibani et al., 2006, Christoforidis, 2011, Rink et al., 2008, Hill et al., 1955).

3.6.1 Approaches to Stroke Induction in Canine Models

The first embolic model of cerebral ischaemia was described in the dog in 1955 using autologous blood clots (Hill et al., 1955). Because of the anatomical structure of the coW, this model involves the injection of optimally sized emboli into the ICA to induce vascular occlusion of the MCA. Autologous clots are prepared using a mixture of the experimental animal's blood and bovine thrombin (Liu et al., 2012). This method of inducing cerebral ischaemia mimics the human condition most accurately and is amenable to studies investigating the efficacy of novel thrombolytic therapies or thrombectomy devices. However, despite clinical applicability, the canine ICA is extremely tortuous, forming a petrous loop prior to articulation with the coW, with high variability in convolution between animals (Zu et al., 2013). Therefore, the relative size and location of the lesion vary because of the distal injection of emboli and variations in vascular architecture. Further, MCAo via ICA autologous clot injection produces significantly smaller lesions than those seen clinically, given the aforementioned extensive leptomeningeal collateral circulation in canines (Zu et al., 2013, Atchaneeyasakul et al., 2016, Symon, 1960). More recently, adaptations have been made to the model to address this, including alterations to the route of embolus administration, where cells are injected via the BA or VA rather than ICA (Qureshi et al., 2004). VA occlusion may, however, be contraindicated because of forceful collateral blood flow, preventing embolus anchorage (Atchaneeyasakul et al., 2016). The

BA is relatively straight and easy to navigate compared with the ICA, and occlusion produces a significant and defined hemispheric lesion. The benefit of this route may, however, be outweighed by significant mortality and neurological deficit associated with BA occlusion, requiring prolonged intensive care (Atchaneeyasakul et al., 2016, Qureshi et al., 2004). The most significant disadvantage associated with the embolic technique of cerebral ischaemia is the relative variation in vascular diameter and organisation between different dog breeds (Atchaneeyasakul et al., 2016). This is of particular relevance as mixed breeds are among the most commonly used canine species, and variation between individual experimental animals may significantly limit reproducibility and experimental outcomes.

An alternative method of MCAo in the canine model is the coil occlusion method (Christoforidis et al., 2011, Rink et al., 2008). This method involves the use of a soft platinum coil, clinically used to treat intracranial aneurysms (Rink et al., 2008). The coil is inserted through a micro-catheter and advanced through the vasculature to the target vessel, allowing for precise positioning and coil detachment, inducing a permanent occlusion, or transient occlusion with vessel recanalisation following coil removal. Coil access to the MCA is typically achieved via the VA or PCA, as access via the ICA is complicated because of its convoluted structure (Rink et al., 2008, Christoforidis et al., 2011). Comprehensive imaging techniques are required for coil guidance and to ensure sufficient vascular occlusion (Flecknell, 1996). Several studies have reported endovascular coil MCA access via the femoral artery using C-arm fluoroscopy guidance (Flecknell, 1996), which allows for catheterisation of the vasculature comparable to that in humans undergoing angiographic guided procedures.

The advanced neuroimaging techniques used in the endovascular coil model offer a number of benefits to translation. Angiographic guidance in the dog offers significant superiority when compared with commonly used rodent models of endovascular MCAo, where the relatively small size of the cranial arteries limits procedural evaluation and confirmation of occlusion. The use of image guidance in these studies enables specificity in coil placement and thus yields a highly specified and reproducible lesion, offering advantages when compared with embolic methods. Further, the large size of the canine brain is compatible with non-specialised, clinical imaging equipment, representing an appropriate model for validation of clinical stroke imaging. Nevertheless, the benefits of neurointerventional approaches are not without challenges. The use of advanced imaging techniques requires sophisticated skills and complex understanding of the canine cerebrovascular system. PCA micro-catheter access may be influenced by breed of dog and thus not achievable in all species. Further, MCA cannulation may not always be possible because of variations in relative vascular architecture in individual subjects. Despite the clinical relevance of vasospasm in the canine model, this can be an issue when advancing the coil and can lead to vascular perforation, especially in the BA, which is predisposed to spasm (Rink et al., 2008, Christoforidis et al., 2011). Extreme care must be taken in this instance to halt advancement, and wait for spasm to resolve, following which coil movement must be limited to purposeful advancement as quickly as possible. Despite challenges, the endovascular access to MCAo achievable in canine models completely circumvents the need for transorbital access and enucleation or craniotomy, and disruption of the temporalis muscle. Therefore, endovascular techniques significantly eliminate the occurrence of head trauma and iatrogenic injury commonly associated with direct vascular approaches.

3.6.2 Outcome Measures in Canine Stroke Models

The majority of canine studies to date have focused on the use of MRI and other imaging techniques to determine lesion volume as an indication of stroke severity (Zu et al., 2013, Shaibani et al., 2006). Neurobehavioural assessment has been performed by several groups to determine deficits in neurological function following cerebral ischaemia (Christoforidis et al., 2011, Boulos et al., 2010). A canine stroke score has been developed to enable clinical assessment, which specifically measures canine vocalisation, consciousness, gait, behaviour, and sensory and motor function, and has been successfully correlated with infarct volume (Boulos et al., 2010).

3.6.3 Considerations in Canine Stroke Models

Although canine models offer distinct advantages, particularly in relation to the route of vascular occlusion, such species are associated with high purchase costs, and access to an appropriate institution where advanced imaging techniques are available may not be viable (Hasiwa et al., 2011). Further, the use of canines for neuroscientific research is mired with ethical complications, especially in Western cultures, where dogs are domestic companion animals. Therefore, the use of canine species is often limited, and alternative large species may need to be considered.

3.7 FELINE STROKE MODELS

Although less commonly used than canines, several feline models of cerebral ischaemia have been described (Watson et al., 1997, Moonen et al., 1991, Combs et al., 1990, Zauner et al., 1995, Di et al., 1997). Of all the large animals commonly used for investigation of cerebral ischaemia, cats are comparatively the smallest species. Despite this, the feline brain has a

gyrencephalic structure with high white to grey matter ratio and large vessel diameter (Smith et al., 2001), favouring their use over rodents, mice and other small animals in line with the desired experimental outcomes.

Early models of focal ischaemia in the cat were produced by occluding the MCA via a transorbital approach (Watson et al., 1997, Moonen et al., 1991, Zauner et al., 1995, Combs et al., 1990, Di et al., 1997). This method involves supraorbital and periorbital incision and subsequent enucleation, enabling periorbital craniotomy and direct access to the MCA. Permanent MCAo is subsequently achieved through electrocautery or microvascular clip application. Direct vascular access achievable in this model produces a defined and reproducible lesion. However, the need for enucleation diminishes the ability to perform postoperative functional assessment, similar to that described for NHPs. In early studies, the relative accessibility to mixed breed cats, in addition to their gyrencephalic brain, favoured them as models to investigate cerebral ischaemia compared with rodents. These early studies were instrumental to understanding the effects of insulin on the brain following ischaemia and subsequent BBB disruption (Combs et al., 1990). However, similar to other large animal species, cats have a rich vascular collateralisation and there is high variability in cerebrovascular structure between individual animals. As with dogs, this is extremely prevalent between experimental animals because of frequent experimental mixed breed use.

For the past decade, feline models of stroke have not been used, and there has been an increased tendency to use larger animals with a greater brain mass and/or genetic similarity closer to that of the human for enhanced translation. Although body weight and phylogeny do not predict translational success, larger brains allow for easier surgical manipulation, which in turn enhances experimental outcome. The decline in feline models may also be a

result of the relative ethical considerations associated with the use of cats, which, similar to canines, are domestic companion animals.

3.8 PORCINE STROKE MODELS

Porcine models offer distinct advantages because of the presence of cerebral sulci and gyri, large intracranial vessel diameter, and relative white to grey matter proportion (Gralla et al., 2006, Kobayashi et al., 2012). The aforementioned presence of the rete mirabile in pigs, however, renders endovascular methods of occlusion unfeasible, and thus direct vascular access is often required (Ashwini et al., 2008, Sakoh et al., 2000, Watanabe et al., 2007, (STAIR), 1999).

3.8.1 Approaches to Stroke Induction in Porcine Models

A transorbital vascular approach to MCAo has been described in pigs as a method of inducing cortical infarction (Sakoh et al., 2000, Watanabe et al., 2007), allowing for the investigation of discrepancies in CBV and flow. Occlusion of the MCA can be achieved by either permanent electrocautery or transient micro-clip application (Sakoh et al., 2000, Watanabe et al., 2007, (STAIR), 1999). However, this model is associated with variable lesion volume and limited reproducibility (Sakoh et al., 2000), with the transorbital approach to MCAo described restricting the surgical field of view and thus vessel visualisation. Therefore, porcine models require frontotemporal and pterional craniotomy approaches to optimise vascular access because of their relatively large size and skull anatomy (Platt et al., 2014). Transcranial approaches offer a distinct advantage compared with transorbital methods, including avoiding the need for enucleation or intraorbital decompression, thus preventing loss of vision and the development of postoperative complications such as

infection of the dead space following eyeball removal (Imai et al., 2006). Further, frontotemporal approaches to MCAo benefit vascular approach and orientation by increasing the visual field available, improving surgical access and visibility.

Several studies have described MCAo in the miniature pig using a frontotemporal craniotomy approach with a single-entry burr hole drilled in the skull and Kerrison forceps used to widen the field to achieve vascular visualisation (Imai et al., 2006). In this model, direct electrocautery of the MCA is performed proximal to the origin of the lenticulostriate artery and opposing ends of the vessel occluded to ensure complete cessation of blood flow. Miniature pig species also have significantly thinner skulls than commonly used large domesticated porcine species, potentiating a reduction in surgical duration (Cui et al., 2013). It must be recognised, however, that the removal of bone and subsequent dural incision required for this approach may have implications for outcome measures, such as ICP, because of disruption of intracranial dynamics (Imai et al., 2006). Further, permanent vascular cauterisation of the MCA may lead to disruption of the BBB. Although transient occlusion may be possible in this model, it has not been adequately addressed and requires further investigation. To overcome the need for craniotomy and associated damage to the dura, a model has been established in which small-diameter sodium alginate microspheres are injected extracranially to induce occlusion of the skull base rete mirabile (Cui et al., 2013). This method produces a defined cortical lesion and complete unilateral occlusion of the rete mirabile, as evident on MRI. Further research on the use of extravascular microspheres is needed to determine the reproducibility and clinical applicability of the model.

The vascular diameter of pigs favours them for models testing novel thrombectomy devices that are otherwise not feasible in small animals (Gralla et al., 2006, Gross, 1997). Several porcine models of vascular occlusion have been used to investigate the efficacy of new generation thrombectomy devices, with variable success (Chueh et al., 2013, Nogueira et al., 2012). The testing of devices in these models involves the injection of autologous emboli into extracranial vessels, such as the ascending pharyngeal artery (APA). Advanced neuroimaging techniques are required for the successful generation of these models in order to assess vascular dimensions prior to clot synthesis and administration. It must be reiterated that the small diameter of vessels comprising the rete in pigs is not conducive to embolic models of MCAo, and thus stroke is only achievable via occlusion of large-diameter extracranial vessels (Ringer et al., 2004). Further, the porcine model is contraindicated for use in studies evaluating combined tPA treatment, as pigs exhibit a high resistance to recombinant tPA (Yakovlev et al., 1995).

Pigs also represent the only large animal species, aside from NHPs, that have been used to successfully model photothrombotic stroke (Kuluz et al., 2007). Initially described in piglets, this method was developed as an approach to paediatric focal cerebral ischaemia. Because of skull thickness, photothrombosis in porcine species requires craniotomy by transorbital or transcranial means to enable vascular access and application of the light source. This method of occlusion produces a defined lesion with consistent infarction in both grey and white matter, platelet activation, and occlusive thrombus formation (Kuluz et al., 2007). Photothrombotic occlusion eliminates cerebrovascular trauma that may be associated with microvessel clip application and removal required for vascular recanalisation. Although this method offers high reproducibility, there is some question regarding the artificial means by which occlusion is induced, with atypical lesion features observed that are not seen clinically

(Durukan and Tatlisumak, 2007). These findings, however, appear consistent between species using photothrombotic models.

3.8.2 Outcome Measures in Porcine Stroke Models

The majority of porcine studies use lesion volume as a measure of outcome following stroke, with neuroimaging commonly used as a means of quantification (Kuluz et al., 2007). MRI and positron emission tomography (PET) scanning of the pig brain produces images of high resolution, which may benefit morphometric analysis, an advantage because of high clinical translatability. Several automatic labelling and processing routines for MRI have been developed specifically for pigs, which offer efficient and unbiased analysis of infarct volume (Conrad et al., 2014, Saikali et al., 2010). In relation to porcine neurobehavioural assessment, pigs have significant cognitive abilities and are capable of learning behavioural tasks in relatively short periods of time (Gieling et al., 2011). Neurological assessment in ischaemic porcine models has been performed using established canine neurological function scales, with minor amendments allowing the evaluation of limb and facial paralysis, consciousness, and visual field defects (Cui et al., 2013). A plethora of studies have determined differences in gait and locomotor patterns in pigs on various floor surfaces (Thorup et al., 2007, Applegate et al., 1988, Wachenfelt et al., 2008); however, few have investigated changes in gait characteristics following stroke (Duberstein et al., 2014). The full spectrum of porcine neurological deficits following cerebral infarction and discrepancies in normal/abnormal behaviour have, however, not yet been adequately assessed, and further investigation is required (Nielsen et al., 2009, Schook et al., 2005).

3.8.3 Considerations in Porcine Stroke Models

One disadvantage to using porcine species to model cerebral ischaemia is their relative use for the purpose of longitudinal survival studies. Pigs are predisposed to rapid weight gain, and thus food intake must be strictly monitored to prevent excessive weight increase, which may alter experimental outcomes (Lawrence et al., 2012). Despite this, the use of porcine stroke models offers several translational advantages, in addition to the inherent neuroanatomical similarities to the human. The relative ethical challenges and high purchase costs associated with the use of canines and NHPs are significantly less pronounced in pigs (Kobayashi et al., 2012). Further, the use of porcine models may also prove advantageous for neurobehavioural and cognitive assessment because of their relatively superior cognition and ability to learn tasks rapidly.

3.9 OVINE STROKE MODELS

The large gyrencephalic brain of the sheep, comparable with that of the human, has facilitated the development of several ovine models of cerebral ischaemia. As with porcine models, the complex cerebrovascular architecture of the rete mirabile in ruminant species renders endovascular methods of MCAo unfeasible, and transcranial approaches are required. Nevertheless, a comparison between the cerebrovasculature of sheep, humans and rodents was recently conducted to determine implications for translation to cerebrovascular diseases (Hoffmann et al., 2014). In rodents, vast interarterial anastomoses are present, which may prevent cortical infarction upon distal occlusion of the MCA. Cortical anastomoses are less frequent in humans and ovine species, providing partial explanation as to why occlusion of the MCA has devastating clinical repercussions (Hoffmann et al., 2014), thus highlighting the translational value of sheep as an experimental species.

3.9.1 Approaches to Stroke Induction in Ovine Models

The first model of ovine MCAo was developed to address ongoing translational failures and limitations in other large animal models (Boltze et al., 2008). This seminal work described a model of permanent MCAo via direct electrocautery, with access achieved via pterional craniotomy, necessitating incision of the temporalis muscle at its insertion point (Boltze et al., 2008). This model offers significant advantages compared with transorbital approaches and avoids the need for enucleation, permitting postoperative assessment of binocular vision. Further, this approach is associated with significantly enhanced survival, allowing longer observation periods compared with many other large animal species, where proximal MCAo is associated with premature mortality. However, it must be noted that enhanced survival in this model is likely attributable to the fact that the craniotomy site is left open, effectively providing surgical decompression at the time of stroke induction, and thus preventing elevations in ICP, which is obviously a contraindication for measurement of intracranial dynamics in this model. Further, incision of the temporalis is contentious, given the effect on limited mastication.

More recently, a new model has been developed by our group, which permits the study of transient occlusion while maintaining intracranial dynamics (Wells et al., 2012). This model requires removal of the coronoid process of the mandible to allow skull base exposure and pterional craniotomy (Wells et al., 2012). MCAo is achieved via direct electrocautery or aneurysm clip application, which enables reperfusion. After MCAo, the dura is closed, and the bone removed from the area of the craniotomy is reinserted and sealed watertight with dental cement to restore intracranial dynamics. This method of access benefits studies investigating physiological outcome measures such as ICP, which were not achievable in the original model. As previously mentioned, the strong fibrous tentorium cerebelli of the

sheep mimics the human meningeal features, benefiting the use of ruminant species for investigating the development of ICP following stroke. However, the relative mortality (approximately 30%) in this model is high owing to the development of excessive pressures, often in excess of 40 mmHg, leading to tonsillar herniation (Wells et al., 2012) and thus mimicking the burden of mortality associated with clinical stroke. Further, the complete removal of the coronoid process prevents postoperative survival, and animals must be maintained under anaesthesia for the entire duration of the experiment. This increases the cost and technical expertise required because of the need to keep animals physiologically stable and under a surgical level of general anaesthesia throughout the study (Wells et al., 2012, Wells et al., 2015). Clearly, a modified surgical approach that permits animal survival and recovery post-stroke induction would be desirable to study the long-term effects of transient occlusion in the ovine model.

Although ovine models have been used successfully to measure cerebral oedema and ICP, there is some question regarding the craniotomy approach in relation to disruption of intracranial dynamics when compared with non-invasive methods. The relative CSF production and resorption rate following dural opening is at present unknown, which has implications for experimental outcome. Irrespective of this, ovine permanent MCAo studies have shown significant elevations in ICP (>40 mmHg) within 24 hours following craniotomy (Wells et al., 2015), suggesting that despite the loss of CSF upon dural excision, the methods used to achieve dural and skull closure following vascular access prevent ongoing leakage of CSF (thereby allowing CSF to reaccumulate), leading to the pathological development of elevated ICP.

The transcranial access described in the ovine model favours investigation of behaviour compared with transorbital approaches, as binocular vision is left intact. This is particularly beneficial in survival models where ICP is a primary outcome, as excessive increases in pressure can compress the optic nerve, leading to pupillary dilation and anisocoria, commonly used to assess neurological deterioration clinically (Chen et al., 2011). Further, the length of the ICA may benefit transcranial approaches to MCAo, as the proximal MCA is more easily accessible than in other large animal species, allowing for better visualisation and vessel access, thereby favouring reproducibility (Kapoor et al., 2003).

3.9.2 Outcome Measures in Ovine Stroke Models

Primary assessment of outcome following stroke in the ovine model is similar to that of the pig, and imaging techniques remain the preferred method of determining infarct volume as an indicator of outcome. Behavioural phenotyping of sheep has been performed, allowing for the development of a neurobehavioural score system, which has subsequently been correlated with lesion volume (Boltze et al., 2008). This neurologic score point system assesses functional deficits that are characteristically seen in large animals following MCAo, such as ataxia, state of consciousness, torticollis, fetlock flexion/weakness, hemi-standing and hopping reactions. Such assessment is typically carried out by a trained veterinarian to subjectively assess the animal's response. It must be acknowledged, however, that assessment of sensory function in ovine models is contraindicated, as sheep rapidly habituate to nociceptive stimulation. Further, to date, a comprehensive method to objectively quantify kinematics in the sheep does not exist; thus, a method that enables rigorous assessment of motor function following stroke is required.

3.9.3 Considerations in Ovine Stroke Models

The use of ruminants offers distinct advantages over other large animal models, as sheep display similar haematological properties to those seen in humans and NHPs (Boltze et al., 2011). However, very little is known at present regarding the metabolic and molecular pathways following cerebral infarction, which is a major downfall when compared with other large animal models, where this is well characterised. Nevertheless, as with pigs, the relative ethical challenges associated with the use of canines and NHPs are significantly less prevalent in sheep, as is purchase cost and availability.

3.10 ADVANTAGES AND LIMITATIONS OF LARGE ANIMAL MODELS

As highlighted throughout this chapter, large animal models provide significant benefits in improving clinical translation, including the utilisation of sophisticated imaging technologies, similarities in neuroanatomical structure, and wide spectrum of clinically relevant data recording and analysis options. Key advantages and limitations of large animal models are summarised in Table 3.1.

However, while this chapter has highlighted the many advantages of large animal species and their ability to better mimic human ischaemic stroke, there are also a number of disadvantages that affect the ability to pursue large animal studies. Foremost is the significant expense of not only the large animals themselves, but also the technical support and infrastructure required to appropriately house and care for the animals, as well as performing the experiments themselves.

Table 3.1 Summary of advantages and limitations of large animal models of stroke

Advantages	Disadvantages
Brain more closely resembles the human	Difficult to handle
Higher proportion white matter	Higher purchase and maintenance cost of animals
Gyrencephalic structure	Higher costs of facilities required to perform procedures and house animals
Strong tentorium cerebelli	
Relative cortical organisation	Longer gestation time and life span
Ability to use clinically relevant outcome measures, such as MRI, PET/CT	Transgenic selection and production of transgenic strains limited
Ability to use clinically relevant equipment for anaesthesia, physiological monitoring, surgical procedures	Poor availability of physiological databases
	Ethical considerations higher
	Behavioural assessment more cumbersome
Ability to undertake chronic/co-morbidity studies	Increased anatomical variability
Increased clinical translation	Limited access to species appropriate antibodies

Procedures often require access to specialised facilities with operating theatres, housing and imaging equipment capable of accommodating large animals, often comparable to clinical spaces. In addition, specialised surgical instruments, along with clinical anaesthetic and monitoring equipment, are required. Extensive surgical skill and technical expertise is necessary for the vast majority of large animal injury models to produce lesions of consistent size, while also obviating iatrogenic brain injury. Large animal model studies may be further hampered as access to specific species may be difficult in some countries. For example, the use of ovine species in Australia and New Zealand is common because of high availability; however, the use of some porcine species is limited by stringent quarantine laws. Therefore, appropriate experimental species must be selected carefully, taking into consideration not only the injury type and surgical procedure required, but also species availability and access to an appropriate surgical facility.

Further, longer life spans of large species mean that chronic studies take considerably longer than smaller animals (Agoston, 2017). However, this may also offer the opportunity to study

stroke in concert with co-morbidities. Biochemical and molecular data are less readily available for larger animal species, as are functional outcome tests to characterise effects of therapeutic intervention on neurological outcome. Further, acquiring antibodies for routine immunohistochemistry or western blotting is more challenging than for rodent counterparts. Indeed, the vast majority of biological assays are optimised in rats and mice, which has implications for the validity and reliability of data when protocols are adjusted for application in larger animals. Nevertheless, such assays are possible using large animal tissues although may require extensive optimisation and different retrieval/extraction protocols compared with rodent tissue. Finally, the rete mirabile, present in some species, may influence CBF after acute brain injury, although this has not yet been characterised.

While rodents will always have a valuable place in studies of acute brain injury, especially in initial characterisation and screening of potential therapeutic interventions, the use of large animal models is becoming increasingly important to improve the chances of successful translation. Indeed, one could argue that the emphasis on rodent models of acute brain injury over recent decades has hampered our ability to identify the critical injury factors associated with stroke and its complications, and our ability to develop a therapeutic intervention that will prove efficacious in a clinical setting.

3.11 CONCLUSIONS

Large animal models are a key step in the stroke translational framework. Following initial discovery studies in rodents to identify novel therapeutic agents or pathophysiological mechanism/pathways of outstanding promise, these should then be assessed in an appropriate large animal model to enhance the likelihood of successful clinical translation.

04

Study Synopsis, Aims and Hypotheses

4.0 INTRODUCTION

Following ischaemic stroke, aberrant release of neuropeptide SP initiates the development of neurogenic inflammation (Turner et al., 2006, Turner et al., 2011, Turner and Vink, 2012, Turner and Vink, 2014, Yu et al., 1997). This is associated with increased BBB permeability, development of cerebral oedema and persistent neurological deficits. It has been extensively demonstrated in rodent stroke studies that blocking the action of SP with an NK1-R antagonist reduces BBB permeability and cerebral oedema and improves functional deficits (Turner and Vink, 2014, Turner and Vink, 2013, Turner and Vink, 2012). Therefore, NK1-R antagonist treatment may represent a novel approach to treating cerebral oedema and elevated ICP post-stroke. However, given the poor translation from rodent studies to the clinic, evaluation of the NK1-R antagonist in an intermediate, large animal stroke model is required prior to clinical trial in order to improve the likelihood of clinical efficacy.

4.1 STAIR GUIDELINES: SUITABILITY OF A LARGE ANIMAL MODEL

To address the limitations of past studies and advocate for more rigorous preclinical screening, the Stroke Therapy Academic Industry Roundtable (STAIR) guidelines were formulated to improve the quality of preclinical stroke studies, with the goal of increasing successful clinical translation. However, a systematic review conducted in 2003 found that out of over 1000 novel therapies for stroke, only one was successful in translation (tPA, O'Collins et al., 2006). Further, only five of 550 trials evaluated met the interpretation of the STAIR guidelines. This highlights the need for adherence to STAIR recommendations to improve direct linkage between animal models and the clinical situation. The studies in this thesis were therefore designed to address the STAIR guidelines and increase the likelihood of successful translation of the NK1-R antagonist through use of a clinically relevant large

animal model. Specifically, because of the primary outcome measures of interest (ICP and cerebral oedema) and availability of large animal species in Australia, an ovine model was chosen. A brief discussion of STAIR criterion the proposed ovine model aims to address, with particular reference to the relevant thesis chapters, is provided below.

4.1.1 Replication in a Second Species

It is strongly recommended that the efficacy of putative therapies be established in two species prior to clinical assessment. More specifically, once initial efficacy has been demonstrated in rodent models, promising therapeutic agents should ideally be screened in larger animal species whose brains bear closer similarity to that of humans. The efficacy of NK1-R antagonist treatment in rodent stroke models has been clearly establish, therefore this thesis seeks to address whether such treatment is also efficacious in an ovine stroke model (Chapters 6 and 8).

Following from seminal work conducted by Boltze et al. (2008), in 2012 our group first proposed the use of sheep to investigate the evolution of ischaemic injury, in particular elevated ICP, following permanent stroke (Wells et al., 2012). Neuroanatomically, the large gyrencephalic structure, with high ratio of white to grey matter, cortical organisation and strong tentorium cerebelli, make sheep an ideal species to model stroke and investigate the development of cerebral oedema and ICP. This is of particular relevance given that vasogenic oedema develops predominantly in the white matter of the brain, which has direct implications when determining the efficacy of the NK1-R antagonist in targeting oedema genesis. Our group has previously demonstrated that sheep exhibit extensive cerebral oedema and elevations in ICP following permanent MCAo (Wells et al., 2015), further highlighting their value as a translational species to model ischaemic stroke.

4.1.2 Dose of Drug and Pharmacokinetics

Unfortunately, preclinical pharmacokinetic studies are often not pursued because of extensive cost. This limits the ability to successfully translate pre-clinical dosing regimens to clinical studies, as although a drug may prove effective in rodent stroke models, it may not be feasible, or safe, to simply extrapolate dosing to humans (Bracken, 2009, Perel et al., 2007). Efficacious treatment outcomes obtained in large animal species may, however, be more predictive of clinical efficacy given their more comparable size. Irrespective of this, pharmacokinetics and pharmacodynamics vary considerably between species due to differences in metabolism. Generation of dose–response curves is thus critical in both small and large animal studies for effective clinical translation. Pharmacokinetic data for the NK1-R antagonist obtained following administration in the sheep is therefore presented in Chapter 8 of the thesis.

4.1.3 Testing in Permanent and Transient Stroke Models

When modelling stroke, the STAIR guidelines strongly recommend duration of ischaemia be taken into consideration. In the past, the vast majority of studies have adopted permanent stroke models; however, the development of cerebral oedema is more prominent following transient stroke. Further, the majority of clinical ischaemic stroke cases involve an element of reperfusion whereby recanalisation may occur, either spontaneously or purposefully through intervention. In addition, as cerebral oedema peaks between 3- and 5-days post-ictus (Battey et al., 2014, Hacke et al., 1996), this necessitates study of the evolution of injury beyond the acute phase. This is often not possible in permanent stroke models because of the severity of injury, with high mortality rates and ethical limitations precluding permanent survival models. Prior to this doctorate, a survival model of transient stroke in the sheep was lacking, limiting the evaluation of injury evolution. This highlights the need for well-

characterised ovine permanent, and transient, stroke models to further enhance their translational value as an experimental species and enable the reliable screening of novel therapies targeting oedema genesis. Therefore, this thesis developed an ovine model of transient stroke with reperfusion, with studies outlined in this thesis encompassing both permanent (Chapter 6) and transient (Chapters 7–9) stroke.

4.1.4 Consideration of Sex and Age Differences

The established model of ovine stroke characterised by Wells et al. in 2012 involved permanent occlusion of the MCA (Wells et al., 2012). Because of the severity of the resultant infarct and ethical requirements, animals were kept under general anaesthesia for the duration of the experiment (±24 hours), prior to euthanasia (Chapter 6). This, unfortunately, has inherent limitations, including the use of only female animals because of the inability to catheterise the convoluted urethra of male sheep. STAIR guidelines, however, dictate gender as an important consideration given sex differences in stroke mechanisms and therapeutic response. To address this, studies in this thesis (Chapters 7–9) have sought to characterise response to injury and treatment in both male and female sheep.

Further, given the population in which stroke is most prevalent is adults over the age of 65, the age of animals used in preclinical studies is of relevance. The average life span of sheep is 10–12 years, with domesticated sheep primarily raised for wool, meat and occasionally dairy production. However, because of reduced fertility, tooth wear and disease susceptibility, the mean age of animal culling is 5 years (Munoz et al., 2019, Hoffman and Valencak, 2020). Further, the average age of animals used for research purposes is approximately 3 years, where animals are generally only aged at the researchers' request and are often culled earlier because of the aforementioned wellbeing considerations.

Accordingly, sheep aged 18–36 months were used in this study. Animals in this age bracket are reaching skeletal maturity, and can be considered comparable to young adults (Cake et al., 2006). However, given limited research into the equivalence of human to ovine age, this is largely anecdotal, and further research is required to draw meaningful comparisons, especially in regard to neurological maturity equivalencies (Hoffman and Valencak, 2020).

4.1.5 Consideration of a Clinically Useful Therapeutic Window

The STAIR guidelines indicate the necessity of a clinically useful therapeutic window, that is, the duration after stroke in which a treatment is efficacious. The therapeutic window for thrombolysis (Ma et al., 2019) and mechanical thrombectomy (Albers et al., 2018, Nogueira et al., 2018, Berkhemer et al., 2015, Smith and Yan, 2015, Goyal et al., 2016, Goyal et al., 2015) has increased significantly in recent years. However, following vessel recanalisation, it is essential that treatments targeting secondary complications are effective when administered beyond the acute phase post-stroke. The ability to study longer time-points following stroke is essential not only to elucidate the temporal profile of key injury factors such as cerebral oedema and elevated ICP, but also to meaningfully determine the therapeutic window of any novel treatment. We have specifically addressed this criterion by assessing administration of the NK1-R antagonist both early and late after stroke (Chapter 8) in the ovine transient stroke model.

4.1.6 Physiological Monitoring and Neuroimaging

It is strongly recommended that physiological variables be recorded to limit variability in infarct volume. The large size of the sheep allows for application of clinical equipment for the accurate assessment of physiological parameters including blood pressure, blood gases, blood electrolytes and CBF. Further, invasive neuromonitoring can be carried out, including

the application of clinical devices to measure brain tissue oxygenation ($PbtO_2$) and ICP, in addition to high resolution CT and MRI. This enables more accurate quantification of infarct volume, comparable to clinical assessment. Accordingly, studies within this thesis include physiological monitoring, encompassing blood pressure and arterial blood gas/electrolyte analysis (Chapters 6–9), invasive neuromonitoring and neuroimaging (Chapters 6–8).

4.1.7 Functional Outcome

Finally, in determining the efficacy of therapies clinically, it is vital to determine how treatment influences long-term function. Indeed, functional outcome is often the major endpoint in clinical trials. As per the STAIR guidelines, the ultimate goal of preclinical assessment is to show that, in concert with tissue endpoints, functional neurological outcomes are also improved in treated populations. Specifically, it is recommended that the effect of treatment on functional outcome is assessed for a minimum of 28 days following stroke onset. Functional assessment typically aims to assess behavioural outcomes, including both motor and sensory domains. Obtaining measures of functional motor outcome is particularly paramount given the standard for functional assessment via clinical scoring, where clinical evaluation via the modified Rankin Scale (mRS) and National Institutes of Health Stroke Scale (NIHSS) remain the most routinely used methods for assessing stroke severity worldwide (Chalos et al., 2020). The amenable nature of sheep enables ease of handling, neurological assessment and advanced quantitative biomechanical assessment. However, comprehensive assessment of ovine functional kinematics following stroke has previously been lacking. To address the lack of functional assessment, a novel approach to evaluate motor function in sheep post-stroke was developed and is described in Chapter 9.

4.2 HYPOTHESES AND AIMS

The overarching goal of this thesis was to examine the effect of NK1-R antagonist treatment on cerebral oedema and elevated ICP following stroke in a clinically relevant ovine model. The specific aims and respective hypotheses were as follows:

AIM 1. To determine the effect of NK1-R antagonist treatment or decompressive craniectomy surgery on ICP following permanent stroke in an ovine model. This aim sought to evaluate three different treatment regimens of the NK1-R antagonist (EU-C-001, PresSuraNeuro) and compare pharmacotherapy with surgical intervention via decompressive craniectomy (DC). This study was performed to determine whether the NK1-R antagonist could be as effective in reducing ICP as surgical intervention with DC. In addition, this study sought to determine the most effective NK1-R antagonist treatment regimen to reduce ICP following permanent stroke in the ovine model.

AIM 2. To develop a survival model of transient MCAo in the sheep. Prior to the thesis, methods to induce transient stroke in the ovine model were incompatible with survival because of the surgical approach used. Therefore, the purpose of this study was to modify the surgical approach to transient MCAo so that sheep were able to be recovered for long-term assessment (28 days) following stroke onset.

AIM 3. To determine the temporal profile of cerebral oedema and ICP following transient stroke in an ovine model. To evaluate the efficacy of the NK1-R antagonist, it was first essential to characterise the course of cerebral oedema and elevated ICP development for 7 days following stroke with reperfusion in the ovine model. In addition, both males and females were utilised in this aim, given that urinary catheterisation was not

required, allowing investigation of sex differences in the temporal profile following stroke.

AIM 4. To determine the efficacy of NK1-R antagonist treatment, administered either early or late following stroke, in reducing cerebral oedema and elevated ICP following transient stroke in an ovine model. For this aim we sought to determine the efficacy of NK1-R antagonist treatment in a clinically relevant therapeutic window following transient ovine MCAo. Specifically, we sought to determine if the NK1-R antagonist could produce a clinically meaningful reduction in ICP when administered either early (before elevated ICP was established) or late (when ICP was already elevated) post-stroke. Further, we also sought to assess whether any differences in response to treatment between genders were apparent.

AIM 5. To develop a novel method to assess motor outcome following stroke in an ovine model. For this aim, we sought to develop a method to quantitatively assess functional outcome and recovery following ovine stroke. To achieve this in a robust and clinically relevant manner, we sought to carry out motion capture to assess the gait and kinematics of experimental animals. Given limited research in this area, this necessitated the development of a novel method of assessment, and significant troubleshooting and ongoing optimisation.

Hypothesis 1. NK1-R antagonist treatment will reduce cerebral oedema and ICP, comparable to decompressive craniectomy, at 24 hours following permanent stroke in the ovine model.

Hypothesis 2. The development of cerebral oedema and elevated ICP in the ovine transient stroke model will be comparable to that seen clinically, peaking within 3–5 days of stroke onset.

Hypothesis 3. NK1-R antagonist treatment will reduce cerebral oedema and elevated ICP, measured at 6 days following transient stroke, with reperfusion in the ovine model.

Hypothesis 4. Kinematic evaluation of animals pre- and post-transient stroke in the ovine model will provide a quantitative and reliable method in which motor function following stroke can be assessed.

05

Study Design and Methodology

5.0 INTRODUCTION

Although specific procedures are discussed within each experimental chapter, a comprehensive overview of methods undertaken, especially those beyond the scope and detail of publication, are provided below.

5.1 STUDY DESIGN

A total of 125 (40 M, 78 F) merino sheep (*Ovis aries*) were used in this thesis. Animals were sourced from a single farm in Gum Greek, South Australia and were aged 18 – 36 months, with a weight range of 60.38±6.67 kgs. Castrated wethers and ewes with either very small or no horns were used preferentially as they were easier to position and operate upon given the temporal/parietal surgical approach. All animals were transported from the farm in groups of 6-12 on days not exceeding 35 °C to the South Australian Health and Medical Research Institute (SAHMRI) Preclinical, Imaging and Research Laboratories (PIRL). On arrival, animals were examined by a veterinarian for general wellbeing and absence of neurofunctional deficit (Boltze et al., 2008). Sheep were treated prophylactically with antiparasitic ivermectin administered intramuscularly (0.25 mg/kg, Ivomec 0.8 g/L) and cydectin administered by oral drench (0.1% Moxidectin), and examined for presence of nasal bot fly larvae and itchmite. Thereafter, animals were housed in groups of 20-30 in outdoor paddocks with free access to water and grazing pastures. All animals were acclimatised to pasture for a minimum of 7 days, following which they were transported to smaller yard housing to undergo acclimatisation to bucket feeding and human contact for an additional 7 days prior to commencing experimental procedures.

A minimum of 6 animals were randomised into relevant treatment groups for each of the

thesis aims. ICP (Chapters 6-8), MRI (cerebral oedema and infarct volume; Chapters 6-8) and functional assessment (Chapter 9) were the primary outcome measures for this thesis, with secondary outcome measures including the measurement of physiological parameters and immunohistochemistry (IHC). Historical sham data (for example, ICP) was used to determine baseline parameters across aims in order to minimise animal numbers required for ethical purposes (in accordance with the 3R's for the use of animals for scientific research - Replace, Reduce, Refine - guidelines) and reduce experimental costs (Wells et al., 2015, Wells et al., 2012). The breakdown of animal numbers for each experimental group is shown in Table 5.1.

5.2 ETHICS APPROVAL

All studies were approved by The University of Adelaide (M-2014-015; M-2015-018) and SAHMRI (SAM 104, SAM 3, SAM 141) animal ethics committees. Experimentation was conducted in accordance with the Australian National Health and Medical Research Council code of care and use of animals for scientific purposes (8th Edition, 2013), and adhere with the Animal Research Reporting of *In Vivo* Experiments (ARRIVE) guidelines (Percie Du Sert et al., 2020).

Table 5.1 Animal allocations across experimental chapters and aims

Aim and Chapter	Total Number of Animals	Duration of Ischaemia	Survival time point	Treatment	Number Animals per Gender	Method of Brain Tissue Collected	Outcome Measures Assessed		
							ICP	MRI	Functional
Aim 1 (Chapter 6)	34 Merino Sheep	Permanent MCAo	24 hours	Sham	4F	Fixed	Y	Y	N
				Vehicle	6F	Fixed	Y	Y	N
				DC	6F	Fixed	Y	Y	N
				1xNK1	6F	Fixed	Y	Y	N
				2xNK1	6F	Fixed	Y	Y	N
				3xNK1	6F	Fixed	Y	Y	N
Aim 2 and 3 (Chapter 7)	47 Merino Sheep	2hr MCAo	1 day	Vehicle	4M; 5F	Fixed	Y	Y	N
			2 days	Vehicle	5M; 3F	Fixed	Y	Y	N
			3 days	Vehicle	3M; 3F	Fixed	Y	Y	N
			4 days	Vehicle	3M; 3F	Fixed	Y	Y	N
			5 days	Vehicle	3M; 3F	Fixed	Y	Y	N
			6 days	Vehicle	3M; 3F	Fixed	Y	Y	N
			7 days	Vehicle	3M; 3F	Fixed	Y	Y	N
Aim 4 (Chapter 8)	16 Merino Sheep	2hr MCAo	6 days	Vehicle	3M; 3F	Fixed	Y	Y	N
				Early NK1	3M; 3F	Fixed	Y	Y	N
				Late NK1	3M; 3F	Fixed	Y	Y	N
Aim 5 (Chapter 9)	30 Merino Sheep	2hr MCAo	28 days	Vehicle	7M; 6F	Fresh Fixed	N	Y	Y
				Late NK1	6M; 7F	Fresh Fixed	N	Y	Y

5.3 SURGICAL APPROACH TO MCAo

5.3.1 Animal Preparation

Twenty-four hours prior to surgery, all animals were moved to indoor pens where they were individually housed and fasted for a minimum of 12 hours pre-operatively to reduce the risk of intraoperative regurgitation. This also reduced the rate of fermentation and thus development of ruminal tympany due to anaesthetic suppression of eructation, as described in Chapter 3.

5.3.2 Anaesthesia Induction and Maintenance

Animals were transported to a procedure room and induction commenced. For animals in Chapter 6, anaesthesia was induced with intramuscular thiopentone (1000 mg in 20 mL, Jurox Pty Ltd, Australia); whereas those in Chapters 7, 8 and 9, a combination of ketamine (0.05 mL/kg, 100 mg/mL Injection, CEVA, Australia) and diazepam (0.08 mL/kg, 5mg/mL Injection, Pamlin, CEVA, Australia), administered intramuscularly, was used. Change in induction protocol for Chapter 7 onwards was made following observations of poor recovery from anaesthesia with thiopentone in survival animals.

Following induction, animals were positioned supine on a trolley and an endotracheal tube placed via direct laryngoscopy. Wool was shorn from the surgical site and sites of intravenous/arterial access and skin cleaned with 4% chlorhexidine (Beckton-Dickinson E-Z Scrub™, Australia). Protective gel ointment (Poly Visc, Alcon, Australia) was deposited in the eyes to prevent corneal drying due to loss of the blink response under anaesthesia. Animals were then transported to a surgical theatre and mechanical ventilation commenced. The ventilation rate was set to 15 breaths/minute and tidal volume to 10 mL/kg, adjusted

thereafter to normalise oxygen and carbon dioxide tensions. Anaesthesia was maintained via a combination of inhalational isoflurane delivered at 1.5-2 % minimum alveolar concentration (MAC) via vaporiser (Henry Shein, Australia) and intravenous ketamine at 4 mg/kg/hr. To prevent intraoperative hypothermia, a heated breathing circuit (Darvall Anaesthesia, Australia) was used which warmed inspired gas to 38.5 ˚C - 40 ˚C. This was paired with an oesophageal temperature probe to provide closed-loop temperature control.

5.3.3 Cannulation and Fluid Management

An arterial catheter (22 g, Terumo SURFLO®) was inserted in the left hind leg for arterial blood sampling for blood gas and electrolyte analysis. To ensure patency and minimise risk of thrombotic complications, the catheter was regularly flushed (2 mL) via a 500 mL bag of sodium chloride (Baxter Health, Australia) attached to a pressurised bag pump (maintained at 300 mmHg). The pressure bag was used in combination with a standard flow-regulating device allowing fluid to be continually administered at a rate of approximately 3 mL/hr. A cannula (20 g, Terumo SURFLO®) was inserted into the external jugular vein for fluid and ketamine administration. Crystalloid fluids were administered intravenously throughout surgery via continuous infusion with compound sodium lactate at a rate 60 mL/hr (Hartmann’s solution, Baxter Health, Australia).

Figure 5.1. Surgical theatre set up, with surgery in progress. All procedures were carried out aseptically, with animals draped and surgeon scrubbed as shown, and overhead theatre lights positioned to illuminate the operating area.

5.3.2 Induction of Stroke

All surgical procedures were carried out aseptically (Figure 5.1). Two different approaches to accessing the MCA were used in this thesis. The studies outlined in Chapter 6 used a non-survival surgical approach (Wells et al., 2012), whereas the studies outlined in Chapters 7-9 used a modified surgical approach that was compatible with survival (Sorby-Adams et al., 2019a).

5.3.2.1 Non-survival Surgical Approach - Permanent MCAo

To achieve stroke in the non-survival model, animals were placed prone in the sphinx position with their head tilted 90 degrees for a right MCA approach. A 5 cm vertical incision was made running equidistant between the right eye and ear, terminating just below the

zygomatic arch. Underlying branches of the superficial temporal artery were identified and cauterised, and the large fat pad that sits behind the orbit removed to improve visualisation. The temporalis and other muscles of mastication were then stripped from the coronoid process of the mandible and the coronoid subsequently fractured at its base, adjacent to the zygomatic arch (Figure 5.2). Remaining muscles of mastication were stripped to expose the pterion, which comprises the junction of the parietal, sphenoid and frontal bones of the skull. Visualisation of the pterion was necessary to perform a craniotomy with adequate access to the proximal MCA. With the assistance of loupe magnification and a head mounted light source (Surgical Acuity, Wisconsin), a small craniotomy was performed over the junction of the parietal and squamous temporal bones using a high-speed pneumatic drill (Midas Rex® Legend Electric System (ICP), Medtronic, USA) with a 5 mm fluted ball drill bit (Midas Rex® Legend, Medtronic, USA), taking care not to breach the underlying dura. Bone was also removed anteroinferiorly from the greater wing of sphenoid to adequately expose the MCA. The craniotomy was then extended extradurally with a Kerrison rongeur (2 mm, upward facing) anteriorly and inferiorly to provide access to the anterior temporal lobe beneath the underlying dura.

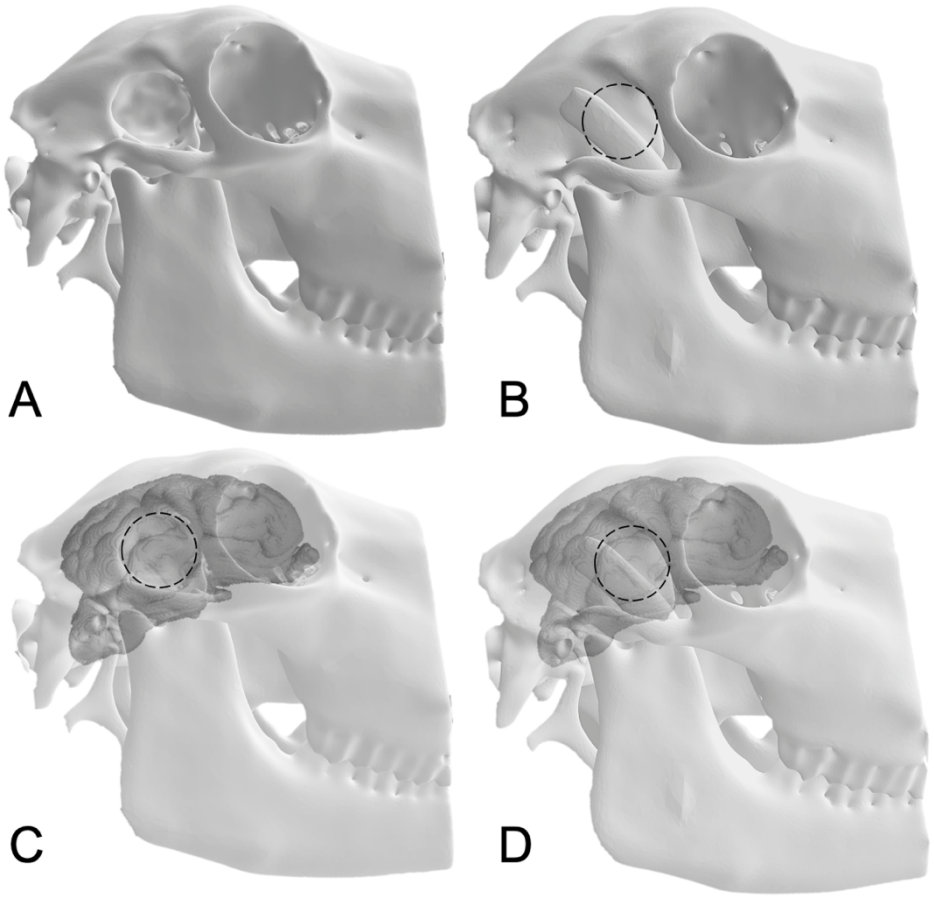

Figure 5.2. Surgical approach to ovine stroke. (A and C) demonstrate the non-survival approach, where the coronoid process is removed and the corresponding craniotomy is unobscured, allowing access to the underlying temporal lobe. (B and D) demonstrate the survival approach, where preservation of the coronoid process impedes access to the underlying skull bones making appropriate craniotomy more challenging. Three-dimensional (3D) reconstruction of the skull was performed using images acquired on a Philips CT and prepared using 3D slicer and MeshMixer. Brain surface image obtained from the McGill Brain Imaging Centre (Brain Surfaces STL; Nitzsche et al., 2015)

5.3.2.2 Survival Surgical Approach - Temporary MCAo with Reperfusion

To maintain the animals' ability to masticate post-operatively, the surgical method to achieve transient stroke necessitated a less invasive approach (developed according to Aim 2). Here, animals were placed on their left side, and head tilted to enable a posterior frontotemporal surgical approach. A 5 cm incision was then made horizontally between the

ear and the orbital rim along the superior temporal fossa. The coronoid process was left intact (Figure 5.2) and displaced laterally using Cloward retractors inserted inferiorly. Underlying muscles of mastication were then stripped from the floor of the cranium as far rostral as the fibrous ring attaching the posterior orbit to the border of the parietal bone, enabling visualisation of the pterion. A craniotomy was performed using the same landmarks and procedures as the non-survival approach (section 5.3.2.1). The anterior component of the craniotomy was frequently the most difficult part of the exposure, and the most critical in order to achieve satisfactory proximal MCA access. This was particularly challenging in the survival approach due to the intact coronoid process impeding access to the underlying skull surface.

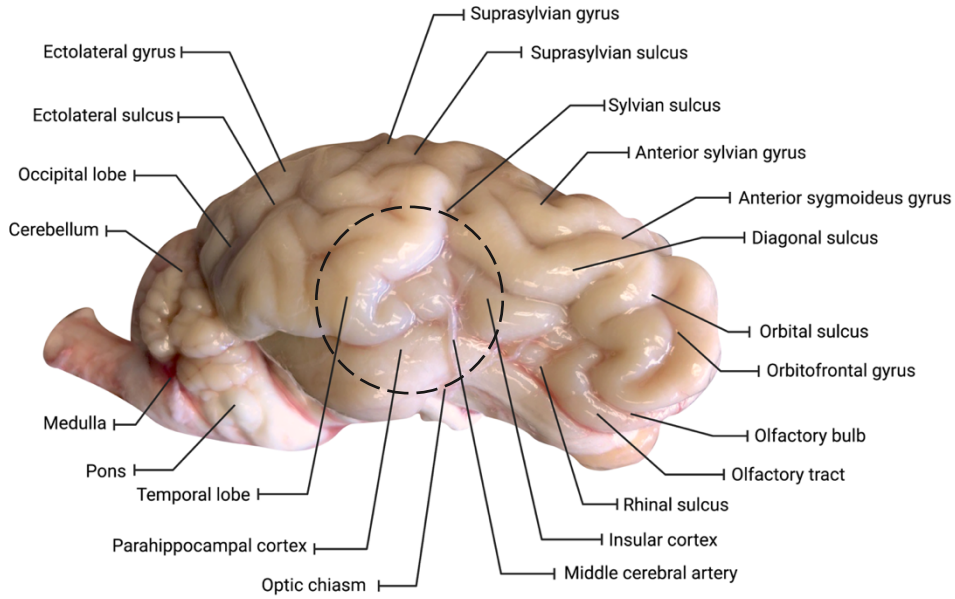

Figure 5.3. Neuroanatomical structure of the lateral surface of the ovine brain. The approximate location of the craniotomy is indicated by the dashed line. The middle cerebral artery can be seen faintly on the cortical surface. During surgery visualisation is optimised with gentle retraction of the temporal lobe.

5.3.2.3 Craniotomy, Durotomy and MCA Occlusion

Once sufficient bony exposure and craniotomy was achieved in both non-survival and survival approaches, a horseshoe-shaped durotomy was performed with an inferiorly based

flap. Ideally, the cortical branches of MCA were seen running subpially on the surface of the brain (Figure 5.3). Branches were then followed proximally, neurosurgical textile pads (patties) inserted over the exposed brain to prevent contusion (Neuray® Surgical Patties, Medtronic, USA), and gentle upwards retraction of the anterior temporal lobe performed to follow each branch to its bifurcation point. Further gentle retraction and careful CSF aspiration from the pre-chiasmatic cistern allowed identification of the proximal MCA where it looped around the optic tract, medial to where the free tentorial edge meets the roof of the cavernous sinus. To include the perforating branches when performing an occlusive MCA stroke, proximal exposure of the artery at its origin was deemed important (see cerebrovasculature in Figure 5.4). At this point of the surgical procedure, the animal was randomised into one of the following experimental groups, according to study aim: 1) Sham: the proximal MCA was dissected but not occluded; 2) Permanent occlusion: the proximal MCA was cauterised with Malis bipolar diathermy forceps (Valleylab Inc., Colorado); or 3) Temporary occlusion with reperfusion: the proximal MCA was occluded for 2 hours with a temporary mini aneurysm clip (Aesculap YASARGIL® Aneurysm Clip, Germany) before being released to achieve reperfusion.

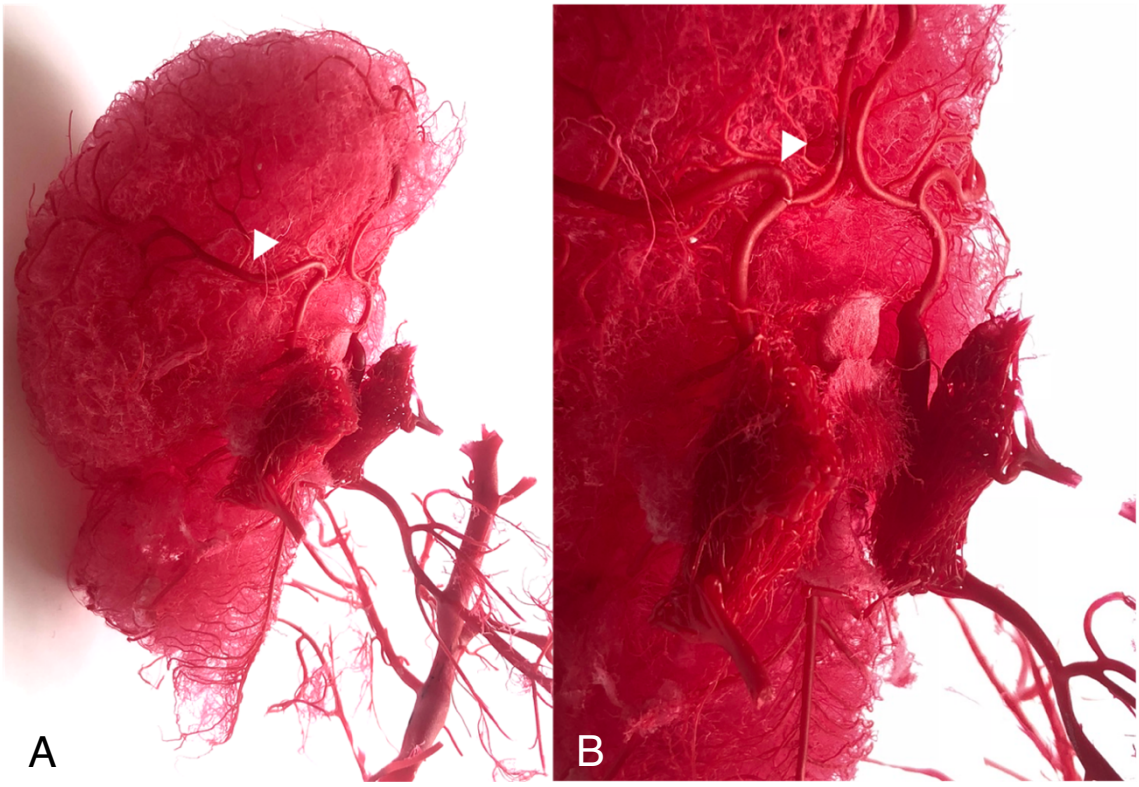

Figure 5.4. The ovine cerebrovasculature. This resin cast shows in intricate detail the complex anatomy of the ovine cerebrovascular system. (A) The lateral aspect of the brain shows the course of the middle cerebral artery (MCA) with branches running along the cortical surface, as indicated by the arrowhead. (B) The inferior aspect of the brain shows in more detail the MCA at its site of bifurcation from the internal carotid artery (ICA). The arrowhead indicates the ideal site of M1 MCA occlusion prior to its division into M2 cortical branches. Also of note is the intricate structure of the rete mirabile, which can be see prior to continuation of the ICA into the circle of Willis (see Figure 3.2, Chapter 3, for diagrammatic representation).

5.3.2.4 Restoring Intracranial Dynamics and Wound Closure

After sham surgery, permanent MCA occlusion, or aneurysm clip release, synthetic dural regeneration matrix (Durepair®, Medtronic, USA) was used to cover the brain and watertight dural closure achieved with ethyl cyanoacrylate (Bostik, Australia). The bone flap from the craniotomy was reinserted and cranioplasty performed with dental acrylic cement (Sledgehammer, Keystone, Germany), which was applied and manipulated into the edges of the craniotomy, restoring the integrity of the cranial cavity and thus homeostasis of ICP dynamics. The surgical site was then treated with 1.0 mL 0.5% local anaesthetic Marcain (Bupivacaine hydrochloride 5 mg/mL, AstraZeneca, Australia) and muscle layers opposed

using 0.1 braided polyglactin suture with tapercutting needle (Vicryl®, ETHICON, Australia) using a horizontal mattress suture technique of wound closure to prevent infection (Kudur, 2009).

5.3.3 Physiological Monitoring

Arterial blood samples (2.0 mL) were collected every 3-4 hours via the indwelling arterial catheter and analysed (Machine AVL Scientific Corporation USA, Manufactured by Hersteller, OPTI Critical Care Analyzer–Model OPTI3, Serial No. OP3-2759) to determine pO_2, pCO_2, bicarbonate, base excess, haematocrit, haemoglobin, pH, Na^+ and K^+ levels. Rectal and oesophageal temperature and end tidal CO_2 ($ETCO_2$) were also measured at this time. A pulse oximeter attached to the side of the mouth enabled continuous measurement of oxygen saturation and pulse rate. Intraoperative pO_2 was maintained at >100 mmHg to ensure adequate oxygenation of the brain to prevent hypoxia and exacerbation of ischaemia. Mean arterial blood pressure (MABP) was maintained at approximately 70-90 mmHg to ensure adequate arterial pressure during reperfusion to ensure sufficient blood return to the area of ischaemia. Physiological pCO_2 was considered 36-44 mmHg; as CO_2 is a potent cerebral vasodilator, it was essential to induce mild hypocapnia (>40 mmHg) to promote moderate brain relaxation and facilitate adequate MCA exposure during surgery, and also to reduce the effects of elevated pCO_2 on ICP. Finally, target pH was ±7.42 to prevent metabolic acidosis (pH <7.41) as metabolic disturbances predispose to respiratory acidosis, resulting in elevations in CO_2. A summary of physiological variables recorded, and normal values, are provided in Table 5.2.

Table 5.2 Physiological variables recorded intraoperatively

Abbreviation	Description	Physiological value
pH	pH	7.42 - 7.46
pO_2	Partial pressure of oxygen	>100 mmHg
pCO_2	Partial pressure of carbon dioxide	36 - 42 mmHg
$ETCO_2$	End tidal/alveolar carbon dioxide	30 - 48 mmHg
BE	Base excess	-2 - +2
SpO_2	Oxygen saturation	>90
HCO_{3-}	Bicarbonate	22 - 33
Hb	Haemoglobin	7.3 - 10
Hct	Haematocrit	23.5 - 33
Na^+	Sodium	130-145
K^+	Potassium	3.9 - 4.1
PR	Pulse rate	60 - 85 beats per minute
rTemp	Rectal temperature	37.5 - 39.5 ºC

Values based on Byrom et al., 2010.

5.3.4 Blood Pressure Monitoring

Given the relationship between MABP, ICP, CPP, and cerebral ischaemia, efforts were made to obtain regular measurements of MABP intraoperatively. Arterial blood pressure (ABP) was monitored continuously via insertion of an indwelling arterial catheter (Chapter 6), or at 5-minute intervals via application of a paediatric blood pressure cuff (Easy Care Cuff, Phillips) on the upper left front limb (Chapters 7-8). Although application of the blood pressure cuff to the limb provided an estimate of blood pressure at regular intervals, measurement via direct catheterisation of the artery enabled recording of accurate physiological measurements in real time, and subsequent correlations to the ICP response. In Chapter 6, where non-survival animals were used, femoral artery catheterisation was achieved via invasive means. This approach, however, was not achievable in survival animals due to permanent occlusion of the femoral artery.

5.3.4.1 Invasive Arterial Blood Pressure Monitoring in Non-survival Animals

Animals were positioned supine on the operating table and hindlimbs extended to expose the ventromedial aspect of the left hindlimb. Using a sterile technique, the femoral artery was palpated, and an incision made using a size 22 scalpel blade along the ventromedial aspect of the hindlimb running laterally. Upon incision, the underlying muscle was dissected using a blunt technique, allowing the femoral artery to be isolated from the adjacent nerve and vein. A 3 cm segment of the artery was located, fascia cleared, and the distal end tied off. A haemostatic clamp (straight mosquito) was subsequently applied to proximal segment of the vessel, a small incision made in the exposed section, and 12 g, 42 cm sterile spinal manometer tube (Baldwin Medical, Australia) inserted into the vessel. A female-taper Luer lock (Becton-Dickinson, Australia) was subsequently attached to the distal end of the catheter, and Codman® Microsensor transducer (Codman & Shurtleff Inc., Massachusetts) attached to the male-taper of the Luer lock. This set-up allowed for simultaneous continuous ABP monitoring (LabChart Reader, ADInstruments, Australia), and sampling of arterial blood for blood gas analysis. The catheter remained *in situ* for the duration of the experiment thereafter.

5.4 INTRACRANIAL PRESSURE MONITORING

The method in which ICP was monitored varied depending on the experimental aim, with differences in the duration of ICP monitoring between survival and non-survival experiments. Those animals in Chapter 6 underwent continuous ICP monitoring throughout the entire 24-hour period following stroke. For animals in Chapters 7 and 8, prior to the pre-determined survival time-point, animals were re-anaesthetised and ICP measured for 3-4 hours only (as discussed in detail in Chapters 7 and 8).

Regardless of ICP monitoring duration, procedures were performed in the same fashion. Burr holes with a diameter of 5 mm were drilled bilaterally into the skull using a handheld, Codman® Cranial Hand Drill (Codman & Shurtleff Inc., Massachusetts), approximately 1 cm lateral to the sagittal suture and 1 cm posterior to the horn buds. Once the skull was breached, the underlying dura was incised, and plastic bolts from a Codman Microsensor™ Skull Bolt Kit for Intraparenchymal Procedures (Codman & Shurtleff Inc., Massachusetts) secured into the burr holes. A Millar strain gauge Codman® Microsensor transducer (Codman & Shurtleff Inc., Massachusetts) was used to measure ICP (the same fabrication as used to monitor ABP) with a range of –50 mmHg to +250 mmHg. The Codman® Microsensor comprises a pressure sensing microchip transducer mounted in a titanium case, with a 1.2 mm diameter tip attached to a 0.7 mm diameter nylon lead measuring 40 cm in length. The nylon lead of the Microsensor was attached to a bridge amplifier and PowerLab data acquisition device (ADInstruments, Australia). LabChart software (ADInstruments, Australia) installed on a computer (Dell, UK) to which the PowerLab and bridge amplifier were connected allowed for the analogue signal from the Codman microsensor to be continually recorded at frequencies of approximately 1 KHz.

Once attached to the bridge amplifier and PowerLab, the Codman Microsensor™ was laid flat, with the tip of the sensor immersed in sterile saline. The device was subsequently zeroed, and two-point pressure checks (0 mmHg, 100 mmHg) performed to ensure transducer accuracy. Following zeroing and checking, the prepared probes were attached to skull bolts and transducers advanced 15 mm into the brain parenchyma to allow continuous recording of ICP for the aforementioned durations. At the conclusion of recording, probes were removed, and two-point checks re-performed to determine extent of drift, if any,

throughout the duration of the experiment. ICP readings from the ipsilateral hemisphere were preferentially used for data analysis.

5.5 POSTOPERATIVE RECOVERY

On completion of intraoperative procedures, animals were removed from anaesthesia and extubated. Thereafter, their post-operative fate was dependent upon the specific experimental aim. Animals in Chapters 7, 8 and 9, once lucid, were transported to post-operative recovery pens. Here they were placed under a forced air warming blanket (Darvall, Australia) and treated with subcutaneous antibiotic Rilexene (Chapter 6 and 7; 1 mL/10 kg every 12 hours, 15 g/100 mL Cephalexin, VIBRAC, Australia) or Depocillin (Chapter 8 and 9; 1 mL/25 kg every 12 hours Procaine benzylpenicillin, Intervet, Australia), non-steroidal anti-inflammatory Carprevine (0.7 mg/kg every 12 hours, 50 mg/mL Carprofen, Norbrook, Australia) and opioid Temgesic (1.0 mL, 300 μg/mL Buprenorphine hydrochloride, Reckin Benckiser, Australia) for pain relief. Note the differences in the antibiotic agent use across studies was due to a change in the preferred antibiotic agent used by SAHMRI PIRL and not researcher preference. Antibiotic and NSAID treatment was continued for 3 days following surgery, with additional opioid and NSAID administered as required thereafter upon veterinary advice.

All animals remained in indoor single pens 7 days post-operatively to allow for close continuous monitoring. Here, they were fed once daily with a combination of feedlot, nuts, grain and lucerne hay (Laucke Mills, South Australia), with free access to water. Clinical evaluation of was performed *bis in die* in accordance with ethical guidelines, more frequently as clinical scoring and animal condition dictated. Specifically, animal wellbeing was

monitored through recording of food consumption and water intake, urine and faeces output, ability to walk and stand unassisted, signs of pain such as the presence of teeth grinding, droopy ears and signs of wound infection such as swelling of the surgical site (see Appendix 5.1 for ovine stroke clinical record sheet, which also details humane endpoint). Animals were weighed weekly or more frequently as required. In addition, continuous animal monitoring was performed via closed-circuit television (CCTV), with researchers able to check on animals remotely via CCTV monitoring software available on personal mobile devices.

5.6 MAGNETIC RESONANCE IMAGING

All animals underwent MRI under general anaesthesia (1.5% isoflurane, Henry Shein, Australia) with time of acquisition varying according to the experimental aims. Images were acquired on a 1.5 Tesla (T) Siemens Syngo2004A Sonata (Siemens AG, Munich, Germany) with a 12-channel head coil. The specific scanning sequences included T_1 magnetisation-prepared rapid acquisition with gradient echo (MPRAGE), T_1 turbo spin echo (TSE), T_2 TSE, T_2 fluid attenuated inversion recovery (FLAIR), T_2 star, diffusion-weighted imaging (DWI, with B_{1000} and B_0 values acquired), DWI apparent diffusion coefficient (ADC), magnetic resonance angiography (MRA) time-of-flight (TOF) and T_1 MPRAGE following contrast administration (details in section 5.6.2). Sequence parameters are summarised in Table 5.3. The level of vital MRI coronal slices in the territory of MCA are shown in Figure 5.6, and corresponding neuroanatomical landmarks in Figure 5.7.

Table 5.3 MRI imaging sequences

Sequence	Orientation	Slice Thickness (mm)	Pixel size	TR (ms)	TE (ms)	FA	NA	IT	Purpose
T_1 MPRAGE	Isometric	1	0.58/0.58	1900	3.93	15	1	1100	Morphology
T_1 TSE	Coronal	5	0.58/0.58	490	9.3	90	2		Morphology
T_1 TSE	Axial	5	0.58/0.58	450	9.3	90	2		Morphology
T_2 TSE	Coronal	5	0.46/0.46	5160	72	150	1		Morphology Parenchyma fluid content
T_2 TSE	Axial	5	0.46/0.46	4000	72	150	1		Morphology Parenchyma fluid content
T_2 FLAIR	Coronal	5	0.46/0.46	8700	162	150	2	2500	Oedema
T_2 star	Coronal	5	0.46/0.46	1050	26	20	1		Haemorrhage
DWI ADC	Coronal	5	1.56/1.56	3600	95	90	10		Infarction
DWI ADC	Axial	5	1.56/1.56	3000	84	90	10		Infarction
DWI TRACE	Coronal	5	1.56/1.56	3600	95	90	10		Infarction
DWI TRACE	Axial	5	1.56/1.56	3000	84	90	10		Infarction
MRA TOF	Isometric	5	0.39/0.39	40	5.16	25	2		Cerebrovascular anatomy
T_1 MPRAGE fs GAD	Isometric	5	0.58/0.58	1900	3.93	15	1	1100	Morphology

FA – flip angle, NA – number of averages, TSE – turbo spin echo, TR – repetition time, TE – echo time, IT – inversion time, TOF – time of flight, GAD – gadolinium.

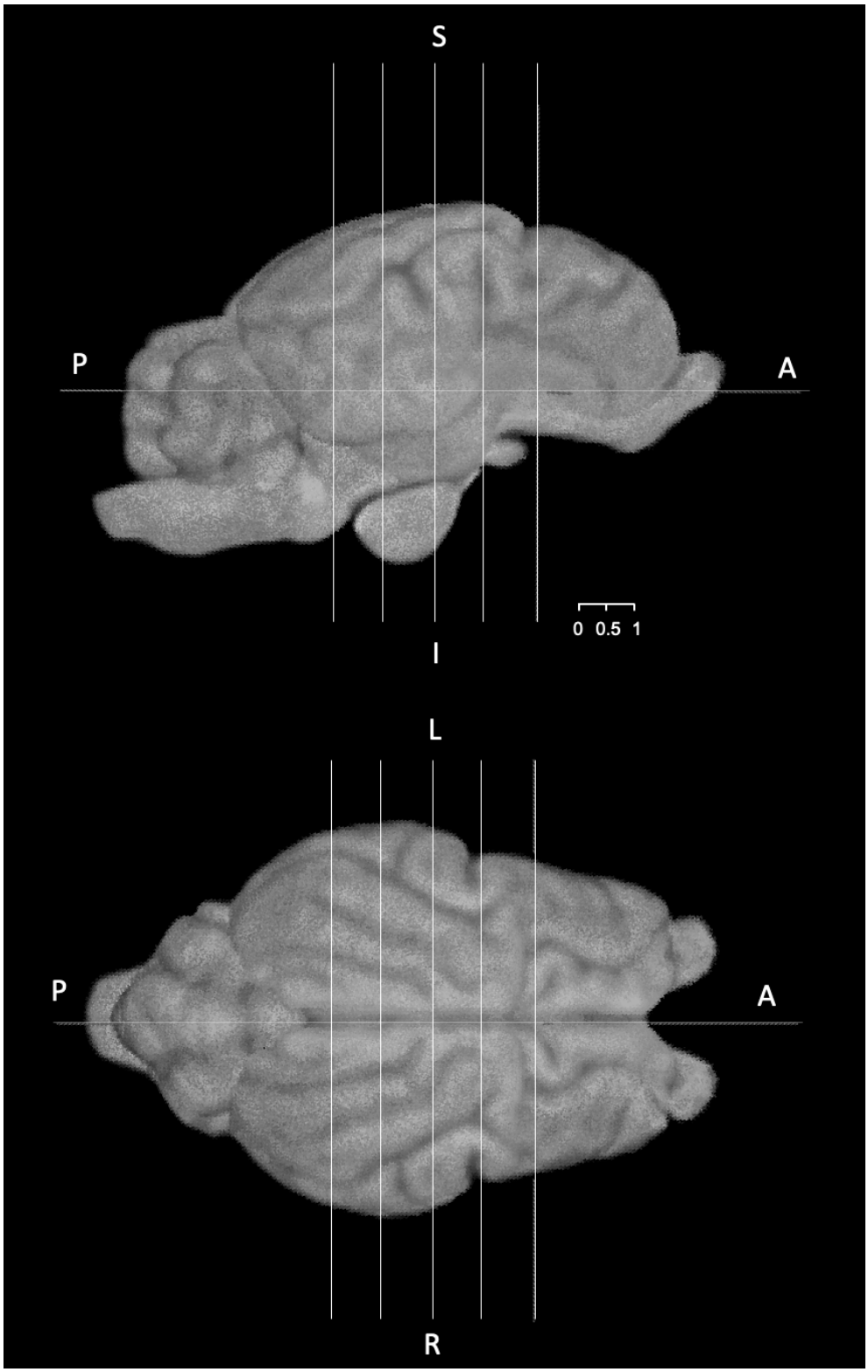

Figure 5.5. Location of vital MRI slices in the coronal plane. Slices in the territory of the middle cerebral artery most commonly affected by stroke are indicated by the vertical white lines. From anterior to posterior slices; A, B, C and D, corresponding neuroanatomical landmarks shown in Figure 5.7. A – anterior, P – posterior, S – superior, I – inferior, L – left, R – right. Figure created from T_1 SPC MRI atlas (Ella and Keller, 2015, Ella et al., 2017, Ella et al., 2019). Scale bar 1 cm.

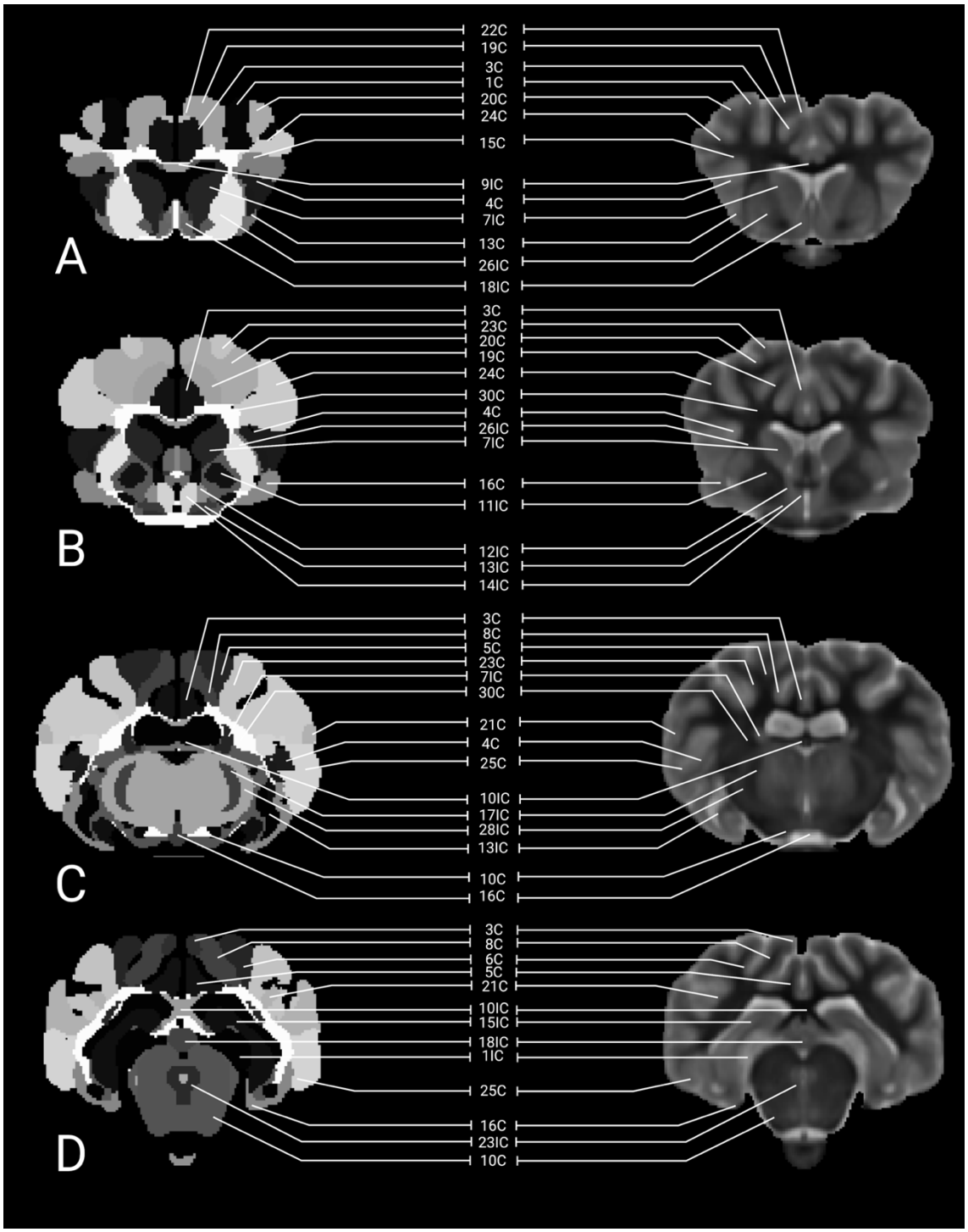

Figure 5.6. Neuroanatomical landmarks of critical coronal sections in the territory of the middle cerebral artery (MCA). The left panel shows an atlas of key neuroanatomical areas, and the right panel shows corresponding brain regions on T_2 weighted slices. Refer to Table 5.4 for corresponding numerical atlas regions.

Table 5.4 Neuroanatomical landmarks of the cortex (C) and inner cortex (IC)

Annotations for cortical structures (C)		Annotations for inner brain structures (IC)	
1	Anterior sygmoideus gyrus	1	Lateral ventricle
2	Cerebellum	2	Fourth ventricle, aqueduct
3	Cingulate gyrus	3	Accumbens
4	Insular cortex	4	Amygdala
5	Ectolateral gyrus	5	Anterior commissure
6	Entolateral gyrus	6	Bed nucleus
7	Gyrus rectus	7	Caudate nucleus
8	Lateral gyrus	8	Claustrum
9	Medulla oblongata	9	Corpus callosum
10	Midbrain	10	Fornix
11	Occipital lobe	11	Globus pallidus
12	Olfactory bulb	12	Globus Pallidus additional structure
13	Olfactory tract	13	Hippocampus
14	Orbital gyrus	14	Hypothalamus
15	Orbitofrontal gyrus	15	Internal capsule
16	Parahippocampal gyrus	16	Lateral septal nucleus
17	Pituitary gland	17	Mamillothalamic tract
18	Pons	18	Medial septal nucleus
19	Postcruciate gyrus	19	Medullary lamina
20	Posterior sygmoideus gyrus	22	Optic tract
21	Posterior sylvian gyrus	23	Periaqueductal grey matter
22	Precruciate gyrus	24	Pineal gland
23	Suprasylvius gyrus	25	Preoptic hypothalamic area
24	Sylvian gyrus	26	Putamen
25	Temporal lobe	28	Thalamus

Atlas regions from Ella et al., 2019.

5.6.3 MRI Analysis of Infarct Volume

Diffusion weighted imaging sequences were used to assess infarct volume (Figure 5.8, A). DWI is able to detect changes in ischaemic brain tissue in as little as 2.5 minutes post-ictus in experimental animals, and is highly sensitive in the hyperacute examination of clinical stroke (Linfante et al., 2001). These sequences enable assessment of the apparent diffusion coefficient (ADC) of water, with a decreased ADC signal corresponding with energy failure,

such as that of ATP dependent pumps during acute stroke and accumulating cytotoxic oedema. When cytotoxic oedema plateaus after the first 24 hours of stroke onset, the ADC evolves to appear bright.

Ergo, these sequences are particularly robust and allow for identification of the evolving infarct. In order to undergo volumetric quantification of the infarct, segmentation tools in ITK-SNAP were used to perform semi-automated segmentation of diffusion-weighted lesions (Figure 9). This consisted of a combination of three-dimensional (3D) active contour segmentation and subsequent manual post-processing of the segmentation while adjusting image thresholds. This semi-automated method was chosen to maximise reproducibility whilst excluding artefacts. The 3D active contour segmentation consisted of multiple steps: First, in the pre-segmentation phase, independent component analysis automatically segmented parts of the DWI image which were subsequently manually identified as foreground or background. To obtain the optimal distinction between foreground and background, thresholds of the image windows were adjusted. After thresholding, a "speed image" with a separate foreground and background was created (Figure 5.9, B). Next, in the active contour phase, seed regions were manually placed within the region of interest (ROI) (Figure 5.9, B, white circle). These seeds were then automatically grown within the ROIs to form the temporary segmentation (Figure 5.9, C). On completion of active contour expansion, the 3D volume segmentation was assessed, and areas not automatically included in the active contour manually included in a follow-up manual segmentation. For a full description of this method please see Yushkevich et al., 2006 and Yushkevich et al., 2019.

Figure 5.7. Infarct segmentation on ITK-SNAP. (A) The DWI sequence of interest is loaded into ITK-SNAP and automatic thresholding applied to better identify the infarct. (B) after thresholding, a 'speed image' is created as shown, and threshold further adjusted to optimise demarcation between the infarct and surrounding tissue. Seeds were then placed in the seed image and grown (circle), allowing the infarct to be segmented from unaffected tissue, as shown by the white overlay in (C). (D) The segmentation can be seen in 3D and volumes exported for analysis, with all images converted to binary for comparison.

5.6.1 MRI Analysis of Cerebral Oedema

T_2 FLAIR images were used to quantify cerebral oedema. Here, the inversion pulse applied to suppress high signals emanating from normal fluid-filled spaces such as ventricles and sulci enables determination of the extent of cerebral oedema by visualisation of areas in the brain of increased parenchymal water content, which appear bright (Figure 5.8, A) (Hudak et al., 2014, Battey et al., 2014).

Quantification of cerebral oedema was thereby achieved via direct measurement of white matter hypersensitivities. The specific approach to analysis, however, changed throughout the course of this thesis. In the initial studies (Chapters 6 and 7), manual segmentation was performed on coronal FLAIR images by an assessor blinded to the treatment group (HOROS v.3.3.6). As an understanding of analysis procedures were developed throughout the course of this doctorate, more comprehensive measures were performed, with updated approach applied in Chapter 8. This involves quantification of the hypersensitive FLAIR region using semi-automated methods described in section 5.6.3. Here, co-registration of oedema FLAIR and infarct DWI segmentations were performed, following which the infarct was subtracted from the oedema volume, thereby providing a quantitative measure of peri-infarct fluid.

In Chapter 8, quantification of the relaxation signal on T_2 scans was also performed to determine parenchymal water content. Here, 8 ROI's measuring 10 mm^2 were drawn in the ipsi- and contra- lateral hemispheres on axial scans at the level of the foramen of Monro. The mean signal intensity for each ROI was recorded, and the average intensity of all ROI's summed for each hemisphere. Signal intensity ratios were then calculated by normalising the signal intensity within the ipsilateral hemisphere to the signal intensity of the contralateral hemisphere. The normalised values in the stroke affected hemisphere were then exported for final interpretation.

5.6.2 MRI Analysis of BBB Permeability

To assess the permeability of the BBB, pre- and post-contrast T_1 MPRAGE series (Figure 5.8, D) were obtained following intravenous administration of 0.1 mL/kg Gadolinium-diethylene-triamine-pentaacetic acid (Gadovist, Gd-DTPA or GAD) (Magnevist, Bayer HealthCare, Germany). Gd-DTP is a large molecule that cannot enter the brain tissue when the BBB is intact (Aksoy et al., 2013). Leakage of GAD into brain tissue thus reflects breakdown and disruption of the barrier, permitting the abnormal movement of water into the brain (Aksoy et al., 2013) Dynamic sequences were unfortunately not obtained in this thesis; therefore, quantification of the influx constant (K_{trans}) was unable to be performed (Varatharaj et al., 2019). Instead, single time point series were used to perform qualitative analysis of pre- and post- contrast images to assess of the extent of GAD extravasation.

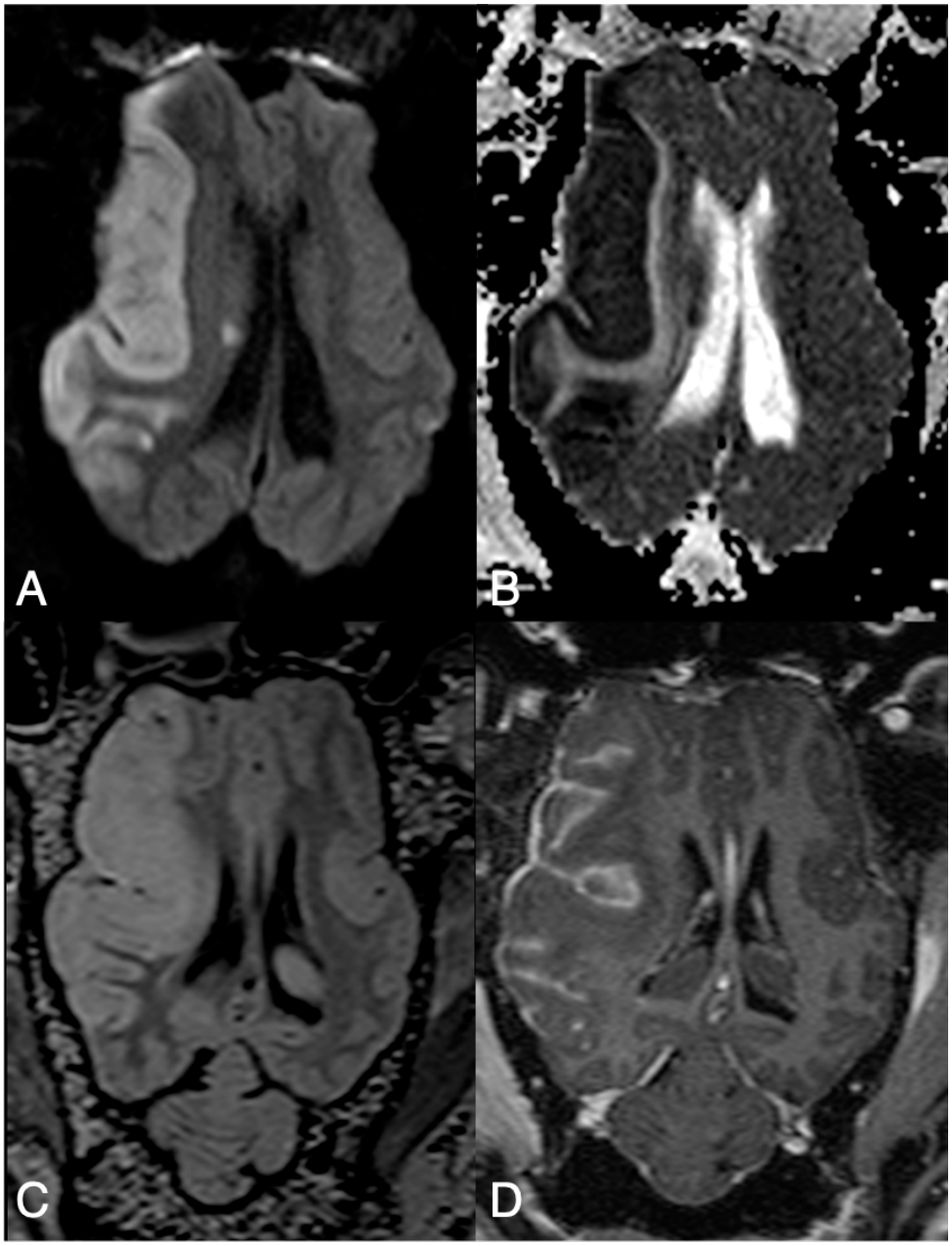

Figure 5.8. MRI sequences used for quantitative analysis 3 days post stroke. (A) Diffusion weighted imaging (DWI) showing the infarct core with cytotoxic oedema (hypertensive) used for quantification of infarct volume. (B) Apparent diffusion coefficient (ADC) maps showing infarct core (hypotensive) and surrounding vasogenic oedema (hypertensive rim). (C) T_2 fluid attenuated inversion recovery (FLAIR) showing infarct and oedema (hypertensive) with evident midline shift used for quantification of oedema. (D) TI MP-RAGE following administration of 0.1 mg/kg Gadovist showing evidence of BBB breakdown identified as the hypertensive rim along sulci and gyri of the stroke affected hemisphere, used for assessment of BBB permeability.

5.6.4 MRI Analysis of Mass Effect

To determine the mass effect of cerebral oedema, T_2 WI were used to determine pathological abnormality in which the degree of midline shift (MLS) was measured. Clinically, elevated ICP is associated with significant MLS and compression or obliteration of the perimesencephalic cisterns, with the degree of MLS being a predictor of poor prognosis and mortality. MLS is therefore regarded as an imaging feature supporting the Munro-Kellie doctrine (Liao et al., 2018). In this thesis, extent of shift from the midline was measured in mm from the septum pellucidum at the level of the foramen of Monro by blinded assesment (HOROS v3.1.1).

5.7 COLLECTION OF BIOLOGICAL FLUIDS

5.7.1 Collection of Cerebrospinal Fluid

CSF was collected via lumbosacral tap prior to induction of stroke and on days 1, 3, 6 thereafter in the cohort from Chapter 9. Note that as collection was performed in animals that did not undergo ICP monitoring there were no concerns regarding multiple CSF draws and the associated effects on ICP measurement accuracy. To obtain samples, animals were induced with a combination diazepam and ketamine as previously described (section 5.3.1). Animals were then placed in the prone position on a surgical table and the sagittal plane of the animal's vertebrae manipulated so that it was perpendicular to the horizontal plane of the table. Palpation of the hips was performed to determine the correct sagittal plane orientation of the spine and the optimal site for CSF collection was identified by the midline depression between the last lumbar and first sacral vertebrae. The area was shorn and cleaned using a 4% chlorhexidine preoperative surgical scrub brush (Beckton-Dickinson E-Z Scrub™, Australia), povidone-iodine applied and site surgically prepared. A 19 g medium bevel point

spinal needle with stylet (BMDi TUTA Healthcare, Australia) was inserted perpendicular to the skin and the needle advanced slowly through the subcutaneous tissue and interarcuate ligament until a sudden drop in resistance was felt indicating the advancement through the dural membrane and entry into the subarachnoid space. The stylet was then removed, and 2 mL of CSF aspirated via a syringe and deposited into a 3 mL tube, the sample placed immediately on ice for 20 minutes, centrifuged (15 mins at 4 °C 3000 relative centrifugal force (RCF)), extracted into 3 x 500 µL aliquots and stored at -80 °C until use.

5.7.2 Collection of Serum

For the animals in Chapter 9, 8.5 mL of whole blood was collected in Serum Separator tubes containing Silica/clot activator (Vacutainer® SST™ II *Advance* Tube, Beckon-Dickinson, Australia), either by direct venepuncture or via indwelling venous jugular catheter. Once filled, the tube was gently inverted 180° and back 5-6 times to ensure mixing of silica activator with the blood. Blood samples were subsequently left to clot at room temperature (not exceeding 25 °C) for 30 minutes. Samples were then centrifuged at 2000 RCF for 15 minutes at 18-25 °C to separate cellular blood components from serum, following which serum was carefully aliquoted in 500 µL samples into pre-labelled Eppendorf tubes and transferred to a -80 °C freezer for storage. Any evidence of haemolysis was carefully documented for future analyses.

5.7.4 Collection of Blood for Pharmacokinetics

To complete pharmacokinetic assessment following NK1-R administration, a subset of animals underwent additional blood collection (*n*=6, 3M, 3F) as detailed in Chapter 8. By direct venepuncture or via indwelling venous catheter, whole blood was collected in K2EDTA tubes (Vacutainer® K2EDTA tubes, Beckon-Dickinson, Australia). Twelve mL

of blood was taken per animal at the following time points; immediately prior to administration and at 4, 8, 12 16, 24, 28 and 48 hours thereafter. Tubes were gently inverted 180° and back 6-8 times to ensure mixing of anticoagulant to avoid microclotting. Immediately following inversion, samples were placed in an ice bath for 20 minutes, after which samples were centrifuged at 1500 RCF for 10 min at 18-25 °C. Immediately following centrifuge, blood was aliquoted into pre labelled 2 mL iobind polypropylene t tubes (PCR clean, Eppendorf™, Australia). Samples were then flash frozen by immersion in liquid nitrogen for approximately 1 minute, following which cryovials were transferred to a -80 °C freezer for storage.

The NK1-R antagonist was subsequently extracted from plasma samples via protein precipitation extraction. Analytes were separated using high-performance liquid chromatography on an ACE C18-AR column, and the eluates monitored by an API4000™ liquid chromatography mass spectroscopy (SCIEX) in positive multiple reaction monitoring mode. The extracts were then assayed against a calibration cure, data analysed via Analyst® software (SCIEX) and processed in Watson LIMS™ (Thermo Scientific).

5.8 NK1-R TREATMENT ADMINISTRATION

For the NK1-R treatment studies (Chapters 6-8), animals were randomised to receive either the NK1 tachykinin receptor antagonist or equal volume of saline vehicle. The NK1-R compound used, EU-C-001, was supplied by PresSuraNeuro (Hoffmann et al., 2005, Australian Patent AU2002328837B2 (under embargo), May 5, 2005). The dose of NK1-R antagonist was chosen based on previous studies in ovine traumatic brain injury (Vink et al., 2017).

The NK1-R dosing regimen differed across the studies, as detailed in Table 5.5. Treatment was delivered via intravenous jugular catheter (18 g, Terumo SURFLO®) at a volume of 1 mL/kg of 1 mg/mL solution (i.e., 65 kg animal was administered 65 mL of prepared EU-C-001). The EU-C-001 is formulated as a powder and prior to administration was dissolved in warmed (37 °C) sterile saline (e.g., 60 mg EU-C-001 dissolved into 60 mL saline) for administration as a slow bolus over approximately 10 minutes via intravenous line.

Table 5.5 NK1-R antagonist administration regimens

Chapter	NK1-R treatment regimens
6	***3 NK1-R treatment groups***
	1 × NK1 - bolus at 4 h post-stroke onset
	2 × NK1 - bolus at 4 h and 9 h post-stroke
	3 × NK1 - bolus at 4 h, 9 h and 14 h post-stroke
8	***Early NK1-R - treatment commenced at 28 h post-stroke***
	Animals treated on days 1, 2 and 3 post-stroke - bolus of NK1-R antagonist administered, followed by up bolus 5 h later
	Late NK1-R - treatment commenced at 124 h post-stroke
	Animals treated on 5 days post-stroke – bolus of NK1-R antagonist, followed up by bolus 5 h later

5.9 PERFUSION

All animals were humanely killed via exsanguination under general anaesthesia (isoflurane 3%) and were perfused with tris-saline (Tris(hydroxymethyl) aminomethane and sodium chloride solution (Sigma-Aldrich, Australia). Animals were laid in a prone position on a post-mortem table, the neck dissected to expose the carotid arteries, and infusion lines inserted bilaterally and secured into place. Heparin (25000 IU heparin in 5 mL saline, Pfizer,

USA), followed by a 10 mL saline flush was administered via jugular catheter to prevent coagulation following exsanguination. A perfusion pump was attached, and at a pressure of 140 mmHg, sheep were perfused with 4 L of chilled tris-saline via the carotid artery lines, after which the jugular veins were incised, ensuring a clean circuit for tris saline to flow through the brain, clearing out blood from the cerebrovasculature.

Following perfusion and confirmation of death, animals were removed from anaesthesia, endotracheal tube cuff-deflated, and extubated. Animals were then rapidly decapitated, and a hexagon marked at boundaries rostral to the highest point of the orbital ridge, lateral to the head of the coronoid, and caudal at the occipital crests using an oscillating saw. The bone was cut along the boundaries of the hexagon at a depth of approximately 1 cm rostrally, and 0.5 cm caudally and laterally. Using an osteotome, the bone was levered, and the skull cap removed, allowing the brain to be separated from the encasing cranium without damage. The tentorium and cranial nerves were incised, and the brain gently removed from the skull. The brain was then placed in a custom brain matrix and sections cut into 0.5-1 cm coronal slices perpendicular to the dorsal surface, starting at the anterior pole and extending to the cerebellum. Sections were placed with the anterior face down in Pre-Load II embedding cassettes (Leica Biosystems, Australia) and labelled accordingly. Tissue was then immersed in 10% neutral-buffered formalin for a minimum of 14 days to allow for fixation and processing for immunohistochemistry (IHC) thereafter.

Critical coronal sections in the region of the MCA are shown in Figure 5.9, with corresponding neuroanatomical regions shown in both fresh and IHC stained slices in Figure 5.10.

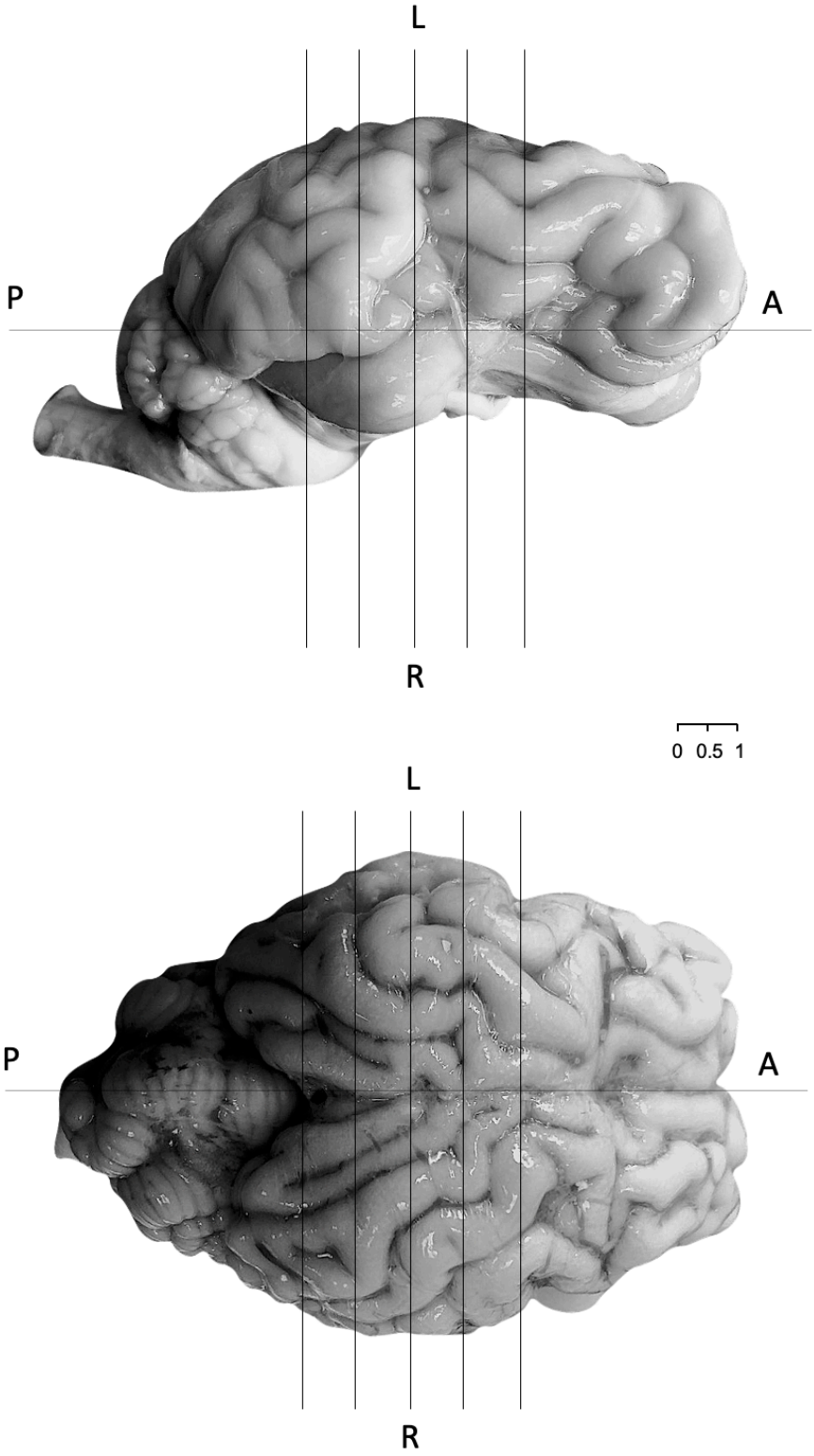

Figure 5.9. Critical coronal brain sections in the territory of the middle cerebral artery (MCA). Locations of sections are indicated by the vertical black line, from anterior to posterior A, B, C and D. Corresponding neuroanatomical landmarks of these sections can be seen in figure 5.9. A – anterior, P – posterior, S- superior, I – inferior, L – left, R – right. Scale bar 1 cm.

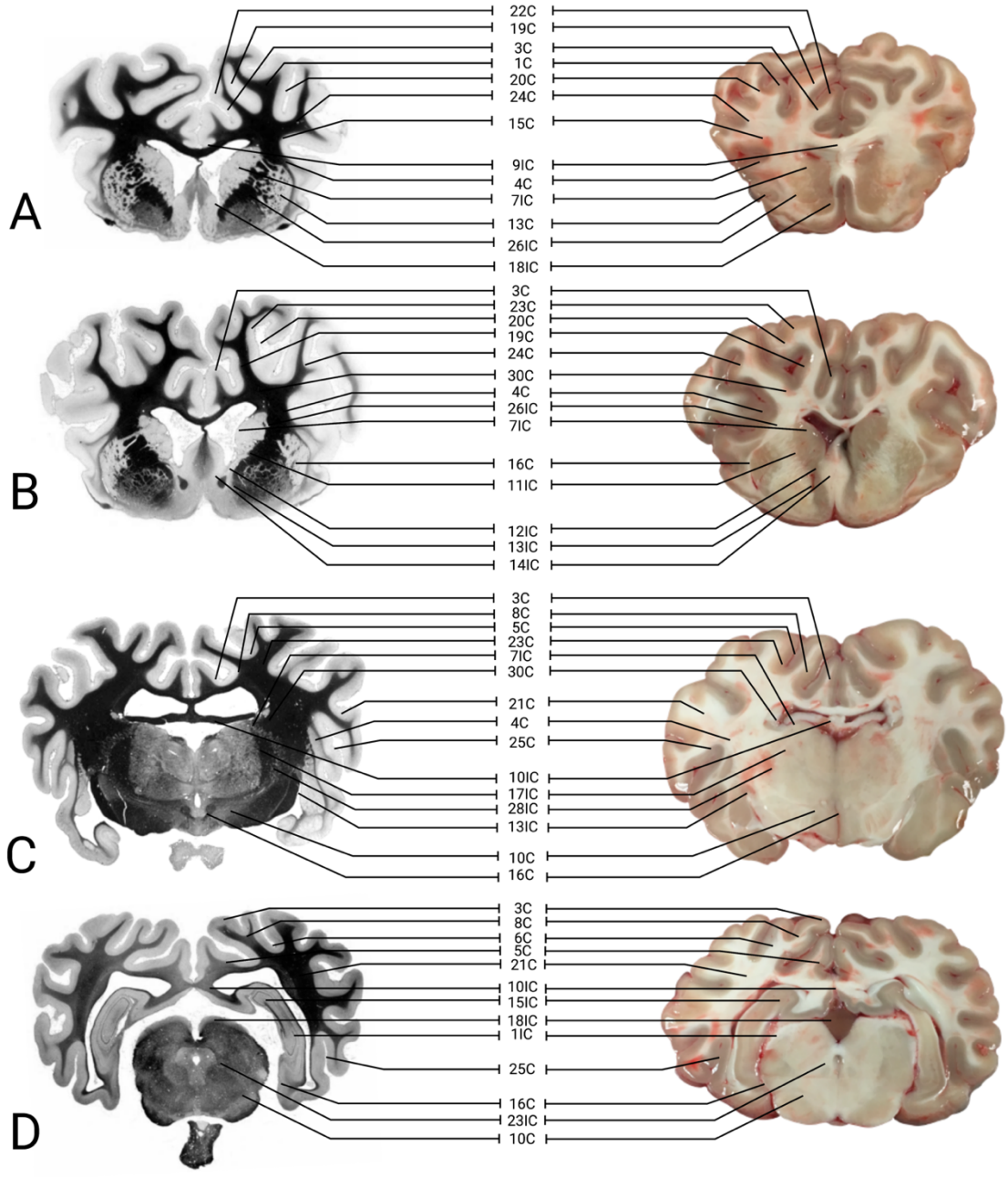

Figure 5.10. Neuroanatomical landmarks of critical coronal sections in the territory of the middle cerebral artery (MCA). The left panel shows the regions on immunohistochemical specimens stained with Weil's myelin stain to better demarcate white matter tracts. The right panel shows regions in fresh brain specimens. Refer to Table 5.4 for corresponding numerical atlas regions. Weil images converted to binary obtained from the University of Wisconsin and Michigan State Comparative Mammalian Brain Collections and National Museum of Health and Medicine Collection. Preparation of images and specimens funded by the National Science Foundation and the National Institutes of Health). Fresh brain images obtained from studies reported herein.

5.10 TTC STAINING

In Chapter 6, 2,3,5-Triphenyltetrazolium chloride (TTC) staining was used to differentiate between metabolically active and inactive brain tissue, in which viable brain tissue stained pink whilst the area of infarct appeared white. A 3% TTC (Sigma-Aldrich, Australia) solution prepared in 10 mL tris-saline was used in which brain slices were immersed. Slices were then placed in a 37 °C water bath and incubated in dark room conditions for a total of 10 minutes on the anterior face and 10 minutes on the posterior face. Anterior and posterior sides of all brain slices were photographed on a flatbed scanner (Canon CanoScan LiDE700F, Canon Inc., Japan) and immersion fixed in 10% neutral-buffered formalin immediately thereafter, as detailed above. Lesion volume was calculated using ImageJ software (Version 1.49v), in which the area of infarct on both the anterior and posterior faces for each slice was calculated and the total area of infarct determined. For the purpose of data analysis, total brain volume was calculated in pixels and area of infarct calculated as a percentage of the whole brain. Due to the infarct being indistinguishable by TTC beyond 3 days following stroke (Mcbride et al., 2015), staining was not repeated for Chapters 7 and 8.

5.11 HISTOPATHOLOGY AND IMMUNOHISTOCHEMISTRY

Fixed brain tissue slices were processed, embedded in paraffin wax and 5-micon coronal sections mounted on silane coated glass slides for histological examination. Haematoxylin and eosin (H&E) staining was used to demarcate the infarct and examine gross pathological abnormalities. Immunohistochemistry (IHC) was used to probe neurogenic inflammation, vasogenic oedema and BBB permeability, with staining details outlined in Table 5.6. Whole

slides were scanned (NanoZoomer 2.0-RS, Hamamatsu Photonics, Japan) and visualised on NDP view software (NDP.view v2.0, Hamamatsu Photonics, Japan) for future assessment.

Table 5.6 Antibody details for immunohistochemistry

Antibody	Dilution	Retrieval	Brand	Catalogue no.
Albumin	1:2000	No retrieval	Dako	A0001
SP	1:5000	Citrate	Abcam	ab14184
Caveolin-1	1:500	EDTA	Cell Signalling Technologies	3238
NK1-R	1:1000	Citrate	Advanced Targeting Systems Pty Ltd	AB-N-33AP

5.12 ENZYME-LINKED IMMUNOSORBENT ASSAY (ELISA)

In Chapter 7, serum and CSF samples were analysed using enzyme-linked immunosorbent assay (ELISA) to determine levels of SP, with plates run according to the manufacturer's instructions (Abcam; KIT-ab133029). All samples were diluted 1:4 in assay buffer for appropriate compliance with each individual plate standard curve. Standards were run along with the serum and CSF samples and the plate immediately analysed following addition of the stop solution using a spectrophotometric microplate reader (Synergy HTX, multi-mode reader). At optical density of 405 nm light absorbance was calculated to give an inverse reading of SP proportional to its captured measure on the plate.

5.13 FUNCTIONAL ASSESSMENT

The assessment of motor function completed in this thesis required a significant period of troubleshooting to determine the most robust method. Firstly, we sought to identify common

deficits observed following ovine stroke in the existing literature, and in our prior studies. Most noticeable was significant deficit of the contralateral fetlock joint, as shown in Figure 5.11. This loss of motor control was seen to affect the distal phalanges, resulting in constant flexion of the joint and impaired gait during forward motion. Postural deficits were also seen, including lowering of the head and shoulders, and behavioral disturbances including circling, apathetic behavior, and reduced food intake.

Figure 5.11. Observable post-stroke motor deficit. Following right middle cerebral artery occlusion, the left forelimb fetlock joint can be seen in partial flexion (foreground of B) compared with the contralateral unaffected limb (foreground of A).

5.13.1 Gait analysis – Hoof Impression Assessment

To assess function of the lower limb and the influence of hemiparesis on gait, we initially sought to emulate commonly used, highly cost-effective rodent gait models, in which animals' paws are painted and animals are encouraged to walk over paper, creating prints

which are used to measure stride length and width. A comparable experiment was designed in which sheep were required to traverse a shallow pit (1 m × 3 m) of semi-soft clay. This necessitated determining the optimum mix of clay and soil to ensure a consistency in which an impression of the hoof could be taken (Figure 5.12A), with the ability to hold its structure when the animal initiated forward movement, whilst simultaneously ensuring it did not dry out. Here, the intention was for hoof impressions to be made in the clay (Figure 5.12B) and measured to provide an estimate of stride length and width, in addition to any differences in weight baring (as indicated by the depth of the impression) pre- and post-stroke. Initial trials of this method, however, proved futile as sheep were completely unwilling to step on the clay, requiring consideration of other methods.

Figure 5.12. Soil and clay combinations for hoof impressions. (A) Determining optimum soil and clay mixtures for hoof impressions using sand, sand and clay, and sand and soil. (B) Once the optimum mixture of sand and clay was determined, the hoof impression of a sheep can be seen.

5.13.2 Gait Analysis – High Speed Cameras

Following failure of hoof impression attempts, quantitative and less tactile means of assessing gait kinematics were considered. Two-dimensional (2D) video analysis of gait, such as use of video cameras, can serve as a means to analyse motion, with systems being adapted using a single camera (Zult et al., 2019). Accordingly, we sought to use a single video camera to measure trajectories of black and white quadrant markers placed at various anatomical locations on the animal to allow us to measure kinematics of the gait cycle.

As sheep are inherently flock animals who spend significant durations engaged in ambulatory grazing (McBride et al., 2016), we sought to design a functional run in which animals could execute forward ambulatory movement during which 2D kinematics could be assessed via video capture. It was imperative the design of the functional testing space was both ethologically suitable for sheep and ensured high quality video data was obtained. It was also important the design was easy to set up, and did not compromise the well-being of the animal, nor the safety of the equipment or personnel working with the animals. Although a functional run was successfully built, unfortunately the camera system trialed did not operate at a sufficient frame rate to accurately capture marker trajectories.

5.13.3 Gait Analysis – Motion Capture

The preferred approach for the kinematic assessment of gait is the use of a three-dimensional (3D) motion analysis system. These systems typically incorporate multiple cameras and active (light-emitting diodes), or passive (retro reflective) markers. The 3D analysis of gait is highly accurate and reliable and is commonly reported in the clinical literature. Assessment of motion using such a system following stroke in the ovine model could provide quantitative and discreet measures relating to stride length, stance duration, swing duration

and joint angle. Accordingly, we sought to use a Vicon Vero motion capture system (Vicon Motion Capture Systems, Oxford, UK) to overcome the challenges associated with 2D video assessment, in conjunction with a standard composite scoring system to allow for assessment of function beyond the scope of kinematic assessment. Detailed methodologies are reported in Chapter 9.

5.14 EXCLUSION CRITERIA

Animals excluded across the studies are summarised in Table 5.5. For Chapter 7, 8 and 9, animals were excluded early in the experimental course, and therefore, replacement animals were produced retrospectively. For Chapter 6, data was unfortunately lost after completion of the experiment, and animals were unable to be regenerated due to lapse of ethics.

Table 5.7 Details of animal exclusions for each study

Chapter	Study total	No. animals excluded	Reason(s)	No. animals included in analysis
Chapter 6	34	8	Significant data loss due to system failure of PACS system where original MRI data was stored. MRI data for a total of 8 animals was lost. There was no premature mortality seen in this study.	26
Chapter 7	47	5	1 animal was excluded due to insufficient reperfusion following MCAo, as seen on MRA, resulting in a permanent rather than a transient occlusion. 4 animals were excluded due to significant anaesthetic difficulties which confounded the experimental course, with animals unstable throughout the induction of stroke surgery, necessitating repeat boluses of ketamine and diazepam and a prolonged increase in the percentage of isoflurane required to maintain surgical levels of anaesthesia, which resulted in significantly lowered MABP, decreased cerebral perfusion pressure and ultimately profound infarct expansion.	42
Chapter 8	18	0	No animals excluded, surgery and post-operative recovery was carried out without complication.	18
Chapter 9	30	2	1 animal was excluded due to permanent MCAo, as identified on MRA, resulting in significant loss of function necessitating euthanasia 24 hours post stroke 1 animal was excluded due to kidney failure, most likely as a result of excessive GAD accumulation. The animal deteriorated over time, and by day 10 post-stroke was significantly impaired, necessitating euthanasia.	28

5.15 STATISTICAL ANALYSES

Data analyses were performed using GraphPad Prism (Chapters 6, 7, 8 and 9) and Stata Corp (Chapter 9). One-way analysis of variance (ANOVA) and Tukey's post-hoc analyses were performed for ICP, cerebral oedema, midline shift and infarct volume. Two-way ANOVAs with Sidak's post-hoc tests were used to determine gender differences where appropriate. Pearson's correlations were also be run to determine the relationship between outcomes measures of interest in each individual chapter. Intraclass Correlation Coefficients (ICC) and mixed effects linear regression models were fitted to assess gait kinematics, and two-way ANOVAs with Friedman post-hoc tests to determine differences in composite scoring in Chapter 9. Data are presented as SEM, SD or 95% CI. A p value <0.05 and an R value >0.04 was considered significant throughout each experimental chapter.

06

NK1-R Antagonist Treatment Comparable to Decompressive Craniectomy in Reducing Intracranial Pressure Following Stroke

Presented as accepted for publication by **SORBY-ADAMS, A. J.**, LEONARD, A. V., HOVING, J. W., YASSI, N., VINK, R., WELLS, A. J. & TURNER, R. J. 2019. NK1-R Antagonist Treatment Comparable to Decompressive Craniectomy in Reducing Intracranial Pressure Following Stroke. *Frontiers in Neuroscience,* 13**,** 681.

Statement of Authorship

Title of Paper	NK1-R Antagonist Treatment Comparable to Decompressive Craniectomy in Reducing Intracranial Pressure Following Stroke
Publication Status	☑ Published ☐ Accepted for Publication ☐ Submitted for Publication ☐ Unpublished and Unsubmitted w ork w ritten in manuscript style
Publication Details	Sorby-Adams, A.J., Leonard, A.V., Hoving, J.W., Yassi, N., Vink, R., Wells, A.J., and Turner, R.J. (2019). NK1-r Antagonist Treatment Comparable to Decompressive Craniectomy in Reducing Intracranial Pressure Following Stroke. *Front Neurosci* 13, 681.

Principal Author

Name of Principal Author (Candidate)	Annabel Sorby-Adams		
Contribution to the Paper	I performed the immunohistochemistry, analysed MRI, pressure, and immunohistochemistry data, wrote the manuscript, and was the main and corresponding author.		
Overall percentage (%)	40%		
Certification:	This paper reports on original research I conducted during the period of my Higher Degree by Research candidature and is not subject to any obligations or contractual agreements with a third party that would constrain its inclusion in this thesis. I am the primary author of this paper.		
Signature		Date	16.03.2021

Co-Author Contributions

By signing the Statement of Authorship, each author certifies that:

i. the candidate's stated contribution to the publication is accurate (as detailed above);

ii. permission is granted for the candidate in include the publication in the thesis; and

iii. the sum of all co-author contributions is equal to 100% less the candidate's stated contribution.

Name of Co-Author	Renee Turner		
Contribution to the Paper	Associate Professor Renee Turner is the head of the Translational Neuropathology Laboratory and primary investigator on this thesis. She oversaw experimental design and performed the surgeries, perfusions and assisted with manuscript preparation and editing.		
Signature		Date	16.03.2021

Name of Co-Author	Anna Leonard		
Contribution to the Paper	Dr Anna Leonard is a member of the Translational Neuropathology Laboratory and on the supervisory panel for this thesis. She was involved in the surgeries and provided intraoperative support, assistance with physiological monitoring and perfusion, in addition to structure and editing of the manuscript.		
Signature		Date	16.03.2021

Name of Co-Author	Nawaf Yassi		
Contribution to the Paper	Associate Professor Nawaf Yassi is a neuroradiologist from the Royal Melbourne Hospital. He provided expert advice regarding imaging protocols and analysis.		
Signature		Date	16.03.2021

Name of Co-Author	Jan Hoving		
Contribution to the Paper	Dr Jan Hoving is a medical radiologist from the University of Amsterdam. He analysed the MRI infarct volume and provided guidance, assistance and training of protocols.		
Signature		Date	16.03.2021

Name of Co-Author	Robert Vink		
Contribution to the Paper	Professor Robert Vink was the past head of the Translational Neuropathology Laboratory. He oversaw experimental design.		
Signature		Date	16.03.2021

Name of Co-Author	Adam Wells		
Contribution to the Paper	Dr Adam Wells pioneered the non-recovery approach to ovine stroke in the Translational Neuropathology Laboratory in his doctoral studies. He provided expert advice regarding experimental design.		
Signature		Date	16.03.2021

6.0 ABSTRACT

Background and Purpose: The morbidity and early mortality associated with stroke is largely attributable to cerebral oedema and elevated intracranial pressure (ICP). Existing pharmacotherapies do not target the underlying pathophysiology and are often ineffective in sustainably lowering ICP, whilst decompressive craniectomy (DC) surgery is lifesaving yet with surgical/peri-operative risk and increased morbidity in the elderly. Accordingly, there is an urgent need for therapies that directly target the mechanisms of oedema genesis. Neurogenic inflammation, mediated by substance P (SP) binding to the tachykinin NK1 receptor (NK1-R), is associated with blood-brain barrier (BBB) disruption, cerebral oedema and poor outcome post-stroke. NK1-R antagonist treatment ameliorates BBB dysfunction and cerebral oedema in rodent stroke models. However, treatment has not been investigated in a large animal model, an important step towards clinical translation. Consequently, the current study compared the efficacy of NK1-R antagonist treatment to DC surgery in reducing ICP post-stroke in a clinically relevant ovine model.

Methods: Anaesthetised female Merino sheep (65±6 kg, 18-36 months) underwent sham surgery (*n*=4) or permanent middle cerebral artery occlusion (*n*=22). Stroke animals were randomised into one of 5 treatments: 1 × NK1-R bolus (4h), 2 × NK1-R bolus (4h; 9h), 3 × NK1-R bolus (4h; 9h; 14h), DC surgery (performed at 4h) or saline vehicle. ICP, blood pressure and blood gases were monitored for 24h post-stroke. At 24h post-stroke anaesthetised animals underwent MRI, followed by perfusion, removal and processing of brains for histological assessment.

Results: Two × NK1-R, 3 × NK1-R administration or DC surgery significantly ($p<0.05$) reduced ICP compared to vehicle. 1× NK1-R was ineffective in sustainably lowering ICP. On MRI, midline shift and cerebral oedema were more marked in vehicles compared to NK1-R treatment groups.

Conclusion: Two or 3 boluses of NK1-R antagonist treatment reduced ICP comparable to DC surgery, suggesting it may provide a novel alternative to invasive surgery for management of elevated ICP post-stroke.

6.1 INTRODUCTION

Elevated intracranial pressure (ICP) arising as a result of malignant cerebral oedema is the leading cause of death in the first week following stroke (Hacke et al., 1996). Despite the devastating impact of elevated ICP on patient outcome, clinical management remains sub-optimal. Pharmacological options for ICP management are limited, and while osmotic therapies (including mannitol and hypertonic saline) are used in some centres (Zhang et al., 2018), there is no evidence that these therapies are independently effective in improving outcome. Furthermore, the efficacy of other pharmacological interventions including corticosteroids and barbiturates remain ambiguous for the treatment of post-stroke cerebral oedema (Brogan and Manno, 2015). In selected patients with malignant middle cerebral artery (MCA) territory infarction, surgical intervention with decompressive craniectomy (DC) may be required. This procedure rapidly alleviates pressure by removing a large portion of the skull and opening the dura overlying the swollen brain, thereby providing space for the oedematous brain to swell freely until cerebral oedema resolves, typically beyond the first week following stroke (Xiao-Feng et al., 2005). However, although this procedure reduces compression on cerebral structures and the risk of life-threatening tonsillar herniation, it is also associated with increased morbidity in those aged greater than 60 years, the patient population in which stroke is most prevalent (Jüttler et al., 2007, Das et al., 2019). It is clear that current pharmacological and surgical interventions are inadequate as they target the symptoms, rather than the underlying cause of cerebral oedema and concomitant rise in ICP (Bardutzky and Schwab, 2007, Simard et al., 2007). An enhanced understanding of the mechanisms that underlie the genesis of cerebral oedema and raised ICP is thus critical for the development of more targeted and effective treatments.

Although factors associated with the pathogenesis of cerebral oedema are not completely understood, neurogenic inflammation has been identified as a potential therapeutic target (Corrigan et al., 2016a, Stumm et al., 2001, Turner et al., 2006). Neurogenic inflammation is a neurally-mediated process involving the release of neuropeptides, including substance P (SP) and calcitonin gene-related peptide, which initiate vasodilation, increased microvascular permeability and oedema (Hokfelt et al., 2000). Although well established as a precipitant of oedema development within peripheral tissues such as the skin and lungs (Alves et al., 1999), neurogenic inflammation remained largely unexplored as a potential mechanism of cerebral oedema development (Lewis et al., 2013, Sorby-Adams et al., 2017). This was until studies depleting neuropeptides or blocking the action of neuropeptide SP at the tachykinin NK1 receptor (NK1-R), to which SP binds preferentially, showed a ubiquitous role for this process in the genesis of cerebral oedema following stroke and traumatic brain injury (TBI) (Nimmo et al., 2004, Donkin et al., 2009, Turner et al., 2011b, Turner and Vink, 2014, Turner et al., 2006, Turner and Vink, 2012, Vink et al., 2003, Corrigan et al., 2016a). Specifically, increased SP immunoreactivity within the penumbral perivascular tissue is associated with profound BBB disruption and cerebral oedema at 24 hours post-stroke and poor functional outcomes up to 7 days following middle cerebral artery occlusion (MCAo) in rats, with NK1-R blockade ameliorating these effects (Turner et al., 2011b, Turner and Vink, 2012, Turner and Vink, 2014, Corrigan et al., 2016a). Increased plasma SP levels have also been reported clinically following severe acute ischaemic stroke, elevated levels of which were associated with increased mortality (Lorente et al., 2016). Comparable alterations in SP levels have also been observed in clinical TBI correlating with injury severity and mortality (Lorente et al., 2015).

The cumulative evidence from these studies suggests an important role for SP in the development of cerebral oedema and poor outcome following acute CNS injury. However, pre-clinical evaluation of the NK1-R antagonist has been limited to small animal stroke models, with the most extensive screening to date performed in small and large animal models of TBI. Whilst rodent species are essential for establishing basic biological processes, it is often difficult to obtain clinically relevant outcome measures, thereby limiting clinical translation. Given the extremely poor translation of stroke neuroprotectants from the laboratory to the clinic (Xu and Pan, 2013), evaluation of promising therapies in a large, intermediate species is essential. Species such as sheep are an ideal candidate for such studies due to the ability to utilise clinically relevant outcome measures in addition to similarities in neuroanatomical structure, including gyrencephalic cerebral organisation and significant portion of white matter (Sorby-Adams et al., 2018). Of particular relevance when investigating elevated ICP; however, is the strong tentorium cerebelli of the sheep, separating supra- and infra- tentorial compartments, bearing structural similarity to that of the human (Dostovic et al., 2016). In the setting of clinical malignant cerebral oedema, this leads to compartmentalisation of pressure within the supratentorial space, tonsillar herniation, and ultimately often fatal compression of the brain stem as the brain attempts to alleviate dangerously elevated ICP. Indeed, ovine stroke models replicate key clinical hallmarks following stroke including elevated ICP, cerebral oedema, midline shift and tonsillar herniation (Wells et al., 2012, Wells et al., 2015, Sorby-Adams et al., 2018). As such, the aim of the present study was to determine the effect of inhibition of SP with an NK1-R antagonist, compared to DC surgery, on ICP following permanent ischaemic stroke in an ovine model.

6.2 MATERIALS AND METHODS

6.2.1 Experimental Procedure

All experimental procedures were approved by the Animal Ethics Committees of the University of Adelaide (M-2011-240) and South Australian Health and Medical Research Institute (SAHMRI; SAM104) and conducted according to guidelines established for the use of animals in experimental research as outlined by the Australian National Health and Medical Research Council code of practice for the care and use of animals for scientific purposes (8th edition, 2013).

6.2.2 Animals and Experimental Design

Female merino sheep (*n*=26) aged 18–24 months old (65±6 kg) were allocated to the study. Animals were randomised into either sham surgery or permanent MCA occlusion (MCAo). Following induction of stroke, animals were then further randomised into one of the following groups: 1) saline vehicle treatment at 4 hours post-stroke (*n*=6); 2) 1 × bolus NK1-R antagonist at 4 hours post-stroke (*n* =3); 3) 2 × boluses of NK1-R antagonist at 4 hours and 9 hours post-stroke (*n* =3); 4) 3 × boluses of NK1-R antagonist at 4-, 9- and 14-hours post-stroke (*n*=6); or 5) decompressive craniectomy (*n*=5) at 4 hours post-stroke. Note that the dose for the NK1-R antagonist treatment was the same across all the NK1-R treatment groups, the only difference was the number of boluses that each group received, either one (1 × NK1-R), two (2 × NK1-R) or three (3 × NK1-R) boluses. The NK1-R antagonist used in the study was a test compound supplied by PresSuraNeuro (Hoffmann et al., 2005, Australian Patent AU2002328837B2, May 5, 2005), prepared at a concentration of 1 mg/mL in warmed saline (37 °C) and administered at a dose of 1 mL/kg via an indwelling jugular venous catheter, as per previous studies in our laboratory (Vink et al., 2017).

6.2.3 Anaesthesia and Physiological Monitoring

Anaesthesia was induced with intravenous thiopentone (1000 mg in 20 mL, Jurox Pty Ltd, Australia) and maintained with 1.5% inhalational isoflurane (Veterinary Companies of Australia Pty Ltd, Australia) in a mixture of oxygen and room air (500:5000 mL/min), plus intravenous ketamine (Parnell Australia Pty Ltd, Australia) infusion at 4 mg/kg/hr via a femoral venous line. These two anaesthetic agents were used in combination to avoid the intrinsic neuroprotective properties of either above certain doses, and to maintain a twilight general anaesthesia (Schifilliti et al., 2010, Hudetz and Pagel, 2010). With the animal supine, an arterial catheter was placed in the right femoral artery for continuous blood pressure monitoring and periodic arterial blood gas sampling, and a venous catheter inserted for anaesthetic and fluid administration. The animal was then placed prone in the sphinx position, a burr hole drilled in the right parietal bone posterior to the coronal suture and approximately 20 mm from the sagittal suture, dura perforated, and skull bolts secured. A Codman microsensor ICP probe (Codman & Shurtleff Inc., Massachusetts) was introduced into the bolt, calibrated, and inserted intraparenchymally to measure ICP within the supratentorial compartment. Using LabChart Reader (v 8.1.1), mean arterial blood pressure (MABP) and ICP were continuously recorded throughout the 24-hour monitoring period. Arterial blood gas sampling was conducted prior to MCAo or sham surgery and at hourly intervals throughout the monitoring period until the completion of the experiment to maintain physiological pO_2, pCO_2 and pH.

6.2.4 Surgical Approach to MCAo

We have previously described the surgical approach to proximal MCAo in detail (Wells et al., 2015, Wells et al., 2012). Briefly, a 5 cm vertical incision was made posterior to the right eye, terminating at the zygomatic arch. The underlying muscle was retracted, coronoid

process removed, and the skull revealed. A small craniotomy was performed at the junction of the parietal and squamous temporal bones with a high-speed pneumatic drill using a 5 mm cutting burr (Midas Rex® Legend, Medtronic, USA). All intra-dural work was carried out with loupe magnification and a head mounted light source (Surgical Acuity, Wisconsin). A horse-shoe shaped durotomy was performed with an inferiorly based flap allowing for gentle upward retraction of the anterior temporal lobe to achieve visualisation of the proximal MCA. Animals then either underwent sham surgery in which the proximal MCA was dissected but not occluded, or permanent MCA in which the proximal MCA was occluded via Malis bipolar diathermy forceps (Valleylab Inc., Colorado). The exposed brain was irrigated with saline during surgery to prevent dehydration of the cerebral cortex. After completion of sham or MCAo surgery the dura was approximated, and synthetic dura (Durepair®, Medtronic, USA) interleaved under the existing dura (in the case of dural retraction following incision) and closed watertight with ethyl cyanoacrylate (Bostik, Australia). Once dural closure was confirmed and no leakage of CSF observed, the craniotomy site was reinforced with dental acrylic cement (Lang Dental, IL) that was manipulated into the edge of the craniotomy and the wound closed in layers, maintaining the shape of the cranial cavity and importantly, the homeostasis of ICP dynamics. For animals allocated to the DC group, at 4h following stroke the wound was opened, dental acrylic removed, and the craniotomy site widened (3 cm x 6 cm) to allow for decompression. A dural pouch was created using Durepair to expand the intracranial cavity, after which the bone was left off and the overlying skin sutured closed, simulating clinical DC and expansile duraplasty. For all groups, the head was then returned to a neutral position for monitoring under general anaesthesia.

6.2.5 Magnetic Resonance Imaging

At 24 hours following stroke or sham surgery onset animals were placed under general anaesthesia (3% isoflurane) in a 1.5 Tesla Siemens Sonata (Siemens AG, Munich, Germany) magnetic resonance imaging (MRI) scanner. The scanning sequence included time-of-flight magnetic resonance angiography (TOF MRA; TR 26.0 ms, TE 3.69 ms, slice thickness 0.50 mm, slices per slab 48), diffusion weighted imaging (DWI; TR 5600.0 ms, TE 80 ms, slice thickness 3.0 mm, slices per slab 25), fluid attenuated inversion recovery (FLAIR; TR 5000.0 ms, TE 386 ms, slice thickness 0.9 mm, slices per slab 96), T_1 (TR 2300.0 ms, TE 2.58ms, slice thickness 0.9 mm, slices per slab 96) and T_2 (TR 3200 ms, TE 410 ms, slice thickness 0.9 mm, slices per slab 96) weighted images.

The degree of midline shift on MRI was used as a marker of the amount of expansion of the infarcted hemisphere, indicative of cerebral oedema. Extent of shift from the midline was assessed using axial T_2 weighted scans and measured in mm from the septum pellucidum at the level of the foramen of Monro (HOROS DICOM image viewer v3.1.1). To calculate cerebral oedema, coronal FLAIR images were analysed using HOROS (v3.1.1). After optimal adjustment of brightness and contrast, oedema volume was determined from sequences using computer-aided manual tracing of the hyperintense lesion by a blinded assessor. The areas were then summed and multiplied by the slice thickness to give a total volume in cm^3.

To calculate infarct volume, segmentation tools in ITK-SNAP (v 3.7) were used to perform semi-automated segmentation of the MRI diffusion lesions using diffusion-weighted images (Yushkevich et al., 2006). A combination of “three-dimensional active contour segmentation” and subsequent manual post-processing of the segmentation while adjusting

image thresholds was performed to maximise reproducibility whilst excluding artefacts. The "three-dimensional active contour segmentation" consisted of multiple steps: First, in the pre-segmentation phase, independent component analysis automatically segmented parts of the DWI image and these were manually identified as foreground or background. To obtain an optimal distinction between foreground and background, thresholds of the image windows were adjusted. After thresholding, a "speed image" with a separate foreground and background was created. Next, in the active contour phase, seed regions were manually placed within the region of interest (ROI). These seeds were then automatically grown within the ROIs to form the temporary segmentation. Subsequently, areas that were not automatically included in the "active contour segmentation", were manually included in the follow-up infarct segmentation. The total volume of the segmentation was exported and reported in cm^3 for analysis.

6.2.6 Histological Examination

Following MRI, intravenous heparin (5000 I.U./5mL; Pfizer, New York) was administered and animals euthanised via common carotid perfusion fixation with cold TRIS-buffered saline under isoflurane anaesthesia. The brains were subsequently removed and sliced into 10 mm coronal slices using a custom-made matrix. Sections were then immersion fixed in 10% neutral-buffered formalin for a minimum of 14 days prior to being processed, embedded in paraffin wax and sectioned coronally at 5-micron intervals for histological examination by haematoxylin and eosin (H&E), albumin (1:2000, Dako Pty Ltd; A0001), SP (1:5000 citrate retrieval, Abcam Pty Ltd; ab14184), NK1-R (1:1000 citrate retrieval, Advanced Targeting Systems Pty Ltd; AB-N-33AP) and caveolin-1 (cav-1; 1:1000 EDTA retrieval, Cell Signalling Technologies Pty Ltd; 3238) immunohistochemistry.

6.2.7 Statistical Analysis

All data are expressed as mean ± SD. Physiological data (arterial blood pressure, pH, pO_2, pCO_2) were analysed using one-way analysis of variance (ANOVA) followed by Tukey's post-hoc tests (Prism v.8.0.1, GraphPad, California). Values were averaged for each treatment group across all time points and reported as a single value. Raw ICP and MABP data underwent a logarithmic exponential transformation as previously described and were expressed as geometric mean ± SD (Wells et al., 2015, Matthews et al., 1990). ICP was analysed by two-way ANOVA and lesion volume, cerebral oedema and midline shift data were analysed by one-way ANOVA, all followed by Tukey's post-hoc tests. A p-value of <0.05 was considered significant. Correlations were performed between cerebral oedema and midline shift; ICP and cerebral oedema; to determine the relationship between these variables, with an R-value >0.04 considered significant throughout.

6.3 RESULTS

6.3.1 Surgery, Mortality and Physiological Parameters

All experimental procedures were carried out without complication and there was no premature mortality or unexpected events in any of the groups. Basic physiological parameters are expressed in Table 6.1. For all groups, there was no statistically significant difference in pO_2, pCO_2, or pH at any of the time-points following stroke. However, there was a statistically significant difference in MABP between sham, 1 × NK1-R ($p=0.02$) DC ($p=0.02$) and 3 × NK1-R ($p=0.006$) treatment groups.

Table 6.1 Basic physiological parameters

Group	pCO_2 (mmHg) ± SD	pO_2 (mmHg) ± SD	MABP (mmHg) ± SD	pH (-log [H^+]) ± SD
Sham	43±8.41	113±14.09	79±8.78	7.48±0.039
Vehicle	40±6.09	127±31.28	104±10.17	7.46±0.062
1× NK1-R	36±2.55	138±25.06	112±10.18	7.51±0.033
2 × NK1-R	43±6.56	149±33.99	98±5.81	7.45±0.031
3 × NK1-R	37±2.34	135±20.53	111±15.66	7.52±0.018
DC	42±3.78	150±17.22	108±10.65	7.45±0.082

6.3.2 Intracranial Pressure

ICP remained physiologically stable across all time points in sham animals (9±3 mmHg). At both 4- and 9-hours post-stroke, there was no significant difference in ICP between sham or any of the stroke groups. By 14 hours following injury, ICP in vehicle animals was significantly elevated (24±11 mmHg) compared with shams (10±3 mmHg) (p=0.019). However, no difference in ICP was seen between vehicle or any of the treatment groups at this time-point (Figure 6.1).

ICP in vehicle animals continued to rise and by 19 hours post-stroke measured 32±11 mmHg, which was significantly elevated (p=0.0002) compared with shams recording an ICP of 13±6 mmHg. Following intervention, by 19 hours there was a significant reduction in ICP seen in 2 × NK1-R (18±4 mmHg; p=0.013), 3 × NK1-R (17±7 mmHg; p=0.015) and DC (19±11 mmHg; p=0.042) treated animals compared with vehicle. Conversely, there was no reduction (p>0.05) in ICP seen following 1 × NK1-R treatment (31±9 mmHg) compared with vehicle, with ICP remaining significantly elevated compared with sham (p=0.002).

By the 24-hour post-stroke time-point, ICP in vehicle animals had continued to rise (39±7 mmHg) and remained significantly elevated compared with shams (12±8 mmHg; p<0.001), DC (23±12 mmHg; p=0.013), 2 × NK1-R (20±6 mmHg; p<0.001) and 3 × NK1-R (19±7 mmHg; p<0.005) treated animals. ICP continued to rise in the 1 × NK1-R treatment group

(35±9 mmHg) and remained significantly elevated compared with both shams ($p<0.001$) and 2 × NK1-R ($p=0.029$) treatment animals. ICP in 2 × NK1-R and 3 × NK1-R treatment groups was comparable ($p>0.05$) with DC across all time points following stroke. No rebound increases in ICP were observed following 2 × NK1-R or 3 × NK1-R treatment at any time-point post-stroke.

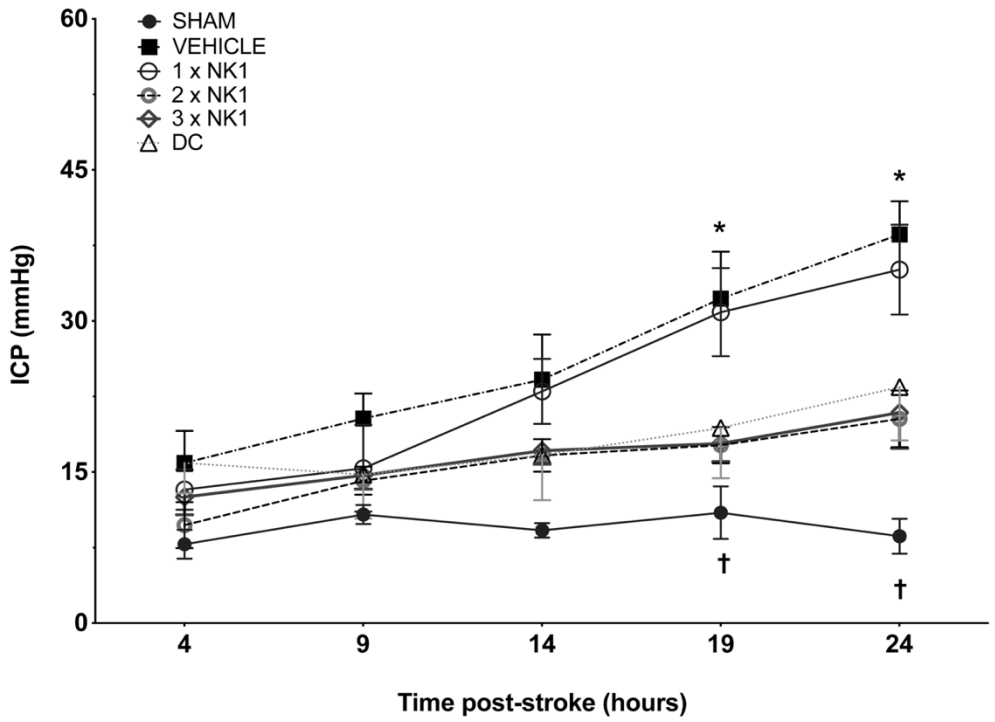

Figure 6.1. 24-hour ICP following middle cerebral artery occlusion. There was no significant difference in sham ICP across any of the time points. At 14 h post-stoke ICP was elevated in vehicle animals compared with shams ($p<0.05$) and by 19 h post-stroke, ICP was significantly elevated in vehicle ($p<0.001$) and 1× NK1-R ($p<0.01$) treated animals when compared with 2 × NK1-R ($p<0.05$), 3 × NK1-R ($p<0.05$) and DC treatment groups ($p<0.05$). By 24 h, ICP remained significantly elevated in vehicle animals compared with sham ($p<0.0001$), 2 × NK1-R ($p<0.01$), 3 × NK1-R ($p<0.01$) and DC ($p<0.05$) treatment groups. ICP also remained elevated at 24 h post-stroke in 1 × NK1-R treatment groups compared with sham ($p<0.001$) and 2 × NK1-R ($p<0.05$). Data presented as mean ± SD. *=$p<0.05$ compared to sham; †=$p<0.05$ compared with vehicle.

6.3.3 MRI

MRI was unremarkable in sham animals (n=4) with no evidence of cerebral oedema, midline shift or infarction (Figure 6.2 A). At 24 hours, all stroke animals showed evidence of hyperintensity on T_2 weighted and FLAIR images in the territory of the MCA, indicative of the infarct core and surrounding vasogenic oedema (Figure 6.2). In addition, DC treated animals showed evidence of transcalvarial herniation through the craniectomy site (Figure 6.2 D). No animals showed evidence of tonsillar herniation or brain stem compression on MRI (data not shown).

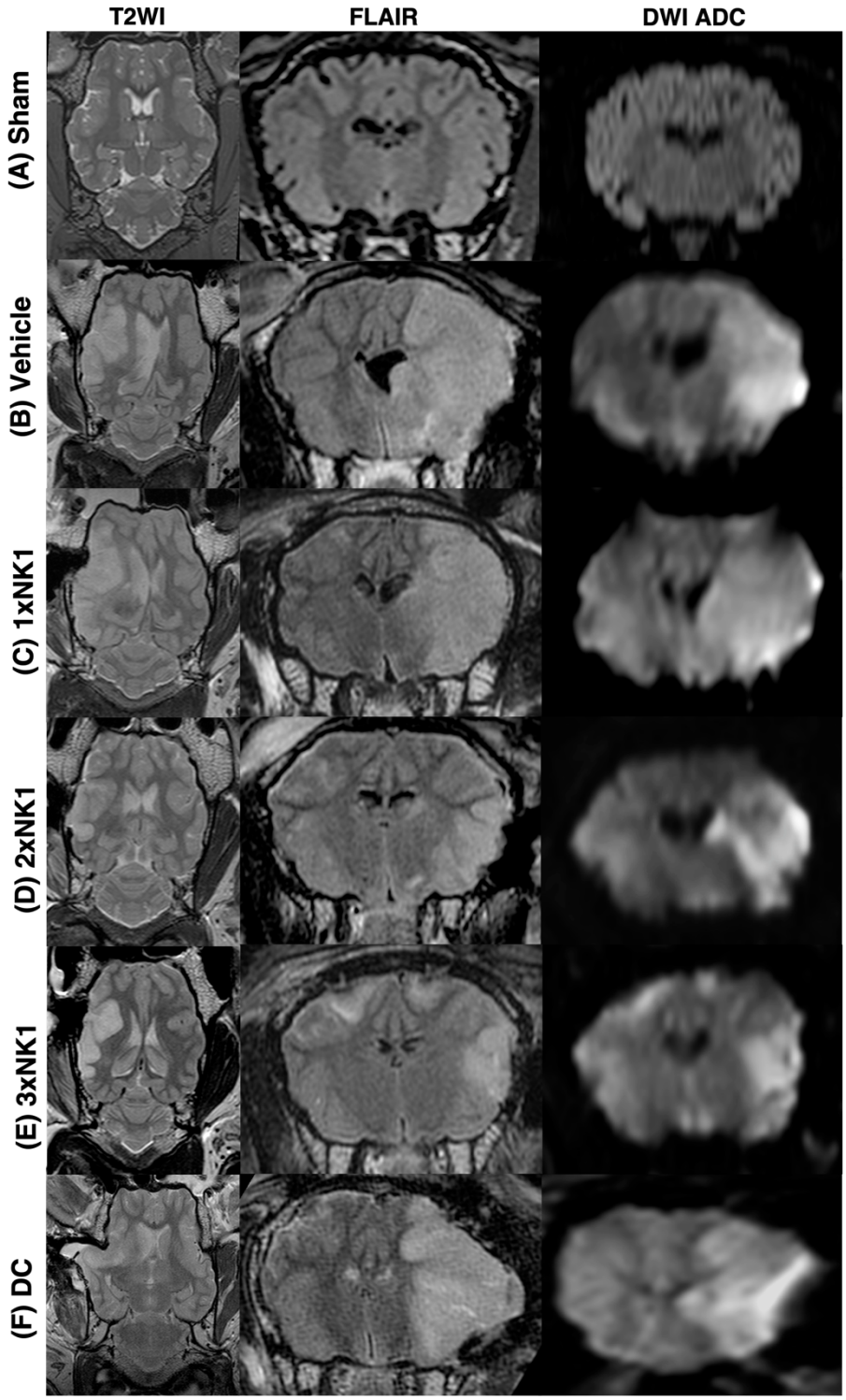

Figure 6.2. MRI findings 24h post middle cerebral artery occlusion. There was no evidence of hyperintensity, or tissue deformation, seen in sham animals (A). Midline shift was evident in all stroke animals as seen on axial T_2 weighted images (B-D). Cerebral oedema as shown in coronal FLAIR MRI images was greater in vehicle (B), DC (F) and 1 × NK1-R (C) groups compared with 2 × NK1-R (D) and 3 × NK1-R (E) groups. This was associated with a smaller lesion volume as shown in DWI MRI images in the coronal plane. Note the transcalvarial herniation through the craniotomy site in DC treated animals (F).

Cerebral oedema calculated on FLAIR MRI (Figure 6.3, Table 6.2) was reduced in DC ($p=0.012$) and 1 × NK1-R treatment groups ($p=0.042$) when compared with vehicle (Fig.3A). However, treatment with 2 × NK1-R ($p=0.001$) and 3 × NK1-R ($p=0.001$) was associated with a more significant reduction in cerebral oedema volume compared with vehicle (Figure 6.3 A). Midline shift was evident in all stroke animals (Table 6.2) with no statistical significance seen between groups ($p=0.2$; Figure 6.3 B). Nevertheless, there was a moderate positive relationship between the volume of cerebral oedema and the amount of midline shift ($r=0.46$; Figure 6.3 C). No significant differences ($p=0.17$) were observed in infarct volume across any of the treatment groups following stroke, as measured on DWI MRI (Figure 6.3 D).

Table 6.2 MRI characteristics post middle cerebral artery occlusion

Treatment	Oedema FLAIR MRI (cm3)	Midline Shift T_2 (mm)	Infarct DWI MRI (cm3)
Vehicle			
86	19.48	1.8	33.9
87	36.45	3.5	24.5
60	20.96	3	25.9
66	31.14	2	34.4
57	27.61	3.5	20.1
59	23.32	3.4	56.5
Mean±SD	25.56±6.10	2.87±0.71	32.55±11.85
1 × NK1			
69	10.84	1.8	22.1
75	21.51	3.2	23
88	11.44	2.2	12.7
Mean±SD	14.60±6.0	2.40±0.72	19.27±5.70
2 × NK1			
70	4.230	0.8	8.3
72	3.520	0.5	17.2
91	11.789	2.6	34.7
Mean±SD	6.51±4.58	1.30±1.14	20.07±13.43
3 × NK1			
71	5.49	1.8	11.6
73	13.50	2.7	20.7
74	7.56	0.7	10.6
76	8.33	1.1	20.8
89	18.23	4.1	32.1
90	16.27	1.7	23.7
Mean±SD	11.56±5.17	2.02±1.23	19.92±8.0
DC			
101	19.38	2.6	26.8
102	15.46	2.9	23.7
105	15.74	1	16.6
106	12.80	1.4	15.6
107	8.36	1.8	24
Mean±SD	14.35±4.08	1.94±0.78	21.34±4.95

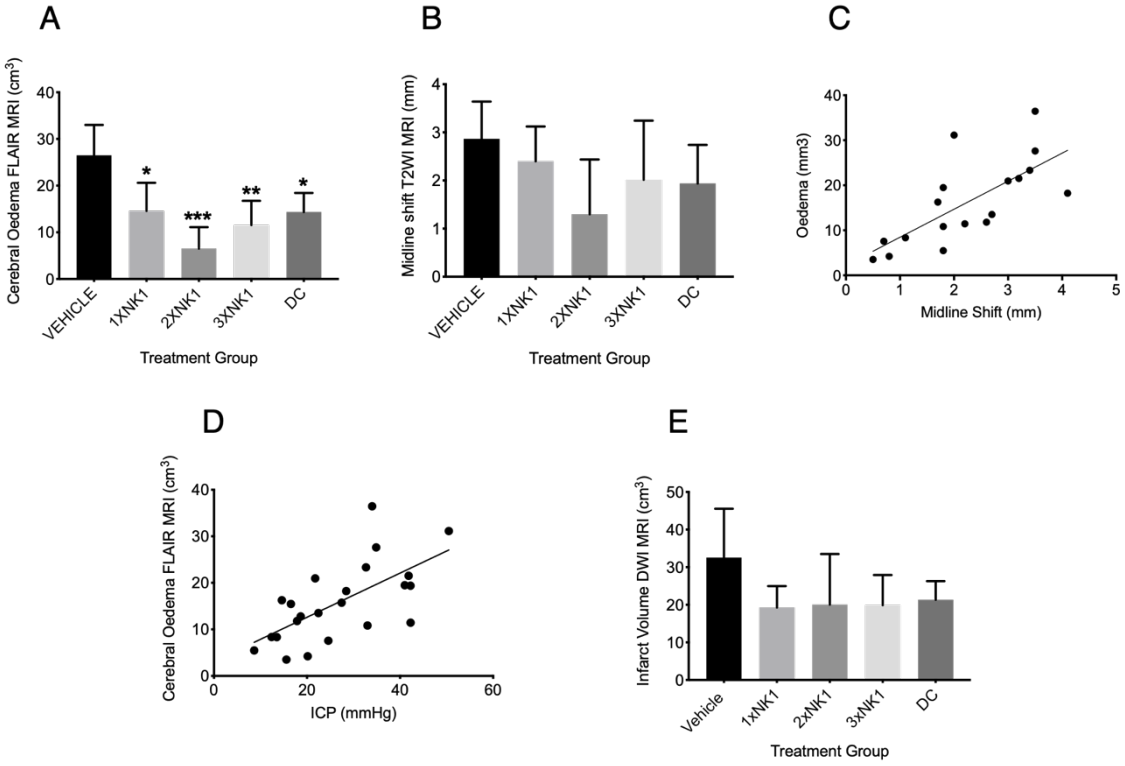

Figure 6.3. Cerebral oedema and infarct volume findings at 24 hours post middle cerebral artery occlusion. (A) Cerebral oedema volume, as measured on FLAIR MRI, was decreased in 1 × NK1-R ($p<0.05$), 2 × NK1-R ($p<0.001$), 3 × NK1-R ($p<0.01$) and DC ($p<0.05$) treatment groups when compared with vehicle. (B) There was no difference in midline shift in any of the vehicle or treatment groups post-stroke. (C) Despite this, there was a relative moderate positive correlation between cerebral oedema and midline shift. (D) There was also a moderate positive correlation between cerebral oedema and ICP measured at 24 h post-stroke. (E) There was no significant difference in infarct volume as measured on DWI MRI between any treatment groups. *$p<0.05$, **$p<0.01$, ***$p<0.001$ compared with vehicle.

6.3.4 Histological Analysis

6.3.4.1 H&E

There was no evidence of tissue injury or infarction in sham tissue (Figure 6.4 A). Following stroke (Figure 6.4 B) there was marked tissue pallor and loss of grey-white matter differentiation, indicative of infarction within the MCA territory of the right hemisphere. 1 × NK1-R (Figure 6.4 C) treatment tissue was comparable with vehicles, however there was

an increased preservation of tissue, in particular the sub-cortical white matter, in the 2 × NK1-R (Figure 6.4 D), 3 × NK1-R (Figure 6.4 E) and DC (Figure 6.4 F) treated groups.

6.3.4.2 Albumin

There was minimal evidence of albumin extravasation in sham tissue (Figure 6.4 A). Following stroke, marked albumin extravasation, indicative of BBB breakdown and subsequent vasogenic cerebral oedema formation, was observed both macroscopically within the infarcted territory and microscopically in the perivascular tissue of the infarct in vehicles (Figure 6.4 B), 1 × NK1-R (Figure 6.4 C) and DC (Figure 6.4 F), when compared with sham (Figure 6.4 A), 2 × NK1-R (Figure 6.4 D) and 3 × NK1-R (Figure 6.4 E) treatment groups.

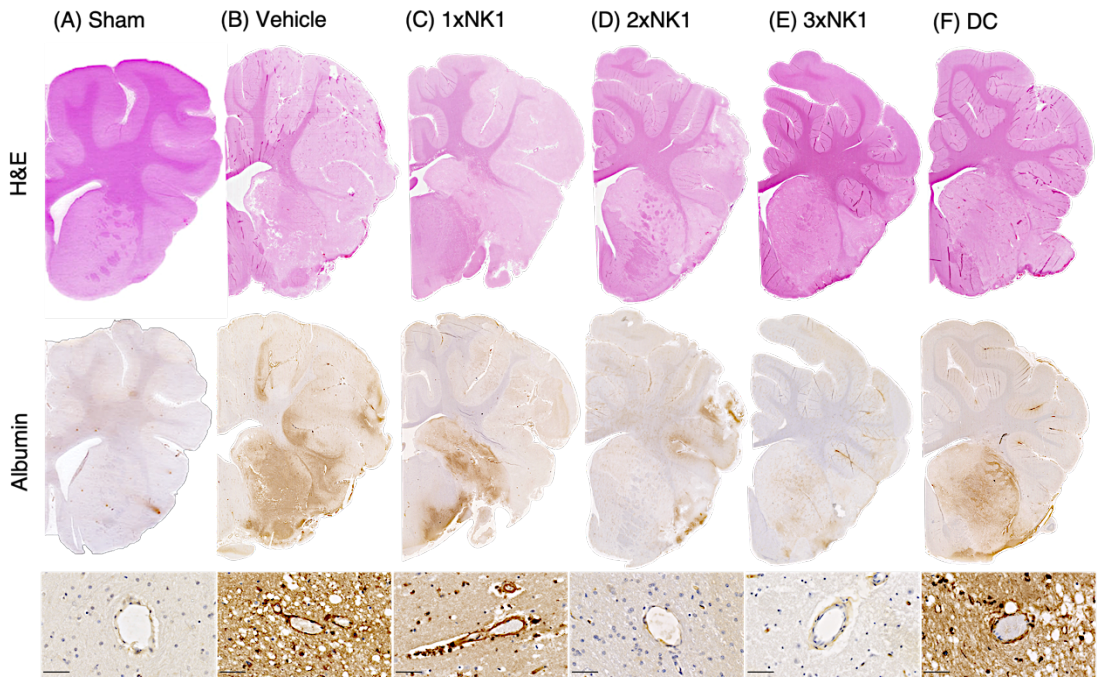

Figure 6.4. Haematoxylin and Eosin staining and albumin immunoreactivity in (A) sham, (B) vehicle, (C) 1 × NK1-R, (D) 2 × NK1-R, (E) 3 × NK1-R and (F) DC animals. H&E staining shows evidence of pallor and reduction of grey-white matter differentiation, which is especially prominent in vehicle and 1 × NK1-R treated animals. Enhanced albumin extravasation was seen macroscopically in vehicle, 1 × NK1-R and DC treated animals compared with sham, 2 × NK1-R and 3 × NK1-R treatment groups. This pattern of albumin staining is consistent with the perivascular staining in microscopic images. Scale bar 50 µm, 40 × magnification.

6.3.4.3 Substance P

There was low to no observable immunoreactivity of SP in sham tissue (Figure 6.5 A). Furthermore, similarly low levels of SP immunoreactivity were observed in the infarcted hemisphere of vehicle and each of the treatment groups following stroke.

6.3.4.4 NK1-R

Low levels of perivascular NK1-R immunoreactivity were observed in sham tissue (Figure 6.5 B). Following stroke, an increase in perivascular NK1-R immunoreactivity was observed

in vehicle and DC treated groups, which was not observed in any of the NK1-R treatment groups.

6.3.4.5 Caveolin-1

Little to no perivascular cav-1 immunoreactivity was observed in sham tissue (Figure 6.5 C). Following stroke, a marked increase in perivascular cav-1 immunoreactivity was observed in vehicles, 1 × NK1-R and DC tissue when compared with sham, 2 × NK1-R and 3 × NK1-R tissue.

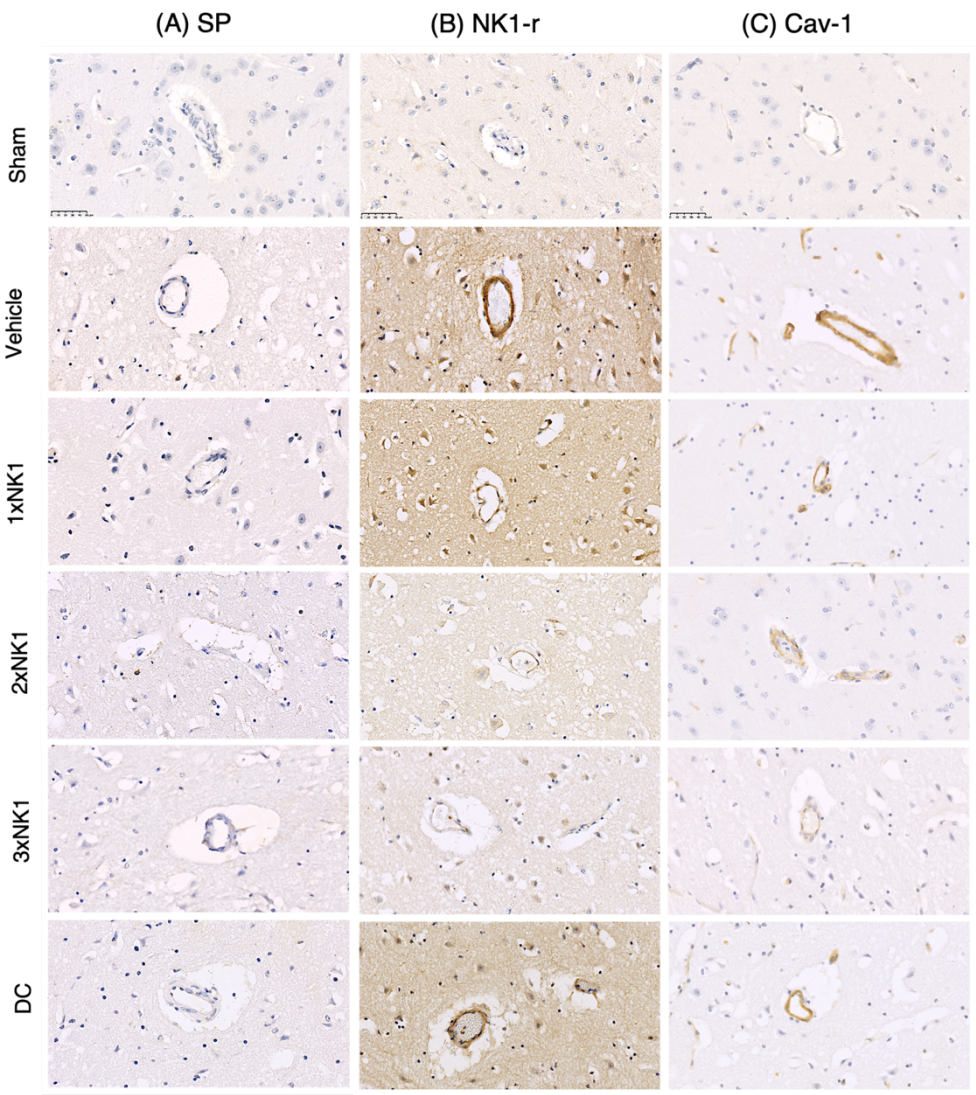

Figure 6.5. Substance P (SP), NK1 receptor (NK1-R) and caveolin-1 (cav-1) immunoreactivity. There was no identifiable increase in SP, NK1-R or cav-1 immunoreactivity in sham animals. (A) Low levels of SP immunoreactivity were seen perivascularly in vehicle, 1 × NK1-R, 2 × NK1-R, 3 × NK1-R and DC groups. (B) This was concordant with an increase in NK1-R immunoreactivity, which was most prominent in vehicle, 1 × NK1-R and DC animals. (C) Cav-1 immunoreactivity was significantly enhanced in 1 × NK1-R, 2 × NK1-R and DC treatment groups when compared with vehicle and 1 × NK1-R. Scale bar: 50 μm, 40 × magnification.

6.4 DISCUSSION

In this study we have demonstrated that administration of 2 or 3 boluses of an NK1-R antagonist is effective in reducing ICP following stroke in a clinically relevant ovine model. This reduction in ICP following treatment was associated with improved BBB integrity, as shown by albumin immunohistochemistry, and a trend towards reduction in the volume of cerebral oedema in the infarcted hemisphere. These findings corroborate previous experimental (Turner et al., 2011, Turner and Vink, 2014, Turner and Vink, 2012, Turner et al., 2006, Nimmo et al., 2004, Donkin et al., 2009, Vink et al., 2003, Corrigan et al., 2012, Corrigan et al., 2016b) and clinical (Lorente et al., 2016, Lorente et al., 2015) studies to further support the role of SP in the pathogenesis of elevated ICP, cerebral oedema and increased permeability of the BBB following acute CNS injury. Indeed, the reduction in ICP following treatment observed in this study is consistent with findings in an ovine model of TBI (Vink et al., 2017). Taken together, we have now successfully demonstrated the efficacy of NK1-R antagonist treatment for the reduction of cerebral oedema and its consequences in both rodent and sheep models of stroke (Turner and Vink, 2012, Turner and Vink, 2014, Turner et al., 2011, Turner et al., 2006) and TBI (Donkin et al., 2009, Vink et al., 2017, Corrigan et al., 2012, Corrigan et al., 2016b). Taken together these findings clearly demonstrate that SP release is a ubiquitous feature of acute CNS injury and that blockade of this pathway is able to preserve BBB integrity and halt the development of cerebral oedema and subsequent rise in ICP.

Despite the clear treatment effect of blocking the NK1-R to reduce ICP in this study, we did not observe a significant increase in perivascular SP immunoreactivity within the infarcted territory in any of the treatment groups following stroke. This is in keeping with previous

findings in a rodent model of MCAo (Turner, 2007), where minimal SP immunoreactivity was observed following permanent MCAo, yet profound perivascular staining was identified following transient stroke with reperfusion. These observations are most likely due to the fact that in the setting of permanent MCAo, the release and peak in SP occurs acutely due to the severity of the ischaemic insult. As such, SP has likely been degraded by the time of tissue harvest at 24 hours post-stroke. In comparison, in previous rodent transient MCAo studies, perivascular SP immunoreactivity was observed primarily in the penumbral tissue. The relative proportion of penumbra to ischaemic core is likely to be much less following permanent compared with transient MCAo due to the extensive collateral failure associated with longer durations of ischaemia. Not surprisingly, this suggests the magnitude and timing of SP release in the neurogenic inflammatory response is dependent upon the duration and severity of the ischaemic insult (Corrigan et al., 2016b). Indeed, following vascular occlusion, temporary changes in transient receptor potential channels of c-fibres as a result of alterations in temperature, pH and ligand binding instigates release of SP (Hokfelt et al., 1975). When there is no reperfusion, compromised cells undergo ischaemic necrosis quickly with associated acute changes in cellular function, leading to a rapid return of receptor channel potential and decrease in SP release. Comparatively, in the setting of transient MCAo, compromised cells in the penumbra experience long durations of electrical silence and alterations in neuronal function, leading to sustained activation of c- fibres and persistent SP release (Astrup et al., 1981, Hofmeijer and Van Putten, 2012, Turner, 2007). Taken together, these findings may provide an explanation as to why SP was not observed on IHC in this study.

We did not observe any effect on infarct volume following NK1-R antagonist treatment, irrespective of the number of boluses administered. This is not surprising considering that

we used a permanent stroke model and given that the NK1-R antagonist is targeting BBB disruption rather than other pathways in the ischaemic injury cascade. A transient stroke model with reperfusion followed by delivery of an NK1-R antagonist may, however, yield different results on infarct volume. Nevertheless, we also did not observe an effect on infarct volume at 24 hrs following 2-hour MCAo thread occlusion in our rodent studies (Turner et al, 2011). In these previous rat studies, however, we did demonstrate that increased perivascular SP immunoreactivity was associated with increased BBB permeability, profound cerebral oedema and persistent functional deficits (Turner et al., 2011, Turner et al., 2006, Turner and Vink, 2012, Turner and Vink, 2014).

In the present study we have identified that increased BBB permeability was sustained to 24 hours post-stroke in vehicle-treated animals, as identified by increased albumin extravasation. Furthermore, the corresponding increase in perivascular caveolin-1 immunoreactivity in the vehicle group may provide an explanation for persistent changes in barrier permeability seen. Caveolae are invaginations of the plasma membrane present in endothelial cells, including those that comprise the BBB, with a key role in regulating transcytosis of large molecules, including albumin, across the barrier (Abbott et al., 2006). Cav-1 is an integral protein for caveolae formation, with upregulation associated with enhanced albumin extravasation and the development of vasogenic cerebral oedema (Nag et al., 2007). Furthermore, cav-1 is upregulated following rodent cortical cold injury and feline TBI, despite maintenance of TJ integrity (Nag et al., 2007, Povlishock et al., 1978), suggesting that physical breakdown of the barrier through loss of TJ is not necessary for the development of cerebral oedema. The NK1-R is located within caveolae, suggesting that its activation may play a role in regulating transcytosis (Kubale et al., 2007, Monastyrskaya et al., 2005). Indeed, this is consistent with the observation of reduced barrier permeability

following NK1-R antagonist administration in previous studies (Turner and Vink, 2012, Turner and Vink, 2014, Turner et al., 2011, Vink et al., 2017, Corrigan et al., 2016a, Donkin et al., 2007). It is proposed that SP release following acute CNS injury leads to NK1-R activation, including those receptors located within the caveolae of endothelial cells, which facilitates enhanced transcytosis of albumin across the barrier, altering the osmotic gradient and leading to the development of vasogenic oedema. Inhibition of transcytosis-mediated albumin extravasation through administration of the NK1-R antagonist diminishes alterations in the osmotic gradient across the barrier, thus preventing the abnormal accumulation of water in the parenchyma and subsequent development of oedema and rise in ICP.

As previously mentioned, in this study we were able to reliably measure changes in ICP throughout the 24-hour monitoring period. Clinical studies investigating fluctuations in ICP following malignant MCA stroke have recorded pressures as high as 43 mmHg in patients who ultimately died, compared with 28 mmHg in survivors (Hacke et al., 1996). In the present study pressures as high as 50 mmHg were recorded in vehicle animals, however, 2 or 3 boluses of the NK1-R antagonist were sufficient to diminish ICP to less than 30 mmHg. Furthermore, 2 × NK1-R animals recorded pressures of less than 20 mmHg throughout the 24-hour monitoring period, with the exception of one animal, and 3 boluses of the antagonist was sufficient to maintain pressures below 25 mmHg, again with the exception of one animal who recorded a maximum pressure of 28 mmHg. One dose of the NK1-R antagonist, however, was insufficient to produce a treatment effect with pressures averaging 35 mmHg. These findings suggest that multiple boluses of the NK1-R antagonist is a potentially viable therapeutic strategy to reduce elevated ICP following stroke, with the ability to bring about

a clinically-meaningful and sustainable reduction in pressure comparable to that observed in surviving patients (Hacke et al., 1996).

Furthermore, the reduction in ICP we observed with repeated NK1-R boluses was comparable to surgical decompression, which is encouraging given the limitations of current available pharmacotherapies used for ICP management, often necessitating early DC. DC performed prior to onset of clinical signs and herniation has been shown to yield improved functional outcomes; however, if surgery is performed when there is evidence of clinical deterioration, it may be too late to yield beneficial outcomes (Shah et al., 2019). Furthermore, although DC is the most powerful tool currently available to combat elevated ICP, the procedure is highly invasive, thus benefits remain controversial, and the long-term implications of this procedure on ICP dynamics are not well understood (Lilja-Cyron et al., 2019, Shah et al., 2019, Funchal et al., 2018). A pooled analysis of the randomised control trials DECIMAL, HAMLET, and DESTINY compared early DC with conventional medical management of patients with evidence of MCA territory infarction and NIHSS >15/20 (Vahedi et al., 2007a, Vahedi et al., 2007b, Geurts et al., 2013, Jüttler et al., 2007, Hofmeijer et al., 2009). These studies found that DC significantly reduced fatality rates and improved functional outcome compared with conventional pharmacotherapy alone. However, whilst some studies report reduced mortality and improved survival, it was at the cost of a higher number of individuals moderately to severely disabled (Kurland et al., 2015, Vahedi et al., 2007a). This becomes an issue of increasing concern given that DC is associated with higher mortality rates in those aged greater than 60 years of age, the most prevalent stroke patient population (Hofmeijer et al., 2009, Benjamin et al., 2018). The correlation between age and functional outcome remains an extremely important pre-treatment prognostic factor in deciding if patients should undergo DC (Chen et al., 2007), highlighting the need for

development of new therapies that can be administered to a wider patient population in a safe and timely manner, eliminating the need for surgical decompression and associated morbidity. In this study we have demonstrated that repeated dosing of NK1-R antagonist treatment was able to reduce ICP comparable to DC surgery, thus providing an alternate treatment strategy, circumventing the need for invasive surgery.

6.4.1 Limitations

Although we have established that the NK1-R antagonist is an effective strategy to lower ICP and have previously determined that the ovine model is viable candidate for the screening of promising novel therapeutics, we must acknowledge the limitations of the study. Due to the invasive nature of the surgery and significant deficits that ensued following permanent MCAo, animals were required to be maintained under anaesthesia for the duration of the experiment. We recognise that human patients are rarely under the influence of anaesthesia at onset of stroke, and that the use of anaesthetic agents may affect outcome measures. Despite this, the agents used for induction and maintenance were chosen to reduce any potential neuroprotective or damaging effects, as previously described in detail (Wells et al., 2015). Indeed, as ketamine is known for its neuroprotective properties, and inhalation isoflurane for its sub-neuroprotection and association with reduced blood pressure, the combination was used to bring about a countering effect. The synergistic use of these agents permitted adequate anaesthesia with controlled MABP whilst preventing inadvertent neuroprotection as a confounding factor, an important consideration when modelling acute ischaemic stroke. It must be acknowledged, however, that we did observe significant differences in MABP across several of the groups. Nevertheless, these alterations in blood pressure did not follow the same pattern as the alterations in ICP so it is therefore unlikely that they significantly contributed to the observed treatment effects. The differences in

MABP observed between groups most likely reflects both the within group and between group heterogeneity in the amount of isoflurane required to maintain twilight anaesthesia during surgery whilst balancing ketamine dosing to maintain adequate blood pressure. Furthermore, only female animals were used in the present study due to the inherent need for catheterisation of animals during long-duration anaesthesia. Females were selected preferentially over males upon veterinary advice given the difficulty in catheterising the highly convoluted male urethra, and thus we were unable to determine gender discrepancies.

Though we were able to establish a significant increase in ICP following ovine stroke, MRI findings were not strongly associated with ICP. We acknowledge that the small sample sizes in this study may have led to a low statistical power. Furthermore, it must be noted that this is frequently seen in clinical stroke cases, where MRI and CT findings are not always a good predictor of ICP. MRI was not possible in the entire cohort, leading to uneven group sizes. Despite a larger cohort available for ICP in both treatment and vehicle groups, only animals with matching ICP/MRI data were included, leading to variations in group sizes. Furthermore, the reliable measurement of cerebral oedema on MRI at a single time-point is somewhat contentious, as the hyperintensity of vasogenic oedema is difficult to distinguish from the ischaemic lesion itself. The measurement of the entire FLAIR lesion volume therefore includes areas of infarction as well as oedema and is thus an indirect measure of oedema volume. A more robust approach to measuring oedema volume would be to perform sequential MRI's and evaluate the change in diffusion lesion volume across times points following reperfusion, which was not feasible in this study due to cost. It should also be acknowledged that whilst MRI findings did not correlate with ICP, we were able to observe MRI features similar to that seen clinically, including transcalvarial herniation in DC treated animals and reduced midline shift. Finally, testing of multiple NK1-R antagonists was not

feasible in this study given the time and cost involved in conducting sheep experiments. However, in our rodent studies of TBI we have previously tested 2 different NK1-R antagonists and recorded comparable results (Donkin, 2006) which provided the basis for the use of the agent in the present study.

For future studies we will work alongside the animal ethics committee of the South Australian Health and Medical Research Institute to develop a survival model of transient MCAo which obviates the need for long duration anaesthesia, allowing for the study of conscious animals following induction of stroke and assessment of long-term functional changes.

6.5 CONCLUSIONS

Use of multiple boluses of an NK1-R antagonist is effective in lowering ICP following ovine stroke, producing a reduction in pressure that is comparable to decompressive surgery. We propose that the mechanism by which the NK1-R antagonist is exerting its action to reduce pressure is largely via caveolae mediated albumin transcytosis. Administration of the NK1-R is thus preventing abnormal albumin extravasation from the vasculature to the brain parenchyma and ameliorating the subsequent development of vasogenic oedema and concomitant rise in ICP. These findings suggest that NK1-R antagonist treatment may represent a novel intervention for the management of elevated ICP following stroke.

Acknowledgements

The authors would like to thank Sunthara Rajan Perumal for the acquisition of the MRI and Shenyi Peng, Tony Nguyen and Martina Kontos for their contribution to the MRI analysis.

We would also like to acknowledge the facilities and scientific and technical assistance of the National Imaging Facility, a National Collaborative Research Infrastructure Strategy (NCRIS) capability, at LARIF, SAHMRI.

Sources of Funding

This work was supported by the National Health and Medical Research Council (NHMRC; Project grant GNT1082556) and by the NeuroSurgical Research Foundation (Adelaide, Australia). RJT was supported by an NHMRC Post-Doctoral Training Fellowship. AJW was supported by an NHMRC Post-Graduate Fellowship.

07

Determining the Temporal Profile of Intracranial Pressure Changes Following Transient Stroke in an Ovine Model

.

Presented as accepted for publication by **SORBY-ADAMS, A. J.**, LEONARD, A. V., ELMS, L. E., MARIAN, O. C., HOVING, J. W., YASSI, N., VINK, R., THORNTON, E. & TURNER, R. J. 2019. Determining the Temporal Profile of Intracranial Pressure Changes Following Transient Stroke in an Ovine Model.

Frontiers in Neuroscience, 13**,** 587.

Statement of Authorship

Title of Paper	Determining the temporal profile of intracranial pressure changes following transient stroke in an ovine model
Publication Status	☑ Published ☐ Accepted for Publication ☐ Submitted for Publication ☐ Unpublished and Unsubmitted w ork w ritten in manuscript style
Publication Details	Sorby-Adams, A.J., Leonard, A.V., Elms, L.E., Marian, O.C., Hoving, J.W., Yassi, N., Vink, R., Thornton, E., and Turner, R.J. (2019). Determining the Temporal Profile of Intracranial Pressure Changes Following Transient Stroke in an Ovine Model. *Front Neurosci* 13, 587.

Principal Author

Name of Principal Author (Candidate)	Annabel Sorby-Adams		
Contribution to the Paper	I conducted the surgeries, performed the immunohistochemistry, analysed the data, am the first and corresponding author and main contributor to the manuscript.		
Overall percentage (%)	50%		
Certification:	This paper reports on original research I conducted during the period of my Higher Degree by Research candidature and is not subject to any obligations or contractual agreements with a third party that would constrain its inclusion in this thesis. I am the primary author of this paper.		
Signature		Date	16.03.2021

Co-Author Contributions

By signing the Statement of Authorship, each author certifies that:

i. the candidate's stated contribution to the publication is accurate (as detailed above);

ii. permission is granted for the candidate in include the publication in the thesis; and

iii. the sum of all co-author contributions is equal to 100% less the candidate's stated contribution.

Name of Co-Author	Renee Turner		
Contribution to the Paper	Associate Professor Renee Turner is the head of the Translational Neuropathology Laboratory and primary investigator on this thesis. She oversaw experimental design, surgical training, intraoperative support, manuscript preparation and editing.		
Signature		Date	16.03.2021

Name of Co-Author	Anna Leonard		
Contribution to the Paper	Dr Anna Leonard is a member of the Translational Neuropathology Laboratory and on the supervisory panel for this thesis. She provided input regarding the experimental design, structure and editing of the manuscript.		
Signature		Date	16.03.2021

Name of Co-Author	Levi Elms		
Contribution to the Paper	Mr Levi Elms was an honours student in the Translational Neuropathology Laboratory in 2018. He provided assistance in preparing and analysing ELISA plates.		
Signature		Date	16.03.2021

Name of Co-Author	Oana Marian		
Contribution to the Paper	Miss Oana Marian was a Research Assistant in the Translational Neuropathology Laboratory from 2017-2019. She provided intraoperative theatre assistance, postoperative care for the animals and assistance with perfusions.		
Signature		Date	16.03.2021

Name of Co-Author	Dr Emma Thornton		
Contribution to the Paper	Dr Emma Thornton was a member of the Translational Neuropathology Laboratory and previous supervisor on this thesis (2016-2018). She provided intraoperative assistance, monitoring intracranial pressure and assistance with perfusions.		
Signature		Date	16.03.2021

Name of Co-Author	Nawaf Yassi		
Contribution to the Paper	Associate Professor Nawaf Yassi is a neuroradiologist from the Royal Melbourne Hospital. He provided expert advice regarding imaging protocols and analysis.		
Signature		Date	16.03.2021

Name of Co-Author	Jan Hoving		
Contribution to the Paper	Dr Jan Hoving is a medical radiologist from the University of Amsterdam. He analysed the MRI infarct volume and provided guidance, assistance and training of protocols.		
Signature		Date	16.03.2021

Name of Co-Author	Robert Vink		
Contribution to the Paper	Professor Robert Vink was the past head of the Translational Neuropathology Laboratory. He oversaw experimental design.		
Signature		Date	16.03.2021

7.0 ABSTRACT

Background and Purpose: Cerebral oedema and elevated intracranial pressure (ICP) are the leading cause of death in the first week following stroke. Despite this, current treatments are limited and fail to address the underlying mechanisms of swelling, highlighting the need for targeted treatments. When screening promising novel agents, it is essential to use clinically relevant large animal models to increase the likelihood of successful clinical translation. As such, we sought to develop a survival model of transient middle cerebral artery occlusion (tMCAo) in the sheep and subsequently characterise the temporal profile of cerebral oedema and elevated ICP following stroke in this novel, clinically relevant model.

Methods: Merino sheep (27M; 31F) were anaesthetised and subject to 2 hours tMCAo with reperfusion or sham surgery. Following surgery, animals were allowed to recover and returned to their home pens. At preselected time points ranging from 1 to 7 days post-stroke, animals were re-anaesthetised, ICP measured for 4 hours, followed by imaging with MRI to determine cerebral oedema, midline shift and infarct volume (FLAIR, T_2, DWI). Animals were subsequently euthanised, and their brain removed for immunohistochemical analysis. Serum and cerebrospinal fluid samples were also collected and analysed for substance P (SP) using ELISA.

Results: ICP and MRI scans were normal in sham animals. Following stroke, ICP rose gradually over time and by 5 days was significantly ($p<0.0001$) elevated above sham levels. Profound cerebral oedema was observed as early as 2 days post-stroke and continued to evolve out to 6 days, resulting in significant midline shift which was most prominent at 5

days post-stroke ($p<0.01$), in keeping with increasing ICP. Serum SP levels were significantly elevated ($p<0.01$) by 7 days post tMCAo.

Conclusion: We have successfully developed a survival model of ovine tMCAo and characterised the temporal profile of ICP. Peak ICP elevation, cerebral oedema and midline shift occurred at day 5-6 following stroke, accompanied by an elevation in serum SP. Our findings suggest that novel therapeutic agents screened in this model targeting cerebral oedema and elevated ICP would most likely be effective when administered prior to 5 days, or as early as possible following stroke onset.

7.1 INTRODUCTION

Worldwide, over 17 million people suffer a stroke each year, of which one third will die and one third will remain permanently disabled as a result (Feigin et al., 2017). Cerebral ischaemia initiates a cascade of interrelated events precipitating brain tissue injury and cell death (Ayata and Ropper, 2002). Of these secondary injury processes, increased microvascular permeability and loss of structural integrity of the blood-brain barrier (BBB) are key to the development of cerebral oedema, a pathological state in which fluid abnormally accumulates in the extracellular space of the cerebral parenchyma, resulting in an overall increase in brain volume. This leads to a subsequent rise in intracranial pressure (ICP), which has devastating consequences including infarct expansion, displacement of brain tissue, tonsillar herniation and death (Steiner et al., 2001c, Raslan and Bhardwaj, 2007, Kim et al., 2015, Battey et al., 2014).

Stroke patients often exhibit a progressive and slow evolution of brain injury, with cerebral oedema and elevated ICP presenting some days following initial insult to tissue, most commonly around 3-5 days following onset (Hewitt and Ellory, 2012). Despite the devastating impact of cerebral oedema and elevated ICP, however, existing treatments fail to address the underlying pathophysiology, thereby limiting their efficacy (Battey et al., 2014). Novel therapies that target the underlying cause of swelling and prevent the evolution of cerebral oedema are urgently required to improve post-stroke outcomes. To this end, our laboratory has identified that the tachykinin neuropeptide substance P (SP) is a key mediator of BBB dysfunction and development of cerebral oedema following stroke (Turner et al., 2006, Turner et al., 2011, Turner and Vink, 2012) and traumatic brain injury (TBI) (Vink et al., 2003, Nimmo et al., 2004, Donkin et al., 2009, Corrigan et al., 2012). Specifically, SP

release leads to neurogenic inflammation, manifesting following acute central nervous system (CNS) injury as increased BBB permeability and the development of cerebral oedema. Furthermore, we have established that blockade of the receptor for SP, the tachykinin NK1 receptor (NK1-R), reduces both BBB permeability and cerebral oedema in rodent models of stroke (Turner and Vink, 2012, Turner et al., 2011, Turner and Vink, 2014) and TBI (Donkin et al., 2009, Corrigan et al., 2016a, Corrigan et al., 2012), suggesting that this is a common feature of acute brain injury.

An enhanced understanding of the underlying pathophysiology of cerebral oedema and elevated ICP following stroke is essential in guiding the development of more effective therapies, and pre-clinical stroke studies are an essential step in this process. However, the poor clinical translation of stroke therapies from the laboratory to the clinic to date has emphasised the importance of appropriate species and model selection (Casals et al., 2011). The use of large intermediate species for these studies is an essential step in the pre-clinical phase to improve translation to the clinic due to similarities in neuroanatomical structure, such as a large gyrencephalic brain that is closer in similarity to that of the human compared with many widely adopted small animal models. In light of this, a number of large animal species are used as pre-clinical stroke models, including sheep (Wells et al., 2015, Wells et al., 2012, Boltze et al., 2008), dogs (Christoforidis et al., 2011, Qureshi et al., 2004, Boulos et al., 2011, Cameron et al., 2008), pigs (Platt et al., 2014, Sakoh et al., 2000, Watanabe et al., 2007) and non-human primates (D'Ambrosio et al., 2004, Nehls et al., 1986, Tagaya et al., 1997, Furuichi et al., 2007, Yuji et al., 2001), each with their own inherent advantages and disadvantages (Sorby-Adams et al., 2018). Although gyrencephalic non-human primates are of significant value in modelling the human condition, the extensive cost, housing requirements and ethical considerations may preclude their use in large scale studies. Pigs

are a widely used experimental species in models of cardiovascular (Kamoi et al., 2014, Suzuki et al., 2011) and traumatic brain injury (TBI) studies worldwide (Pfenninger et al., 1989, Duhaime et al., 2000, Lighthall, 1988, Manley et al., 2006, Ross et al., 1994), however, the Yucatan mini-pig is not available in Australia, and the rapidly increasing bodyweight of other strains can make long-term studies difficult. Sheep are an accessible experimental species and have been used extensively to model a number of neurological conditions, including non-accidental head injury (Anderson et al., 2014, Sandoz et al., 2012), TBI (Vink et al., 2008, Vink et al., 2017) and Huntington's Disease (Reid et al., 2013, Morton et al., 2014). Although sheep have earned a reputation as unintelligent animals, the evidence is quite to the contrary, as sheep demonstrate excellent facial recognition, executive decision making and emotional processing, often comparable to humans on equivalent tasks (Morton and Avanzo, 2011, Keith et al., 2007, Tate et al., 2006). Specifically, the high proportion of white to grey matter in the sheep brain is of particular benefit when studying the pathophysiology of oedema and ICP, given that oedematous fluid predominantly accumulates in the white matter following ischaemic stroke (Jha, 2003, Mahajan and Bhagat, 2016). The strong fibrous tentorium cerebelli of the sheep, comparable with that of the human, also prevents the brain from moving downwards to accommodate increased volume of the oedematous brain, resulting in persistent elevations in ICP, midline shift and herniation of the brain, all of which are seen clinically. Additional advantages of large animal models, including sheep, are the ability to obtain multiple serum and cerebrospinal fluid (CSF) samples from an individual animal over time which is not possible in rodents, as well as using clinical physiological monitoring equipment and MRI. As such, large animal stroke models, such as the sheep, are an excellent additional screening tool following evaluation in rodents and prior to progression to clinical trials.

There are two models of ovine middle cerebral artery occlusion (MCAo) currently in use (Boltze et al., 2008, Wells et al., 2012) both of which involve permanent occlusion of the MCA. In the Boltze model (Boltze et al, 2008) the craniotomy is left open so that animals are effectively given decompression at the time of stroke, allowing for the investigation of long-term time-points without premature mortality, although intracranial pressure dynamics cannot be investigated. Conversely, in the Wells model (Wells et al., 2015, Wells et al., 2012) the craniotomy is closed following MCAo so that the evolution of ICP can be accurately studied. However, survival time-points beyond 24hrs are not possible in this model due to the resulting malignant MCA infarction and ethical requirement to maintain animals under anaesthesia for the duration of the experiment. As such, there is a clear requirement for an ovine MCAo stroke model where the MCA is temporarily occluded to study the effects of reperfusion injury and longer time-points following stroke onset. Furthermore, there is an increasing incidence of patients who successfully recanalise following stroke onset. This is largely due to the increased use of endovascular clot retrieval for reperfusion of large strokes, such as occlusion of the internal carotid artery (ICA) or M1 segment of the MCA (Goyal et al., 2016). The mechanical recanalisation of the MCA produced in a transient MCAo model closely aligns with the vascular reperfusion achieved with endovascular thrombectomy, and thus may be more representative of the evolving human condition.

Accordingly, the aims of the present study were to: 1) develop a survival model of ovine MCAo stroke with reperfusion; and 2) characterise the temporal profile of intracranial pressure changes following stroke; and 3) determine the contribution of SP to BBB permeability and cerebral oedema that develops in this model. By determining the clinical

course of ICP following ovine MCAo, an optimal time window for administration of therapeutic agents targeting elevated ICP due to cerebral oedema can be established.

7.2 MATERIALS AND METHODS

7.2.1 Ethics Statement

All experimental procedures were approved by the Animal Ethics Committees of The University of Adelaide (M-2014-015) and South Australian Health and Medical Research Institute (SAHMRI; SAM 3; SAM 141). Experiments were conducted in accordance with the Australian National Health and Medical Research Council (NHMRC) code of practice for the care and use of animals for scientific purposes (8th edition, 2013).

7.2.2 Experimental Design

A total of 58 (*n*=27M;31F) merino sheep (weight range 65±7kg; age 18-36 months) were used in this study. Animals (3M and 3F/time point) were pre-operatively randomised to daily post-stroke survival time points ranging from day 1 to day 7. Animals allocated to the stroke groups underwent two surgeries: tMCAo surgery with recovery, and ICP monitoring on the designated day post-stroke. An additional group of animals underwent the surgical procedure without MCAo and acted as sham controls (*n*=4F). These animals had ICP continuously recorded for 4 hours immediately following the sham surgical procedure. Finally, an additional follow-up cohort of 12 animals (*n*=6F;6M) underwent stroke surgery and were included to obtain serum and CSF samples over the 7-day post-stroke time-course. This was not possible in the main stroke cohort due to the risk that repeat CSF sampling might potentiate changes in intracranial dynamics leading to inaccurate measurements of ICP. All animals were group housed in conventional sheep paddocks for a minimum of 2 weeks prior

to surgery to allow for acclimatisation. Animals were then moved to individual indoor pens 48 hours prior to surgery and fasted overnight for a minimum of 12 hours prior to the procedure.

7.2.3 Experimental Procedure

7.2.3.1 Animal Preparation and Anaesthesia

Anaesthesia was induced with a combination of intravenous ketamine (0.05 mL/kg, 100 mg/kg Injection, CEVA, Australia) and diazepam (0.08 mL/kg, 5 mg/mL injection, Pamlin, CEVA, Australia). Following induction, animals were intubated via endotracheal tube insertion to ensure airway patency for ventilation. Animals were then positioned on an operating table on their left side, with hind limbs exposed for arterial access. An arterial catheter was inserted in the left hind leg for blood gas sampling and a cannula inserted into the external jugular vein for fluid and drug administration. Intraoperative anaesthesia was maintained via a combination of inhalational isoflurane (Henry Shein, Australia; 1.5-2.0%) in 100% oxygen and intravenous (jugular) ketamine at an infusion rate of 4 mg/kg/hr. Crystalloid fluids were administered throughout surgery via continuous intravenous infusion with compound sodium lactate (Baxter Health, Australia) to assist hydration and ionic balance. In addition, intraarterial sodium chloride (Baxter Health, Australia) was infused at a rate sufficient to ensure arterial catheter patency. Following surgery, animals were recovered and treated with subcutaneous antibiotic Rilexine (1 mL/10kg every 12 hours, 15 g/100 mL Cephalexin, VIBRAC, Australia), NSAID Carprieve (0.7 mg/kg, 50 mg/mL every 12 hours, Carprofen, Norbrook, Australia) and opioid Temgesic (1.0 mL, 324 μg/mL Buprenorphine hydrochloride, one dose post-operatively, Reckin Benckiser, Australia) for pain relief. Antibiotic and NSAID treatment were continued for a minimum of 3 days

following surgery, with additional opioid and/or NSAID administered as required thereafter for pain management.

7.2.3.2 Surgical Approach

A model of ovine stroke was modified from previously published works (Wells et al., 2015, Wells et al., 2012) in order to achieve tMCAo with reperfusion (Figure 7.1). This modification enabled the recovery of animals from surgery and the study of longer time-points (beyond 24 hours) following stroke. In this particular approach, it was necessary to keep the coronoid process of the mandible intact and preserve the surrounding temporalis muscle to ensure animals were able to masticate following surgery. To achieve this, a 5 cm horizontal incision was made posterior to the orbital rim of the right eye and terminating anterior to the ear. Upon incision, the temporalis muscle was retracted, and the coronoid process elevated to expose the underlying skull. Cloward retractors (Codman & Shurtleff Inc., Massachusetts) were inserted, and blades adjusted to provide space for a small craniotomy to be drilled at the junction of the parietal and squamous temporal bones with a high-speed pneumatic drill using a 5 mm cutting burr (Midas Rex, Medtronic, MN). Following craniotomy, a horseshoe durotomy was performed, the brain exposed, and the anterior temporal lobe gently retracted to expose the right proximal MCA. A small amount of CSF was aspirated to ensure sufficient visualisation of the proximal MCA; however, this was kept to a minimum to reduce the impact on intracranial volume. Gentle dissection of the MCA from the arachnoid mater was performed to allow for a temporary aneurysm clip (Aesculap, Germany) to be applied proximal to the MCA bifurcation using a clip applicator (YASARGIL® Aneurysm clip system, Germany). Successful clipping of the MCA resulted in an immediate decrease in vessel calibre, confirming reduced blood flow. The dura was then gently re-opposed onto the brain and the craniotomy site filled with sterile saline to

prevent dehydration of the underlying cortical tissue, and the surgical site draped. The clip was left *in situ* for 2 hours and subsequently removed with clip applicators to achieve reperfusion. Visual confirmation of reperfusion was noted when the calibre of the vessel increased, and blood returned to the distal MCA. Successful reperfusion also was confirmed on magnetic resonance angiography (MRA) performed at the pre-selected timepoints.

Following reperfusion, the dura was approximated and interleaved with synthetic dura (Durepair®, Medtronic, USA) to cover the exposed brain. Dural closure was then achieved with ethyl cyanoacrylate (Bostik, Australia), and the bone previously removed reinserted into the craniotomy site and reinforced with dental acrylic cement (Sledgehammer, Keystone, Germany) to create a watertight seal, thus restoring intracranial dynamics. The surgical site was then treated with 1.0 mL 0.5% local anaesthetic Marcain (bupivacaine hydrochloride 5 mg/mL, AstraZeneca, Australia) and closed using a 0.1 Vicryl braided polyglactin Suture (ETHICON, Australia) using the horizontal mattress suture technique of wound closure to minimise risk of infection. The animal was removed from anaesthesia, extubated, transferred to a post-operative recovery pen and pain relief administered. Mean arterial blood pressure (MABP) was monitored at 5-minute intervals throughout surgery via application of a paediatric blood pressure cuff (Easy Care Cuff, Phillips) on the upper left front limb. Blood samples (Machine AVL Scientific Corporation USA, Manufactured by Hersteller, OPTI Critical Care Analyzer–Model OPTI3, Serial No. OP3-2759) were acquired hourly via arterial catheter sampling to determine pO_2, pCO_2, haematocrit, haemoglobin, pH, Na^+ and K^+ levels. End tidal CO_2 was also recorded at regular intervals. Animals were maintained on a heating pad throughout all surgical procedures and rectal temperature checked hourly to ensure maintenance of body temperature within normal ovine limits (37.5-39.0 °C).

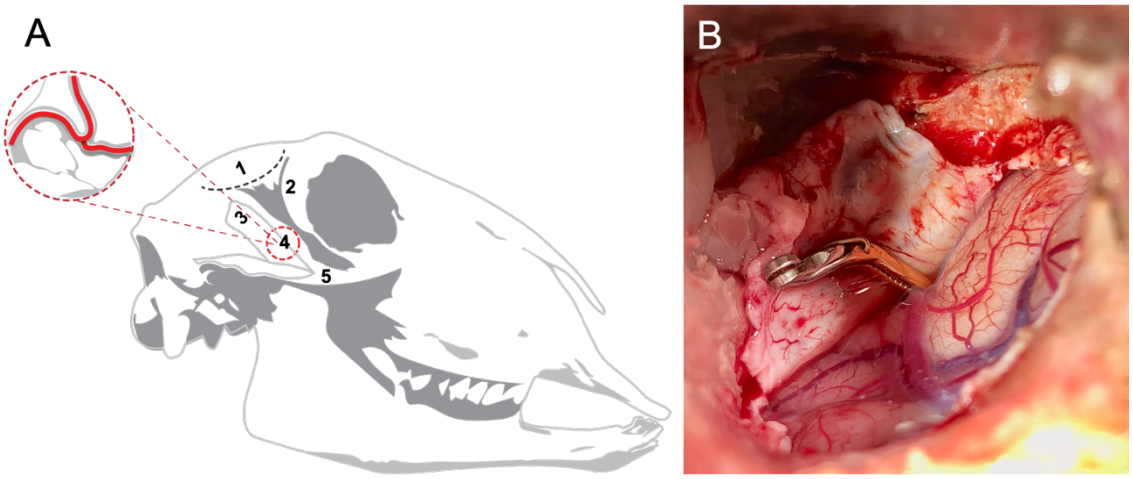

Figure 7.1. Surgical approach to ovine transient middle cerebral artery occlusion. (A) Surgical approach showing site of incision (1; black dotted line) posterior to the orbital rim (2) and superior to the coronoid process (3). This approach enabled the skull base to be accessed without disrupting the coronoid process or zygomatic arch (5), allowing for craniotomy (4) and direct access to the MCA, whilst ensuring post-operative recovery of the animal and the ability to masticate following the procedure. (B) Superior view of craniotomy site showing the aneurysm clip applied to the proximal MCA.

7.2.2.3 ICP Measurement

At 4 hours prior to the pre-determined post-stroke time-point, or immediately following surgery in shams, anaesthetised (using aforesaid isoflurane and ketamine maintenance protocols) animals were placed prone in the sphinx position on the operating table. Bilateral burr holes were drilled into the left and right parietal bone, posterior to the coronal suture and approximately 10 mm from the sagittal suture. The dura was perforated, and skull bolts secured, following which Codman microsensor ICP probes (Codman & Shurtleff Inc., Massachusetts) were inserted to an approximate depth of 15 mm into the brain parenchyma and ICP recorded continuously for a period of 4 hours post time of MCAo or sham surgery (LabChart Reader, ADInstruments, v. 8.1.1). Two-point checks (0mmHg, 100mmHg) were performed prior to insertion of probes and at the end of the recording period to confirm measurement accuracy. ICP readings that were selected for final analysis (left or right) were based on calibration data, with readings preferentially selected from the right hemisphere probe. Raw ICP data underwent a logarithmic exponential transformation as previously

described and was expressed as geometric mean ± SEM (Wells et al., 2015a, Matthews et al., 1990).

7.2.2.4 Magnetic Resonance Imaging

Following the 4-hour ICP monitoring period, animals were moved to a 1.5 Tesla Siemens Syngo2004A (Siemens AG, Munich, Germany) MRI scanner, during which they were maintained under general anaesthesia (3% isoflurane). Sequences were acquired including time-of-flight magnetic resonance angiography (TOF MRA; TR 26 ms, TE 3.69 ms, slice thickness 0.50 mm), diffusion weighted imaging (DWI; TR 5600 ms, TE 80 ms, slice thickness 3.0 mm), fluid attenuated inversion recovery (FLAIR; TR 5000 ms, TE 386 ms, slice thickness 0.9 mm), T_1 weighted imaging (TR 2300 ms, TE 2.58ms, slice thickness 0.9 mm) and T_2 weighted imaging (TR 3200 ms, TE 410 ms, slice thickness 0.9 mm). T_1 weighted post-contrast images were also acquired following intravenous administration of 0.1 mL/kg gadolinium-diethylene-triamine-pentaacetic acid (GAD) (Magnevist, Bayer HealthCare, Germany) to determine the extent of BBB breakdown on MRI.

The degree of midline shift was used as a surrogate marker for the anatomical sequelae of cerebral oedema. Shift from the midline was assessed using axial T_2 weighted scans and measured in mm from the septum pellucidum at the level of the foramen of Monro (HOROS DICOM image viewer v3.1.1). To calculate cerebral oedema, coronal FLAIR images were analysed using HOROS DICOM image viewer (v3.1.1). After optimal adjustment of brightness and contrast, oedema volume was determined from sequences using computer-aided manual tracing of the hyperintense lesion by a blinded assessor. The areas were then summed and multiplied by the slice thickness to give a total volume in cm^3.

To calculate infarct volume, segmentation tools in ITK-SNAP (v 3.7) were used to perform semi-automated segmentation of the MRI diffusion lesions, in which a separate foreground and background was created using diffusion-weighted images (Yushkevich et al., 2006). A combination of "three-dimensional active contour segmentation" and subsequent manual post-processing of the segmentation while adjusting image thresholds was performed to maximize reproducibility whilst excluding artefacts. The "three-dimensional active contour segmentation" consisted of multiple steps: First, in the pre-segmentation phase, independent component analysis automatically segmented parts of the DWI image and these were manually identified as foreground or background. To obtain an optimal distinction between foreground and background, thresholds of the image windows were adjusted. After thresholding, a "speed image" with a separate foreground and background was created. Next, in the active contour phase, seed regions were manually placed within the region of interest (ROI). These seeds were then automatically grown within the ROIs to form the temporary segmentation. Subsequently, areas that were not automatically included in the "active contour segmentation" were manually included in the follow-up infarct segmentation. The total volume of the segmentation was exported and reported in cm^3 for analysis.

7.2.2.5 Perfusion and Histological Examination

Following MRI, intravenous heparin (5000 I.U./5mL; Pfizer, NY) was administered and animals humanely euthanised via common carotid perfusion fixation with cold TRIS-buffered saline under isoflurane anaesthesia. The brains were subsequently removed and sliced into 10 mm coronal slices using a custom-made sheep brain matrix. Sections were then immersion fixed in 10% neutral-buffered formalin for a minimum of 14 days prior to being processed, embedded in paraffin wax and sectioned coronally at 5-micron intervals for immunohistochemistry for albumin, SP, and caveolin-1 (Table 1).

Table 7.1 Immunohistochemistry protocols

Antibody	Dilution	Retrieval	Brand	Catalogue no.
Albumin	1:2000	No retrieval	Dako	A0001
SP	1:5000	Citrate	Abcam	ab14184
Caveolin-1	1:500	EDTA	Cell Signaling Technologies	3238

7.2.2.6 Serum and CSF Collection

Blood samples were collected (Vacutainer® SST™ II Advance Tube, Beckton-Dickinson, Australia) from animals (*n*=12, 6M;6F) pre-injury and at 4, 8, 12 and 16 hours post stroke and on days 1, 3, 5, and 7 via jugular venepuncture. Following collection, samples were centrifuged (15 mins at 2000 RCF) and serum extracted into 10 x 500 µl aliquots and stored at -80 °C. CSF was collected via lumbosacral tap prior to induction of stroke and on days 1, 3 and 6 thereafter. Note that this was performed in the follow up cohort, and these animals did not undergo ICP monitoring so there were no concerns regarding multiple CSF draws and the associated effects on ICP measurement accuracy. Prior to collection, animals were induced with combination diazepam and ketamine as previously described. The animals were then placed in the prone position on a surgical table and the sagittal plane of the animal's vertebrae was manipulated so that it was perpendicular to the horizontal plane of the bench. The animal was shaved to allow for clear access to the lumbosacral joint and appropriate visualisation of landmarks. Palpation of the hips was performed to determine the correct sagittal plane orientation of the spine and the optimal site for CSF collection was determined via identification of the midline depression between the last lumbar and first sacral vertebrae. The area was cleaned using a 4% chlorhexidine preoperative surgical scrub brush (Becton-Disckinson E-Z Scrub™, Australia), povidone-iodine applied and site surgically prepared. A spinal needle with stylet (BMDi TUTA Healthcare, Australia) was inserted perpendicular to the skin and the needle advanced slowly through the subcutaneous tissue and interarcuate ligament until a sudden drop in resistance was felt indicating the

advancement through the dural membrane and entry into the subarachnoid space. The stylet was then removed, and 2 mL of CSF aspirated via a syringe and deposited into a 3 mL container; sample placed immediately on ice for 20 minutes, centrifuged (15 mins at 3000 RCF), extracted into 3 x 500 µL aliquots and stored at -80 °C.

7.2.2.7 Analysis of Serum and CSF

Serum and CSF samples were used to quantify expression of SP using enzyme-linked immunosorbent assay (ELISA) according to the manufacturer's instructions (Abcam; KIT-ab133029). All samples were diluted 1:4 in assay buffer for appropriate compliance with each individual plate standard curve. Standards, serum and CSF test samples were run, and the plate immediately analysed following addition of stop solution using a spectrophotometric microplate reader (Synergy HTX, multi-mode reader). At optical density of 405 nm light absorbance was calculated to give an inverse reading of SP proportional to its captured measure on the plate.

7.2.3 Statistical Analysis

All data are expressed as mean ± SEM. Physiological data (MABP, pH, pO2, pCO2) were analysed using one-way analysis of variance (ANOVA) followed by Tukey's post-hoc tests (Prism v.8.0.1, GraphPad, California). ICP, infarct volume, cerebral oedema and midline shift data were analysed by one-way ANOVA with multiple comparisons followed by Tukey's post-hoc tests. ELISA evaluation was performed for each plate using individually generated standard curves and an R value of 0.9709 was accepted to improve the efficacy of inter-plate accuracy. ELISA values were then analysed via one-way ANOVA with Tukey's post-hoc. Pearson's correlations were run between midline shift and cerebral oedema, cerebral oedema and ICP and midline shift and ICP to determine the relationship between

variables. A two-way ANOVA with Sidak's multiple comparison test was run to determine gender differences in physiological variables during both surgery and ICP monitoring. Gender discrepancies were also established for infarct volume, cerebral oedema, midline shift and ICP in addition to CSF and serum SP via two-way ANOVA with Sidak's post-hoc. A p-value <0.05 and R-value >0.04 were considered significant throughout.

7.3 RESULTS

7.3.1 Surgery, Mortality and Post-operative Course

There was no premature mortality of animals seen in the present study. One animal was excluded due to insufficient reperfusion following MCAo as seen on MRA, resulting in a permanent rather than a transient occlusion (Figure 7.2). In all other animals, temporary occlusion of the MCA with reperfusion was successfully performed. A further 4 animals were excluded due to significant anaesthetic difficulties which confounded the experimental course (*n*=2 in 2 days group; *n*=2 in 3 days group). Specifically, the excluded animals were unstable throughout the induction of stroke surgery, necessitating repeat boluses of ketamine and diazepam and an increased rate of isoflurane to maintain surgical levels of anaesthesia, which resulted in significantly lowered MABP, decreased cerebral perfusion pressure and ultimately profound infarct expansion.

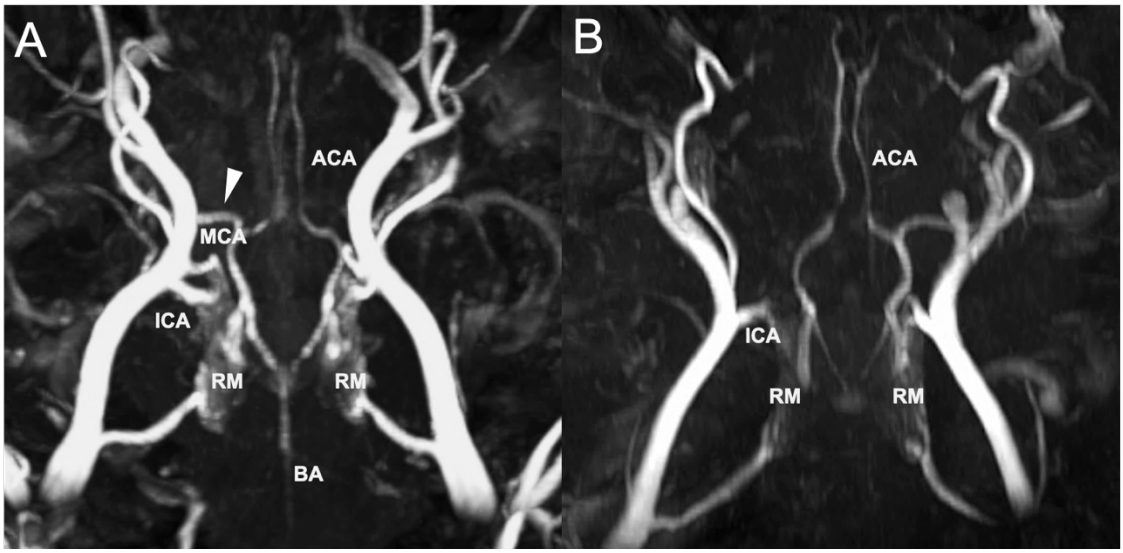

Figure 7.2. Middle cerebral artery (MCA) reperfusion following transient MCA occlusion (MCAo) (A) compared with permanent MCAo (B) on time-of-flight magnetic resonance angiography. Evidence of vessel patency, indicated by the white arrow, following clip removal in transient MCAo animals compared with permanent MCAo animals, where the vessel cannot be visualised MRA (data not reported). MCA-middle cerebral artery; ACA-anterior cerebral artery; ICA-internal carotid artery; BA-basilar artery; RM-rete mirabile.

All animals were able to use their jaw and masticate following surgery. A comprehensive behavioural analysis was beyond the scope of this study; however, all animals in the ICP cohort were observed for jaw alignment and eating behaviour, the presence/absence of fetlock weakness and demeanour throughout the post-stroke period. Nine of 42 animals demonstrated evidence of jaw misalignment following stroke surgery, which persisted to the end of the experiment in 3/9 animals. Although 25/42 animals showed reduced food intake post-stroke, as compared to their pre-stroke daily intake, body weight remained within acceptable limits (15%). Fourteen of 42 animals showed weakness of the fetlock joint following stroke, manifesting as knuckling, which was most commonly observed on day 1 and typically resolved by day 4 post-stroke. An alteration in demeanour, as demonstrated by a lowered head position and droopy ears, was observed in 26/42 animals and was most prevalent at days 5-7 post-stroke, coinciding with elevated ICP.

7.3.2 Physiological Parameters

Physiological variables for pCO_2, MABP and pH were within normal limits for all groups throughout the duration of the experiment (Table 7.2). As animals were maintained on 100% oxygen (6.0 L/min) through the course of surgery and ICP monitoring this resulted in pO_2 values that were significantly above the normal range of 90-100 mmHg. These observations, however, were observed across all experimental groups. No significant differences ($p>0.05$; Table 7.2) between pO_2, pCO_2 and pH were observed between groups during stroke surgery or the 4-hour period of ICP monitoring. There was, however, a statistically significant decrease in MABP during the ICP monitoring period seen at 1-day post-stroke compared with 4 ($p=0.04$) and 7 ($p=0.01$) days.

Table 7.2 Surgical and intracranial pressure monitoring physiological parameters

PCO_2 (mmHg) ± SEM

	Surgery Day			*ICP Monitoring*		
Group	Male	Female	All animals	Male	Female	All animals
Sham		43.19±3.43				
1 Day	41.19±3.39	39.83±2.07	40.51±1.80	36.08±1.61	37.42±2.32	36.75±1.30
2 Day	43.83±2.05	45.25±2.84	44.54±1.60	38.33±1.02	41.42±2.14	39.88±1.27
3 Day	46.58±1.72	46.25±1.50	46.42±1.02	47.28±2.98	40.25±1.75	44.47±2.43
4 Day	46.81±3.13	43.0±3.47	44.90±2.26	42.89±0.45	38.17±4.19	40.53±2.16
5 Day	50.08±3.17	44.33±2.51	47.21±2.22	41.58±0.79	39.58±2.19	40.58±1.13
6 Day	45.42±2.38	41.33±1.62	43.38±1.58	47.75±1.75	42.83±1.96	45.29±1.61
7 Day	47.67±1.88	44.08±2.24	45.80±3.76	42.75±2.89	46.25±0.88	44.50±1.56

MABP (mmHg) ± SEM

	Surgery Day			*ICP Monitoring*		
Group	Male	Female	All animals	Male	Female	All animals
Sham		79.35±6.27				
1 Day	84.61±12.54	86.17±8.80	85.39±6.86	97.25±8.76	77.64±8.54	87.44±7.01
2 Day	74.17±0.87	92.92±4.01	106.98±25.30	88.50±11.35	107.39±17.88	96.44±10.66
3 Day	75.42±5.47	91.42±4.03	83.42±4.69	93.75±14.42	99.88±12.63	96.20±8.97
4 Day	92.75±3.82	84.17±3.99	88.46±3.13	116.33±10.19	127.50±6.91	121.92±6.05*
5 Day	96.75±1.32	80.97±13.45	88.86±7.00	117.92±7.58	104.75±1.98	111.33±4.58
6 Day	78.67±9.04	91.17±2.98	119.56±6.87	122.67±2.85	108.42±5.21	115.54±4.15
7 Day	114.17±11.28	84.25±10.31	99.21±9.56	137.42±17.12	116.75±10.33	127.08±10.07*

(continued)

	PO_2 (mmHg) ± SEM					
	Surgery Day			*ICP Monitoring*		
Group	Male	Female	All animals	Male	Female	All animals
Sham		112.77±5.75				
1 Day	213.94±50.81	213.08±66.77	213.51±37.52	294.36±64.89	191.64±38.27	243±40.78
2 Day	200.17±37.13	83.67±10.83	141.92±31.27	166.67±14.21	250.92±62.62	208.79±34.34
3 Day	289.50±96.27	187.0±38.56	238.25±51.73	241.81±126.13	237.38±72.13	240.03±72.76
4 Day	193.00±73.93	113.50±8.75	153.25±37.74	304.67±47.92	163.0±17.10	233.83±39.00
5 Day	193.83±30.12	188.47±57.77	191.15±29.16	228.17±70.65	251.33±29.37	239.75±34.61
6 Day	342.33±101.85	217.58±76.33	279.96±63.39	319.56±122.91	422.67±57.68	371.11±64.95
7 Day	172.08±79.94	116.50±8.62	144.29±38.04	313.03±83.77	280.83±48.43	296.93±43.87

	pH ± SEM					
	Surgery Day			*ICP Monitoring*		
Group	Male	Female	All animals	Male	Female	All animals
Sham		7.46±0.02				
1 Day	7.43±0.03	7.44±0.01	7.43±0.01	7.42±0.01	7.42±0.03	7.42±0.01
2 Day	7.43±0.02	7.45±0.04	7.44±0.02	7.43±0.03	7.48±0.03	7.45±0.02
3 Day	7.41±0.04	7.41±0.01	7.41±0.02	7.39±0.04	7.41±0.03	7.40±0.02
4 Day	7.41±0.02	7.44±0.02	7.42±0.02	7.35±0.05	7.48±0.02	7.41±0.04
5 Day	7.38±0.02	7.43±0.07	7.40±0.02	7.47±0.02	7.43±0.07	7.45±0.03
6 Day	7.39±0.03	7.45±0.01	7.42±0.02	7.40±0.02	7.44±0.03	7.42±0.02
7 Day	7.40±0.02	7.42±0.02	7.41±0.01	7.48±0.02	7.44±0.03	7.46±0.02

7.3.4 Intracranial Pressure

ICP remained within normal limits for the duration of the 4-hour monitoring period in sham animals (8±2 mmHg). From 1 to 4 days following tMCAo, ICP levels were comparable with sham ($p>0.05$; Figure 7.3). However, by 5 days post-stroke, ICP was significantly elevated (28±10 mmHg; $p<0.0001$) from sham levels and post-stroke days 1-4 ($p<0.0001$). ICP remained significantly elevated out to 6 days post-stroke when compared with shams (25±5 mmHg; $p=0.0001$) and 1 ($p=0.0001$), 2 ($p=0.0003$), 3 ($p=0.03$) and 4 day ($p=0.0007$) post-stroke time points. By 7 days, ICP began to decline (18±2 mmHg; $p=0.02$ when compared with 5 days) but remained significantly elevated compared with sham ($p=0.04$), although not significantly different ($p>0.05$) from recordings on days 1, 2, 3, 4 and 6 post-stroke.

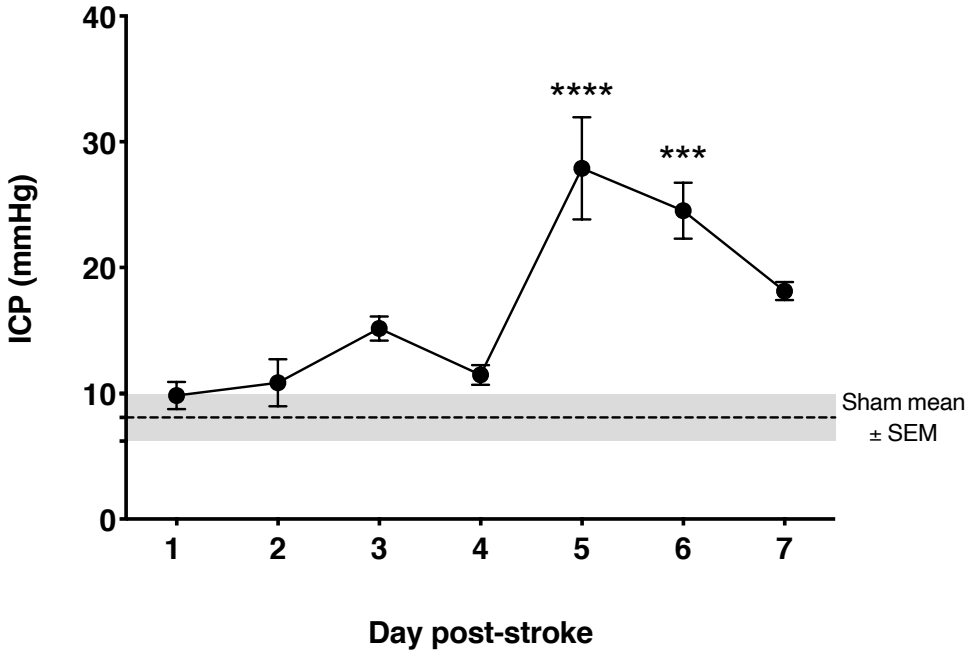

Figure 7.3. Temporal profile of ICP following transient middle cerebral artery occlusion. ICP was significantly elevated at 5 days ($p<0.001$) and 6 days ($p<0.05$) post-stroke when compared with shams. By 7 days, ICP began to normalise, though remained elevated compared with sham ($p<0.05$). ****$p<0.0001$; ***$p<0.001$ compared with sham. *n*=6/time-point, *n*=4 sham.

7.3.5 MRI

MRI was normal in sham animals, with no evidence of infarction, cerebral oedema or midline shift observed (data not shown). At each time-point following stroke, there was evidence of MCA recanalisation following clip removal as seen on MRA, with the exception of one animal that was excluded due to persistent MCAo (Figure 7.2). All stroke animals showed evidence of hyperintensity on T_2 weighted and FLAIR images in the MCA territory, indicative of the infarct core and surrounding extracellular oedema (Figure 7.4). There was no significant difference in infarct volume at any of the time points post-stroke as measured on DWI MRI (Figure 7.5 A).

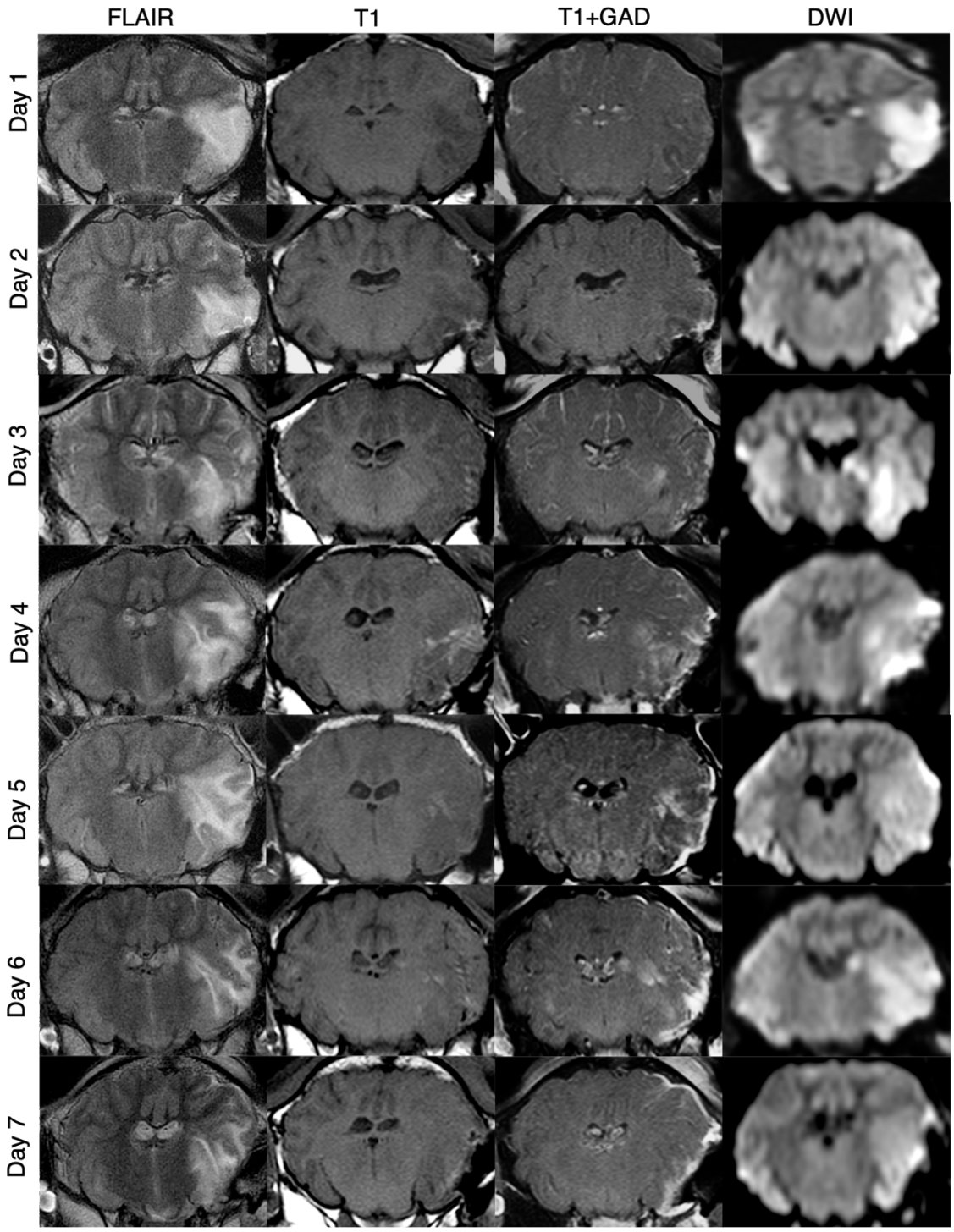

Figure 7.4. MRI findings post transient middle cerebral artery occlusion. Cerebral oedema, as shown in coronal FLAIR MRI images, evolved from 1-6 days following stroke, beginning to resolve by 7 days. This evolution in cerebral oedema was associated with enhanced extravasation of Gadolinium (GAD) across the BBB as seen on T_1 weighted post-contrast series when compared with pre-contrast T_1 series. Lesion volume, as shown in DWI MRI images, was comparable across time-points following stroke.

Cerebral oedema evolved over time from 1 to 6 days post tMCAo, with the largest volume of cerebral oedema seen at 5 (8.86±2.03 cm^3) and 6 days (7.01±0.9 cm^3). This increase in the volume of oedema was accompanied by increased extravasation of GAD across the barrier, as seen in T_1 post-contrast sequences, indicative of BBB breakdown (Figure 7.4). However, although a qualitative evolution of cerebral oedema post-stroke was apparent (Figure 7.4), accompanied by increased GAD contrast, there was no statistically significant difference between time-points (Figure 7.5 B; $p>0.05$). Midline shift was evident in all stroke animals. The degree of midline shift evolved over time following stroke (Figure 7.5 C) and was most prominent at 5 days post-stroke (3.92±0.59 mm) when compared with 1 ($p=0.002$) and 7 days ($p=0.04$), in keeping with ICP findings. No animals showed evidence of tonsillar herniation or brain stem compression on MRI (data not shown).

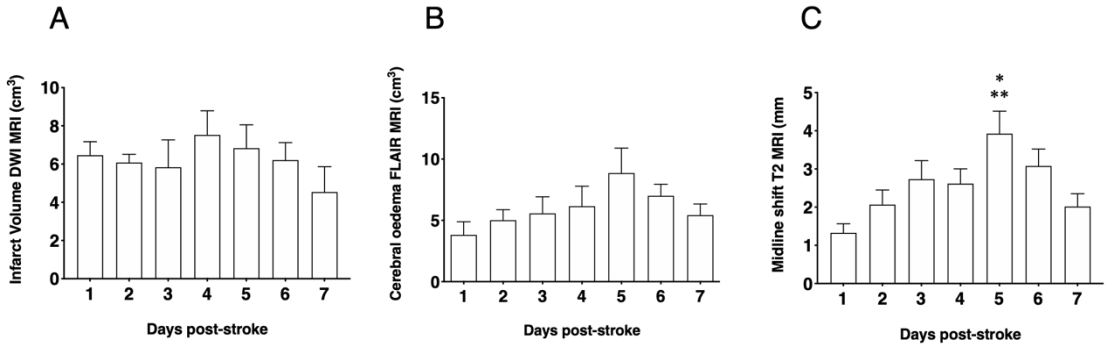

Figure 7.5. Quantification of infarct volume, cerebral oedema and midline shift on MRI. There was no significant difference ($p>0.05$) in infarct volume at any of the time-points following stroke. The evolution of cerebral oedema showed a similar pattern to intracranial pressure; however, changes were not significant ($p>0.05$). Midline shift was significantly greater at 5 days when compared with 1 (<0.01) and 7 ($p<0.05$) days post-stroke. Data shown as mean ± SEM. * $p<0.05$ compared with 7 days, ** $p<0.01$ compared with 1 day.

Despite the fact that cerebral oedema findings were not significantly different between time points, there was a moderate positive correlation seen between midline shift and cerebral oedema calculations ($r=0.49$; Figure 7.6 A). However, there was no positive correlation seen

between ICP and cerebral oedema (r=0.23; Figure 7.6 B) or ICP and midline shift (r=0.20; Figure 7.6 C). *n*=6/time-point.

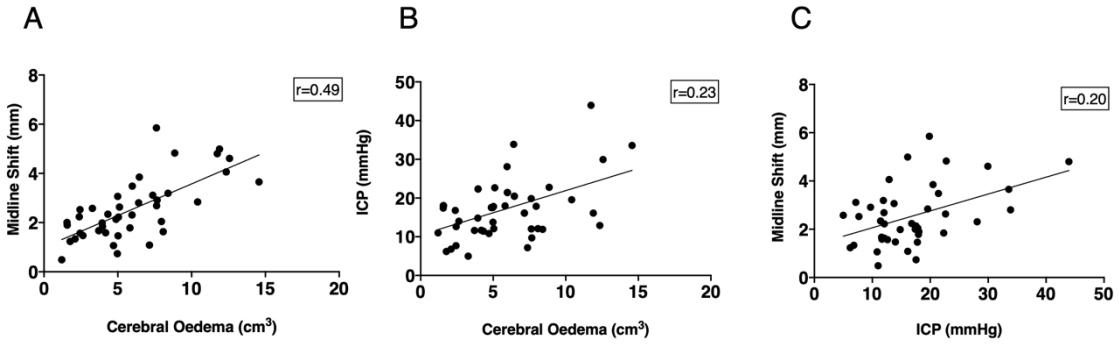

Figure 7.6. Relationship between ICP, cerebral oedema, midline shift and infarct volume. There was a moderate positive correlation seen between cerebral oedema and midline shift (r=0.49). Despite this, there was no correlation seen between ICP and cerebral oedema (r=0.23), or ICP and midline shift (r=0.20). Note data from all time points was used for comparison between variables.

7.3.6 Substance P ELISA

A reduction in serum SP was observed between 4 and 16 hours following transient MCAo, however, changes were not significant (p>0.05; Figure 7.7). At 7 days post-stroke, SP levels were significantly elevated compared with 4 (p=0.04), 8 (p=0.008), 12 (p=0.003) and 16 hours (p=0.002) and 1 day (p=0.04) following occlusion. Despite a qualitative increase, the concentration of serum SP at day 7 was not significantly elevated (p>0.05) when compared with pre-stroke measurements. Despite a relative increase in SP seen in the serum post-stroke, no significant changes (p>0.05) in SP levels in the CSF (Figure 7.7) were observed at any time-point following MCAo.

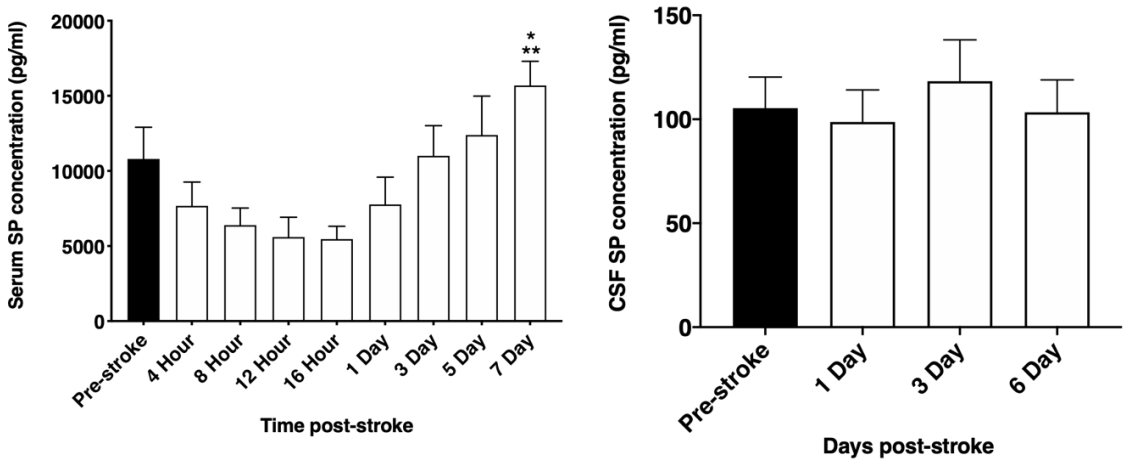

Figure 7.7. Temporal profile of serum and cerebrospinal fluid Substance P (SP) levels following stroke. At 7 days post-stroke, SP in the serum was significantly elevated compared with levels seen at 4 hours ($p<0.05$), 8, 12, 16 hours ($p<0.01$) and 1 day ($p<0.05$) following stroke. Furthermore, despite a qualitative increase, SP concentration pre-stroke was comparable with day 7. In the CSF, there was no significant difference seen in SP levels at days 1, 3 and 6 post-stroke ($p>0.05$). Data shown as mean ± SEM. * $p<0.05$ compared with 4 hours and 1 day; **$p<0.01$ compared to 8 hours, 12 hours and 16 hours. *n*=12/time-point serum; *n*=8/time-point CSF.

7.3.7 Gender comparisons

No differences in pCO_2, pO2, MABP or pH were seen between sexes during either stroke surgery or ICP monitoring ($p>0.05$; Table 7.2). There was no significant difference in ICP between male and female animals at any of the post-stroke time-points ($p=0.93$; Figure 7.8 A). Furthermore, there was no significant difference in infarct volume ($p=0.79$; Figure 7.8 B), cerebral oedema ($p=0.41$; Figure 7.8 C) or midline shift ($p=0.39$; Figure 7.8 D) seen between sexes following stroke. SP levels in the serum were not significantly different between males and females ($p=0.41$; Figure 8D). However, there was a significant increase in SP seen in the CSF of females when compared with males, pre-stroke ($p=0.002$), and at 1 ($p<0.0001$), 3 ($p<0.0001$) and 6 ($p=0.002$) day post-stroke time-points, although there were no significant within group differences observed in the females at any time-point pre- or post-stroke ($p=0.18$).

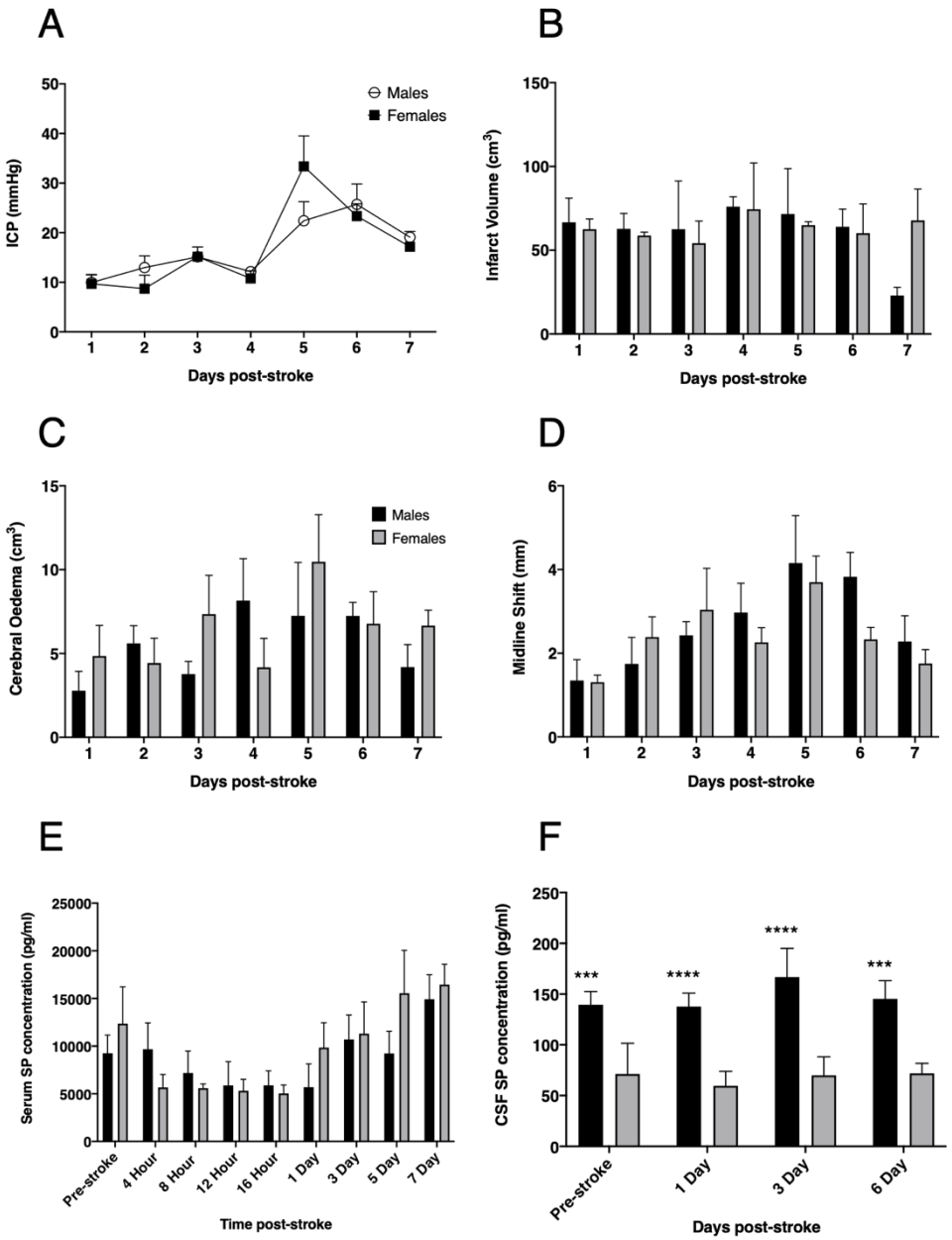

Figure 7.8. Sex differences post middle cerebral artery occlusion. There was no significant difference in ICP seen between sexes at any of the post-stroke time points ($p>0.05$). Furthermore, there was no significant difference seen between males and females in infarct volume, cerebral oedema or midline shift ($p>0.05$). SP levels in the serum were not significantly different between sexes ($p>0.05$) but were significantly elevated in the CSF of female animals compared with males at both pre- and post-stroke time points ($p<0.01$). Data shown as mean ±SEM. ***$p<0.01$, ****$p<0.0001$ females compared with males. *n*=3/time-point ICP infarct volume, midline shift and oedema; *n*=6/time-point for serum; *n*=4/time-point CSF.

7.3.8 Immunohistochemistry

7.3.8.1 Albumin

There was minimal evidence of albumin extravasation in sham tissue (Figure 7.9 S). Following stroke, marked albumin extravasation, indicative of BBB breakdown and subsequent vasogenic cerebral oedema formation, was observed both macroscopically within the infarcted territory and microscopically in the perivascular tissue of the infarct, which was most prominent at 4-, 5- and 6-days post-stroke.

7.3.8.2 Substance P

Little to no perivascular SP immunoreactivity was observed in sham tissue (Figure 7.10, Substance P, S). Following stroke, a marked increase in perivascular SP immunoreactivity was observed in tissue at 5 and 6 days, which remained evident at 7 days, although less pronounced.

7.3.8.3 Caveolin-1

Low levels of caveolin-1 immunoreactivity were observed in sham tissue (Figure 7.10, Caveolin-1, S). Following stroke, an increase in perivascular caveolin-1 immunoreactivity was observed, which was particularly evident at 5- and 6-days post stroke.

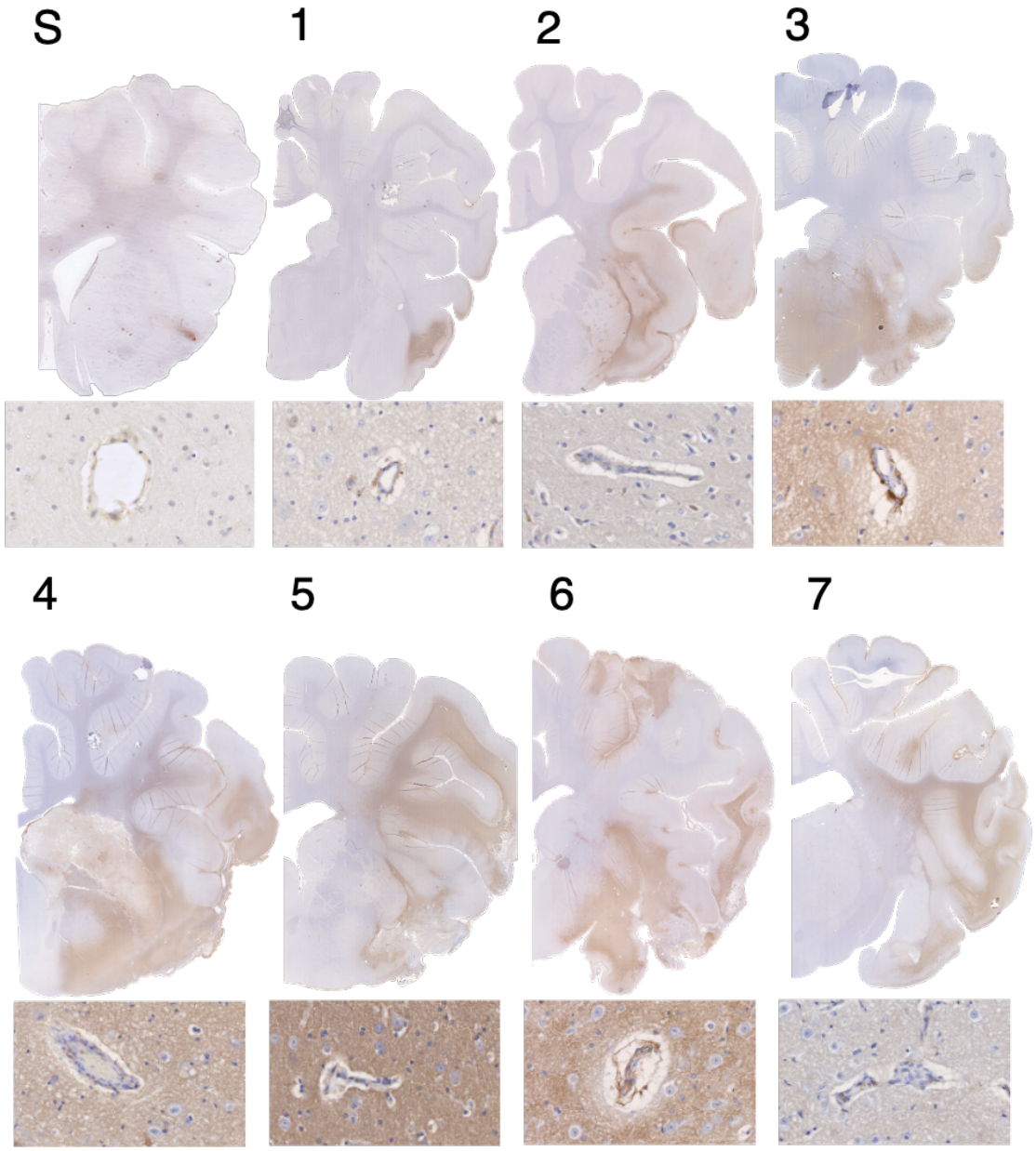

Figure 7.9. Albumin immunoreactivity in sham (S) and post-stroke animals at 1 (1), 2 (2), 3 (3), 4 (4), 5 (5), 6 (6) and 7 days (7) post-stoke. Enhanced albumin extravasation evolved over time following stroke and was most prominent at 4-6 days post transient MCAo. This pattern of albumin staining is consistent with perivascular staining seen microscopically. Microscopic images scale bar 100 μm, 40 × magnification.

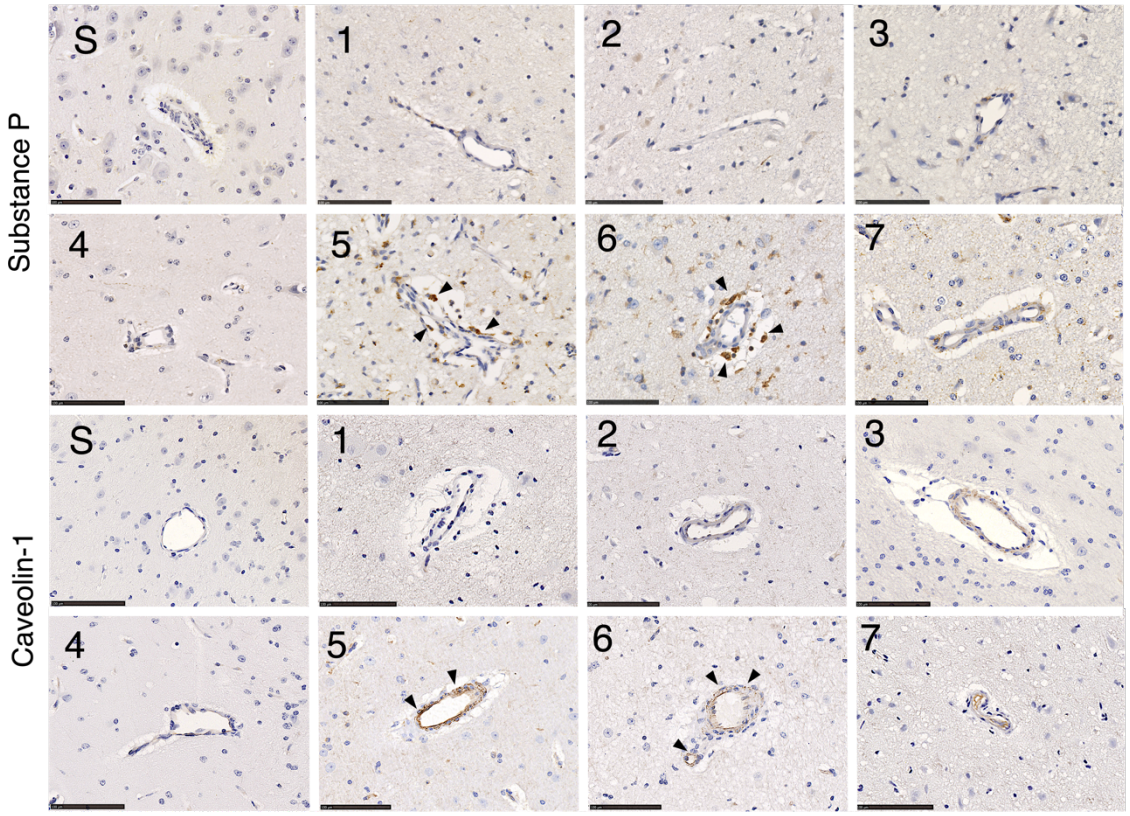

Figure 7.10. Substance P (SP) and caveolin-1 immunoreactivity. There was no identifiable immunoreactivity of SP or caveolin-1 in sham animals (S). Low levels of SP immunoreactivity were seen perivascularly at 1-4 days post stroke. At 5 and 6 days following transient MCAo, there was an increase in SP seen in the perivascular tissue of the ischaemic penumbra in the affected hemisphere. This increase in SP was concordant with an increase in caveolin-1 immunoreactivity perivascularly, which was most evident at 5-6 days. Arrows indicate increased immunoreactivity of SP and cav-1 seen surrounding vessels. Scale bar 100 µm, 40 × magnification.

7.4 DISCUSSION

This study is the first to describe a surgical approach to ovine tMCAo with reperfusion. Through this study we have successfully developed a model that conserves tissue and permits post-operative recuperation, allowing for investigation of the pathophysiology of ischaemic stroke, in particular post-stroke complications such as BBB disruption, development of cerebral edema and elevated ICP. This method of transient stroke induction provides a clinically relevant model in which promising novel treatments targeting stroke and its complications can be screened. Using this model, we have successfully characterised the temporal profile of ICP out to 7 days post-stroke.

Although a number of studies have reported raised ICP following transient stroke in small animal models (Beard et al., 2015, Murtha et al., 2015) and large animal species at early time-points (Wells et al., 2015) this study is the first in which ICP was recorded out to 7 days post-stoke in a large gyrencephalic species. We have established that ICP peaks at 5-6 days following ovine transient MCAo. These findings are comparable with human patients, where ICP is shown to peak 3-5 days post-stroke, indicating that our model reliably replicates the clinical situation (Battey et al., 2014). The modest difference in the time course between the ovine model and humans may reflect the additional time taken to restore intracranial dynamics following surgery due to CSF aspiration required for optimal visualisation of the proximal MCA. Indeed, a closed skull approach to MCAo where ICP dynamics are maintained through the induction of stroke may yield a timeline of ICP changes that directly align with clinical pathogenesis; however, this was not possible due to the complex ovine extracranial anastomosis, the rete mirabile, which precludes endovascular

access via the ICA for insertion of a balloon catheter, autologous clot or other occlusive agent.

Regardless, at 5-6 days post-stroke this study consistently observed elevated ICP readings above 20 mmHg. Clinically, ICP readings of ≥20 mmHg warrant investigation for possible treatment and intervention (Battey et al., 2014, Lavinio and Menon, 2011), as persistently elevated ICP is associated with poor outcome following ischaemic stroke, widely accepted as being attributable to the development of oedema in the cerebral parenchyma (Ayata and Ropper, 2002). Despite this, conflicting studies have reported an elevation of ICP in the absence of cerebral oedema following small ischaemic stroke in rats (Beard et al., 2015, Murtha et al., 2015). However, the underlying pathophysiology of increased ICP was not reported and requires further investigation. Furthermore, in the case of larger hemispheric strokes seen clinically, such as that of proximal MCA or ICA occlusion, there is a positive correlation between cerebral oedema and elevated ICP (Engelhorn et al., 2002). We did not, however, observe such a relationship, which may reflect within group variability and the different cohorts that were required to populate the time course. Further, when measuring elevated ICP following stroke, the influence of autoregulation must also be taken into consideration. The ability to maintain cerebral homeostasis plays an important role in moderating the pathogenesis of elevated ICP. A loss of autoregulation has been shown to enhance the progression of ischaemia and development of cerebral oedema, and thus plays an important role during MCA reperfusion (Dohmen et al., 2007). It is proposed that autoregulation may be enhanced early following stroke, and become dampened at 6 days post-stroke (Reinhard et al., 2012), in keeping with our observations of significantly elevated ICP at 6 days post-stroke. Elevated ICP is associated with a decreased ability to autoregulate

following head injury, indicating a strong positive correlation between the two (Reinhard et al., 2012).

We observed an evolution of cerebral oedema over time following stroke, although changes were not significant between time-points. Nevertheless, as previously stated it is widely accepted that the increased volume of the brain as a result of cerebral oedema positively correlates with subsequent elevations in ICP (Battey et al., 2014, Brogan and Manno, 2015, Beard et al., 2015). The development of vasogenic cerebral oedema in particular occurs following loss of integrity of the BBB, permitting the abnormal extravasation of proteins across the damaged barrier. This creates an osmotic drive pulling water from the vasculature into the extracellular cerebral parenchyma, leading to an overall increase in brain volume and concomitant rise in ICP (Battey et al., 2014). Our study was able to confirm that there was disruption to BBB via visualisation of GAD within the brain parenchyma, suggesting that the cerebral oedema seen was vasogenic in nature. This finding was substantiated by the increased extravasation of albumin following tMCAo, which was most prominent at 5-6 days post-stroke. Albumin is unable to cross the intact barrier under physiological conditions due to its large size and structure (Quinlan et al., 2005). Previous studies have established that albumin crosses the barrier via the transcellular pathway, facilitated by caveolae (Abbott et al., 2006), of which caveolin-1 (cav-1) is an integral component (Nag et al., 2007). Indeed, increased barrier permeability in association with caveolin-1 upregulation has been observed in the absence of tight junction breakdown, confirming the integral role of caveolae in maintenance of barrier integrity (Povlishock et al., 1978, Nag et al., 2007). Our immunohistochemistry findings of increased cav-1 immunoreactivity at 5-6 days post-stroke corroborate this, providing a potential mechanism that may be driving sustained barrier permeability and evolution of cerebral oedema. Furthermore, the

volumetric enlargement of the brain as a result of vasogenic oedema leads to displacement of cerebral tissue and subsequent shift of the midline, a critical state in which compression of adjacent brain structures precedes potentially fatal tonsillar herniation (Huttner and Schwab, 2009). We observed significant midline shift at 5 days following stroke in keeping with elevated ICP. Taken together, our findings of enhanced GAD, albumin and cav-1 immunoreactivity at 5-6 days post-stroke suggest a loss of barrier integrity at this time-point, precipitating the development of vasogenic cerebral oedema, extensive midline shift and the subsequent rise in ICP.

We also demonstrated that serum SP levels were increased at 7 days following stroke when compared with pre-stroke values. This followed a non-significant decline in serum SP at 4 hours which continued to decline up to 16 hours following injury. This suggests a peak increase in the levels of serum SP may occur ahead of the 4 hour-post-stroke sampling time-point. Indeed, rodent TBI studies reported an early peak in plasma SP levels at 30 minutes post-injury but a decline by 5 hours post-injury (Donkin and Vink, 2010) Similarly, SP levels were increased in serum samples obtained within 12 hours following the onset of both clinical stroke (Bruno et al., 2003, Lorente et al., 2016) and TBI (Lorente et al., 2015), with higher levels associated with early mortality. Although some discrepancy between experimental and clinical time-points exists, it is important to acknowledge that it is difficult to draw firm comparisons given the complications in obtaining clinical samples at acute time-points. We also examined SP levels in the CSF following stroke, though observed no differences at 1-, 3- or 6-day time-points. Although females consistently had higher CSF SP levels compared with males at all post-stroke time-points, there was no significant change in these levels post-stroke. This suggests that females have higher baseline levels of SP. Indeed, gender differences in the SP response have previously been observed (Pittenger et

al., 2016, Simões et al., 2018). A comprehensive sampling regimen, including sampling at 4- and 6-days post-stroke for serum and 4- and 5-days post-stroke for CSF, would be required to provide a detailed time-course of changes in SP in the serum and CSF in the setting of ischaemic stroke, and may reveal changes beyond those observed in the current cohort. Nevertheless, the increase in serum SP levels observed, in conjunction with the increased barrier permeability and vasogenic oedema seen with albumin IHC and MRI, support a potential role for SP in the genesis of cerebral oedema and development of elevated ICP in this model. Indeed, our rodent stroke studies support this (Turner and Vink, 2012, Turner and Vink, 2014, Turner et al., 2011, Turner et al., 2006, Corrigan et al., 2016a, Corrigan et al., 2012) and corroborates our recent work demonstrating the efficacy of NK1-R antagonist treatment in reducing ICP in an ovine model of permanent MCAo (Sorby-Adams et al, 2019b). Taken together, these findings suggest that neurogenic inflammation occurs following ischaemic stroke and may contribute to the increased BBB permeability and elevated ICP observed, suggesting that blocking the action of SP with a tachykinin NK1-R antagonist may be an effective strategy to mitigate these post-stroke complications and improve outcome.

7.4.1 Limitations and future directions

Although the findings of this study demonstrate successful model development and clearly show the evolution of ICP following stroke, several limitations must be acknowledged. It must firstly be recognised that human patients are rarely under anaesthesia when suffering a stroke. This is of particular importance due to the implied effects of anaesthesia, both protective and deleterious. Ketamine has been shown to have neuroprotective effects (Hudetz and Pagel, 2010), whilst isoflurane is associated with respiratory depression, decreased MABP and thus diminished oxygen supply to neuronal cells (Murr et al., 1993),

exacerbating cerebral ischaemia. These limitations have been discussed in detail in our previous studies (Wells et al., 2015, Wells et al., 2012), however due to the nature of the surgical procedure, anaesthesia is unavoidable (Lin et al., 1997). The decision to maintain animals on a combination of ketamine and isoflurane was made on the basis of prolonged duration (4-5 hours) of surgical procedures. The anaesthetic combination produces a countering effect, eliminating the neuroprotective effect of pure ketamine and the respiratory distress associated with pure isoflurane, thus reducing confounding factors of either anaesthetic agent administered alone (Schifilliti et al., 2010).

There was a large within group variability, particularly for the MRI parameters, observed at each of the time-points following stroke. This may reflect differences in collateral flow or autoregulation capacity within the individual animals. Indeed, there is a considerable degree of variation in the severity and timing of cerebral oedema in human patients following stroke. Variability may also be attributable to the severity of stroke in addition to the relative age of the sheep compared with the greater stroke population. In this study we used sheep aged 18-36 months, which are the equivalent to mid-adulthood in humans, whereas clinical stroke most commonly occurs in those over 60 years of age. Furthermore, the exclusion of experimental animals due to anaesthetic complications or lack of reperfusion decreased the total sample size. This could be addressed by increasing the overall sample size for each group to increase statistical power. It must also be acknowledged that we used different cohorts of animals to generate the stroke ICP data, sham ICP data and serum/CSF for the ELISAs. This led to an inability to run true correlations between groups, for example between the SP and ICP datasets, limiting the conclusions we can draw regarding the potential relationship between serum/CSF SP and ICP. Furthermore, there was some discrepancy seen between elevated ICP and oedema at 5-6 days in the first cohort, and

elevated serum SP seen at 7 days in the second cohort. Our findings suggest that SP is involved in the evolution of oedema, however, given that different cohorts were used in this study it was difficult to establish a definitive relationship between the two. As such, the differences in the time course of SP elevations and increased ICP are most likely attributable to the different cohorts used for each of these outcome measures.

In order to reduce the number of animals required we utilised a historical cohort of sham animals that underwent sham surgery immediately followed by ICP monitoring. We acknowledge that we would have preferentially used the same regimen as the stroke cohort, but it was not possible to generate an additional sham control cohort for this study alone. When measuring ICP, values would ideally be obtained from the same animal from 1-7 days post stroke to look at the evolution of pressure intrinsic to that animal. This could be addressed through the use of a telemetric system to remotely and non-invasively measure ICP. As sheep are quadrupeds, however, some questions remain regarding the impact of head position, in particular when feeding, on ICP measurements obtained using this method. Furthermore, the use of individual cohorts of animals allowed us to harvest the brain at specific time-points following stroke and perform IHC accordingly, an important aspect to understanding the evolution of the injury.

The reliable measurement of cerebral oedema on MRI at a single time-point is somewhat contentious, as the hyperintensity of vasogenic oedema is difficult to distinguish from the lesion itself. The measurement of the entire FLAIR lesion volume therefore includes areas of infarction as well as oedema and is therefore an indirect measure of oedema volume. A more robust approach to measuring oedema would be to undergo sequential MRI's and evaluate the change in diffusion lesion volume between 2 time points following reperfusion,

which was not feasible in this study due to cost. Furthermore, although GAD was utilised, T_1 weighted MRI images were only taken at a single time-point following administration. As such, it is difficult to obtain a quantitative measure of GAD extravasation across the barrier. A more robust approach to this would be to obtain dynamic contrast enhanced (DCE) and dynamic susceptibility contrast (DSC) sequences to obtain quantitative, clinically relevant measurements of barrier permeability. Finally, although gender differences were examined in this study the hormonal status of the female animals at the time of stroke and monitoring period was not known.

7.5 CONCLUSIONS

In this study, we have successfully developed a surgical approach to tMCAo with reperfusion in the sheep that permits recovery and the examination of long-term time-points following stroke. In this novel model we have determined the temporal profile of ICP, showing that ICP peaks at 5-6 days following stroke, in conjunction with midline shift, an evolution of cerebral oedema, increased serum SP levels, enhanced SP immunoreactivity and increased albumin extravasation. These results suggest a putative role for SP in BBB disruption and the subsequent genesis of cerebral oedema and associated rise in ICP following stroke. As such, agents targeting elevated ICP and cerebral oedema would be most effective when administered prior to 6 days post-stroke, or as early as possible following stroke-onset. We conclude that this ovine model provides a promising platform to screen novel treatments targeting post-stroke complications and verify treatment efficacy prior to clinical assessment.

Acknowledgements

This study was supported by funding from the NHMRC (Project Grant 1082556) and the NeuroSurgical Research foundation (Australia). The authors would like to thank Sunthara Rajan Perumal for the acquisition of the MRI. We would also like to acknowledge the facilities and technical assistance of the National Imaging Facility, a National Collaborative Research Infrastructure Strategy (NCRIS) capability, at LARIF, South Australian Health and Medical Research Institute (SAHMRI).

08

Elevated Intracranial Pressure Following Transient Stroke: The NK1 Tachykinin Receptor as a Potential Therapeutic Target

.

Prepared in publication format by **SORBY-ADAMS, A. J.**, MARIAN, O.C., BILECKI., I.M., ELMS., L.E., LEONARD, A.V., VINK, R., & TURNER, R. J.

Statement of Authorship

Title of Paper	Elevated intracranial pressure following transient stroke: the NK1 tachykinin receptor as a potential therapeutic target
Publication Status	☐ Published ☐ Accepted for Publication ☐ Submitted for Publication ☑ Unpublished and Unsubmitted w ork w ritten in manuscript style
Publication Details	Publication prepared in manuscript style

Principal Author

Name of Principal Author (Candidate)	Annabel Sorby-Adams		
Contribution to the Paper	I conducted the surgeries, analysed the data and am the first author and main contributor to the manuscript.		
Overall percentage (%)	60%		
Certification:	This paper reports on original research I conducted during the period of my Higher Degree by Research candidature and is not subject to any obligations or contractual agreements with a third party that would constrain its inclusion in this thesis. I am the primary author of this paper.		
Signature		Date	16.03.2021

Co-Author Contributions

By signing the Statement of Authorship, each author certifies that:

i. the candidate's stated contribution to the publication is accurate (as detailed above);

ii. permission is granted for the candidate in include the publication in the thesis; and

iii. the sum of all co-author contributions is equal to 100% less the candidate's stated contribution.

Name of Co-Author	Renee Turner		
Contribution to the Paper	Associate Professor Renee Turner is the head of the Translational Neuropathology Laboratory and primary supervisor on this thesis. She oversaw experimental design, data analysis, manuscript preparation and editing.		
Signature		Date	16.03.2021

Name of Co-Author	Anna Leonard		
Contribution to the Paper	Dr Anna Leonard is a member of the Translational Neuropathology Laboratory and on the supervisory panel for this thesis. She assisted in drafting the manuscript.		
Signature		Date	16.03.2021

Name of Co-Author	Levi Elms		
Contribution to the Paper	Mr Levi Elms was an honours student in the Translational Neuropathology Laboratory in 2018. He provided assistance collecting blood samples for pharmacokinetics.		
Signature		Date	16.03.2021

Name of Co-Author	Oana Marian		
Contribution to the Paper	Miss Oana Marian was a Research Assistant in the Translational Neuropathology Laboratory from 2017-2019. She provided intraoperative theatre assistance, postoperative care for the animals, assistance with perfusions, and collection of blood for pharmacokinetics.		
Signature		Date	16.03.2021

Name of Co-Author	Isabella Bilecki		
Contribution to the Paper	Miss Isabella Bilecki was an honours student in the Translational Neuropathology Laboratory in 2018 and remains a current PhD student. She provided assistance collecting blood samples for pharmacokinetics.		
Signature		Date	16.03.2021

Name of Co-Author	Robert Vink		
Contribution to the Paper	Professor Robert Vink was the past head of the Translational Neuropathology Laboratory. He oversaw experimental design.		
Signature		Date	16.03.2021

8.0 ABSTRACT

Background and Purpose: Following stroke, substance P (SP)-mediated neurogenic inflammation has been linked to profound blood-brain barrier (BBB) disruption, cerebral oedema, elevated intracranial pressure (ICP) and poor functional outcome. SP elicits its effects by binding the NK1 tachykinin receptor (NK1-R), with administration of an NK1-R antagonist ameliorating barrier dysfunction and cerebral oedema following stroke in rodent models. Due to a plethora of neuroprotectants developed in rodents failing clinical trials, stroke academic and industry guidelines now suggest screening promising novel agents in large animal species to improve the likelihood of successful translation. Accordingly, this study examined the efficacy of NK1-R antagonist treatment in reducing cerebral oedema and ICP in a clinically relevant ovine model of transient middle cerebral artery occlusion (MCAo).

Methods: Merino sheep (12M; 12F; 61±6 kg; 18-36 months) were anaesthetised and subject to 2 hours MCAo with reperfusion. Animals were randomly allocated into one of the following regimens, in which 2 boluses of the NK1-R antagonist (1 mg/kg) were given 5 hours apart: early treatment at 1-3 days post stroke (*n*=6), delayed treatment at 5 days post stroke (*n*=6) or saline vehicle (*n*=6). At 6 days post stroke, when elevated ICP is known to be established in this model, animals were re-anaesthetised and ICP measured for 3 hrs, followed by MRI to evaluate infarct volume (DWI), cerebral oedema (FLAIR) and parenchymal water content (T_2), and also to confirm vascular reperfusion (MRA). Following MRI, anaesthetised animals were euthanased, and brains removed for immunohistochemical analysis of albumin, caveolin-1 and claudin-5. An additional cohort of animals (*n*=6) underwent MCAo and late treatment administration only, following which whole blood

samples were obtained at four-hourly intervals for the assessment of NK1-R antagonist pharmacokinetics.

Results: ICP was significantly decreased following both early and delayed administration of the NK1-R antagonist compared with vehicles ($p<0.05$). Profound cerebral oedema was observed in vehicle treated animals at 6 days, in keeping with the elevated ICP. Cerebral oedema and midline shift were significantly reduced following both NK1-R treatment regimens ($p<0.05$). Marked perivascular caveolin-1 and albumin reactivity was observed in vehicle animals, with a decrease in reactivity seen following both early and late treatment. Pharmacodynamic assessment of the NK1-R was variable for C_{max} and 50% C_{max}. The T_{max}, however, was comparable for all animals, with a maximum peak at 8 hours, and a $t_{1/2}$ of 11 hours post-administration.

Conclusion: This study demonstrates that NK1-R antagonist treatment is an efficacious novel therapy for cerebral oedema and elevated ICP following stroke in an ovine model. Specifically, treatment is able to both prevent increases in ICP when administered early (1-3d) post-stroke, and also reduce established ICP when administered in a delayed (5d) fashion. This provides compelling evidence for future clinical evaluation of NK1-R antagonist treatment in the management of cerebral oedema and ICP following stroke.

8.1 INTRODUCTION

Cerebral oedema and concomitant rise in intracranial pressure (ICP) account for a mortality rate of up to 80% in the first week following middle cerebral artery (MCA) stroke (Hacke et al., 1996). Surmounting oedema typically peaks within 3 to 5 days post-ictus, with the deleterious effect of space-occupying swelling leading to secondary neurological deterioration and irreversible brain tissue damage (Thorén et al., 2017, Jüttler et al., 2007). Conservative pharmacological management, such as osmotherapeutics, aim to reduce oedema via rheological mechanisms (Brogan and Manno, 2015). In the setting of blood-brain barrier (BBB) breakdown, however, therapy is largely ineffective and may be associated with rebound oedema, necessitating surgical intervention via decompressive hemicraniectomy (DC) (Jüttler et al., 2007, Mori et al., 2001). Whilst early DC (within 48 hours of stroke onset) improves survival, it is associated with increased risk of transcalvarial herniation, haematoma, and morbidity in the elderly (Gopalakrishnan et al., 2018). Ergo, determining an optimal treatment solution for post-stroke cerebral oedema represents an urgent unmet need in the field of neurointensive medicine.

Identification of molecular pathways underlying the pathogenesis of cerebral oedema is essential in developing novel therapeutics which halt or prevent oedema progression. Attenuating neurogenic inflammation has been identified as one such strategy to combat cerebral oedema and elevated ICP post-stroke (Turner et al., 2011b, Turner and Vink, 2012, Sorby-Adams et al., 2017, Sorby-Adams et al., 2019b, Turner and Vink, 2007). In the setting of cerebral ischaemia, neurogenic inflammation occurs via noxious stimulation of sensory c-fibers present in high densities around cerebral blood vessels, leading to the aberrant release of neuropeptide substance P (SP) (Harrison and Geppetti, 2001, Hokfelt et al., 2000). Pre-clinical studies have shown that elevated perivascular SP is associated with increased

BBB breakdown, cerebral oedema, elevated ICP, and poor functional outcome following stroke in experimental models (Sorby-Adams et al., 2019a, Turner et al., 2006, Turner et al., 2011a). SP preferentially binds the neurokinin 1 tachykinin receptor (NK1-R), a G-protein coupled receptor expressed along endothelial cells of the BBB (Johnson et al., 2017). NK1 receptors are particularly abundant within endothelial caveolae, which facilitate paracellular transport across the barrier. Following stroke, it is proposed that binding of SP to the NK1-R compromises BBB integrity by increasing transport of osmotically active molecules such as albumin across the barrier (Vink and van den Heuvel, 2010). This drives an abnormal accumulation of water in the cerebral parenchyma and consequent rise in ICP. Administration of a NK1-R antagonist has subsequently been shown to reduce BBB permeability, cerebral oedema and functional deficits following stroke in rodent models (Turner et al., 2011a, Turner and Vink, 2014, Turner and Vink, 2012, Corrigan et al., 2016), further supporting the role of neurogenic inflammation in the pathogenesis of secondary injury post-stroke.

Unfortunately, however, numerous novel stroke therapeutic agents developed in rodents have failed to demonstrate efficacy in clinical trials, calling for more rigorous pre-clinical screening in accordance with the Stroke Therapy Academic and Industry Roundtable (STAIR) guidelines (O'Collins et al., 2006, (STAIR), 1999). For promising therapeutics such as the NK1-R antagonist, it is suggested that, prior to clinical evaluation, screening in a large animal species is performed to increase the likelihood of successful clinical translation (Fisher et al., 2009). Furthermore, advances in the acute management of stroke have highlighted the need for more ‘reperfusion-centric’ pre-clinical stroke research (Kuan and Sun, 2015). This is particularly relevant given the extended window for vascular recanalisation interventions (Broderick and Hill, 2021). Indeed, the tissue plasminogen

activator (tPA) thrombolysis window has expanded in selected patients well beyond 4.5h, and endovascular clot retrieval has shown efficacious outcomes up to 24h post-stroke in patients selected by multimodal imaging, for example perfusion-core mismatch detected on either CT perfusion or MRI (Nogueira et al., 2018, Ma et al., 2019, Albers et al., 2017, Thomalla et al., 2020). This has been game-changing for stroke management, with more patients than ever receiving reperfusion intervention. Restoration of blood flow and re-oxygenation of ischaemic tissue can, however, exacerbate tissue injury and trigger deleterious complications including exacerbation of haemorrhagic transformation, flow-no reflow phenomena and post-stroke cerebral oedema (Eltzschig and Eckle, 2011, Kloner et al., 2018). Re-initiation of blood flow can also cause ischaemia/reperfusion (I/R) injury and consequent accumulation of reactive oxygen species (ROS), inflammation, apoptosis, and increased permeability of the BBB, thereby exacerbating development of oedema. Clinically relevant, large animal models encompassing both permanent and transient occlusion are thus required to appropriately replicate the clinical scenario, establish the development of oedema, and provide a window for therapeutic intervention with anti-oedema agents.

We have previously determined the course of cerebral oedema and elevated ICP following both permanent (Wells et al., 2015) and transient stroke in a clinically-relevant ovine model (Sorby-Adams et al., 2019a). Specifically, following permanent MCA occlusion, significant cerebral oedema and elevated ICP was observed within 24 hours of stroke onset, whereas following 2-hour MCAo occlusion with reperfusion, ICP was shown to be significantly elevated at 5- and 6-days post-ictus, accompanied by profound midline shift. To determine the efficacy of NK1-R antagonism we subsequently assessed NK1-R treatment following permanent MCAo, showing that treatment administration produced reductions in ICP comparable to DC (Sorby-Adams et al., 2019b). However, whether NK1-R antagonist

treatment is also effective in stroke with a component of reperfusion has not yet been assessed. As such, this study sought to evaluate the efficacy of NK1-R antagonism following transient MCA occlusion in an ovine stroke model. Given the delayed nature of cerebral oedema and ICP development, two different treatment regimens were assessed to determine if the NK1-R antagonist could produce a clinically meaningful reduction in cerebral oedema and ICP when administered either early (before elevated ICP was established) or late (when ICP was already elevated), post-stroke. Furthermore, we also sought to assess the pharmacokinetics of the NK1-R following late administration, and to assess whether any differences in response to treatment between genders were apparent.

8.2 MATERIALS AND METHODS

8.2.1 Ethics Statement

This study was approved by the South Australian Health and Medical Research Institute (SAHMRI) Animal Ethics Committee (SAM 141, SAM 3). All experiments were conducted in accordance with the Australian National Health and Medical Research Council code of care and use of animals for scientific purposes (8th Edition, 2013).

8.2.2 Experimental Design

Twenty-four merino sheep (*Ovis aries*) were used in this study (12M;12F; 61±6 kg; 18-36 months old). Animals were sourced from a single farm in Gum Greek, South Australia, and transported to the SAHMRI Preclinical Imaging Research Laboratories (PIRL), where they were acclimated for 2 weeks in conventional outdoor paddocks prior to experimental procedures. Animals were pre-operatively randomised to one of the following treatment

regimens: early NK1-R treatment at 1-3 days post stroke (*n*=6), delayed NK1-R treatment at 5 days post stroke (*n*=6), or saline vehicle (*n*=6). The experimental timeline was as follows: induction of stroke on day 0; early (1-3 days) or late (5 days) NK1-R treatment; ICP monitoring (6 days). An additional cohort of animals (*n*=3M;3F, 18-36 months) underwent delayed treatment following which repeat collection of whole blood was performed at 4 hourly intervals for pharmacokinetic assessment of the NK1-R antagonist compound.

8.2.3 Surgical Approach

8.2.3.1 Preoperative Preparation

Animals were fasted for 12 hours preoperatively to reduce intraoperative regurgitation. Anaesthesia was induced via intramuscular administration of ketamine (0.05 mL/kg, 100 mg/kg Injection, CEVA, Australia) and diazepam (0.08 mL/kg, 5 mg/mL Injection, Pamlin, CEVA, Australia). Animals were intubated, and a jugular catheter (18 g, Terumo SURFLO®) inserted for delivery of intraoperative (1000 mL Hartmann's solution, Baxter Health, Australia) and post-operative (as required) crystalloid fluids. Animals were moved to a surgical theatre and placed on their left side on an operating table. Anaesthesia was maintained throughout surgery with inhalational isoflurane (1.5-2.0 % minimum alveolar concentration (MAC); mixed in 3 L of air and 500 mL of oxygen; Henry Schein, Australia) and continuous ketamine infusion via jugular line (4 mg/kg/hr). An arterial catheter (20 g, Terumo SURFLO®) was placed in the distal hindlimb to yield arterial blood gas samples. The catheter was regularly flushed (2 mL) via a 500 mL bag of sodium chloride (Baxter Health, Australia) attached to a pressurised bag pump (maintained at 300 mmHg). A paediatric blood pressure cuff (Easy Care Cuff, Phillips) was placed on the proximal

forelimb for a non-invasive measure of ABP which was manually recorded at 5-minute intervals.

8.2.3.2 Intraoperative Procedures

MCA occlusion with reperfusion surgery was performed as previously described in detail (Sorby-Adams et al., 2019a). Briefly, a pterional craniotomy was performed, dura incised, MCA visualised, and an aneurysm clip (Aesculap YASARGIL® Aneurysm Clip, Germany) applied to the proximal MCA and left *in situ* for 2 hours, after which it was removed to allow reperfusion. The dura was subsequently closed watertight with a synthetic dural regeneration matrix (Durepair®, Medtronic, USA) and superglue (Bostik, Australia), and a cranioplasty performed using autologous bone and dental cement (Sledgehammer, Keystone, Germany) to restore intracranial dynamics. The muscle was reopposed using a horizontal mattress suture technique, and the incision site treated with 1.0 mL 0.5% subcutaneous local anaesthetic Marcain (Bupivacaine hydrochloride 5 mg/mL, AstraZeneca, Australia). Hourly arterial blood samples were obtained and analysed (Machine AVL Scientific Corporation USA, Manufactured by Hersteller, OPTI Critical Care Analyzer–Model OPTI3, Serial No. OP3-2759) to ensure sodium, potassium, haematocrit, haemoglobin, bicarbonate, carbon dioxide and oxygen levels were maintained within normal physiological limits.

8.2.3.3 Postoperative Recovery

Animals were removed from anaesthesia, extubated and transported to a post-operative recovery pen. Once lucid, subcutaneous non-steroidal anti-inflammatory (NSAID; 0.7 mg/kg, 50 mg/mL every 12 hours, Carprofen, Norbrook, Australia) and intramuscular Buprenorphine (Temgesic, 1.0 mL, 300 ug/ml Buprenorphine hydrochloride, Reckin

Benckiser, Australia) were administered for pain relief, and intramuscular Depocillin for antibiotic cover (1 mL/25 kg every 12 hrs Procaine benzylpenicillin, Intervet, Australia). NSAID and antibiotic treatment was continued for 3 days post-operatively, and as required thereafter. All animals were assessed twice daily for clinical signs of stroke, in addition to general wellbeing, including urine and faecal output, food and water intake, and signs of apathy. Animals remained in indoor housing for the duration of the experiment and monitored remotely via closed-circuit television for 24-hour assessment.

8.2.4 NK1-R Administration

The dose of NK1-R antagonist was chosen based on previous studies following ovine permanent MCAo, where NK1-R antagonist treatment was initiated at 4 hours following stroke, with a subsequent bolus administered 5 hours later (Sorby-Adams et al., 2019). Animals herein were treated with 2 boluses, 5 hours apart, of 1 mg/kg NK1-R-antagonist as follows: early treatment on days 1, 2 and 3 post-stroke (n=6), delayed treatment at 5 days post-stroke (n=6) or saline vehicle (n=6). The NK1-R antagonist, supplied by PresSuraNeuro (EU-C-001, Hoffmann et al., 2005, Australian Patent AU2002328837B2 (under embargo), May 5, 2005), was warmed to ±37 °C and administered as slow bolus via jugular catheter (18 g, Terumo SURFLO®). Vehicle animals received an equal volume (1 mL/kg) of saline (Baxter Health, Australia), also via jugular catheter.

8.2.5 Intracranial Pressure Monitoring

All animals underwent ICP monitoring at 6 days following stroke. Animals were re-anaesthetised with ketamine (0.05 mL/kg, 100 mg/kg Injection, CEVA, Australia) and diazepam (0.08 mL/kg, 5mg/ml Injection, Pamlin, CEVA, Australia), and maintained with isoflurane (1.5-1.75% MAC, Henry Shein, Australia). Animals were placed in the sphinx

position on the operating table, and bilateral burr holes (5 mm) drilled using a Codman® Cranial Hand Drill (Codman & Shurtleff Inc., Massachusetts), approximately 1 cm lateral to the sagittal suture and 1 cm posterior to the horn buds. The underlying dura was incised, and plastic bolts from a Codman Microsensor™ Skull Bolt Kit for Intraparenchymal Procedures (Codman & Shurtleff Inc., Massachusetts) secured into the burr holes. Codman Microsensor™ transducers attached to a bridge amplifier and PowerLab data acquisition device (ADInstruments, Australia) were used to measure ICP. Transducers underwent two-point calibration checks to ensure accuracy (0 mmHg and 100 mmHg), following which they were advanced through skull bolts approximately 15 mm into the cerebral parenchyma. ICP was recorded for a duration of 3 hrs. Transducers were subsequently removed, and two-point checks re-performed to determine drift, if any. Physiological variables were recorded hourly throughout the monitoring period as previously described (section 8.2.3.2). Given that CO_2 is a potent cerebral vasodilator, efforts were made to maintain pCO_2 within physiological limits (36-44 mmHg), and also to prevent metabolic acidosis (pH <7.41) to reduce any predisposition to respiratory acidosis and thus potential elevation of CO_2.

8.2.6 Magnetic Resonance Imaging

8.2.6.1 Image Acquisition

Following ICP recording, animals were transported to a 1.5 T Siemens Syngo2004A (Siemens AG, Munich, Germany) MRI scanner for neuroimaging. Anaesthesia was maintained via inhalational isoflurane (3% MAC) and the following sequences acquired: time-of-flight magnetic resonance angiography (TOF MRA; TR 26 ms, TE 3.69 ms, slice thickness 0.50 mm), diffusion weighted imaging (DWI; TR 5600 ms, TE 80 ms, slice thickness 3.0 mm), fluid attenuated inversion recovery (FLAIR; TR 5000 ms, TE 386 ms, slice thickness 0.9 mm), T_1 weighted imaging (TR 2300 ms, TE 2.58ms, slice thickness 0.9

mm) and T_2 weighted imaging (TR 3200 ms, TE 410 ms, slice thickness 0.9 mm). T_1 weighted post-contrast images were also acquired following intravenous administration of 1 mL/kg gadolinium-diethylene-triamine-pentaacetic acid (Gadolinium) (Magnevist, Bayer HealthCare, Germany) to determine the extent of BBB breakdown on MRI.

8.2.6.2 Image Analysis

Infarct volume and cerebral oedema were calculated using segmentation tools in ITK-SNAP (v 3.7), as previously described (Sorby-Adams et al., 2019a, Yushkevich et al., 2006). DWI sequences were used to perform semi-automated three-dimensional (3D) quantification of the lesion. To determine cerebral oedema, 3D quantification of hyperintensities were calculated using FLAIR sequences. As MRI was only acquired at a single time point, DWI volumes were subtracted from FLAIR to provide a measure of peri-infarct oedema. Midline shift was used as a surrogate marker of cerebral oedema and was assessed using axial T_2 weighted scans and measured as the distance in mm from the septum pellucidum at the level of the foramen of Monro (HOROS DICOM image viewer v3.1.1).

To determine parenchymal water content, quantification of the relaxation signal was performed on axial T_2 scans at the level of the foramen of Monro. Here, eight regions of interest (ROI's) measuring 10 mm^2 were drawn in the ipsilateral and contralateral hemispheres. The mean signal intensity for each ROI was summed, and the average intensity for all ROI's reported for each hemisphere. Signal intensity ratios were then calculated by normalising the signal intensity within the stroke hemisphere to the signal intensity of the contralateral hemisphere. The normalised values in the stroke affected hemisphere were then exported for final interpretation.

8.2.7 Immunohistochemistry

Following MRI, animals were humanely euthanased via common carotid artery perfusion fixation with cold TRIS-buffered saline and bilateral jugular exsanguination under isoflurane anaesthesia (3%) following administration of intravenous heparin (5000 I.U./5mL; Pfizer, New York). The brains were removed and sliced into 10 mm coronal sections, following which they were immersion fixed in 10% neutral-buffered formalin for a minimum of 14 days prior to being processed, embedded in paraffin wax and sectioned coronally at 5-micron intervals. Histological examination was performed via albumin (1:2000, Dako Pty Ltd; A0001), caveolin-1 (cav-1; 1:1000 EDTA retrieval, Cell Signalling Technologies Pty Ltd; 3238) and claudin-5 (1:500 EDTA retrieval, Invitrogen Pty Ltd; 35-2500) immunohistochemistry (IHC) to examine vasogenic oedema, transcellular BBB permeability and paracellular BBB permeability respectively.

8.2.8 Pharmacokinetics

A separate cohort of animals underwent blood collection for pharmacokinetic (PK) measurement of the NK1-R antagonist EU-C-001 (n=6, 3M, 3F). All animals underwent stroke surgery as described (section 8.2.3.2) and were administered 2 × doses of the NK1-R antagonist at the late time point, 5 days following stroke onset. Blood samples were collected 5 minutes prior to treatment administration, and at 4, 8, 12, 16, 24 and 28 hours thereafter. Whole blood was collected in K2EDTA tubes (BD Vacutainer® K2EDTA tubes), with 12 mL of blood collected per animal, per time point (total 84 mL collected over the 28-hour sampling period). Tubes were gently inverted 180° to ensure mixing of anticoagulant to avoid microclotting. Samples were then placed in an ice bath for 20 minutes and centrifuged at 1500 RCF for 10 min at 18-25 °C. Plasma was aliquoted into 2 mL LoBind polypropylene

tubes (PCR clean, Eppendorf™, Australia) and samples flash frozen by liquid nitrogen immersion and transferred to a -80 °C freezer.

EU-C-001 and its desmethyl metabolite were subsequently extracted from plasma samples via protein precipitation extraction. Analytes were separated using high-performance liquid chromatography on an ACE C18-AR column, and the eluates monitored by an API4000™ liquid chromatography mass spectroscopy (SCIEX) in positive multiple reaction monitoring mode. The extracts were then assayed against a calibration cure, data analysed via Analyst® software (SCIEX) and processed in Watson LIMS™ (Thermo Scientific). The lowest limit of quantification (LLOQ) of the EU-C-001 compound was calculated as 0.200 ng/mL.

8.2.9 Statistical Analysis

Data are expressed as mean ± SD. Data was tested for normality using the Shapiro-Wilk normality test, or by assessing Q-Q plots of residuals. Physiological data (arterial blood pressure, pH, pO_2, pCO_2) were analysed using one-way analysis of variance (ANOVA) followed by Tukey's post-hoc tests (Prism v.8.0.1, GraphPad, CA). Values were averaged for each treatment group during surgery and ICP monitoring and reported as a single value. ICP measurements underwent logarithmic exponential transformation as previously described (Wells et al., 2015, Matthews et al., 1990). Values were reported at hourly intervals for 3 hours and expressed as geometric mean ± SD and analysed by two-way ANOVA. Cerebral perfusion pressure (CPP) was calculated by subtracting hourly ICP measurements from mean arterial blood pressure (MABP). MRI parameters (lesion volume, cerebral oedema, midline shift and T_2 prolongation) were analysed by one-way ANOVA, all followed by Tukey's post-hoc tests. To determine the effect of gender on all outcome measures, two-way ANOVA's with Sidak's post-hoc tests were performed. Correlations

were also run between cerebral oedema and infarct volume; cerebral oedema and midline shift; oedema and T_2 prolongation; ICP and cerebral oedema; to determine if a relationship was present. A p-value <0.05 and R value >0.4 were considered significant throughout.

8.3 RESULTS

8.3.1 Surgery, Mortality and Postoperative Course

There was no premature mortality observed throughout the experimental course, with all animals surviving to terminal experimental endpoints. Reperfusion was achieved in all animals, as confirmed by MRA (data not shown). Animals were observed for behavioural and neurological deficits following stroke surgery. Evidence of subdued demeanour was reported, although this was observed irrespective of treatment group (data not shown). The most common deficit observed was reduced food and water intake (*n*=6), which was most apparent at 5 (*n*=6) and 6 days (*n*=6) post-stroke. Other deficits included lowering of the head and drooping of the ears (*n*=2) and teeth grinding (*n*=3) on day 1 post-stroke. A subset of animals also displayed motor deficit, identified as a weakness in the contralateral fetlock joint following stroke, which was most prevalent at 1-3 days following stroke (*n*=3).

8.3.2 Physiological Parameters

Physiological parameters for pCO_2 ($F_{2, 15}$ =2.745, p=0.096), pO_2 ($F_{2, 15}$ =3.053, p=0.077), pH ($F_{2, 15}$ =1.612, p=0.232) and MABP ($F_{2, 15}$ =1.926, p=0.180) were comparable between all groups throughout transient MCAo surgery (p>0.05), irrespective of gender (p>0.05). During ICP monitoring, pH ($F_{2, 15}$ =1.985, p=0.172) and pO_2 ($F_{2, 15}$ =0.1043, p=0.902) levels were normal between groups and comparable between genders (p>0.05). However, blood pressure in vehicle animals was significantly higher compared with the late treatment

group ($F_{2, 15}$ =10.36, p=0.002), although no differences were observed between male and female animals (p>0.05). PCO_2 was also higher in vehicle animals compared with early ($F_{2, 15}$ =18.86, p=0.0016) and late ($F_{2, 15}$ =18.86, p<0.0001) treatment groups, but no effects of gender were observed (p>0.05). A summary of all physiological variables obtained during surgery and ICP monitoring is provided in Table 8.1.

Table 8.1 Physiological variables (Data expressed as mean +/- SD)

	pCO_2 (mmHg)					
	Surgery Day			*ICP Monitoring*		
	Males	Females	All animals	Males	Females	All animals
Vehicle	45±4	41±3	43±4	44±3	42±3	43±3
Early NK1	39±5	41±1	40±3	38±1	38±1	38±1
Late NK1	37±4	40±4	38±4	35±1	37±1	36±1
	MABP (mmHg)					
	Surgery Day			*ICP Monitoring*		
	Males	Females	All animals	Males	Females	All animals
Vehicle	79±16	91±5	85±12	123±5	108±9	116±10
Early NK1	87±17	82±8	84±12	107±7	96±12	101±11
Late NK1	75±10	73±5	74±7	92±3	93±6	93±4
	pO_2 (mmHg)					
	Surgery Day			*ICP Monitoring*		
	Males	Females	All animals	Males	Females	All animals
Vehicle	333±188	218±132	275±158	320±213	423±100	371±159
Early NK1	288±148	255±73	241±105	250±97	440±66	345±128
Late NK1	419±48	376±70	397±59	307±96	450±82	378±112
	pH					
	Surgery Day			*ICP Monitoring*		
	Males	Females	All animals	Males	Females	All animals
Vehicle	7.39±0.05	7.45±0.02	7.42±0.05	7.40±0.03	7.44±0.06	7.42±0.05
Early NK1	7.47±0.05	7.44±0.04	7.46±0.04	7.48±0.01	7.44±0.12	7.46±0.08
Late NK1	7.45±0.01	7.44±0.03	7.45±0.02	7.47±0.06	7.52±0.05	7.49±0.05

8.3.3 Intracranial Pressure

At 6 days post-stroke, a sustained elevation in ICP was seen in vehicle animals (Figure 8.1A). During the first hour of monitoring, ICP was 17.73 ± 6.70 mmHg, levels significantly higher than those recorded in sham animals (9 ± 3 mmHg) in our previous studies (Sorby-Adams et al 2019). Elevated ICP in vehicle animals was sustained throughout the second

(20.06 ± 5.41 mmHg) and final hour (24.51 ± 5.45 mmHg) of ICP recording. In comparison, early NK1-R antagonist treatment (1-3 days post-stroke) brought about a significant reduction in ICP compared with vehicles ($F_{2, 44}$ =28.06). This was evident during the second (ICP 11.50 ± 3.93 mmHg, p=0.022), and third (ICP 13.06 ± 3.34, p=0.0002) hour of ICP monitoring. Late NK1-R antagonist treatment also reduced ICP, sustaining a reduction throughout the first (9.21 ± 4.09 mmHg, p=0.006), second (9.63 ± 4.11 mmHg, p=0.0005), and final hour (11.43 ± 1.97 mmHg, p<0.0001) of ICP recording. There were no differences (p>0.05) in treatment efficacy between the early and late NK1-R treatment regimens. Despite differences in ICP response between vehicle and treatment animals, no differences in CPP were seen across any of the treatment groups ($F_{2, 44}$=0.930, p>0.05, CPP 84.76 ±16.41 mmHg, Figure 8.1B). Furthermore, the observed differences in ICP and CPP were seen irrespective of gender, with comparable CPP and ICP recordings seen in both male and female animals, and across all treatment groups (p>0.05, data not shown).

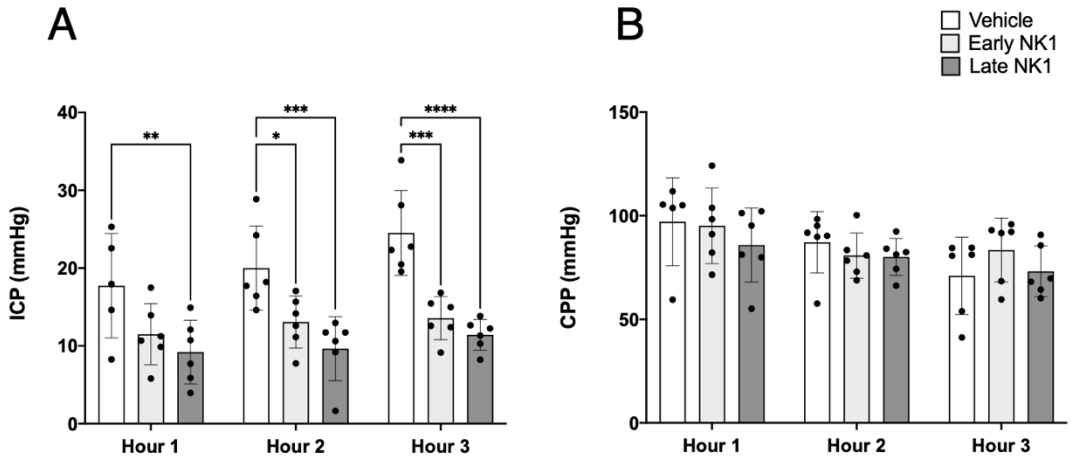

Figure 8.1. Intracranial pressure (ICP) and cerebral perfusion pressure (CPP). (A) At 6 days post-stoke, ICP was elevated in vehicle animals. Early NK1 treatment administered from 1-3 days following stroke brought about a reduction in ICP compared with vehicle, which was evident in the second (p<0.05) and third (p<0.001) hour of ICP recording. Delayed treatment at 5 days also brought about a significant reduction in ICP, which was evident throughout the first (p<0.01), second (p<0.001) and third (p<0.0001) monitoring hour. (B) No difference in CPP was observed between treatment groups at any time-point (p>0.05). Data presented as mean ± SD. *=p<0.05, **=p <0.01, *** =p<0.001 and ****=p<0.0001 compared to vehicle.

8.3.4 MRI

Infarct volume, calculated on DWI MRI, was comparable in both vehicle and NK1-treated animals ($F_{2, 15}$ =3.207, p>0.05; Figure 8.2A). Cerebral oedema, assessed on FLAIR, was reduced following both early ($F_{2, 15}$ =3.207, p=0.040) and late ($F_{2, 15}$ =3.207, p=0.049) NK1-R antagonist administration when compared with vehicles (Figure 8.2B). This was accompanied by a significant reduction in T_2 midline shift in both early ($F_{2, 15}$ =12.99, p=0.001, 1.03 ± 0.49 mm) and late ($F_{2, 15}$ =12.99, p=0.001, 1.12 ± 0.64 mm) treatment animals compared with vehicles (3.07 ± 1.08 mm; Figure 8.2C). Despite a reduction in oedema and midline shift, the amount of water in the ipsilateral hemisphere, as measured by T_2 prolongation, was only reduced following late ($F_{2, 15}$ =3.68, p=0.043), but not early NK1-R antagonist $F_{2, 15}$ =3.68, p=0.228) treatment (Figure 8.2D). Nevertheless, there was a qualitative increase in gadolinium extravasation across the BBB seen in vehicle animals compared with both the early and late NK1-R treatment groups (Figure 8.5). No gender differences were observed with respect to infarct volume, oedema or T_2 prolongation (p>0.05). However, there was a significant difference in midline shift within the vehicle group, with male animals having a greater shift from the midline compared with females (p=0.039, data not shown). Gender differences in midline shift were not observed in either of the NK1-R antagonist treatment groups (p>0.05).

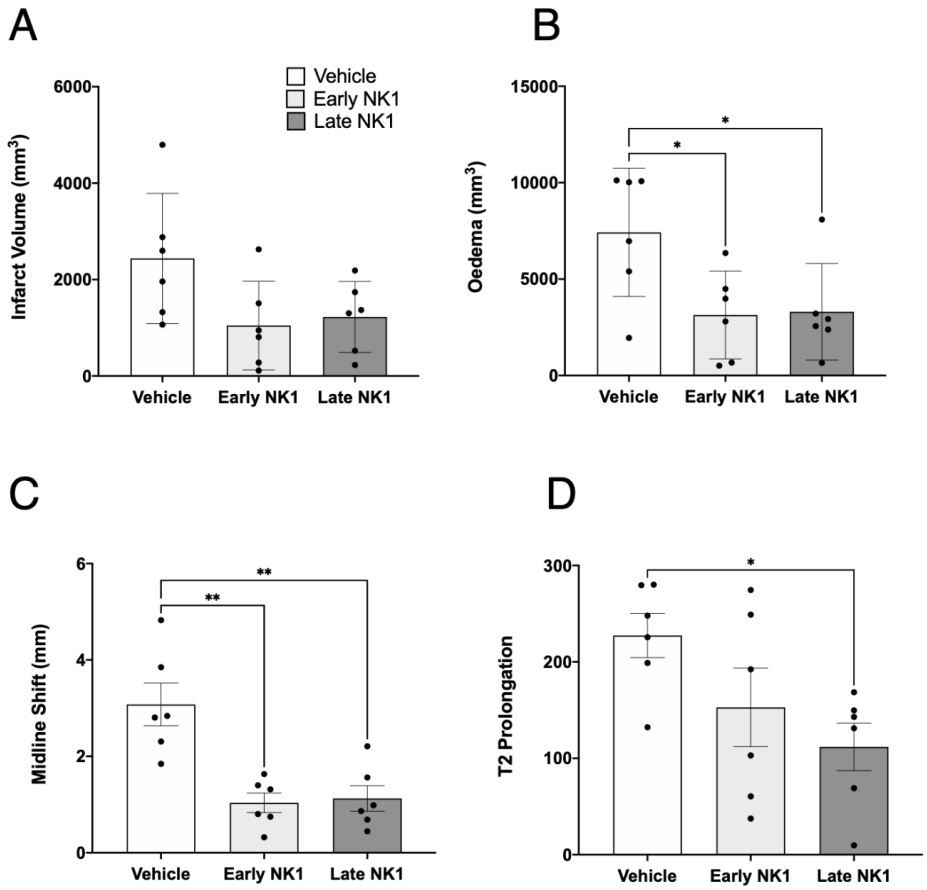

Figure 8.2. Infarct volume, cerebral oedema, midline shift and T_2 prolongation on MRI. (A) No differences ($p>0.05$) in infarct volume between vehicle and NK1-R antagonist groups were observed. (B) Cerebral oedema was reduced following both early ($p<0.05$) and late ($p<0.05$) NK1-R antagonist treatment, (C) accompanied by a reduction in midline shift seen in early ($p<0.01$) and late ($p<0.01$) treatment groups respectively. (D) Despite a reduction in oedema volume, water content in the stroke effected hemisphere was only reduced in late treatment animals ($p<0.05$) compared with vehicle. Data presented as mean ± SD. *=$p<0.05$, **=$p<0.01$, compared to vehicle.

In determining the relationship between outcome measures assessed, there was a poor correlation seen between infarct volume and oedema (r=0.046; Figure 8.3A). The relationship between oedema and midline shift, however, was strong (r=0.658; Figure 8.3B), and there was a moderate relationship between oedema and T_2 prolongation (r=0.548; Figure 8.3C). Despite observed relationships between MRI parameters, there was a poor relationship seen between ICP and oedema volume (r=0.310; Figure 8.3D).

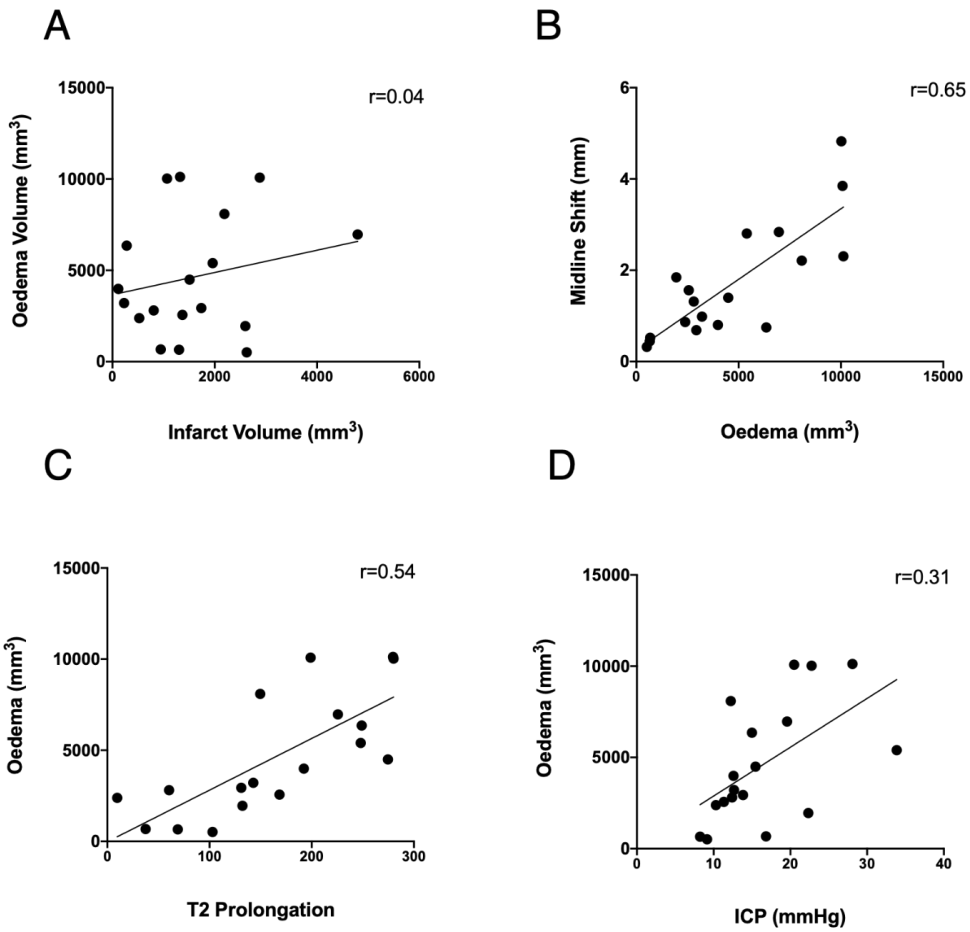

Figure 8.3. Correlations between outcome measures. (A) There was no relationship observed between infarct volume and oedema. (B) A positive relationship was seen between oedema and midline shift, and (C) oedema and T_2 prolongation signal. (D) No significant relationship was observed between oedema and ICP.

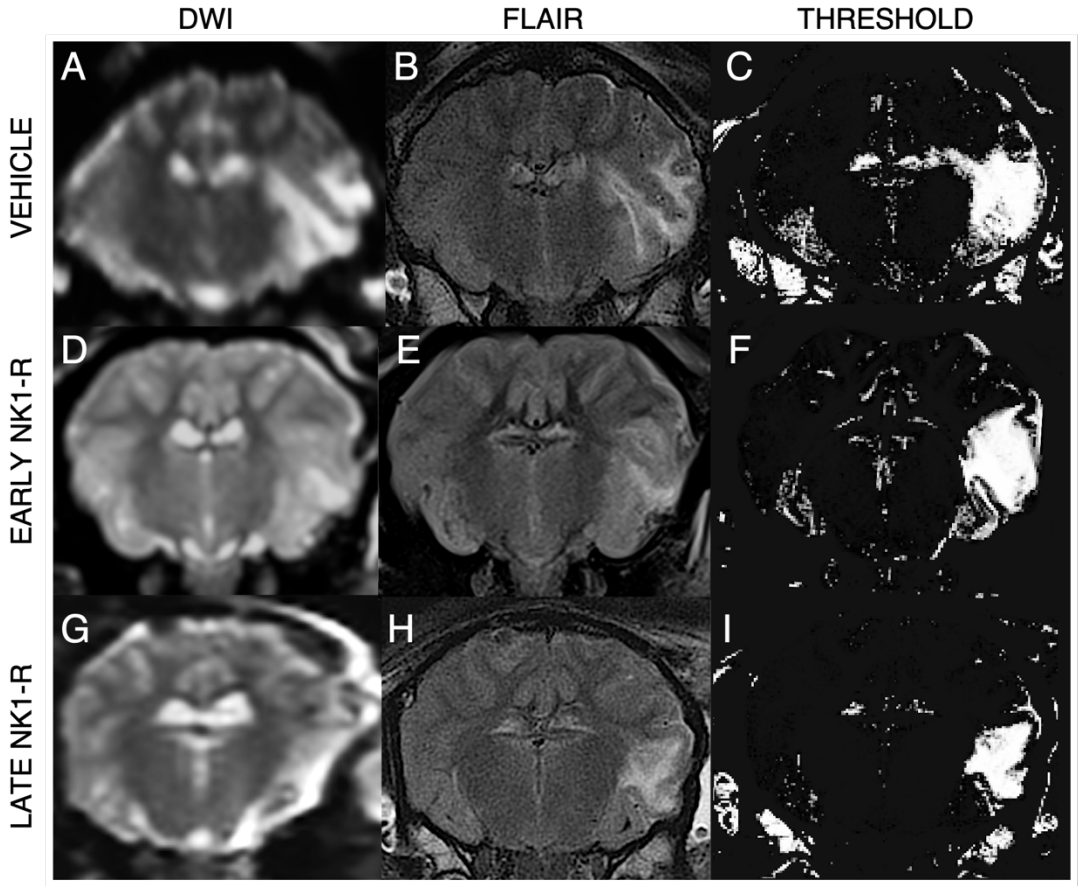

Figure 8.4. MRI findings following stroke. (A, D, G) Coronal DWI images indicate the lesion area which was comparable across all groups. (B, E, H) FLAIR images show a visible and significant reduction in cerebral oedema following both early (E) and late (H) NK1-R antagonist administration compared with vehicles (B). (C, F, I) Cerebral oedema was quantified by threshold adjustment and semi-automated three-dimensional segmentation.

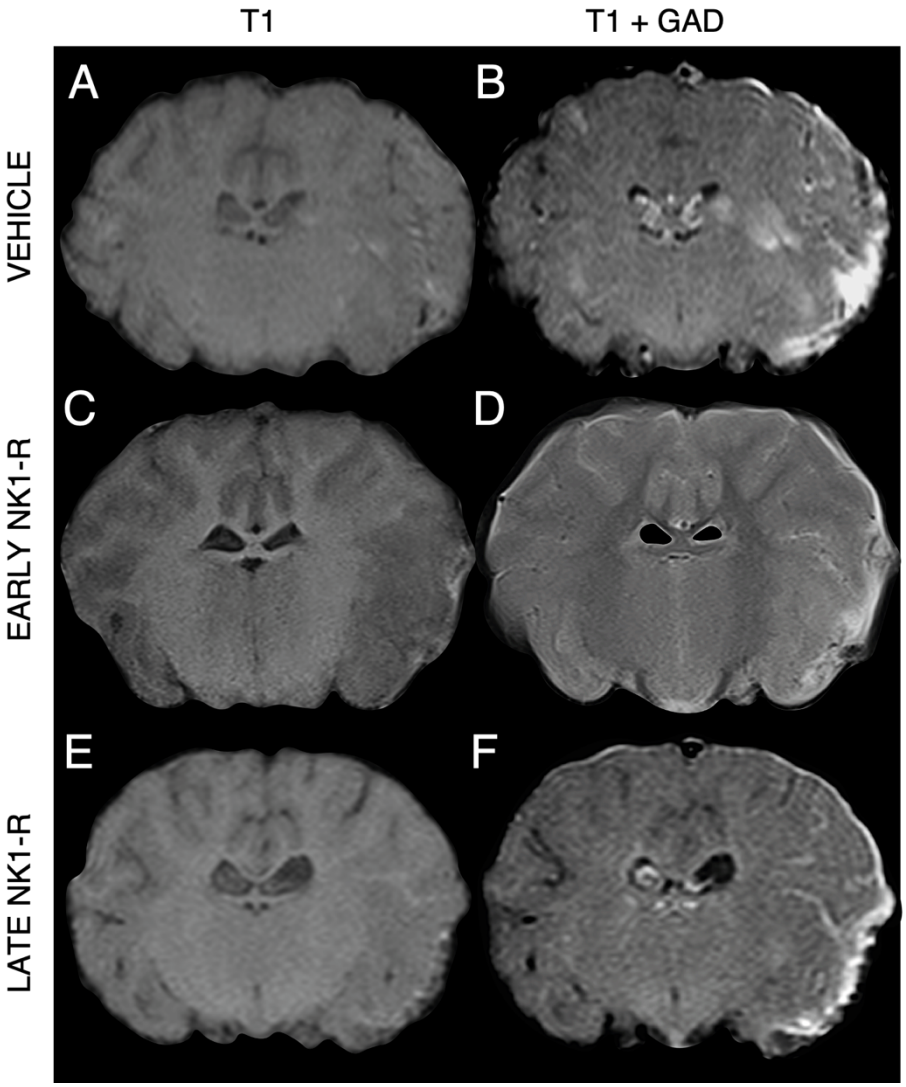

Figure 8.5. Pre and post gadolinium T_1 images. (A, C, E) T_1 images were comparable between treatment groups prior to gadolinium administration. (B, D, F) Following gadolinium administration, a bright rim was evident along the stroke affected hemisphere in territory of the MCA. Gadolinium extravasation into the parenchymal tissue was evident in vehicle treated animals (B), however there was less leakage evident in both the early (D) and late (F) NK1-R treatment groups.

8.3.4 Immunohistochemistry

8.3.4.2 Albumin

In sham animals, minimal albumin reactivity was observed, with weak staining localised to the vascular lumen (Figure 8.6, Albumin, Sham). Following stroke in vehicle animals,

marked albumin reactivity was observed. This was seen in the parenchyma, although it was significantly enhanced in the perivascular space. In both early and late NK1-R antagonist treatment animals, there was a reduction in both parenchymal and perivascular albumin reactivity observed.

8.3.4.1 Caveolin-1

Caveolin-1 immunoreactivity was not detected in sham tissue (Figure 8.6, Caveolin-1, Sham). Following stroke, an increase in perivascular caveolin-1 immunoreactivity was observed in vehicle animals. In both early and late NK1 treatment animals, however, there was decreased reactivity within the perivascular tissue. Furthermore, there appeared to be enhanced white blood cell extravasation in stroke animals, although this was greatest in vehicle animals.

8.3.4.2 Claudin-5

Endothelial tight junction protein claudin-5 was identified in sham animals, circumscribing vessels within the brain parenchyma (Figure 8.6, Claudin-5, Sham). Following stroke, a loss of claudin-5 immunoreactivity was observed, which was consistent across vehicle and NK1-R treatment animals.

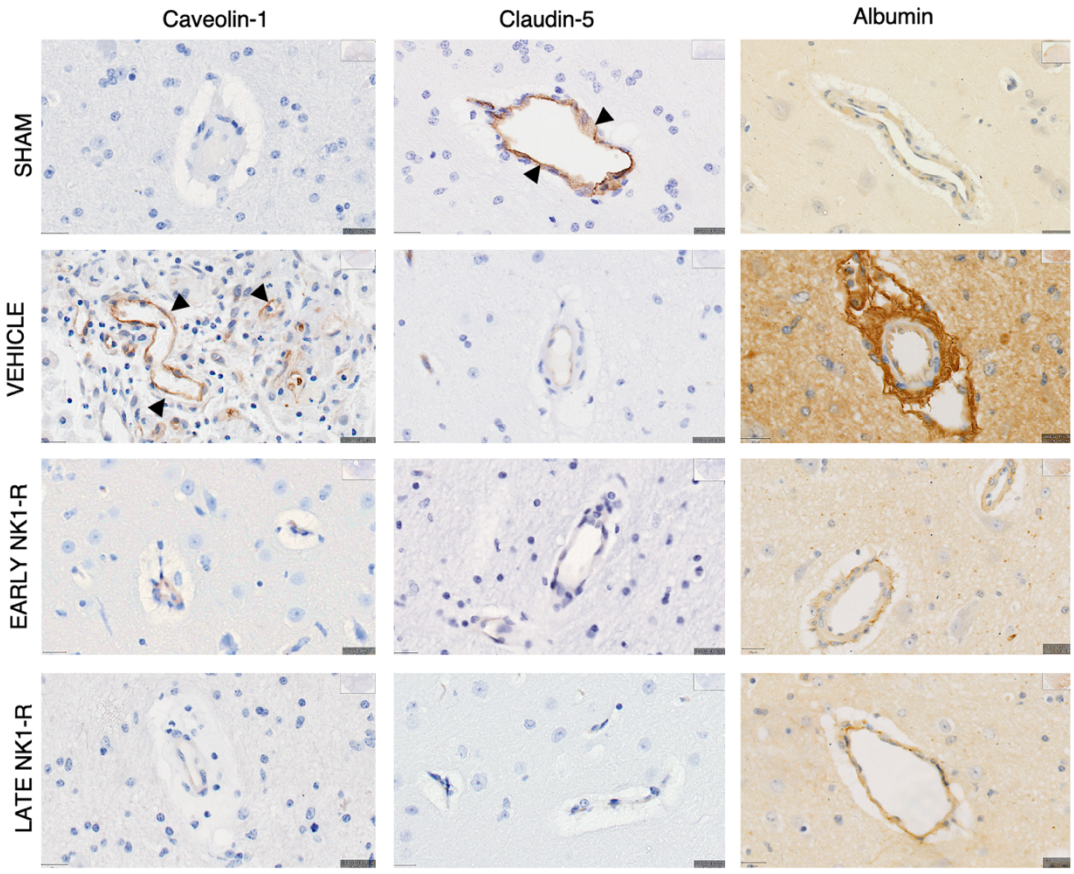

Figure 8.6. Immunohistochemical findings of caveolin-1, claudin-5 and albumin. Vehicle animals showed marked caveolin 1 and albumin reactivity. Following both early and late NK1-R treatment regimens, reactivity of caveolin-1 and albumin was reduced, comparable to sham. Claudin-5 reactivity was observed in sham animals, although no differences were observed between vehicle and treatment animals. Scale bar 100 µm, 40 × magnification.

8.3.5 Pharmacokinetics

The level of EU-C-001 in the plasma was below the limit of quantification (BLQ) prior to treatment administration (Figure 8.5, A). The maximum concentration (C_{max}; Figure 8.5C) and 50% C_{max} (Figure 8.5D) calculated across time points was highly variable between animals; however, the timing of the maximum (T_{max}; Figure 8.5E) was consistent, with highest peak seen at 8 hours following administration. The half-life ($t_{1/2}$) was less variable with an approximate average of 11 hours (Figure 8.5F). Furthermore, a constant decrease in plasma concentration was observed following the T_{max} at 8 hours, with a relative return to

baseline between 20 and 28 hours (Figure 8.5A). Male and female animals had comparable PK concentrations (Figure 8.5B).

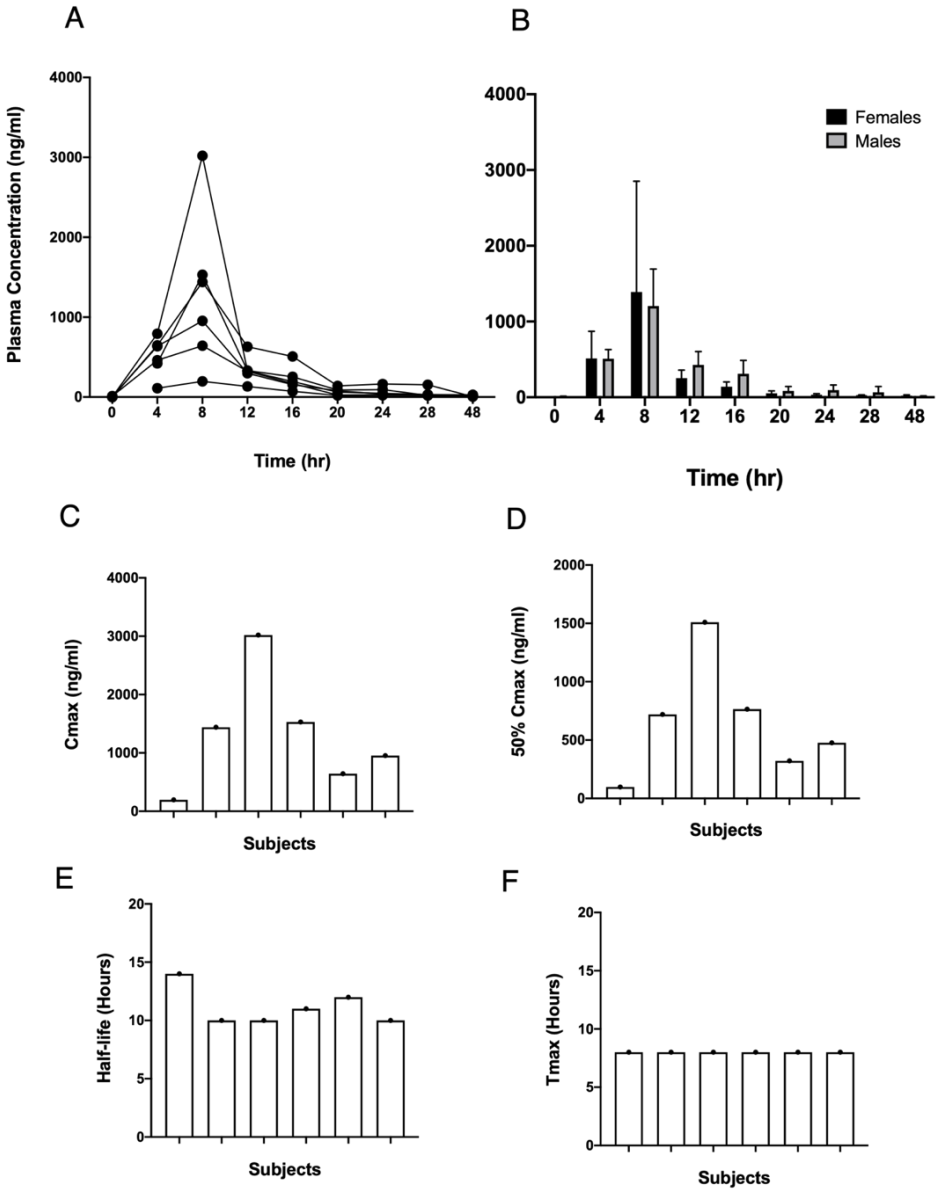

Figure 8.7. Plasma concentration of EU-C-001 following late treatment administration. (A) plasma concentration over time, (B) difference in male and female plasma concentration, (C) maximum concentration, (D) 50% of the maximum concentration, (E) half-life and (F) time to maximum concentration for each of the animals following treatment administration.

8.10 DISCUSSION

This study demonstrates the efficacy of NK1-R antagonist administration to reduce cerebral oedema and ICP following stroke with reperfusion in a clinically relevant large animal model. A significant and sustained reduction in ICP at 6 days post-stroke was observed following treatment, accompanied by a decrease in cerebral oedema and midline shift. More specifically, NK1-R antagonist administered either early (1-3d) post-stroke, before the onset cerebral oedema and elevated ICP, or in a delayed fashion (5d) post-ictus, when significant cerebral oedema and elevated ICP are established, were both shown to be effective in substantially reducing pressure.

In the neurointensive care unit, ICP in excess of 20 mmHg is classified as 'high' and is considered the threshold for intervention (Robba and Citerio, 2019). In vehicle animals, this study observed intracranial hypertension in excess of 24 mmHg. As per clinical guidelines, the current stepwise approach to treatment first seeks to minimise pressure conservatively, with therapy intensity modulated in accordance with the ICP response (Robba and Citerio, 2019). Conservative strategies to reduce ICP, however, almost consistently fail (Jüttler et al., 2007). This is largely due to their predominant mechanism of action, with intervention aimed at alleviating symptoms, rather than targeting the underlying cause of oedema genesis. When BBB integrity is compromised, as is established in this model and frequently reported in the clinical literature, pharmacological management with osmotherapeutic agents can paradoxically worsen injury, aggravating pressure differentials and causing devastating shifts of brain tissue (Schwarz et al., 1998, Chen et al., 2019, Jüttler et al., 2007, Manno et al., 1999). Decompressive surgery is thus often necessitated, albeit with numerous contraindications, inherent risk of post-operative complications, and maximal efficacy only achieved within 48 hours of stroke onset. Clinical management of ICP must also not be at

the expense of CPP. If pressure autoregulation is preserved, higher CPP (70 mmHg) is tolerated and may reduce ICP whilst maintaining cerebral blood flow to ischaemic tissue. If pressure autoregulation is not preserved, however, elevated CPP increases cerebral blood volume, resulting in an adverse rise in ICP (Robba and Citerio, 2019).

The reduction in ICP observed in this study thus addresses several limitations to current approaches to ICP management. Firstly, NK1-R antagonist administration produced a significant and sustained reduction in ICP following early treatment administration at 1-3 days. Although treatment ceased at 3 days, reduction in ICP and oedema remained at 6 days, suggesting that treatment is efficacious in maintaining barrier permeability, whilst not associated with rebound oedema commonly reported for existing pharmacological agents. Secondly, we established that treatment was effective when administered both early and in a delayed fashion, increasing benefits to patients presenting with cerebral oedema and elevated ICP in the days following stroke onset. Thirdly, as treatment is administered intravenously, this circumvents the need for invasive surgery, minimising risks of transcalvarial herniation and morbidity in the elderly associated with DC. Finally, NK1-R administration maintained CPP at approximately 80 mmHg in both treatment regimens, meaning that the reduction in ICP we observed was not at the expense of CPP, thereby avoiding further tissue compromise due to ischaemia.

The reduction in ICP observed following NK1-R antagonist treatment in this study supports findings from our previous work in which treatment was administered following permanent ovine stroke (Sorby-Adams et al., 2019). Taken together, these results suggest NK1-R antagonist treatment is effective in reducing ICP in the setting of both complete and partial MCA territory occlusion. Nevertheless, the inability to perform repeat, daily measurements

to determine the clinical course of ICP in real time must be acknowledged as a limitation of this study. The ICP system we used, although clinically applied, is not telemetric, meaning that animals were anaesthetised for the duration of ICP recording. Furthermore, anaesthesia and adequate animal positioning were necessary given the position of the head can significantly influence ICP dynamics (Ng et al., 2004). Given the need to open the skull and underlying dura to install the intraparenchymal probes, there was also a small amount (<1 mL) of CSF leakage. Previous studies investigating CSF dynamics in sheep report a formation rate of approximately 7.8±0.7 mL/h at an average resting pressure of 11.9±1.4 cmH_2O, with CSF formation constant over a wide range of CSF pressures (Mollanji et al., 2001). Although we have not observed CSF leakage in any of our experiments, in performing ICP recording on a single day, when ICP is known to be elevated, we sought to reduce the influence of repeat dural opening and thereby increase the validity of our findings. Finally, throughout the ICP monitoring period, pCO_2 was significantly higher in vehicles compared with treatment animals. Given the inverse relationship between pCO_2, CBF and pCO_2, this may have influenced ICP recordings. Nevertheless, no differences in CPP were seen between any of the experimental groups.

The results of this study suggest that the reduction in ICP observed was a result of attenuated cerebral oedema. Although we did not observe a strong correlation between cerebral oedema and ICP, reduced cerebral oedema and associated midline shift was observed in both early and late NK1-R antagonist treatment groups. However, a significant reduction in parenchymal water content was only observed in the late treatment group. The ability to accurately assess intracerebral water content is a significant benefit of large animal species. This is especially evident given the propensity for vasogenic oedema to develop in the white matter (Simard et al., 2007). Neglect of white matter pathology has been amplified by the

continued use of rodent experimental models, where relative white to grey matter ratio is considerably less than that of humans and large, gyrencephalic species (Dewar, 1999). Furthermore, the brains of larger animal species lend themselves to superior quality MRI studies (Sorby-Adams et al., 2018, West and Kaiser, 2020). Neuroimaging remains central to the assessment of clinical stroke, with perfusion and diffusion sequences particularly important. Indeed, a paradigm shift from 'time is brain' to 'imaging is brain' has been proposed, with imaging increasingly used to guide stroke intervention (Puig et al., 2020). Evidence of perfusion-diffusion 'mismatch', where a hypointense lesion is identifiable on DWI apparent diffusion coefficient images, but not FLAIR, indicates patient eligibility for intervention, whereas visualisation on both FLAIR and DWI denotes in-eligibility, as the infarct is beyond the window for effective thrombolysis (Mcgarry et al., 2020). In this study, we utilised clinically comparable scanning sequences (FLAIR, DWI, T_2) to quantify infarct and oedema volume and quantify changes in parenchymal water dynamics. However, one limitation of our imaging protocol was a lack of sequential scanning across post-stroke time-points. In clinical studies, scans obtained within 24 hours of stroke onset are deemed necessary to determine the evolution of ischaemic injury on subsequent scans. As MRI was only obtained at 6 days in the present study, it was difficult to reliably and accurately delineate the infarct from the surrounding oedema and thus examine evolution of the injury. Given infarct volume is a major predictor of the extent and clinical severity of cerebral oedema (Thorén et al., 2020), sequential imaging is highly advised for future studies to better evaluate accumulating oedema and thus the effect of treatment.

In line with our previous work, the attenuation of cerebral oedema with NK1-R antagonist treatment observed in this study is most likely due to inhibition of transcytosis-mediated albumin extravasation via caveolae (Sorby-Adams et al., 2019a, Corrigan et al., 2016). This

is supported by our histological findings, where NK1-R antagonist administration was shown to decrease albumin and caveolin-1 immunoreactivity. NK1-R are expressed within endothelial caveolae, whereby upon SP biding, caveolae undergo internalisation (Bowden et al., 1994, Kubale et al., 2007). Aberrant SP release, as seen following ischaemic stroke, leads to upregulation of NK1-R expression and increased caveolae formation. The main structural component of caveolae, caveolin-1, is directly involved in shuttling albumin from the abluminal to basolateral cell surface, resulting in an increase in parenchymal concentration. As albumin accounts for up to 80% of colloid osmotic pressure, its accumulation in the brain abnormally draws water into the parenchyma, resulting in an increase in total brain volume and subsequent rise in pressure (Gounden et al., 2021). Our findings of comparable claudin-5 immunoreactivity between vehicle and treatment animals further suggests a putative role of caveolae, suggesting the NK1-R is targeting paracellular, rather than transcellular transport across the BBB. Thus, unlike current pharmacotherapies used in the clinical management of cerebral oedema and elevated ICP, the NK1-R antagonist is directly targeting the mechanisms underlying the development of oedema. It is, however, important to note we did not perform quantification of histological findings. This may provide more insight into discreet differences between groups and represents an avenue for future analysis.

In addition to its role in facilitating albumin transport, SP has been shown to increases neutrophil adhesion to vascular endothelial cells, leading to increased leukocyte recruitment (Bost and Pascual, 1992, Ho et al., 1997, Johnson et al., 2017, Lai et al., 1998). In vehicle animals, we observed significant white blood cell infiltration in the infarct core, as identified by haematoxylin counter-staining. Although white blood cells were observed in the parenchyma of all stroke animals, these appeared to be more prevalent in vehicle animals.

Increased expression of NK1-R by leukocytes is proposed to occur via upregulation of pro-inflammatory cytokines following stroke onset, sensitising cells to the effects of SP (Rasley et al., 2002, Marriott and Bost, 2000). Consequent leukocyte extravasation via adhesion molecules ensues, promoting cell migration and surmounting neuroinflammation. SP has also been shown to increase the inflammatory responses of resident glial cells, such as microglia (Burmeister et al., 2017, Martinez and Philipp, 2016, Lim et al., 2017). Although not performed in this study, investigation of microglial activation may provide insight into the interaction of SP with other neuronal cell lines (Johnson et al., 2017). Further analysis should also be directed at exploring the effects of treatment on integrity of other BBB constituents (immunoglobulin G, Zona-occludens-1, matrix metalloproteinases), and neuroinflammation (microglia, astrocytes, pro-inflammatory cytokines) in order to further elucidate the mechanisms of NK1-R antagonist treatment following transient ischaemic stroke.

Although the efficacy of NK1-R antagonism has been demonstrated in prior models of permanent stroke in both rodents and sheep, this was the first to perform pharmacodynamic assessment of the EU-C-001 compound. Analysis in a large animal species is beneficial given their significant blood volume comparable to humans (sheep: ±4 L; humans: ±5 L), allowing for multiple blood draws, mimicking studies performed clinically. Ruminants have an intermediary metabolic clearance, and despite anatomical variation of their gastrointestinal system, metabolism is largely analogous between poly- and mono-gastric species (Toutain et al., 2010). Our findings demonstrated a peak concentration of EU-C-001 in the plasma 8 hours following administration, with levels still present at 12 and 16 hours, decreasing at 20 hours. Although the oestrous cycle was not determined in this particular cohort of animals, no significant differences were observed between male and female

animals in pharmacokinetic response. This provides critical evidence regarding the normal clearance from the plasma, with no evidence of a secondary adsorption or distribution peak seen up to 48 hours following administration. Given PK analyses were performed in animals receiving the late treatment regimen, this may provide explanation as to why outcomes were most improved in late, compared with early treatment regimens. In animals receiving treatment at 1-3 days post-stroke, although repeat dosing was performed, washout could have occurred by 6 days when ICP recording and MRI was performed. Nevertheless, if treatment attenuated secondary injury mechanisms and the development of neurogenic inflammation in the first 1-3 days following stroke, efficacious outcomes are still plausible when assessed at 6 days, as shown by the response to ICP and oedema reported herein. Whilst investigation of PK within both regimens is desirable, it was beyond the scope of the current study. Furthermore, although pharmacodynamic findings provided key evidence regarding the bioavailability of the NK1-R antagonist, it is possible that peak concentrations were missed due to the 4-hourly time-points for blood collection (for example, the maximum peak could have been at 2 hours). Future compartmental analysis of pharmacokinetics could be warranted to determine availability of EU-C-001 in the brain versus the plasma, in addition to evaluating clearance levels in the kidneys.

8.9 CONCLUSIONS

This study demonstrated that NK1-R antagonist treatment was effective in reducing ICP when given either before or after the establishment of elevated pressure, accompanied by significant reductions in cerebral oedema and midline shift. Taken together, the findings from this study provide compelling evidence for NK1-R antagonist treatment as a novel

therapy for the treatment of cerebral oedema and elevated ICP following transient stroke which warrants clinical investigation.

Sources of Funding

This work was supported by the National Health and Medical Research Council (NHMRC; Project grant GNT1082556) and by the NeuroSurgical Research Foundation (Adelaide, Australia).

09

A Novel Approach to Assessing Functional Outcome in an Ovine Model of Ischaemic Stroke

Chapter prepared in publication format by **SORBY-ADAMS, A.J.**, MARIAN, O.C., BILECKI, I.M., ELMS, L.E., CAMARGO, J., LEONARD, A.V., CROWTHER, R.G., TURNER, R.J. and JONES, C.F.

Statement of Authorship

Title of Paper	A novel approach to assessing functional outcome in an ovine model of ischaemic stroke
Publication Status	☐ Published ☐ Accepted for Publication ☐ Submitted for Publication ☑ Unpublished and Unsubmitted w ork w ritten in manuscript style
Publication Details	Publication prepared in manuscript style

Principal Author

Name of Principal Author (Candidate)	Annabel Sorby-Adams
Contribution to the Paper	I conducted the surgeries, designed the experiment, performed the behavioural assessment, analysed the data and am the first author and main contributor to the manuscript.
Overall percentage (%)	46%
Certification:	This paper reports on original research I conducted during the period of my Higher Degree by Research candidature and is not subject to any obligations or contractual agreements with a third party that would constrain its inclusion in this thesis. I am the primary author of this paper.
Signature	Date 16.03.2021

Co-Author Contributions

By signing the Statement of Authorship, each author certifies that:

i. the candidate's stated contribution to the publication is accurate (as detailed above);
ii. permission is granted for the candidate in include the publication in the thesis; and
iii. the sum of all co-author contributions is equal to 100% less the candidate's stated contribution.

Name of Co-Author	Renee Turner
Contribution to the Paper	Associate Professor Renee Turner is the head of the Translational Neuropathology Laboratory and primary supervisor on this thesis. She oversaw experimental design and manuscript preparation and editing. Her overall contribution was 6%.
Signature	Date 16.03.2021

Name of Co-Author	Claire Jones
Contribution to the Paper	Dr Claire Jones is an engineer on the supervisory panel for this thesis. She provided guidance regarding experimental design, development of mathematical coding for analysis and editing the manuscript. Her overall contribution was 10% Analysis, interpretation and presentation of data.
Signature	Date 16.03.2021

Name of Co-Author	Levi Elms		
Contribution to the Paper	Mr Levi Elms was an honours student in the Translational Neuropathology Laboratory in 2018. He provided intraoperative theatre assistance, behavioural assessment, postoperative care and perfusion.		
Signature		Date	16.03.2021

Name of Co-Author	Oana Marian		
Contribution to the Paper	Miss Oana Marian was a Research Assistant in the Translational Neuropathology Laboratory from 2017-2019. She provided intraoperative theatre assistance, postoperative care for the animals, assistance in perfusions, and behavioural assessment.		
Signature		Date	16.03.2021

Name of Co-Author	Isabella Bilecki		
Contribution to the Paper	Miss Isabella Bilecki was an honours student in the Translational Neuropathology Laboratory in 2018 and is now a PhD student. She provided intraoperative theatre assistance, behavioural assessment, postoperative care and perfusion. Her overall contribution was 8%.		
Signature		Date	16.03.2021

Name of Co-Author	Jonathan Camargo Leyva		
Contribution to the Paper	Mr Jonathan Camargo Leyva is a doctoral student in the department of robotics from the Georgia Institute of Technology. He provided guidance in analysis and development of mathematical coding.		
Signature		Date	16.03.2021

Name of Co-Author	Robert Crowther		
Contribution to the Paper	Dr Robert Crowther is a senior lecturer in Biomechanics University of South Australia. He provided guidance regarding experimental design and assisted in pilot studies.		
Signature		Date	16.03.2021

9.0 ABSTRACT

Background and Purpose: Motor impairment is a common feature of ischaemic stroke. When determining the therapeutic value of novel interventions, assessment of function is thus imperative. The poor clinical translation of treatments developed in rodent models of stroke has led to the increased use of large animals. The ability to accurately assess function in these species, however, remains a significant hurdle. This study aimed to develop a method to assess motor function using motion capture in addition to developing a neurological outcome assessment scale in a clinically relevant ovine stroke model.

Methods: Merino sheep (*Ovis aries*, 13M;13F, 18-36 months) were anaesthetised and subjected to 2 hours middle cerebral artery occlusion (MCAo) with reperfusion. Animals underwent baseline assessment 8, 5 and 3 days pre-operatively, and at 3 days post-stroke. Neurological assessment was carried out to determine changes in animal demeanour and neurological status pre- and post- stroke. To assess gait, 10 infrared cameras (Vicon Motion Systems Ltd. Oxford, UK) operating at a frame rate of 200 Hz measured the trajectories of 42 retro-reflective markers placed at defined anatomical locations. Kinematic parameters including stride, stance and swing duration, and limb joint angles were then calculated using MATLAB® (MathWorks Inc., Natick, MA). Intraclass Correlation Coefficients (ICC's) were used to assess the repeatability of each outcome of interest across baseline trials. The average of all baselines compared to 3-day post-stroke parameters were used to assess changes in kinematics following MCAo using linear mixed models.

Results: Motion capture assessment of baseline trials was reliable for the majority of assessed variables (ICC >0.50). Following stroke, kinematics measures were significantly

reduced ($p<0.05$); these included forward velocity, position of the head relative to the torso, and stance and stride duration of the forelimbs. Neurological assessment was able to indicate changes in animal impairment following injury, such as differences in gait, posture, appetite, postural reactions, and circling behaviours.

Conclusion: This study has developed a reproducible method of functional assessment following stroke in an ovine model. Using both motion capture and composite scoring allowed for the comprehensive evaluation of post-stroke deficits. This method has the potential to be applied to other large animal models of acute central nervous system injury to reliably measure changes in gait and demeanor.

9.1 INTRODUCTION

Stroke is a leading cause of death and the principal cause of adult neurological disability worldwide (Gorelick, 2019, Johnson et al., 2019). New approaches to reperfusion have extended the previously narrow window for intervention (Ma et al., 2019, Albers et al., 2018), resulting in reduced mortality, yet a higher incidence of patients facing persistent neurological impairment (Ballester et al., 2019). To improve functional outcomes in the increasing number of patients who survive stroke, new therapies targeting secondary injury and neurological recovery mechanisms are urgently required (Chollet et al., 2014).

Animal models are an essential step in the development of novel stroke therapeutic agents, with restoration of function a key indicator of a treatment's efficacy. However, the translation of pre-clinical findings to clinically efficacious stroke therapies has to date been largely ineffective (Kringe et al., 2020). This may, in part, be a consequence of pre-clinical experimental design, with the vast majority of failed trials being conducted in rodents, with many studies lacking comprehensive functional assessment (O'Collins et al., 2006). Due to their potential for enhanced clinical translation, large animal species are becoming increasingly used as a screening tool once initial therapeutic efficacy has been demonstrated in small animals (Hainsworth et al., 2017, Sorby-Adams et al., 2018a, Herrmann et al., 2019, Eaton and Wishart, 2017). Species such as dogs, pigs, sheep, and non-human primates (NHP's) have been used to model stroke, each with their own inherent benefits and disadvantages (see Sorby-Adams et al., 2018 for review). Porcine species commonly used in America, such as the Yucatan mini pig, are not readily available in other countries such as Australia. The routine use of NHP's remains expensive and ethically challenging, with strict housing requirements restricting their use to a few specialised laboratories (Sorby-

Adams et al., 2018). In comparison, the relative availability, amenable nature, and comparable neuroanatomy of sheep make them a promising species in which to model stroke (Wells et al., 2015, Wells et al., 2012, Boltze et al., 2008, Sorby-Adams et al., 2019a, Sorby-Adams et al., 2019b). Motor deficits have been documented following ovine middle cerebral artery (MCA) occlusion, including noticeable hemiplegia of the contralateral limbs and general apathetic behaviour (Sorby-Adams et al., 2019a, Boltze et al., 2008). These deficits are comparable to those seen clinically, where malignant MCA occlusion often presents as unilateral hemiplegia and hemiparesis, and resultant compensatory reliance on unaffected ipsilateral limbs (Nogles and Galuska, 2020, Jones, 2017). Post-stroke clinical assessment of upper limb function is often carried out using exams such as the National Institute of Health Stroke Scale (NIHSS), the Fugl-Meyer assessment and the Wolf motor function test (Quinn et al., 2009, Vliet et al., 2020). Lower limb differences in gait kinematics can also serve as a quantitative means of determining asymmetry and extent of neurological deficit, with studies demonstrating a significant increase in swing duration, and decrease in gait speed and stride length following stroke onset (Alexander et al., 2009, Rozanski et al., 2019).

Assessment of functional deficits in animal stroke models is essential in determining their relevance to clinical disability and enabling the evaluation of novel therapeutics. In rodents, this encompasses composite scores such as the Bederson scale and Modified Neurological Severity Score (mNSS), motor function tests such as rotarod, cylinder test, ledged beam, grid walking, reaching chamber and staircase test, and systems to assess gait such as the Catwalk and DigiGait (Schaar et al., 2010). Equivalent functional assessment in large animals presents a new set of challenges. Firstly, unlike their small animal counterparts, neurological exams are not well described for ungulate species. Although neurological exams for quadrupeds do exist, standard clinical tasks such as grip and grasp reflexes cannot

be assessed (Boltze et al., 2008, Cui et al., 2013). Secondly, tests developed for rodents are often difficult to translate to large animals due to the need for significant upscaling, whilst others are completely inappropriate for large species (e.g., rotarod). Thirdly, the relative size and strength of large animals requires the construction of robust systems that are both adaptable for use in farming environments and able to withstand a higher level of physical demand. It is also essential that such systems enable safe handling of the animal throughout assessment to ensure both animal and handler wellbeing. The development of a method to mitigate these challenges could lend itself to detection of both acute and long-term functional changes post-stroke.

In sheep, assessment of kinematics using motion capture serves as a quantitative means to assess gait, with systems being adapted for use in ovine musculoskeletal, orthopaedic and spinal cord-injury (SCI) models (Safayi et al., 2014, Safayi et al., 2015, Safayi et al., 2016, Wilson et al., 2017). In these studies, retro-reflective markers are placed on distinct anatomical locations allowing for the assessment of joint angles, stride length, and duration of stance, stride and swing. In large animal stroke models, gait assessment using motion capture has the potential to enhance functional assessment, and could be used alone, or in conjunction with conventional scoring systems. Accordingly, the objectives of this study were to develop a method to assess gait kinematics using motion capture in an ovine model of stroke, in addition to use of a composite scoring system. Specifically, the aims were to: 1) assess the repeatability of gait kinematics obtained using motion capture across baseline trials; 2) determine if a change in gait kinematics was detected 3-days post stroke; and, 3) develop a composite scoring system to assess function pre- and post-stroke.

9.2 MATERIALS AND METHODS

9.2.1 Ethics

This study was approved by the South Australian Health and Medical Research Institute (SAHMRI) Animal Ethics Committee (SAM 3). A total of 26 adult Merino sheep (*Ovis aries*) (57±4 kgs, 18-36 months,) were used (*n*=13F; 13M). All animals were obtained from a single farm in Gum Creek, South Australia. Six months prior to commencing the study, animals were moved from the farm to the research facility (SAHMRI Preclinical Imaging and Research Facility (PIRL)), where on arrival they were examined by a veterinarian and judged to be healthy prior to inclusion in the study based on complete physical and orthopaedic examinations. They were fed once daily by facility staff to gradually acclimatise animals to human proximity, until they underwent staged habituation and surgical procedures, as described below (section 9.2.4).

9.2.2 Experimental Design

To determine the repeatability of both motion capture and composite scoring, pre-stroke, baseline assessment was carried out on three occasions; 8-, 5- and 3- day prior to stroke induction. To compare pre- and post-stroke parameters, assessment was also carried out 3 days following stroke onset.

9.2.3 Motion Capture Assessment

9.2.3.1 System Design Ethological Considerations

The system designed for motion capture sought to take advantage of the inherent flight zone of ungulates, defined as the distance in which a person can approach an animal before it moves away (Grandin, 1999, Grandin, 1987, Grandin, 1997). The positioning of the eyes in the lateral aspect of the skull results in a wide visual field allowing sheep to move in a flock

and assess the surrounding environment for threats, yet results in a blind spot directly behind and directly in front of them. Studies have shown working along the edge of an animal's flight zone at approximately 90 degrees allows for ease of movement (Kilgour, 1971, Kilgour, 1972). Consideration of the flight zone was thus incorporated in the system design to improve animal handling and welfare.

9.2.3.2 System Fabrication

A functional run measuring 10 m × 5 m × 1.5 m was fabricated using standard building and farming equipment (Figure 9.1A). One length of the run was defined as the capture volume (the space in which cameras can detect movement of the subject), with the other perimeters allowing for the continuous movement of the animal. The capture area comprised a 10 cm high wooden platform over which the animal walked, covered by matte rubber matting (2 ply Natural Insertion Rubber, Clark Rubber, Australia). Ramps (1 m) on either end allowed smooth transition to/from the platform. The capture area was enclosed with matte, galvanised steel fencing (Cyclone Ringlock™, Australia) comprising six horizontal wires of graduated spacing with a wire diameter of 2.5 mm and 0.9 m total fence height (Figure 9.1B). For the remaining periphery of the run, robust, galvanised steel interlocking 1.1 m high fencing was used. The run was enclosed in a large building, with limited external light sources to limit environmental light for optimised motion capture.

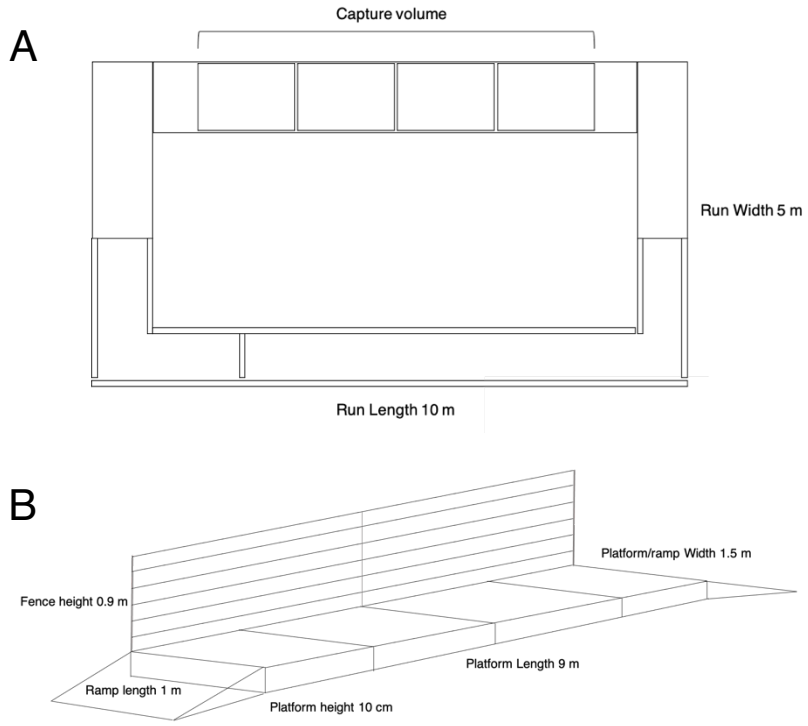

Figure 9.1. Orthographic and perspective views of the functional run. (A) Orthographic view of the run demonstrates the peripheries of the run allowing for continuous movement and the capture area. (B) Perspective view of the capture area shows elevated platform, ramping, and fencing used to contain animals as they execute forward movement.

Animals were encouraged to walk forwards through the run, with a researcher with whom the sheep was familiar walking behind them at a consistent pace. As the sheep turned the corners of the run, the researcher appeared in their visual field along the edge of their flight zone, encouraging continuous forward movement. Animals executed movement at their own pace, thus this design did not artificially alter gait asymmetry. This design also allowed for the synchronised capture of force through an integrated force plate which was built into the platform (data not reported herein).

9.2.3.3 Hardware

Ten motion capture cameras (Vicon Vero, Vicon Motion System Ltd., Oxford, UK) were placed equidistant around the periphery of the capture area, five on either side, approximately 1 m back from a fence line (Figure 9.2). Vicon Nexus software (v2.10) was used to capture marker data at a frame rate of 200 Hz. An additional video camera (Vicon Vue, Vicon, Oxford, UK) operating at a frame rate of 60 Hz captured video data to be superimposed to the motion capture data for quality control when post-processing.

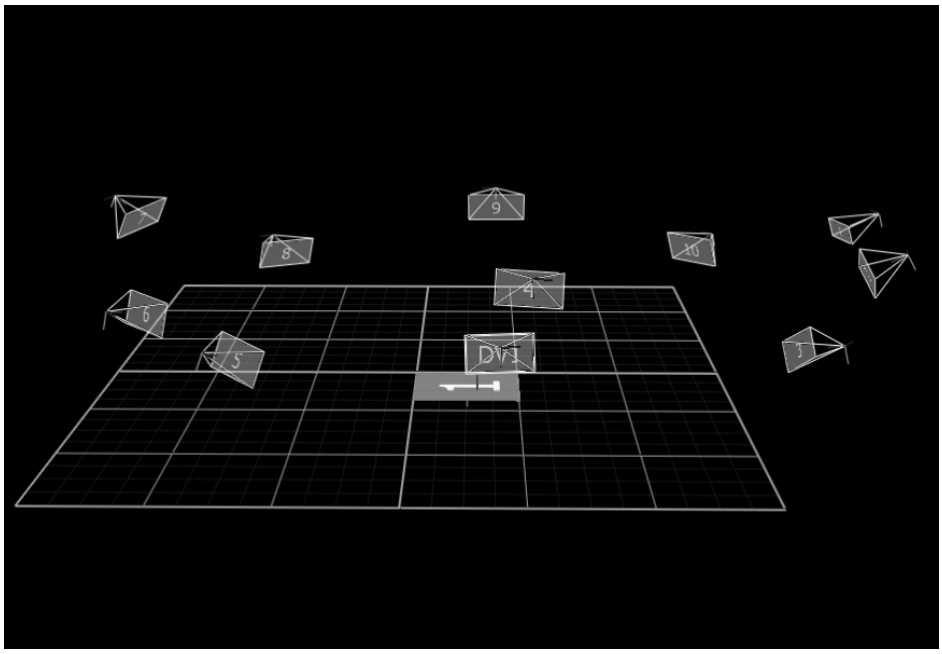

Figure 9.2. The camera positions and 3D capture volume shown on the Vicon Nexus interface. Grey rectangles represent position of each infrared camera (1 – 10) and video camera (DV1). The rectangle with number 1 indicates the position of the force plate. The final three-dimensional (3D) capture volume was 5 m in length x 5 m in width x 2 m in height.

9.2.4 Acclimation and Habituation

To familiarise animals to their surroundings, animals underwent staged acclimatisation prior to baseline assessment. On arrival to the facility, animals were initially group housed in outdoor paddocks, then moved to undercover pens, where they were housed in groups of

six. Four weeks prior to surgery, they were then separated into pairs, following which they underwent a three-stage habituation protocol.

In the first stage of habituation, pairs of animals (housed together) were allowed to roam the functional area without a handler for 30 minutes on five consecutive days. In the second phase, individual animals traversed the run in a clockwise direction (30 minutes for five consecutive days), with a handler walking behind them to encourage forward movement. In the third phase, the animals were additionally trained to step into, and out of, a modified transport crate; grain (Laucke Mills, South Australia) was used to encourage animals to step into the crate without handler intervention. Both acclimatisation and testing were carried out by four trained handlers familiar to the sheep.

9.2.5 Anatomical Landmarks

Spherical retro-reflective markers (9 mm and 15 mm diameter; B&L Engineering, California, USA) were non-invasively attached to 42 anatomical landmarks (Figure 9.3) using hooked Velcro® (Velcro USA Inc, Manchester, NH, US). The opposing loop surface of the Velcro® was adhered to the animal using superglue (Bostik, Australia). To ensure consistent marker placing, 6 days prior to baseline testing, animals were intubated and anaesthetised (isoflurane, 1.5% minimum alveolar concentration (MAC), Henry Schein, Australia), anatomical locations palpated, and landmarks tattooed using a handheld tattoo gun and India ink (Windsor and Newton, Australia). Animals were shorn at 2-week intervals to facilitate marker removal and reattachment to the skin to reduce obstruction by long wool. Sites of marker attachment are summarised in Table 9.1.

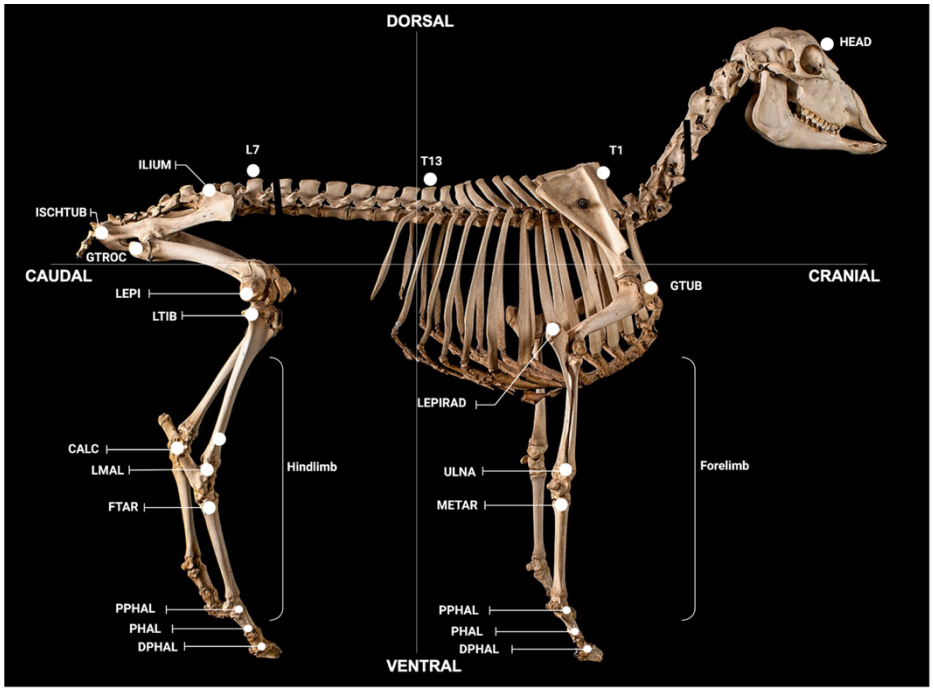

Figure 9.3. Anatomical locations for assessment. Retro-reflective markers attached to each location were 15 mm in diameter, with the exception of markers on the PHAL, PHAL and DPHAL, which were 9 mm. Figure adapted from a sheep skeleton on display at the Museum of Veterinary Anatomy, Faculty of Veterinary Medicine and Animal Science, University of São Paulo, Brazil.

Table 9.1 Sites of marker attachment

Position	Acronym	Anatomical location of attachment
Global	HEAD	On the head between the eyes
	T1	Spinous process of T1
	T13	Spinous process of T13
	L7	Spinous process of L7
Forelimb	GTUB	Greater tubercle of the humerus
	LEPIRAD	Lateral epicondyle of the radius
	ULNA	Distal tubercule of the ulna
	METAR	Proximal tubercule of the metatarsal
	PPHAL	Forelimb proximal phalange
	PHAL	Forelimb phalange
	DPHAL	Forelimb distal phalange
Hindlimb	ILIUM	Iliac crest
	ISCHTUB	Ischial tuberosity
	GTROC	Greater trochanter of the femur
	LEPI	Lateral epicondyle of the femur
	LTIB	Lateral condyle of the tibia
	TIB	Tibia
	LMAL	Lateral malleolus
	FTAR	Fused tarsal of the metacarpus
	PPHAL	Hindlimb proximal phalange
	PHAL	Hindlimb phalange
	DPHAL	Hindlimb distal phalange

9.2.5 Surgical Approach

9.2.5.1 Preoperative Preparation

Animals were moved indoors pre-operatively and fasted for 12 hours. Anaesthesia was induced with intramuscular ketamine and diazepam as per previous studies (Sorby-Adams et al., 2019a). A jugular catheter (18 g, Terumo SURFLO®) was inserted for delivery of intraoperative crystalloid fluids (Hartmann's, Baxter Health, Australia). Anaesthesia was maintained with inhalational isoflurane (1.5-2.0 % MAC in in 3 L of air and 500 mL of oxygen, Henry Schein, Australia) and continuous ketamine infusion (4 mg/kg/hr) via jugular line. An arterial catheter (20 g, Terumo SURFLO®) was placed in the distal hindlimb to yield arterial blood gas samples. A paediatric blood pressure cuff (Easy Care Cuff, Phillips) was placed on the proximal forelimb for a non-invasive measure of arterial blood pressure (ABP), which was manually recorded at 5-minute intervals.

9.2.5.2 Intraoperative Procedures

Stroke surgery was performed as previously described (Sorby-Adams et al., 2019a). Briefly, an incision was made between the right ear and orbital rim, coronoid process of the mandible lateralised, and skull based exposed to perform a small craniotomy using a pneumatic drill (Midas Rex® Legend Electric System (ICP), Medtronic USA). A 2 cm skull flap was removed, underlying dura breached, proximal MCA located, and an aneurysm clip (Aesculap YASARGIL® Aneurysm Clip, Germany) placed over the diameter of the vessel which remained *in situ* for 2 hours. The clip was subsequently removed to achieve reperfusion, dura closed watertight with synthetic matrix (Durepair®, Medtronic, USA) and superglue (Bostik, Australia), cranioplasty performed using dental cement (Sledgehammer, Keystone, Germany), and surgical site closed in layers using polyglactin suture (Vicryl®,

ETHICON). Arterial blood samples were obtained at hourly intervals intra-operatively to maintain the animal within normal physiological limits.

9.2.5.3 Postoperative Recovery

Animals were removed from anaesthesia and placed in a metabolism crate to limit excessive lateral movement of the head. Once lucid, subcutaneous non-steroidal anti-inflammatory (NSAID, 0.7 mg/kg, 50 mg/mL every 12 hours, Carprofen, Norbrook, Australia) and intramuscular Buprenorphine (Temgesic, 1.0 mL, 300 μg/ml Buprenorphine hydrochloride, Reckin Benckiser, Australia) was administered for pain relief, and intramuscular Depocillin for antibiosis (1 mL/25 kg every 12 hours Procaine benzylpenicillin, Intervet, Australia). NSAID and antibiotic treatment was continued for 3 days post-operatively, and as required thereafter. Assessment was carried out *bis in die* to determine animal wellbeing, including urine and faecal output, food and water intake, and signs of apathy. Animals remained in indoor housing for 3 days post-operatively, where they were also monitored remotely via closed-circuit television.

9.2.6 Motion Capture Data Collection

On testing days, the Vicon system was calibrated, and the global coordinate system (GCS) set to the upper right corner of the force plate using a light emitting diode wand (Vicon Active Wand, Vicon Motion System Ltd., Oxford, UK). Animals were placed into the modified transport crate in their home pen, reflective markers attached to anatomical locations, and animals moved to the functional testing space where they completed a minimum of 20 traverses of the functional run. Once motion capture was complete, animals were placed in the transport crate, reflective markers removed, and returned to their home pen with free access to food and water.

9.2.7 Motion Capture Data Post-processing

Post-processing of motion capture data was performed using Vicon Nexus software (version 2.10, Vicon Motion System Ltd., Oxford, UK). Five trials in which the animal maintained a consistent walking pace without running or trotting were reconstructed, and markers labelled. Spline and cyclic algorithms were used to fill all visible gaps (Vicon Motion System Ltd., Oxford, UK). A fourth order, zero lag, low pass Butterworth filter was applied with a cut off frequency of 10 Hz. Data were exported to C3D format and further processed with custom MATLAB® code (Mathworks, Natick, MA, USA, Appendix 9.1).

Parameters of interest were classified into *global* and *limb-specific. Global* parameters correspond to the outcome measures pertaining the entire trial, e.g. forward velocity. These outcomes were reported as average values across trials ± SD (Table 9.2). For the notation, the z axis corresponds to the vertical direction with the positive axis pointing up, the y axis corresponds to the direction of the progression, and the x-axis corresponds to the lateral direction of the animal (left/right) with the positive axis pointing to the right side.

Table 9.2 Global outcome measures

Outcome	Direction	Measure	Purpose
Mean Absolute Velocity T1	Forward	Velocity of T1	Determine velocity of forward movement
Mean Head to T1	Left/right	Position of the head in relation to T1	Determine preference for side of the run (left or right)
Mean Head to T1	Vertical	Position of the head in relation to T1	Determine lowering of the head
Mean T1 to T13	Vertical	Position of T1 in relation to T13	Determine lowering of the neck
Mean T1 to L7	Vertical	Position T13 in relation to L7	Determine lowering of the back

Limb-specific parameters were computed from the observation of the kinematic data of each limb within its corresponding gait cycle. For each trial, the gait cycles were identified following the method from (Ghoussayni et al., 2004). Changes in the velocity of each limb's hoof marker (DPHAL) were detected in the vertical and progression directions, determining when the marker stopped moving (entering stance phase) or started moving (entering swing phase). One gait cycle per limb was extracted from each trial to calculate kinematic measures of interest using two-dimensional (2D) planar analysis in the Cartesian coordinate system of the sagittal plane (Figure 9.5). Joint angles were defined between two vectors. The METAR/FTAR, PPHAL, and PHAL were used to determine the fetlock angle of the fore and hind limbs. The LEPIRAD, ULNA, METAR, and PPHAL and the TIB, LMAL, FTAR and PPHAL, were used to determine the angle of the carpus and tarsus, respectively. The GTUB, LEPIRAD, and ULNA and the GTROC, LEPI, LTIB, and LMAL were used to determine the angle of the elbow and stifle, respectively. The primary outcomes assessed, and their purpose, are summarised in Table 9.3.

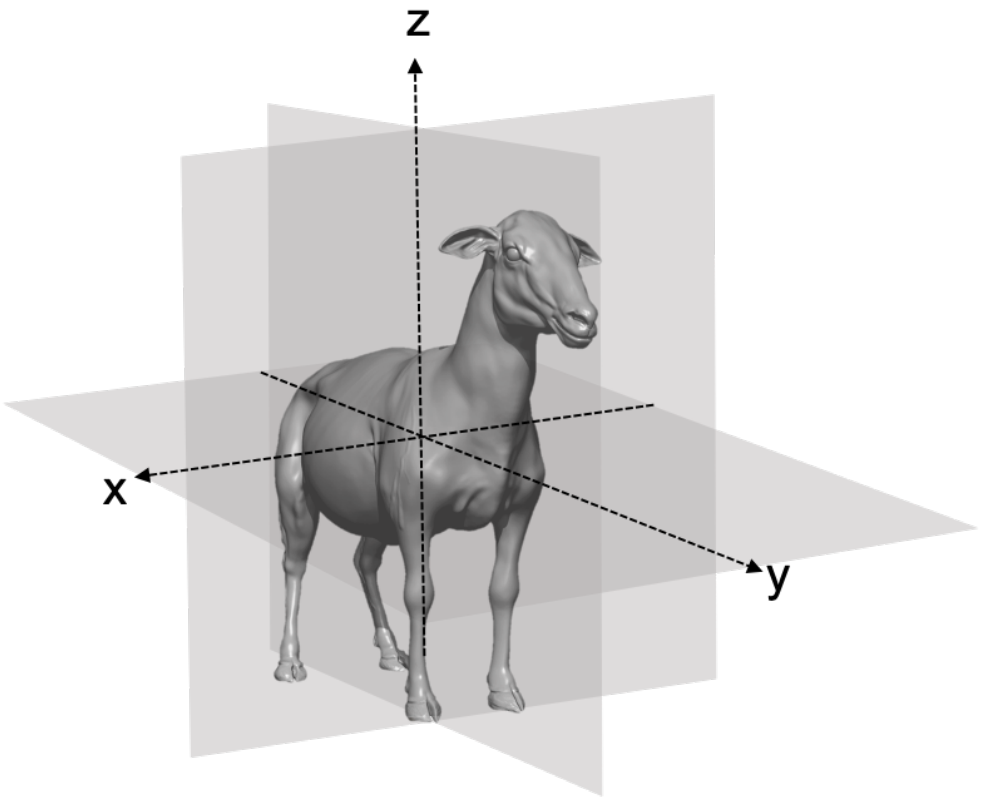

Figure 9.4. Ovine movement in the Cartesian coordinate system. The z axis corresponds to the vertical direction (up and down), the y axis corresponds to the direction of the progression (forward), and the x-axis corresponds to the lateral direction of the animal (left/right).

Table 9.3 Limb-specific outcome measures

Outcome	Direction	Marker(s) used	Variables Measured	Purpose
Stance Duration (s)	Vertical	DPHAL (each limb)	Duration from end of swing to beginning of a new swing cycle	Determine stance duration
Swing Duration (s)	Vertical	DPHAL (each limb)	Duration from beginning of swing to beginning of stance	Determine swing duration
Stride Duration (s)	Vertical	DPHAL (each limb)	Duration from entering swing to ending stance	Determine stride duration
Hoof Lateral Deviation (cm)	Left/right	DPHAL (each limb)	Lateral (outward) deviation of distal limb	
Hoof Forward Swing Velocity (m/s)	Forward	DPHAL (each limb)	The speed at which the animal is moving the limb forwards during swing	The speed (m/s) the animal is lifting or dragging the limb during swing
Hoof Vertical Swing Velocity (m/s)	Vertical	DPHAL (each limb)	The speed at which the animal is lifting the hoof upwards during swing	The speed (m/s) the animal is lifting or dragging the limb during swing
Range Hoof Height in Swing (cm)	Vertical	DPHAL (each limb)	Range of upwards movement of the hoof during swing	The amount (cm) the animal is lifting or dragging the limb during swing
Stride Length (cm)	Vertical	DPHAL (each limb)	The length of the stride from stance to swing	Determine length of stride
Distance Matching Limb during stance (cm)	Left/right	Forelimb DPHAL and Hindlimb DPHAL	Distance between limbs	Determine splay of limbs pre- and post-stroke
Forelimb Fetlock Angle Stance (º)	Vertical	Forelimb PHAL, PPHAL and METAR	Maximum, minimum and range of joint during stance	Determine forelimb ipsi- versus contra-lateral lower limb deficit
Forelimb Fetlock Angle in Swing (º)	Vertical	Forelimb PHAL, PPHAL and METAR	Maximum, minimum and range of joint during stance	Determine forelimb ipsi- versus contra-lateral lower limb deficit
Carpal Angle in Stance (º)	Vertical	METAR, PPHAL, LEPIRAD and ULNA	Maximum, minimum and range of joint during stance	Determine forelimb ipsi- versus contra-lateral mid limb deficit

(continued)

Outcome	Direction	Marker(s) used	Variables Measured	Purpose

Carpal Angle in Swing (º)	Vertical	METAR, PPHAL, LEPIRAD and ULNA	Maximum, minimum and range of joint during stance	Determine forelimb ipsi- versus contra-lateral mid limb deficit
Elbow Angle in Stance (º)	Vertical	LEPIRAD, ULNA and GTUB	Maximum, minimum and range of joint during stance	Determine forelimb ipsi- versus contra-lateral upper limb deficit
Elbow Angle in Swing (º)	Vertical	LEPIRAD, ULNA and GTUB	Maximum, minimum and range of joint during stance	Determine forelimb ipsi- versus contra-lateral upper limb deficit
Hindlimb Fetlock Angle in Stance (º)	Vertical	Hindlimb PHAL, PPHAL and FTAR	Maximum, minimum and range of joint during stance	Determine hindlimb ipsi- versus contra-lateral lower limb deficit
Hindlimb Fetlock Angle in Swing (º)	Vertical	Hindlimb PHAL, PPHAL and FTAR	Maximum, minimum and range of joint during stance	Determine hindlimb ipsi- versus contra-lateral lower limb deficit
Tarsal Angle in Stance (º)	Vertical	FTAR, PPHAL, TIB and LMAL	Maximum, minimum and range of joint during stance	Determine hindlimb ipsi- versus contra-lateral mid limb deficit
Tarsal Angle in Swing (º)	Vertical	FTAR, PPHAL, TIB and LMAL	Maximum, minimum and range of joint during stance	Determine hindlimb ipsi- versus contra-lateral mid limb deficit
Stifle Angle in Stance (º)	Vertical	LTIB, LMAL, GTROC and LEPI	Maximum, minimum and range of joint during stance	Determine hindlimb ipsi- versus contra-lateral upper limb deficit
Stifle Angle in Swing (º)	Vertical	LTIB, LMAL, GTROC and LEPI	Maximum, minimum and range of joint during stance	Determine hindlimb ipsi- versus contra-lateral upper limb deficit
Ratio Stance to Stride (%)	Vertical	DPHAL (each limb)	Ratio of time in stance compared with stride	
Ratio Swing to Stride (%)	Vertical	DPHAL (each limb)	Ratio of time in swing compared with stride	
Ratio Stance to Swing (%)	Vertical	DPHAL (each limb)	Ratio of time in stance compared with swing	

9.2.8 Neurological Scoring Assessment

A 12 criteria neurological assessment score was adapted from previous work (Boltze et al., 2008). Assessment was based on the common system for neurologic dysfunctions in large animals (Lorenz et al., 2010). This study, however, specifically focused on the functional deficits observed in animals following MCAO, including changes in state of activity, behaviour, and motor dysfunction (Table 9.4). A score of 0 was considered normal, with a possible total score of 25 indicating severe deficit.

Scoring took place approximately 2 hours prior to commencing motion capture procedures. Each examination was scored at time of assessment and simultaneously recorded on three cameras (GoPro HERO6) positioned anteriorly, posteriorly and laterally to the assessment space. Observations of level of consciousness and position of the head gave a score for animal demeanour (Table 9.4, criteria 1). Animals who were in a state of stupor or were comatose warranted euthanasia, and no further investigations were performed. Abnormalities in animal behaviour were assessed by accumulating scores for presence of torticollis, food debris in the mouth indicating inability to properly masticate, general ataxia or dysmetria in limb movements, evidence of abnormal flexion at the fetlock and/or carpus joints, and circling (Table 9.4, criteria's 2, 3, 4 and 5, respectively). Circling behaviours (Table 9.4, criteria 6) were monitored prior to animal handling on assessment days by undisturbed video recording of the animal for 10 minutes within their home pen environment.

Table 9.4 Neurological scoring system

Criteria	Assessment	Score
1	**State of Activity/Consciousness**	**0 – 3**
	Normal	0
	Apathetic	1
	Stupor	2
	Comatose	1
2	**Presence of Food Debris in the Mouth**	**0 – 1**
	No food	0
	Food present	1
3	**Presence of Torticollis**	**0 – 1**
	Absent	0
	Present	1
4	**Partial Flexion of Fetlock and/or Carpus**	**0 – 1**
	Absent	0
	Present	1
5	**Ataxia/Dysmetria**	**0 – 3**
	Normal	0
	Dysmetric limb movement	1
	Staggering	2
	Animal falls down	3
6	**Circling Movements**	**0 – 2**
	None	0
	Occasional	1
	Continuous	2
7	**Hemi-standing**	**0 – 4**
	Immediate adjustment of both limbs	0
	Delayed adjustment of hindlimb	1
	Delayed adjustment of forelimb	2
	Delayed adjustment of both limbs	3
	No adjustment of both limbs	4
	Knuckling limb on hoof release	+ 0.25/limb
8	**Forelimb Lateral and Medial Hopping**	**0 – 2**
	Normal response/immediate adjustment	0
	Delayed adjustment	1
	No adjustment	2
	Knuckling limb on hoof release	+ 0.25/limb
9	**Limb Medial Adjustment "Lateral Dragging"**	**0 – 2**
	Normal response/immediate adjustment	0
	Delayed adjustment	1
	No adjustment	2
	Partial correction	+ 0.25/limb
10	**Forced Forelimb Movement "Wheelbarrowing"**	**0 – 2**
	Normal response/immediate adjustment	0
	Drifting to side	1
	Animal falls down	2

Three postural reaction tests (Table 9.4; Criteria 7-9) were conducted by forcefully shifting the animal's weight over their centre of gravity on individual limbs and assessing their ability to correct the movement. Criteria 7 refers to "hemi-standing", which evaluated the animal's ability to correct and co-ordinate fore- and hind- limbs during a lateral movement on the left and right side of the body. Criteria 8 encompassed "lateral dragging", which involved the forced lateral movement of each individual limb and assessment of the animal's ability to return the limb back to the medial starting position. Quarter scores were also given where animals dragged a limb on return or if correction back to original position was only partial. Criteria 9 refers the "hopping reaction" which assessed forelimbs individually to determine the animal's ability to correct the limb during lateral movement. Forced forward movement of the animal on both forelimbs ("wheelbarrowing", criteria 10) assessed for any sideways deviation, indicative of hemineglect and potential hemiparesis. Additional quarter scores were allocated in criteria 7 and 8 if the animal exhibited abnormal reactions beyond observed delays, including the inability of the animal to fully extend a held limb upon release, causing 'knuckling' on ground. Criteria 10 was reported independently, and scores for hemi-standing, hopping, and lateral drag were incorporated into measures for the contralateral and ipsilateral side of the body.

9.2.9 Statistics

9.2.9.1 Motion Capture

Statistical analysis for motion capture was performed with Stata (version 15.1, StataCorp, College Station, TX). Descriptive statistics are presented for each outcome as mean and standard deviations (SD). Analysis of variance (ANOVA) models were used to determine if there was a difference between the three baseline measures (8-, 3- and 1-day pre stroke) for each variable. Intraclass Correlation Coefficients (ICC) were used to describe the

repeatability of each outcome of interest. For stride-related measures, two ICC values were derived; one un-adjusted and one adjusted for the potential confounding effect of walking speed (measured as mean absolute velocity at T1). Interpretation of ICC values was <0.50 poor; 0.50-0.75 fair; 0.75-0.90 good; >0.90 excellent (Koo and Li, 2016).

Mixed effects linear regression models were fitted to determine the change in gait-related measures from baseline to 3 days post-stroke. For ease of interpretation in the models, a single baseline measure was used comprised of the mean of the three baseline measures. A random effect of sheep was used to account for the correlation between repeated or multiple measures on the same animal. Fixed effects were time (pre-, post-stroke), limb (left, right), and a time-by-limb interaction term. The interaction term was necessary as the right sided stroke was expected to cause left-sided deficits (with potential right-sided compensation) thus producing a side-dependent effect of time. For models in which the interaction term was not significant, the baseline to post-stroke comparisons within limb are interpreted with caution. Two models were fitted for each stride measurement; the first un-adjusted and the second adjusted for velocity. For the velocity outcome measure, only an unadjusted model was fitted. Estimates of the difference between baseline and post-stroke were derived for each limb. Results are presented as p-value, mean difference and 95% confidence intervals (CI). $p<0.05$ was considered statistically significant.

9.2.9.2 Neurological Scoring

Neurological examination scores were analysed using Prism (version 9.0, GraphPad, CA). Friedman, non-parametric, one-way ANOVAs were performed with repeated measures and Dunn's post hoc test for multiple comparisons. All score values are expressed as mean and 95% CI. A value of $p<0.05$ was considered statistically significant throughout.

9.3 RESULTS

Two animals were euthanised before the experimental endpoint and excluded from the study. Specifically, one animal had an unsuccessful reperfusion of the MCA resulting in a permanent stroke, and the other had kidney failure leading to seizures. As such, twenty-four animals reached the experimental endpoint and were included in the final analysis.

9.3.1 Motion Capture

9.3.1.1 Baseline Repeatability Analysis of Global Parameters

No statistically significant differences were detected for any of the global measures across the three baseline sessions (all $p \geq 0.05$) (Table 9.5). The repeatability of forward velocity was poor (ICC <0.50), with animals walking at variable speeds between sessions. The mean walking speed across all baseline trials was 1.28 m/s, however, despite poor repeatability, the SD was low for all animals (+/- 0.20 m/s). Repeatability of measures in the vertical plane were good (all ICC > 0.70), with the position of the head in relation to T1, T1 to T13, and T13 to L7, consistent across baseline testing sessions. The position of the head to T1 in the left/right axis was also repeatable (ICC >0.50), with animals consistently holding their head slightly to the right of the run (approximately 3 cm). Repeatable variables are denoted with an asterix (*) in Table 9.5.

Table 9.5 Baseline global parameters (mean +/- SD)

Variable	Direction	Baseline 1	Baseline 2	Baseline 3	P-value baselines	Mean (SD) of three baselines	ICC (95% CI)
Mean Absolute Velocity T1 (m/s)	Forward	1.31 (0.17)	1.26 (0.24)	1.27 (0.21)	0.656	1.28 (0.20)	0.41 (0.20, 0.66)
Mean Head to T1 (cm)	Left/right	2.68 (6.22)	4.16 (6.26)	3.35 (5.79)	0.707	3.39 (6.04)	0.58 (0.36, 0.76) *
Mean Head to T1 (cm)	Vertical	9.75 (4.59)	10.41 (3.39)	9.53 (4.31)	0.751	9.89 (4.10)	0.70 (0.51, 0.84) *
Mean T1 to T13 (cm)	Vertical	-0.54 (1.14)	-0.43 (1.10)	-0.56 (1.07)	0.919	-0.51 (1.09)	0.74 (0.56, 0.86) *
Mean T1 to L7 (cm)	Vertical	-3.10 (1.49)	-3.04 (1.44)	-3.25 (1.50)	0.875	-3.13 (1.46)	0.80 (0.66, 0.90) *

* = ICC >0.50

9.3.1.1 Baseline Repeatability Analysis of Limb Parameters

There was no significant difference between baseline trials for all limb-related variables ($p>0.11$). Repeatability was good for some, but not all, of the recorded measures (highlighted by an asterix (*) in Table 9.6). To allow for comparison between post-stroke trials, the outcome measures for each individual limb are described herein.

For the forelimbs, the majority of outcome measures were reproducible. Specifically for the left forelimb, the variables that reported fair to good repeatability included swing duration, hoof vertical swing, range hoof height and stride length. Joint angles were also repeatable, with the exception of the minimum fetlock angle in swing. When adjusted for velocity, the ICC increased for all variables, and stride duration which was previously considered un-repeatable across trials was subsequently considered fair. For the right forelimb, all joint angles were repeatable, with ICC values increasing when adjusted for velocity. Swing and stride duration, hoof lateral deviation, vertical swing and height range were also repeatable, but only after velocity adjustment.

The repeatability of hindlimb parameters was similar to that of the forelimbs (Table 9.7). In the left hindlimb, repeatable variables un-adjusted for velocity included swing duration, hoof vertical swing, hoof height range, and stride length. All hindlimb angles were repeatable. When adjusted for velocity, the ICC increased for all variables, and hoof forward swing and stride duration became repeatable measures. For the right hindlimb, variables repeatable in the un-adjusted model included swing duration, hoof vertical swing, hoof height range, and stride length. Joint angles were all repeatable, with the exception of the minimum fetlock angle during swing. When adjusted for velocity, the ICC for all variables increased, and both stride duration and hoof forward swing were repeatable. The distance between the matching limbs during stance were also considered repeatable for the fore- and hind- limbs when both adjusted and un-adjusted for velocity.

Table 9.6 Baseline forelimb parameters (mean +/- SD)

Left Forelimb

Variable	*Baseline 1*	*Baseline 2*	*Baseline 3*	*Mean baselines*	*P-value*	*Unadjusted ICC and 95% CI*	*Adjusted ICC and 95% CI*
Stance Duration (s)	0.40 (0.07)	0.42 (0.09)	0.41 (0.09)	0.41 (0.01)	0.580	0.41 (0.20, 0.66)	0.45 (0.24, 0.69)
Swing Duration (s)	0.35 (0.02)	0.36 (0.03)	0.36 (0.02)	0.36 (0.00)	0.433	0.60 (0.39, 0.78) *	0.67 (0.47, 0.82) *
Stride Duration (s)	0.75 (0.08)	0.78 (0.11)	0.77 (0.11)	0.77 (0.01)	0.553	0.45 (0.24, 0.69)	0.59 (0.38, 0.77) *
Ratio Stance To Stride (%)	0.52 (0.04)	0.53 (0.05)	0.52 (0.05)	0.52 (0.01)	0.644	0.36 (0.16, 0.63)	0.28 (0.09, 0.60)
Ratio Swing To Stride (%)	0.48 (0.04)	0.47 (0.05)	0.48 (0.05)	0.48 (0.01)	0.644	0.36 (0.16, 0.63)	0.28 (0.09, 0.60)
Ratio Stance To Swing (%)	1.11 (0.18)	1.16 (0.19)	1.12 (0.21)	1.13 (0.02)	0.642	0.34 (0.14, 0.62)	0.28 (0.10, 0.60)
Hoof Lateral Deviation (cm)	7.29 (1.98)	7.47 (2.31)	7.45 (2.59)	7.40 (0.08)	0.959	0.40 (0.19, 0.65)	0.41 (0.20, 0.66)
Hoof Forward Swing Velocity (m/s)	2.77 (0.15)	2.68 (0.25)	2.71 (0.21)	2.72 (0.03)	0.378	0.44 (0.22, 0.68)	0.42 (0.20, 0.67)
Hoof Vertical Swing Velocity (m/s)	0.39 (0.08)	0.35 (0.08)	0.36 (0.10)	0.37 (0.02)	0.275	0.64 (0.44, 0.80) *	0.70 (0.51, 0.84) *
Range Hoof Height in Swing (cm)	7.16 (1.54)	6.39 (1.59)	6.63 (2.08)	6.73 (0.33)	0.305	0.74 (0.56, 0.86) *	0.78 (0.62, 0.88) *
Stride Length (cm)	98.44 (5.15)	96.51 (6.17)	98.64 (6.31)	97.88 (0.96)	0.399	0.73 (0.56, 0.86) *	0.82 (0.68, 0.91) *
Minimum Forelimb Fetlock Angle Stance (º)	4.10 (10.78)	5.82 (8.63)	5.47 (8.43)	5.12 (0.75)	0.799	0.56 (0.35, 0.76) *	0.54 (0.31, 0.75) *
Maximum Forelimb Fetlock Angle Stance (º)	19.51 (10.98)	21.01 (8.81)	20.93 (8.56)	20.47 (0.70)	0.83	0.53 (0.31, 0.74) *	0.50 (0.27, 0.72) *
Range Forelimb Fetlock Angle in Stance (º)	15.41 (4.18)	15.18 (3.21)	15.46 (3.20)	15.35 (0.12)	0.962	0.63 (0.43, 0.80) *	0.63 (0.43, 0.80) *
Minimum Forelimb Fetlock Angle in Swing (º)	-29.70 (10.51)	-26.87 (7.91)	-27.49 (8.31)	-28.04 (1.22)	0.527	0.43 (0.21, 0.68)	0.43 (0.21, 0.69)
Maximum Forelimb Fetlock Angle in Swing (º)	12.00 (11.16)	13.48 (9.42)	13.08 (8.78)	12.84 (0.63)	0.867	0.56 (0.35, 0.75) *	0.52 (0.29, 0.74) *
Range Forelimb Fetlock Angle in Swing (º)	41.70 (6.60)	40.35 (5.80)	40.57 (5.63)	40.88 (0.59)	0.713	0.68 (0.49, 0.83) *	0.69 (0.49, 0.83) *
Minimum Carpal Angle in Stance (º)	-13.90 (4.43)	-14.74 (4.57)	-14.78 (5.10)	-14.47 (0.41)	0.766	0.71 (0.53, 0.84) *	0.72 (0.54, 0.85) *
Maximum Carpal Angle in Stance (º)	-1.74 (4.94)	-2.29 (5.10)	-2.42 (4.90)	-2.15 (0.30)	0.883	0.78 (0.63, 0.89) *	0.79 (0.63, 0.89) *
Range Carpal Angle in Stance (º)	12.15 (3.49)	12.45 (3.84)	12.36 (3.45)	12.32 (0.12)	0.959	0.68 (0.49, 0.83) *	0.72 (0.54, 0.85) *
Minimum Carpal Angle in Swing (º)	-77.34 (8.01)	-74.86 (8.16)	-77.88 (10.11)	-76.72 (1.32)	0.463	0.75 (0.59, 0.87) *	0.81 (0.66, 0.90) *
Maximum Carpal Angle in Swing (º)	-3.19 (4.75)	-3.96 (5.26)	-4.18 (4.74)	-3.77 (0.43)	0.766	0.81 (0.66, 0.90) *	0.81 (0.66, 0.90) *
Range Carpal Angle in Swing (º)	74.15 (6.85)	70.90 (7.44)	73.71 (8.37)	72.95 (1.44)	0.289	0.73 (0.55, 0.86) *	0.82 (0.68, 0.90) *
Minimum Elbow Angle in Stance (º)	51.94 (5.22)	51.97 (4.71)	51.92 (5.99)	51.94 (0.02)	1.000	0.80 (0.65, 0.89) *	0.85 (0.73, 0.92) *
Maximum Elbow Angle in Stance (º)	76.21 (5.88)	76.88 (5.93)	77.23 (5.99)	76.78 (0.43)	0.833	0.89 (0.80, 0.94) *	0.89 (0.80, 0.95) *
Range Elbow Angle in Stance (º)	24.27 (3.81)	24.92 (4.38)	25.31 (4.49)	24.83 (0.43)	0.694	0.70 (0.52, 0.84) *	0.82 (0.69, 0.91) *
Minimum Elbow Angle in Swing (º)	52.92 (5.47)	53.22 (4.70)	53.23 (6.07)	53.12 (0.14)	0.976	0.81 (0.67, 0.90) *	0.85 (0.74, 0.92) *
Maximum Elbow Angle in Swing (º)	95.89 (6.37)	94.50 (6.28)	95.41 (6.75)	95.27 (0.58)	0.757	0.80 (0.65, 0.89) *	0.82 (0.68, 0.91) *
Range Elbow Angle in Swing (º)	42.97 (4.60)	41.28 (5.31)	42.18 (5.07)	42.16 (0.69)	0.515	0.74 (0.56, 0.86) *	0.73 (0.56, 0.86) *

* = ICC >0.50

(continued)

Right Forelimb							
Variable	*Baseline 1*	*Baseline 2*	*Baseline 3*	*Mean baselines*	*P-value*	*Unadjusted ICC and 95% CI*	*Adjusted ICC and 95% CI*
Stance Duration (s)	0.40 (0.07)	0.42 (0.10)	0.42 (0.09)	0.41 (0.01)	0.569	0.47 (0.25, 0.70)	0.48 (0.27, 0.71)
Swing Duration (s)	0.36 (0.02)	0.36 (0.03)	0.36 (0.02)	0.36 (0.00)	0.431	0.37 (0.17, 0.64)	0.53 (0.31, 0.74) *
Stride Duration (s)	0.75 (0.08)	0.79 (0.12)	0.78 (0.11)	0.77 (0.01)	0.501	0.46 (0.24, 0.69)	0.59 (0.37, 0.77) *
Ratio Stance To Stride (%)	0.52 (0.04)	0.53 (0.06)	0.53 (0.05)	0.52 (0.00)	0.823	0.46 (0.24, 0.69)	0.30 (0.10, 0.60)
Ratio Swing To Stride (%)	0.48 (0.04)	0.47 (0.06)	0.47 (0.05)	0.48 (0.00)	0.823	0.46 (0.24, 0.69)	0.30 (0.10, 0.60)
Ratio Stance To Swing (%)	1.11 (0.18)	1.15 (0.23)	1.15 (0.21)	1.13 (0.02)	0.736	0.46 (0.24, 0.69)	0.30 (0.11, 0.60)
Hoof Lateral Deviation (cm)	7.59 (2.54)	7.21 (2.98)	7.07 (2.71)	7.29 (0.22)	0.795	0.49 (0.28, 0.71)	0.51 (0.29, 0.72) *
Hoof Forward Swing Velocity (m/s)	2.74 (0.19)	2.64 (0.23)	2.71 (0.23)	2.70 (0.04)	0.311	0.28 (0.10, 0.59)	0.45 (0.22, 0.69)
Hoof Vertical Swing Velocity (m/s)	0.37 (0.07)	0.34 (0.07)	0.36 (0.08)	0.36 (0.01)	0.438	0.49 (0.27, 0.71)	0.60 (0.39, 0.78) *
Range Hoof Height in Swing (cm)	6.63 (1.35)	6.27 (1.37)	6.54 (1.69)	6.48 (0.16)	0.679	0.65 (0.45, 0.81) *	0.70 (0.51, 0.84) *
Stride Length (cm)	97.83 (5.45)	96.30 (6.12)	98.14 (6.50)	97.44 (0.81)	0.539	0.69 (0.50, 0.84) *	0.80 (0.66, 0.90) *
Minimum Forelimb Fetlock Angle Stance (º)	5.59 (8.26)	8.40 (8.30)	5.34 (7.73)	6.42 (1.39)	0.363	0.61 (0.40, 0.79) *	0.62 (0.41, 0.79) *
Maximum Forelimb Fetlock Angle Stance (º)	21.03 (9.15)	23.03 (9.26)	20.80 (9.11)	21.60 (1.00)	0.662	0.65 (0.45, 0.81) *	0.67 (0.48, 0.82) *
Range Forelimb Fetlock Angle in Stance (º)	15.43 (3.79)	14.62 (3.35)	15.46 (3.96)	15.18 (0.39)	0.683	0.74 (0.56, 0.86) *	0.75 (0.58, 0.87) *
Minimum Forelimb Fetlock Angle in Swing (º)	-26.96 (9.28)	-25.34 (10.05)	-25.82 (8.92)	-26.05 (0.68)	0.833	0.73 (0.55, 0.86) *	0.73 (0.55, 0.86) *
Maximum Forelimb Fetlock Angle in Swing (º)	13.96 (7.68)	15.59 (8.15)	13.77 (7.97)	14.43 (0.82)	0.691	0.57 (0.36, 0.76) *	0.61 (0.40, 0.79) *
Range Forelimb Fetlock Angle in Swing (º)	40.92 (5.80)	40.93 (7.05)	39.59 (7.14)	40.48 (0.64)	0.730	0.70 (0.51, 0.84) *	0.70 (0.51, 0.84) *
Minimum Carpal Angle in Stance (º)	-16.97 (5.58)	-18.73 (5.75)	-17.46 (5.25)	-17.70 (0.75)	0.533	0.82 (0.68, 0.90) *	0.84 (0.71, 0.92) *
Maximum Carpal Angle in Stance (º)	-3.27 (4.25)	-4.59 (5.02)	-3.87 (4.22)	-3.90 (0.54)	0.606	0.85 (0.73, 0.92) *	0.84 (0.72, 0.92) *
Range Carpal Angle in Stance (º)	13.70 (3.83)	14.14 (4.01)	13.58 (3.61)	13.80 (0.24)	0.869	0.66 (0.47, 0.82) *	0.70 (0.52, 0.84) *
Minimum Carpal Angle in Swing (º)	-79.86 (7.27)	-78.27 (7.76)	-79.72 (8.40)	-79.30 (0.72)	0.745	0.78 (0.63, 0.88) *	0.84 (0.72, 0.92) *
Maximum Carpal Angle in Swing (º)	-5.16 (4.64)	-6.38 (4.86)	-5.47 (4.73)	-5.66 (0.52)	0.660	0.88 (0.78, 0.94) *	0.89 (0.80, 0.94) *
Range Carpal Angle in Swing (º)	74.70 (7.10)	71.89 (6.78)	74.25 (8.29)	73.64 (1.23)	0.387	0.71 (0.52, 0.84) *	0.79 (0.64, 0.89) *
Minimum Elbow Angle in Stance (º)	53.51 (6.59)	54.30 (6.46)	53.52 (7.87)	53.77 (0.37)	0.908	0.76 (0.60, 0.87) *	0.77 (0.61, 0.88) *
Maximum Elbow Angle in Stance (º)	77.33 (8.49)	76.95 (8.07)	77.10 (8.14)	77.13 (0.16)	0.987	0.85 (0.74, 0.92) *	0.86 (0.75, 0.93) *
Range Elbow Angle in Stance (º)	23.82 (5.88)	22.65 (5.57)	23.58 (4.66)	23.36 (0.50)	0.737	0.58 (0.36, 0.76) *	0.61 (0.41, 0.79) *
Minimum Elbow Angle in Swing (º)	54.66 (6.60)	55.85 (6.54)	55.14 (7.93)	55.20 (0.49)	0.845	0.78 (0.62, 0.88) *	0.79 (0.63, 0.89) *
Maximum Elbow Angle in Swing (º)	96.14 (8.20)	96.51 (8.16)	95.47 (8.76)	96.03 (0.43)	0.911	0.85 (0.73, 0.92) *	0.85 (0.74, 0.92) *
Range Elbow Angle in Swing (º)	41.48 (5.58)	40.67 (6.52)	40.33 (5.20)	40.83 (0.49)	0.779	0.69 (0.50, 0.83) *	0.69 (0.50, 0.83) *
Distance Matching Limb during stance (cm)	51.12 (2.71)	50.98 (3.12)	51.73 (2.59)	51.28 (0.33)	0.623	0.56 (0.34, 0.76) *	0.52 (0.29, 0.74) *

* = ICC >0.50

Table 9.7 Baseline hindlimb parameters (mean +/- SD)

Left Hindlimb

Variable	*Baseline 1*	*Baseline 2*	*Baseline 3*	*Mean baselines*	*P-value*	*Unadjusted ICC and 95% CI*	*Adjusted ICC and 95% CI*
Stance Duration (s)	0.42 (0.07)	0.44 (0.10)	0.43 (0.09)	0.43 (0.01)	0.678	0.43 (0.22, 0.68)	0.47 (0.24, 0.70)
Swing Duration (s)	0.34 (0.03)	0.34 (0.03)	0.34 (0.03)	0.34 (0.00)	0.883	0.54 (0.33, 0.74) *	0.66 (0.47, 0.82) *
Stride Duration (s)	0.76 (0.09)	0.78 (0.12)	0.77 (0.11)	0.77 (0.01)	0.737	0.46 (0.24, 0.69)	0.62 (0.41, 0.79) *
Ratio Stance To Stride (%)	0.55 (0.04)	0.56 (0.04)	0.55 (0.05)	0.55 (0.00)	0.735	0.42 (0.20, 0.67)	0.35 (0.14, 0.64)
Ratio Swing To Stride (%)	0.45 (0.04)	0.44 (0.04)	0.45 (0.05)	0.45 (0.00)	0.735	0.42 (0.20, 0.67)	0.35 (0.14, 0.64)
Ratio Stance To Swing (%)	1.24 (0.19)	1.29 (0.20)	1.25 (0.22)	1.26 (0.02)	0.667	0.40 (0.19, 0.65)	0.32 (0.12, 0.62)
Hoof Lateral Deviation (cm)	7.66 (2.86)	6.86 (2.12)	6.68 (2.04)	7.07 (0.43)	0.324	0.12 (0.01, 0.61)	0.11 (0.01, 0.63)
Hoof Forward Swing Velocity (m/s)	2.89 (0.21)	2.83 (0.31)	2.88 (0.27)	2.87 (0.03)	0.722	0.39 (0.18, 0.65)	0.66 (0.46, 0.82) *
Hoof Vertical Swing Velocity (m/s)	0.25 (0.06)	0.24 (0.06)	0.24 (0.07)	0.24 (0.01)	0.718	0.50 (0.28, 0.72) *	0.67 (0.48, 0.83) *
Range Hoof Height in Swing (cm)	4.35 (0.97)	4.10 (0.94)	4.10 (1.09)	4.18 (0.12)	0.615	0.61 (0.40, 0.79) *	0.72 (0.54, 0.85) *
Stride Length (cm)	97.90 (5.99)	96.33 (5.93)	98.72 (5.77)	97.67 (0.99)	0.378	0.62 (0.41, 0.79) *	0.73 (0.54, 0.85) *
Minimum Hindlimb Fetlock Angle Stance (º)	3.68 (8.29)	0.67 (6.97)	1.96 (7.31)	2.12 (1.24)	0.395	0.53 (0.31, 0.73) *	0.52 (0.31, 0.73) *
Maximum Hindlimb Fetlock Angle Stance (º)	20.41 (9.09)	17.60 (8.82)	18.98 (8.00)	19.02 (1.15)	0.541	0.56 (0.34, 0.75) *	0.56 (0.35, 0.76) *
Range Hindlimb Fetlock Angle in Stance (º)	16.73 (5.44)	16.93 (4.79)	17.02 (4.99)	16.90 (0.12)	0.980	0.69 (0.50, 0.83) *	0.69 (0.50, 0.83) *
Minimum Hindlimb Fetlock Angle in Swing (º)	-31.51 (8.65)	-33.72 (6.22)	-30.96 (7.49)	-32.04 (1.19)	0.420	0.53 (0.31, 0.73) *	0.55 (0.33, 0.75) *
Maximum Hindlimb Fetlock Angle in Swing (º)	10.58 (7.78)	7.33 (9.01)	9.35 (7.13)	9.11 (1.34)	0.377	0.52 (0.31, 0.73) *	0.56 (0.34, 0.75) *
Range Hindlimb Fetlock Angle in Swing (º)	42.09 (6.22)	41.05 (8.01)	40.31 (6.26)	41.15 (0.74)	0.668	0.50 (0.28, 0.72) *	0.67 (0.47, 0.82) *
Minimum Tarsal Angle in Stance (º)	28.01 (7.37)	27.95 (6.83)	27.14 (8.61)	27.70 (0.40)	0.909	0.84 (0.71, 0.91) *	0.83 (0.70, 0.91) *
Maximum Tarsal Angle in Stance (º)	63.41 (6.57)	62.82 (7.05)	63.08 (9.01)	63.10 (0.24)	0.965	0.73 (0.56, 0.86) *	0.75 (0.58, 0.87) *
Range Tarsal Angle in Stance (º)	35.40 (5.51)	34.86 (5.33)	35.94 (5.51)	35.41 (0.44)	0.796	0.72 (0.54, 0.85) *	0.75 (0.58, 0.87) *
Minimum Tarsal Angle in Swing (º)	28.01 (7.37)	27.98 (6.82)	27.20 (8.59)	27.73 (0.38)	0.916	0.84 (0.71, 0.92) *	0.84 (0.71, 0.92) *
Maximum Tarsal Angle in Swing (º)	77.93 (6.84)	77.24 (7.98)	76.59 (9.09)	77.25 (0.56)	0.845	0.61 (0.40, 0.78) *	0.73 (0.54, 0.85) *
Range Tarsal Angle in Swing (º)	49.92 (5.15)	49.25 (7.25)	49.39 (6.95)	49.53 (0.29)	0.933	0.51 (0.29, 0.72) *	0.64 (0.43, 0.80) *
Minimum Stifle Angle in Stance (º)	-69.42 (14.76)	-68.28 (14.05)	-67.92 (14.30)	-68.54 (0.65)	0.931	0.85 (0.73, 0.92) *	0.85 (0.74, 0.92) *
Maximum Stifle Angle in Stance (º)	-46.58 (13.23)	-44.31 (14.18)	-44.44 (14.87)	-45.12 (1.05)	0.825	0.81 (0.66, 0.90) *	0.84 (0.71, 0.92) *
Range Stifle Angle in Stance (º)	22.85 (4.81)	23.96 (4.58)	23.48 (5.27)	23.42 (0.46)	0.736	0.61 (0.40, 0.78) *	0.60 (0.39, 0.78) *
Minimum Stifle Angle in Swing (º)	-81.80 (13.70)	-80.80 (13.65)	-79.57 (15.07)	-80.72 (0.93)	0.862	0.79 (0.64, 0.89) *	0.85 (0.73, 0.92) *
Maximum Stifle Angle in Swing (º)	-37.38 (14.23)	-34.78 (13.99)	-34.18 (14.51)	-35.46 (1.41)	0.712	0.84 (0.72, 0.92) *	0.85 (0.73, 0.92) *
Range Stifle Angle in Swing (º)	44.42 (5.04)	46.02 (6.55)	45.39 (4.84)	45.26 (0.66)	0.605	0.52 (0.30, 0.73) *	0.71 (0.51, 0.85) *

* = ICC >0.50

(continued)

Right Hindlimb

Variable	*Baseline 1*	*Baseline 2*	*Baseline 3*	*Mean baselines*	*P-value*	*Unadjusted ICC and 95% CI*	*Adjusted ICC and 95% CI*
Stance Duration (s)	0.42 (0.07)	0.44 (0.09)	0.44 (0.10)	0.43 (0.01)	0.729	0.46 (0.24, 0.69)	0.49 (0.27, 0.71)
Swing Duration (s)	0.34 (0.03)	0.34 (0.03)	0.34 (0.03)	0.34 (0.00)	0.785	0.58 (0.37, 0.77) *	0.69 (0.50, 0.83) *
Stride Duration (s)	0.76 (0.09)	0.78 (0.11)	0.78 (0.11)	0.77 (0.01)	0.692	0.47 (0.25, 0.70)	0.62 (0.41, 0.79) *
Ratio Stance To Stride (%)	0.55 (0.04)	0.55 (0.05)	0.55 (0.06)	0.55 (0.00)	0.909	0.49 (0.27, 0.71)	0.48 (0.26, 0.71)
Ratio Swing To Stride (%)	0.45 (0.04)	0.45 (0.05)	0.45 (0.06)	0.45 (0.00)	0.909	0.49 (0.27, 0.71)	0.48 (0.26, 0.71)
Ratio Stance To Swing (%)	1.24 (0.19)	1.28 (0.22)	1.28 (0.28)	1.27 (0.02)	0.820	0.44 (0.22, 0.68)	0.41 (0.19, 0.66)
Hoof Lateral Deviation (cm)	7.74 (1.59)	7.71 (2.06)	7.25 (2.13)	7.56 (0.23)	0.620	0.33 (0.13, 0.63)	0.30 (0.10, 0.62)
Hoof Forward Swing Velocity (m/s)	2.90 (0.22)	2.83 (0.29)	2.86 (0.23)	2.86 (0.03)	0.569	0.40 (0.19, 0.66)	0.68 (0.48, 0.83) *
Hoof Vertical Swing Velocity (m/s)	0.23 (0.06)	0.22 (0.06)	0.22 (0.06)	0.22 (0.00)	0.786	0.59 (0.37, 0.78) *	0.80 (0.65, 0.90) *
Range Hoof Height in Swing (cm)	3.96 (0.83)	3.71 (0.78)	3.87 (0.98)	3.85 (0.10)	0.615	0.61 (0.40, 0.79) *	0.76 (0.59, 0.88) *
Stride Length (cm)	98.04 (5.69)	96.88 (6.02)	97.94 (6.27)	97.63 (0.52)	0.767	0.66 (0.47, 0.82) *	0.74 (0.56, 0.86) *
Minimum Hindlimb Fetlock Angle Stance (º)	3.50 (8.58)	0.50 (6.64)	2.66 (7.61)	2.25 (1.26)	0.391	0.60 (0.39, 0.78) *	0.60 (0.39, 0.78) *
Maximum Hindlimb Fetlock Angle Stance (º)	20.68 (9.73)	18.10 (7.16)	20.44 (9.23)	19.77 (1.16)	0.545	0.67 (0.47, 0.82) *	0.67 (0.47, 0.82) *
Range Hindlimb Fetlock Angle in Stance (º)	17.19 (4.96)	17.60 (3.84)	17.78 (4.56)	17.52 (0.25)	0.896	0.75 (0.58, 0.87) *	0.75 (0.58, 0.87) *
Minimum Hindlimb Fetlock Angle in Swing (º)	-31.36 (7.82)	-31.77 (6.67)	-29.69 (7.32)	-30.93 (0.91)	0.585	0.39 (0.18, 0.65)	0.48 (0.25, 0.71)
Maximum Hindlimb Fetlock Angle in Swing (º)	10.82 (9.34)	8.19 (6.77)	11.28 (8.74)	10.12 (1.36)	0.401	0.66 (0.46, 0.81) *	0.66 (0.46, 0.82) *
Range Hindlimb Fetlock Angle in Swing (º)	42.18 (6.70)	39.96 (7.76)	40.98 (7.26)	41.05 (0.91)	0.578	0.63 (0.43, 0.80) *	0.79 (0.64, 0.89) *
Minimum Tarsal Angle in Stance (º)	24.61 (6.60)	24.46 (7.20)	24.23 (7.05)	24.43 (0.16)	0.982	0.77 (0.60, 0.88) *	0.77 (0.60, 0.88) *
Maximum Tarsal Angle in Stance (º)	59.87 (7.37)	61.04 (8.54)	60.60 (7.43)	60.50 (0.48)	0.874	0.65 (0.44, 0.81) *	0.67 (0.47, 0.82) *
Range Tarsal Angle in Stance (º)	35.26 (5.16)	36.58 (5.63)	36.37 (5.36)	36.06 (0.58)	0.664	0.76 (0.60, 0.87) *	0.75 (0.58, 0.87) *
Minimum Tarsal Angle in Swing (º)	24.63 (6.41)	24.68 (7.12)	24.38 (7.11)	24.56 (0.13)	0.987	0.76 (0.59, 0.87) *	0.76 (0.58, 0.87) *
Maximum Tarsal Angle in Swing (º)	73.76 (6.84)	74.52 (8.96)	74.23 (8.00)	74.17 (0.32)	0.946	0.62 (0.41, 0.79) *	0.69 (0.50, 0.84) *
Range Tarsal Angle in Swing (º)	49.13 (4.90)	49.85 (6.63)	49.85 (5.74)	49.61 (0.34)	0.884	0.68 (0.49, 0.83) *	0.72 (0.53, 0.85) *
Minimum Stifle Angle in Stance (º)	-71.48 (13.23)	-71.00 (14.49)	-70.55 (13.52)	-71.01 (0.39)	0.972	0.91 (0.84, 0.96) *	0.91 (0.84, 0.96) *
Maximum Stifle Angle in Stance (º)	-48.67 (11.71)	-47.69 (12.99)	-47.31 (13.78)	-47.89 (0.58)	0.931	0.84 (0.71, 0.92) *	0.88 (0.77, 0.94) *
Range Stifle Angle in Stance (º)	22.81 (4.62)	23.31 (5.23)	23.24 (5.03)	23.12 (0.22)	0.932	0.62 (0.41, 0.79) *	0.67 (0.47, 0.82) *
Minimum Stifle Angle in Swing (º)	-84.25 (11.65)	-83.32 (14.27)	-82.52 (14.29)	-83.36 (0.72)	0.905	0.87 (0.76, 0.93) *	0.91 (0.83, 0.95) *
Maximum Stifle Angle in Swing (º)	-39.31 (11.24)	-38.23 (12.90)	-37.47 (12.59)	-38.34 (0.77)	0.872	0.87 (0.76, 0.93) *	0.87 (0.76, 0.93) *
Range Stifle Angle in Swing (º)	44.94 (5.18)	45.09 (6.13)	45.05 (6.71)	45.03 (0.06)	0.996	0.64 (0.44, 0.80) *	0.73 (0.55, 0.85) *
Distance Matching Limb during stance (cm)	89.01 (6.85)	88.73 (8.15)	89.58 (9.63)	89.11 (0.36)	0.937	0.59 (0.38, 0.77) *	0.70 (0.51, 0.84) *

* = ICC >0.50

9.3.1.2 Baseline Versus Post-stroke Analysis of Global Parameters

Following stroke, all global parameters were significantly reduced compared to pre-stroke (Table 9.8). Animals walked more slowly, on average reducing the mean forward velocity of T1 by 0.28 m/s following stroke onset ($p<0.001$). Animals also held their head more to the centre of the run throughout the gait cycle, with the position of the head to T1 in the left/right plane closer to 0 (centre of the run) compared with pre-stroke. The vertical position of the head, in relation to T1, was on average 8.21 cm lower 3 days following stroke. T1 in relation to T13 was also 1.88 cm lower, and T1 to L7 2.27 cm lower, indicating lowering of the thorax following stroke onset.

Table 9.8 Baseline compared to post-stroke global parameters (mean +/- SD)

Variable	Direction	Mean (SD) of three baselines	Post-stroke	Mean difference (95% CI)	P-value
Mean Absolute Velocity T1 (m/s)	Forward	1.28 (0.20)	1.00 (0.18)	-0.28 (-0.35, -0.22)	<0.001 *
Mean Head to T1 (cm)	Left/right	3.39 (6.04)	0.61 (4.79)	-2.72 (-5.42, -0.02)	0.049 *
Mean Head to T1 (cm)	Vertical	9.89 (4.10)	1.69 (7.29)	-8.21 (-10.73, -5.68)	<0.001 *
Mean T1 to T13 (cm)	Vertical	-0.51 (1.09)	-2.40 (1.56)	-1.88 (-2.47, -1.30)	<0.001 *
Mean T1 to L7 (cm)	Vertical	-3.13 (1.46)	-5.40 (1.82)	-2.27 (-2.88, -1.67)	<0.001 *

* = $p<0.05$

9.3.1.2 Baseline Versus Post-stroke Analysis of Limb Parameters

Following stroke, deficit of the left forelimb (contralateral to the lesion) was the most frequently observed limb-specific change although was not observed in all animals (Figure 9.4). Although analyses were performed on both hind- and fore-limbs, to focus on deficits observed qualitatively, only forelimbs results are reported herein. Hindlimb parameters can be found in Appendix 9.2. Furthermore, time-by-limb interactions to determine the effect of time (pre- versus post- stroke) on sided limb deficit are reported in Appendix 9.3. Parameters for which both the interaction term (time*side) (Appendix 9.3) and the time term (Table 9.9)

were statistically significant are considered statistically reliable and reported as such. Parameters for which the interaction term (time*side) (Appendix 9.2) was not statistically significant, but the time term was (Table 9.9) are interpreted as suggestive of deficit.

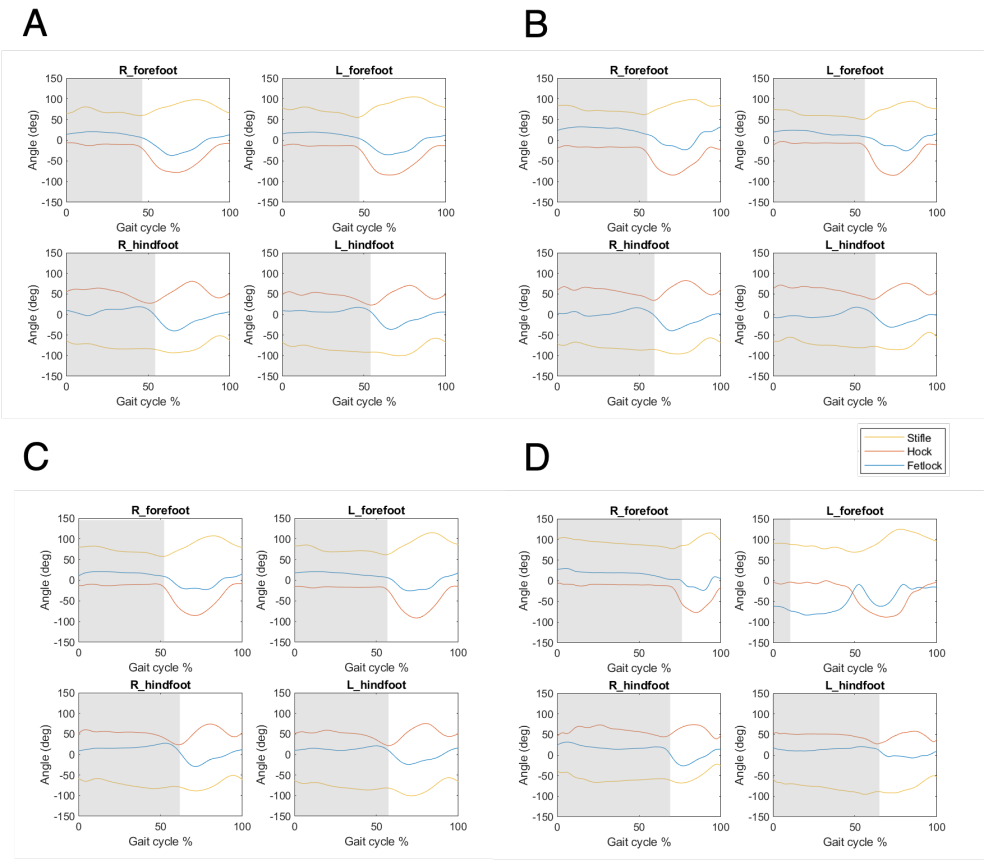

Figure 9.5. Joint exemplar data over 0-100 % of the gait cycle for 2 different animals. Shaded grey indicates the stance phase. A, B) joint angles pre stroke and C, D) joint angles 3 days following stroke. A, C) This animal did not display significant change of the fetlock joint angle pattern following stroke, as identified by the blue line in the left forefoot. B, D) In comparison, this animal displayed significant fetlock dysfunction, with a decreased left fetlock angle throughout the cycle and a reduction of left stance duration.

For the left forelimb, following stroke, on average the stance (13 s), swing (0.2 s) and stride (15 s) duration were longer than pre-stroke. An increase in the ratio of stance to stride (0.6%) and stance to swing (32%) and decrease in swing to stride (-0.6%) was also observed. Lateral deviation of the hoof was also less (-1 cm), as was forward (-31 m/s) and vertical (-0.04 m/s) swing velocity, and the range of the hoof height during swing (-0.62). Stride length (90 cm)

was considerably reduced following stroke compared with pre-stroke (97 cm). Joint angles were also influenced, including a reduction in the range of the fetlock (-3.9 º) and carpus (-2.8 º) during swing, an increase in the minimum (6 º) and maximum (5 º) angle of the elbow during stance, and increase in the maximum angle of the elbow during swing (5 º). When adjusted for velocity, the duration in stance and stride remained longer than pre-stroke, as did the increased ratio of stance to stride, and decreased ratio of swing to stride. Lateral deviation of the hoof remained reduced following adjustment, as did decreased range of flexion-extension of the elbow during stance. When both un-adjusted and adjusted for velocity, no differences were observed for minimum, maximum or range of the fetlock or stifle joint angles.

For the right limb, stroke resulted in an increase in stance (14 s), swing (2 s), and stride (15 s) duration, and decrease in stride length (-7 cm). This resulted in an increased ratio of stance to stride (0.6) and stance to swing (0.33), and decrease in swing to stride (-0.6). A reduction in hoof lateral deviation (-1.4 cm), hoof forward swing velocity (-0.3 m/s), range in the hoof height during swing (-0.7 cm) and increase in hoof vertical swing velocity (0.05 m/s) were also observed. Regarding joint angles, the minimum angle of the fetlock was increased during swing (2 º), although the range was reduced (- 3 º). The minimum angle of the carpus was increased during swing (3 º) and range decreased (-3 º). Following adjustment for velocity, differences in stance, stride, ratio of stance to stride, swing to stride and stance to swing remained, as did hoof lateral deviation, vertical swing velocity, and hoof height range. No differences were observed for joint angles when adjusted for velocity. The distance between the left and right forelimbs during stance was also reduced following stroke (- 3 cm).

Parameters observed to have a significant interaction between time and limb side (Appendix 9.3) included hoof forward swing velocity, range of the fetlock angle during swing, and maximum carpal angle during swing. The interaction remained significant for these variables following adjustment for velocity. Further, the interaction term for the range of the elbow during stance was significant following velocity adjustment. It was, however, not significant when unadjusted.

Table 9.9 Baseline compared to post-stroke fore-limb parameters (mean +/- SD)

Left Forelimb *Variable*	*Mean Baselines*	*Post-stroke*	*Mean difference un-adjusted (95% CI)*	*P-value un-adjusted*	*Mean difference adjusted (95% CI)*	*P-value adjusted*
Stance Duration (s)	0.41 (0.01)	0.54 (0.11)	0.13 (0.11, 0.16)	<0.001 *	0.02 (0.00, 0.05)	0.037 *
Swing Duration (s)	0.36 (0.00)	0.38 (0.04)	0.02 (0.01, 0.03)	<0.001 *	0.00 (-0.01, 0.01)	0.851
Stride Duration (s)	0.77 (0.01)	0.92 (0.13)	0.15 (0.12, 0.18)	<0.001 *	0.03 (0.00, 0.05)	0.028 *
Ratio Stance To Stride (%)	0.52 (0.01)	0.58 (0.04)	0.06 (0.05, 0.07)	<0.001 *	0.02 (0.00, 0.03)	0.018 *
Ratio Swing To Stride (%)	0.48 (0.01)	0.42 (0.04)	-0.06 (-0.07, -0.05)	<0.001 *	-0.02 (-0.03, -0.00)	0.018 *
Ratio Stance To Swing (%)	1.13 (0.02)	1.44 (0.23)	0.31 (0.24, 0.39)	<0.001 *	0.06 (-0.01, 0.14)	0.096
Hoof Lateral Deviation (cm)	7.40 (0.08)	6.39 (2.04)	-1.02 (-1.88, -0.16)	0.020 *	-1.10 (-2.13, -0.07)	0.036 *
Hoof Forward Swing Velocity (m/s)	2.72 (0.03)	2.42 (0.25)	-0.31 (-0.38, -0.23)	<0.001 *	-0.05 (-0.12, 0.03)	0.240
Hoof Vertical Swing Velocity (m/s)	0.37 (0.02)	0.32 (0.09)	-0.04 (-0.07, -0.02)	0.003 *	-0.03 (-0.07, 0.00)	0.061
Range Hoof Height in Swing (cm)	6.73 (0.33)	6.10 (1.89)	-0.62 (-1.20, -0.03)	0.038 *	-0.56 (-1.27, 0.15)	0.124
Stride Length (cm)	97.88 (0.96)	90.60 (5.41)	-7.41 (-9.25, -5.58)	<0.001 *	-1.50 (-3.34, 0.33)	0.109
Minimum Forelimb Fetlock Angle Stance (º)	5.12 (0.75)	4.16 (9.73)	-1.01 (-5.06, 3.03)	0.624	0.57 (-4.09, 5.24)	0.810
Maximum Forelimb Fetlock Angle Stance (º)	20.47 (0.70)	19.73 (9.89)	-0.83 (-4.90, 3.24)	0.689	-0.38 (-5.21, 4.46)	0.879
Range Forelimb Fetlock Angle in Stance (º)	15.35 (0.12)	15.57 (4.10)	0.18 (-1.60, 1.96)	0.841	-0.77 (-2.94, 1.39)	0.485
Minimum Forelimb Fetlock Angle in Swing (º)	-28.04 (1.22)	-24.69 (11.23)	3.17 (-0.96, 7.30)	0.132	3.26 (-1.54, 8.05)	0.183
Maximum Forelimb Fetlock Angle in Swing (º)	12.84 (0.63)	12.21 (9.22)	-0.73 (-4.74, 3.28)	0.721	0.94 (-3.76, 5.63)	0.696
Range Forelimb Fetlock Angle in Swing (º)	40.88 (0.59)	36.90 (7.81)	-3.90 (-6.62, -1.18)	0.005 *	-2.17 (-5.45, 1.11)	0.195
Minimum Carpal Angle in Stance (º)	-14.47 (0.41)	-15.47 (4.77)	-1.01 (-3.98, 1.96)	0.506	-0.98 (-4.49, 2.53)	0.584
Maximum Carpal Angle in Stance (º)	-2.15 (0.30)	-4.31 (4.91)	-2.15 (-4.85, 0.54)	0.118	-0.49 (-3.77, 2.79)	0.769
Range Carpal Angle in Stance (º)	12.32 (0.12)	11.16 (2.99)	-1.15 (-3.24, 0.95)	0.283	0.55 (-1.91, 3.01)	0.663
Minimum Carpal Angle in Swing (º)	-76.72 (1.32)	-75.37 (6.58)	1.42 (-1.71, 4.54)	0.374	0.70 (-3.10, 4.51)	0.717
Maximum Carpal Angle in Swing (º)	-3.77 (0.43)	-5.18 (5.30)	-1.40 (-4.54, 1.74)	0.383	-0.00 (-3.79, 3.78)	0.999
Range Carpal Angle in Swing (º)	72.95 (1.44)	70.19 (6.41)	-2.81 (-5.58, -0.05)	0.046 *	-0.61 (-3.93, 2.71)	0.719
Minimum Elbow Angle in Stance (º)	51.94 (0.02)	57.92 (6.73)	6.00 (0.55, 11.45)	0.031 *	4.84 (-1.64, 11.33)	0.143
Maximum Elbow Angle in Stance (º)	76.78 (0.43)	81.98 (6.87)	5.18 (-0.07, 10.43)	0.053 *	2.08 (-4.06, 8.22)	0.507
Range Elbow Angle in Stance (º)	24.83 (0.43)	24.05 (3.86)	-0.82 (-3.21, 1.57)	0.503	-3.03 (-5.81, -0.25)	0.033 *
Minimum Elbow Angle in Swing (º)	53.12 (0.14)	58.82 (6.46)	5.71 (0.54, 10.87)	0.030 *	3.50 (-2.66, 9.66)	0.265
Maximum Elbow Angle in Swing (º)	95.27 (0.58)	100.21 (7.49)	4.88 (-0.49, 10.25)	0.075	2.92 (-3.40, 9.23)	0.365
Range Elbow Angle in Swing (º)	42.16 (0.69)	41.40 (4.61)	-0.83 (-3.12, 1.46)	0.479	-0.91 (-3.67, 1.85)	0.518

* = p<0.05

(continued)

Right forelimb						
Variable	*Mean Baselines*	*Post-stroke*	*Mean difference un-adjusted (95% CI)*	*P-value un-adjusted*	*Mean difference adjusted (95% CI)*	*P-value adjusted*
Stance Duration (s)	0.41 (0.01)	0.55 (0.11)	0.14 (0.11, 0.16)	<0.001 *	0.03 (0.00, 0.05)	0.020 *
Swing Duration (s)	0.36 (0.00)	0.38 (0.02)	0.02 (0.01, 0.02)	0.002 *	-0.00 (-0.01, 0.01)	0.567
Stride Duration (s)	0.77 (0.01)	0.92 (0.13)	0.15 (0.12, 0.18)	<0.001 *	0.03 (0.00, 0.05)	0.039 *
Ratio Stance To Stride (%)	0.52 (0.00)	0.59 (0.04)	0.06 (0.05, 0.08)	<0.001 *	0.02 (0.01, 0.04)	0.004 *
Ratio Swing To Stride (%)	0.48 (0.00)	0.41 (0.04)	-0.06 (-0.08, -0.05)	<0.001 *	-0.02 (-0.04, -0.01)	0.004 *
Ratio Stance To Swing (%)	1.13 (0.02)	1.47 (0.28)	0.33 (0.25, 0.41)	<0.001 *	0.08 (0.01, 0.16)	0.033 *
Hoof Lateral Deviation (cm)	7.29 (0.22)	5.88 (1.57)	-1.43 (-2.29, -0.57)	0.001 *	-1.51 (-2.54, -0.48)	0.004 *
Hoof Forward Swing Velocity (m/s)	2.70 (0.04)	2.41 (0.18)	-0.30 (-0.37, -0.22)	<0.001 *	-0.03 (-0.11, 0.04)	0.363
Hoof Vertical Swing Velocity (m/s)	0.36 (0.01)	0.30 (0.06)	-0.05 (-0.08, -0.02)	<0.001 *	-0.04 (-0.08, -0.01)	0.023 *
Range Hoof Height in Swing (cm)	6.48 (0.16)	5.71 (1.20)	-0.78 (-1.36, -0.19)	0.009 *	-0.72 (-1.43, -0.01)	0.048 *
Stride Length (cm)	97.44 (0.81)	90.52 (5.57)	-7.05 (-8.88, -5.22)	<0.001 *	-1.14 (-2.98, 0.70)	0.224
Minimum Forelimb Fetlock Angle Stance (º)	6.42 (1.39)	5.87 (8.97)	-0.37 (-4.42, 3.67)	0.856	1.21 (-3.46, 5.88)	0.611
Maximum Forelimb Fetlock Angle Stance (º)	21.60 (1.00)	21.57 (9.46)	0.11 (-3.96, 4.17)	0.959	0.56 (-4.27, 5.40)	0.820
Range Forelimb Fetlock Angle in Stance (º)	15.18 (0.39)	15.71 (4.29)	0.48 (-1.30, 2.26)	0.596	-0.47 (-2.64, 1.69)	0.669
Minimum Forelimb Fetlock Angle in Swing (º)	-26.05 (0.68)	-23.78 (8.87)	2.32 (-1.80, 6.45)	0.270 *	2.41 (-2.39, 7.20)	0.325
Maximum Forelimb Fetlock Angle in Swing (º)	14.43 (0.82)	13.32 (9.07)	-0.99 (-5.00, 3.02)	0.629	0.68 (-4.02, 5.38)	0.777
Range Forelimb Fetlock Angle in Swing (º)	40.48 (0.64)	37.10 (6.51)	-3.31 (-6.03, -0.60)	0.017 *	-1.58 (-4.86, 1.70)	0.345
Minimum Carpal Angle in Stance (º)	-17.70 (0.75)	-17.55 (4.79)	0.13 (-2.84, 3.10)	0.933	0.15 (-3.36, 3.67)	0.931
Maximum Carpal Angle in Stance (º)	-3.90 (0.54)	-5.18 (3.49)	-1.28 (-3.98, 1.41)	0.351	0.38 (-2.90, 3.66)	0.821
Range Carpal Angle in Stance (º)	13.80 (0.24)	12.37 (3.32)	-1.41 (-3.50, 0.68)	0.186	0.28 (-2.18, 2.74)	0.822
Minimum Carpal Angle in Swing (º)	-79.30 (0.72)	-76.25 (6.76)	3.08 (-0.05, 6.20)	0.054 *	2.36 (-1.44, 6.17)	0.224
Maximum Carpal Angle in Swing (º)	-5.66 (0.52)	-6.14 (3.72)	-0.47 (-3.61, 2.66)	0.767	0.92 (-2.87, 4.71)	0.634
Range Carpal Angle in Swing (º)	73.64 (1.23)	70.12 (5.74)	-3.55 (-6.31, -0.79)	0.012 *	-1.35 (-4.67, 1.97)	0.427
Minimum Elbow Angle in Stance (º)	53.77 (0.37)	56.38 (9.20)	2.52 (-2.93, 7.97)	0.366	1.36 (-5.12, 7.85)	0.681
Maximum Elbow Angle in Stance (º)	77.13 (0.16)	81.20 (8.27)	3.98 (-1.27, 9.23)	0.137	0.88 (-5.26, 7.02)	0.778
Range Elbow Angle in Stance (º)	23.36 (0.50)	24.82 (7.63)	1.46 (-0.93, 3.86)	0.230	-0.75 (-3.53, 2.03)	0.598
Minimum Elbow Angle in Swing (º)	55.20 (0.49)	57.95 (8.95)	2.65 (-2.51, 7.82)	0.314	0.45 (-5.71, 6.60)	0.887
Maximum Elbow Angle in Swing (º)	96.03 (0.43)	99.29 (8.73)	3.14 (-2.23, 8.51)	0.252	1.17 (-5.14, 7.49)	0.716
Range Elbow Angle in Swing (º)	40.83 (0.49)	41.34 (7.18)	0.49 (-1.80, 2.78)	0.677	0.40 (-2.36, 3.16)	0.775
Distance Matching Limb during stance (cm)	51.28 (0.33)	47.51 (2.87)	-3.84 (-5.92, -1.77)	<0.001 *	-0.62 (-2.92, 1.67)	0.595

* = $p<0.05$

9.3.2 Neuroscore Assessment

Total neurological scores of 0 were typically seen in all animals across the three baseline sessions, with the exception of minor abnormalities in postural reactions ($p>0.05$, Figure 9.5, A). Following stroke, scores at 3 days were significantly higher when compared to pre-injury assessment, indicating considerable deficit ($p<0.0001$).

Assessment of demeanour incorporated both head posture and overall state of consciousness, with 21 of the 24 animals displaying evidence of apathy 3 days following stroke. This was significantly different to pre-stroke assessment, where demeanour appeared normal in all animals across baseline sessions ($p<0.0001$, Figure 9.5, B). Circling behaviour was observed in 6 animals' post-stroke, with consistent movement in a clockwise direction documented (towards side of lesion). Quantitative behavioural changes incorporating circling, torticollis, flexion of the fetlock, and dysmetria, however, were not significantly different between pre- and post-stroke assessments ($p>0.05$, Figure 9.5, C).

Regarding postural reactions, following stroke lateral drifting of was observed in 14/24 animals assessed via "wheelbarrowing" ($p<0.05$, Figure 9.5, C). Considering left and right sided reactions, there was a significant difference seen in the ipsilateral limbs following stroke when compared to baseline ($p<0.05$, Figure 9.5, E). This was significantly more pronounced in the contralateral, stroke affected limbs ($p<0.0001$, Figure 9.5, F).

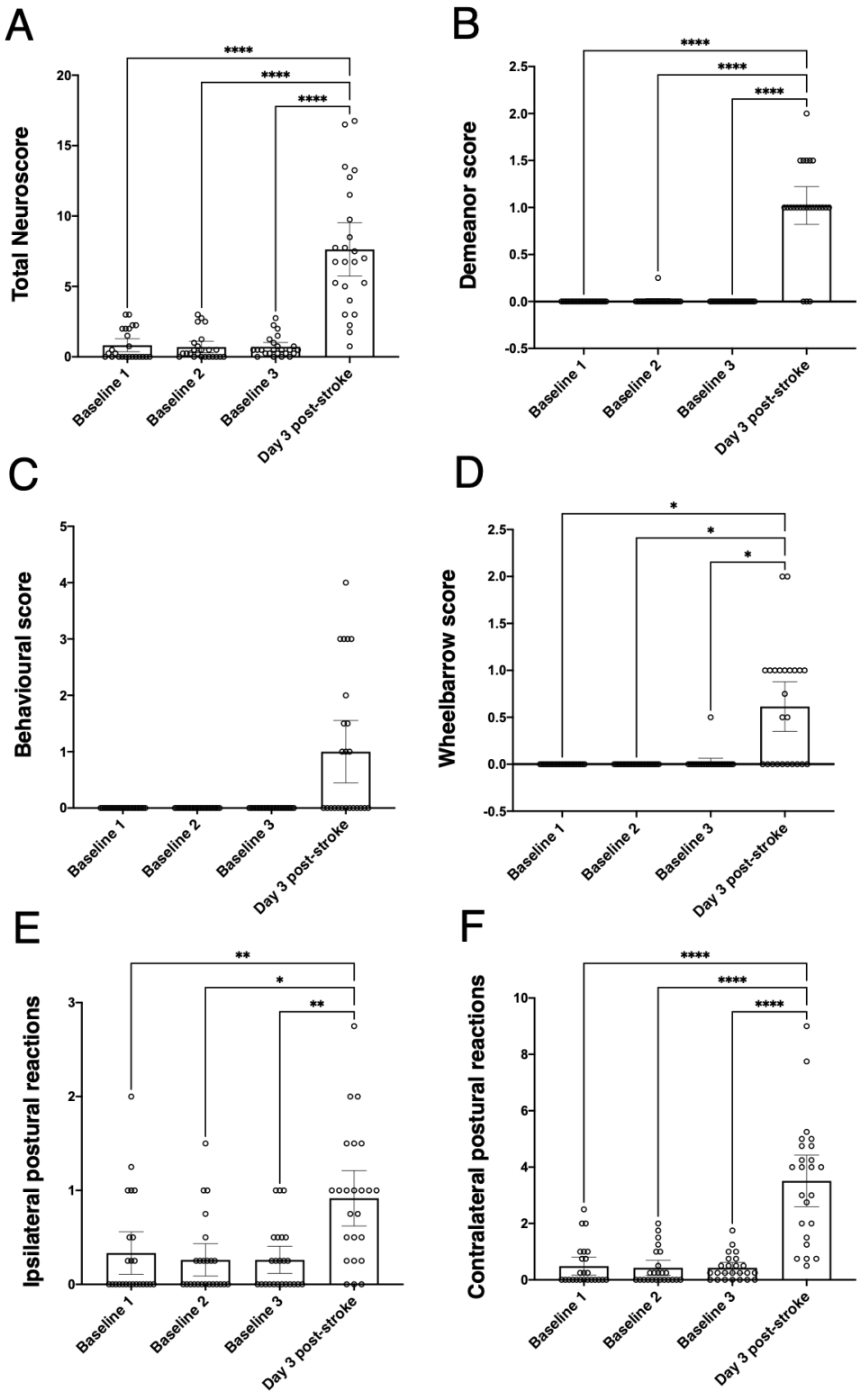

Figure 9.6. Neurological scores across baseline and post-stroke testing sessions. (A) total neuroscore, and scores for (B) demeanour, (C) behaviour, (D) "wheelbarrowing", (E) ipsilateral postural reactions and (F) contralateral postural reactions. * $p<0.05$, ** $p<0.01$, *** $p<0.001$, **** $p<0.0001$.

9.10 DISCUSSION

In this study we present a comprehensive approach to assessing functional outcome in an ovine model of stroke. First, using motion capture, we developed a method to assess gait kinematics. We have shown this approach to be repeatable in healthy animals through comparison of baseline pre-stroke trials and subsequently used these findings to assess changes in gait 3 days following stroke. Second, through adaptation of a neurological assessment score, we characterised the pre- and post-stroke response of animals, beyond the scope of kinematic assessment, including animal circling, behaviour, demeanour and postural reactions. Taken together, this approach to functional assessment provides an opportunity for the evaluation of medical and surgical interventions following stroke, and their contribution to function in a large animal model.

9.10.1 Repeatability of Motion Capture

In this study we showed that the position of the head in relation to T1, T13 and L7 across baseline trials had good repeatability, with animals consistently walking with their head upright, and slightly towards the right. Although the average speed of walking was comparable across animals with a low reported standard deviation, velocity had poor repeatability. This may have subsequently influenced limb specific parameters of interest. Indeed, it is well established that gait patterns change as a function of velocity (Fukuchi et al., 2019, Broom et al., 2017). This is true under physiological conditions and factoring in all velocity-related changes when assessing gait in disease is especially challenging. Previous studies suggest observation of gait characteristics when speed is not controlled leads to variable speeds from trial to trial, which is often significantly impacted following experimental intervention. This is true for both experimental animals (Herbin et al., 2007, Neckel et al., 2013, Batka et al., 2014, Machado et al., 2015) and human participants (Van

Iersel et al., 2007, Keene et al., 2016, Astephen Wilson, 2012). Neglect of velocity has also been proposed to lead to oversimplification of analysis and loss of potentially valuable data (Broom et al., 2017). The repeatability of limb-specific measures of interest reported herein improved when adjusted for walking speed via regression analysis. Such use of regression-based analysis has been suggested as a robust approach to translational gait analysis (Batka et al., 2014, Broom et al., 2017). This suggests our method is reproducible and enables application in various experimental conditions and environments, especially those where velocity is not a controlled measure.

Previous studies have used treadmills for functional assessment in sheep (Safayi et al., 2015, Safayi et al., 2016, Wilson et al., 2017). Although this offers the advantage of controlling walking speed, the selected speed of the treadmill has been shown to directly influence walking patterns (Parvataneni et al., 2009, Chen et al., 2005, Riley et al., 2007). Importantly, faster speed has been shown to facilitate a more normal walking pattern following stroke in humans (Brouwer et al., 2009). Given the unilateral effects of MCAo, the ability to accurately assess deficits of symmetry is imperative. Although we did not detect differences in symmetry in the aggregate data presented herein, allowing animals to walk at their own pace may enable more accurate assessment of asymmetric gait following stroke, which can retrospectively be adjusted for velocity. Further, for humans, treadmill tasks are also often used as a means of post-stroke rehabilitation (Tyrell et al., 2011). Ergo, speed-controlled treadmill tasks could improve functional outcome via incidental rehabilitation, obscuring accurate assessment of intervention. Enabling animals to walk at their own pace also allowed us to determine the ‘comfortable’ walking speed pre and post injury: an important consideration from an animal welfare perspective. Thus, adjusting for velocity during post-

processing is of benefit from both ethical and experimental perspectives and favours the generation of more reliable data.

In addition to accounting for velocity, assessing the variation across baseline trials allowed us to determine the reliability of findings following onset of injury. This provided important information regarding the utility of motion capture for functional assessment in large animal species. Across the three baseline sessions, we observed good repeatability of most, but not all, limb-specific outcome measures. Repeatability of human gait kinematics using motion capture in multiple laboratories is high (ICC >0.80), suggesting motion capture is a valuable tool across a range of environments and in different species (Charlton et al., 2020). Although most measures reported were repeatable, the few that were not varied between limb and side of the body. Specifically, all joint angles were repeatable with the exception of the left fore and right hindlimb minimum fetlock angle during swing, which was observed when both adjusted and unadjusted for velocity. The retro-reflective markers on the distal limbs were smaller (9 mm) than the other markers (15 mm) due to the close proximity placement on the hooves. Due to reduced spatial resolution, these markers frequently required more extensive gap filling during post-processing. This may have introduced more error, potentially confounding experimental results. Other fetlock angle parameters, however, were repeatable throughout baseline testing, including the minimum fetlock angle during swing for both the right fore and left hindlimb. Discrepancy may thus also represent variation of animal behaviour during overland walking. Future analyses should aim to improve data capture for the distal forelimbs and focus on assessing repeatable measures reported herein to accurately evaluate stroke and the benefit of interventions on gait kinematics.

The baseline gait outcomes reported in this study were generally consistent with other gait assessments performed in healthy sheep. Shelton and colleagues reported a stride length of approximately 1 m in mature female sheep, comparable to the present study (~98 cm for all limbs) (Shelton et al., 2011). The duration of the gait cycle phases was also consistent with previous studies as summarised in Table 9.10 (Agostinho et al., 2012, Safayi et al., 2015, Tapper et al., 2004, Tapper et al., 2006, Wilson et al., 2017, Kim and Breur, 2008)

Table 9.10 Stride, swing and stance duration in clinically healthy sheep

	Forelimb (L/R where applicable)			**Hindlimb (L/R where applicable)**		
Study	*Stance duration (s)*	*Swing Duration (s)*	*Stride duration (s)*	*Stance duration (s)*	*Swing Duration (s)*	*Stride duration (s)*
Present study	0.41	0.36	0.77	0.43	0.34	0.77
Tapper 2004	-	-	-	-	-	- / 0.98
Tapper 2006	-	-	-	-	-	- / 0.94
Agostinho 2012	0.41	0.28	0.70	0.43	0.27	0.69
Safayi 2015	0.46	0.37	0.84	0.47	0.37	0.84
Wilson 2017	0.51/0.49	0.33/0.34	0.84	0.49	0.35	0.84
Kim 2008	0.55	0.27	0.82	0.57	0.25	0.82

Limb joint flexion and extension throughout walking gait has also been reported in the ovine gait literature. Previous studies have primarily focused on the upper hind limb (stifle and hock joints). Tapper et al (2004) observed a minimum stifle flexion of -77 and maximum of -43 degrees, with a range of 34 degrees in healthy female Suffolk sheep. These values were reported over the entire gait cycle. Conversely, we observed a minimum stifle angle of -68 degrees in stance and -80 degrees in swing in the left hindlimb, and -71 in stance and -83 in

swing for the right hindlimb. We also observed a maximum stifle angle of -45 in stance and -35 in swing for the left hindlimb, and maximum of -47 and -38 for stance and swing respectively for the right hindlimb. Ergo, the range of motion of both the left and right stifle during stance was 23, however, during swing was 45.

There is limited published data regarding the fetlock angle of ruminants. The fetlock angle of horses has, however, been extensively researched (Peham et al., 2006, Crevier-Denoix et al., 2013). During cantering (+/- 8.3 m/s) on a synthetic surface, Crevier-Denoix and colleagues reported a minimum angle of the equine fetlock of 97 degrees in the leading limb and 95 for the trailing limb during stance. The maximal fetlock angle was 166 for the leading at 165 degrees for the trailing limb. This equates to a range of motion of 69 degrees for the leading and 70 for the trailing limb (Crevier-Denoix et al., 2013). During walking (+/- 2.2 m/s), Peham et al., reported an approximate minimum joint angle of 140 and maximum of 220 degrees, equating to a range of 80 degrees (Peham et al., 2006). At an average velocity of 1.2 m/s, our study observed a minimum fetlock angle of 5 degrees and maximum of 20 during stance in the left forelimb, and minimum of 6 degrees and maximum of 21 for the right forelimb. This equates to a range of motion of 15 degrees for both limbs. Although these values differ from those reported in the equine literature, differences may reflect allocation of flexion direction. Indeed, when observing the overall pattern of the gait cycle of the equine fetlock, the gait signature was qualitatively comparable to the sheep (Peham et al., 2006, Crevier-Denoix et al., 2013, Butcher and Ashley-Ross, 2002).

9.10.2 Post-stroke Motion Capture Assessment

We observed a significant reduction in forward velocity following stroke. A reduction of the head position in relation to T1, T1 to T13, and T1 to L7, was also observed, indicating significant lowering of the head and thorax post-ictus. These findings are potentially indicative of motor deficit and/or of animal apathy. Indeed, post-stroke apathy, mood and emotional disturbances are common clinically, where patients often present with a loss of motivation and initiative (Van Dalen et al., 2013). Conducting cognitive tasks may provide a more accurate measure of motivation, with systems developed for use in sheep (Sorby-Adams et al., 2021, McBride et al., 2016, Morton and Avanzo, 2011, Knolle et al, 2019). Although not reported herein, cognitive assessment represents an avenue for future assessment.

With regard to limb specific parameters, swing, stance and stride durations were substantially longer post-stroke than any reported values in clinically healthy animals, both in this study (statistically significant) and others (Agostinho et al., 2012, Safayi et al., 2015, Tapper et al., 2004, Tapper et al., 2006, Wilson et al., 2017, Kim and Breur, 2008). The increases observed effected both forelimbs irrespective of whether ipsi- or conta- lateral to the lesion. Animals also spent a significantly longer duration in stance compared with both swing and stride. This, in conjunction with decreased velocity, indicates that animals were less willing/able to execute forward movement. Furthermore, lateral deviation of the hoof in both left and right limbs was less than pre-stroke, as were forward and lateral swing velocity; indicating a slower pace and more ‘drag’ of the limb

Dysfunction of the left forelimb, contralateral to the lesion, was qualitatively observed following stroke herein and in previous studies (Sorby-Adams et al., 2019a, Boltze et al., 2008a). This was not, however, uniform in all animals, as shown in the exemplar data for

two different animals in Figure 9.5. This study observed no statistically significant differences in joint angle minimum, maximum and range for this limb, with the exception of the range of the elbow joint. It is important to note that the minimum angle of the elbow had low repeatability across baseline sessions, so the significance of this finding is questionable. Further, although gait durations were reduced, comparable findings of joint angle minimum, maximum and range for were observed in the right forelimb. Indeed, when comparing the left and right forelimbs, aggregate deficits are almost identical to the right. This suggests an overall reduction in animal well-being, rather than the unilateral, stroke specific deficit that was anticipated.

Adjusting for velocity reduced the mean difference between pre- and post-stroke for most outcomes, although significant differences remained. These findings were true of stance, stride and hoof lateral deviation irrespective of limb. This suggests that the change in gait parameters seen following stroke may reflect a change in gait signature due to the underlying pathology, not just a change in velocity. However, although these changes remained, they were not as anticipated. As per the exemplar data, if significant sided deficit was present, a reduction in stance of the effected limb due to hemiparesis and inability to execute motor control, and subsequent compensatory increase in stride of the unaffected limb would be expected. Indeed, the lack of significant differences between pre and post stroke joint angles was unexpected, particularly of the fetlock. Although fetlock paresis was observed during testing, deficit was not pronounced for every animal. Furthermore, if deficit was present, it was not consistent for every step of the gait cycle. Consequently, although we observed a qualitative loss of motor control of the left fetlock, it appears we have not accurately captured this deficit in this model, or so few animals displayed deficit such that findings were not significant. Moreover, of the 20 trials collected throughout testing, only 5 were post-

processed due to the significant time commitment. This suggests further trials may be necessary to increase the likelihood of accurately detecting sided deficit.

9.10.3 Neuroscore

Using the modified neuroscore, this study observed significant dysfunction following stroke onset, in keeping with previous studies (Boltze et al., 2008). Animals displayed evidence of abnormal movement of the thoracic limbs, and both ipsi- and contra- lateral postural reactions. Alterations in demeanour, including lowering of the head, were observed following stroke onset, in keeping with kinematic findings. Animals were also regarded as being apathetic, however, no sheep were reported as being in a state of stupor or comatose. Despite promising findings, the post-operative course may be a potential confounder of animal demeanour, and this finding may not be a reliable measure of cerebral ischaemia (Freret et al., 2011). In comparison, postural disturbances are a reliable indicator of veterinary neurological dysfunction, including stroke (Thomsen et al., 2016). Postural reactions in large animal species, however, are difficult to obtain because of their large size, requiring significant manual handling. Slight variability was consequently observed in baseline postural reaction tests. This likely reflects the fact that on occasion, animals were unwilling to perform the task, lying down or showing no desire to respond to the perturbation.

When assessing the thoracic limbs, we observed a significant deficit during wheelbarrowing. Fourteen animals displayed evidence of deficit, stumbling or knuckling during forward movement, with an additional 2 animals unable to coordinate movement of the limbs at all, and subsequently falling over. In evaluating ipsi- versus contra-lateral deficit, postural reaction tests to determine conscious proprioceptive positioning were performed, including

hopping and lateral drag. Although deficits were comparably more significant in the left forelimb, statistically significant differences were also observed in the right following stroke onset when compared to baseline. These findings support the motion capture findings, suggesting global deficit, rather than limb specific changes.

9.10.4 Limitations of This Method

There were several limitations in this study. Firstly, markers attached to areas with more overlying tissue were prone to skin motion artefact. Marker pins inserted directly into the bone eliminate skin motion artefact, although this was not possible in this study due to the number of markers and duration of post-stroke assessment, as pins can be painful and increase likelihood of infection. Skin motion artefact was minimised by selecting marker positions with minimal overlying soft tissue, not performing analysis of joints/bones with substantial overlying muscle mass, and tattooing the skin to make marker placement repeatable. Tattooing was, however, less distinguishable over the superficial bones of the distal limb, so reattachment of markers at these sites may have been more variable. Secondly, we only performed 2D analysis predominantly in the sagittal plane. Three-dimensional joint angle analysis provides more comprehensive (i.e. rotations about three axes) and accurate (i.e. relative to anatomical coordinate systems rather than a global coordinate system) joint angle assessment. We were limited in our approach due to the relative size of the animal, where given the number of joints assessed, there was insufficient space on rigid bodies to place additional markers. Future analyses should focus on only assessing outcomes of relevance and where possible, ensuring markers are placed on rigid bodies. Thirdly, due to 2D analysis, any deviation from straight line walking in the forward direction (y axis in the global coordinate system) could lead to errors in sagittal plane measures. This was minimised by limiting the width of the run (1.5 m), using only one gait cycle per trial for

which the animal was walking over the centre of the motion capture field, and discarding trials where animals deviated from straight line walking. Finally, for both motion capture and neuroscore, we only reported one occasion post-stroke. To accurately capture the temporal profile of post-stroke gait changes, functional studies should, ideally, mimic the clinical scenario where assessment is performed up to 90 days following stroke onset.

9.11 CONCLUSIONS

Functional outcome a major endpoint in stroke clinical trials, and an essential consideration in pre-clinical stoke models. In this study we developed a comprehensive method to assess function following stroke in a clinically-relevant ovine model. Following stroke, animals exhibited deficit, observed both kinematically via motion capture and via composite scoring. This method enables the assessment of novel therapeutics on stroke outcome and has the potential to be applied to other large animal models of central nervous system injury including traumatic brain injury, Alzheimer's disease, Parkinson's disease and Huntington's disease.

Acknowledgements

This study was supported by funding from the National Health and Medical Research Council (NHMRC; RJT) Australia (Project grant 1082556; RJT) and Brain Foundation, Australia (RJT). We would like to thank the generous support provided by Logemas: Alex Muir, Chris Muir, Denny Wells and Max Cowan, and VICON.

10

General Discussion

10.0 INTRODUCTION

This thesis characterised a clinically relevant model of ovine stroke in which the efficacy of an NK1-R antagonist (EU-C-001) was investigated. In Chapter 6, we successfully demonstrated that 2 doses of the NK1-R significantly reduced ICP post-stroke, comparable to decompressive craniectomy. In Chapter 7, we demonstrated that cerebral oedema and ICP rose in a delayed fashion following ovine stroke with reperfusion, peaking at 5-6 days, comparable to the clinical scenario. In Chapter 8, we determined that the NK1-R antagonist was able to successfully sustain a reduction in ICP compared with vehicle when given both acutely (1-3 days) and in a delayed fashion (5 days) post transient stroke. Finally, in Chapter 9, we developed a novel method of ovine functional assessment, assessing gait kinematics using motion capture, in addition to development of a neuroscore to assess deficits beyond the scope of biomechanical assessment. Using these methods, we were able to successfully detect behavioural changes following stroke onset. Taken together, these findings highlight the relevance of NK1-R antagonism as a viable treatment for cerebral oedema and concomitant rise in ICP post-stroke. This general discussion will summarise and integrate the main findings across doctoral chapters, highlighting the contribution of research to the field, and suggest avenues for future analyses.

10.1 NK1-R ANTAGONIST TREATMENT REDUCES ICP - IRRESPECTIVE OF REPERFUSION STATUS OR TREATMENT WINDOW

This thesis observed marked increases in ICP following ischaemic stroke under both permanent and transient stroke conditions. Following permanent MCAo (Chapter 6), ICP began to rise by 14 hours post-ictus (24 mmHg) and continued to rise unabated, reaching 32

mmHg at 19 hours, and 39 mmHg by the terminal 24-hour endpoint. These findings corroborate previous studies in our ovine model, where ICP was significantly elevated following permanent, but not transient MCAo at 24 hours post-stroke (Wells et al., 2015) . To examine more sub-acute time-points after stroke with reperfusion (Chapter 7), this thesis observed a significant increase in ICP at 5 (28 mmHg) and 6 days (25 mmHg) post-ictus, which began to resolve at 7 days. Across the studies reported herein, both permanent and transient stroke animals reported ICP values significantly higher than sham operated animals (10 mmHg).

The finding of aggravated ICP following complete MCA occlusion, and delayed increases following temporary/partial arterial obstruction, support the human literature where raised ICP characteristically presents within 2-5 days of stroke onset following failure of cerebral autoregulation (Hacke et al., 1996). In the neurointensive care unit, ICP in excess of 20 mmHg is associated with an increased risk of herniation, death and disability, necessitating appropriate intervention (Jeon et al., 2014, Pinto et al., 2020). Clinical management of intracranial hypertension is typically approached in a step wise manner (Chapter 1) seeking first to consider general management approaches to reduce ICP (hypertension) and avoid factors that aggravate or precipitate elevation of ICP (inadequate venous drainage) (Jeon et al., 2014). Osmotherapeutic agents are typically administered in an attempt to reverse osmotic drive, albeit associated with transient effects and increased likelihood of rebound oedema (Brogan and Manno, 2015, Cho, 2007, Maioriello et al., 2002, Burgess et al., 2016). In patients with MMCAI, elevated ICP is resistant to conservative management, with mortality ranging up to 70%-80% with medical treatment alone (Hacke et al., 1996, Qureshi et al., 2003, Berrouschot et al., 1998).

When intracranial hypertension is refractory to medical management (remaining between 20-25 mmHg), surgical intervention with DC is warranted. DC reduces ICP, relieves tissue shifts, and improves mortality when performed within 48 hours of stroke (Vahedi et al., 2007a, Vahedi et al., 2007b, Geurts et al., 2013, Jüttler et al., 2007, Hofmeijer et al., 2009). Indeed, DC is superior to other treatment modalities used to manage elevated ICP, bringing about at 19 mmHg reduction in pressure when compared with hyperventilation (6 mmHg), mannitol (8 mmHg), barbiturates (8 mmHg), hypothermia (10 mmHg), hypertonic saline (15 mmHg), or CSF drainage (15 mmHg) (Schreckinger and Marion, 2009). Despite unequivocal effects on survival, DC is associated with an increased risk of perioperative injury and morbidity in the elderly. With a lack of efficacious pharmacological interventions, however, it remains the current best-approach to clinical management. Replicating the clinical scenario in this thesis, ICP was shown to be attenuated following pterional DC performed 2 hours after stroke onset (Chapter 6). Following DC, pressure rose slightly, yet was maintained below 19 mmHg (-10 mmHg compared with vehicle) for the duration of the 24-hour monitoring period.

Attenuated ICP following DC in this model subsequently provided a clinically relevant measure in which we were able to compare outcomes following NK1-R administration. When treatment was administered following permanent stroke, we observed a significant reduction in ICP following 2 (18 mmHg) and 3 (17 mmHg) doses of the NK1-R antagonist at 19 hours post-ictus. This reduction was sustained for both regimens (2 doses 20 mmHg: 3 doses 19 mmHg), with ICP comparable to DC and with no rebound cerebral oedema or elevated ICP observed. Indeed, the most remarkable finding of this study was the fact that NK1-R antagonist treatment was able to reduce ICP to the same extent as DC surgery. However, a single bolus of the NK1-R antagonist was insufficient to produce a sustained

effect on ICP. The lack of treatment effect seen in the single bolus NK1-R group may be due to the need for the drug to sufficiently saturate binding sites in different body compartments. Given that NK1-R are ubiquitously expressed throughout the body, initial dosing may cause preferential distribution and saturation of compartments such as the gastrointestinal tract. The first dose may thus be required for initial loading to saturate non-brain compartments, with the second dose able to bring about a treatment effect in the target organ, which in this study is the brain. However, the significant reduction in ICP following 2 × and 3 × doses of the NK1-R antagonist administered intravenously suggest it is a promising therapeutic strategy to reduce elevated ICP following stroke, due to its ability to produce a clinically-meaningful and sustained reduction in pressure, whilst at the same time circumventing the need for invasive surgery with inherent post-operative risks (Hacke et al., 1996).

Given the increased rate of vascular recanalisation following stroke due to the increased uptake of endovascular clot retrieval and extended window for thrombolysis in select patients, there is a need for reperfusion-centric pre-clinical research. Accordingly, we also investigated the efficacy of NK1-R administration following transient stroke (Chapter 8). The clinical course of elevated ICP was determined in Chapter 7, where increased ICP was observed at 5-6 days post stroke. This time-course was subsequently used to guide administration of the NK1-R antagonist following stroke with reperfusion (Chapter 8). A significant reduction in ICP was observed when treatment was administered prior to onset of elevated ICP (administration on days 1-3) and following delayed onset when elevated ICP was already established at 5 days post-stroke. When ICP was measured at 6 days, early NK1-R treatment maintained ICP at 13 mmHg, and late treatment at 11 mmHg, compared with vehicle animals who reported ICP as high as 24 mmHg during the same period. The ability to produce a significant reduction in ICP with treatment administered in a more delayed

fashion was a particularly promising finding of this study. Indeed, the most significant limitation to current stroke intervention is time, hence the stroke mantra 'time is brain' (Saver, 2006). Prompt diagnosis of stroke subtype is key to expedite treatment and improve outcomes for those affected (Marchese et al., 2016, Yew and Cheng, 2015). Time to treatment onset can be significantly extended for those living in rural communities, which is costly in terms of outcome (Ader et al., 2019). The importance of treatment timing is also relevant for the management of post-stroke cerebral oedema. DC performed too soon after ictus may cause unnecessary surgical iatrogenic injury, whereas surgery performed after signs of herniation have developed may be of little value with an increased risk of complications (Jeon et al., 2014). The significant reduction in ICP observed following late NK1-R antagonist administration suggests that treatment is directly targeting the mechanisms underlying increased barrier permeability and consequent development of space-occupying cerebral oedema. Therefore, the ability to produce a significant and sustained reduction in ICP following intravenous administration of a novel pharmacotherapy, such as the NK1-R antagonist, is potentially of great clinical significance.

10.2 NK1-R ANTAGONIST TREATMENT REDUCES CEREBRAL OEDEMA AND MIDLINE SHIFT

Across the studies reported in this thesis, considerable cerebral oedema was observed within the infarcted MCA territory on FLAIR MRI following onset of ischaemia, consistent with elevated ICP. It is largely accepted clinically that elevations in ICP following stroke onset arise as a consequence of malignant fluid accumulation within the non-expansile cranial cavity (Ropper and Shafran, 1984, Simard et al., 2007). Following permanent MCA infarction (Chapter 6), untreated vehicle animals presented with significant cerebral oedema

and associated midline shift at 24 hours post-stroke. Furthermore, animals who underwent DC displayed evidence of significant transcalvarial herniation on MRI. This is comparable with clinical stroke, where the brain is shown to expand out of the skull defect created by the craniectomy (Liao et al., 2015). Ergo, despite a significant reduction in ICP following DC, pressure relief is achieved solely via mechanical means and, as anticipated, DC treatment does not significantly reduce the underlying pathology driving the development of cerebral oedema and elevated ICP. In comparison, 2 × or 3 × doses of the NK1-R antagonist brought about a significant and sustained reduction in cerebral oedema and a reduction in midline shift when compared with vehicles.

Congruent with elevated ICP shown in Chapter 7, an evolution of cerebral oedema was also observed following transient stroke, which was maximal at 5-6 days. This was accompanied by a significant increase in midline shift at 5 days (when compared with 1 day post stroke), and an increase in extravasation of gadolinium across the BBB. The finding of enhanced gadolinium is of particular importance given its clinical use as a marker of BBB permeability in stroke (Kassner et al., 2009, Kassner et al., 2011, Merali et al., 2015, Wardlaw et al., 2008, Wardlaw et al., 2009, Vidarsson et al., 2009). Contrast-based MRI accurately enables *in vivo* mapping of gadolinium, which given its large molecular weight (550 Da) can be used as a marker of BBB permeability in real time (Montagne et al., 2016). Following NK1-R administration, a decrease in gadolinium extravasation within the infarcted hemisphere was observed, which was a consistent feature following both the early and late treatment regimens. Furthermore, NK1-R antagonist administration was associated with a significant reduction in cerebral oedema and midline shift following both early (1-3 days) and delayed (5 days) treatment. This was accompanied by a decrease in hemispheric water content which, despite a trend towards a reduction in the early NK1-R group, was only statistically

significant in the late NK1-R antagonist treatment group. Taken together, the findings of reduced oedema volume following treatment administration in both permanent and transient stroke models suggest the reduction in cerebral oedema observed is occurring as a result of decreased fluid accumulation in the cerebral hemispheres.

In keeping with significant cerebral oedema, all stroke animals also exhibited significant infarction of the MCA territory on DWI MRI (Chapters 6, 7 and 8). Lesion volume was greatest following permanent MCAo (Chapter 6), accompanied by tonsillar herniation in several animals, whereas lesion volume following transient stroke was comparably less (Chapters 7 and 8). However, in all animals the infarct typically involved the temporal lobe and insula, and subcortical structures such as the hippocampus, thalamus, putamen and caudate nucleus. This is comparable to areas typically involved in MMCAI clinically (Heiss, 2016, Thomalla et al., 2003, Walcott et al., 2014, Nogles and Galuska, 2020). Taken together, these findings highlight the value of the ovine model, and its ability to replicate key aspects of clinical stroke. It is important to note that although cerebral oedema was reduced following NK1-R antagonist treatment in our models (Chapters 6 and 8), no treatment effect on infarct volume was observed following either permanent or transient stroke. Nevertheless, these findings are consistent with previous rodent studies where no effect on infarct volume was observed following NK1-R antagonist treatment, as measured at 24 hours following transient MCAo (Turner et al., 2011a). Such findings are not surprising considering the NK1-R antagonist is targeting mechanisms underlying barrier disruption and downstream cerebral oedema, rather than other pathways in the ischaemic injury cascade.

Furthermore, across the studies reported in this thesis (Chapters 7 and 8), we did not observe a difference in response to either injury or NK1-R antagonist administration between male

and female animals. Although the female oestrous cycle was not monitored in these studies, this provides compelling evidence regarding the clinical potential for this therapy for both male and female stroke patients.

10.3 MECHANISMS UNDERLYING NK1-R ANTAGONIST TREATMENT EFFICACY POST-ISCHAEMIC STROKE

To probe the mechanisms underlying the reductions in ICP and cerebral oedema observed, immunohistochemical analyses were also performed to elucidate changes in neurogenic inflammation (SP, NK1-R) and BBB (caveolin-1, albumin and claudin-5) markers (Chapters 6-8). Following stroke, increased SP immunoreactivity in vehicle animals was observed following transient MCAo at 5 and 6 days (Chapter 7) post-stroke. However, no SP reactivity was observed following permanent occlusion at 24 hours (Chapter 6) post-ictus. Consequently, no changes in SP expression between vehicle and NK1-R treatment were observed, as all animals had undergone permanent infarction (Chapter 6). These findings are consistent with previous IHC studies in rodents, where SP was only observed following stroke with reperfusion, but not where there was persistent arterial occlusion (Turner et al., 2011b, Turner et al., 2006, Turner and Vink, 2012, Turner and Vink, 2014). It is postulated that in stroke with a reperfusion component, compromised penumbral cells in ischaemic tissue experience long durations of electrical silence and alterations in neuronal function, leading to sustained activation of c-fibres and persistent SP release (Astrup et al., 1981, Hofmeijer and Van Putten, 2012, Turner, 2007). The physical exertion of pressure on c-fibres as a consequence of accumulating vasogenic oedema may also lead to their mechanical stimulation, whereby release of SP occurs in a vicious cycle. Indeed, prior studies in rodents have observed that increased SP immunoreactivity was seen as early as 5

hours following transient stroke, yet was most pronounced at 24 hours (Turner, 2007). Conversely, cells exposed to permanent ischaemia undergo rapid necrosis where, after 24 hours, all compromised cells have succumbed to the persistent cerebral ischaemia. In the early stages of ischaemia and cytotoxic oedema, acidosis likely promotes c-fibre stimulation and SP release. However, as cytotoxic oedema plateaus, a prompt return of receptor channel potential occurs leading to decreased SP release. Ergo, SP release likely occurs early following permanent stroke, compared with the sustained release observed following transient occlusion. This may explain the absence of SP observed following permanent stroke (Chapter 6), as by the time tissue was harvested at 24 hours, SP was no longer detectable.

Following transient ovine stroke (Chapter 7), peak SP immunoreactivity was observed 5-6 days post-ictus, with SP localised to the perivascular tissue, suggesting the source was c-fibres ensheathing the vasculature (Edvinsson et al., 1983). This corroborates previous IHC findings in rodent models of both stroke and TBI (Turner et al., 2011b, Turner et al., 2006, Turner and Vink, 2012, Turner and Vink, 2014). SP has also been reported in serum collected from both ischaemic and haemorrhagic stroke patients (Lorente et al., 2016, Lorente et al., 2020). In non-surviving patients following ICH, SP was significantly elevated at 4-, 6- and 8-days following haemorrhage onset (Lorente et al., 2020). Similarly, elevated serum SP levels were observed as early as 12 hours following ischaemic stroke, with significantly elevated levels observed in patients who died, as compared with those who survived. A trend towards elevated serum SP at 3-7 days following transient stroke was observed in this thesis. However, no significant differences were seen within the CSF at 1-, 3- and 6-days following onset (Chapter 7), when compared with pre-stroke baseline samples. This highlights the variability in SP response depending on both the fluid or tissue used for analysis, and that

timing of sample collection is crucial to detecting any changes. One potential explanation for this is that the peak of SP release may not be accurately captured in our studies due to timing of sample collection post-stroke, whereby SP release may have occurred at time-points which weren't captured in our sampling timeline. In addition, given that SP is a small peptide, it is susceptible to rapid degradation. Indeed, unbound SP becomes rapidly hydrolysed by peptidases, specifically p-endopeptidase in the extracellular fluid and angiotensin-converting hormone in the blood plasma (Kream et al., 1985). Consequently, the half-life of SP ranges from seconds to minutes in extracellular fluid, while in extracted plasma SP remains stable for hours (Suvas, 2017, Skidgel et al., 1984, Skidgel and Erdos, 1987).

Although a marked SP response was not seen following permanent stroke, significant NK1-R immunoreactivity was observed at 24 hours following permanent MCAo (Chapter 6). A subsequent decrease in NK1-R immunoreactivity was also observed following 2 × and 3 × boluses of the NK1-R antagonist (Chapter 6). This suggests competitive binding of the antagonist to the receptor, thereby preventing SP docking. Characteristically, SP binds the NK1-R, initiating G-protein subunit disassociation and activation of secondary messenger pathways depending on cell type, including phospholipase C, adenyl cyclase and phospholipase A_2 (Steinhoff et al., 2014, Monastyrskaya et al., 2005). Upon binding, the receptor ligand complex is rapidly internalised and undergoes disassociation (Martinez and Philipp, 2016). The ultimate fate of the endocytosed complex thereafter depends on the stimulation conditions of the surrounding environment (Martinez and Philipp, 2016). Low concentrations of SP lead to receptor degradation and recycling to the cell surface, facilitated by the β-arrestin pathway (Mcconalogue et al., 1999). The cellular response to SP is then rapidly attenuated due to NK1-R endocytosis, desensitisation, and depletion of high-affinity

membrane bound receptors (Steinhoff et al., 2014, Mcconalogue et al., 1999). Conversely, high concentrations of SP and sustained incubation initiates NK1-R ubiquitination and degradation (Steinhoff et al., 2014).

Following stroke, aberrant SP release leads to NK1-R upregulation (Turner, 2007, Nishimura et al., 1994). In endothelial cells such as those lining the BBB, SP has been shown to activate transcription factors such as nuclear-factor (NF)-AT and NF-κB (Quinlan et al., 1999), with NF-κB being a major regulator of NK1-R expression during neurogenic inflammation. Indeed, a putative NF-κB binding site has been identified in the promoter of the human NK1-R gene, which has been confirmed experimentally (Takahashi et al., 1992, Simeonidis et al., 2003). The magnitude of SP release thus likely determines the extent of NK1-R upregulation in endothelial cells of the BBB. This is supported by the findings reported in this thesis, where the significant increase in NK1-R reactivity was primarily observed in the perivascular tissue following permanent stroke (Chapter 6). Furthermore, NK1-R upregulation has also been reported in other models of acute CNS injury, where following TBI, increased NK1-R expression has been observed in vehicle animals (Li et al., 2019). During inflammation, increased release of SP from afferent c-fibres has also been shown to cause NK1-R upregulation in the dorsal horn (Zieglgänsberger, 2019). Given the rapid degradation of unbound SP, the findings of this thesis suggest that identification of the NK1-R may be a more robust measure of neurogenic inflammation. Indeed a decrease in SP, in conjunction with a significant increase in NK1-R internalisation, has previously been observed (Cipriani et al., 2011). Nevertheless, further investigation into the relative concentrations of both SP and NK1-R is warranted to further elucidate the timing of the receptor-ligand interactions and subsequent activation of downstream injury pathways.

The mechanisms of SP/NK1-R receptor internalisation is an important feature or neurogenic inflammation and increased barrier permeability. SP-induced stimulation of the NK1-R has been shown to cause relocation of protein kinase C-α to caveolae and subsequent caveolar internalisation (Mineo et al., 1998). Endocytosis of the NK1-R/SP complex thus likely occurs via caveolae, facilitated by the principal structural protein caveolin-1 (Williams and Lisanti, 2004). Indeed, a marked increase in perivascular caveolin-1 expression was observed in the thesis studies (Chapters 6 and 7), which was consistent in both permanent and transient models. The greatest reactivity was seen in permanent vehicle animals at 24 hours, and in transient vehicle animals at 5-6 days following stroke onset. Following administration of the NK1-R antagonist in permanent stroke, a reduction in caveolin-1 reactivity was observed, which was most pronounced in the 2 × and 3 × dose treatment groups (Chapter 6). Following transient stroke, we also noted a marked reduction in perivascular caveolin-1 in both early and late treatment regimens (Chapter 8). In the brain, caveolin-1 is generally expressed at a low level. However, upon SP binding, the NK1-R localises to caveolae via lipid rafts in the plasma membrane, following which the receptor ligand complex is internalised. Ergo, upregulation of NK1-R following stroke may cause an aberrant increase in caveolae-formation. Indeed, studies have shown that the NK1-R is co-expressed within endothelial caveolae, further supporting a dynamic relationship (Kubale et al., 2007, Vink et al., 2017, Cipriani et al., 2011, Monastyrskaya et al., 2005). Caveolin-1 is also suggested to be involved in signalling activities of long-duration, suggesting a sustained upregulation of caveolae following NK1-R activation (Monastyrskaya et al., 2005).

This thesis also observed increased caveolin-1 reactivity in conjunction with marked albumin extravasation, which was a consistent feature of both permanent and transient stroke (Chapters 6-8). Enhanced parenchymal albumin suggests extensive barrier breakdown, in

keeping with our MRI finings of increase gadolinium extravasation post-ictus. Following administration of the NK1-R antagonist in permanent stroke animals, a marked reduction in parenchymal albumin was observed. As with caveolin-1, the most pronounced reduction in albumin was seen in animals who received 2 × and 3 × treatment doses (Chapter 6). In transient stroke, albumin extravasation was greatest at 4-6 days post-stroke, and was observed to localise both within the brain parenchyma (Chapter 7) and the perivascular space (Chapter 8). NK1-R antagonist administration significantly reduced albumin within the infarcted hemisphere, with comparable findings observed for both the early and late NK1-R antagonist treatment regimens (Chapter 8). Functionally, albumin maintains colloid osmotic pressure across the endothelial barrier, and its concentration gradient is critical in the regulation of fluid balance (Minshall et al., 2000). Given the findings of this thesis, it is proposed that increased albumin in the parenchyma following stroke is facilitated by caveolin mediated transcytosis. Indeed, the albumin docking protein 60-kD glycoprotein (gp60) is localised to endothelial caveolae. Upon albumin binding gp60, the gp60/albumin domain interacts with caveolin-1 via the heterotrimeric GTP binding protein G_i (Minshall et al., 2000). The activation of albumin and its receptor subsequently facilitates migration of vesicles from the apical to the basolateral endothelial cell surface, and consequent accumulation of albumin in interstitial fluid. Ergo, our finding of enhanced caveolin-1 and albumin reactivity post-stroke, which is subsequently attenuated following NK1-R antagonist administration, suggest that caveolin-1/NK1-R interactions are a key contributor to the increased BBB permeability seen following cerebral ischaemia (Figure 10.1). Although loss of TJ integrity is also hypothesised to precipitate oedema formation, we did not observe any changes in claudin-5 expression following NK1-R antagonist administration in transient MCAo animals (Chapter 8), further supporting a leading role of caveolae in mediating albumin transcytosis.

In the setting of post-stroke oedema, it is largely accepted that the albumin that accumulates within the brain parenchyma is derived from the vasculature due its high plasma concentration (Gounden et al., 2021, Weaving et al., 2016). However, in the permanent stroke model reported herein, the marked parenchymal albumin observed is contentious given that there is no active blood flow to the ischaemic region. This suggests that the albumin is derived from a compartment other than the vasculature. Indeed, increasing evidence suggests that the fluid in vasogenic oedema may be partially derived from the CSF rather than the vasculature alone (Mestre et al., 2020). Our finding of increased albumin reactivity following permanent MCAo suggests neurogenic inflammation may cause an upregulation of caveolin-1 mediated albumin transcytosis in endothelial cells comprising both the blood-brain and blood-CSF (BCSF) barriers. Indeed, the choroid plexus displays a high rate of vesicular transport activity, suggesting movement across the barrier is primary mediated by transcytosis, facilitated in part by caveolae (Praetorius and Damkier, 2017). If the BBB/BCSF barrier integrity is compromised, albumin may consequently be upregulated in the circulating CSF. Indeed, the albumin CSF quotient is often used as a marker of BBB integrity clinically (Musaeus et al., 2020, Akaishi et al., 2015), with elevated levels in the CSF indicative of barrier breakdown and subsequent extravasation from the blood to the CSF (Gounden et al., 2021, Akaishi et al., 2015). Previous studies have also documented caveolin-1 and NK1-R immunoreactivity in the choroid plexus (Maeno et al., 1993, Mantyh et al., 1988, Mantyh et al., 1989, Nag et al., 2007). Although not investigated in this thesis, examining the relationship between NK1/SP, BCSF barrier permeability and albumin transcytosis may provide further insight into the genesis of vasogenic oedema following stroke.

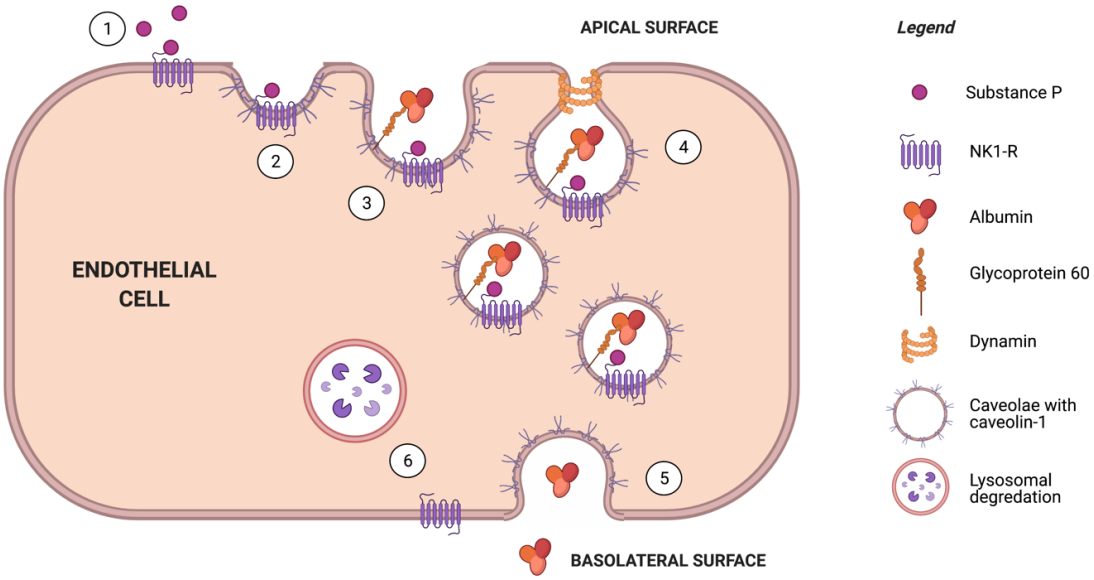

Figure 10.1. Proposed mechanism of NK1-R facilitated caveolin-mediated albumin transcytosis facilitating vasogenic oedema formation. 1) SP released from perivascular c-fibres binds NK1-R embedded in the endothelial plasma membrane. 2) The receptor ligand complex is co-localised to lipid-raft caveolae. 3) Albumin is bound 60-kD glycoprotein (gp60) colocalised with caveolin-1 to endothelial cell apical plasma membrane caveolae. 4) the NK1-R/SP and albumin/gp60 complexes are rapidly endocytosed with dynamin facilitating caveolar budding. 5) The caveolae containing albumin migrates to the basolateral surface, where albumin is exocytosed into the extracellular parenchymal space. 6) The NK1-R/SP complex is disassociated and either degraded or recycled, depending on SP concentration.

10.4 NK1-R ANTAGONIST PHARMACOKINETICS

To establish the molecular pharmacokinetics of the NK1-R antagonist following administration of 2 × doses at 5 days following stroke onset (late NK1-R antagonist treatment regimen), multiple whole blood samples were drawn at 4 hourly intervals. Peak NK1-R concentration was observed in the blood at 8 hours following administration (Chapter 8), which began to decline thereafter, with levels returning to baseline within 24 hours of first dosage. Administration of the NK1-R antagonist intravenously was elected to ensure that the delivery mode was feasible in the clinical stroke setting.

Previous studies have extensively shown that NK1-R antagonists are able to cross the BBB, depending on their inherent structure (Garcia-Recio and Gascón, 2015, Muñoz and Coveñas, 2020) Peptide based NK1-R antagonists are unable to cross the BBB and show poor potency, whereas non-peptide molecules show a high affinity for the NK1-R and an ability to cross the BBB (Muñoz and Coveñas, 2020). Previous studies have evaluated the barrier permeability of EU-C-001 compared with other NK1-R antagonists, with EU-C-001 shown to cross the barrier and thus elicit an effect on cerebrovascular endothelial cells (Donkin et al., 2011). Taken together, this further highlights the validity of NK1-R treatment for post-stroke oedema, with the timing of dosing and rate of clearance reported herein potentially able to inform clinical application.

10.5 DEVELOPMENT OF A NOVEL APPROACH TO MEASURING FUNCTION FOLLOWING OVINE STROKE

Given the promising findings of Chapters 6-8 in which the NK1-R was shown to bring about a significant and sustained reduction in ICP in both permanent and transient stroke animals, we sought to assess the effect of treatment on functional outcome. Given the lack of established methods to evaluate motor function in sheep, a comprehensive approach to assessment was subsequently developed in Chapter 9. This study used motion capture to assess gait kinematics, in conjunction with a modified neuroscore to assess variables beyond the scope of biomechanical assessment.

Assessment of kinematics across baseline trials was shown to be a reliable method to assess gait signatures for the majority of outcome measures of interest. Following stroke, a significant change in several outcomes of interest were detected. Specifically, these included

decreased walking speed, lowering of the head and first thoracic vertebra, and a significant increase in stance, swing and stride duration of the forelimbs. Despite these findings, we did not detect a significant change in joint angle variables across all animals, despite qualitative identification of deficit of the left forelimb both in Chapter 9 and in previous studies (Sorby-Adams et al., 2019a). It is important to note that some animals were qualitatively more substantially affected than others; some exhibited persistent flexion of the fetlock joint; some occasionally 'knuckled' on the joint during forward motion; and others appeared completely unaffected. Subgroup analysis targeting animals which were substantially, partially or seemingly unaffected by transient MCAo may provide more insight into the variability of injury response and the gait parameters which most effectively distinguish severity and quality of motor deficit.

Correlation of kinematic findings with neuroscore may also enhance the stratification of response to injury. Indeed, significant post-stroke deficits were detected via composite scoring (Chapter 9). Specifically, after stroke onset animals displayed significant impairment in demeanor, willingness and ability to initiate forward movement, and ability to correct and detect conscious proprioceptive positioning during postural reaction tests. Following stroke onset, patients often present with unilateral deficits including hemiplegia and hemiparesis. Via neuroscore, a marked left sided deficit was observed on postural reaction tests. However, we also observed deficit of the right forelimb when compared with baseline. This suggests an overall impaired demeanour with animals less willing to adjust limbs during forced movement rather than an indication of asymmetric neuromotor function.

Animals also show evidence of spontaneous functional recovery following stroke, similar to humans and rodents, therefore timing, duration and number of post-stroke assessments is

important given there are critical periods for detecting even mild impairment. For both kinematic and neuroscore assessment, we chose to assess animals 3 days following stroke to reduce the influence of post-operative analgesia and recovery on function, although we may not be capturing maximal deficit at 3 days post injury. Ergo, determining changes in gait kinematics at other post-stroke time-points suggests an avenue for future assessment.

10.6 LIMITATIONS AND FUTURE DIRECTIONS

Large animal models of stroke represent a promising avenue for improving the clinical translation of novel stroke therapeutics (Chapter 3). Nevertheless, as identified in each individual chapter, the thesis studies and indeed ovine stroke models are not without their own limitations. Notable is the significant time and resources expended generating experimental animals and performing analyses, inherent in large animal studies. This was especially evident in Chapter 9 given significant training durations required to habituate animals, which was a limitation both financially and in terms of physical demand. Furthermore, despite promising treatment effects, the small sample size within groups across all studies reported herein must be acknowledged as a potential limitation, although deemed necessary to reduce extensive experimental costs, and reduce animal numbers in accordance with the ARRIVE guidelines (Percie Du Sert et al., 2020).

The promising findings of this thesis, however, provide an exciting opportunity for future analyses. Indeed, some studies are underway using tissue collected throughout this PhD, and other possible avenues remain as yet unexplored. Projects underway using data collected throughout this thesis include those focusing on molecular mechanisms, functional outcomes, and MRI. Regarding molecular analyses, all experimental animals underwent

extensive biological fluid and tissue collection. The ability to yield significant volumes of both blood and CSF is a significant advantage of the ovine model, allowing for comprehensive assessment across time points in the same experimental animals. Indeed, for animals in Chapter 9, extensive serum, plasma and CSF samples were collected prior to stroke and at multiple time-points thereafter. Although initial SP ELISA analysis has been carried out on serum and CSF (Chapter 7), samples are currently undergoing metabolomic assessment via mass spectroscopy to evaluate key molecules involved in the ischaemic cascade following ovine stroke. Fresh brain samples, serum and CSF for each of these animals are also in the process of undergoing thorough molecular analysis to investigate key molecules involved in regulating BBB integrity, including caveolins, claudins, neuroinflammatory cells (microglia, monocytes), MMP's (MMP2, MMP9) and both pro- (IL-6, IL-17, IL-1β, TNF-α, IFN-γ) and anti-inflammatory (IL-10, IL-4) cytokines.

For functional analyses, Chapter 9 presents four time points in which function was assessed: 8-, 5- and 1- day pre-stroke, and 3 days post-stroke. These sessions were chosen to assess repeatability across baseline sessions and subsequently determine if the method developed was able to detect changes in behaviour and kinematics 3-days following stroke (with 3 days post stroke chosen to reduce the impact of post-surgical course on outcome). In addition to these reported time points, however, all animals also underwent testing at 1-, 5-, 7-, 14-, 21- and 28-days post-ictus. In this cohort, 12 of the animals also received the late NK1-R antagonist treatment regimen at 5 days. Unfortunately, due to the significant time spent post-processing and optimising coding procedures, I was unable to include this data in the final thesis due to time restraints. Future analysis should focus on assessing the effect of treatment on outcomes using the method described herein. Animals on whom biomechanics assessment was carried out also underwent comprehensive MRI sequencing pre-stroke and

at days 1-, 6- and 28-days post stroke. These studies occurred following an upgrade to a 3T MRI machine at the SAHMRI PIRL facility. In addition to sequences obtained in previous studies (T_1, T_2, FLAIR, DWI, MRA) animals underwent diffusion susceptibility contrast (DSC) and dynamic contrast enhancement (DCE) imaging to comprehensively assess dynamics of the barrier and how it is influenced, both with and without treatment. We also undertook resting functional MRI (fMRI) and diffusion tractography imaging (DTI). These sequences are currently being processed, with the goal to characterise functional brain regions affected by stroke and correlate regions of interest with behavioral outcomes.

In addition to assessments already underway, the sheep model of stroke provides a platform in which other novel therapeutics can be assessed. Evaluating the response to stroke in aged and co-morbid animals could provide an opportunity for future studies, especially given the correlation between stroke and increasing age. Furthermore, although we performed functional assessment of motor recovery, we did not assess cognition. Cognitive models of executive function have been developed in sheep (Sorby-Adams et al., 2021, McBride et al., 2016, Morton and Avanzo, 2011, Knolle et al, 2019), which may be able to be applied to stroke models to determine the effect of infarction and cerebral oedema on cognitive outcome. The assessment of later time points following onset of injury may also provide insight into the mechanisms underlying secondary neurodegeneration to subsequently determine if a positive effect of treatment can be seen on both long term cognitive and motor function, as well as other stroke complications such as pneumonia.

10.7 SUMMARY OF KEY CONTRIBUTIONS

The collective findings of this thesis provide compelling evidence regarding the utility of NK1-R antagonist treatment in the management of cerebral oedema and elevated ICP following ischaemic stroke, as follows:

1) Characterised clinically relevant neuroimaging (MRI) and neurophysiological (ICP) outcomes following stroke in a large animal model. This has enabled the accurate characterisation of the ovine response to both complete and partial MCA occlusion.
2) Intravenous administration with an NK1-R antagonist produced a clinically meaningful reduction in ICP following complete MCA occlusion, bringing about a reduction in pressure comparable to DC, all whilst circumventing the need for invasive surgery.
3) Developed an ovine model of transient stroke, compatible with survival, in which marked cerebral oedema and elevated ICP were observed 5-6 days following stroke. This provides a model in which putative therapeutics targeting oedema can be assessed in line with current stroke research guidelines.
4) Demonstrated NK1-R administration abates a rise in ICP following stroke with reperfusion when administered both early, and in a delayed fashion. Given the heterogenous nature of stroke, this provides compelling evidence that treatment will be effective across a broad range of stroke patients.
5) Developed an innovative method to assess functional and kinematic outcomes following ovine stroke, enabling the future assessment of interventions on long term recovery.
6) Demonstrated that the post-stroke elevation in ICP and oedema is associated with an increase in BBB permeability, which is likely facilitated by caveolae-mediated albumin transcyotsis as a result of aberrant SP release and subsequent NK1-R upregulation.

10.5 CONCLUSION

This thesis has established that NK1-R antagonist treatment is effective in reducing cerebral oedema and ICP following stroke in a clinically relevant ovine model. Here, we have shown that following permanent stroke, NK1-R antagonist treatment significantly reduces ICP, comparable with DC surgery. A significant reduction in both cerebral oedema and ICP was also observed with NK1-R antagonist administration following transient stroke, when given either before (1-3d) or after (5d) the development of space-occupying oedema and elevated ICP. Taken together, these studies support the role of SP and neurogenic inflammation in the development of cerebral oedema following stroke. This dataset supports advancement of NK1-R antagonist treatment for cerebral oedema and elevated ICP to evaluation in clinical stroke. Indeed, the experimental work in this thesis has formed a strong pre-clinical basis for the assessment of the NK1-R antagonist in clinical trials, with Phase II trials currently underway in Australia (Melbourne), the United Kingdom (Cambridge) and the United States of America.

11

Reference List

(STAIR), S. T. A. I. R. 1999. Recommendations for standards regarding preclinical neuroprotective and restorative drug development. *Stroke,* 30**,** 2752-8.

ABBOTT, N. J., RONNBACK, L. & HANSSON, E. 2006. Astrocyte-endothelial interactions at the blood-brain barrier. *Nature Reviews Neuroscience,* 7**,** 41-53.

ACHARYA, A. B. & WROTEN, M. 2020. Wernicke Aphasia. *StatPearls.* Treasure Island (FL).

ADER, J., WU, J., FONAROW, G. C., SMITH, E. E., SHAH, S., XIAN, Y., BHATT, D. L., SCHWAMM, L. H., REEVES, M. J., MATSOUAKA, R. A. & SHETH, K. N. 2019. Hospital distance, socioeconomic status, and timely treatment of ischemic stroke. *Neurology,* 93**,** e747-e757.

AGARWAL, S., SCOFFINGS, D. J., JONES, P. S., MARRAPU, S. T., BARRY, P. J., O'BRIEN, E. W., BARON, J. C. & WARBURTON, E. A. 2013. Interaction of age with the ischaemic penumbra, leptomeningeal collateral circulation and haemodynamic variables in acute stroke: a pilot study. *Journal of Neurology, Neurosurgery and Psychiatry,* 84**,** 271-6.

AGOSTINHO, F. S., RAHAL, S. C., ARAÚJO, F. A. P., CONCEIÇÃO, R. T., HUSSNI, C. A., EL-WARRAK, A. O. & MONTEIRO, F. O. B. 2012. Gait analysis in clinically healthy sheep from three different age groups using a pressure-sensitive walkway. *BMC Veterinary Research,* 8**,** 87.

AGOSTON, D. V. 2017. How to Translate Time? The Temporal Aspect of Human and Rodent Biology. *Frontiers in Neurology,* 8**,** 92.

AKAISHI, T., NARIKAWA, K., SUZUKI, Y., MITSUZAWA, S., TSUKITA, K., KURODA, H., NAKASHIMA, I., FUJIHARA, K. & AOKI, M. 2015. Importance of the quotient of albumin, quotient of immunoglobulin G and Reibergram in inflammatory neurological disorders with disease-specific patterns of blood–brain barrier permeability. *Neurology and Clinical Neuroscience,* 3**,** 94-100.

AKSOY, D., BAMMER, R., MLYNASH, M., VENKATASUBRAMANIAN, C., EYNGORN, I., SNIDER, R. W., GUPTA, S. N., NARAYANA, R., FISCHBEIN, N. & WIJMAN, C. A. 2013. Magnetic resonance imaging profile of blood-brain barrier injury in patients with acute intracerebral hemorrhage. *Journal of the American Heart Association,* 2**,** e000161.

ALBERS, G. W., LANSBERG, M. G., KEMP, S., TSAI, J. P., LAVORI, P., CHRISTENSEN, S., MLYNASH, M., KIM, S., HAMILTON, S., YEATTS, S. D., PALESCH, Y., BAMMER, R., BRODERICK, J. & MARKS, M. P. 2017. A multicenter randomized controlled trial of endovascular therapy following imaging evaluation for ischemic stroke (DEFUSE 3). *International Journal of Stroke,* 12**,** 896-905.

ALBERS, G. W., MARKS, M. P., KEMP, S., CHRISTENSEN, S., TSAI, J. P., ORTEGA-GUTIERREZ, S., MCTAGGART, R. A., TORBEY, M. T., KIM-TENSER, M., LESLIE-MAZWI, T., SARRAJ, A., KASNER, S. E., ANSARI, S. A., YEATTS, S. D., HAMILTON, S., MLYNASH, M., HEIT, J. J., ZAHARCHUK, G., KIM, S., CARROZZELLA, J., PALESCH, Y. Y., DEMCHUK, A. M., BAMMER, R., LAVORI, P. W., BRODERICK, J. P. & LANSBERG, M. G. 2018. Thrombectomy for Stroke at 6 to 16 Hours with Selection by Perfusion Imaging. *New England Journal of Medicine,* 378**,** 708-718.

ALEXANDER, L. D., BLACK, S. E., PATTERSON, K. K., GAO, F., DANELLS, C. J. & MCILROY, W. E. 2009. Association Between Gait Asymmetry and Brain Lesion Location in Stroke Patients. *Stroke,* 40**,** 537-544.

ALVES, R. V., CAMPOS, M. M., SANTOS, A. R. & CALIXTO, J. B. 1999. Receptor subtypes involved in tachykinin-mediated edema formation. *Peptides,* 20**,** 921-7.

AMARA, S. G., JONAS, V., ROSENFELD, M. G., ONG, E. S. & EVANS, R. M. 1982. Alternative RNA processing in calcitonin gene expression generates mRNAs encoding different polypeptide products. *Nature,* 298**,** 240-4.

ANDERSON, R. W., SANDOZ, B., DUTSCHKE, J. K., FINNIE, J. W., TURNER, R. J., BLUMBERGS, P. C., MANAVIS, J. & VINK, R. 2014. Biomechanical studies in an ovine model of non-accidental head injury. *Journal of Biomechanics,* 47**,** 2578-83.

ANDRADE, A. F. D., PAIVA, W. S., AMORIM, R. L. O. D., FIGUEIREDO, E. G., ALMEIDA, A. N. D., BROCK, R. S., BOR-SENG-SHU, E. & TEIXEIRA, M. J. 2011. Continuous ventricular cerebrospinal fluid drainage with intracranial pressure monitoring for management of posttraumatic diffuse brain swelling. *Arquivos de Neuro-Psiquiatria,* 69**,** 79-84.

ANNUNZIATA, P., CIONI, C., SANTONINI, R. & PACCAGNINI, E. 2002. Substance P antagonist blocks leakage and reduces activation of cytokine-stimulated rat brain endothelium. *Journal of Neuroimmunology,* 131**,** 41-9.

ANTHONY, D. C., FERGUSON, B., MATYZAK, M. K., MILLER, K. M., ESIRI, M. M. & PERRY, V. H. 1997. Differential matrix metalloproteinase expression in cases of multiple sclerosis and stroke. *Neuropathology and Applied Neurobiology,* 23**,** 406-15.

APPLEGATE, A. L., CURTIS, S. E., GROPPEL, J. L., MCFARLANE, J. M. & WIDOWSKI, T. M. 1988. Footing and gait of pigs on different concrete surfaces. *Journal of Animal Science,* 66**,** 334-41.

ARANAKE, A., MASHOUR, G. A. & AVIDAN, M. S. 2013. Minimum alveolar concentration: ongoing relevance and clinical utility. *Anaesthesia,* 68**,** 512-22.

ASAHI, M., WANG, X., MORI, T., SUMII, T., JUNG, J. C., MOSKOWITZ, M. A., FINI, M. E. & LO, E. H. 2001. Effects of matrix metalloproteinase-9 gene knock-out on the proteolysis of blood-brain barrier and white matter components after cerebral ischaemia. *Journal of Neuroscience,* 21**,** 7724-32.

ASHWINI, C. A., SHUBHA, R. & JAYANTHI, K. S. 2008. Comparative anatomy of the circle of Willis in man, cow, sheep, goat, and pig. *Neuroanatomy,* 7**,** 54-85.

ASTEPHEN WILSON, J. L. 2012. Challenges in dealing with walking speed in knee osteoarthritis gait analyses. *Clinical Biomechanics,* 27**,** 210-212.

ASTRUP, J., SIESJO, B. K. & SYMON, L. 1981. Thresholds in cerebral ischaemia - the ischaemic penumbra. *Stroke,* 12**,** 723-5.

ATCHANEEYASAKUL, K., GUADA, L., RAMDAS, K., WATANABE, M., BHATTACHARYA, P., RAVAL, A. P. & YAVAGAL, D. R. 2016. Large animal canine endovascular ischaemic stroke models: A review. *Brain Research Bulletin,* 127**,** 134-140.

AVAN, A., DIGALEH, H., DI NAPOLI, M., STRANGES, S., BEHROUZ, R., SHOJAEIANBABAEI, G., AMIRI, A., TABRIZI, R., MOKHBER, N., SPENCE, J. D. & AZARPAZHOOH, M. R. 2019. Socioeconomic status and stroke incidence, prevalence,

mortality, and worldwide burden: an ecological analysis from the Global Burden of Disease Study 2017. *BMC Medicine,* 17**,** 191.

AYATA, C. & ROPPER, A. H. 2002. Ischaemic brain oedema. *Journal of Clinical Neuroscience,* 9**,** 113-24.

BAKTHAVACHALAM, P. & SHANMUGAM, P. S. T. 2017. Mitochondrial dysfunction – Silent killer in cerebral ischaemia. *Journal of the Neurological Sciences,* 375**,** 417-423.

BALLABH, P., BRAUN, A. & NEDERGAARD, M. 2004. The blood-brain barrier: an overview: structure, regulation, and clinical implications. *Neurobiology of Disease,* 16**,** 1-13.

BALLESTER, B. R., MAIER, M., DUFF, A., CAMEIRÃO, M., BERMÚDEZ, S., DUARTE, E., CUXART, A., RODRÍGUEZ, S., SAN SEGUNDO MOZO, R. M. & VERSCHURE, P. F. M. J. 2019. A critical time window for recovery extends beyond one-year post-stroke. *Journal of Neurophysiology,* 122**,** 350-357.

BARDUTZKY, J. & SCHWAB, S. 2007. Antiedema therapy in ischaemic stroke. *Stroke,* 38**,** 3084-3094.

BATKA, R. J., BROWN, T. J., MCMILLAN, K. P., MEADOWS, R. M., JONES, K. J. & HAULCOMB, M. M. 2014. The Need for Speed in Rodent Locomotion Analyses. *The Anatomical Record,* 297**,** 1839-1864.

BATTEY, T. W., KARKI, M., SINGHAL, A. B., WU, O., SADAGHIANI, S., CAMPBELL, B. C., DAVIS, S. M., DONNAN, G. A., SHETH, K. N. & KIMBERLY, W.

T. 2014. Brain edema predicts outcome after nonlacunar ischaemic stroke. *Stroke,* 45**,** 3643-8.

BAYLISS, W. 1901. On the origin from the spinal cord of the vaso-dilator fibres of the hind-limb, and on the nature of these fibres. *The Journal of Physiology.,* 26**,** 173-209.

BAZZONI, G. & DEJANA, E. 2004. Endothelial cell-to-cell junctions: molecular organization and role in vascular homeostasis. *Physiological Reviews,* 84**,** 869-901.

BEARD, D. J., MCLEOD, D. D., LOGAN, C. L., MURTHA, L. A., IMTIAZ, M. S., VAN HELDEN, D. F. & SPRATT, N. J. 2015. Intracranial Pressure Elevation Reduces Flow through Collateral Vessels and the Penetrating Arterioles they Supply. a Possible Explanation for 'Collateral Failure' and Infarct Expansion after Ischaemic Stroke. *Journal of Cerebral Blood Flow & Metabolism,* 35**,** 861-872.

BEEZ, T., MUNOZ-BENDIX, C., STEIGER, H. J. & BESEOGLU, K. 2019. Decompressive craniectomy for acute ischaemic stroke. *Critical Care,* 23**,** 209.

BEGLEY, D. J. & BRIGHTMAN, M. W. 2003. Structural and functional aspects of the blood-brain barrier. *Progress in Drug Research,* 61**,** 39-78.

BELL, A. H., MILLER, S. L., CASTILLO-MELENDEZ, M. & MALHOTRA, A. 2020. The Neurovascular Unit: Effects of Brain Insults During the Perinatal Period. *Frontiers in Neuroscience,* 13.

BENJAMIN, E. J., VIRANI, S. S., CALLAWAY, C. W., CHAMBERLAIN, A. M., CHANG, A. R., CHENG, S., CHIUVE, S. E., CUSHMAN, M., DELLING, F. N., DEO, R.,

DE FERRANTI, S. D., FERGUSON, J. F., FORNAGE, M., GILLESPIE, C., ISASI, C. R., JIMÉNEZ, M. C., JORDAN, L. C., JUDD, S. E., LACKLAND, D., LICHTMAN, J. H., LISABETH, L., LIU, S., LONGENECKER, C. T., LUTSEY, P. L., MACKEY, J. S., MATCHAR, D. B., MATSUSHITA, K., MUSSOLINO, M. E., NASIR, K., O'FLAHERTY, M., PALANIAPPAN, L. P., PANDEY, A., PANDEY, D. K., REEVES, M. J., RITCHEY, M. D., RODRIGUEZ, C. J., ROTH, G. A., ROSAMOND, W. D., SAMPSON, U. K. A., SATOU, G. M., SHAH, S. H., SPARTANO, N. L., TIRSCHWELL, D. L., TSAO, C. W., VOEKS, J. H., WILLEY, J. Z., WILKINS, J. T., WU, J. H., ALGER, H. M., WONG, S. S. & MUNTNER, P. 2018. Heart Disease and Stroke Statistics-2018 Update: A Report From the American Heart Association. *Circulation,* 137**,** e67.

BERECZKI, D. N., MIHÁLKA, L. S., SZATMÁRI, S., FEKETE, K. R., DI CESAR, D., FÜLESDI, B. L., CSIBA, L. S. & FEKETE, I. N. 2003. Mannitol Use in Acute Stroke. *Stroke,* 34**,** 1730-1735.

BERKHEMER, O. A., FRANSEN, P. S. S., BEUMER, D., VAN DEN BERG, L. A., LINGSMA, H. F., YOO, A. J., SCHONEWILLE, W. J., VOS, J. A., NEDERKOORN, P. J., WERMER, M. J. H., VAN WALDERVEEN, M. A. A., STAALS, J., HOFMEIJER, J., VAN OOSTAYEN, J. A., LYCKLAMA À NIJEHOLT, G. J., BOITEN, J., BROUWER, P. A., EMMER, B. J., DE BRUIJN, S. F., VAN DIJK, L. C., KAPPELLE, L. J., LO, R. H., VAN DIJK, E. J., DE VRIES, J., DE KORT, P. L. M., VAN ROOIJ, W. J. J., VAN DEN BERG, J. S. P., VAN HASSELT, B. A. A. M., AERDEN, L. A. M., DALLINGA, R. J., VISSER, M. C., BOT, J. C. J., VROOMEN, P. C., ESHGHI, O., SCHREUDER, T. H. C. M. L., HEIJBOER, R. J. J., KEIZER, K., TIELBEEK, A. V., DEN HERTOG, H. M., GERRITS, D. G., VAN DEN BERG-VOS, R. M., KARAS, G. B., STEYERBERG, E. W., FLACH, H. Z., MARQUERING, H. A., SPRENGERS, M. E. S., JENNISKENS, S. F. M.,

BEENEN, L. F. M., VAN DEN BERG, R., KOUDSTAAL, P. J., VAN ZWAM, W. H., ROOS, Y. B. W. E. M., VAN DER LUGT, A., VAN OOSTENBRUGGE, R. J., MAJOIE, C. B. L. M. & DIPPEL, D. W. J. 2015. A Randomized Trial of Intraarterial Treatment for Acute Ischaemic Stroke. *New England Journal of Medicine,* 372**,** 11-20.

BERROUSCHOT, J., STERKER, M., BETTIN, S., KÖSTER, J. & SCHNEIDER, D. 1998. Mortality of space-occupying ('malignant') middle cerebral artery infarction under conservative intensive care. *Intensive Care Medicine,* 24**,** 620-623.

BERTRAND, C. & GEPPETTI, P. 1996. Tachykinin and kinin receptor antagonists: therapeutic perspectives in allergic airway disease. *Trends in Pharmacological Sciences,* 17**,** 255-9.

BLACK, P. H. 2002. Stress and the inflammatory response: a review of neurogenic inflammation. *Brain, Behavior and Immunity,* 16**,** 622-53.

BOLTZE, J., FÖRSCHLER, A., NITZSCHE, B., WALDMIN, D., HOFFMANN, A., BOLTZE, C. M., DREYER, A. Y., GOLDAMMER, A., REISCHAUER, A., HARTIG, W., GEIGER, K. D., BARTHEL, H., EMMRICH, F. & GILLE, U. 2008. Permanent Middle Cerebral Artery Occlusion in Sheep: A Novel Large Animal Model of Focal Cerebral Ischaemia. *Journal of Cerebral Blood Flow & Metabolism,* 28**,** 1951-1964.

BOLTZE, J., NITZSCHE, B., GEIGER, K. D. & SCHOON, H. A. 2011. Histopathological Investigation of Different MCAO Modalities and Impact of Autologous Bone Marrow Mononuclear Cell Administration in an Ovine Stroke Model. *Translational Stroke Research,* 2**,** 279-93.

BOST, K. L. & PASCUAL, D. W. 1992. Substance P: a late-acting B lymphocyte differentiation cofactor. *American Journal of Physiology,* 262**,** C537-45.

BOULOS, A. S., DESHAIES, E. M., DALFINO, J. C., FEUSTEL, P. J., POPP, A. J. & DRAZIN, D. 2010. Tamoxifen as an effective neuroprotectant in an endovascular canine model of stroke. *Journal of Neurosurgery,* 114**,** 1117-1126.

BOWDEN, J. J., GARLAND, A. M., BALUK, P., LEFEVRE, P., GRADY, E. F., VIGNA, S. R., BUNNETT, N. W. & MCDONALD, D. M. 1994. Direct observation of substance P-induced internalization of neurokinin 1 (NK1) receptors at sites of inflammation. *Proceedings of the National Academy of Sciences of the United States of America,* 91**,** 8964-8.

BRACKEN, M. B. 2009. Why animal studies are often poor predictors of human reactions to exposure. *Journal of the Royal Society of Medicine,* 102**,** 120-122.

BRODERICK, J. P. & HILL, M. D. 2021. Advances in Acute Stroke Treatment 2020. *Stroke,* 52**,** 729-734.

BROGAN, M. & MANNO, E. 2015. Treatment of Malignant Brain Edema and Increased Intracranial Pressure After Stroke. *Current Treatment Options in Neurology,* 17**,** 1-11.

BROOM, L., ELLISON, B. A., WORLEY, A., WAGENAAR, L., SÖRBERG, E., ASHTON, C., BENNETT, D. A., BUCHMAN, A. S., SAPER, C. B., SHIH, L. C., HAUSDORFF, J. M. & VANDERHORST, V. G. 2017. A translational approach to capture gait signatures of neurological disorders in mice and humans. *Scientific Reports,* 7.

BROUWER, B., PARVATANENI, K. & OLNEY, S. J. 2009. A comparison of gait biomechanics and metabolic requirements of overground and treadmill walking in people with stroke. *Clinical Biomechanics,* 24**,** 729-734.

BRUNO, G., TEGA, F., BRUNO, A., GRAF, U., CORELLI, F., MOLFETTA, R. & BARUCCO, M. 2003. The role of substance P in cerebral ischaemia. *International Journal of Immunopathology and Pharmacology,* 16**,** 67-72.

BUCINSKAITE, V., BRODDA-JANSEN, G., STENFORS, C., THEODORSSON, E. & LUNDEBERG, T. 1998. Increased concentrations of calcitonin gene-related peptide-like immunoreactivity in rat brain and peripheral tissue after ischaemia: correlation to flap survival. *Neuropeptides,* 32**,** 179-83.

BULLOCH, K., MILNER, T. A., PRASAD, A., HSU, M., BUZSAKI, G. & MCEWEN, B. S. 1998. Induction of calcitonin gene-related peptide-like immunoreactivity in hippocampal neurons following ischaemia: a putative regional modulator of the CNS injury/immune response. *Experimental Neurology,* 150**,** 195-205.

BURMEISTER, A. R., JOHNSON, M. B., CHAUHAN, V. S., MOERDYK-SCHAUWECKER, M. J., YOUNG, A. D., COOLEY, I. D., MARTINEZ, A. N., RAMESH, G., PHILIPP, M. T. & MARRIOTT, I. 2017. Human microglia and astrocytes constitutively express the neurokinin-1 receptor and functionally respond to substance P. *Journal of Neuroinflammation,* 14.

BURGESS, S., ABU-LABAN, R. B., SLAVIK, R. S., VU, E. N. & ZED, P. J. 2016. A Systematic Review of Randomized Controlled Trials Comparing Hypertonic Sodium

Solutions and Mannitol for Traumatic Brain Injury: Implications for Emergency Department Management. *Annals of Pharmacotherapy,* 50**,** 291-300.

BUTCHER, M. T. & ASHLEY-ROSS, M. A. 2002. Fetlock joint kinematics differ with age in Thoroughbred [was thoroughbred] racehorses. *Journal of Biomechanics,* 35**,** 563-71.

BYROM, M. J., BANNON, P. G., WHITE, G. H. & NG, M. K. C. 2010. Animal models for the assessment of novel vascular conduits. *Journal of Vascular Surgery,* 52**,** 176-195.

CAI, B. & WANG, N. 2016. Large Animal Stroke Models vs. Rodent Stroke Models, Pros and Cons, and Combination? *Acta Neurochirurgica Supplement,* 121**,** 77-81.

CAI, H., XU, X., LIU, Z., WANG, Q., FENG, G., LI, Y., XU, C., LIU, G. & LI, Z. 2010. The effects of calcitonin gene-related peptide on bFGF and AQP4 expression after focal cerebral ischaemia reperfusion in rats. *Pharmazie,* 65**,** 274-8.

CAKE, M. A., GARDNER, G. E., BOYCE, M. D., LOADER, D. & PETHICK, D. W. 2006. Forelimb bone growth and mineral maturation as potential indices of skeletal maturity in sheep. *Australian Journal of Agricultural Research,* 57**,** 699-706.

CAMERON, R., GREG, C., AMIR, A., MARINOS, K., VALERIE, B., SASHWATI, R., SAVITA, K., ANDREW, S., MICHAEL, K. & CHANDAN, K. S. 2008. Minimally invasive neuroradiologic model of preclinical transient middle cerebral artery occlusion in canines. *Proceedings of the National Academy of Sciences,* 105**,** 14100.

CAMPOS, M. M. & CALIXTO, J. B. 2000. Neurokinin mediation of edema and inflammation. *Neuropeptides,* 34**,** 314-22.

CAO, T., PINTER, E., AL-RASHED, S., GERARD, N., HOULT, J. R. & BRAIN, S. D. 2000. Neurokinin-1 receptor agonists are involved in mediating neutrophil accumulation in the inflamed, but not normal, cutaneous microvasculature: an in vivo study using neurokinin-1 receptor knockout mice. *Journal of Immunology,* 164**,** 5424-9.

CARROLL, G. L. & HARTSFIELD, S. M. 1996. General Anesthetic Techniques in Ruminants. *Veterinary Clinics of North America: Food Animal Practice,* 12**,** 627-661.

CARTER, J. & STORY, D. A. 2013. Veterinary and human anaesthesia: an overview of some parallels and contrasts. *Anesthesia and Intensive Care,* 41**,** 710-8.

CASALS, J. B., PIERI, N. C., FEITOSA, M. L., ERCOLIN, A. C., ROBALLO, K. C., BARRETO, R. S., BRESSAN, F. F., MARTINS, D. S., MIGLINO, M. A. & AMBROSIO, C. E. 2011. The use of animal models for stroke research: a review. *Comparative Medicine,* 61**,** 305-13.

CHALOS, V., VAN DER ENDE, N. A. M., LINGSMA, H. F., MULDER, M. J. H. L., VENEMA, E., DIJKLAND, S. A., BERKHEMER, O. A., YOO, A. J., BRODERICK, J. P., PALESCH, Y. Y., YEATTS, S. D., ROOS, Y. B. W. E. M., VAN OOSTENBRUGGE, R. J., VAN ZWAM, W. H., MAJOIE, C. B. L. M., VAN DER LUGT, A., ROOZENBEEK, B., DIPPEL, D. W. J., BERKHEMER, O. A., FRANSEN, P. S. S., BEUMER, D., VAN DEN BERG, L. A., LINGSMA, H. F., YOO, A. J., SCHONEWILLE, W. J., ALBERT VOS, J., NEDERKOORN, P. J., WERMER, M. J. H., VAN WALDERVEEN, M. A. A., STAALS, J., HOFMEIJER, J., VAN OOSTAYEN, J. A., LYCKLAMA A NIJEHOLT, G. J., BOITEN, J., BROUWER, P. A., EMMER, B. J., DE BRUIJN, S. F., VAN DIJK, L. C., KAPPELLE, L. J., LO, R. H., VAN DIJK, E. J., DE VRIES, J., DE KORT, P. L. M., VAN ROOIJ, W. J. J., VAN DEN BERG, J. S. P., VAN HASSELT, B. A. A. M., AERDEN, L. A. M.,

DALLINGA, R. J., VISSER, M. C., BOT, J. C. J., VROOMEN, P. C., ESHGHI, O., SCHREUDER, T. H. C. M. L., HEIJBOER, R. J. J., KEIZER, K., TIELBEEK, A. V., DEN HERTOG, H. M., GERRITS, D. G., VAN DEN BERG-VOS, R. M., KARAS, G. B., STEYERBERG, E. W., FLACH, H. Z., MARQUERING, H. A., SPRENGERS, M. E. S., JENNISKENS, S. F. M., BEENEN, L. F. M., VAN DEN BERG, R., KOUDSTAAL, P. J., VAN ZWAM, W. H., ROOS, Y. B. W. E. M., VAN DER LUGT, A., VAN OOSTENBRUGGE, R. J., MAJOIE, C. B. L. M. & DIPPEL, D. W. J. 2020. National Institutes of Health Stroke Scale. *Stroke,* 51**,** 282-290.

CHANG, M. L., YANG, J., KEM, S., KLAIDMAN, L., SUGAWARA, T., CHAN, P. H. & ADAMS JR, J. D. 2002. Nicotinamide and ketamine reduce infarct volume and DNA fragmentation in rats after brain ischaemia and reperfusion. *Neuroscience Letters,* 322**,** 137-140.

CHANG, R., LIU, X., LI, S. & LI, X. J. 2015. Transgenic animal models for study of the pathogenesis of Huntington's disease and therapy. *Drug Design, Development and Therapy,* 9**,** 2179-88.

CHARLTON, J. M., BIRMINGHAM, T. B., LEITCH, K. M. & HUNT, M. A. 2020. Knee-specific gait biomechanics are reliable when collected in multiple laboratories by independent raters. *Journal of Biomechanics***,** 110182.

CHAU, C. Y. C., MEDIRATTA, S., MCKIE, M. A., GREGSON, B., TULU, S., ERCOLE, A., SOLLA, D. J. F., PAIVA, W. S., HUTCHINSON, P. J. & KOLIAS, A. G. 2020. Optimal Timing of External Ventricular Drainage after Severe Traumatic Brain Injury: A Systematic Review. *Journal of Clinical Medicine,* 9**,** 1996.

CHEN, C. C., CHO, D. Y. & TSAI, S. C. 2007. Outcome of and prognostic factors for decompressive hemicraniectomy in malignant middle cerebral artery infarction. *Journal of Clinical Neuroscience,* 14**,** 317-21.

CHEN, G., PATTEN, C., KOTHARI, D. H. & ZAJAC, F. E. 2005. Gait differences between individuals with post-stroke hemiparesis and non-disabled controls at matched speeds. *Gait & Posture,* 22**,** 51-56.

CHEN, H., SONG, Z. & DENNIS, J. A. 2019. Hypertonic saline versus other intracranial pressure-lowering agents for people with acute traumatic brain injury. *Cochrane Database of Systematic Reviews*.

CHEN, J. W., GOMBART, Z. J., ROGERS, S., GARDINER, S. K., CECIL, S., & BULLOCK, R. M. 2011. Pupillary reactivity as an early indicator of increased intracranial pressure: The introduction of the Neurological Pupil index. *Surgical Neurology International*, 2**,** 82

CHEN, Y., MERZDORF, C., PAUL, D. L. & GOODENOUGH, D. A. 1997. COOH terminus of occludin is required for tight junction barrier function in early Xenopus embryos. *Journal of Cell Biology,* 138**,** 891-9.

CHILEUITT, L., LEBER, K., MCCALDEN, T. & WEINSTEIN, P. R. 1996. Induced hypertension during ischaemia reduces infarct area after temporary middle cerebral artery occlusion in rats. *Surgical Neurology International,* 46**,** 229-34.

CHO, J., KIM, Y. H., HAN, H. S. & PARK, J. 2007. Accumulated mannitol and aggravated cerebral edema in a rat model of middle cerebral artery infarction. *Journal of the Korean Neurosurgical Society*. 4**,** 337–341.

CHOLLET, F., CRAMER, S. C., STINEAR, C., KAPPELLE, L. J., BARON, J. C., WEILLER, C., AZOUVI, P., HOMMEL, M., SABATINI, U., MOULIN, T., TARDY, J., VALENTI, M., MONTGOMERY, S. & ADAMS, H. 2014. Pharmacological therapies in post stroke recovery: recommendations for future clinical trials. *Journal of Neurology,* 261**,** 1461-1468.

CHRISTENSEN, M. S., PAULSON, O. B., OLESEN, J., ALEXANDER, S. C., SKINHØJ, E., DAM, W. H. & LASSEN, N. A. 1973. Cerebral Apoplexy (Stroke) Treated With or Without Prolonged Artificial Hyperventilation: 1. Cerebral Circulation, Clinical Course, and Cause of Death. *Stroke,* 4**,** 568-619.

CHRISTOFORIDIS, G. A., RINK, C., KONTZIALIS, M. S., MOHAMMAD, Y., KOCH, R. M., ABDULJALIL, A. M., BERGDALL, V. K., ROY, S., KHANNA, S., SLIVKA, A. P., KNOPP, M. V. & SEN, C. K. 2011. An endovascular canine middle cerebral artery occlusion model for the study of leptomeningeal collateral recruitment. *Investigative Radiology,* 46**,** 34-40.

CHUEH, J. Y., KUHN, A. L., WAKHLOO, A. K. & GOUNIS, M. J. 2013. Experimental Models of Vascular Occlusions for Evaluation of Thrombectomy Devices. *Cardiovascular Engineering and Technology,* 4**,** 309-322.

CIPRIANI, G., SERBOIU, C. S., GHERGHICEANU, M., SIMONETTA FAUSSONE-PELLEGRINI, M. & VANNUCCHI, M. G. 2011. NK receptors, Substance P, Ano1

expression and ultrastructural features of the muscle coat in Cav-1−/− mouse ileum. *Journal of Cellular and Molecular Medicine,* 15**,** 2411-2420.

CLARK, A. W., KREKOSKI, C. A., BOU, S. S., CHAPMAN, K. R. & EDWARDS, D. R. 1997. Increased gelatinase A (MMP-2) and gelatinase B (MMP-9) activities in human brain after focal ischaemia. *Neuroscience Letters,* 238**,** 53-6.

CLAXTON-GILL, M. S., CORNICK-SEAHORN, J. L., GAMBOA, J. C. & BOATRIGHT, B. S. 1993. Suspected malignant hyperthermia syndrome in a miniature pot-bellied pig anaesthetised with isoflurane. *Journal of the American Veterinary Medical Association,* 203**,** 1434-6.

CLÉMENT, T., RODRIGUEZ-GRANDE, B. & BADAUT, J. 2020. Aquaporins in brain edema. *Journal of Neuroscience Research,* 98**,** 9-18.

COMBS, D. J., DEMPSEY, R. J., KUMAR, S. & DONALDSON, D. 1990. Focal cerebral infarction in cats in the presence of hyperglycemia and increased insulin. *Metabolic Brain Disease,* 5**,** 169-178.

CONRAD, M. S., SUTTON, B. P., DILGER, R. N. & JOHNSON, R. W. 2014. An In Vivo Three-Dimensional Magnetic Resonance Imaging-Based Averaged Brain Collection of the Neonatal Piglet (Sus scrofa). *PLOS ONE,* 9**,** e107650.

COOK, A. M., MORGAN JONES, G., HAWRYLUK, G. W. J., MAILLOUX, P., MCLAUGHLIN, D., PAPANGELOU, A., SAMUEL, S., TOKUMARU, S., VENKATASUBRAMANIAN, C., ZACKO, C., ZIMMERMANN, L. L., HIRSCH, K. &

SHUTTER, L. 2020. Guidelines for the Acute Treatment of Cerebral Edema in Neurocritical Care Patients. *Neurocritical Care,* 32**,** 647-666.

COOK, D. J. & TYMIANSKI, M. 2011. Translating promising preclinical neuroprotective therapies to human stroke trials. *Expert Review of Cardiovascular Therapy,* 9**,** 433-49.

COOK, D. J. & TYMIANSKI, M. 2012. Nonhuman primate models of stroke for translational neuroprotection research. *Neurotherapeutics,* 9**,** 371-9.

CORRIGAN, F., LEONARD, A., GHABRIEL, M., VAN DEN HEUVEL, C. & VINK, R. 2012. A substance P antagonist improves outcome in female Sprague Dawley rats following diffuse traumatic brain injury. *CNS Neuroscience & Therapeutics,* 18**,** 513-5.

CORRIGAN, F., MANDER, K. A., LEONARD, A. V. & VINK, R. 2016a. Neurogenic inflammation after traumatic brain injury and its potentiation of classical inflammation. *Journal of Neuroinflammation,* 13**,** 264.

CORRIGAN, F., VINK, R. & TURNER, R. J. 2016b. Inflammation in acute CNS injury: a focus on the role of substance P. *British Journal of Pharmacology,* 173**,** 703-15.

CREVIER-DENOIX, N., FALALA, S., HOLDEN-DOUILLY, L., CAMUS, M., MARTINO, J., RAVARY-PLUMIOEN, B., VERGARI, C., DESQUILBET, L., DENOIX, J. M., CHATEAU, H. & POURCELOT, P. 2013. Comparative kinematic analysis of the leading and trailing forelimbs of horses cantering on a turf and a synthetic surface. *Equine Veterinary Journal,* 45**,** 54-61.

CUI, Y., TIAN, Y., TANG, Y., JIA, L., WU, A., PENG, P., YANG, J., DU, H., WANG, X. & WU, L. 2013. Application of sodium alginate microspheres in ischaemic stroke modeling in miniature pigs. *Neural Regeneration Research,* 8**,** 1473-1480.

CYRINO, L. A., CARDOSO, R. C., HACKL, L. P. & NICOLAU, M. 2002. Effect of quercetin on plasma extravasation in rat CNS and dura mater by ACE and NEP inhibition. *Phytotherapy Research,* 16**,** 545-9.

D'AMBROSIO, A. L., SUGHRUE, M. E., MOCCO, J., MACK, W. J., KING, R. G., AGARWAL, S. & CONNOLLY, E. S. 2004. A modified transorbital baboon model of reperfused stroke. *Methods in Enzymology,* 386**,** 60-73.

DAS, S., MITCHELL, P., ROSS, N. & WHITFIELD, P. C. 2019. Decompressive Hemicraniectomy in the Treatment of Malignant Middle Cerebral Artery Infarction: A Meta-Analysis. *World Neurosurgery,* 123**,** 8-16.

DAVIS, S. M. & DONNAN, G. A. 2004. Steroids for Stroke: Another Potential Therapy Discarded Prematurely? *Stroke,* 35**,** 230-231.

DE CRESPIGNY, A. J., D'ARCEUIL, H. E., MAYNARD, K. I., HE, J., MCAULIFFE, D., NORBASH, A., SEHGAL, P. K., HAMBERG, L., HUNTER, G., BUDZIK, R. F., PUTMAN, C. M. & GONZALEZ, R. G. 2005. Acute studies of a new primate model of reversible middle cerebral artery occlusion. *Journal of Stroke and Cerebrovascular Disease,* 14**,** 80-7.

DEEPTHI, S., SUSEELAMMA, D., PRAMOD KUMAR, D., SARADADEVI, S. S. & SUBHADRADEVI, V. 2016. Comparative study of formation of circle of Willis in human and sheep brain. *Journal of the Anatomical Society of India,* 65**,** S16-S19.

DEL ZOPPO, G. J., COPELAND, B. R., HARKER, L. A., WALTZ, T. A., ZYROFF, J., HANSON, S. R. & BATTENBERG, E. 1986. Experimental acute thrombotic stroke in baboons. *Stroke,* 17**,** 1254-65.

DEMOPOULOS, H. B., FLAMM, E. S., PIETRONIGRO, D. D. & SELIGMAN, M. L. 1980. The free radical pathology and the microcirculation in the major central nervous system disorders. *Acta Physiologica Scandinavica Supplementum,* 492**,** 91-119.

DEWAR, D., YAM, P. & MCCULLOCH, J. 1999. Drug development for stroke: importance of protecting cerebral white matter. *European Journal of Pharmacology,* 375**,** 41-50.

DI, X., BULLOCK, R., WATSON, J., FATOUROS, P., CHENARD, B., WHITE, F. & CORWIN, F. 1997. Effect of CP101,606, a novel NR2B subunit antagonist of the N-methyl-D-aspartate receptor, on the volume of ischaemic brain damage off cytotoxic brain edema after middle cerebral artery occlusion in the feline brain. *Stroke,* 28**,** 2244-51.

DIENER, H. C., LEES, K. R., LYDEN, P., GROTTA, J., DAVALOS, A., DAVIS, S. M., SHUAIB, A., ASHWOOD, T., WASIEWSKI, W., ALDERFER, V., HARDEMARK, H. G., RODICHOK, L., SAINT, I. & INVESTIGATORS, I. I. 2008. NXY-059 for the treatment of acute stroke: pooled analysis of the SAINT I and II Trials. *Stroke,* 39**,** 1751-8.

DIRNAGL, U., IADECOLA, C. & MOSKOWITZ, M. A. 1999. Pathobiology of ischaemic stroke: an integrated view. *Trends in Neurosciences,* 22**,** 391-397.

DOBRIVOJEVIC, M., SPIRANEC, K. & SINDIC, A. 2015. Involvement of bradykinin in brain edema development after ischaemic stroke. *European Journal of Physiology,* 467**,** 201-12.

DOHMEN, C., BOSCHE, B., GRAF, R., REITHMEIER, T., ERNESTUS, R. I., BRINKER, G., SOBESKY, J. & HEISS, W. D. 2007. Identification and clinical impact of impaired cerebrovascular autoregulation in patients with malignant middle cerebral artery infarction. *Stroke,* 38**,** 56.

DONKIN, J. D. 2006. *The effects of the neuropeptide substance P on outcome following experimental traumatic brain injury in rats.* University of Adelaide.

DONKIN, J. J., CERNAK, I., BLUMBERGS, P. C. & VINK, R. 2011. A substance P antagonist reduces axonal injury and improves neurologic outcome when administered up to 12 hours after traumatic brain injury. *Journal of Neurotrauma,* 28**,** 217-24.

DONKIN, J. J., NIMMO, A. J., CERNAK, I., BLUMBERGS, P. C. & VINK, R. 2009. Substance P is associated with the development of brain edema and functional deficits after traumatic brain injury. *Journal of Cerebral Blood Flow & Metabolism,* 29**,** 1388-98.

DONKIN, J. J., TURNER, R. J., HASSAN, I. & VINK, R. 2007. Substance P in traumatic brain injury. *Progress in Brain Research,* 161**,** 97-109.

DONKIN, J. J. & VINK, R. 2010. Mechanisms of cerebral edema in traumatic brain injury: therapeutic developments. *Current Opinion in Neurology,* 23**,** 293-299.

DOSTOVIC, Z., DOSTOVIC, E., SMAJLOVIC, D., IBRAHIMAGIC, O. C. & AVDIC, L. 2016. Brain Edema After Ischaemic Stroke. *Medical Archives,* 70**,** 339-341.

DOYLE, K. P., SIMON, R. P. & STENZEL-POORE, M. P. 2008. Mechanisms of ischaemic brain damage. *Neuropharmacology,* 55**,** 310-8.

DUBERSTEIN, K. J., PLATT, S. R., HOLMES, S. P., DOVE, C. R., HOWERTH, E. W., KENT, M., STICE, S. L., HILL, W. D., HESS, D. C. & WEST, F. D. 2014. Gait analysis in a pre- and post-ischaemic stroke biomedical pig model. *Physiology & Behavior,* 125**,** 8-16.

DUBOIS, J., BENDERS, M., BORRADORI-TOLSA, C., CACHIA, A., LAZEYRAS, F., HA-VINH LEUCHTER, R., SIZONENKO, S. V., WARFIELD, S. K., MANGIN, J. F. & HUPPI, P. S. 2008. Primary cortical folding in the human newborn: an early marker of later functional development. *Brain,* 131**,** 2028-41.

DUHAIME, A. C., MARGULIES, S. S., DURHAM, S. R., O'ROURKE, M. M., GOLDEN, J. A., MARWAHA, S. & RAGHUPATHI, R. 2000. Maturation-dependent response of the piglet brain to scaled cortical impact. *Journal of Neurosurgery,* 93**,** 455-62.

DURUKAN, A. & TATLISUMAK, T. 2007. Acute ischaemic stroke: Overview of major experimental rodent models, pathophysiology, and therapy of focal cerebral ischaemia. *Pharmacology, Biochemistry and Behavior,* 87**,** 179-197.

EATON, S. L. & WISHART, T. M. 2017. Bridging the gap: large animal models in neurodegenerative research. *Mammalian Genome,* 28**,** 324-337.

EBNER, K., MUIGG, P., SINGEWALD, G. & SINGEWALD, N. 2008. Substance P in stress and anxiety: NK-1 receptor antagonism interacts with key brain areas of the stress circuitry. *Annals of the New York Academy of Sciences,* 1144**,** 61-73.

EBNER, K., RUPNIAK, N. M., SARIA, A. & SINGEWALD, N. 2004. Substance P in the medial amygdala: emotional stress-sensitive release and modulation of anxiety-related behavior in rats. *Proceedings of the National Academy of Sciences of the United States of America,* 101**,** 4280-5.

EBNER, K. & SINGEWALD, N. 2006. The role of substance P in stress and anxiety responses. *Amino Acids,* 31**,** 251-72.

EBNET, K., AURRAND-LIONS, M., KUHN, A., KIEFER, F., BUTZ, S., ZANDER, K., BRICKWEDDE, M.-K. M. Z., SUZUKI, A., IMHOF, B. A. & VESTWEBER, D. 2003. The junctional adhesion molecule (JAM) family members JAM-2 and JAM-3 associate with the cell polarity protein PAR-3: a possible role for JAMs in endothelial cell polarity. *Journal of Cell Science,* 116**,** 3879-3891.

ECONOMOS, A. C. 1980. Taxonomic differences in the mammalian life span-body weight relationship and the problem of brain weight. *Gerontology,* 26**,** 90-8.

EDVINSSON, L., MACKENZIE, E. T. & MCCULLOCH, J. 1993. *Cerebral Blood Flow & Metabolism*, Raven Press.

EDVINSSON, L., ROSENDAL-HELGESEN, S. & UDDMAN, R. 1983. Substance P: localization, concentration and release in cerebral arteries, choroid plexus and dura mater. *Cell and Tissue Research,* 234**,** 1-7.

EISENBERG, H. M., FRANKOWSKI, R. F., CONTANT, C. F., MARSHALL, L. F. & WALKER, M. D. 1988. High-dose barbiturate control of elevated intracranial pressure in patients with severe head injury. *Journal of Neurosurgery,* 69**,** 15-23.

ELLA, A., BARRIERE, D. A., ADRIAENSEN, H., PALMER, D. N., MELZER, T. R., MITCHELL, N. L. & KELLER, M. 2019. The development of brain magnetic resonance approaches in large animal models for preclinical research. *Animal Frontiers,* 9**,** 44-51.

ELLA, A., DELGADILLO, J. A., CHEMINEAU, P. & KELLER, M. 2017. Computation of a high-resolution MRI 3D stereotaxic atlas of the sheep brain. *Journal of Comparative Neurology,* 525**,** 676-692.

ELLA, A. & KELLER, M. 2015. Construction of an MRI 3D high resolution sheep brain template. *Magnetic Resonance Imaging,* 33**,** 1329-1337.

ELTZSCHIG, H. K. & ECKLE, T. 2011. Ischemia and reperfusion—from mechanism to translation. *Nature Medicine,* 17**,** 1391-1401.

ENGELHORN, T., VON KUMMER, R., REITH, W., FORSTING, M. & DOERFLER, A. 2002. What is effective in malignant middle cerebral artery infarction: Reperfusion, craniectomy, or both? An experimental study in rats. *Stroke,* 33**,** 617-622.

FALK, D. & GIBSON, K. R. 2001. *Evolutionary Anatomy of the Primate Cerebral Cortex*, Cambridge University Press.

FANNING, A. S., JAMESON, B. J., JESAITIS, L. A. & ANDERSON, J. M. 1998. The tight junction protein ZO-1 establishes a link between the transmembrane protein occludin and the actin cytoskeleton. *Journal of Biological Chemistry,* 273**,** 29745-53.

FEIGIN, V. L., NGUYEN, G., CERCY, K., JOHNSON, C. O., ALAM, T., PARMAR, P. G., ABAJOBIR, A. A., ABATE, K. H., ABD-ALLAH, F., ABEJIE, A. N., ABYU, G. Y.,

ADEMI, Z., AGARWAL, G., AHMED, M. B., AKINYEMI, R. O., AL-RADDADI, R., AMINDE, L. N., AMLIE-LEFOND, C., ANSARI, H., ASAYESH, H., ASGEDOM, S. W., ATEY, T. M., AYELE, H. T., BANACH, M., BANERJEE, A., BARAC, A., BARKER-COLLO, S. L., BARNIGHAUSEN, T., BARREGARD, L., BASU, S., BEDI, N., BEHZADIFAR, M., BEJOT, Y., BENNETT, D. A., BENSENOR, I. M., BERHE, D. F., BONEYA, D. J., BRAININ, M., CAMPOS-NONATO, I. R., CASO, V., CASTANEDA-ORJUELA, C. A., RIVAS, J. C., CATALA-LOPEZ, F., CHRISTENSEN, H., CRIQUI, M. H., DAMASCENO, A., DANDONA, L., DANDONA, R., DAVLETOV, K., DE COURTEN, B., DEVEBER, G., DOKOVA, K., EDESSA, D., ENDRES, M., FARAON, E. J. A., FARVID, M. S., FISCHER, F., FOREMAN, K., FOROUZANFAR, M. H., GALL, S. L., GEBREHIWOT, T. T., GELEIJNSE, J. M., GILLUM, R. F., GIROUD, M., GOULART, A. C., GUPTA, R., GUPTA, R., HACHINSKI, V., HAMADEH, R. R., HANKEY, G. J., HARERI, H. A., HAVMOELLER, R., HAY, S. I., HEGAZY, M. I., HIBSTU, D. T., JAMES, S. L., JEEMON, P., JOHN, D., JONAS, J. B., JOZWIAK, J., KALANI, R., KANDEL, A., KASAEIAN, A., KENGNE, A. P., KHADER, Y. S., KHAN, A. R., KHANG, Y. H., KHUBCHANDANI, J., KIM, D., KIM, Y. J., KIVIMAKI, M., KOKUBO, Y., KOLTE, D., KOPEC, J. A., KOSEN, S., KRAVCHENKO, M., KRISHNAMURTHI, R., KUMAR, G. A., LAFRANCONI, A., LAVADOS, P. M., et al. 2018. Global, Regional, and Country-Specific Lifetime Risks of Stroke, 1990 and 2016. *New England Journal of Medicine,* 379**,** 2429-2437.

FEIGIN, V. L., NORRVING, B. & MENSAH, G. A. 2017. Global Burden of Stroke. *Circulation Research,* 120**,** 439.

FELDMAN, Z., KANTER, M. J., ROBERTSON, C. S., CONTANT, C. F., HAYES, C., SHEINBERG, M. A., VILLAREAL, C. A., NARAYAN, R. K. & GROSSMAN, R. G. 1992.

Effect of head elevation on intracranial pressure, cerebral perfusion pressure, and cerebral blood flow in head-injured patients. *Journal of Neurosurgery,* 76**,** 207-211.

FISHER, M., FEUERSTEIN, G., HOWELLS, D. W., HURN, P. D., KENT, T. A., SAVITZ, S. I. & LO, E. H. 2009. Update of the stroke therapy academic industry roundtable preclinical recommendations. *Stroke,* 40**,** 2244-50.

FLECKNELL, P. 2016a. Chapter 2 - Managing and Monitoring Anaesthesia. *Laboratory Animal Anaesthesia (Fourth Edition).* Boston: Academic Press.

FLECKNELL, P. 2016b. Chapter 4 - Analgesia and Post-Operative Care. *Laboratory Animal Anaesthesia (Fourth Edition).* Boston: Academic Press.

FLECKNELL, P. A. 1996. *Laboratory animal anaesthesia,* London, Academic Press Ltd.

FLURI, F., SCHUHMANN, M. K. & KLEINSCHNITZ, C. 2015. Animal models of ischaemic stroke and their application in clinical research. *Drug Design, Development and Therapy,* 9**,** 3445-54.

FREEMAN, W. D. 2015. Management of Intracranial Pressure. *Neurocritical Care,* 21**,** 1299-323.

FRERET, T., SCHUMANN-BARD, P., BOULOUARD, M. & BOUET, V. 2011. On the importance of long-term functional assessment after stroke to improve translation from bench to bedside. *Experimental & Translational Stroke Medicine,* 3**,** 6.

FUKUCHI, C. A., FUKUCHI, R. K. & DUARTE, M. 2019. Effects of walking speed on gait biomechanics in healthy participants: a systematic review and meta-analysis. *Systematic Reviews,* 8.

FUNCHAL, B. F., ALVES, M. M., SURIANO, I. C., CHADDAD-NETO, F. E., FERRAZ, M. & SILVA, G. S. 2018. Intracranial pressure following decompressive hemicraniectomy for malignant cerebral infarction: clinical and treatment correlations. *Arquivos de Neuropsiquiatria,* 76**,** 812-815.

FURUICHI, Y., MAEDA, M., MATSUOKA, N., MUTOH, S. & YANAGIHARA, T. 2007. Therapeutic time window of tacrolimus (FK506) in a nonhuman primate stroke model: Comparison with tissue plasminogen activator. *Experimental Neurology,* 204**,** 138-146.

FURUSE, M., FUJIMOTO, K., SATO, N., HIRASE, T., TSUKITA, S. & TSUKITA, S. 1996. Overexpression of occludin, a tight junction-associated integral membrane protein, induces the formation of intracellular multilamellar bodies bearing tight junction-like structures. *Journal of Cell Science,* 109**,** 429-35.

FURUSE, M., HATA, M., FURUSE, K., YOSHIDA, Y., HARATAKE, A., SUGITANI, Y., NODA, T., KUBO, A. & TSUKITA, S. 2002. Claudin-based tight junctions are crucial for the mammalian epidermal barrier: a lesson from claudin-1–deficient mice. *Journal of Cell Biology,* 156**,** 1099-1111.

FURUSE, M., HIRASE, T., ITOH, M., NAGAFUCHI, A., YONEMURA, S., TSUKITA, S. & TSUKITA, S. 1993. Occludin: a novel integral membrane protein localizing at tight junctions. *Journal of Cell Biology,* 123**,** 1777-88.

FURUSE, M., SASAKI, H., FUJIMOTO, K. & TSUKITA, S. 1998. A Single Gene Product, Claudin-1 or -2, Reconstitutes Tight Junction Strands and Recruits Occludin in Fibroblasts. *Journal of Cell Biology,* 143**,** 391-401.

GABRIELIAN, L., HELPS, S. C., THORNTON, E., TURNER, R. J., LEONARD, A. V. & VINK, R. 2013. Substance P antagonists as a novel intervention for brain edema and raised intracranial pressure. *Acta Neurochirurgica Supplement,* 118**,** 201-4.

GABRIELIAN, L., WISLLSHIRE, L. W., HELPS, S. C., VAN DEN HEUVEL, C., MATHIAS, J. L. & VINK, R. 2011. Intracranial pressure changes following traumatic brain injury in rats: lack of significant change in the absence of mass lesions or hypoxia. *Journal of Neurotrauma,* 28**,** 2103-2111.

GARCIA-RECIO, S. & GASCÓN, P. 2015. Biological and Pharmacological Aspects of the NK1-Receptor. *BioMed Research International,* 2015**,** 1-14.

GEORGIADIS, A. L. & SUAREZ, J. I. 2003. Hypertonic saline for cerebral edema. *Current Neurology and Neuroscience Reports,* 3**,** 524-30.

GEURTS, M., VAN DER WORP, H. B., KAPPELLE, L. J., AMELINK, G. J., ALGRA, A. & HOFMEIJER, J. 2013. Surgical decompression for space-occupying cerebral infarction: outcomes at 3 years in the randomized HAMLET trial. *Stroke,* 44**,** 2506.

GHOUSSAYNI, S., STEVENS, C., DURHAM, S. & EWINS, D. 2004. Assessment and validation of a simple automated method for the detection of gait events and intervals. *Gait & Posture,* 20**,** 266-272.

GIBSON, K. R., RUMBAUGH, D. & BERAN, M. 2001. Bigger is better: primate brain size in relationship to cognition. *In:* FALK, D. & GIBSON, K. R. *Evolutionary Anatomy of the Primate Cerebral Cortex.* Cambridge: Cambridge University Press.

GIELING, E. T., NORDQUIST, R. E. & VAN DER STAAY, F. J. 2011. Assessing learning and memory in pigs. *Animal Cognition,* 14**,** 151-73.

GONZALEZ-MARISCAL, L., NAMORADO, M. C., MARTIN, D., LUNA, J., ALARCON, L., ISLAS, S., VALENCIA, L., MURIEL, P., PONCE, L. & REYES, J. L. 2000. Tight junction proteins ZO-1, ZO-2, and occludin along isolated renal tubules. *Kidney International,* 57**,** 2386-402.

GOODE, T., O'CONNOR, T., HOPKINS, A., MORIARTY, D., O'SULLIVAN, G. C., COLLINS, J. K., O'DONOGHUE, D., BAIRD, A. W., O'CONNELL, J. & SHANAHAN, F. 2003. Neurokinin-1 receptor (NK-1R) expression is induced in human colonic epithelial cells by proinflammatory cytokines and mediates proliferation in response to substance P. *Journal of Cellular Physiology,* 197**,** 30-41.

GOPALAKRISHNAN, M. S., SHANBHAG, N. C., SHUKLA, D. P., KONAR, S. K., BHAT, D. I. & DEVI, B. I. 2018. Complications of Decompressive Craniectomy. *Frontiers in Neurology,* 9.

GORELICK, P. B. 2019. The global burden of stroke: persistent and disabling. *Lancet Neurology,* 18**,** 417-418.

GOTTESMAN, R. F. & HILLIS, A. E. 2010. Predictors and assessment of cognitive dysfunction resulting from ischaemic stroke. *Lancet Neurology,* 9**,** 895-905.

GOUNDEN, V., VASHISHT, R. & JIALAL, I. 2021. Hypoalbuminemia. *StatPearls.* Treasure Island (FL).

GOYAL, M., DEMCHUK, A. M., MENON, B. K., EESA, M., REMPEL, J. L., THORNTON, J., ROY, D., JOVIN, T. G., WILLINSKY, R. A., SAPKOTA, B. L., DOWLATSHAHI, D., FREI, D. F., KAMAL, N. R., MONTANERA, W. J., POPPE, A. Y., RYCKBORST, K. J., SILVER, F. L., SHUAIB, A., TAMPIERI, D., WILLIAMS, D., BANG, O. Y., BAXTER, B. W., BURNS, P. A., CHOE, H., HEO, J.-H., HOLMSTEDT, C. A., JANKOWITZ, B., KELLY, M., LINARES, G., MANDZIA, J. L., SHANKAR, J., SOHN, S.-I., SWARTZ, R. H., BARBER, P. A., COUTTS, S. B., SMITH, E. E., MORRISH, W. F., WEILL, A., SUBRAMANIAM, S., MITHA, A. P., WONG, J. H., LOWERISON, M. W., SAJOBI, T. T. & HILL, M. D. 2015. Randomized Assessment of Rapid Endovascular Treatment of Ischaemic Stroke. *New England Journal of Medicine,* 372**,** 1019-1030.

GOYAL, M., MENON, B. K., VAN ZWAM, W. H., DIPPEL, D. W. J., MITCHELL, P. J., DEMCHUK, A. M., DÁVALOS, A., MAJOIE, C. B. L. M., VAN DER LUGT, A., DE MIQUEL, M. A., DONNAN, G. A., ROOS, Y. B. W. E. M., BONAFE, A., JAHAN, R., DIENER, H. C., VAN DEN BERG, L. A., LEVY, E. I., BERKHEMER, O. A., PEREIRA, V. M., REMPEL, J., MILLÁN, M., DAVIS, S. M., ROY, D., THORNTON, J., ROMÁN, L. S., RIBÓ, M., BEUMER, D., STOUCH, B., BROWN, S., CAMPBELL, B. C. V., VAN OOSTENBRUGGE, R. J., SAVER, J. L., HILL, M. D. & JOVIN, T. G. 2016. Endovascular thrombectomy after large-vessel ischaemic stroke: a meta-analysis of individual patient data from five randomised trials. *The Lancet,* 387**,** 1723-1731.

GRALLA, J., SCHROTH., G., REMONDA, L., FLEISCHMANN, A., FANDINO, J., SLOTBOOM, J. & BREKENFELD, C. 2006. A dedicated animal model for mechanical thrombectomy in acute stroke. *American Journal of Neuroradiology,* 27**,** 1357-61.

GRANDE, P. O. & ROMNER, B. 2012. Osmotherapy in brain edema: a questionable therapy. *Journal of Neurosurgical Anesthesiology,* 24**,** 407-12.

GRANDIN, T. 1987. Animal handling. *Veterinary Clinics of North America: Food Animal Practice,* 3**,** 323-38.

GRANDIN, T. 1997. Assessment of stress during handling and transport. *Journal of Animal Science,* 75**,** 249-57.

GRANDIN, T. 1999. Safe handling of large animals. *Occupational Medicine,* 14**,** 195-212.

GREENE, S. A. 2002. Chapter 32 - Anaesthesia for the Patient with Neurologic Disease. *Veterinary Anaesthesia and Pain Management Secrets.* Philadelphia: Hanley & Belfus.

GREENE, S. A. & BENSON, G. J. 2002. Chapter 45 - Porcine Anaesthesia. *Veterinary Anaesthesia and Pain Management Secrets.* Philadelphia: Hanley & Belfus.

GREIF, D. M. & EICHMANN, A. 2014. Vascular biology: Brain vessels squeezed to death. *Nature,* 508**,** 50-1.

GRINDLINGER, G. A., SKAVDAHL, D. H., ECKER, R. D. & SANBORN, M. R. 2016. Decompressive craniectomy for severe traumatic brain injury: clinical study, literature review and meta-analysis. *Springerplus,* 5**,** 1605.

GROSS, D. R. 1997. Thromboembolic phenomena and the use of the pig as an appropriate animal model for research on cardiovascular devices. *International Journal of Artificial Organs,* 20**,** 195-203.

GU, Y., ZHENG, G., XU, M., LI, Y., CHEN, X., ZHU, W., TONG, Y., CHUNG, S. K., LIU, K. J. & SHEN, J. 2012. Caveolin-1 regulates nitric oxide-mediated matrix metalloproteinases activity and blood-brain barrier permeability in focal cerebral ischaemia and reperfusion injury. *Journal of Neurochemistry,* 120**,** 147-56.

GUPTA, R., CONNOLLY, E. S., MAYER, S. & ELKIND, M. S. V. 2004. Hemicraniectomy for Massive Middle Cerebral Artery Territory Infarction. *Stroke,* 35**,** 539-543.

GUZIK, A., DRUZBICKI, M. & WOLAN-NIERODA, A. 2018. Assessment of two gait training models: conventional physical therapy and treadmill exercise, in terms of their effectiveness after stroke. *Hippokratia,* 22**,** 51-59.

HAARMANN, A., DEIS, A., PROCHASKA, J., FOERCH, C., WEKSLER, B., ROMERO, I., COURAUD, P.-O., STOLL, G., RIECKMANN, P. & BUTTMANN, M. 2010. Evaluation of Soluble Junctional Adhesion Molecule-A as a Biomarker of Human Brain Endothelial Barrier Breakdown. *PLOS ONE,* 5**,** e13568.

HACKE, W., SCHWAB, S., HORN, M., SPRANGER, M., DE GEORGIA, M. & VON KUMMER, R. 1996. 'Malignant' middle cerebral artery territory infarction: clinical course and prognostic signs. *Archives of Neurology,* 53**,** 309-15.

HAINSWORTH, A. H., ALLAN, S. M., BOLTZE, J., CUNNINGHAM, C., FARRIS, C., HEAD, E., IHARA, M., ISAACS, J. D., KALARIA, R. N., LESNIK OBERSTEIN, S. A. M. J., MOSS, M. B., NITZSCHE, B., ROSENBERG, G. A., RUTTEN, J. W., SALKOVIC-PETRISIC, M. & TROEN, A. M. 2017. Translational models for vascular cognitive impairment: a review including larger species. *BMC Medicine,* 15**,** 16-16.

HAKIM, A. M. 1998. Ischaemic penumbra: the therapeutic window. *Neurology,* 51**,** S44-6.

HALL, L. W., CLARKE, K. W. & TRIM, C. M. 2001. Chapter 14 - Anaesthesia of the pig. *Veterinary Anaesthesia (Tenth Edition).* Oxford: W.B. Saunders.

HANKO, J., HARDEBO, J. E., KAHRSTROM, J., OWMAN, C. & SUNDLER, F. 1985. Calcitonin gene-related peptide is present in mammalian cerebrovascular nerve fibres and dilates pial and peripheral arteries. *Neuroscience Letters,* 57**,** 91-5.

HARRISON, S. & GEPPETTI, P. 2001. Substance P. *International Journal of Biochemistry & Cell Biology,* 33**,** 555-576.

HARTINGS, J. A., ROLLI, M. L., LU, X. C. & TORTELLA, F. C. 2003. Delayed secondary phase of peri-infarct depolarizations after focal cerebral ischaemia: relation to infarct growth and neuroprotection. *Journal of Neuroscience,* 23**,** 11602-10.

HARUTJUNYAN, L., HOLZ, C., RIEGER, A., MENZEL, M., GROND, S. & SOUKUP, J. 2005. Efficiency of 7.2% hypertonic saline hydroxyethyl starch 200/0.5 versus mannitol 15% in the treatment of increased intracranial pressure in neurosurgical patients - a randomized clinical trial. *Critical Care,* 9**,** R530-40.

HASENOHRL, R. U., SOUZA-SILVA, M. A., NIKOLAUS, S., TOMAZ, C., BRANDAO, M. L., SCHWARTING, R. K. & HUSTON, J. P. 2000. Substance P and its role in neural mechanisms governing learning, anxiety and functional recovery. *Neuropeptides,* 34**,** 272-80.

HASIWA, N., BAILEY., J., CLAUSING, P., DANESHIAN, M., EILERAAS, M., FARKAS, S., GYERTYÁN, I., HUBRECHT, R., KOBEL, W., KRUMMENACHER, G., LEIST, M., LOHI, H., MIKLÓSI, A., OHL, F., OLEJNICZAK, K., SCHMITT, G., SINNETT-SMITH, P., SMITH, D., WAGNER, K., YAGER, J. D., ZURLO, J. & HARTUNG, T. 2011. Critical evaluation of the use of dogs in biomedical research and testing in Europe. *Alternatives to Aminal Medicine,* 28**,** 326-40.

HAUER, E. M., STARK, D., STAYKOV, D., STEIGLEDER, T., SCHWAB, S. & BARDUTZKY, J. 2011. Early continuous hypertonic saline infusion in patients with severe cerebrovascular disease. *Critical Care Medicine,* 39**,** 1766-72.

HAWKINS, B. T. & DAVIS, T. P. 2005. The blood-brain barrier/neurovascular unit in health and disease. *Pharmacological Reviews,* 57**,** 173-85.

HEISS, W. D. 2016. Malignant MCA Infarction: Pathophysiology and Imaging for Early Diagnosis and Management Decisions. *Cerebrovascular Diseases,* 41**,** 1-7.

HENDRICKSON, D. A. & BAIRD, A. N. 2013. *Turner and McIlwraith's Techniques in Large Animal Surgery,* Somerset, United States, Wiley.

HERBIN, M., HACKERT, R., GASC, J. P. & RENOUS, S. 2007. Gait parameters of treadmill versus overground locomotion in mouse. *Behavioural Brain Research,* 181**,** 173-179.

HERRMANN, A. M., MECKEL, S., GOUNIS, M. J., KRINGE, L., MOTSCHALL, E., MÜLLING, C. & BOLTZE, J. 2019. Large animals in neurointerventional research: A systematic review on models, techniques and their application in endovascular procedures for stroke, aneurysms and vascular malformations. *Journal of Cerebral Blood Flow & Metabolism,* 39**,** 375-394.

HEWITT, A. & ELLORY, C. 2012. Brain oedema, intracranial pressure and cerebral blood flow. *Surgery (Oxford),* 30**,** 102-106.

HILL, N. C., MILLIKAN, C. H., WAKIM, K. G. & SAYRE, G. P. 1955. Studies in cerebrovascular disease. VII. Experimental production of cerebral infarction by intracarotid injection of homologous blood clot; preliminary report. *Proceedings ot the Staff Meetings of the Mayo Clinic,* 30**,** 625-33.

HIROUCHI, Y., SUZUKI, E., MITSUOKA, C., JIN, H., KITAJIMA, S., KOHJIMOTO, Y., ENOMOTO, M. & KUGINO, K. 2007. Neuroimaging and histopathological evaluation of delayed neurological damage produced by artificial occlusion of the middle cerebral artery in Cynomolgus monkeys: establishment of a monkey model for delayed cerebral ischaemia. *Experimental and Toxicologic Pathology,* 59**,** 9-16.

HO, W. Z., LAI, J. P., ZHU, X. H., UVAYDOVA, M. & DOUGLAS, S. D. 1997. Human monocytes and macrophages express substance P and neurokinin-1 receptor. *Journal of Immunology,* 159**,** 5654-60.

HOFFMAN, J. M. & VALENCAK, T. G. 2020. A short life on the farm: aging and longevity in agricultural, large-bodied mammals. *GeroScience,* 42**,** 909-922.

HOFFMANN, A., STOFFEL, M. H., NITZSCHE, B., LOBSIEN, D., SEEGER, J., SCHNEIDER, H. & BOLTZE, J. 2014. The ovine cerebral venous system: comparative anatomy, visualization, and implications for translational research. *PLOS ONE,* 9**,** e92990.

HOFMAN, M. A. 1983. Energy Metabolism, Brain Size and Longevity in Mammals. *The Quarterly Review of Biology,* 58**,** 495-512.

HOFMEIJER, J., KAPPELLE, L. J., ALGRA, A., AMELINK, G. J., VAN GIJN, J. & VAN DER WORP, H. B. 2009. Surgical decompression for space-occupying cerebral infarction (the Hemicraniectomy After Middle Cerebral Artery infarction with Life-threatening Edema Trial [HAMLET]): a multicentre, open, randomised trial. *Lancet Neurology,* 8**,** 326-333.

HOFMEIJER, J. & VAN PUTTEN, M. J. A. M. 2012. Ischaemic cerebral damage: An appraisal of synaptic failure. *Stroke,* 43**,** 607-615.

HOKFELT, T., BROBERGER, C., XU, Z. Q., SERGEYEV, V., UBINK, R. & DIEZ, M. 2000. Neuropeptides--an overview. *Neuropharmacology,* 39**,** 1337-56.

HOKFELT, T., KELLERTH, J. O., NILSSON, G. & PERNOW, B. 1975. Substance P: localisation in the central nervous system and in some primary sensory neurones. *Science,* 190**,** 889 - 890.

HOLLAND, J. P., SYDSERFF, S. G., TAYLOR, W. A. & BELL, B. A. 1994. Calcitonin gene-related peptide reduces brain injury in a rat model of focal cerebral ischaemia. *Stroke,* 25**,** 2058-9.

HONIG, A., ELIAHOU, R. & AURIEL, E. 2017. Confined anterior cerebral artery infarction manifesting as isolated unilateral axial weakness. *Journal of the Neurological Sciences,* 373**,** 18-20.

HOWELLS, D. W., PORRITT, M. J., REWELL, S. S., O'COLLINS, V., SENA, E. S., VAN DER WORP, H. B., TRAYSTMAN, R. J. & MACLEOD, M. R. 2010. Different strokes for different folks: the rich diversity of animal models of focal cerebral ischaemia. *Journal of Cerebral Blood Flow & Metabolism,* 30**,** 1412-31.

HUANG, H., BHUIYAN, M. I. H., JIANG, T., SONG, S., SHANKAR, S., TAHERI, T., LI, E., SCHREPPEL, P., HINTERSTEININGER, M., YANG, S.-S., LIN, S.-H., MOLYNEAUX, B. J., ZHANG, Z., ERKER, T. & SUN, D. 2019. A Novel Na +-K +-Cl−Cotransporter 1 Inhibitor STS66* Reduces Brain Damage in Mice After Ischaemic Stroke. *Stroke,* 50**,** 1021-1025.

HUANG, J. M., MOCCO, J., CHOUDHRI, T. F., POISIK, A., POPILSKIS, S. J., EMERSON, R., DELAPAZ, R. L., KHANDJI, A. G., PINSKY, D.J. & CONNOLLY, E. S. 2000. A modified transorbital baboon model of reperfused stroke. *Stroke,* 31**,** 3054-63.

HUDAK, A. M., PENG, L., MARQUEZ DE LA PLATA, C., THOTTAKARA, J., MOORE, C., HARPER, C., MCCOLL, R., BABCOCK, E. & DIAZ-ARRASTIA, R. 2014. Cytotoxic and vasogenic cerebral oedema in traumatic brain injury: Assessment with FLAIR and DWI imaging. *Brain Injury,* 28**,** 1602-1609.

HUDETZ, J. A. & PAGEL, P. S. 2010. Neuroprotection by ketamine: a review of the

experimental and clinical evidence. *Journal of Cardiothoracic and Vascular Anaesthesia,* 24**,** 131-142.

HUI, C., TADI, P. & PATTI, L. 2020. Ischaemic Stroke. *StatPearls.* Treasure Island (FL).

HUSKEY, S. E. W., DEAN, B. J., BAKHTIAR, R., SANCHEZ, R. I., TATTERSALL, F. D., RYCROFT, W., HARGREAVES, R., WATT, A. P., CHICCHI, G. G., KEOHANE, C., HORA, D. F. & CHIU, S.-H. L. 2003. Brain penetration of aprepitant, a substance p receptor antagonist, in ferrets. *Drug Metabolism and Disposition,* 31**,** 785-791.

HUTTNER, H. B. & SCHWAB, S. 2009. Malignant middle cerebral artery infarction: clinical characteristics, treatment strategies, and future perspectives. *Lancet Neurology,* 8**,** 949-958.

IBRAHIM, M. A. & PREUSS, C. V. 2020. Antiemetic Neurokinin-1 Receptor Blockers. *StatPearls.* Treasure Island (FL).

IMAI, H., KONNO, K., NAKAMURA, M., SHIMIZU, T., KUBOTA, C., SEKI, K., HONDA, F., TOMIZAWA, S., TANAKA, Y., HATA, H. & SAITO, N. 2006. A new model of focal cerebral ischaemia in the miniature pig. *Journal of Neurosurgery,* 104**,** 123-32.

INOUE, T., KIMURA, M., UCHIDA, J., NISHINO, K., KUMAGAI, T., TANIGUCHI, J. & IMAMURA, F. 2017. Aprepitant for the treatment of breakthrough chemotherapy-induced nausea and vomiting in patients receiving moderately emetogenic chemotherapy.

IRVINE, H. J., OSTWALDT, A. C., BEVERS, M. B., DIXON, S., BATTEY, T. W., CAMPBELL, B. C., DAVIS, S. M., DONNAN, G. A., SHETH, K. N., JAHAN, R., SAVER,

J. L., KIDWELL, C. S. & KIMBERLY, W. T. 2018. Reperfusion after ischaemic stroke is associated with reduced brain edema. *Journal of Cerebral Blood Flow & Metabolism,* 38**,** 1807-1817.

ITOH, C., KIMURA, K. & WAKAYAMA, S. 2016. Comparison of intraclass correlation coefficient and the coefficient of multiple correlation in the reliability of gait analysis. *Physiotherapy,* 102**,** e83.

ITOH, M., NAGAFUCHI, A., YONEMURA, S., KITANI-YASUDA, T., TSUKITA, S. & TSUKITA, S. 1993. The 220-kD protein colocalizing with cadherins in non-epithelial cells is identical to ZO-1, a tight junction-associated protein in epithelial cells: cDNA cloning and immunoelectron microscopy. *Journal of Cell Biology,* 121**,** 491-502.

JEON, S. B., KOH, Y., CHOI, H. A. & LEE, K. 2014. Critical Care for Patients with Massive Ischaemic Stroke. *Journal of Stroke,* 16**,** 146.

JESSEN, N. A., MUNK, A. S. F., LUNDGAARD, I. & NEDERGAARD, M. 2015. The Glymphatic System: A Beginner's Guide. *Neurochemical Research,* 40**,** 2583-2599.

JHA, S. 2003. Cerebral Edema and its Management. *Medical Journal Armed Forces India,* 59**,** 326-331.

JIANG, X., ANDJELKOVIC, A. V., ZHU, L., YANG, T., BENNETT, M. V. L., CHEN, J., KEEP, R. F. & SHI, Y. 2018. Blood-brain barrier dysfunction and recovery after ischaemic stroke. *Progress in Neurobiology,* 163-164**,** 144-171.

JIAO, H., WANG, Z., LIU, Y., WANG, P. & XUE, Y. 2011. Specific role of tight junction proteins claudin-5, occludin, and ZO-1 of the blood-brain barrier in a focal cerebral ischaemic insult. *Journal of Molecular Neuroscience,* 44**,** 130-9.

JOHNSON, C. O., NGUYEN, M., ROTH, G. A., NICHOLS, E., ALAM, T., ABATE, D., ABD-ALLAH, F., ABDELALIM, A., ABRAHA, H. N., ABU-RMEILEH, N. M., ADEBAYO, O. M., ADEOYE, A. M., AGARWAL, G., AGRAWAL, S., AICHOUR, A. N., AICHOUR, I., AICHOUR, M. T. E., ALAHDAB, F., ALI, R., ALVIS-GUZMAN, N., ANBER, N. H., ANJOMSHOA, M., ARABLOO, J., ARAUZ, A., ÄRNLÖV, J., ARORA, A., AWASTHI, A., BANACH, M., BARBOZA, M. A., BARKER-COLLO, S. L., BÄRNIGHAUSEN, T. W., BASU, S., BELACHEW, A. B., BELAYNEH, Y. M., BENNETT, D. A., BENSENOR, I. M., BHATTACHARYYA, K., BIADGO, B., BIJANI, A., BIKBOV, B., BIN SAYEED, M. S., BUTT, Z. A., CAHUANA-HURTADO, L., CARRERO, J. J., CARVALHO, F., CASTAÑEDA-ORJUELA, C. A., CASTRO, F., CATALÁ-LÓPEZ, F., CHAIAH, Y., CHIANG, P. P. C., CHOI, J.-Y. J., CHRISTENSEN, H., CHU, D.-T., CORTINOVIS, M., DAMASCENO, A. A. M., DANDONA, L., DANDONA, R., DARYANI, A., DAVLETOV, K., DE COURTEN, B., DE LA CRUZ-GÓNGORA, V., DEGEFA, M. G., DHARMARATNE, S. D., DIAZ, D., DUBEY, M., DUKEN, E. E., EDESSA, D., ENDRES, M., FARAON, E. J. A., FARZADFAR, F., FERNANDES, E., FISCHER, F., FLOR, L. S., GANJI, M., GEBRE, A. K., GEBREMICHAEL, T. G., GETA, B., GEZAE, K. E., GILL, P. S., GNEDOVSKAYA, E. V., GÓMEZ-DANTÉS, H., GOULART, A. C., GROSSO, G., GUO, Y., GUPTA, R., HAJ-MIRZAIAN, A., HAJ-MIRZAIAN, A., HAMIDI, S., HANKEY, G. J., HASSEN, H. Y., HAY, S. I., HEGAZY, M. I., HEIDARI, B., HERIAL, N. A., HOSSEINI, M. A., HOSTIUC, S., IRVANI, S. S. N., ISLAM, S. M. S., JAHANMEHR, N., JAVANBAKHT, M., et al.

2019. Global, regional, and national burden of stroke, 1990–2016: a systematic analysis for the Global Burden of Disease Study 2016. *The Lancet Neurology,* 18**,** 439-458.

JOHNSON, M. B., YOUNG, A. D. & MARRIOTT, I. 2017. The Therapeutic Potential of Targeting Substance P/NK-1R Interactions in Inflammatory CNS Disorders. *Frontiers in Cellular Neuroscience,* 10.

JONES, T. A. 2017. Motor compensation and its effects on neural reorganization after stroke. *Nature Reviews Neuroscience,* 18**,** 267-280.

JOO, F. 1993. The blood-brain barrier in vitro: the second decade. *Neurochemistry International,* 23**,** 499-521.

JUUL, R., AAKHUS, S., BJORNSTAD, K., GISVOLD, S. E., BRUBAKK, A. O. & EDVINSSON, L. 1994. Calcitonin gene-related peptide (human alpha-CGRP) counteracts vasoconstriction in human subarachnoid haemorrhage. *Neuroscience Letters,* 170**,** 67-70.

JÜTTLER, E., SCHWAB, S., SCHMIEDEK, P., UNTERBERG, A., HENNERICI, M., WOITZIK, J., WITTE, S., JENETZKY, E. & HACKE, W. 2007. Decompressive Surgery for the Treatment of Malignant Infarction of the Middle Cerebral Artery (DESTINY): a randomized, controlled trial. *Stroke,* 38**,** 2518.

KALOGERIS, T., BAINES, C. P., KRENZ, M. & KORTHUIS, R. J. 2012. Cell biology of ischaemia/reperfusion injury. *International Review of Cell and Molecular Biology,* 298**,** 229-317.

KAMOI, S., PRETTY, C., DOCHERTY, P., SQUIRE, D., REVIE, J., CHIEW, Y. S., DESAIVE, T., SHAW, G. M. & CHASE, J. G. 2014. Continuous Stroke Volume Estimation

from Aortic Pressure Using Zero Dimensional Cardiovascular Model: Proof of Concept Study from Porcine Experiments. *PLOS ONE,* 9.

KAPOOR, K., KAK, V. K. & SINGH, B. 2003. Morphology and Comparative Anatomy of Circulus Arteriosus Cerebri in Mammals. *Anatomia, Histologia, Embryologia,* 32**,** 347-355.

KASSELL, N. F., PEERLESS, S. J., DRAKE, C. G., BOARINI, D. J. & ADAMS, H. P. 1980. Treatment of ischaemic deficits from cerebral vasospasm with high dose barbiturate therapy. *Neurosurgery,* 7**,** 593-7.

KASSNER, A., MANDELL, D. M. & MIKULIS, D. J. 2011. Measuring permeability in acute ischemic stroke. *Neuroimaging Clinics of North America,* 21**,** 315-25, x-xi.

KASSNER, A., ROBERTS, T. P. L., MORAN, B., SILVER, F. L. & MIKULIS, D. J. 2009. Recombinant Tissue Plasminogen Activator Increases Blood-Brain Barrier Disruption in Acute Ischemic Stroke: An MR Imaging Permeability Study. *American Journal of Neuroradiology,* 30**,** 1864-1869.

KAVELAARS, A., BROEKE, D., JEURISSEN, F., KARDUX, J., MEIJER, A., FRANKLIN, R., GELFAND, E. W. & HEIJNEN, C. J. 1994. Activation of human monocytes via a non-neurokinin substance P receptor that is coupled to Gi protein, calcium, phospholipase D, MAP kinase, and IL-6 production. *Journal of Immunology,* 153**,** 3691-9.

KEENE, D. J., MOE-NILSSEN, R. & LAMB, S. E. 2016. The application of multilevel modelling to account for the influence of walking speed in gait analysis. *Gait & Posture,* 43**,** 216-219.

KEITH, M. K., ANA, P. D. C., ANDREA, E. L., MICHAEL, R. H. & JON, W. P. 2007. Sheep don't forget a face. *Nature,* 447**,** 346.

KHATIBI, N. H., JADHAV, V., CHARLES, S., CHIU, J., BUCHHOLZ, J., TANG, J. & ZHANG, J. H. 2011. Capsaicin Pre-treatment Provides Neurovascular Protection Against Neonatal Hypoxic-Ischaemic Brain Injury in Rats. *Intracerebral Hemorrhage Research.* Springer Vienna.

KIENING, K., HÄRTL, R., UNTERBERG, A., SCHNEIDER, G.-H., BARDT, T. & LANKSCH, W. 1997. Brain tissue pO2-monitoring in comatose patients: Implications for therapy. *Neurological Research,* 19**,** 233-240.

KILGOUR, R. 1971. Animal behaviour and scientific management. *New Zealand Veterinary Journal,* 19**,** 188-9.

KILGOUR, R. 1972. Animal behaviour in intensive systems and its relationship to disease and production. *Australian Veterinary Journal,* 48**,** 94-8.

KIM, D. K., OH, E. K., SUMMERS, B. A., PRABHAKAR, N. R. & KUMAR, G. K. 2001. Release of substance P by low oxygen in the rabbit carotid body: evidence for the involvement of calcium channels. *Brain Research,* 892**,** 359-69.

KIM, H., JIN, S. T., KIM, Y. W., KIM, S. R., PARK, I. S. & JO, K. W. 2015. Predictors of malignant brain edema in middle cerebral artery infarction observed on CT angiography. *Journal of Clinical Neuroscience,* 22**,** 554-560.

KIM, J. & BREUR, G. J. 2008. Temporospatial and kinetic characteristics of sheep walking on a pressure sensing walkway. *Canadian Journal of Veterinary Research,* 72**,** 50-55.

KIMBERLY, W. T., BATTEY, T. W., PHAM, L., WU, O., YOO, A. J., FURIE, K. L., SINGHAL, A. B., ELM, J. J., STERN, B. J. & SHETH, K. N. 2014. Glyburide is associated with attenuated vasogenic edema in stroke patients. *Neurocritical Care,* 20**,** 193-201.

KIMBERLY, W. T., BEVERS, M. B., VON KUMMER, R., DEMCHUK, A. M., ROMERO, J. M., ELM, J. J., HINSON, H. E., MOLYNEAUX, B. J., SIMARD, J. M. & SHETH, K. N. 2018. Effect of IV glyburide on adjudicated edema endpoints in the GAMES-RP Trial. *Neurology,* 91**,** e2163-e2169.

KITANO, H., KIRSCH, J. R., HURN, P. D. & MURPHY, S. J. 2007. Inhalational anesthetics as neuroprotectants or chemical preconditioning agents in ischaemic brain. *Journal of Cerebral Blood Flow & Metabolism,* 27**,** 1108-1128.

KITO, G., NISHIMURA, A., SUSUMU, T., NAGATA, R., KUGE, Y., YOKOTA, C. & MINEMATSU, K. 2001. Experimental thromboembolic stroke in cynomolgus monkey. *Journal of Neuroscience Methods,* 105**,** 45-53.

KJARTANSSON, J. & DALSGAARD, C. J. 1987. Calcitonin gene-related peptide increases survival of a musculocutaneous critical flap in the rat. *European Journal of Pharmacology,* 142**,** 355-8.

KLEINMAN, J. E., HONG, J., IADAROLA, M., GOVONI, S. & GILLIN, C. J. 1985. Neuropeptides in human brain—postmortem studies. *Progress in Neuro-Psychopharmacology and Biological Psychiatry,* 9**,** 91-95.

KLINTWORTH, G. K. 1968. The comparative anatomy and phylogeny of the tentorium cerebelli. *The Anatomical Record,* 160**,** 635-42.

KLONER, R. A., KING, K. S. & HARRINGTON, M. G. 2018. No-reflow phenomenon in the heart and brain. *American Journal of Physiology-Heart and Circulatory Physiology,* 315**,** H550-H562.

KNOLLE, F., GONCALVES, R., DAVIES, E., DUFF, A. & MORTON, J. 2019. Response-inhibition during problem solving in sheep. *International Journal of Comparative Psychology,* 32.

KOBAYASHI, E., HISHIKAWA, S., TERATANI, T. & LEFOR, A. T. 2012. The pig as a model for translational research: overview of porcine animal models at Jichi Medical University. *Transplantation Research,* 1**,** 1-9.

KOENIG, M. A., BRYAN, M., LEWIN, J. L., 3RD, MIRSKI, M. A., GEOCADIN, R. G. & STEVENS, R. D. 2008. Reversal of transtentorial herniation with hypertonic saline. *Neurology,* 70**,** 1023-9.

KOMAROVA, Y. & MALIK, A. B. 2010. Regulation of endothelial permeability via paracellular and transcellular transport pathways. *Annual Review of Physiology,* 72**,** 463-93.

KONAN, L. M., REDDY, V. & MESFIN, F. B. 2020. Neuroanatomy, Cerebral Blood Supply. *StatPearls.* Treasure Island (FL).

KOO, T. K. & LI, M. Y. 2016. A Guideline of Selecting and Reporting Intraclass Correlation Coefficients for Reliability Research. *Journal of Chiropractic Medicine,* 15**,** 155-163.

KOTWICA, Z., HARDEMARK, H. G. & PERSSON, L. 1991. Intracranial pressure changes following middle cerebral artery occlusion in rats. *Research in Experimental Medicine,* 191**,** 99-104.

KREAM, R. M., SCHOENFELD, T. A., MANCUSO, R., CLANCY, A. N., EL-BERMANI, W. & MACRIDES, F. 1985. Precursor forms of substance P (SP) in nervous tissue: detection with antisera to SP, SP-Gly, and SP-Gly-Lys. *Proceedings of the National Academy of Sciences,* 82**,** 4832-4836.

KRINGE, L., SENA, E. S., MOTSCHALL, E., BAHOR, Z., WANG, Q., HERRMANN, A. M., MÜLLING, C., MECKEL, S. & BOLTZE, J. 2020. Quality and validity of large animal experiments in stroke: A systematic review. *Journal of Cerebral Blood Flow & Metabolism,* 40**,** 2152-2164.

KRISHNASWAMY, A., KLEIN, J. P. & KAPADIA, S. R. 2009. Clinical cerebrovascular anatomy. *Catheterization and Cardiovascular Interventions***,** NA-NA.

KUAN, C. & SUN, Y. 2015. Towards reperfusion-centric preclinical stroke research: outside the box of "reperfusion injury". *Neural Regeneration Research,* 10**,** 534.

KUBALE, V., ABRAMOVIC, Z., POGACNIK, A., HEDING, A., SENTJURC, M. & VRECL, M. 2007. Evidence for a role of caveolin-1 in neurokinin-1 receptor plasma-membrane localization, efficient signaling, and interaction with beta-arrestin 2. *Cell Tissue Research,* 330**,** 231-45.

KUGE, Y., YOKOTA, C., TAGAYA, M., HASEGAWA, Y., NISHIMURA, A., KITO, G., TAMAKI, N., HASHIMOTO, N., YAMAGUCHI, T. & MINEMATSU, K. 2001. Serial changes in cerebral blood flow and flow-metabolism uncoupling in primates with acute thromboembolic stroke. *Journal of Cerebral Blood Flow & Metabolism,* 21**,** 202-10.

KULUZ, J. W., PRADO, R., HE, D., ZHAO, W., DIETRICH, W. D. & WATSON, B. 2007. New pediatric model of ischaemic stroke in infant piglets by photothrombosis: acute changes in cerebral blood flow, microvasculature, and early histopathology. *Stroke,* 38**,** 1932-7.

KURLAND, D. B., KHALADJ-GHOM, A., STOKUM, J. A., CARUSILLO, B., KARIMY, J. K., GERZANICH, V., SAHUQUILLO, J. & SIMARD, J. M. 2015. Complications Associated with Decompressive Craniectomy: A Systematic Review. *Neurocritical Care,* 23**,** 292.

LABAT-GEST, V. & TOMASI, S. 2013. Photothrombotic ischaemia: a minimally invasive and reproducible photochemical cortical lesion model for mouse stroke studies. *Journal of Visualized Experiments,* 76**,** 50370.

LAI, J. P., DOUGLAS, S. D. & HO, W. Z. 1998. Human lymphocytes express substance P and its receptor. *Journal of Neuroimmunology,* 86**,** 80-6.

LAKHAN, S. E., KIRCHGESSNER, A., TEPPER, D. & LEONARD, A. 2013. Matrix metalloproteinases and blood-brain barrier disruption in acute ischaemic stroke. *Frontiers in Neurology,* 4**,** 32.

LALETIN, V. S. & BYKOV, Y. N. 2015. General anesthetics as a factor of effective neuroprotection in ischaemic stroke models. *Biomeditsinskaya Khimiya,* 61**,** 440-8.

LAMAGNA, C., MEDA, P., MANDICOURT, G., BROWN, J., GILBERT, R. J. C., JONES, E. Y., KIEFER, F., RUGA, P., IMHOF, B. A. & AURRAND-LIONS, M. 2005. Dual Interaction of JAM-C with JAM-B and αMβ2Integrin: Function in Junctional Complexes and Leukocyte Adhesion. *Molecular Biology of the Cell,* 16**,** 4992-5003.

LANGE, M., ENKHBAATAR, P., TRABER, D. L., COX, R. A., JACOB, S., MATHEW, B. P., HAMAHATA, A., TRABER, L. D., HERNDON, D. N. & HAWKINS, H. K. 2009. Role of calcitonin gene-related peptide (CGRP) in ovine burn and smoke inhalation injury. *Journal of Applied Physiology,* 107**,** 176-84.

LANGFITT, T. W., TANNANBAUM, H. M. & KASSEL, N. 1966. The etiology of acute brain swelling following experimental head injury. *Journal of Neurosurgery,* 24**,** 47-56.

LAVINIO, A. & MENON, D. K. 2011. Intracranial pressure: Why we monitor it, how to monitor it, what to do with the number and what's the future? *Current Opinion in Anaesthesiology,* 24**,** 117-123.

LAWRENCE, T. L. J., FOWLER, V. R. & NOVAKOFSKI, J. E. 2012. *Growth of Farm Animals, 3rd Edition*, CABI.

LE LAY, S. & KURZCHALIA, T. V. 2005. Getting rid of caveolins: phenotypes of caveolin-deficient animals. *Biochimica et Biophysica Acta,* 1746**,** 322-33.

LEEMAN, S. E. & FERGUSON, S. L. 2000. Substance P: an historical perspective. *Neuropeptides,* 34**,** 249-254.

LEGAT, F. J., GRIESBACHER, T., SCHICHO, R., ALTHUBER, P., SCHULIGOI, R., KERL, H. & WOLF, P. 2002. Repeated subinflammatory ultraviolet B irradiation increases substance P and calcitonin gene-related peptide content and augments mustard oil-induced neurogenic inflammation in the skin of rats. *Neuroscience Letters,* 329**,** 309-13.

LEWIS, K. M., TURNER, R. J. & VINK, R. 2013. Blocking neurogenic inflammation for the treatment of acute disorders of the central nervous system. *International Journal of Inflammation,* 578480.

LI, P. C., CHEN, W. C., CHANG, L. C. & LIN, S. C. 2008. Substance P acts via the neurokinin receptor 1 to elicit bronchoconstriction, oxidative stress, and upregulated ICAM-1 expression after oil smoke exposure. *American Journal of Physiology-Lung Cellular and Molecular Physiology,* 294**,** L912-L920.

LI, Q., WU, X., YANG, Y., ZHANG, Y., HE, F., XU, X., ZHANG, Z., TAO, L. & LUO, C. 2019. Tachykinin NK1 receptor antagonist L-733,060 and substance P deletion exert neuroprotection through inhibiting oxidative stress and cell death after traumatic brain injury in mice. *The International Journal of Biochemistry & Cell Biology,* 107**,** 154-165.

LI, W. & YANG, S. 2016. Targeting oxidative stress for the treatment of ischaemic stroke: Upstream and downstream therapeutic strategies. *Brain Circulation,* 2**,** 153-163.

LI, X. J. & LI, S. 2012. Influence of Species Differences on the Neuropathology of Transgenic Huntington's Disease Animal Models. *Journal of Genetics and Genomics,* 39**,** 239-245.

AO, C. C., TSAI, Y. H., CHEN, Y. L., HUANG, K. C., CHIANG, I. J., WONG, J. M. & XIAO, F. 2015. Transcalvarial brain herniation volume after decompressive craniectomy is the difference between two spherical caps. *Medical Hypotheses,* 84**,** 183-8.

LIAO, C. C., CHEN, Y. F. & XIAO, F. 2018. Brain Midline Shift Measurement and Its Automation: A Review of Techniques and Algorithms. *International Journal of Biomedical Imaging,* 2018**,** 1-13.

LIANG, D., BHATTA, S., GERZANICH, V. & SIMARD, J. M. 2007. Cytotoxic edema: mechanisms of pathological cell swelling. *Neurosurgical Focus,* 22**,** E2.

LIEBESKIND, D. S., JÜTTLER, E., SHAPOVALOV, Y., YEGIN, A., LANDEN, J. & JAUCH, E. C. 2019. Cerebral Edema Associated With Large Hemispheric Infarction. *Stroke,* 50**,** 2619-2625.

LIGHTHALL, J. W. 1988. Controlled cortical impact: a new experimental brain injury model. *Journal of Neurotrauma,* 5**,** 1-15.

LILJA-CYRON, A., ANDRESEN, M., KELSEN, J., ANDREASEN, T. H., FUGLEHOLM, K. & JUHLER, M. 2019. Long-Term Effect of Decompressive Craniectomy on Intracranial Pressure and Possible Implications for Intracranial Fluid Movements. *Neurosurgery,* 1**,** 231-240.

LIM, J. E., CHUNG, E. & SON, Y. 2017. A neuropeptide, Substance-P, directly induces tissue-repairing M2 like macrophages by activating the PI3K/Akt/mTOR pathway even in the presence of IFNγ. *Scientific Reports,* 7.

LIN, H. C., PUROHIT, R. C. & POWE, T. A. 1997. Anaesthesia in sheep with propofol or with xylazine-ketamine followed by halothane. *Veterinary Surgery,* 26**,** 247-52.

LINFANTE, I., LLINAS, R. H., SCHLAUG, G., CHAVES, C., WARACH, S. & CAPLAN, L. R. 2001. Diffusion-Weighted Imaging and National Institutes of Health Stroke Scale in the Acute Phase of Posterior-Circulation Stroke. *Archives of Neurology,* 58.

LINKENHOKER, J. R., BURKHOLDER, T. H., LINTON, C. G. G., WALDEN, A., ABUSAKRAN-MONDAY, K. A., ROSERO, A. P. & FOLTZ, C. J. 2010. Effective and Safe Anaesthesia for Yorkshire and Yucatan Swine with and without Cardiovascular Injury and Intervention. *Journal of the American Association for Laboratory Animal Science,* 49**,** 344-351.

LIU, S., HU, W. X., ZU, Q. Q., LU, S. S., XU, X. Q., SUN, L., ZHOU, W. Z. & SHI, H. B. 2012. A novel embolic stroke model resembling lacunar infarction following proximal middle cerebral artery occlusion in beagle dogs. *Journal of Neuroscience Methods,* 209**,** 90-6.

LIU, Z., LIU, Q., CAI, H., XU, C., LIU, G. & LI, Z. 2011. Calcitonin gene-related peptide prevents blood-brain barrier injury and brain edema induced by focal cerebral ischaemia reperfusion. *Regulatory Peptides,* 171**,** 19-25.

LO, A. C., CHEN, A. Y., HUNG, V. K., YAW, L. P., FUNG, M. K., HO, M. C., TSANG, M. C., CHUNG, S. S. & CHUNG, S. K. 2005. Endothelin-1 Overexpression Leads to Further Water Accumulation and Brain Edema after Middle Cerebral Artery Occlusion via Aquaporin 4 Expression in Astrocytic End-Feet. *Journal of Cerebral Blood Flow & Metabolism,* 25**,** 998-1011.

LO, E. H., SINGHAL, A. B., TORCHILIN, V. P. & ABBOTT, N. J. 2001. Drug delivery to damaged brain. *Brain Research Reviews,* 38**,** 140-8.

LORENTE, L., MARTIN, M. M., ALMEIDA, T., HERNANDEZ, M., RAMOS, L., ARGUESO, M., CACERES, J. J., SOLE-VIOLAN, J. & JIMENEZ, A. 2015. Serum substance P levels are associated with severity and mortality in patients with severe traumatic brain injury. *Critical Care,* 19**,** 192.

LORENTE, L., MARTÍN, M. M., ALMEIDA, T., PÉREZ-CEJAS, A., RAMOS, L., ARGUESO, M., RIAÑO-RUIZ, M., SOLÉ-VIOLÁN, J., HERNÁNDEZ, M. & JIA, X. 2016. Serum Levels of Substance P and Mortality in Patients with a Severe Acute Ischaemic Stroke. *International Journal of Molecular Sciences,* 17**,** 991.

LORENTE, L., MARTÍN, M. M., GONZÁLEZ-RIVERO, A. F., PÉREZ-CEJAS, A., SABATEL, R., RAMOS-GÓMEZ, L., ARGUESO, M., CÁCERES, J. J., SOLÉ-VIOLÁN, J., JIMÉNEZ, A. & GARCÍA-MARÍN, V. 2020. Serum substance P levels and early mortality of spontaneous intracerebral haemorrhage patients. *Journal of Stroke and Cerebrovascular Diseases,* 29**,** 104893.

LORENZ, M. D., COATES, J. & KENT, M. 2010. *Handbook of Veterinary Neurology,* Philadelphia, Elsevier.

LU, T. S., AVRAHAM, H. K., SENG, S., TACHADO, S. D., KOZIEL, H., MAKRIYANNIS, A. & AVRAHAM, S. 2008. Cannabinoids inhibit HIV-1 Gp120-mediated insults in brain microvascular endothelial cells. *Journal of Immunology,* 181**,** 6406-16.

MA, H., CAMPBELL, B. C. V., PARSONS, M. W., CHURILOV, L., LEVI, C. R., HSU, C., KLEINIG, T. J., WIJERATNE, T., CURTZE, S., DEWEY, H. M., MITEFF, F., TSAI, C. H., LEE, J. T., PHAN, T. G., MAHANT, N., SUN, M. C., KRAUSE, M., STURM, J.,

GRIMLEY, R., CHEN, C. H., HU, C. J., WONG, A. A., FIELD, D., SUN, Y., BARBER, P. A., SABET, A., JANNES, J., JENG, J. S., CLISSOLD, B., MARKUS, R., LIN, C. H., LIEN, L. M., BLADIN, C. F., CHRISTENSEN, S., YASSI, N., SHARMA, G., BIVARD, A., DESMOND, P. M., YAN, B., MITCHELL, P. J., THIJS, V., CAREY, L., MERETOJA, A., DAVIS, S. M. & DONNAN, G. A. 2019. Thrombolysis Guided by Perfusion Imaging up to 9 Hours after Onset of Stroke. *New England Journal of Medicine,* 380**,** 1795-1803.

MACDONALD, R. L., PLUTA, R. M. & ZHANG, J. H. 2007. Cerebral vasospasm after subarachnoid hemorrhage: the emerging revolution. *Nature Clinical Practice Neurology,* 3**,** 256-63.

MACHADO, A. S., DARMOHRAY, D. M., FAYAD, J., MARQUES, H. G. & CAREY, M. R. 2015. A quantitative framework for whole-body coordination reveals specific deficits in freely walking ataxic mice. *eLife,* 4.

MACK, W. J., KING, R. G., HOH, D. J., COON, A. L., DUCRUET, A. F., HUANG, J., MOCCO, J., WINFREE, C. J., D'AMBROSIO, A. L., NAIR, M. N., SCIACCA, R. R. & CONNOLLY, E. S., JR. 2003. An improved functional neurological examination for use in nonhuman primate studies of focal reperfused cerebral ischaemia. *Neurological Research,* 25**,** 280-4.

MAEDA, M., TAKAMATSU, H., FURUICHI, Y., NODA, A., AWAGA, Y., TATSUMI, M., YAMAMOTO, M., ICHISE, R., NISHIMURA, S. & MATSUOKA, N. 2005. Characterization of a novel thrombotic middle cerebral artery occlusion model in monkeys that exhibits progressive hypoperfusion and robust cortical infarction. *Journal of Neuroscience Methods,* 146**,** 106-15.

MAENO, H., KIYAMA, H. & TOHYAMA, M. 1993. Distribution of the substance P receptor (NK-1 receptor) in the central nervous system. *Molecular Brain Research,* 18**,** 43-58.

MAGGI, C. A. 1995. The mammalian tachykinin receptors. *General Pharmacology,* 26**,** 911-44.

MAHAJAN, S. & BHAGAT, H. 2016. Cerebral oedema: Pathophysiological mechanisms and experimental therapies. *Journal of Neuroanaesthesiology and Critical Care,* 03**,** S22-S28.

MAIORIELLO, A. V., CHALJUB, G., NAUTA, H. J. & LACROIX, M. 2002. Chemical shift imaging of mannitol in acute cerebral ischaemia. Case report. *Journal of Neurosurgery,* 97**,** 687-91.

MAMA, K. 2002. Chapter 4 - Fluid Therapy A2 - Greene, Stephen A. *Veterinary Anaesthesia and Pain Management Secrets.* Philadelphia: Hanley & Belfus.

MANDALANENI, K., RAYI, A. & JILLELLA, D. V. 2020. Stroke Reperfusion Injury. *StatPearls.* Treasure Island (FL).

MANLEY, G. T., ROSENTHAL, G., LAM, M., MORABITO, D., YAN, D., DERUGIN, N., BOLLEN, A., KNUDSON, M. M. & PANTER, S. S. 2006. Controlled cortical impact in swine: pathophysiology and biomechanics. *Journal of Neurotrauma,* 23**,** 128-39.

MANNO, E. M., ADAMS, R. E., DERDEYN, C. P., POWERS, W. J. & DIRINGER, M. N. 1999. The effects of mannitol on cerebral edema after large hemispheric cerebral infarct. *Neurology,* 52**,** 583-7.

MANSOUR, N., DESOUZA, R. M., SIKORSKI, C., KAHANA, M. & FRIM, D. 2013. Role of barbiturate coma in the management of focally induced, severe cerebral edema in children. *Journal of Neurosurgery Pediatrics,* 12**,** 37-43.

MANTYH, C. R., GATES, T. S., ZIMMERMAN, R. P., WELTON, M. L., PASSARO, E. P., JR., VIGNA, S. R., MAGGIO, J. E., KRUGER, L. & MANTYH, P. W. 1988. Receptor binding sites for substance P, but not substance K or neuromedin K, are expressed in high concentrations by arterioles, venules, and lymph nodules in surgical specimens obtained from patients with ulcerative colitis and Crohn disease. *Proceedings of the National Academy of Sciences of the United States of America,* 85**,** 3235-9.

MANTYH, P., GATES, T., MANTYH, C. & MAGGIO, J. 1989. Autoradiographic localization and characterization of tachykinin receptor binding sites in the rat brain and peripheral tissues. *The Journal of Neuroscience,* 9**,** 258-279.

MARCHESE, G., PROCHAZKA, B. & WIDIMSKY, P. 2016. The importance of time: Time delays in acute stroke. *Cor et Vasa,* 58**,** e225-e232.

MARION, D. W., PUCCIO, A., WISNIEWSKI, S. R., KOCHANEK, P. M., DIXON, C. E., BULLIAN, L. & CARLIER, P. G. 2002. Effect of hyperventilation on extracellular concentrations of glutamate, lactate, pyruvate, and local cerebral blood flow in patients with severe traumatic brain injury. *Critical Care Medicine,* 30**,** 2619-2625.

MARKOWITZ, S., SAITO, K. & MOSKOWITZ, M. A. 1987. Neurogenically mediated leakage of plasma protein occurs from blood vessels in dura mater but not brain. *Journal of Neuroscience,* 7**,** 4129-36.

MARKUS, H. S. 2016. Stroke: causes and clinical features. *Medicine,* 44**,** 515-520.

MARKUS, H. S. 2004. Cerebral perfusion and stroke. *Journal of Neurology, Neurosurgery & Psychiatry,* 75**,** 353-361.

MARRIOTT, I. & BOST, K. L. 2000. IL-4 and IFN-γ Up-Regulate Substance P Receptor Expression in Murine Peritoneal Macrophages. *The Journal of Immunology,* 165**,** 182-191.

MARTINEZ, A. N. & PHILIPP, M. T. 2016. Substance P and Antagonists of the Neurokinin-1 Receptor in Neuroinflammation Associated with Infectious and Neurodegenerative Diseases of the Central Nervous System. *Journal of Neurological Neuromedicine,* 1**,** 29-36.

MARSHALL, J. W. B. & RIDLEY, R. M. 2003. Assessment of Cognitive and Motor Deficits in a Marmoset Model of Stroke. *Institute of Laboratory Animal Research Journal,* 44**,** 153-160.

MARTIN-PADURA, I., LOSTAGLIO, S., SCHNEEMANN, M., WILLIAMS, L., ROMANO, M., FRUSCELLA, P., PANZERI, C., STOPPACCIARO, A., RUCO, L., VILLA, A., SIMMONS, D. & DEJANA, E. 1998. Junctional adhesion molecule, a novel member of the immunoglobulin superfamily that distributes at intercellular junctions and modulates monocyte transmigration. *Journal of Cell Biology,* 142**,** 117-27.

MARTÍN-ARAGÓN BAUDEL, M. A. S., POOLE, A. V. & DARLISON, M. G. 2017. Chloride co-transporters as possible therapeutic targets for stroke. *Journal of Neurochemistry,* 140**,** 195-209.

MATHE, A. A., AGREN, H., LINDSTROM, L. & THEODORSSON, E. 1994. Increased concentration of calcitonin gene-related peptide in cerebrospinal fluid of depressed patients. A possible trait marker of major depressive disorder. *Neuroscience Letters,* 182**,** 138-42.

MATOS CASANO, H. A., TADI, P. & CIOFOAIA, G. A. 2020. Anterior Cerebral Artery Stroke. *StatPearls.* Treasure Island (FL).

MATTHEWS, J. N., ALTMAN, D. G., CAMPBELL, M. J. & ROYSTON, P. 1990. Analysis of serial measurements in medical research. *British Medical Journal,* 300**,** 230.

MAY, A. & GOADSBY, P. J. 2001a. Pharmacological opportunities and pitfalls in the therapy of migraine. *Current Opinions in Neurology,* 14**,** 341-5.

MAY, A. & GOADSBY, P. J. 2001b. Substance P receptor antagonists in the therapy of migraine. *Expert Opinion on Investigational Drugs,* 10**,** 673-8.

MCBRIDE, D. W., KLEBE, D., TANG, J. & ZHANG, J. H. 2015. Correcting for Brain Swelling's Effects on Infarct Volume Calculation After Middle Cerebral Artery Occlusion in Rats. *Translational Stroke Research,* 6**,** 323-338.

MCBRIDE, S. D., PERENTOS, N. & MORTON, A. J. 2016. A mobile, high-throughput semi-automated system for testing cognition in large non-primate animal models of Huntington disease. *Journal of Neuroscience Methods,* 265**,** 25-33.

MCCONALOGUE, K., DÉRY, O., LOVETT, M., WONG, H., WALSH, J. H., GRADY, E. F. & BUNNETT, N. W. 1999. Substance P-induced Trafficking of β-Arrestins. *Journal of Biological Chemistry,* 274**,** 16257-16268.

MCGARRY, B. L., DAMION, R. A., CHEW, I., KNIGHT, M. J., HARSTON, G. W., CARONE, D., JEZZARD, P., SITARAM, A., MUIR, K. W., CLATWORTHY, P. & KAUPPINEN, R. A. 2020. A Comparison of T2 Relaxation-Based MRI Stroke Timing Methods in Hyperacute Ischemic Stroke Patients: A Pilot Study. *Journal of Central Nervous System Disease,* 12**,** 117957352094331.

MCINTOSH, T. K., VINK, R., SOARES, H., HAYES, R. & SIMON, R. 1990. Effect of noncompetitive blockade of N-methyl-D-aspartate receptors on the neurochemical sequelae of experimental brain injury. *Journal of Neurochemisty,* 55**,** 1170-9.

MCLATCHIE, L. M., FRASER, N. J., MAIN, M. J., WISE, A., BROWN, J., THOMPSON, N., SOLARI, R., LEE, M. G. & FOORD, S. M. 1998. RAMPs regulate the transport and ligand specificity of the calcitonin-receptor-like receptor. *Nature,* 393**,** 333-9.

MEDINA, R., RAHNER, C., MITIC, L. L., ANDERSON, J. M. & VAN ITALLIE, C. M. 2000. Occludin localization at the tight junction requires the second extracellular loop. *Journal of Membrane Biology,* 178**,** 235-47.

MERALI, Z., WONG, T., LEUNG, J., GAO, M. M., MIKULIS, D. & KASSNER, A. 2015. Dynamic contrast-enhanced MRI and CT provide comparable measurement of blood-brain barrier permeability in a rodent stroke model. *Magnetic Resonance Imaging,* 33**,** 1007-12.

MESTRE, H., DU, T., SWEENEY, A. M., LIU, G., SAMSON, A. J., PENG, W., MORTENSEN, K. N., STÆGER, F. F., BORK, P. A. R., BASHFORD, L., TORO, E. R., TITHOF, J., KELLEY, D. H., THOMAS, J. H., HJORTH, P. G., MARTENS, E. A., MEHTA, R. I., SOLIS, O., BLINDER, P., KLEINFELD, D., HIRASE, H., MORI, Y. &

NEDERGAARD, M. 2020. Cerebrospinal fluid influx drives acute ischaemic tissue swelling. *Science,* 367**,** 7171.

MICHINAGA, S. & KOYAMA, Y. 2015. Pathogenesis of Brain Edema and Investigation into Anti-Edema Drugs. *International Journal of Molecular Sciences,* 16**,** 9949-9975.

MINEO, C., YING, Y. S., CHAPLINE, C., JAKEN, S. & ANDERSON, R. G. W. 1998. Targeting of Protein Kinase Cα to Caveolae. *Journal of Cell Biology,* 141**,** 601-610.

MINSHALL, R. D., TIRUPPATHI, C., VOGEL, S. M., NILES, W. D., GILCHRIST, A., HAMM, H. E. & MALIK, A. B. 2000. Endothelial Cell-Surface Gp60 Activates Vesicle Formation and Trafficking via Gi-Coupled Src Kinase Signaling Pathway. *Journal of Cell Biology,* 150**,** 1057-1070.

MOJTAHEDZADEH, M., AHMADI, A., MAHMOODPOOR, A., BEIGMOHAMMADI, M. T., ABDOLLAHI, M., KHAZAEIPOUR, Z., SHAKI, F., KUOCHAKI, B. & HENDOUEI, N. 2014. Hypertonic saline solution reduces the oxidative stress responses in traumatic brain injury patients. *Journal of Research in Medical Sciences,* 19**,** 867-74.

MOLLANJI, R., PAPAICONOMOU, C., BOULTON, M., MIDHA, R. & JOHNSTON, M. 2001. Comparison of cerebrospinal fluid transport in fetal and adult sheep. *American Journal of Physiology: Regulatory, Integrative and Comparative Physiology,* 281**,** R1215-23.

MONASTYRSKAYA, K., HOSTETTLER, A., BUERGI, S. & DRAEGER, A. 2005. T The NK1 receptor localizes to the plasma membrane microdomains, and its activation is dependent on lipid raft integrity. *Journal of Biological Chemistry,* 280**,** 7135-7146.

MONTAGNE, A., TOGA, A. W. & ZLOKOVIC, B. V. 2016. Blood-Brain Barrier Permeability and Gadolinium. *JAMA Neurology,* 73**,** 13.

MONTANER, J., MOLINA, C. A., MONASTERIO, J., ABILLEIRA, S., ARENILLAS, J. F., RIBO, M., QUINTANA, M. & ALVAREZ-SABIN, J. 2003. Matrix metalloproteinase-9 pretreatment level predicts intracranial hemorrhagic complications after thrombolysis in human stroke. *Circulation,* 107**,** 598-603.

MOONEN, C. T., PEKAR, J., DE VLEESCHOUWER, M. H., VAN GELDEREN, P., VAN ZIJL, P. C. & DESPRES, D. 1991. Restricted and anisotropic displacement of water in healthy cat brain and in stroke studied by NMR diffusion imaging. *Magnetic Resonance in Medicine,* 19**,** 327-332.

MORENO, M. J., COHEN, Z., STANIMIROVIC, D. B. & HAMEL, E. 1999. Functional calcitonin gene-related peptide type 1 and adrenomedullin receptors in human trigeminal ganglia, brain vessels, and cerebromicrovascular or astroglial cells in culture. *Journal of Cerebral Blood Flow & Metabolism,* 19**,** 1270-8.

MORI, K., AOKI, A., YAMAMOTO, T., HORINAKA, N. & MAEDA, M. 2001. Aggressive decompressive surgery in patients with massive hemispheric embolic cerebral infarction associated with severe brain swelling. *Acta Neurochirurgica,* 143**,** 483-91.

MORTON, A. J. & AVANZO, L. 2011. Executive Decision-Making in the Domestic Sheep.(Research Article). *PLOS ONE,* 6**,** e15752.

MORTON, A. J., RUDIGER, S. R., WOOD, N. I., SAWIAK, S. J., BROWN, G. C., MCLAUGHLAN, C. J., KUCHEL, T. R., SNELL, R. G., FAULL, R. L. M. & BAWDEN,

C. S. 2014. Early and progressive circadian abnormalities in Huntington's disease sheep are unmasked by social environment. *Human Molecular Genetics,* 23**,** 3375-3383.

MOUNT, C. A. & J, M. D. 2021. Cerebral Perfusion Pressure. *StatPearls.* Treasure Island (FL).

MUIR, K. W. 2013. Stroke. *Medicine,* 41**,** 169-174.

MUIZELAAR, J. P., WEI, E. P., KONTOS, H. A. & BECKER, D. P. 1983. Mannitol causes compensatory cerebral vasoconstriction and vasodilation in response to blood viscosity changes. *Journal of Neurosurgery,* 59**,** 822-8.

MUN-BRYCE, S. & ROSENBERG, G. A. 1998. Gelatinase B modulates selective opening of the blood-brain barrier during inflammation. *American Journal of Physiology,* 274**,** R1203-11.

MUNAKOMI, S. & J, M. D. 2020. Brain Herniation. *StatPearls.* Treasure Island (FL).

MUNOZ, C. A., CAMPBELL, A. J. D., HEMSWORTH, P. H. & DOYLE, R. E. 2019. Evaluating the welfare of extensively managed sheep. *PLOS ONE,* 14**,** e0218603.

MURR, R., SCHURER, L., BERGER, S., ENZENBACH, R., PETER, K. & BAETHMANN, A. 1993. Effects of isoflurane, fentanyl, or thiopental anaesthesia on regional cerebral blood flow and brain surface PO2 in the presence of a focal lesion in rabbits. *Anesthesia & Analgesia,* 77**,** 898-907.

MURTHA, L. A., MCLEOD, D. D., PEPPERALL, D., MCCANN, S. K., BEARD, D. J., TOMKINS, A. J., HOLMES, W. M., MCCABE, C., MACRAE, I. M. & SPRATT, N. J.

2015. Intracranial Pressure Elevation after Ischaemic Stroke in Rats: Cerebral Edema is not the only Cause, and Short-Duration Mild Hypothermia is a Highly Effective Preventive Therapy. *Journal of Cerebral Blood Flow & Metabolism,* 35**,** 2109-2109.

MUSAEUS, C. S., GLEERUP, H. S., HØGH, P., WALDEMAR, G., HASSELBALCH, S. G. & SIMONSEN, A. H. 2020. Cerebrospinal Fluid/Plasma Albumin Ratio as a Biomarker for Blood-Brain Barrier Impairment Across Neurodegenerative Dementias. *Journal of Alzheimer's Disease,* 75**,** 429-436.

MUÑOZ, M. & COVEÑAS, R. 2020. The Neurokinin-1 Receptor Antagonist Aprepitant: An Intelligent Bullet against Cancer? *Cancers,* 12**,** 2682.

NAG, S., VENUGOPALAN, R. & STEWART, D. J. 2007. Increased caveolin-1 expression precedes decreased expression of occludin and claudin-5 during blood-brain barrier breakdown. *Acta Neuropathologica,* 114**,** 459-69.

NANDA, B. S. & GETTY, R. 1975. Arteria intercarotica caudalis and its homologue in the domestic animals. *Anatomischer Anzeiger,* 137**,** 110-5.

NAVARRO-OROZCO, D. & SANCHEZ-MANSO, J. C. 2020. Neuroanatomy, Middle Cerebral Artery. *StatPearls.* Treasure Island (FL).

NAWROTH, C., LANGBEIN, J., COULON, M., GABOR, V., OESTERWIND, S., BENZ-SCHWARZBURG, J. & VON BORELL, E. 2019. Farm Animal Cognition—Linking Behavior, Welfare and Ethics. *Frontiers in Veterinary Science,* 6.

NECKEL, N. D., DAI, H. & BREGMAN, B. S. 2013. Quantifying changes following spinal cord injury with velocity dependent locomotor measures. *Journal of Neuroscience Methods,* 214**,** 27-36.

NEHLS, D. G., CARTWRIGHT, M. & SPETZLER, R. F. 1986. Experimental primate stroke model. *Neurosurgery,* 18**,** 388.

NEUMAR, R. W. 2000. Molecular mechanisms of ischaemic neuronal injury. *Annals of Emergency Medicine,* 36**,** 483-506.

NG, I., LIM, J. & WONG, H. B. 2004. Effects of head posture on cerebral hemodynamics: its influences on intracranial pressure, cerebral perfusion pressure, and cerebral oxygenation. *Neurosurgery,* 54**,** 593-7.

NIELSEN, T. R., KORNUM, B. R., MOUSTGAARD, A., GADE, A., LIND, N. M. & KNUDSEN, G. M. 2009. A novel spatial Delayed Non-Match to Sample (DNMS) task in the Gottingen minipig. *Behavioral Brain Research,* 196**,** 93-8.

NIMMO, A. J., CERNAK, I., HEATH, D. L., HU, X., BENNETT, C. J. & VINK, R. 2004. Neurogenic inflammation is associated with development of edema and functional deficits following traumatic brain injury in rats. *Neuropeptides,* 38**,** 40-7.

NING, M., FURIE, K. L., KOROSHETZ, W. J., LEE, H., BARRON, M., LEDERER, M., WANG, X., ZHU, M., SORENSEN, A. G., LO, E. H. & KELLY, P. J. 2006. Association between tPA therapy and raised early matrix metalloproteinase-9 in acute stroke. *Neurology,* 66**,** 1550-5.

NISHIMURA, A., TAKASHIMA, S., MITO, T. & BECKER, L. E. 1994. Aberrant distribution of tyrosine hydroxylase and substance P in infants with brain stem infarction. *Acta Paediatrica Japonica,* 36**,** 355-360.

NITTA, T., HATA, M., GOTOH, S., SEO, Y., SASAKI, H., HASHIMOTO, N., FURUSE, M. & TSUKITA, S. 2003. Size-selective loosening of the blood-brain barrier in claudin-5-deficient mice. *Journal of Cell Biology,* 161**,** 653-60.

NITZSCHE, B., FREY, S., COLLINS, L. D., SEEGER, J., LOBSIEN, D., DREYER, A., KIRSTEN, H., STOFFEL, M. H., FONOV, V. S. & BOLTZE, J. 2015. A stereotaxic, population-averaged T1w ovine brain atlas including cerebral morphology and tissue volumes. *Frontiers in Neuroanatomy,* 9**,** 69.

NOGLES, T. E. & GALUSKA, M. A. 2020. Middle Cerebral Artery Stroke. *StatPearls.* Treasure Island (FL).

NOGUEIRA, R. G., JADHAV, A. P., HAUSSEN, D. C., BONAFE, A., BUDZIK, R. F., BHUVA, P., YAVAGAL, D. R., RIBO, M., COGNARD, C., HANEL, R. A., SILA, C. A., HASSAN, A. E., MILLAN, M., LEVY, E. I., MITCHELL, P., CHEN, M., ENGLISH, J. D., SHAH, Q. A., SILVER, F. L., PEREIRA, V. M., MEHTA, B. P., BAXTER, B. W., ABRAHAM, M. G., CARDONA, P., VEZNEDAROGLU, E., HELLINGER, F. R., FENG, L., KIRMANI, J. F., LOPES, D. K., JANKOWITZ, B. T., FRANKEL, M. R., COSTALAT, V., VORA, N. A., YOO, A. J., MALIK, A. M., FURLAN, A. J., RUBIERA, M., AGHAEBRAHIM, A., OLIVOT, J. M., TEKLE, W. G., SHIELDS, R., GRAVES, T., LEWIS, R. J., SMITH, W. S., LIEBESKIND, D. S., SAVER, J. L., JOVIN, T. G. &

INVESTIGATORS, D. T. 2018. Thrombectomy 6 to 24 Hours after Stroke with a Mismatch between Deficit and Infarct. *New England Journal of Medicine,* 378**,** 11-21.

NOGUEIRA, R. G., LEVY, E. I., GOUNIS, M. & SIDDIQUI, A. H. 2012. The Trevo device: preclinical data of a novel stroke thrombectomy device in two different animal models of arterial thrombo-occlusive disease. *Journal of Neurointerventional Surgery,* 4**,** 295-300.

O'COLLINS, V. E., MACLEOD, M. R., DONNAN, G. A., HORKY, L. L., VAN DER WORP, B. H. & HOWELLS, D. W. 2006. 1,026 experimental treatments in acute stroke. *Annals of Neurology,* 59**,** 467-77.

O'DONNELL, M. E., CHEN, Y. J., LAM, T. I., TAYLOR, K. C., WALTON, J. H. & ANDERSON, S. E. 2013. Intravenous HOE-642 reduces brain edema and Na uptake in the rat permanent middle cerebral artery occlusion model of stroke: evidence for participation of the blood-brain barrier Na/H exchanger. *Journal of Cerebral Blood Flow & Metabolism,* 33**,** 225-34.

O'DONNELL, M. E., TRAN, L., LAM, T. I., LIU, X. B. & ANDERSON, S. E. 2004. Bumetanide inhibition of the blood-brain barrier Na-K-Cl cotransporter reduces edema formation in the rat middle cerebral artery occlusion model of stroke. *Journal of Cerebral Blood Flow & Metabolism,* 24**,** 1046-56.

OCHFELD, E., NEWHART, M., MOLITORIS, J., LEIGH, R., CLOUTMAN, L., DAVIS, C., CRINION, J. & HILLIS, A. E. 2010. Ischaemia in broca area is associated with broca aphasia more reliably in acute than in chronic stroke. *Stroke,* 41**,** 325-30.

OGUN, S. A. & ODUSOTE, K. A. 2001. Effectiveness of high dose dexamethasone in the treatment of acute stroke. *West African Journal of Medicine,* 20**,** 1-6.

OHTORI, S., TAKAHASHI, K., CHIBA, T., YAMAGATA, M., SAMEDA, H. & MORIYA, H. 2002. Substance P and calcitonin gene-related peptide immunoreactive sensory DRG neurons innervating the lumbar intervertebral discs in rats. *Annals of Anatomy,* 184**,** 235-40.

OKU, R., SATOH, M., FUJII, N., OTAKA, A., YAJIMA, H. & TAKAGI, H. 1987. Calcitonin gene-related peptide promotes mechanical nociception by potentiating release of substance P from the spinal dorsal horn in rats. *Brain Research,* 403**,** 350-4.

OLSEN, T. S., SKRIVER, E. B. & HERNING, M. 1985. Cause of cerebral infarction in the carotid territory. Its relation to the size and the location of the infarct and to the underlying vascular lesion. *Stroke,* 16**,** 459-66.

OMEIS, I., NEIL, J. A., MURALI, R. & ABRAHAMS, J. M. 2008. Treatment of cerebral vasospasm with biocompatible controlled-release systems for intracranial drug delivery. *Neurosurgery,* 63**,** 1011-9.

ORSER, B. A., PENNEFATHER, P. S. & MACDONALD, J. F. 1997. Multiple mechanisms of ketamine blockade of N-methyl-D-aspartate receptors. *Anesthesiology,* 86**,** 903-17.

OTSUKA, M. & YOSHIOKA, K. 1993. Neurotransmitter functions of mammalian tachykinins. *Physiological Reviews,* 73**,** 229-308.

OVBIAGELE, B., GOLDSTEIN, L. B., HIGASHIDA, R. T., HOWARD, V. J., JOHNSTON, S. C., KHAVJOU, O. A., LACKLAND, D. T., LICHTMAN, J. H., MOHL,

S., SACCO, R. L., SAVER, J. L., TROGDON, J. G., AMERICAN HEART ASSOCIATION ADVOCACY COORDINATING, C. & STROKE, C. 2013. Forecasting the future of stroke in the United States: a policy statement from the American Heart Association and American Stroke Association. *Stroke,* 44**,** 2361-75.

ÖZUGUR, S., KUNZ, L. & STRAKA, H. 2020. Relationship between oxygen consumption and neuronal activity in a defined neural circuit. *BMC Biology,* 18.

PAPAGIANNI, M., TZIOMALOS, K., KOSTAKI, S., ANGELOPOULOU, S.-M., CHRISTOU, K., BOUZIANA, S. D., VERGOU, M., DIDANGELOS, T., SAVOPOULOS, C. & HATZITOLIOS, A. I. 2018. Treatment with Mannitol is Associated with Increased Risk for In-Hospital Mortality in Patients with Acute Ischaemic Stroke and Cerebral Edema. *American Journal of Cardiovascular Drugs,* 18**,** 397-403.

PARTON, R. G. & SIMONS, K. 2007. The multiple faces of caveolae. *Nature Reviews Molecular Cell Biology,* 8**,** 185-94.

PARVATANENI, K., PLOEG, L., OLNEY, S. J. & BROUWER, B. 2009. Kinematic, kinetic and metabolic parameters of treadmill versus overground walking in healthy older adults. *Clinical Biomechanics,* 24**,** 95-100.

PASCOE, P. J. 2012. Chapter 17 - Perioperative Management of Fluid Therapy A2 - DiBartola, Stephen P. *Fluid, Electrolyte, and Acid-Base Disorders in Small Animal Practice (Fourth Edition).* Saint Louis: W.B. Saunders.

PATEL, P. M., DRUMMOND, J. C. & COLE, D. J. 1991. Induced hypertension during restoration of flow after temporary middle cerebral artery occlusion in the rat: Effect on neuronal injury and edema. *Surgical Neurology,* 36**,** 195-201.

PEHAM, C., GIRTLER, D., KICKER, C. & LICKA, T. 2006. Raising heels of hind hooves changes the equine coffin, fetlock and hock joint angle: a kinematic evaluation on the treadmill at walk and trot. *Equine Veterinary Journal,* 38**,** 427-430.

PELOSI, P., CROCI, M., RAVAGNAN, I., TREDICI, S., PEDOTO, A., LISSONI, A. & GATTINONI, L. 1998. The effects of body mass on lung volumes, respiratory mechanics, and gas exchange during general anaesthesia. *Anesthesia & Analgesia,* 87**,** 654-60.

PERCIE DU SERT, N., HURST, V., AHLUWALIA, A., ALAM, S., AVEY, M. T., BAKER, M., BROWNE, W. J., CLARK, A., CUTHILL, I. C., DIRNAGL, U., EMERSON, M., GARNER, P., HOLGATE, S. T., HOWELLS, D. W., KARP, N. A., LAZIC, S. E., LIDSTER, K., MACCALLUM, C. J., MACLEOD, M., PEARL, E. J., PETERSEN, O. H., RAWLE, F., REYNOLDS, P., ROONEY, K., SENA, E. S., SILBERBERG, S. D., STECKLER, T. & WÜRBEL, H. 2020. The ARRIVE guidelines 2.0: Updated guidelines for reporting animal research. *PLOS Biology,* 18**,** e3000410.

PEREL, P., ROBERTS, I., SENA, E., WHEBLE, P., BRISCOE, C., SANDERCOCK, P., MACLEOD, M., MIGNINI, L. E., JAYARAM, P. & KHAN, K. S. 2007. Comparison of treatment effects between animal experiments and clinical trials: systematic review. *British Medical Journal,* 334**,** 197.

PERSIDSKY, Y., RAMIREZ, S. H., HAORAH, J. & KANMOGNE, G. D. 2006. Blood-brain barrier: structural components and function under physiologic and pathologic conditions. *Journal of Neuroimmune Pharmacology,* 1**,** 223-36.

PETTY, M. A. & WETTSTEIN, J. G. 1999. White matter ischaemia. *Brain Research Reviews,* 31**,** 58-64.

PFENNINGER, E. G., REITH, A., BREITIG, D., GRUNERT, A. & AHNEFELD, F. W. 1989. Early changes of intracranial pressure, perfusion pressure, and blood flow after acute head injury. Part 1: An experimental study of the underlying pathophysiology. *Journal of Neurosurgery,* 70**,** 774-9.

PHILIP, M., BENATAR, M., FISHER, M. & SAVITZ, S. I. 2009. Methodological quality of animal studies of neuroprotective agents currently in phase II/III acute ischaemic stroke trials. *Stroke,* 40**,** 577-81.

PINTO, V. L., TADI, P. & ADEYINKA, A. 2020. Increased Intracranial Pressure. *StatPearls.* Treasure Island (FL).

PITTENGER, S. T., SWALVE, N., CHOU, S., SMITH, M. D., HOONAKKER, A. J., PUDIAK, C. M., FLECKENSTEIN, A. E., HANSON, G. R. & BEVINS, R. A. 2016. Sex differences in neurotensin and substance P following nicotine self-administration in rats. *Synapse,* 70**,** 336-346.

PLATT, S. R., HOLMES, S. P., HOWERTH, E. W., DUBERSTEIN, K. J., DOVE, C. R., KINDER, H. A., WYATT, E. L., LINVILLE, A. V., LAU, V. W., STICE, S. L., HILL, W. D., HESS, D. C. & WEST, F. D. 2014. Development and characterization of a Yucatan miniature biomedical pig permanent middle cerebral artery occlusion stroke model. *Experimental & Translational Stroke Medicine,* 6**,** 5.

POVLISHOCK, J. T., BECKER, D. P., SULLIVAN, H. G. & MILLER, J. D. 1978. Vascular permeability alterations to horseradish peroxidase in experimental brain injury. *Brain Research,* 153**,** 223-239.

PRAETORIUS, J. & DAMKIER, H. H. 2017. Transport across the choroid plexus epithelium. *American Journal of Physiology-Cell Physiology,* 312**,** C673-C686.

PUIG, J., SHANKAR, J., LIEBESKIND, D., TERCENO, M., NAEL, K., DEMCHUK, A. M., MENON, B., DOWLATSHAHI, D., LEIVA-SALINAS, C., WINTERMARK, M., THOMALLA, G., SILVA, Y., SERENA, J., PEDRAZA, S. & ESSIG, M. 2020. From "Time is Brain" to "Imaging is Brain": A Paradigm Shift in the Management of Acute Ischemic Stroke. *Journal of Neuroimaging*.

QIZILBASH, N., LEWINGTON, S. L. & LOPEZ-ARRIETA, J. M. 2002. Corticosteroids for acute ischaemic stroke. *Cochrane Database of Systematic Reviews***,** Cd000064.

QUINLAN, G. J., MARTIN, G. S. & EVANS, T. W. 2005. Albumin: biochemical properties and therapeutic potential. *Hepatology,* 41**,** 1211-1219.

QUINLAN, K. L., NAIK, S. M., CANNON, G., ARMSTRONG, C. A., BUNNETT, N. W., ANSEL, J. C. & CAUGHMAN, S. W. 1999. Substance P activates coincident NF-AT- and NF-kappa B-dependent adhesion molecule gene expression in microvascular endothelial cells through intracellular calcium mobilization. *Journal of Immunology,* 163**,** 5656-65.

QUINN, T., PAOLUCCI, S., SUNNERHAGEN, K., SIVENIUS, J., WALKER, M., TONI, D. & LEES, K. 2009. Evidence-based stroke rehabilitation: an expanded guidance document from the european stroke organisation (ESO) guidelines for management of ischaemic stroke and transient ischaemic attack 2008. *Journal of Rehabilitation Medicine,* 41**,** 99-111.

QURESHI, A. I., BOULOS, A. S., HANEL, R. A., SURI, M. F., YAHIA, A. M., ALBERICO, R. A. & HOPKINS, L. N. 2004. Randomized comparison of intra-arterial and

intravenous thrombolysis in a canine model of acute basilar artery thrombosis. *Neuroradiology,* 46**,** 988-95.

QURESHI, A. I., SUAREZ, J. I., YAHIA, A. M., MOHAMMAD, Y., UZUN, G., SURI, M. F., ZAIDAT, O. O., AYATA, C., ALI, Z. & WITYK, R. J. 2003. Timing of neurologic deterioration in massive middle cerebral artery infarction: a multicenter review. *Critical Care Medicine,* 31**,** 272-7.

RABINSTEIN, A. A. 2020. Update on Treatment of Acute Ischaemic Stroke. *Continuum (Minneapolis Minnesota),* 26**,** 268-286.

RAJSIC, S., GOTHE, H., BORBA, H. H., SROCZYNSKI, G., VUJICIC, J., TOELL, T. & SIEBERT, U. 2019. Economic burden of stroke: a systematic review on post-stroke care. *The European Journal of Health Economics,* 20**,** 107-134.

RAMNATH, R. D. & BHATIA, M. 2006. Substance P treatment stimulates chemokine synthesis in pancreatic acinar cells via the activation of NF-κB. *American Journal of Physiology-Gastrointestinal and Liver Physiology,* 291**,** G1113-G1119.

RASLAN, A. & BHARDWAJ, A. 2007. Medical management of cerebral edema. *Neurosurgical Focus,* 22**,** E12.

RASLEY, A., BOST, K. L., OLSON, J. K., MILLER, S. D. & MARRIOTT, I. 2002. Expression of functional NK-1 receptors in murine microglia. *Glia,* 37**,** 258-267.

REGOLI, D., BOUDON, A. & FAUCHERE, J. L. 1994. Receptors and antagonists for substance P and related peptides. *Pharmacological Reviews,* 46**,** 551-99.

REHNI, A. K., SINGH, T. G., JAGGI, A. S. & SINGH, N. 2008. Pharmacological preconditioning of the brain: a possible interplay between opioid and calcitonin gene related peptide transduction systems. *Pharmacological Reports,* 60**,** 904-13.

REID, S. J., PATASSINI, S., HANDLEY, R. R., RUDIGER, S. R., MCLAUGHLAN, C. J., OSMAND, A., JACOBSEN, J. C., MORTON, A. J., WEISS, A., WALDVOGEL, H. J., MACDONALD, M. E., GUSELLA, J. F., BAWDEN, C. S., FAULL, R. L. M. & SNELL, R. G. 2013. Further molecular characterisation of the OVT73 transgenic sheep model of Huntington's disease identifies cortical aggregates. *Journal of Huntington's Disease,* 2**,** 279.

REINHARD, M., RUTSCH, S. & HETZEL, A. 2012. Cerebral autoregulation in acute ischaemic stroke. *Perspectives in Medicine,* 1**,** 194.

REIS, P. A., ALBUQUERQUE, C. F. G. D., MARON-GUTIERREZ, T., SILVA, A. R. & NETO, H. C. D. C. F. 2017. Role of Nitric Oxide Synthase in the Function of the Central Nervous System under Normal and Infectious Conditions. *Nitric Oxide Synthase - Simple Enzyme-Complex Roles.* InTech.

RIBEIRO-DA-SILVA, A. & HOKFELT, T. 2000. Neuroanatomical localisation of Substance P in the CNS and sensory neurons. *Neuropeptides,* 34**,** 256-71.

RIEBOLD, T. 2002. Chapter 43 - Ruminant Anaesthesia A2 - Greene, Stephen A. *Veterinary Anaesthesia and Pain Management Secrets.* Philadelphia: Hanley & Belfus.

RIEGLER, M., CASTAGLIUOLO, I., SO, P. T., LOTZ, M., WANG, C., WLK, M., SOGUKOGLU, T., COSENTINI, E., BISCHOF, G., HAMILTON, G., TELEKY, B.,

WENZL, E., MATTHEWS, J. B. & POTHOULAKIS, C. 1999. Effects of substance P on human colonic mucosa in vitro. *American Journal of Physiology,* 276**,** G1473-83.

RILEY, P. O., PAOLINI, G., DELLA CROCE, U., PAYLO, K. W. & KERRIGAN, D. C. 2007. A kinematic and kinetic comparison of overground and treadmill walking in healthy subjects. *Gait & Posture,* 26**,** 17-24.

RINGER, A. J., GUTERMAN, L. R. & HOPKINS, L. N. 2004. Site-specific thromboembolism: a novel animal model for stroke. *American Journal of Neuroradiology,* 25**,** 329-32.

RINK, C., CHRISTOFORIDIS, G., ABDULJALIL, A., KONTZIALIS, M., BERGDALL, V., ROY, S., SEN, C. K 2008. Minimally invasive neuroradiologic model of preclinical transient middle cerebral artery occlusion in canines. *Proceedings of the National Academy of Sciences of the United States of America,* 105**,** 14100-14105.

ROBBA, C. & CITERIO, G. 2019. How I manage intracranial hypertension. *Critical Care,* 23.

ROBBINS, N. M. & SWANSON, R. A. 2014. Opposing effects of glucose on stroke and reperfusion injury: acidosis, oxidative stress, and energy metabolism. *Stroke,* 45**,** 1881-6.

ROBERTS, I. & SYDENHAM, E. 2012. Barbiturates for acute traumatic brain injury. *Cochrane Database of Systematic Reviews,* 12**,** CD000033.

ROBERTSON, S. A. 2002. Chapter 2 - Oxygenation and Ventilation A2 - Greene, Stephen A. *Veterinary Anaesthesia and Pain Management Secrets.* Philadelphia: Hanley & Belfus.

ROITBERG, B., KHAN, N., TUCCAR, E., KOMPOLITI, K., CHU, Y., ALPERIN, N., KORDOWER, J. H. & EMBORG, M. E. 2003. Chronic ischaemic stroke model in cynomolgus monkeys: behavioral, neuroimaging and anatomical study. *Neurology Research,* 25**,** 68-78.

ROPPER, A. H. 2014. Management of raised intracranial pressure and hyperosmolar therapy. *Practical Neurology,* 14**,** 152-8.

ROPPER, A. H. & SHAFRAN, B. 1984. Edema after stroke. Clinical syndrome and intracranial pressure. *Archives of Neurology,* 41**,** 26-29.

ROSELL, A., CUADRADO, E., ORTEGA-AZNAR, A., HERNANDEZ-GUILLAMON, M., LO, E. H. & MONTANER, J. 2008. MMP-9-positive neutrophil infiltration is associated to blood-brain barrier breakdown and basal lamina type IV collagen degradation during hemorrhagic transformation after human ischaemic stroke. *Stroke,* 39**,** 1121-6.

ROSENBERG, G. A., ESTRADA, E. Y. & DENCOFF, J. E. 1998. Matrix metalloproteinases and TIMPs are associated with blood-brain barrier opening after reperfusion in rat brain. *Stroke,* 29**,** 2189-95.

ROSENFELD, M. G., MERMOD, J. J., AMARA, S. G., SWANSON, L. W., SAWCHENKO, P. E., RIVIER, J., VALE, W. W. & EVANS, R. M. 1983. Production of a novel neuropeptide encoded by the calcitonin gene via tissue-specific RNA processing. *Nature,* 304**,** 129-35.

ROSNER, J., REDDY, V. & LUI, F. 2020. Neuroanatomy, Circle of Willis. *StatPearls.* Treasure Island (FL).

ROSS, D. T., MEANEY, D. F., SABOL, M. K., SMITH, D. H. & GENNARELLI, T. A. 1994. Distribution of forebrain diffuse axonal injury following inertial closed head injury in miniature swine. *Experimental Neurology,* 126(2)**,** 291-299.

ROSSI, J. 2009. Nonhuman primate research: the wrong way to understand needs and necessity. *American Journal of Bioethics,* 9**,** 21-3.

ROTH, G. & DICKE, U. 2005. Evolution of the brain and intelligence. *Trends in Cognive Science,* 9**,** 250-7.

ROWE, R. K., HARRISON, J. L., THOMAS, T. C., PAULY, J. R., ADELSON, P. D. & LIFSHITZ, J. 2013. Using anesthetics and analgesics in experimental traumatic brain injury. *Lab Animal,* 42**,** 286-91.

ROZANSKI, G. M., HUNTLEY, A. H., CROSBY, L. D., SCHINKEL-IVY, A., MANSFIELD, A. & PATTERSON, K. K. 2019. Lower limb muscle activity underlying temporal gait asymmetry post-stroke. Cold Spring Harbor Laboratory.

RUPNIAK, N. M. & KRAMER, M. S. 1999. Discovery of the antidepressant and anti-emetic efficacy of substance P receptor (NK1) antagonists. *Trends in Pharmacological Sciences,* 20**,** 485-90.

SACCO, R. L., KASNER, S. E., BRODERICK, J. P., CAPLAN, L. R., CONNORS, J. J., CULEBRAS, A., ELKIND, M. S., GEORGE, M. G., HAMDAN, A. D., HIGASHIDA, R. T., HOH, B. L., JANIS, L. S., KASE, C. S., KLEINDORFER, D. O., LEE, J. M., MOSELEY, M. E., PETERSON, E. D., TURAN, T. N., VALDERRAMA, A. L. & VINTERS, H. V. 2013. An updated definition of stroke for the 21st century: a statement for

healthcare professionals from the American Heart Association/American Stroke Association. *Stroke,* 44**,** 2064-89.

SAFAYI, S., JEFFERY, N. D., FREDERICKS, D. C., VILJOEN, S., DALM, B. D., REDDY, C. G., WILSON, S., GILLIES, G. T. & HOWARD, M. A. 2014. Biomechanical performance of an ovine model of intradural spinal cord stimulation. *Journal of Medical Engineering & Technology,* 38**,** 269-273.

SAFAYI, S., JEFFERY, N. D., SHIVAPOUR, S. K., ZAMANIGHOMI, M., ZYLSTRA, T. J., BRATSCH-PRINCE, J., WILSON, S., REDDY, C. G., FREDERICKS, D. C., GILLIES, G. T. & HOWARD, M. A., 3RD 2015. Kinematic analysis of the gait of adult sheep during treadmill locomotion: Parameter values, allowable total error, and potential for use in evaluating spinal cord injury. *Journal of the Neurological Sciences,* 358**,** 107-12.

SAFAYI, S., MILLER, J. W., WILSON, S., SHIVAPOUR, S. K., OELFKE, T. F., FORD, A. L., KLARMANN STAUDT, A., ABODE-IYAMAH, K., REDDY, C. G., JEFFERY, N. D., FREDERICKS, D. C., GILLIES, G. T. & HOWARD III, M. A. 2016. Treadmill measures of ambulation rates in ovine models of spinal cord injury and neuropathic pain. *Journal of Medical Engineering & Technology,* 40**,** 72-79.

SAIKALI, S., MEURICE, P., SAULEAU, P., ELIAT, P. A., BELLAUD, P., RANDUINEAU, G., VERIN, M. & MALBERT, C. H. 2010. A three-dimensional digital segmented and deformable brain atlas of the domestic pig. *Journal of Neuroscience Methods,* 192**,** 102-9.

SAITOU, M., FURUSE, M., SASAKI, H., SCHULZKE, J. D., FROMM, M., TAKANO, H., NODA, T. & TSUKITA, S. 2000. Complex phenotype of mice lacking occludin, a component of tight junction strands. *Molecular Biology of the Cell,* 11**,** 4131-42.

SAKOH, M., RØHL, L., GYLDENSTED, C., GJEDDE, A. & OSTERGAARD, L. 2000. Cerebral blood flow and blood volume measured by magnetic resonance imaging bolus tracking after acute stroke in pigs: comparison with (15)OH(2)O positron emission tomography. *Stroke,* 31**,** 1958.

SANDERCOCK, P. A. & SOANE, T. 2011. Corticosteroids for acute ischaemic stroke. *Cochrane Database of Systematic Reviews,* 2011**,** Cd000064.

SANDOZ, B., DUTSHKE, J., LIU, Q., MANAVIS, J., FINNIE, J. W., VINK, R. & ANDERSON, R. W. 2012. In vivo biomechanical response of ovine heads to shaken baby syndrome events. *Computer Methods in Biomechanical and Biomedical Engineering,* 15, 293-4.

SAVER, J. L. 2006. Time is brain-quantified. *Stroke,* 37**,** 263-6.

SAVER, J. L., JOHNSTON, K. C., HOMER, D., WITYK, R., KOROSHETZ, W., TRUSKOWSKI, L. L. & HALEY, E. C. 1999. Infarct volume as a surrogate or auxiliary outcome measure in ischaemic stroke clinical trials. The RANTTAS Investigators. *Stroke,* 30**,** 293-8.

SCHAAR, K. L., BRENNEMAN, M. M. & SAVITZ, S. I. 2010. Functional assessments in the rodent stroke model. *Experimental & Translational Stroke Medicine,* 2**,** 13.

SHELTON, T. J., PETER BECK, J., BLOEBAUM, R. D. & BACHUS, K. N. 2011. Percutaneous osseointegrated prostheses for amputees: Limb compensation in a 12-month ovine model. *Journal of Biomechanics,* 44**,** 2601-2606.

SCHIFILLITI, D., GRASSO, G., CONTI, A. & FODALE, V. 2010. Anaesthetic-Related Neuroprotection Intravenous or Inhalational Agents? *CNS Drugs,* 24**,** 893-907.

SCHOOK, L., BEATTIE, C., BEEVER, J., DONOVAN, S., JAMISON, R., ZUCKERMANN, F., NIEMI, S., ROTHSCHILD, M., RUTHERFORD, M. & SMITH, D. 2005. Swine in biomedical research: creating the building blocks of animal models. *Animal Biotechnology,* 16**,** 183-90.

SCHRATZBERGER, P., REINISCH, N., PRODINGER, W. M., KAHLER, C. M., SITTE, B. A., BELLMANN, R., FISCHER-COLBRIE, R., WINKLER, H. & WIEDERMANN, C. J. 1997. Differential chemotactic activities of sensory neuropeptides for human peripheral blood mononuclear cells. *Journal of Immunology,* 158**,** 3895-901.

SCHRECKINGER, M. & MARION, D. W. 2009. Contemporary Management of Traumatic Intracranial Hypertension: Is There a Role for Therapeutic Hypothermia? *Neurocritical Care,* 11**,** 427-436.

SCHUBERT, W., FRANK, P. G., RAZANI, B., PARK, D. S., CHOW, C. W. & LISANTI, M. P. 2001. Caveolae-deficient endothelial cells show defects in the uptake and transport of albumin in vivo. *Journal of Biological Chemistry,* 276**,** 48619-22.

SCHWAB, S., SPRANGER, M., SCHWARZ, S. & HACKE, W. 1997. Barbiturate coma in severe hemispheric stroke: useful or obsolete? *Neurology,* 48**,** 1608-13.

SCHWARTZ, A. E. & PILE-SPELLMAN, J. 2011. New model of reperfused stroke by occlusion of the anterior cerebral artery in baboons. *Acta Neurochirurgica,* 153**,** 327-331.

SCHWARTZ, L. M., JENNINGS, R. B. & REIMER, K. A. 1997. Premedication with the opioid analgesic butorphanol raises the threshold for ischaemic preconditioning in dogs. *Basic Research in Cardiology,* 92**,** 106-14.

SCHWARZ, S., GEORGIADIS, D., ASCHOFF, A. & SCHWAB, S. 2002. Effects of body position on intracranial pressure and cerebral perfusion in patients with large hemispheric stroke. *Stroke,* 33**,** 497-501.

SCHWARZ, S., SCHWAB, S., BERTRAM, M., ASCHOFF, A. & HACKE, W. 1998. Effects of hypertonic saline hydroxyethyl starch solution and mannitol in patients with increased intracranial pressure after stroke. *Stroke,* 29**,** 1550-5.

SEVERINI, C., IMPROTA, G., FALCONIERI-ERSPAMER, G., SALVADORI, S. & ERSPAMER, V. 2002. The tachykinin peptide family. *Pharmacological Reviews,* 54**,** 285-322.

SHAH, A., ALMENAWER, S. & HAWRYLUK, G. 2019. Timing of Decompressive Craniectomy for Ischaemic Stroke and Traumatic Brain Injury: A Review. *Frontiers in Neurology,* 10**,** 11-11.

SHAH, S. & KIMBERLY, W. T. 2016. Today's Approach to Treating Brain Swelling in the Neuro Intensive Care Unit. *Seminars in Neurology,* 36**,** 502-507.

SHAIBANI, A., KHAWAR, S., SHIN, W., CASHEN, T. A., SCHIRF, B., ROHANY, M., KAKODKAR, S. & CARROLL, T. J. 2006. First Results in an MR Imaging-Compatible Canine Model of Acute Stroke. *American Journal of Neuroradiology,* 27**,** 1788.

SHAO, B., ZHOU, Y. L., WANG, H. & LIN, Y. S. 2015. The role of calcitonin gene-related peptide in post-stroke depression in chronic mild stress-treated ischaemic rats. *Physiology & Behavior,* 139**,** 224-30.

SHELTON, T. J., PETER BECK, J., BLOEBAUM, R. D. & BACHUS, K. N. 2011. Percutaneous osseointegrated prostheses for amputees: Limb compensation in a 12-month ovine model. *Journal of Biomechanics,* 44**,** 2601-2606.

SHETH, K., ELM, J., HINSON, H., MOLYNEAUX, B., BESLOW, L., SZE, G., OSTWALDT, A.-C., DEL ZOPPO, G., SIMARD, J., JACOBSON, S. & KIMBERLY, W. 2016a. GAMES (Glyburide Advantage in Malignant Edema and Stroke) RP: A Phase II Study Toward Preventing Edema After Ischaemia (S7.004). *Neurology,* 86**,** S7.004.

SHETH, K. N., ELM, J. J., MOLYNEAUX, B. J., HINSON, H., BESLOW, L. A., SZE, G. K., OSTWALDT, A. C., DEL ZOPPO, G. J., SIMARD, J. M., JACOBSON, S. & KIMBERLY, W. T. 2016b. Safety and efficacy of intravenous glyburide on brain swelling after large hemispheric infarction (GAMES-RP): a randomised, double-blind, placebo-controlled phase 2 trial. *Lancet Neurology,* 15**,** 1160-9.

SIESJO, B. K., KATSURA, K. & KRISTIAN, T. 1996. Acidosis-related damage. *Advances in Neurology,* 71**,** 234-6.

SIFAT, A. E., VAIDYA, B. & ABBRUSCATO, T. J. 2017. Blood-Brain Barrier Protection as a Therapeutic Strategy for Acute Ischaemic Stroke. *American Association of Pharmaceutical Scientists Journal,* 19**,** 957-972.

SIMARD, J., SAHUQUILLO, J., SHETH, K., KAHLE, K. & WALCOTT, B. 2011. Managing Malignant Cerebral Infarction. *Current Treatment Options in Neurology,* 13**,** 217-229.

SIMARD, J. M., CHEN, M., TARASOV, K. V., BHATTA, S., IVANOVA, S., MELNITCHENKO, L., TSYMBALYUK, N., WEST, G. A. & GERZANICH, V. 2006. Newly expressed SUR1-regulated NC(Ca-ATP) channel mediates cerebral edema after ischaemic stroke. *Nature Medicine,* 12**,** 433-40.

SIMARD, J. M., KENT, T. A., CHEN, M., TARASOV, K. V. & GERZANICH, V. 2007. Brain oedema in focal ischaemia: molecular pathophysiology and theoretical implications. *Lancet Neurology,* 6**,** 258-268.

SIMEONIDIS, S., CASTAGLIUOLO, I., PAN, A., LIU, J., WANG, C.-C., MYKONIATIS, A., PASHA, A., VALENICK, L., SOUGIOULTZIS, S., ZHAO, D. & POTHOULAKIS, C. 2003. Regulation of the NK-1 receptor gene expression in human macrophage cells via an NF- B site on its promoter. *Proceedings of the National Academy of Sciences,* 100**,** 2957-2962.

SIMON, R. P. 2006. Acidotoxicity trumps excitotoxicity in ischaemic brain. *Archives of Neurology,* 63**,** 1368-71.

SIMS, N. R. & ANDERSON, M. F. 2002. Mitochondrial contributions to tissue damage in stroke. *Neurochemistry International,* 40**,** 511-26.

SIMÕES, A. L. B., SILVA, G. A. R., GIORGETTO, C., DE CASSIA DO CARMO-CAMPOS, E., DIAS, F. J. & FAZAN, V. P. S. 2018. Substance P in Dorsal Root Ganglion Neurons in Young and Adult Rats, after Nociceptive Stimulation during the Neonatal Period. *Anatomical Record,* 301**,** 849-861.

SKIDGEL, R. A., ENGELBRECHT, S., JOHNSON, A. R. & ERDÖS, E. G. 1984. Hydrolysis of substance p and neurotensin by converting enzyme and neutral endopeptidase. *Peptides,* 5**,** 769-76.

SKIDGEL, R. A. & ERDOS, E. G. 1987. Cleavage of peptide bonds by angiotensin I converting enzyme. *Agents and Actions Supplements,* 22**,** 289-96.

SMITH, J. M., JAMES, M. F., BOCKHORST, K. H. J., SMITH, M. I., BRADLEY, D. P., PAPADAKIS, N. G., CARPENTER, T. A., PARSONS, A. A., LESLIE, R. A., HALL, L. D. & HUANG, C. L. H. 2001. Investigation of feline brain anatomy for the detection of cortical spreading depression with magnetic resonance imaging. *Journal of Anatomy,* 198**,** 537-554.

SMITH, L. J. 2002. Chapter 23 - Hypotension A2 - Greene, Stephen A. *Veterinary Anaesthesia and Pain Management Secrets.* Philadelphia: Hanley & Belfus.

SMITH, W. S. & YAN, B. 2015. REVASCAT Trial. *Stroke,* 46**,** 3012-3013.

SMRCKA, M., OGILVY, C. S., CROW, R. J., MAYNARD, K. I., KAWAMATA, T. & AMES, A. 1998. Induced hypertension improves regional blood flow and protects against infarction during focal ischaemia: time course of changes in blood flow measured by laser Doppler imaging. *Neurosurgery,* 42**,** 617-24.

SOFRONIEW, M. V. 2000. Astrocyte failure as a cause of CNS dysfunction. *Molecular Psychiatry,* 5**,** 230-232.

SORBY-ADAMS, A. J., LEONARD, A. V., ELMS, L. E., MARIAN, O. C., HOVING, J. W., YASSI, N., VINK, R., THORNTON, E. & TURNER, R. J. 2019a. Determining the Temporal Profile of Intracranial Pressure Changes Following Transient Stroke in an Ovine Model. *Frontiers in Neuroscience,* 13**,** 587.

SORBY-ADAMS, A. J., LEONARD, A. V., HOVING, J. W., YASSI, N., VINK, R., WELLS, A. J. & TURNER, R. J. 2019b. NK1-r Antagonist Treatment Comparable to Decompressive Craniectomy in Reducing Intracranial Pressure Following Stroke. *Frontiers in Neuroscience,* 13**,** 681.

SORBY-ADAMS, A. J., MARCOIONNI, A. M., DEMPSEY, E. R., WOENIG, J. A. & TURNER, R. J. 2017. The Role of Neurogenic Inflammation in Blood-Brain Barrier Disruption and Development of Cerebral Oedema Following Acute Central Nervous System (CNS) Injury. *International Journal of Molecular Sciences,* 18**,** 1788.

SORBY-ADAMS, A. J., SCHNEIDER, W. T., GONCALVES, R. P., KNOLLE, F. & MORTON, A. J. 2021. Measuring executive function in sheep (Ovis aries) using visual stimuli in a semi-automated operant system. *Journal of Neuroscience Methods,* 351**,** 109009.

SORBY-ADAMS, A. J., VINK, R. & TURNER, R. J. 2018. Large animal models of stroke and traumatic brain injury as translational tools. *American Journal of Physiology Regulatory, Integrative and Comparative Physiology,* 315**,** R165-R190.

SOUZA, D. G., MENDONÇA, V. A., CASTRO, M. S. D. A., POOLE, S. & TEIXEIRA, M. M. 2002. Role of tachykinin NK receptors on the local and remote injuries following ischaemia and reperfusion of the superior mesenteric artery in the rat. *British Journal of Pharmacology,* 135**,** 303-312.

STAMATOVIC, S. M., JOHNSON, A. M., KEEP, R. F. & ANDJELKOVIC, A. V. 2016. Junctional proteins of the blood-brain barrier: New insights into function and dysfunction. *Tissue Barriers,* 4**,** e1154641.

STEINHOFF, M. S., VON MENTZER, B., GEPPETTI, P., POTHOULAKIS, C. & BUNNETT, N. W. 2014. Tachykinins and Their Receptors: Contributions to Physiological Control and the Mechanisms of Disease. *Physiological Reviews,* 94**,** 265-301.

STEINER, L. A. & ANDREWS, P. J. 2006. Monitoring the injured brain: ICP and CBF. *British Journal of Anaesthesia,* 97**,** 26-38.

STEINER, T., PILZ, J., SCHELLINGER, P., WIRTZ, R., FRIEDERICHS, V., ASCHOFF, A. & HACKE, W. 2001a. Multimodal online monitoring in middle cerebral artery territory stroke. *Stroke,* 32**,** 2500-6.

STEINER, T., RINGLEB, P. & HACKE, W. 2001b. Treatment options for large hemispheric stroke. *Neurology,* 57**,** S61-8.

STEINER, T., WEBER, R. & KRIEGER, D. 2001c. Increased intracerebral pressure following stroke. *Current Treatment Options in Neurology,* 3**,** 441-450.

STOCCHETTI, N., MAAS, A. I., CHIEREGATO, A. & VAN DER PLAS, A. A. 2005. Hyperventilation in head injury: a review. *Chest,* 127**,** 1812-27.

STOKUM, J. A., GERZANICH, V. & SIMARD, J. M. 2016. Molecular pathophysiology of cerebral edema. *Journal of Cerebral Blood Flow & Metabolism,* 36**,** 513-38.

STUMM, R., CULMSEE, C., SCHAFER, M. K., KRIEGLSTEIN, J. & WEIHE, E. 2001. Adaptive plasticity in tachykinin and tachykinin receptor expression after focal cerebral ischaemia is differentially linked to gabaergic and glutamatergic cerebrocortical circuits and cerebrovenular endothelium. *Journal of Neuroscience,* 21**,** 798-811.

SUGAWARA, T. & CHAN, P. H. 2003. Reactive oxygen radicals and pathogenesis of neuronal death after cerebral ischaemia. *Antioxidants & Redox Signaling,* 5**,** 597-607.

SURANI, S., LOCKWOOD, G., MACIAS, M. Y., GUNTUPALLI, B. & VARON, J. 2015. Hypertonic saline in elevated intracranial pressure: past, present, and future. *Journal of Intensive Care Medicine,* 30**,** 8-12.

SUTOO, D., YABE, K. & AKIYAMA, K. 1999. Quantitative imaging of substance P in the human brain using a brain mapping analyzer. *Neuroscience Research,* 35**,** 339-46.

SUVAS, S. 2017. Role of Substance P Neuropeptide in Inflammation, Wound Healing, and Tissue Homeostasis. *Journal of Immunology,* 199**,** 1543-1552.

SUZUKI, Y., YEUNG, A. C. & IKENO, F. 2011. The representative porcine model for human cardiovascular disease. *Journal of Biomedicine and Biotechnology,* 2011**,** 195483.

SYMON, L. 1960. Observations on the leptomeningeal collateral circulation in dogs. *Journal of Physiology,* 154**,** 1-14.

TAGAYA, M., LIU, K. F., COPELAND, B., SEIFFERT, D., ENGLER, R., GARCIA, J. H., & DEL ZOPPO, G. J. 1997. DNA scission after focal brain ischaemia: Temporal differences in two species. *Stroke,* 28**,** 1245-1254.

TAKAHASHI, K., TANAKA, A., HARA, M. & NAKANISHI, S. 1992. The primary structure and gene organization of human substance P and neuromedin K receptors. *European Journal of Biochemistry,* 204**,** 1025-1033.

TAM, C. & BRAIN, S. D. 2004. The assessment of vasoactive properties of CGRP and adrenomedullin in the microvasculature: a study using in vivo and in vitro assays in the mouse. *Journal Molecular Neuroscience,* 22**,** 117-24.

TANG, H. B., INOUE, A., IWASA, M., HIDE, I. & NAKATA, Y. 2006. Substance P release evoked by capsaicin or potassium from rat cultured dorsal root ganglion neurons is conversely modulated with bradykinin. *Journal of Neurochemistry,* 97**,** 1412-1418.

TAPPER, J. E., FUKUSHIMA, S., AZUMA, H., THORNTON, G. M., RONSKY, J. L., SHRIVE, N. G. & FRANK, C. B. 2006. Dynamic in vivo kinematics of the intact ovine stifle joint. *Journal of Orthopaedic Research,* 24**,** 782-792.

TAPPER, J. E., RONSKY, J. L., POWERS, M. J., SUTHERLAND, C., MAJIMA, T., FRANK, C. B. & SHRIVE, N. G. 2004. In vivo measurement of the dynamic 3-D kinematics of the ovine stifle joint. *Journal of Biomechanical Engineering,* 126**,** 301-5.

TATE, A. J., FISCHER, H., LEIGH, A. E. & KENDRICK, K. M. 2006. Behavioural and Neurophysiological Evidence for Face Identity and Face Emotion Processing in Animals. *Philosophical Transactions: Biological Sciences,* 361**,** 2155-2172.

THOMALLA, G., BOUTITIE, F., MA, H., KOGA, M., RINGLEB, P., SCHWAMM, L. H., WU, O., BENDSZUS, M., BLADIN, C. F., CAMPBELL, B. C. V., CHENG, B., CHURILOV, L., EBINGER, M., ENDRES, M., FIEBACH, J. B., FUKUDA-DOI, M., INOUE, M., KLEINIG, T. J., LATOUR, L. L., LEMMENS, R., LEVI, C. R., LEYS, D., MIWA, K., MOLINA, C. A., MUIR, K. W., NIGHOGHOSSIAN, N., PARSONS, M. W., PEDRAZA, S., SCHELLINGER, P. D., SCHWAB, S., SIMONSEN, C. Z., SONG, S. S., THIJS, V., TONI, D., HSU, C. Y., WAHLGREN, N., YAMAMOTO, H., YASSI, N., YOSHIMURA, S., WARACH, S., HACKE, W., TOYODA, K., DONNAN, G. A., DAVIS, S. M., GERLOFF, C., ACOSTA, B. R., AEGIDIUS, K., ALBIKER, C., ALEGIANI, A., ALMENDROTE, M., ALONSO, A., ALTHAUS, K., AMARENCO, P., AMIRI, H., ANDERS, B., ANICULAESEI, A., APPLETON, J., ARENILLAS, J., BACK, C., BÄHR, C., BARDUTZKY, J., BARONNET-CHAUVET, F., BATHE-PETERS, R., BAYER-KARPINSKA, A., BECERRA, J. L., BECK, C., BELCHÍ GUILLAMON, O., BENOIT, A., BERHOUNE, N., BINDILA, D., BIRCHENALL, J., BLANC-LASSERRE, K., BLANCO GONZALES, M., BOBINGER, T., BODECHTEL, U., BODIGUEL, E., BOJARYN, U., BONNET, L., BOUAMRA, B., BOURGEOIS, P., BOUTITIE, F., BREUER, L., BREYNAERT, L., BROUGHTON, D., BROUNS, R., BRUGIRARD, S., BRUNEEL, B., BUGGLE, F., CAKMAK, S., CALLEJA, A., CALVET, D., CARRERA, D., CHEN, H.-C.,

CHENG, B., CHERIPELLI, B., CHO, T. H., CHOE, C.-U., CHOY, L., CHRISTENSEN, H., CIATIPIS, M., et al. 2020. Intravenous alteplase for stroke with unknown time of onset guided by advanced imaging: systematic review and meta-analysis of individual patient data. *The Lancet,* 396**,** 1574-1584.

THOMALLA, G. T. J., KUCINSKI, T., SCHODER, V., FIEHLER, J., KNAB, R., ZEUMER, H., WEILLER, C. & RÖTHER, J. 2003. Prediction of Malignant Middle Cerebral Artery Infarction by Early Perfusion- and Diffusion-Weighted Magnetic Resonance Imaging. *Stroke,* 34**,** 1892-1899.

THOMAS, A. D., DETILLEUX, J., FLECKNELL, P. & SANDERSEN, C. 2017. Impact of Stroke Therapy Academic Industry Roundtable (STAIR) Guidelines on Peri-Anaesthesia Care for Rat Models of Stroke: A Meta-Analysis Comparing the Years 2005 and 2015. *PLOS ONE,* 21**,** p.e0170243.

THOMSEN, B., GAROSI, L., SKERRITT, G., RUSBRIDGE, C., SPARROW, T., BERENDT, M. & GREDAL, H. 2016. Neurological signs in 23 dogs with suspected rostral cerebellar ischaemic stroke. *Acta Veterinaria Scandinavica,* 58**,** 40.

THORÉN, M., AZEVEDO, E., DAWSON, J., EGIDO, J. A., FALCOU, A., FORD, G. A., HOLMIN, S., MIKULIK, R., OLLIKAINEN, J., WAHLGREN, N. & AHMED, N. 2017. Predictors for Cerebral Edema in Acute Ischemic Stroke Treated With Intravenous Thrombolysis. *Stroke,* 48**,** 2464-2471.

THORÉN, M., DIXIT, A., ESCUDERO-MARTÍNEZ, I., GDOVINOVÁ, Z., KLECKA, L., RAND, V.-M., TONI, D., VILIONSKIS, A., WAHLGREN, N. & AHMED, N. 2020. Effect

of Recanalization on Cerebral Edema in Ischemic Stroke Treated With Thrombolysis and/or Endovascular Therapy. *Stroke,* 51**,** 216-223.

THORUP, V. M., TOGERSEN, F. A., JORGENSEN, B. & JENSEN, B. R. 2007. Biomechanical gait analysis of pigs walking on solid concrete floor. *Animal,* 1**,** 708-15.

TONEATTO, S., FINCO, O., VAN DER PUTTEN, H., ABRIGNANI, S. & ANNUNZIATA, P. 1999. Evidence of blood-brain barrier alteration and activation in HIV-1 gp120 transgenic mice. *Aids,* 13**,** 2343-8.

TORNAVACA, O., CHIA, M., DUFTON, N., ALMAGRO, L. O., CONWAY, D. E., RANDI, A. M., SCHWARTZ, M. A., MATTER, K. & BALDA, M. S. 2015. ZO-1 controls endothelial adherens junctions, cell–cell tension, angiogenesis, and barrier formation. *Journal of Cell Biology,* 208**,** 821-838.

TOUTAIN, P. L., FERRAN, A. & BOUSQUET-MELOU, A. 2010. Species differences in pharmacokinetics and pharmacodynamics. *Handbook of Experimental Pharmacology***,** 19-48.

TOYODA, K. 2012. Anterior cerebral artery and Heubner's artery territory infarction. *Frontiers of Neurology and Neuroscience,* 30**,** 120-2.

TRAYSTMAN, R. J. 2003. Animal models of focal and global cerebral ischaemia. *Institute for Laboratory Animal Research,* 44**,** 85-95.

TREADWELL, S. & THANVI, B. 2010. *Malignant middle cerebral artery (MCA) infarction: Pathophysiology, diagnosis and management*.

TU, Z., YANG, W., YAN, S., GUO, X. & LI, X.-J. 2015. CRISPR/Cas9: a powerful genetic engineering tool for establishing large animal models of neurodegenerative diseases. *Molecular Neurodegeneration,* 10.

TURNER, R. J. 2007. *Characterising the role of substance P in acute ischaemic stroke,* The University of Adelaide.

TURNER, R. J. & VINK, R. 2007. Inhibition of neurogenic inflammation as a novel treatment for ischemic stroke. *Drug News Perspect,* 20**,** 221-6.

TURNER, R. J., BLUMBERGS, P. C., SIMS, N. R., HELPS, S. C., RODGERS, K. M. & VINK, R. 2006. Increased substance P immunoreactivity and edema formation following reversible ischaemic stroke. *Acta Neurochirurgica Supplement,* 96**,** 263-6.

TURNER, R. J., HELPS, S. C., THORNTON, E. & VINK, R. 2011. A substance P antagonist improves outcome when administered 4 h after onset of ischaemic stroke. *Brain Research,* 1393**,** 84-90.

TURNER, R. J. & SHARP, F. R. 2016. Implications of MMP9 for Blood Brain Barrier Disruption and Hemorrhagic Transformation Following Ischaemic Stroke. *Frontiers in Cellular Neuroscience,* 10**,** 56.

TURNER, R. J. & VINK, R. 2012. Combined tissue plasminogen activator and an NK1 tachykinin receptor antagonist: an effective treatment for reperfusion injury following acute ischaemic stroke in rats. *Neuroscience,* 220**,** 1-10.

TURNER, R. J. & VINK, R. 2013. The role of substance P in ischaemic brain injury. *Brain Science,* 3**,** 123-42.

TURNER, R. J. & VINK, R. 2014. NK1 tachykinin receptor treatment is superior to capsaicin pre-treatment in improving functional outcome following acute ischaemic stroke. *Neuropeptides,* 48**,** 267-72.

TYRELL, C. M., ROOS, M. A., RUDOLPH, K. S. & REISMAN, D. S. 2011. Influence of Systematic Increases in Treadmill Walking Speed on Gait Kinematics After Stroke. *Physical Therapy,* 91**,** 392-403.

VAHEDI, K., HOFMEIJER, J., JUETTLER, E., VICAUT, E., GEORGE, B., ALGRA, A., AMELINK, G. J., SCHMIEDECK, P., SCHWAB, S., ROTHWELL, P. M., BOUSSER, M.-G., VAN DER WORP, H. B. & HACKE, W. 2007a. Early decompressive surgery in malignant infarction of the middle cerebral artery: a pooled analysis of three randomised controlled trials. *Lancet Neurology,* 6**,** 215-222.

VAHEDI, K., VICAUT, E., MATEO, J., KURTZ, A., ORABI, M., GUICHARD, J. P., BOUTRON, C., COUVREUR, G., ROUANET, F., TOUZÉ, E., GUILLON, B., CARPENTIER, A., YELNIK, A., GEORGE, B., PAYEN, D. & BOUSSER, M. G. 2007b. Sequential-design, multicenter, randomized, controlled trial of early decompressive craniectomy in malignant middle cerebral artery infarction (DECIMAL Trial). *Stroke,* 38**,** 2506.

VAN DALEN, J. W., VAN CHARANTE, E. P. M., NEDERKOORN, P. J., VAN GOOL, W. A. & RICHARD, E. 2013. Poststroke Apathy. *Stroke,* 44**,** 851-860.

VAN IERSEL, M. B., OLDE RIKKERT, M. G. M. & BORM, G. F. 2007. A method to standardize gait and balance variables for gait velocity. *Gait & Posture,* 26**,** 226-230.

VARATHARAJ, A., LILJEROTH, M., DAREKAR, A., LARSSON, H. B. W., GALEA, I. & CRAMER, S. P. 2019. Blood–brain barrier permeability measured using dynamic contrast-enhanced magnetic resonance imaging: a validation study. *The Journal of Physiology,* 597**,** 699-709.

VARTY, G. B., COHEN-WILLIAMS, M. E. & HUNTER, J. C. 2003. The antidepressant-like effects of neurokinin NK1 receptor antagonists in a gerbil tail suspension test. *Behavoiural Pharmacology,* 14**,** 87-95.

VIDARSSON, L., THORNHILL, R. E., LIU, F., MIKULIS, D. J. & KASSNER, A. 2009. Quantitative permeability magnetic resonance imaging in acute ischemic stroke: how long do we need to scan? *Magnetic Resonance Imaging,* 27**,** 1216-1222.

VINK, R., BHATIA, K. D. & REILLY, P. L. 2008. The relationship between intracranial pressure and brain oxygenation following traumatic brain injury in sheep. *Acta Neurochirurgica Supplement,* 102**,** 189-92.

VINK, R., DONKIN, J. J., CRUZ, M. I., NIMMO, A. J. & CERNAK, I. 2004. A substance P antagonist increases brain intracellular free magnesium concentration after diffuse traumatic brain injury in rats. *Journal of the American College of Nutrition,* 23**,** 538S-540S.

VINK, R., GABRIELIAN, L. & THORNTON, E. 2017. The Role of Substance P in Secondary Pathophysiology after Traumatic Brain Injury. *Frontiers in Neurology,* 8.

VINK, R. & VAN DEN HEUVEL, C. 2010. Substance P antagonists as a therapeutic approach to improving outcome following traumatic brain injury. *Neurotherapeutics,* 7**,** 74-80.

VINK, R., YOUNG, A., BENNETT, C. J., HU, X., CONNOR, C. O., CERNAK, I. & NIMMO, A. J. 2003. Neuropeptide release influences brain edema formation after diffuse traumatic brain injury. *Acta Neurochirurgica Supplement,* 86**,** 257-60.

VIRANI, S. S., ALONSO, A., BENJAMIN, E. J., BITTENCOURT, M. S., CALLAWAY, C. W., CARSON, A. P., CHAMBERLAIN, A. M., CHANG, A. R., CHENG, S., DELLING, F. N., DJOUSSE, L., ELKIND, M. S. V., FERGUSON, J. F., FORNAGE, M., KHAN, S. S., KISSELA, B. M., KNUTSON, K. L., KWAN, T. W., LACKLAND, D. T., LEWIS, T. T., LICHTMAN, J. H., LONGENECKER, C. T., LOOP, M. S., LUTSEY, P. L., MARTIN, S. S., MATSUSHITA, K., MORAN, A. E., MUSSOLINO, M. E., PERAK, A. M., ROSAMOND, W. D., ROTH, G. A., SAMPSON, U. K. A., SATOU, G. M., SCHROEDER, E. B., SHAH, S. H., SHAY, C. M., SPARTANO, N. L., STOKES, A., TIRSCHWELL, D. L., VANWAGNER, L. B., TSAO, C. W., AMERICAN HEART ASSOCIATION COUNCIL ON, E., PREVENTION STATISTICS, C. & STROKE STATISTICS, S. 2020. Heart Disease and Stroke Statistics-2020 Update: A Report From the American Heart Association. *Circulation,* 141**,** e139-e596.

VISHWANATH, R. & MUKHERJEE, R. 1996. Substance P promotes lymphocyte-endothelial cell adhesion preferentially via LFA-1/ICAM-1 interactions. *Journal of Neuroimmunology,* 71**,** 163-171.

VLIET, R., SELLES, R. W., ANDRINOPOULOU, E. R., NIJLAND, R., RIBBERS, G. M., FRENS, M. A., MESKERS, C. & KWAKKEL, G. 2020. Predicting Upper Limb Motor Impairment Recovery after Stroke: A Mixture Model. *Annals of Neurology,* 87**,** 383-393.

WACHENFELT, H. V., PINZKE, S., NILSSON, C., OLSSON, O. & EHLORSSON, C. J. 2008. Gait analysis of unprovoked pig gait on clean and fouled concrete surfaces. *Biosystems Engineering,* 101**,** 376-382.

WALCOTT, B. P., MILLER, J. C., KWON, C. S., SHETH, S. A., HILLER, M., CRONIN, C. A., SCHWAMM, L. H., SIMARD, J. M., KAHLE, K. T., KIMBERLY, W. T. & SHETH, K. N. 2014. Outcomes in severe middle cerebral artery ischemic stroke. *Neurocritical Care,* 21**,** 20-6.

WANG, X., CAO, C., HUANG, J., YAO, J., HAI, T., ZHENG, Q., WANG, X., ZHANG, H., QIN, G., CHENG, J., WANG, Y., YUAN, Z., ZHOU, Q., WANG, H. & ZHAO, J. 2016. One-step generation of triple gene-targeted pigs using CRISPR/Cas9 system. *Scientific Reports,* 6**,** 20620.

WARDLAW, J. M., DOUBAL, F., ARMITAGE, P., CHAPPELL, F., CARPENTER, T., MUÑOZ MANIEGA, S., FARRALL, A., SUDLOW, C., DENNIS, M. & DHILLON, B. 2009. Lacunar stroke is associated with diffuse blood-brain barrier dysfunction. *Annals of Neurology,* 65**,** 194-202.

WARDLAW, J. M., FARRALL, A., ARMITAGE, P. A., CARPENTER, T., CHAPPELL, F., DOUBAL, F., CHOWDHURY, D., CVORO, V. & DENNIS, M. S. 2008. Changes in Background Blood–Brain Barrier Integrity Between Lacunar and Cortical Ischemic Stroke Subtypes. *Stroke,* 39**,** 1327-1332.

WATANABE, H., SAKOH, M., ANDERSEN, F., RODELL, A., SØRENSEN, J. C., ØSTERGAARD, L., MOURIDSEN, K. & CUMMING, P. 2007. Statistical mapping of effects of middle cerebral artery occlusion (MCAO) on blood flow and oxygen consumption in porcine brain. *Journal of Neuroscience Methods,* 160**,** 109-115.

WATSON, J. C., DOPPENBERG, E. M., BULLOCK, M. R., ZAUNER, A., RICE, M.R., ABRAHAM, D. & YOUNG, H. F. 1997. Effects of the Allosteric Modification of Hemoglobin on Brain Oxygen and Infarct Size in a Feline Model of Stroke. *Stroke,* 28**,** 1624-1630.

WAY, M. & HILL, G. E. 2011. Intraoperative end-tidal carbon dioxide concentrations: what is the target? *Anesthesiology Research and Practice,* 2011**,** 271539.

WEAVING, G., BATSTONE, G. F. & JONES, R. G. 2016. Age and sex variation in serum albumin concentration: an observational study. *Annals of Clinical Biochemistry,* 53**,** 106-111.

WEDEL, D. J., IAIZZO, P. A. & MILDE, J. H. 1991. Desflurane is a trigger of malignant hyperthermia in susceptible swine. *Anesthesiology,* 74**,** 508-12.

WELLS, A. J., VINK, R., BLUMBERGS, P. C., BROPHY, B. P., HELPS, S. C., KNOX, S. J. & TURNER, R. J. 2012. A surgical model of permanent and transient middle cerebral artery stroke in the sheep. *PLOS ONE,* 7**,** e42157.

WELLS, A. J., VINK, R., HELPS, S., KNOX, S. J., BLUMBERGS, P. C. & TURNER, R. J. 2015a. Elevated Intracranial Pressure and Cerebral Edema following Permanent MCA Occlusion in an Ovine Model. *PLOS ONE,* 10**,** e0130512.

WEST, F. & KAISER, E. 2020. Large animal ischemic stroke models: replicating human stroke pathophysiology. *Neural Regeneration Research,* 15**,** 1377.

WEST, G. A., GOLSHANI, K. J., DOYLE, K. P., LESSOV, N. S., HOBBS, T. R., KOHAMA, S. G., PIKE, M. M., KROENKE, C. D., GRAFE, M. R., SPECTOR, M. D., TOBAR, E. T., SIMON, R. P. & STENZEL-POORE, M. P. 2009. A new model of cortical stroke in the rhesus macaque. *Journal of Cerebral Blood Flow & Metabolism,* 29**,** 1175-86.

WIJDICKS, E. F., SHETH, K. N., CARTER, B. S., GREER, D. M., KASNER, S. E., KIMBERLY, W. T., SCHWAB, S., SMITH, E. E., TAMARGO, R. J. & WINTERMARK, M. 2014. Recommendations for the management of cerebral and cerebellar infarction with swelling: a statement for healthcare professionals from the American Heart Association/American Stroke Association. *Stroke,* 45**,** 1222-38.

WILKINSON, D. 2009. Trade-offs in suffering and wellbeing: the utilitarian argument for primate stroke research. *American Journal of Bioethics,* 9**,** 19-21.

WILLIAMS, T. M. & LISANTI, M. P. 2004. The caveolin proteins. *Genome Biology,* 5**,** 214.

WILSON, S., ABODE-IYAMAH, K. O., MILLER, J. W., REDDY, C. G., SAFAYI, S., FREDERICKS, D. C., JEFFERY, N. D., DEVRIES-WATSON, N. A., SHIVAPOUR, S. K., VILJOEN, S., DALM, B. D., GIBSON-CORLEY, K. N., JOHNSON, M. D., GILLIES, G. T. & HOWARD, M. A. 2017. An ovine model of spinal cord injury. *The Journal of Spinal Cord Medicine,* 40**,** 346-360.

WINTERMARK, M., ALBERS, G. W., BRODERICK, J. P., DEMCHUK, A. M., FIEBACH, J. B., FIEHLER, J., GROTTA, J. C., HOUSER, G., JOVIN, T. G., LEES, K. R., LEV, M. H., LIEBESKIND, D. S., LUBY, M., MUIR, K. W., PARSONS, M. W., VON KUMMER, R., WARDLAW, J. M., WU, O., YOO, A. J., ALEXANDROV, A. V., ALGER, J. R., AVIV, R. I., BAMMER, R., BARON, J. C., CALAMANTE, F., CAMPBELL, B. C., CARPENTER, T. C., CHRISTENSEN, S., COPEN, W. A., DERDEYN, C. P., HALEY, E. C., JR., KHATRI, P., KUDO, K., LANSBERG, M. G., LATOUR, L. L., LEE, T. Y., LEIGH, R., LIN, W., LYDEN, P., MAIR, G., MENON, B. K., MICHEL, P., MIKULIK, R., NOGUEIRA, R. G., OSTERGAARD, L., PEDRAZA, S., RIEDEL, C. H., ROWLEY, H. A., SANELLI, P. C., SASAKI, M., SAVER, J. L., SCHAEFER, P. W., SCHELLINGER, P. D., TSIVGOULIS, G., WECHSLER, L. R., WHITE, P. M., ZAHARCHUK, G., ZAIDAT, O. O., DAVIS, S. M., DONNAN, G. A., FURLAN, A. J., HACKE, W., KANG, D. W., KIDWELL, C., THIJS, V. N., THOMALLA, G., WARACH, S. J., STROKE IMAGING, R. & VIRTUAL INTERNATIONAL STROKE TRIALS ARCHIVE -IMAGING, I. 2013. Acute Stroke Imaging Research Roadmap II. *Stroke,* 44**,** 2628-39.

WITHERSPOON, B. & ASHBY, N. E. 2017. The Use of Mannitol and Hypertonic Saline Therapies in Patients with Elevated Intracranial Pressure: A Review of the Evidence. *Nursing Clinics of North America,* 52**,** 249-260.

WOLLMAN, S. B. & ORKIN, L. R. 1968. Postoperative human reaction time and hypocarbia during anaesthesia. *British Journal of Anaesthesia,* 40**,** 920-6.

WONG, V. & GUMBINER, B. M. 1997. A synthetic peptide corresponding to the extracellular domain of occludin perturbs the tight junction permeability barrier. *Journal of Cell Biology,* 136**,** 399-409.

WOODRUFF, T. M., THUNDYIL, J., TANG, S. C., SOBEY, C. G., TAYLOR, S. M. & ARUMUGAM, T. V. 2011. Pathophysiology, treatment, and animal and cellular models of human ischaemic stroke. *Molecular Neurodegeneration,* 6**,** 11.

WU, D., CHEN, J., WANG, B., ZHANG, M., SHI, J., MA, Y., ZHU, Z., YAN, F., HE, X., LI, S., DORNBOS III, D., DING, Y. & JI, X. 2016. Endovascular ischaemic stroke models of adult rhesus monkeys: a comparison of two endovascular methods. *Scientific Reports,* 6**,** 31608.

WU, H. E., SCHWASINGER, E. T., HONG, J. S. & TSENG, L. F. 2005. Pretreatment with antiserum against dynorphin, substance P, or cholecystokinin enhances the morphine-produced anti-allodynia in the sciatic nerve ligated mice. *Neuroscience Letters,* 386**,** 46-51.

XIA, C. F., YIN, H., BORLONGAN, C. V., CHAO, J. & CHAO, L. 2004. Adrenomedullin gene delivery protects against cerebral ischaemic injury by promoting astrocyte migration and survival. *Human Gene Therapy,* 15**,** 1243-54.

XIAO-FENG, Y., YU, Y., WEI-WEI, H., GU, L., JIN-FANG, X., XUE-QUN, Z. & WEI-GUO, L. 2005. Is decompressive craniectomy for malignant middle cerebral artery infarction of any worth? *Journal of Zhejiang University Science B,* 6**,** 644-649.

XU, S. Y. & PAN, S. Y. 2013. The failure of animal models of neuroprotection in acute ischaemic stroke to translate to clinical efficacy. *Medical Science Monitor Basic Research,* 19**,** 37-45.

YAKOVLEV, S. A., RUBLENKO, M. V., IZDEPSKY, V. I. & MAKOGONENKO, E. M. 1995. Activating effect of the plasminogen activators on plasminogens of different mammalia species. *Thrombosis Research,* 79**,** 423-8.

YAN, S., LI, S. & LI, X.-J. 2019. Use of large animal models to investigate Huntington's diseases. *Cell Regeneration,* 8**,** 9-11.

YANG, S., JIN, H., ZHU, Y., WAN, Y., ZHU, L. & HU, B. 2017. Diverse functions and mechanisms of pericytes in ischemic stroke. *Current Neuropharmacol*, 15**,** 892-905.

YANG, X. F., YAO, Y., HU, W. W., LI, G., XU, J. F., ZHAO, X. Q. & LIU, W. G. 2005. Is decompressive craniectomy for malignant middle cerebral artery infarction of any worth? *Journal of Zhejiang University Science B,* 6**,** 644-9.

YANG, Y. & ROSENBERG, G. A. 2011. Blood–Brain Barrier Breakdown in Acute and Chronic Cerebrovascular Disease. *Stroke,* 42**,** 3323-3328.

YEW, K. S. & CHENG, E. M. 2015. Diagnosis of acute stroke. *American Family Physician,* 91**,** 528-36.

YOUNG, W. L. & STONE, J. G. 1994. Special Anesthetic Considerations for Management of Cerebral Aneurysm Clipping. *New Trends in Management of Cerebro-Vascular Malformations: Proceedings of the International Conference Verona, Italy, June 8–12, 1992.* Vienna: Springer Vienna.

YU, Z., CHENG, G., HUANG, X., LI, K. & CAO, X. 1997. Neurokinin-1 receptor antagonist SR140333: a novel type of drug to treat cerebral ischaemia. *NeuroReport,* 8**,** 2117-9.

YUJI, K., CHIAKI, Y., MASAFUMI, T., YASUHIRO, H., AKIRA, N., GO, K., NAGARA, T., NAOTO, H., TAKENORI, Y. & KAZUO, M. 2001. Serial Changes in Cerebral Blood Flow and Flow–Metabolism Uncoupling in Primates With Acute Thromboembolic Stroke. *Journal of Cerebral Blood Flow & Metabolism,* 21**,** 202.

YUSHKEVICH, P. A., PASHCHINSKIY, A., OGUZ, I., MOHAN, S., SCHMITT, J. E., STEIN, J. M., ZUKIĆ, D., VICORY, J., MCCORMICK, M., YUSHKEVICH, N., SCHWARTZ, N., GAO, Y. & GERIG, G. 2019. User-Guided Segmentation of Multi-modality Medical Imaging Datasets with ITK-SNAP. *Neuroinformatics,* 17**,** 83-102.

YUSHKEVICH, P. A., PIVEN, J., HAZLETT, H. C., SMITH, R. G., HO, S., GEE, J. C. & GERIG, G. 2006. User-guided 3D active contour segmentation of anatomical structures: Significantly improved efficiency and reliability. *NeuroImage,* 31**,** 1116-1128.

ZACEST, A. C., VINK, R., MANAVIS, J., SARVESTANI, G. T. & BLUMBERGS, P. C. 2010. Substance P immunoreactivity increases following human traumatic brain injury. *Acta Neurochirurgica Supplement,* 106**,** 211-6.

ZAUNER, A., BULLOCK, R., DI, X. & YOUNG, H. F. 1995. Brain oxygen, CO2, pH, and temperature monitoring: evaluation in the feline brain. *Neurosurgery,* 37**,** 1168-1176.

ZIEGLGÄNSBERGER, W. 2019. Substance P and pain chronicity. *Cell and Tissue Research,* 375**,** 227-241.

ZHANG, J. Y., YAN, G. T., LIAO, J., DENG, Z. H., XUE, H., WANG, L. H. & ZHANG, K. 2011a. Leptin attenuates cerebral ischaemia/reperfusion injury partially by CGRP expression. *European Journal of Pharmacology,* 671**,** 61-9.

ZHANG, S., HE, W. B. & CHEN, N. H. 2014. Causes of death among persons who survive an acute ischaemic stroke. *Current Neurology and Neuroscience Reports,* 14**,** 467.

ZHANG, W., NEAL, J., LIN, L., DAI, F., HERSEY, D. P., MCDONAGH, D. L., SU, F. & MENG, L. 2018. Mannitol in Critical Care and Surgery Over 50+ Years: A Systematic Review of Randomized Controlled Trials and Complications With Meta-Analysis. *Journal of Neurosurgical Anesthesiology*, 31**,** 273-284.

ZHANG, Y., IRWIN, M. G., LU, Y., MEI, B., ZUO, Y. M., CHEN, Z. W. & WONG, T. M. 2011b. Intracerebroventricular administration of morphine confers remote cardioprotection--role of opioid receptors and calmodulin. *European Journal of Pharmacology,* 656**,** 74-80.

ZHANG, Z. H., FANG, X. B., XI, G. M., LI, W. C., LING, H. Y. & QU, P. 2010. Calcitonin gene-related peptide enhances CREB phosphorylation and attenuates tau protein phosphorylation in rat brain during focal cerebral ischaemia/reperfusion. *Biomedicine & Pharmacotherapy,* 64**,** 430-6.

ZHU, C. Z. & AUER, R. N. 1995. Graded hypotension and MCA occlusion duration: effect in transient focal ischaemia. *Journal of Cerebral Blood Flow & Metabolism,* 15**,** 980-8.

ZIVIN, J. A., FISHER, M., DEGIROLAMI, U., HEMENWAY, C. C. & STASHAK, J. A. 1985. Tissue plasminogen activator reduces neurological damage after cerebral embolism. *Science,* 230**,** 1289-92.

ZU, Q. Q., LIU, S., XU, X. Q., LU, S. S., SUN, L. & SHI, H. B. 2013. An endovascular canine stroke model: middle cerebral artery occlusion with autologous clots followed by ipsilateral internal carotid artery blockade. *Laboratory Investigation,* 93**,** 760-7.

ZULT, T., ALLSOP, J., TABERNERO, J. & PARDHAN, S. 2019. A low-cost 2-D video system can accurately and reliably assess adaptive gait kinematics in healthy and low vision subjects. *Scientific Reports,* 9.

12

Appendices

Appendix 3.1 Recommended pre-anaesthetic treatment regimens for feline, canine, porcine, ovine and non-human primate species.

Drug	Cat	Dog	Pig	Sheep	NHP
Acepromazine	Acepromazine 0.05–0.2 mg/kg i.m. Light to moderate sedation	0.1–0.25 mg/kg i.m. Light to moderate sedation	0.2 mg/kg i.m. Moderate sedation, no analgesia	0.05–0.1 mg/kg i.m. Moderate sedation, no analgesia	0.2 mg/kg i.m. Moderate sedation, no immobilization
Acepromazine + buprenorphine	0.05 mg/kg i.m. + 0.01 mg/kg i.m. Heavy sedation immobilization	0.07 mg/kg i.m. + 0.009 mg/kg i.m. Heavy sedation, immobilization, some analgesia	–	–	–
Acepromazine + morphine	0.05 mg/kg i.m. + 0.1 mg/kg i.m. Heavy sedation immobilization	–	–	–	–
Alphaxalone/ alphadolone	9 mg/kg i.m. Moderate to heavy sedation	–	6 mg/kg i.m. Sedation	–	12–18 mg/kg i.m. Heavy sedation, favorable for small primates, marmosets
Atropine	Atropine 0.05 mg/kg sc or i.m. Anticholinergic	Atropine 0.05 mg/kg sc or i.m. Anticholinergic	0.05 mg/kg sc or i.m. Anticholinergic, can reduce salivary secretions	–	0.05 mg/kg sc or i.m. Anticholinergic, reduce bradycardia and salivary secretions
Azaperone	–	–	5 mg/kg i.m. Moderate to deep sedation, no analgesia	–	–
Dexmedetom-idine	40 µg/kg sc Light to heavy sedation, mild to moderate analgesia	5–40 µg/kg i.m., sc or i.v. Light to heavy sedation, mild to moderate analgesia	–	12.5 µg/kg i.m. Light to heavy sedation, some analgesia	–
Diazepam	–	–	1–2 mg/kg i.m. Light to moderate sedation	1–2 mg/kg i.m., 1 mg/kg i.v. Light to moderate sedation, highly effective in sheep	1 mg/kg i.m. Light to moderate sedation in small NHPs, not sufficient in larger species

Glycopyrrola-te	0.01 mg/kg i.v., 0.05 mg/kg i.m. Anticholinergic	0.01 mg/kg i.v. Anticholinergic	–	–	–
Ketamine	5–30 mg/kg i.m., 10–20 mg/kg per os Light to heavy sedation, mild to moderate analgesia, immobilization at higher dose i.m	–	10–15 mg/kg i.m. Sedation, immobilization	20 mg/kg i.m. Moderate to heavy sedation, immobilization, some analgesia, highly effective when combined with diazepam	20 mg/kg i.m. Moderate to heavy sedation, immobilization, some analgesia
Ketamine/ acepromazine	–	–	22 mg/kg i.m. + 1 mg/kg i.m. Immobilization	–	5–25 mg/kg i.m. Moderate sedation, immobilization, some analgesia
Medetomidine + butorphanol	-	5–10 µg/kg i.m., sc + 0.1–0.5 mg/kg i.m. Light to heavy sedation,	–	–	–
Medetomidine	10–150 µg/kg i.m. or sc Light to heavy sedation, mild to moderate analgesia	10–80 µg/kg i.m., sc or i.v. Light to heavy sedation, mild to moderate analgesia	Ineffective in many pig strains	25 µg/kg i.m. Light to heavy sedation, some analgesia, used in combination with ketamine produces moderate anaesthesia	–
Medetomidine + midazolam + fentanyl					20 µg/kg + 0.5 mg/kg + 10 µg/kg i.m. Heavy sedation/immobilization (Rhesus monkey/large NHPs)
Metomidate	–	–	2 mg/kg i.m. Moderate to deep sedation	–	
Midazolam	–	–	–	0.5 mg/kg i.v. Moderate sedation	
Pethidine	3–5 mg/kg i.m. or sc Light sedation, mild analgesia	–	–	–	

Tiletamine/zolezepam	–	–	2–4 mg/kg i.m. Moderate to deep sedation	–	
Xylazine	1–2 mg/kg i.m., or sc Light to moderate	1–2 mg/kg i.m. Light to moderate sedation,	Ineffective in many pig strains	0.1 mg/kg i.m. or i.v. (sheep) Light to moderate sedation, some analgesia, used in combination with ketamine produces moderate anaesthesia	0.5 mg/kg i.m. Light to moderate sedation, some analgesia

Scheme: Dose rate, route of administration (per os-orally, i.v-intravenous, sc-subcutaneous, i.m-intramuscular), effect, notes. Table adapted from Flecknell, 2016 *Laboratory Animal Anaesthesia (Fourth Edition).*

Appendix 3.2 Summary of physiological variables of feline, canine, porcine, ovine and non-human primate species.

	Cat	Dog	Pig	Sheep	NHP (Large)
Adult body weight (kg)	3-5	15-20	40-200	60-80	8-12
Body temperature (°C)	38.6	38.3	39	39.1	39
Respiration rate (/min)	26	25	12-18	20	35
Recommended ventilation rate	25-50	15-25 (<20kg) 10-15 (>20kg)	15-25 (<20kg) 10-15 (>20kg)	10-15	20-30 (>5kg)
Resting Heart rate (/min)	150	100	220	75	150

Appendix 3.3 Recommended anaesthetic dose regimens for feline, canine, porcine, ovine and non-human primate species.

Drug	Cat	Dog	Pig	Sheep	NHP
Alphaxalone/ alphadolone	9–12 mg/kg i.v., 18 mg/kg i.m. Surgical anaesthesia 10-15mins	–	6 mg/kg i.m. then 2 mg/kg i.v. Immobilization, surgical anaesthesia, 5-10mins	–	10–12 mg/kg i.v. Surgical anaesthesia 5-10mins, 12–18 mg/kg i.m. Immobilization, anaesthesia, 10-20mins
Alphaxalone	2–5 mg/kg i.v. Surgical anaesthesia 10–15mins	2 mg/kg i.v. Surgical anaesthesia 10–15mins	1–2 mg/kg i/v (after azaperone 1–2 mg/ kg i.m.) Surgical anaesthesia 5–10mins	2–3 mg/kg i.v. (adult) 6 mg/kg i.v. (lamb) Surgical anaesthesia 5–10mins	–
Etorphine/ acepromazine	–	–	–	0.5 ml per 50 kg i.m. (>30 kg) Immobilization, Analgesia 30–40mins	–
Ketamine	–	–	10–15 mg/kg i.m. Sedation, immobilization 20–30mins	–	–
Ketamine/ acepromazine	20 mg/kg i.m. + 0.11 mg/kg i.m. Surgical anaesthesia 20-30mins	–	22 mg/kg + 1.1 mg/kg i.m. Light anaesthesia 20–30mins	–	–
Ketamine/diaz-epam	–	–	10–15 mg/kg i.m. + 0.5–2 mg/kg i.m. Immobilization / light anaesthesia 20–30mins	10–15 mg/kg + 1–2 mg/kg i.m. or 4 mg/kg i.v. + 0.5–1 mg/kg i.v. Light to medium anaesthesia/Surgical anaesthesia 20–30mins	15 mg/kg i.m. + 1 mg/kg i.m. Surgical anaesthesia, 30-40mins

Ketamine/ dexmedetomid-ine	7 mg/kg i.m. + 40 µg/kg i.m. Surgical anaesthesia 30-40mins	2.5–7.5 mg/kg i.m. + 20 µg/kg i.m. Light to medium anaesthesia 30–45mins	–	1 mg/kg i.v. + 12.5 µg/kg i.v. Surgical anaesthesia 30–60mins	5 mg/kg i.m. + 25 µg/kg i.m. Surgical anaesthesia, 30-40mins
Ketamine/ medetomidine	7 mg/kg i.m. + 80 µg/kg i.m. Surgical anaesthesia 30-40mins	2.5–7.5 mg/kg i.m. + 40 µg/kg i.m. Light to medium anaesthesia 30–45mins	10 mg/kg i.m. + 0.08 mg/kg i.m. Immobilization / light anaesthesia 40-90mins	1 mg/kg i.v. + 25 µg/kg i.v. Surgical anaesthesia 30–60mins	5 mg/kg i.m. + 50 µg/kg i.m. Surgical anaesthesia, 30-40mins
Ketamine/ midazolam	10 mg/kg i.m. + 0.2 mg/kg i.m. Surgical anaesthesia 20-30mins	–	10–15 mg/kg i.m. + 0.5–2 mg/kg i.m. Immobilization / light anaesthesia 20–30mins	–	–
Ketamine/xyla-zine	22 mg/kg i.m. + 1.1 mg/kg i.m. Surgical anaesthesia 20-30mins	5 mg/kg i.v. + 1–2 mg/kg i.v. or i.m. Light to medium anaesthesia 30–60mins	–	1 mg/kg i.v. + 25 µg/kg i.v. Surgical anaesthesia 30–60mins	10 mg/kg i.m. + 0.5 mg/kg i.m. Surgical anaesthesia, 30-40mins
Methohexital	4–8 mg/kg i.v. Surgical anaesthesia 5-6mins	4–8 mg/kg i.v. Surgical anaesthesia 4–5mins	5 mg/kg i.v. Surgical anaesthesia 4-5mins	4 mg/kg i.v. Surgical anaesthesia 4–5mins	10 mg/kg i.v. Surgical anaesthesia 4–5mins
Pentobarbital	20–30 mg/kg i.v. Surgical anaesthesia 60-90mins	20–30 mg/kg i.v. Surgical anaesthesia 30–40mins	20–30 mg/kg i.v. Light to surgical anaesthesia 15-60mins	30 mg/kg i.v. Immobilization , anaesthesia 15–30mins	25–35 mg/kg i.v. Surgical anaesthesia 30–60mins
Propanidid	8–16 mg/kg i.v. Surgical anaesthesia 4–6mins	–	–	–	–
Propofol	5–8 mg/kg i.v. Surgical anaesthesia 5–10mins	5–7.5 mg/kg i.v. Surgical anaesthesia 5–10mins	2.5–3.5 mg/kg i.v. (6–8 mg/kg if no premed given) Surgical anaesthesia 5-10mins	4–5 mg/kg i.v. Light anaesthesia 5–10mins	7–8 mg/kg i.v. Surgical anaesthesia 5–10mins
Thiamylal	12–18 mg/kg i.v. Surgical anaesthesia 10-15mins	10–15 mg/kg i.v. Surgical anaesthesia 5–10mins	–	–	–
Thiopental	10–15 mg/kg i.v. Surgical anaesthesia 5–10mins	10–20 mg/kg i.v. Surgical anaesthesia 5–10mins	6–9 mg/kg i.v. Surgical anaesthesia, 5-10mins	10–15 mg/kg i.v. Surgical anaesthesia 5–10mins	15–20 mg/kg i.v. Surgical anaesthesia 5–10mins

Tiletamine/ zolezepam	47.5 mg/kg i.m. + 7.5 mg/kg i.m. Surgical anaesthesia 20–40mins	–	2–4 mg/kg i.m. Immobilization, 6–8 mg/kg i.m. Light anaesthesia, 20-30mins	–	–

Scheme: Dose rate, route of administration (per os-orally, i.v-intravenous, sc-subcutaneous, i.m-intramuscular), effect, notes. Table adapted from Flecknell, 2016 *Laboratory Animal Anaesthesia (Fourth Edition).*

Appendix 3.4 Recommended minimal alveolar concentration (MAC%) of commonly used inhalational anaesthetic agents for use in feline, canine, porcine, ovine and non-human primate species

Drug	Cat	Dog	Pig	Sheep	NHP
Isoflurane	1.6	2.3	1.45-2.04	1.19-1.53	1.28
Halothane	1.0	0.9	-	0.69	0.89–1.15 (depending on size of NHP species)
Desflurane	9.8	7.2	8.28-10.0	-	-
Sevoflurane	2.6	2.3	1-1.5	3.3%	2.0

Adapted from Smith and Swindle, 2008 *Anaesthesia and analgesia in laboratory animals*

Appendix 3.5 Recommended antibiotic and antibacterial treatment regimens in feline, canine, porcine, ovine and non-human primate species

Drug	Cat	Dog	Pig	Sheep	NHP
Amoxcillin	7 mg/kg sc u.i.d	7 mg/kg sc u.i.d	7 mg/kg sc u.i.d	7 mg/kg sc u.i.d	7 mg/kg sc u.i.d
Cephalexin	10 mg/kg sc u.i.d	10 mg/kg sc u.i.d	10 mg/kg sc u.i.d	10 mg/kg sc u.i.d	10 mg/kg sc u.i.d
Chloramphenicol	25 mg/kg sc u.i.d	50 mg/kg sc u.i.d	11 mg/kg sc u.i.d	-	20 mg/kg sc u.i.d
Enrofloxacin	5 mg/kg sc u.i.d.	5 mg/kg sc u.i.d.	2.5 mg/kg sc u.i.d.	-	5 mg/kg sc b.i.d.
Neomycin	10 mg/ml per os u.i.d. in divided doses	10 mg/ml per os u.i.d. in divided doses	11 mg/ml per os u.i.d. in divided doses	11 mg/ml per os u.i.d. in divided doses	10 mg/ml per os u.i.d. in divided doses
Trimethoprim/ sulphonamide	30 mg/kg sc u.i.d.	30 mg/kg sc u.i.d.	15-24 mg/kg sc u.i.d.	15-24 mg/kg sc u.i.d.	30 mg/kg sc u.i.d.

Scheme: dose range (u.i.d-once daily, b.i.d –twice a day, t.i.d-three times a day) application routes (p.o./per os=orally; sc= subcutaneous; i.v.=intravenous; i.m.=intramuscular). Table adapted from Flecknell, 2016 *Laboratory Animal Anaesthesia (Fourth Edition).*

Note that considerable individual and strain variation in response may be encountered, and that it is therefore essential to assess the analgesic effect in each individual animal.

Appendix 3.6 Recommended Analgesic treatment regimes in feline, canine, porcine, ovine and non-human primate species

	Drug	Cat	Dog	Pig	Sheep	NHP
Non-Steroidal Anti Inflammatory Analgetics (NSAIDs)	Aspirin	10–25 mg/kg per os, every 48 hours	10–25 mg/kg per os, every 8 hourly	10–20 mg/kg per os, 4–6 hourly	50–100 mg/kg per os, 6–12 hourly	20 mg/kg per os, 6–8 hourly
	Carprofen	4 mg/kg sc or iv	4 mg/kg iv or sc, once daily 1–2 mg/kg b.i.d. per os, for 7 days	2–4 mg/kg iv or sc, once daily	2–4 mg/kg sc or iv, once daily (2–3 days)	3–4 mg/kg sc u.i.d.
	Flunixin	1 mg/kg sc, daily for up to 5 days	1 mg/kg iv or im, 12 hourly 1 mg/kg per os, daily for up to 3 days	1–2 mg/kg iv or sc, once daily	2 mg/kg iv or sc, once daily	0.5–2 mg/kg sc or iv daily
	Ibuprofen	–	10 mg/kg per os, 24 hourly	–	–	7 mg/kg per os
	Ketoprofen	1 mg/kg sc, once daily for up to 3 days 1 mg/ kg per os, once daily for up to 5 days	2 mg/kg sc, im or iv, once daily for up to 3 days 1 mg/kg per os, daily for 5 days	1–3 mg/kg iv, im, sc, per os, 12 hourly	–	2 mg/kg sc daily
	Meloxicam	0.2 mg/kg u.i.d. sc or 0.3 mg/kg per os, then 0.1 mg/kg sc or per os	0.2 mg/kg u.i.d. sc or per os, then 0.1 mg/kg sc or per os	0.4 mg/kg sc, once daily	0.5 mg/kg iv, sc up to b.i.d. for 1 day, then 0.5 mg/kg per os u.i.d. for 5 days	0.1–0.2 mg/kg u.i.d. sc or per os
	Tolfenamic acid	4 mg/kg sc daily for 2 days	4 mg/kg sc daily for 2 days	–	–	–

	Paracetamol (acetaminophen)	Contra-indicated	15 mg/kg per os, 6–8 hourly	–	–	–
Opioid Analgetics	Buprenorphine	0.005–0.01 mg/kg sc or iv, 8–12 hourly	0.005–0.02 mg/kg im, sc or iv, 6–12 hourly	0.01–0.05 mg/kg im or iv, 6–12 hourly	0.005–0.01 mg/kg im or iv, 4 hourly	0.005–0.01 mg/kg im or iv, 6–12 hourly
	Butorphanol	0.4 mg/kg sc, 3–4 hourly	0.2–0.4 mg/kg sc or im, 3–4 hourly	0.1–0.3 mg/kg im or iv, 4 hourly	0.5 mg/kg im or iv, 2–3 hourly	0.01 mg/kg iv, ?3–4 hourly
	Hydromorphone	0.1 mg/kg im, sc 0.2 2–4 hourly	0.05–0.2 mg/kg im, sc 2–4 hourly	–	–	–
	Morphine	0.3 mg/kg sc, 4 hourly	0.5–5 mg/kg sc or im, 4 hourly	0.2–1 mg/kg im , ?4 hourly	0.2–0.5 mg/kg im, ?4 hourly	1–2 mg/kg sc or im, 4 hourly
	Nalbuphine	1.5–3.0 mg/kg iv, 3 hourly	0.5–2.0 mg/kg sc or im, 3–4 hourly	–	–	–
	Oxymorphone	0.2 mg/kg sc or iv	0.05–0.22 mg/kg im, sc or iv, 2–4 hourly	0.15 mg/kg im 4 hourly	–	0.15 mg/kg im 4–6 hourly
	Pentazocine	–	2 mg/kg im or iv, 4 hourly	2 mg/kg im or iv, 4 hourly	–	2–5 mg/kg im or iv, 4 hourly
	Pethadine (Meperidine)	2–10 mg/kg sc or im, 2–3 hourly	10 mg/kg im, 2–3 hourly	2 mg/kg im or iv, 2–4 hourly	2 mg/kg im or iv, 2–4 hourly	2–4 mg/kg im or iv, 2–4 hourly
	Tramadol	2–4 mg/kg sc	2–5 mg/kg iv or sc, 2–5 mg/kg orally t.i.d.	–	–	? 1–2 mg/kg sc or iv, 2 mg/kg orally ? b.i.d.

Scheme: dose range (u.i.d-once daily, b.i.d –twice a day, t.i.d-three times a day) application routes (po/per os=orally; sc= subcutaneous; iv=intravenous; im=intramuscular); time intervals in which the medication should be repeated to ensure sufficient analgesia. ?-duration of action uncertain. Table adapted from Flecknell, 2016 *Laboratory Animal Anaesthesia (Fourth Edition).*

Appendix 5.1 Clinical record sheet

Project: AEC# Expiration:
Primary Researcher: Annabel Sorby-Adams Animal ID: Surgery Date:
Additional Contact: Pre-op Weight:

1	2	3	4	5	6	7	8	9	10	11	12	13	14	15	16	17	18	19	20	21	22	23	24	25	26	27
Date	Time	Weight	Weight loss (15%)	Pulse rate/min	Temperature	Reduced food/ Intake	Reduced Water Intake	Faeces output	Urine output	Teeth Grinding	Abnormal Respiratory Rate normal: 20-40	Change in Posture / Droopy Ears	Discharge or Swelling at Surgical Site	Abnormal Gait or Limb Paralysis	Sluggish/dilated pupils	Demeanour normal	Standing unassisted	Walking unassisted	TOTAL SCORE	TREATMENTS GIVEN	Antibiotics	NSAID	Pain relief/ OPIOIDS	IV Fluids	Ceton	SIGN

Column 3-6 = Noted Changes **Column 7-11** = **0**–Normal, **1**–Slight Change, **2**-Markedly Changed **Column 12-16 = 0**-No**, 1**-Yes
NOTE: Animals to be checked EVERY 15 MINUTES FOR FIRST 4 HOURS and must be free standing prior to leaving facility
Scores of 3: Require the animal to be checked 3 times per day. 4 or 5 Veterinary Advice Required and Review Treatment
Scores above 6: If there seems to be no improvement in sight Animals will be **humanely kille**

Appendix 9.1 MATLAB code for functional analysis

```
init(); def=defaults;
%Code for Stroke Sheep Gait Analysis

%% SCRIPT DESCRIPTION
% This script produces figures and data from Ovine MoCap Trials. The
script calls markers by name directly allowing for ease of comparison
between limb segments and individual markers

%% TOOLBOXES REQUIRED
% The following Toolboxes must be installed to run this code: MoCap Tools
- Labelling, and EpicToolbox. Scripts are available from JCL via
https://github.com/JonathanCamargo?tab=repositories

%% Stop underscores in titles being subscripted
set(0, 'DefaulttextInterpreter', 'none')

% Use the init.m script to change scope of analysis and file pathway
(containing files to be analysed and folder where results and figures
will be output). init.m allows for modificetion of batch processing via
the batchrun.m script or individal
% files/sessions directly via the script
c3dfiles=f.fileList('Subject',SUBJECT,'Session',SESSION,'Folder','C3D_Fin
al','File',FILE);
c3dfile=c3dfiles{1};
% Results path:
fres=FileManager(resultspath,'PathStructure',{'Subject','Session','Folder
','File'});

%% SCRIPT OUTPUTS
% - figures:  Marker positions and gait cycle (0-100%)
% - .mat file with results

%% LOAD MARKERS
% Ensure the appropriate marker order is listed so that the marker
numbers used throughout processing correspond correctly
orderedMarkerNames={'HEAD','T1','T13','L7','L_GTUB','L_LEPIRAD','L_ULNA',
'L_METAR', 'LF_PPHAL', 'LF_PHAL', 'LF_DPHAL', 'R_GTUB', 'R_LEPIRAD',
'R_ULNA', 'R_METAR', 'RF_PPHAL', 'RF_PHAL', 'RF_DPHAL', 'L_ILIUM',
'L_GTROC', 'L_ISCTUB', 'L_LEPI', 'L_LTIB', 'L_TIB', 'L_CALC', 'L_LMAL',
'L_FTAR','LH_PPHAL', 'LH_PHAL', 'LH_DPHAL', 'R_ILIUM', 'R_GTROC',
'R_ISCTUB', 'R_LEPI', 'R_LTIB', 'R_TIB', 'R_CALC', 'R_LMAL',
'R_FTAR','RH_PPHAL', 'RH_PHAL', 'RH_DPHAL'};
c3dstruct=Vicon.ExtractMarkers(c3dfile); % Import the marker data from
the C3D file, according to their abbreviated names, and reorder as above
c3dstruct=Topics.select(c3dstruct,orderedMarkerNames); % Use the
prescribed ordered names to make sure order is as expected for the rest
of the code
trc=Osim.interpret(c3dstruct,'TRC','table'); % Get the markers ('TRC from
Vicon')
trc{:,2:end}=Vicon.transform(trc{:,2:end},'ViconXYZ'); % Flip y and z
data as Extract markers outputs in Osim Coordinate System

%% Center the Global Coordinate System (GCS) to the middle of the Force
Plate.
% Collection GCS is located at the front right Force Plate. Need to shift
all y-coords by 674/2 = 337mm in the negative direction; shift all x-
```

```
coords by 877/2 = 438.5mm in the negative direction. z-coords remain the
same.

trc{:,2:3:end}= trc{:,2:3:end}- 438.5;% Shift the x axis 438.5mm
trc{:,3:3:end}= trc{:,3:3:end}- 337.0;% Shift the y axis 337.0 mm
Nmarkers = size(trc,2); % From now on the marker data is in the TRC table
FS=1/mean(diff(trc.Header)); % Determine sampling frequency (from Vicon,
200Hz), neccesary for determining velocity
trc{:,2:end}=Vicon.Filter(trc{:,2:end},10/(FS/2)); % Apply 4th order,
zero lag, butterworth filter, cut off frequency 10Hz

%% Compensate for Coordinate System Tilt
[pks1,idx1]=findpeaks(-trc.LF_DPHAL_z,'MinPeakProminence',10);
[pks2,idx2]=findpeaks(-trc.RF_DPHAL_z,'MinPeakProminence',10);
[pks3,idx3]=findpeaks(-trc.LH_DPHAL_z,'MinPeakProminence',10);
[pks4,idx4]=findpeaks(-trc.RH_DPHAL_z,'MinPeakProminence',10);

x1=trc(idx1,{'LF_DPHAL_x','LF_DPHAL_y','LF_DPHAL_z'});
x2=trc(idx2,{'RF_DPHAL_x','RF_DPHAL_y','RF_DPHAL_z'});
x3=trc(idx3,{'LH_DPHAL_x','LH_DPHAL_y','LH_DPHAL_z'});
x4=trc(idx4,{'RH_DPHAL_x','RH_DPHAL_y','RH_DPHAL_z'});
x={x1.Variables;x2.Variables;x3.Variables;x4.Variables};
x=x(cellfun(@(x)size(x,1)>1,x));

c_fun=@(x)polyfit(x(:,2),x(:,3),1);
coeffs=cellfun(c_fun,x,'Uni',0);
tilts=cellfun(@(x)atan(x(1)),coeffs);
R=eul2rotm([mean(tilts),0,0],'xyz');
trc{:,2:end}=Vicon.transform(trc{:,2:end},R);


%% Load model %% JCL added functionality to programatically read the VSK
file and get the sticks
info=f.getFields(c3dfile); info.File=join([info.Subject,{'vsk'}],'.');
vskfile=f.fileList(info); vskfile=vskfile{1};

%% Plot the model at a given position
% Plot the first frame for visualising appropriate body segments
% Comment out when not in use

h1=figure(1); clf
Vicon.model.plot(vskfile,trc(1,:))
view(-450,4)  %adjust this to rotate view
%save figure as .png
info=f.getFields(c3dfile);
info.File=[strrep([info.File{1}, '_VSK'],'.c3d',''), '.png'];
info.Folder='Results';
%info.File=strrep(info.File,'.c3d','.png'); info.Folder='Results';
outfile=fres.genList(info); outfile=outfile{1};
mkdirfile(outfile); saveas(gcf,outfile);

%% Figure: Animation in Real Time View using the VSK

segments=Vicon.model.getSegmentMarkers(vskfile);
sticks=Vicon.model.getSticks(vskfile); % Compute sticks to save time
%Comment out when not in use
%figure(1); clf;
%for i=1:10:size(trc,1)
    %clf;
    %view(-90,1)  %adjust this to rotate view
    %axis([-1000 1000 -500 1000 -1000 1500])
```

```
    %axis equal
   % Vicon.model.plot(vskfile,trc(i,:),sticks)
    %drawnow;
%end
h1=figure(1);
plotAnimation(vskfile,trc);

%% Plot the vertical displacement of distal markers on the fore and hind
limbs
h2= figure(2); clf;
subplot(4,1,1); hold on;
plot(trc.RF_DPHAL_z,'r'); title('R Fore (RF_DPHAL)');
subplot(4,1,2); hold on;
plot(trc.LF_DPHAL_z,'r'); title('L Fore (LF_DPHAL)');
subplot(4,1,3); hold on;
plot(trc.RH_DPHAL_z,'r'); title('R Hind (RH_DPHAL)');
subplot(4,1,4); hold on;
plot(trc.LH_DPHAL_z,'r'); title('L Hind (LH_DPHAL)');
ylabel ('Vertical displacement (mm)')
xlabel ('data point')

% save figures as png
info=f.getFields(c3dfile); info.Folder='figures'; info.Folder='Results';
info.File=[strrep([info.File{1}, '_GaitCyclesRaw'],'.c3d',''), '.png'];
outfile=fres.genList(info); outfile=outfile{1};
mkdirfile(outfile); saveas(h2,outfile,'png');

%output seems to make sense, R fore and L hind in contact together, then
R
%hind and L fore in contact together.

%%  Plot the displacement of distal markers on the fore and hind (Nicer
version with for loop)
legs={'R_forefoot','L_forefoot','R_hindfoot','L_hindfoot'};
distalmarkers={'RF_DPHAL','LF_DPHAL','RH_DPHAL','LH_DPHAL'};
h3=figure(3); clf
gc=trc(:,1); %Copy header
for i=1:numel(distalmarkers)
    x1=GaitCycleFromTRC(trc,'Markers',distalmarkers{i});
    x2=GaitCycleFromTRC(trc,'Markers',distalmarkers{i},'Toeoff',true);
    subplot(4,1,i); hold on;
    plot(trc.Header*200,trc.([distalmarkers{i} '_z']),'r');
title(distalmarkers{i});
    plot(trc.Header*200,x1{:,2},'--'); % Plot the gait cycle from 0 to
100%
    plot(trc.Header*200,x2{:,2},'--');
    gc=[gc x1(:,2) x2(:,2)];
end
ylabel ('Vertical displacement (mm)')
legend('Vertical position','StanceStarts','SwingStarts');

% save figures as png
info=f.getFields(c3dfile); info.Folder='figures'; info.Folder='Results';
info.File=[strrep([info.File{1}, '_GaitCyclesSegmented'],'.c3d',''),
'.png'];
outfile=fres.genList(info); outfile=outfile{1};
mkdirfile(outfile); saveas(h3,outfile,'png');

%% Figure: Plot Vertical Hoof Displacement in Z axis (ASA)
h4= figure(4); clf;
subplot(2,1,1); hold on;
```

```
plot(trc.RF_DPHAL_z,'r'); plot(trc.LF_DPHAL_z,'b'); title('Forelimb
Vertical (z) Hoof Displacement');
legend('R Fore','L Fore');
ylabel ('Displacement (mm)')
subplot(2,1,2); hold on;
plot(trc.RH_DPHAL_z,'r'); plot(trc.LH_DPHAL_z,'b'); title('Hindlimb (z)
Hoof Displacement Hindlimbs');
legend('R Hind','L Hind');
ylabel ('Displacement (mm)')
xlabel ('Data Point')

% save figures as png
info=f.getFields(c3dfile); info.Folder='figures'; info.Folder='Results';
info.File=[strrep([info.File{1}, '_HoofDisplacement_Z'],'.c3d',''),
'.png'];
outfile=fres.genList(info); outfile=outfile{1};
mkdirfile(outfile); saveas(h4,outfile,'png');

%% Figure: Plot Distal Hoof Forward Velocity in Y axis (ASA)
markers=Osim.interpret(trc,'TRC','struct');
RF_DPHAL=markers.RF_DPHAL{:,2:end};
velocity_RF_DPHAL_y = smooth(gradient(RF_DPHAL(:,2),1/FS)/1000); %incl.
conversion mm/s to m/s
accel_RF_DPHAL_y = smooth(gradient(velocity_RF_DPHAL_y(:,1),1/FS)); %
t=markers.RF_DPHAL.Header;

markers=Osim.interpret(trc,'TRC','struct');
LF_DPHAL=markers.LF_DPHAL{:,2:end};
velocity_LF_DPHAL_y = smooth(gradient(LF_DPHAL(:,2),1/FS)/1000); %incl.
conversion mm/s to m/s
accel_LF_DPHAL_y = smooth(gradient(velocity_LF_DPHAL_y(:,1),1/FS)); %

markers=Osim.interpret(trc,'TRC','struct');
RH_DPHAL=markers.RH_DPHAL{:,2:end};
velocity_RH_DPHAL_y = smooth(gradient(RH_DPHAL(:,2),1/FS)/1000); %incl.
conversion mm/s to m/s
accel_RH_DPHAL_y = smooth(gradient(velocity_RH_DPHAL_y(:,1),1/FS)); %

markers=Osim.interpret(trc,'TRC','struct');
LH_DPHAL=markers.LH_DPHAL{:,2:end};
velocity_LH_DPHAL_y = smooth(gradient(LH_DPHAL(:,2),1/FS)/1000); %incl.
conversion mm/s to m/s
accel_LH_DPHAL_y = smooth(gradient(velocity_LH_DPHAL_y(:,1),1/FS)); %

h5 = figure (5); clf; hold on
subplot(2,1,1); hold on
plot(velocity_RF_DPHAL_y(:,1), 'r'); title("Forelimb Foward (y) Hoof
Velocity"); ylabel ('Velocity (m/s)'); hold on
plot(velocity_LF_DPHAL_y(:,1), 'b');
legend('R Fore','L Fore');
subplot(2,1,2); hold on
plot(velocity_RH_DPHAL_y(:,1), 'r'); title("Hindlimb Foward (y) Hoof
Velocity"); ylabel ('Velocity (m/s)'); hold on
plot(velocity_LH_DPHAL_y(:,1), 'b');
legend('R Hind','L Hind');
xlabel ('time (s)');

% save figures as png
info=f.getFields(c3dfile); info.Folder='figures'; info.Folder='Results';
info.File=[strrep([info.File{1}, '_HoofVelocityForward_Y'],'.c3d',''),
'.png'];
```

```
outfile=fres.genList(info); outfile=outfile{1};
mkdirfile(outfile); saveas(h5,outfile,'png');

%% Figure: Plot Distal Hoof Vertical Velocity in Z axis (ASA)
markers=Osim.interpret(trc,'TRC','struct');
RF_DPHAL=markers.RF_DPHAL{:,2:end};
velocity_RF_DPHAL_z = smooth(gradient(RF_DPHAL(:,3),1/FS)/1000); %incl.
conversion mm/s to m/s
%accel_RF_DPHAL_z = smooth(gradient(velocity_RF_DPHAL_z(:,1),1/FS)); %
t=markers.RF_DPHAL.Header;

markers=Osim.interpret(trc,'TRC','struct');
LF_DPHAL=markers.LF_DPHAL{:,2:end};
velocity_LF_DPHAL_z = smooth(gradient(LF_DPHAL(:,3),1/FS)/1000); %incl.
conversion mm/s to m/s
%accel_LF_DPHAL_z = smooth(gradient(velocity_LF_DPHAL_z(:,1),1/FS)); %

markers=Osim.interpret(trc,'TRC','struct');
RH_DPHAL=markers.RH_DPHAL{:,2:end};
velocity_RH_DPHAL_z = smooth(gradient(RH_DPHAL(:,3),1/FS)/1000); %incl.
conversion mm/s to m/s
%accel_RH_DPHAL_z = smooth(gradient(velocity_RH_DPHAL_z(:,1),1/FS)); %

markers=Osim.interpret(trc,'TRC','struct');
LH_DPHAL=markers.LH_DPHAL{:,2:end};
velocity_LH_DPHAL_z = smooth(gradient(LH_DPHAL(:,3),1/FS)/1000); %incl.
conversion mm/s to m/s
%accel_LH_DPHAL_z = smooth(gradient(velocity_LH_DPHAL_z(:,1),1/FS)); %

h6 = figure (6); clf; hold on
subplot(2,1,1); hold on
plot(velocity_RF_DPHAL_z(:,1), 'r'); title("Forelimb Vertical (z) Hoof
Velocity"); ylabel ('Velocity (m/s)'); hold on
plot(velocity_LF_DPHAL_z(:,1), 'b');
legend('R Fore','L Fore');
subplot(2,1,2); hold on
plot(velocity_RH_DPHAL_z(:,1), 'r'); title("Hindlimb Vertical (z) Hoof
Velocity"); ylabel ('Velocity (m/s)'); hold on
plot(velocity_LH_DPHAL_z(:,1), 'b');
legend('R Hind','L Hind');
xlabel ('time (s)');

% save figures as png
info=f.getFields(c3dfile); info.Folder='figures'; info.Folder='Results';
info.File=[strrep([info.File{1}, '_HoofVelocityVertical_Z'],'.c3d',''),
'.png'];
outfile=fres.genList(info); outfile=outfile{1};
mkdirfile(outfile); saveas(h6,outfile,'png');

%% Figure: Plot Fetlock Angle (ASA)
markers=Osim.interpret(trc,'TRC','struct');
LF_fetlockangle=jointangle_2D(markers,'LF_PHAL','LF_DPHAL','L_METAR','LF_
PPHAL');
RF_fetlockangle=jointangle_2D(markers,'RF_PHAL','RF_DPHAL','R_METAR','RF_
PPHAL');
LH_fetlockangle=jointangle_2D(markers,'LH_PHAL','LH_DPHAL','L_FTAR','LH_P
PHAL');
RH_fetlockangle=jointangle_2D(markers,'RH_PHAL','RH_DPHAL','R_FTAR','RH_P
PHAL');

h7 = figure (7); clf; hold on
```

```
subplot(2,1,1); hold on
plot(LF_fetlockangle, 'b'); title("Forelimb Fetlock Angle"); ylabel
('Angle (deg)'); hold on
plot(RF_fetlockangle, 'r');
legend('L Fore','R Fore');
subplot(2,1,2); hold on
plot(LH_fetlockangle, 'b'); title("Hindlimb Fetlock Angle"); ylabel
('Angle (deg)'); hold on
plot(RH_fetlockangle, 'r');
legend('L Hind','R Hind');
xlabel ('time (s)');

% save figures as png
info=f.getFields(c3dfile); info.Folder='figures'; info.Folder='Results';
info.File=[strrep([info.File{1}, '_FetlockAngle'],'.c3d',''), '.png'];
outfile=fres.genList(info); outfile=outfile{1};
mkdirfile(outfile); saveas(h7,outfile,'png');

%% Figure: Plot Stifle Angle (ASA)
markers=Osim.interpret(trc,'TRC','struct');
LF_stifleangle=jointangle_2D(markers,'R_LEPIRAD','R_ULNA','R_GTUB','R_LEP
IRAD');
RF_stifleangle=jointangle_2D(markers,'L_LEPIRAD','L_ULNA','L_GTUB','L_LEP
IRAD');
LH_stifleangle=jointangle_2D(markers,'L_LTIB','L_LMAL','L_GTROC','L_LEPI'
);
RH_stifleangle=jointangle_2D(markers,'R_LTIB','R_LMAL','R_GTROC','R_LEPI'
);

h8 = figure (8); clf; hold on
subplot(2,1,1); hold on
plot(LF_stifleangle, 'b'); title("Forelimb Stifle Angle"); ylabel ('Angle
(deg)'); hold on
plot(RF_stifleangle, 'r');
legend('L Fore', 'R Fore');
subplot(2,1,2); hold on
plot(LH_stifleangle, 'b'); title("Hindlimb Stifle Angle"); ylabel ('Angle
(deg)'); hold on
plot(RH_stifleangle, 'r');
legend('L Hind','R Hind');
xlabel ('time (s)');

% save figures as png
info=f.getFields(c3dfile); info.Folder='figures'; info.Folder='Results';
info.File=[strrep([info.File{1}, '_StifleAngle'],'.c3d',''), '.png'];
outfile=fres.genList(info); outfile=outfile{1};
mkdirfile(outfile); saveas(h8,outfile,'png');

%% Figure: Plot Hock Angle (ASA)
markers=Osim.interpret(trc,'TRC','struct');
LF_hockangle=jointangle_2D(markers,'L_METAR','LF_PPHAL','L_LEPIRAD','L_UL
NA');
RF_hockangle=jointangle_2D(markers,'R_METAR','RF_PPHAL','R_LEPIRAD','R_UL
NA');
LH_hockangle=jointangle_2D(markers,'L_FTAR','LH_PPHAL','L_LTIB','L_LMAL')
;
RH_hockangle=jointangle_2D(markers,'R_FTAR','RH_PPHAL','R_LTIB','R_LMAL')
;

h9 = figure (9); clf; hold on
subplot(2,1,1); hold on
```

```
plot(LF_hockangle, 'b'); title("Forelimb Hock Angle"); ylabel ('Angle
(deg)'); hold on
plot(RF_hockangle, 'r');
legend('L Fore','R Fore');
subplot(2,1,2); hold on
plot(LH_hockangle, 'b'); title("Hindlimb Hock Angle"); ylabel ('Angle
(deg)'); hold on
plot(RH_hockangle, 'r');
legend('L Hind','R Hind');
xlabel ('time (s)');

% save figures as png
info=f.getFields(c3dfile); info.Folder='figures'; info.Folder='Results';
info.File=[strrep([info.File{1}, '_HockAngle'],'.c3d',''), '.png'];
outfile=fres.genList(info); outfile=outfile{1};
mkdirfile(outfile); saveas(h9,outfile,'png');

%% Analysis table now contains gait cycle from 0-100% to use for
segmenting data for each limb
trial=struct();
trial.trc=trc;
trial.gc=gc;
%Split the trial data w.r.t gait cycle for each leg independently

strides=[];
for i=1:numel(legs)
    s=segment_gc(trial,'GCtopic','gc','GCChannel',[distalmarkers{i}
'_Strike']); %Split gait cycle
    % Here you can discard the segments that are not good before copying
to
    goodStrides=[];
    for j=1:numel(s)
        % Some if statements to discard each segment?
        % for now lets say that if segment starts or ends with the trial
it
        % is probably bad. % Manually? yes or no?
        if (s{j}.trc.Header(1)==trial.trc.Header(1)) ||
(s{j}.trc.Header(end)==trial.trc.Header(end))
            continue;
        end

        % For convenience on each stride determine the indices of stance
phase and
        % swing phase.
        strikeIdx=find(s{j}.gc.([distalmarkers{i} '_Strike'])==0);
        offIdx=find(s{j}.gc.([distalmarkers{i} '_Off'])==0);
        s{j}.stanceIdx=[strikeIdx(1) offIdx(1)];
        s{j}.swingIdx=[offIdx(1) strikeIdx(2)];
        s{j}.leg=legs{i};
        if numel(goodStrides)>0
            break;
        end
        goodStrides=[goodStrides;s(j)];
    end
    strides=[strides;goodStrides];
end
% strides contains strides based on each individual leg
%% %%%%%%%%%%%%%%%%%%%%% ANALYSIS CODE
%%%%%%%%%%%%%%%%%%%%%%%%%%%%%%%%%%%%
%% A. Analyses / plots that are global in the trial and not stride by
stride basis go here:
```

```
% Forward trajectory velocity, based on pelvis motion (centre point of
ilium) (m/s)
% derive some new points from markers on rigid bodies %
% midpoint of left adn right ilium markers (i.e. centre of pelvis)
globalresults=table();
globalresults.minabsvelocity_midilium_y=nan(1,1);
globalresults.maxabsvelocity_midilium_y=nan(1,1);
globalresults.meanabsvelocity_midilium_y=nan(1,1);
globalresults.rangevelocity_midilium_y=nan(1,1);
globalresults.minabsvelocity_midilium_x=nan(1,1);
globalresults.maxabsvelocity_midilium_x=nan(1,1);
globalresults.meanabsvelocity_midilium_x=nan(1,1);
globalresults.rangevelocity_midilium_x=nan(1,1);
globalresults.minvelocity_midilium_z=nan(1,1);
globalresults.maxvelocity_midilium_z=nan(1,1);
globalresults.meanvelocity_midilium_z=nan(1,1);
globalresults.rangevelocity_midilium_z=nan(1,1);
globalresults.minabsvelocity_T1_y=nan(1,1);
globalresults.maxabsvelocity_T1_y=nan(1,1);
globalresults.meanabsvelocity_T1_y=nan(1,1);
globalresults.rangevelocity_T1_y=nan(1,1);
globalresults.Properties.VariableUnits={'m/s', 'm/s', 'm/s', 'm/s',
'm/s', 'm/s', 'm/s', 'm/s', 'm/s', 'm/s', 'm/s', 'm/s', 'm/s', 'm/s',
'm/s', 'm/s'};

% Head Range w.r.t T1 analysis [Annabel's request]  (cm)
globalresults.MinAbsHeadToT1_x=nan(1,1);
globalresults.MaxAbsHeadToT1_x=nan(1,1);
globalresults.MinHeadToT1_z=nan(1,1);
globalresults.MaxHeadToT1_z=nan(1,1);
globalresults.RangeHeadToT1_x=nan(1,1);
globalresults.RangeHeadToT1_z=nan(1,1);
globalresults.MeanAbsHeadToT1_x=nan(1,1);
globalresults.MeanHeadToT1_z=nan(1,1);
theseunits=repmat({'cm'},1,8);
globalresults.Properties.VariableUnits(end-7:end)=theseunits;
% T1 analysis. Distance of T1 relative to floor, deviation left-right
(cm)
globalresults.MinAbsStrideT1_x=nan(1,1);
globalresults.MaxAbsStrideT1_x=nan(1,1);
globalresults.MinStrideT1_z=nan(1,1);
globalresults.MaxStrideT1_z=nan(1,1);
globalresults.RangeStrideT1_x=nan(1,1);
globalresults.RangeStrideT1_z=nan(1,1);
globalresults.MeanAbsStrideT1_x=nan(1,1);
globalresults.MeanStrideT1_z=nan(1,1);
theseunits=repmat({'cm'},1,8);
globalresults.Properties.VariableUnits(end-7:end)=theseunits;
% T1 Range w.r.t T13 analysis [Annabel's request]  (cm)
globalresults.MinAbsT1ToT13_x=nan(1,1);
globalresults.MaxAbsT1ToT13_x=nan(1,1);
globalresults.MinT1ToT13_z=nan(1,1);
globalresults.MaxT1ToT13_z=nan(1,1);
globalresults.RangeT1ToT13_x=nan(1,1);
globalresults.RangeT1ToT13_z=nan(1,1);
globalresults.MeanAbsT1ToT13_x=nan(1,1);
globalresults.MeanT1ToT13_z=nan(1,1);
theseunits=repmat({'cm'},1,8);
globalresults.Properties.VariableUnits(end-7:end)=theseunits;
% T1 Range w.r.t L7 analysis [Annabel's request]  (cm)
globalresults.MinAbsT1ToL7_x=nan(1,1);
globalresults.MaxAbsT1ToL7_x=nan(1,1);
globalresults.MinT1ToL7_z=nan(1,1);
```

```
globalresults.MaxT1ToL7_z=nan(1,1);
globalresults.RangeT1ToL7_x=nan(1,1);
globalresults.RangeT1ToL7_z=nan(1,1);
globalresults.MeanAbsT1ToL7_x=nan(1,1);
globalresults.MeanT1ToL7_z=nan(1,1);
theseunits=repmat({'cm'},1,8);
globalresults.Properties.VariableUnits(end-7:end)=theseunits;

markers=Osim.interpret(trc,'TRC','struct');
virtualmarkers=struct();
virtualmarkers.mid_ilium=markers.R_ILIUM;
virtualmarkers.mid_ilium{:,2:end}=((markers.L_ILIUM{:,2:end}-
markers.R_ILIUM{:,2:end})/2)+markers.R_ILIUM{:,2:end};

mid_ilium=virtualmarkers.mid_ilium{:,2:end};
velocity_midilium_y = smooth(gradient(mid_ilium(:,2),1/FS)/1000); %incl.
conversion mm/s to m/s
accel_midilium_y = smooth(gradient(velocity_midilium_y(:,1),1/FS)); %
velocity_midilium_x = smooth(gradient(mid_ilium(:,1),1/FS)/1000); %incl.
conversion mm/s to m/s
accel_midilium_x = smooth(gradient(velocity_midilium_x(:,1),1/FS)); %
velocity_midilium_z = smooth(gradient(mid_ilium(:,3),1/FS)/1000); %incl.
conversion mm/s to m/s
accel_midilium_z = smooth(gradient(velocity_midilium_z(:,1),1/FS)); %
t=virtualmarkers.mid_ilium.Header;

%% Figure: Ilium displacement (ASA)

h10 = figure (10); clf; hold on
subplot(3,1,1); hold on
plot(mid_ilium(:,1), 'b'); title("Mid Ilium, x (+ve right)"); ylabel ('x
displacement (mm)')
subplot(3,1,2); hold on
plot(mid_ilium(:,2), 'b'); title("Mid Ilium, y (+ve forward)"); ylabel
('y displacement (mm)')
subplot(3,1,3); hold on
plot(mid_ilium(:,3), 'b'); title("Mid Ilium, z (+ve up)"); ylabel ('z
displacement (mm)')
xlabel ('time (s)');

h11 = figure(11); clf; hold on
subplot(3,1,1); hold on
plot(t,mid_ilium(:,2), 'b'); ylabel ('displ, m/s')
title('Mid-Ilium Displacement')
subplot(3,1,2); hold on
plot(t,velocity_midilium_y, 'b'); ylabel ('velocity, m/s')
title('Mid-Ilium Velocity')
subplot(3,1,3); hold on
plot(t,accel_midilium_y, 'b'); ylabel ('accel, m/s^2')
title('Mid-Ilium Acceleration')
xlabel ('time (s)');

% save figures as png
info=f.getFields(c3dfile); info.Folder='figures'; info.Folder='Results';
info.File=[strrep([info.File{1}, '_MidIliumDispl'],'.c3d',''), '.png'];
outfile=fres.genList(info); outfile=outfile{1};
mkdirfile(outfile); saveas(h10,outfile,'png');

info=f.getFields(c3dfile); info.Folder='figures'; info.Folder='Results';
info.File=[strrep([info.File{1}, '_MidIliumDisplVelAccl'],'.c3d',''),
'.png'];
```

```
outfile=fres.genList(info); outfile=outfile{1};
mkdirfile(outfile); saveas(h11,outfile,'png');

%% Figure: T1 displacement (ASA)

% Forward trajectory velocity, based on T1 motion
markers=Osim.interpret(trc,'TRC','struct');
T1=markers.T1{:,2:end};
velocity_T1_y = smooth(gradient(T1(:,2),1/FS)/1000); %incl. conversion
mm/s to m/s
accel_T1_y = smooth(gradient(velocity_T1_y(:,1),1/FS)); %
t=markers.T1.Header;

h12 = figure (12); clf; hold on
subplot(3,1,1); hold on
plot(T1(:,1), 'b'); title("T1, x (+ve right)"); ylabel ('x displacement
(mm)')
subplot(3,1,2); hold on
plot(T1(:,2), 'b'); title("T1, y (+ve forward)"); ylabel ('y displacement
(mm)')
subplot(3,1,3); hold on
plot(T1(:,3), 'b'); title("T1, z (+ve up)"); ylabel ('z displacement
(mm)')
xlabel ('time (s)');

h13 = figure(13); clf; hold on
subplot(3,1,1); hold on
plot(t,T1(:,2), 'b'); ylabel ('displ, m/s')
title('T1 Displacement')
subplot(3,1,2); hold on
plot(t,velocity_T1_y, 'b'); ylabel ('velocity, m/s')
title('T1 Velocity')
subplot(3,1,3); hold on
plot(t,accel_T1_y, 'b'); ylabel ('accel, m/s^2')
title('T1 Acceleration')
xlabel ('time (s)');

% save figures as png
info=f.getFields(c3dfile); info.Folder='Results';
info.File=[strrep([info.File{1}, '_T1Displ'],'.c3d',''), '.png'];
outfile=fres.genList(info); outfile=outfile{1};
mkdirfile(outfile); saveas(h12,outfile,'png');

info=f.getFields(c3dfile); info.Folder='Results';
info.File=[strrep([info.File{1}, '_T1VelAccl'],'.c3d',''), '.png'];
outfile=fres.genList(info); outfile=outfile{1};
mkdirfile(outfile); saveas(h13,outfile,'png');

% Add global results to the table
globalresults.minabsvelocity_midilium_y(1)=min(abs(velocity_midilium_y));
globalresults.maxabsvelocity_midilium_y(1)=max(abs(velocity_midilium_y));
globalresults.meanabsvelocity_midilium_y(1)=mean(abs(velocity_midilium_y)
);
globalresults.rangevelocity_midilium_y(1)=range(velocity_midilium_y);
globalresults.minabsvelocity_midilium_x(1)=min(abs(velocity_midilium_x));
globalresults.maxabsvelocity_midilium_x(1)=max(abs(velocity_midilium_x));
globalresults.meanabsvelocity_midilium_x(1)=mean(abs(velocity_midilium_x)
);
globalresults.rangevelocity_midilium_x(1)=range(velocity_midilium_x);
globalresults.minvelocity_midilium_z(1)=min(velocity_midilium_z);
globalresults.maxvelocity_midilium_z(1)=max(velocity_midilium_z);
```

```
globalresults.meanvelocity_midilium_z(1)=mean(velocity_midilium_z);
globalresults.rangevelocity_midilium_z(1)=range(velocity_midilium_z);
globalresults.minabsvelocity_T1_y=min(abs(velocity_T1_y));
globalresults.maxabsvelocity_T1_y=max(abs(velocity_T1_y));
globalresults.meanabsvelocity_T1_y=mean(abs(velocity_T1_y));
globalresults.rangevelocity_T1_y=range(velocity_T1_y);

markers=Osim.interpret(trc,'TRC','struct');
% Head Range w.r.t T1 analysis [Annabel's request]  (cm)
head_T1=markers.HEAD{:,2:end}-markers.T1{:,2:end};
% T1 Range to T13 analysis [Annabel's request]  (cm) %%%%%%%
T1_T13=markers.T1{:,2:end}-markers.T13{:,2:end};
% T1 Range to L7 analysis [Annabel's request]  (cm) %%%%%%%
T1_L7=markers.T1{:,2:end}-markers.L7{:,2:end};
% T1 analysis. Distance of T1 to floor, deviation left-right
T1=markers.T1{:,2:end};

%Distance between markers
% Head Range w.r.t T1 analysis [Annabel's request]  (cm)
globalresults.MinAbsHeadToT1_x=min(abs(head_T1(:,1))/10); %(cm)
globalresults.MaxAbsHeadToT1_x=max(abs(head_T1(:,1))/10); %(cm)
globalresults.MinHeadToT1_z=min(head_T1(:,3))/10; %(cm)
globalresults.MaxHeadToT1_z=max(head_T1(:,3))/10; %(cm)
globalresults.RangeHeadToT1_x=range(head_T1(:,1))/10; %(cm)
globalresults.RangeHeadToT1_z=range(head_T1(:,3))/10; %(cm)
globalresults.MeanAbsHeadToT1_x=mean(abs(head_T1(:,1))/10); %(cm)
globalresults.MeanHeadToT1_z=mean(head_T1(:,3))/10; %(cm)
% T1 analysis. Distance of T1 relative to floor, deviation left-right
(cm)
globalresults.MinAbsStrideT1_x=min(abs(T1(:,1))/10); %(cm)
globalresults.MaxAbsStrideT1_x=max(abs(T1(:,1))/10); %(cm)
globalresults.MinStrideT1_z=min(T1(:,3))/10; %(cm)
globalresults.MaxStrideT1_z=max(T1(:,3))/10; %(cm)
globalresults.RangeStrideT1_x=range(T1(:,1))/10; %(cm)
globalresults.RangeStrideT1_z=range(T1(:,3))/10; %(cm)
globalresults.MeanAbsStrideT1_x=mean(abs(T1(:,1))/10); %(cm)
globalresults.MeanStrideT1_z=mean(T1(:,3))/10; %(cm)
% T1 Range w.r.t T13 analysis [Annabel's request]  (cm)
globalresults.MinAbsT1ToT13_x=min(abs(T1_T13(:,1))/10); %(cm)
globalresults.MaxAbsT1ToT13_x=max(abs(T1_T13(:,1))/10); %(cm)
globalresults.MinT1ToT13_z=min(abs(T1_T13(:,3))/10); %(cm)
globalresults.MaxT1ToT13_z=max(T1_T13(:,3))/10; %(cm)
globalresults.RangeT1ToT13_x=range(T1_T13(:,1))/10; %(cm)
globalresults.RangeT1ToT13_z=range(T1_T13(:,3))/10; %(cm)
globalresults.MeanAbsT1ToT13_x=mean(abs(T1_T13(:,1))/10); %(cm)
globalresults.MeanT1ToT13_z=mean(T1_T13(:,3))/10; %(cm)
% T1 Range w.r.t L7 analysis [Annabel's request]  (cm)
globalresults.MinAbsT1ToL7_x=min(abs(T1_L7(:,1)))/10; %(cm)
globalresults.MaxAbsT1ToL7_x=max(abs(T1_L7(:,1)))/10; %(cm)
globalresults.MinT1ToL7_z=min(T1_L7(:,3))/10; %(cm)
globalresults.MaxT1ToL7_z=max(T1_L7(:,3))/10; %(cm)
globalresults.RangeT1ToL7_x=range(T1_L7(:,1))/10; %(cm)
globalresults.RangeT1ToL7_z=range(T1_L7(:,3))/10; %(cm)
globalresults.MeanAbsT1ToL7_x=mean(abs(T1_L7(:,1)))/10; %(cm)
globalresults.MeanT1ToL7_z=mean(T1_L7(:,3))/10; %(cm)

info=f.getFields(c3dfile); info.Folder='Results';
info.File=strrep(info.File{1},'.c3d','.mat');
outfile=fres.genList(info); outfile=outfile{1};
mkdirfile(outfile); save(outfile,'globalresults');

%% Figure: Head displacement (ASA)
```

```
% Forward trajectory velocity, based on Head motion
markers=Osim.interpret(trc,'TRC','struct');
HEAD=markers.HEAD{:,2:end};
velocity_HEAD_y = smooth(gradient(HEAD(:,2),1/FS)/1000); %incl.
conversion mm/s to m/s
accel_HEAD_y = smooth(gradient(velocity_HEAD_y(:,1),1/FS)); %
t=markers.HEAD.Header;

h14 = figure (14); clf; hold on
subplot(3,1,1); hold on
plot(HEAD(:,1), 'b'); title("Head, x (+ve right)"); ylabel ('x
displacement (mm)')
subplot(3,1,2); hold on
plot(HEAD(:,2), 'b'); title("Head, y (+ve forward)"); ylabel ('y
displacement (mm)')
subplot(3,1,3); hold on
plot(HEAD(:,3), 'b'); title("Head, z (+ve up)"); ylabel ('z displacement
(mm)')
xlabel ('time (s)');

h15 = figure(15); clf; hold on
subplot(3,1,1); hold on
plot(t,HEAD(:,2), 'b'); ylabel ('displ, m/s')
title('Head Displacement')
subplot(3,1,2); hold on
plot(t,velocity_HEAD_y, 'b'); ylabel ('velocity, m/s')
title('Head Velocity')
subplot(3,1,3); hold on
plot(t,accel_HEAD_y, 'b'); ylabel ('accel, m/s^2')
title('Head Acceleration')
xlabel ('time (s)');

% save figures as png
info=f.getFields(c3dfile); info.Folder='Results';
info.File=[strrep([info.File{1}, '_HeadDispl'],'.c3d',''), '.png'];
outfile=fres.genList(info); outfile=outfile{1};
mkdirfile(outfile); saveas(h14,outfile,'png');

info=f.getFields(c3dfile); info.Folder='Results';
info.File=[strrep([info.File{1}, '_HeadVelAccl'],'.c3d',''), '.png'];
outfile=fres.genList(info); outfile=outfile{1};
mkdirfile(outfile); saveas(h15,outfile,'png');

%% Figure: T1 w.r.t Head displacement (ASA)

HEAD_T1=markers.HEAD{:,2:end}-markers.T1{:,2:end};

h16 = figure (16); clf; hold on
subplot(3,1,1); hold on
plot(HEAD_T1(:,1), 'b'); title("Head-T1 Distance, x (+ve right)"); ylabel
('x displacement (mm)')
subplot(3,1,2); hold on
plot(HEAD_T1(:,2), 'b'); title("Head-T1 Distance, y (+ve forward)");
ylabel ('y displacement (mm)')
subplot(3,1,3); hold on
plot(HEAD_T1(:,3), 'b'); title("Head-T1 Distance, z (+ve up)"); ylabel
('z displacement (mm)')
xlabel ('time (s)');

% save figures as png
```

```
info=f.getFields(c3dfile); info.Folder='Results';
info.File=[strrep([info.File{1}, '_HeadtoT1Displ'],'.c3d',''), '.png'];
outfile=fres.genList(info); outfile=outfile{1};
mkdirfile(outfile); saveas(h16,outfile,'png');

%% %% Figure: T1 w.r.t T13 displacement (ASA)

T1_T13=markers.T1{:,2:end}-markers.T13{:,2:end};

h17 = figure (17); clf; hold on
subplot(3,1,1); hold on
plot(T1_T13(:,1), 'b'); title("T1-T13 Distance, x (+ve right)"); ylabel
('x displacement (mm)')
subplot(3,1,2); hold on
plot(T1_T13(:,2), 'b'); title("T1-T13 Distance, y (+ve forward)"); ylabel
('y displacement (mm)')
subplot(3,1,3); hold on
plot(T1_T13(:,3), 'b'); title("T1-T13 Distance, z (+ve up)"); ylabel ('z
displacement (mm)')
xlabel ('time (s)');

% save figures as png
info=f.getFields(c3dfile); info.Folder='Results';
info.File=[strrep([info.File{1}, '_T1toT13Displ'],'.c3d',''), '.png'];
outfile=fres.genList(info); outfile=outfile{1};
mkdirfile(outfile); saveas(h17,outfile,'png');

%% Figure: T1 w.r.t L7 displacement (ASA)

T1_L7=markers.T1{:,2:end}-markers.L7{:,2:end};

h18 = figure (18); clf; hold on
subplot(3,1,1); hold on
plot(T1_L7(:,1), 'b'); title("T1-L7 Distance, x (+ve right)"); ylabel ('x
displacement (mm)')
subplot(3,1,2); hold on
plot(T1_L7(:,2), 'b'); title("T1-L7 Distance, y (+ve forward)"); ylabel
('y displacement (mm)')
subplot(3,1,3); hold on
plot(T1_L7(:,3), 'b'); title("T1-L7 Distance, z (+ve up)"); ylabel ('z
displacement (mm)')
xlabel ('time (s)');

% save figures as png
info=f.getFields(c3dfile); info.Folder='Results';
info.File=[strrep([info.File{1}, '_T1toL7Displ'],'.c3d',''), '.png'];
outfile=fres.genList(info); outfile=outfile{1};
mkdirfile(outfile); saveas(h18,outfile,'png');


%% Figure: Fore and hind foot placement as maps of x-y locations
R_forefoot1=markers.RF_DPHAL{:,2:end};
L_forefoot1=markers.LF_DPHAL{:,2:end};
R_hindfoot1=markers.RH_DPHAL{:,2:end};
L_hindfoot1=markers.LH_DPHAL{:,2:end};

h19 = figure(19); clf; hold on
subplot(2,1,1); hold on
plot(R_forefoot1(:,1),R_forefoot1(:,2),'r'); title("Fore foot")
plot(L_forefoot1(:,1),L_forefoot1(:,2),'b');
legend("Right foot", "Left foot")
```

```
subplot(2,1,2); hold on
plot(R_hindfoot1(:,1),R_hindfoot1(:,2),'r'); title("Hind foot")
plot(L_hindfoot1(:,1),L_hindfoot1(:,2),'b');
legend("Right foot", "Left foot")

%% Figure: Trajectory of lowest foot marker for each limb, in global te
%system, x-axis (sideways motion, +ve x to right)
h20 = figure(20); clf; hold on
subplot(6,1,1); hold on
plot(t,R_forefoot1(:,1),'r'); title("Fore: R lateral trajectory, +ve
right")
ylabel ('lateral displ (mm)');
subplot(6,1,2); hold on
plot(t,L_forefoot1(:,1),'b'); title("Fore: L lateral trajectory, +ve
right")
ylabel ('lateral displ (mm)');
subplot(6,1,3); hold on
plot(t,(R_forefoot1(:,1) - L_forefoot1(:,1)), 'k'); title("Fore: R-L,
lateral")
ylabel ('lateral R-L difference (mm)');
subplot(6,1,4); hold on
plot(t,R_hindfoot1(:,1), 'r' ); title("Hind: R lateral trajectory, +ve
right")
ylabel ('vert displ (mm)');
subplot(6,1,5); hold on
plot(t,L_hindfoot1(:,1), 'b' ); title("Hind: L lateral trajectory, +ve
right")
ylabel ('vert displ (mm)');
subplot(6,1,6); hold on
plot(t,(R_hindfoot1(:,1) - L_hindfoot1(:,1)), 'k'); title("Hind: R-L,
lateral")
ylabel ('lateral R-L difference (mm)');
ylabel ('lateral displ (mm)');
xlabel ('time (s)');

%conclusion: x displacement are not cyclic in relation to swing and
stance phase

% save figures as png
info=f.getFields(c3dfile); info.Folder='Results';
info.File=[strrep([info.File{1}, '_HoofPlacementMap'],'.c3d',''),
'.png'];
outfile=fres.genList(info); outfile=outfile{1};
mkdirfile(outfile); saveas(h19,outfile,'png');

info=f.getFields(c3dfile); info.Folder='Results';
info.File=[strrep([info.File{1}, '_HoofPlacementPlots'],'.c3d',''),
'.png'];
outfile=fres.genList(info); outfile=outfile{1};
mkdirfile(outfile); saveas(h20,outfile,'png');

%% B. Leg-Independent analyses
% Results table contains all the result of leg independent analyses
n=numel(strides);
results=table();
results.LegName=cell(n,1); results.Properties.VariableUnits{1}='';
% Calculate durations (s) (Wilson et al., 2019)
results.StanceDuration=nan(n,1);
results.SwingDuration=nan(n,1);
results.StrideDuration=nan(n,1);
results.Properties.VariableUnits(2:4)={'s'};
% Lateral deviation of hoof during swing (cm) [Wilson et al., 2019]
```

```
results.HoofLateralDeviation=nan(n,1);
results.Properties.VariableUnits{5}='cm';
% Velocity of hoof during swing %(m/s) [Wilson et al., 2019]
results.ForwardSwingVelocity=nan(n,1);
results.VerticalSwingVelocity=nan(n,1);
results.Properties.VariableUnits(6:7)={'m/s'};
% Range of hoof height during swing (cm) [Wilson et al., 2019]
results.HoofHeightRange=nan(n,1);
results.Properties.VariableUnits{8}='cm';
% Stride length (cm)
results.StrideLength=nan(n,1); results.Properties.VariableUnits{9}='cm';
% Stance base [requested by Annabel) (cm)
results.DistanceMatchingLimbStance=nan(n,1);
results.Properties.VariableUnits{10}='cm';
% Preliminary 2D joint angle analysis (deg)
results.MinFetlockStance=nan(n,1);
results.MaxFetlockStance=nan(n,1);
results.RangeFetlockStance=nan(n,1);
results.MinFetlockSwing=nan(n,1);
results.MaxFetlockSwing=nan(n,1);
results.RangeFetlockSwing=nan(n,1);
results.MinHockStance=nan(n,1);
results.MaxHockStance=nan(n,1);
results.RangeHockStance=nan(n,1);
results.MinHockSwing=nan(n,1);
results.MaxHockSwing=nan(n,1);
results.RangeHockSwing=nan(n,1);
results.MinStifleStance=nan(n,1);
results.MaxStifleStance=nan(n,1);
results.RangeStifleStance=nan(n,1);
results.MinStifleSwing=nan(n,1);
results.MaxStifleSwing=nan(n,1);
results.RangeStifleSwing=nan(n,1);
results.Properties.VariableUnits(11:28)={'deg'};
% Here for loop the strides and compute every analysis code
for i=1:numel(strides)
   s=strides{i};
   distalmarker=distalmarkers{strcmp(legs,s.leg)};
   markers=Osim.interpret(s.trc,'TRC','struct');
   results.LegName{i}=s.leg;
   %{
   figure(1); % Look at the gait cycle
   thisLegStrike=s.gc.([distalmarkers{i},'_Strike']);
   thisLegOff=s.gc.([distalmarkers{i},'_Off']);
   plot(thisLegStrike); hold on;
   plot(thisLegOff); hold off;
   figure(2); % Look at the animation
   plotAnimation(vskfile,s.trc);
   %}
   %% Calculate durations (s) (Wilson et al., 2019)
   % stance: off-start   % swing: end-off    % duration: end-start
   results.StanceDuration(i)=diff(s.stanceIdx)/FS;
   results.SwingDuration(i)=diff(s.swingIdx)/FS;
   results.StrideDuration(i)=(s.swingIdx(2)-s.stanceIdx(1))/FS;
   %% Lateral deviation of hoof during swing (cm) [Wilson et al., 2019]
   thismarker=markers.(distalmarker){:,2:end};

results.HoofLateralDeviation(i)=range(thismarker(s.swingIdx(1):s.swingIdx
(2),1))/10; %(cm)
   %% (Forward and Vertical) Velocity of hoof during swing (m/s) [Wilson
et al., 2019]
   velocity_y= gradient(thismarker(:,2),1/FS); %(mm/s)
```

```
   results.ForwardSwingVelocity(i)=
mean(abs(velocity_y(s.swingIdx(1):s.swingIdx(2))))/1000; %(m/s)
   velocity_z= gradient(thismarker(:,3),1/FS); %(mm/s)
   results.VerticalSwingVelocity(i)=
mean(abs(velocity_z(s.swingIdx(1):s.swingIdx(2))))/1000; %(m/s)
   %% Range of hoof height during swing (cm) [Wilson et al., 2019]

results.HoofHeightRange(i)=range(thismarker(s.swingIdx(1):s.swingIdx(2),3
))/10; %(cm)
   %% Stride length (cm)

results.StrideLength(i)=range(thismarker(s.stanceIdx(2):s.swingIdx(2),2))
/10; %(cm)
   %% Stance base [requested by Annabel) (cm)
   % (Lateral) Distance between matching limbs (cm) during stance (mean
   % value throughout entire stance phase)
   % forelimbs
   switch s.leg
        case 'L_forefoot'
            matchingLeg='R_forefoot';
        case 'R_forefoot'
           matchingLeg='L_forefoot';
        case 'L_hindfoot'
           matchingLeg='R_hindfoot';
        case 'R_hindfoot'
           matchignLeg='L_hindfoot';
   end

   % Get the distance during stance phase
   matchingMarkerName=distalmarkers{strcmp(legs,matchingLeg)};
   matchingMarkerTbl=markers.(matchingMarkerName);
matchingMarker=matchingMarkerTbl{:,2:end};
   matchingLeg_strikeIdx=find(s.gc.([matchingMarkerName,'_Strike'])==0);
   matchingLeg_offIdx=find(s.gc.([matchingMarkerName,'_Off'])==0);

   % Get indices of stance for the matching leg
   stanceIdx=[matchingLeg_strikeIdx(1)
min([matchingLeg_offIdx(matchingLeg_offIdx>matchingLeg_strikeIdx)
size(s.gc,1)])];

   %% Figure: Limb Distance Distal Markers

   h21 = figure(21);
   if i==1
       clf;
   end

   switch s.leg
        case 'L_forefoot'
           subplot(2,1,1); hold on;
           % s.leg most distal marker
           plot(s.trc{s.stanceIdx(1):s.stanceIdx(2),([distalmarker
'_x'])},s.trc{s.stanceIdx(1):s.stanceIdx(2),([distalmarker '_y'])},'x');
           title("Forelimb Stance")

           % corresponding marker on the contralateral side
           plot(s.trc{stanceIdx(1):stanceIdx(2),([matchingMarkerName
'_x'])},s.trc{stanceIdx(1):stanceIdx(2),([matchingMarkerName
'_y'])},'x');
        case 'R_forefoot'
```

```
        case 'L_hindfoot'
           subplot(2,1,2); hold on;
           % s.leg most distal marker
           plot(s.trc{s.stanceIdx(1):s.stanceIdx(2),([distalmarker
'_x'])},s.trc{s.stanceIdx(1):s.stanceIdx(2),([distalmarker '_y'])},'x');
           title("Hindlimb Stance")

           % corresponding marker on the contralateral side
           plot(s.trc{stanceIdx(1):stanceIdx(2),([matchingMarkerName
'_x'])},s.trc{stanceIdx(1):stanceIdx(2),([matchingMarkerName
'_y'])},'x');

        case 'R_hindfoot'
   end

info=f.getFields(c3dfile); info.Folder='Results';
info.File=[strrep([info.File{1}, '_LimbStanceDist'],'.c3d',''), '.png'];
outfile=fres.genList(info); outfile=outfile{1};
mkdirfile(outfile); saveas(h21,outfile,'png');



   %% Check the animation of strides
   %figure();
   %plotAnimation(vskfile,s.trc(stanceIdx(1):stanceIdx(2),:))
   %plotAnimation(vskfile,s.trc(s.stanceIdx(1):s.stanceIdx(2),:))

   markers=Osim.interpret(s.trc,'TRC','struct');
   x1=mean(thismarker(s.stanceIdx(1):s.stanceIdx(2),:));
   x2=mean(matchingMarker(stanceIdx(1):stanceIdx(2),:));
   results.DistanceMatchingLimbStance(i)=norm(x1-x2)/10; %(cm)

   %% Preliminary 2D joint angle analysis (deg)
   % Fetlock joint (equivalent to ankle or wrist)
   switch s.leg
       % Left Forelimb
       % Phalanx Group = LF_PHAL and LF_DPHAL; Metatarsal Group = L_METAR
and LF_PPHAL
       case 'L_forefoot'

jointangle=jointangle_2D(markers,'LF_PHAL','LF_DPHAL','L_METAR','LF_PPHAL
');
       % Right Forelimb
       % Phalanx Group = RF_PHAL and RF_DPAHL; Metatarsal Group = R_METAR
and RF_PPHAL
       case 'R_forefoot'

jointangle=jointangle_2D(markers,'RF_PHAL','RF_DPHAL','R_METAR','RF_PPHAL
');
       % Left Hindlimb
       % Phalanx Group = LH_PHAL and LH_DPHAL; Tarsal Group = L_FTAR and
LH_PPHAL
       case 'L_hindfoot'

jointangle=jointangle_2D(markers,'LH_PHAL','LH_DPHAL','L_FTAR','LH_PPHAL'
);
       % Right Hindlimb
       % Phalanx Group = RH_PHAL and RH_DPHAL; Tarsal Group = R_FTAR and
RH_PPHAL
       case 'R_hindfoot'
```

```
jointangle=jointangle_2D(markers,'RH_PHAL','RH_DPHAL','R_FTAR','RH_PPHAL'
);
   end
   % During Stance (∞)

results.MinFetlockStance(i)=min(jointangle(s.stanceIdx(1):s.stanceIdx(2))
);

results.MaxFetlockStance(i)=max(jointangle(s.stanceIdx(1):s.stanceIdx(2))
);

results.RangeFetlockStance(i)=range(jointangle(s.stanceIdx(1):s.stanceIdx
(2)));
   % During Swing (∞)

results.MinFetlockSwing(i)=min(jointangle(s.swingIdx(1):s.swingIdx(2)));

results.MaxFetlockSwing(i)=max(jointangle(s.swingIdx(1):s.swingIdx(2)));

results.RangeFetlockSwing(i)=range(jointangle(s.swingIdx(1):s.swingIdx(2)
));

   % Knee/Hock joint (equivalent to knee or elbow)
   switch s.leg
       % Left Forelimb
       % Metatarsal Group = L_METAR and LF_PPHAL; Radius/Ulna group =
L_LEPIRAD and L_ULNA
        case 'L_forefoot'

jointangle=jointangle_2D(markers,'L_METAR','LF_PPHAL','L_LEPIRAD','L_ULNA
');
       % Right Forelimb
       % Metatarsal Group = R_METAR and RF_PPHAL; Radius/Ulna group =
R_LEPIRAD and R_ULNA
        case 'R_forefoot'

jointangle=jointangle_2D(markers,'R_METAR','RF_PPHAL','R_LEPIRAD','R_ULNA
');
        % Left Hindlimb
        % Tarsal Group = L_FTAR and LH_PPHAL; Tibia group = L_LTIB and
L_LMAL
        case 'L_hindfoot'

jointangle=jointangle_2D(markers,'L_FTAR','LH_PPHAL','L_LTIB','L_LMAL');
        % Right Hindlimb
        % Tarsal Group = R_FTAR and RH_PPHAL; Tibia group = R_LTIB and
R_LMAL
        case 'R_hindfoot'

jointangle=jointangle_2D(markers,'R_FTAR','RH_PPHAL','R_LTIB','R_LMAL');
   end
   % During Stance (∞)

results.MinHockStance(i)=min(jointangle(s.stanceIdx(1):s.stanceIdx(2)));

results.MaxHockStance(i)=max(jointangle(s.stanceIdx(1):s.stanceIdx(2)));

results.RangeHockStance(i)=range(jointangle(s.stanceIdx(1):s.stanceIdx(2)
));
   % During Swing (∞)
   results.MinHockSwing(i)=min(jointangle(s.swingIdx(1):s.swingIdx(2)));
   results.MaxHockSwing(i)=mx(jointangle(s.swingIdx(1):s.swingIdx(2)));
```

```
results.RangeHockSwing(i)=range(jointangle(s.swingIdx(1):s.swingIdx(2)));

   % Stifle/Shoulder joint (equivalent to hip or shoulder)
   switch s.leg
       % Left Forelimb
       % Radius/Ulna group = L_LEPIRAD and L_ULNA; Humerus group = L_GTUB
and L_LEPIRAD
        case 'L_forefoot'

jointangle=jointangle_2D(markers,'L_LEPIRAD','L_ULNA','L_GTUB','L_LEPIRAD
');
       % Right Forelimb
       % Radius/Ulna group = R_LEPIRAD and R_ULNA; Humerus group = R_GTUB
and R_LEPIRAD
        case 'R_forefoot'

jointangle=jointangle_2D(markers,'R_LEPIRAD','R_ULNA','R_GTUB','R_LEPIRAD
');
       % Left Hindlimb
       % Tibia group = L_LTIB and L_LMAL; Femur group = L_GTROC and
L_LEPI
        case 'L_hindfoot'

jointangle=jointangle_2D(markers,'L_LTIB','L_LMAL','L_GTROC','L_LEPI');
       % Right Hindlimb
       % Tibia group = R_LTIB and R_LMAL; Femur group = R_GTROC and
R_LEPI
        case 'R_hindfoot'

jointangle=jointangle_2D(markers,'R_LTIB','R_LMAL','R_GTROC','R_LEPI');
   end
   % During Stance (∞)

results.MinStifleStance(i)=min(jointangle(s.stanceIdx(1):s.stanceIdx(2)))
;

results.MaxStifleStance(i)=max(jointangle(s.stanceIdx(1):s.stanceIdx(2)))
;

results.RangeStifleStance(i)=range(jointangle(s.stanceIdx(1):s.stanceIdx(
2)));
   % During Swing (∞)

results.MinStifleSwing(i)=min(jointangle(s.swingIdx(1):s.swingIdx(2)));

results.MaxStifleSwing(i)=max(jointangle(s.swingIdx(1):s.swingIdx(2)));

results.RangeStifleSwing(i)=range(jointangle(s.swingIdx(1):s.swingIdx(2))
);

end
%Save the results table
info=f.getFields(c3dfile); info.Folder='Results';
info.File=strrep(info.File{1},'.c3d','.mat');
outfile=fres.genList(info); outfile=outfile{1};
mkdirfile(outfile); save(outfile,'results','-append');
```

Appendix 9.2 Baseline compared to post-stroke hind-limb parameters (mean +/- SD)

Left hindlimb

Variable	*Mean Baselines*	*Post-stroke*	*Mean difference un-adjusted (95% CI)*	*P-value un-adjusted*	*Mean difference adjusted (95% CI)*	*P-value adjusted*
Stance Duration (s)	0.43 (0.01)	0.56 (0.11)	0.13 (0.10, 0.15)	<0.001 *	0.02 (-0.01, 0.04)	0.132
Swing Duration (s)	0.34 (0.00)	0.37 (0.04)	0.03 (0.02, 0.04)	<0.001 *	0.01 (-0.00, 0.02)	0.061
Stride Duration (s)	0.77 (0.01)	0.93 (0.13)	0.16 (0.13, 0.19)	<0.001 *	0.03 (0.01, 0.05)	0.015 *
Ratio Stance To Stride (%)	0.55 (0.00)	0.60 (0.03)	0.05 (0.03, 0.06)	<0.001 *	0.00 (-0.01, 0.02)	0.599
Ratio Swing To Stride (%)	0.45 (0.00)	0.40 (0.03)	-0.05 (-0.06, -0.03)	<0.001 *	-0.00 (-0.02, 0.01)	0.599
Ratio Stance To Swing (%)	1.26 (0.02)	1.51 (0.22)	0.25 (0.17, 0.32)	<0.001 *	-0.00 (-0.08, 0.07)	0.962
Hoof Lateral Deviation (cm)	7.07 (0.43)	6.55 (1.97)	-0.55 (-1.41, 0.31)	0.208	-0.63 (-1.66, 0.40)	0.231
Hoof Forward Swing Velocity (m/s)	2.87 (0.03)	2.45 (0.27)	-0.43 (-0.50, -0.35)	<0.001 *	-0.17 (-0.24, -0.09)	<0.001 *
Hoof Vertical Swing Velocity (m/s)	0.24 (0.01)	0.21 (0.08)	-0.03 (-0.06, 0.00)	0.056	-0.02 (-0.05, 0.02)	0.319
Range Hoof Height in Swing (cm)	4.18 (0.12)	3.97 (1.35)	-0.22 (-0.80, 0.37)	0.469	-0.16 (-0.87, 0.55)	0.666
Stride Length (cm)	97.67 (0.99)	90.13 (6.06)	-7.70 (-9.53, -5.87)	<0.001 *	-1.79 (-3.63, 0.05)	0.056
Minimum Hindlimb Fetlock Angle Stance (º)	2.12 (1.24)	1.81 (7.61)	-0.35 (-4.39, 3.70)	0.867	1.24 (-3.43, 5.91)	0.603
Maximum Hindlimb Fetlock Angle Stance (º)	19.02 (1.15)	17.28 (7.29)	-1.79 (-5.85, 2.28)	0.389	-1.33 (-6.17, 3.50)	0.589
Range Hindlimb Fetlock Angle in Stance (º)	16.90 (0.12)	15.47 (4.24)	-1.44 (-3.22, 0.34)	0.112	-2.39 (-4.56, -0.23)	0.03 *
Minimum Hindlimb Fetlock Angle in Swing (º)	-32.04 (1.19)	-25.68 (8.63)	6.35 (2.22, 10.47)	0.003 *	6.43 (1.64, 11.23)	0.009 *
Maximum Hindlimb Fetlock Angle in Swing (º)	9.11 (1.34)	7.16 (7.82)	-2.00 (-6.01, 2.02)	0.329	-0.33 (-5.03, 4.37)	0.891
Range Hindlimb Fetlock Angle in Swing (º)	41.15 (0.74)	32.84 (6.18)	-8.34 (-11.06, -5.63)	<0.001 *	-6.61 (-9.89, -3.33)	<0.001 *
Minimum Tarsal Angle in Stance (º)	27.70 (0.40)	27.15 (7.76)	-0.35 (-3.32, 2.62)	0.818	-0.32 (-3.84, 3.19)	0.857
Maximum Tarsal Angle in Stance (º)	63.10 (0.24)	58.01 (9.57)	-5.07 (-7.77, -2.37)	<0.001 *	-3.41 (-6.69, -0.12)	0.042 *
Range Tarsal Angle in Stance (º)	35.41 (0.44)	30.86 (6.08)	-4.72 (-6.81, -2.63)	<0.001 *	-3.03 (-5.49, -0.56)	0.016 *
Minimum Tarsal Angle in Swing (º)	27.73 (0.38)	27.14 (7.59)	-0.38 (-3.51, 2.75)	0.812	-1.09 (-4.90, 2.71)	0.573
Maximum Tarsal Angle in Swing (º)	77.25 (0.56)	70.65 (11.40)	-6.53 (-9.67, -3.39)	<0.001 *	-5.14 (-8.92, -1.35)	0.008 *
Range Tarsal Angle in Swing (º)	49.53 (0.29)	43.51 (7.20)	-6.15 (-8.91, -3.39)	<0.001 *	-3.95 (-7.26, -0.63)	0.02 *
Minimum Stifle Angle in Stance (º)	-68.54 (0.65)	-65.60 (15.97)	3.01 (-2.44, 8.46)	0.279	1.86 (-4.63, 8.34)	0.575
Maximum Stifle Angle in Stance (º)	-45.12 (1.05)	-39.39 (14.56)	5.81 (0.56, 11.06)	0.03 *	2.71 (-3.43, 8.85)	0.387
Range Stifle Angle in Stance (º)	23.42 (0.46)	26.22 (4.98)	2.80 (0.41, 5.19)	0.022 *	0.58 (-2.20, 3.36)	0.68
Minimum Stifle Angle in Swing (º)	-80.72 (0.93)	-74.06 (15.27)	6.69 (1.52, 11.86)	0.011 *	4.48 (-1.68, 10.64)	0.154
Maximum Stifle Angle in Swing (º)	-35.46 (1.41)	-32.70 (14.73)	2.84 (-2.53, 8.21)	0.3	0.87 (-5.44, 7.19)	0.786
Range Stifle Angle in Swing (º)	45.26 (0.66)	41.36 (3.87)	-3.85 (-6.14, -1.56)	0.001 *	-3.94 (-6.70, -1.18)	0.005 *

* = p<0.05

(continued)

Right hindlimb						
Variable	*Mean Baselines*	*Post-stroke*	*Mean difference un-adjusted (95% CI)*	*P-value un-adjusted*	*Mean difference adjusted (95% CI)*	*P-value adjusted*
Stance Duration (s)	0.43 (0.01)	0.56 (0.11)	0.12 (0.10, 0.15)	<0.001 *	0.02 (-0.01, 0.04)	0.184
Swing Duration (s)	0.34 (0.00)	0.37 (0.03)	0.03 (0.02, 0.04)	<0.001 *	0.01 (-0.00, 0.02)	0.148
Stride Duration (s)	0.77 (0.01)	0.92 (0.12)	0.15 (0.12, 0.18)	<0.001 *	0.03 (0.00, 0.05)	0.038 *
Ratio Stance To Stride (%)	0.55 (0.00)	0.60 (0.04)	0.05 (0.03, 0.06)	<0.001 *	0.00 (-0.01, 0.02)	0.57
Ratio Swing To Stride (%)	0.45 (0.00)	0.40 (0.04)	-0.05 (-0.06, -0.03)	<0.001 *	-0.00 (-0.02, 0.01)	0.57
Ratio Stance To Swing (%)	1.27 (0.02)	1.52 (0.26)	0.25 (0.17, 0.32)	<0.001 *	0.00 (-0.07, 0.08)	0.972
Hoof Lateral Deviation (cm)	7.56 (0.23)	5.80 (1.81)	-1.81 (-2.67, -0.95)	<0.001 *	-1.89 (-2.92, -0.86)	<0.001 *
Hoof Forward Swing Velocity (m/s)	2.86 (0.03)	2.46 (0.26)	-0.41 (-0.48, -0.33)	<0.001 *	-0.15 (-0.22, -0.07)	<0.001 *
Hoof Vertical Swing Velocity (m/s)	0.22 (0.00)	0.18 (0.08)	-0.05 (-0.08, -0.02)	0.001 *	-0.04 (-0.08, -0.00)	0.03 *
Range Hoof Height in Swing (cm)	3.85 (0.10)	3.24 (1.22)	-0.64 (-1.23, -0.06)	0.032 *	-0.58 (-1.29, 0.13)	0.109
Stride Length (cm)	97.63 (0.52)	90.33 (6.45)	-7.44 (-9.28, -5.61)	<0.001 *	-1.53 (-3.37, 0.30)	0.102
Minimum Hindlimb Fetlock Angle Stance (º)	2.25 (1.26)	1.38 (8.05)	-0.85 (-4.89, 3.20)	0.681	0.73 (-3.93, 5.40)	0.758
Maximum Hindlimb Fetlock Angle Stance (º)	19.77 (1.16)	19.52 (9.10)	-0.18 (-4.25, 3.88)	0.93	0.27 (-4.56, 5.11)	0.912
Range Hindlimb Fetlock Angle in Stance (º)	17.52 (0.25)	18.15 (4.99)	0.67 (-1.11, 2.45)	0.462	-0.29 (-2.45, 1.88)	0.796
Minimum Hindlimb Fetlock Angle in Swing (º)	-30.93 (0.91)	-24.00 (6.68)	6.95 (2.82, 11.07)	0.001 *	7.03 (2.24, 11.83)	0.004 *
Maximum Hindlimb Fetlock Angle in Swing (º)	10.12 (1.36)	8.84 (8.72)	-1.24 (-5.26, 2.77)	0.544	0.43 (-4.27, 5.12)	0.859
Range Hindlimb Fetlock Angle in Swing (º)	41.05 (0.91)	32.84 (5.43)	-8.19 (-10.90, -5.47)	<0.001 *	-6.46 (-9.74, -3.18)	<0.001 *
Minimum Tarsal Angle in Stance (º)	24.43 (0.16)	23.85 (6.69)	-0.42 (-3.39, 2.55)	0.781	-0.39 (-3.91, 3.12)	0.826
Maximum Tarsal Angle in Stance (º)	60.50 (0.48)	55.07 (7.94)	-5.33 (-8.02, -2.63)	<0.001 *	-3.66 (-6.95, -0.38)	0.029 *
Range Tarsal Angle in Stance (º)	36.06 (0.58)	31.22 (4.90)	-4.91 (-7.00, -2.81)	<0.001 *	-3.21 (-5.67, -0.75)	0.011 *
Minimum Tarsal Angle in Swing (º)	24.56 (0.13)	23.56 (6.64)	-0.83 (-3.96, 2.29)	0.602	-1.55 (-5.36, 2.26)	0.426
Maximum Tarsal Angle in Swing (º)	74.17 (0.32)	66.53 (8.89)	-7.51 (-10.65, -4.37)	<0.001 *	-6.12 (-9.90, -2.33)	0.002 *
Range Tarsal Angle in Swing (º)	49.61 (0.34)	42.97 (5.81)	-6.68 (-9.44, -3.91)	<0.001 *	-4.47 (-7.79, -1.15)	0.008 *
Minimum Stifle Angle in Stance (º)	-71.01 (0.39)	-66.98 (14.54)	4.09 (-1.37, 9.54)	0.142	2.93 (-3.55, 9.41)	0.376
Maximum Stifle Angle in Stance (º)	-47.89 (0.58)	-40.12 (12.71)	7.77 (2.52, 13.02)	0.004 *	4.67 (-1.47, 10.82)	0.136
Range Stifle Angle in Stance (º)	23.12 (0.22)	26.86 (4.81)	3.69 (1.30, 6.08)	0.002 *	1.48 (-1.30, 4.26)	0.298
Minimum Stifle Angle in Swing (º)	-83.36 (0.72)	-75.97 (14.00)	7.41 (2.24, 12.58)	0.005 *	5.20 (-0.96, 11.36)	0.098
Maximum Stifle Angle in Swing (º)	-38.34 (0.77)	-33.28 (13.34)	5.06 (-0.31, 10.43)	0.065	3.10 (-3.22, 9.41)	0.336
Range Stifle Angle in Swing (º)	45.03 (0.06)	42.69 (3.77)	-2.35 (-4.64, -0.06)	0.044 *	-2.43 (-5.19, 0.33)	0.084
Distance Matching Limb during stance (cm)	89.11 (0.36)	79.66 (5.02)	-9.38 (-11.46, -7.31)	<0.001 *	-6.16 (-8.46, -3.87)	<0.001 *

* = $p<0.05$

Appendix 9.3 Interaction between all limbs pre vs post-stroke

Outcome	Overall Unadjusted P-value interaction	Overall Adjusted P-value interaction*
Stance Duration (s)	0.923	0.789
Swing Duration (s)	0.151	0.114
Stride Duration (s)	0.996	0.986
Ratio Stance To Stride (%)	0.181	0.084
Ratio Swing To Stride (%)	0.181	0.084
Ratio Stance To Swing (%)	0.287	0.13
Hoof Lateral Deviation (cm)	0.207	0.208
Hoof Forward Swing Velocity (m/s)	0.027 *	0.002 *
Hoof Vertical Swing Velocity (m/s)	0.677	0.678
Range Hoof Height in Swing (cm)	0.577	0.578
Stride Length (cm)	0.97	0.943
Minimum Fetlock Angle Stance (º)	0.994	0.994
Maximum Fetlock Angle Stance (º)	0.921	0.921
Range Fetlock Angle in Stance (º)	0.337	0.336
Minimum Fetlock Angle in Swing (º)	0.314	0.314
Maximum Fetlock Fetlock Angle in Swing (º)	0.975	0.975
Range Fetlock Angle in Swing (º)	0.01 *	0.009 *
Minimum Carpal/Tarsal Angle in Stance (º)	0.963	0.963
Maximum Carpal/Tarsal Angle in Stance (º)	0.085	0.082
Range Carpal/Tarsal Angle in Stance (º)	0.012 *	0.011 *
Minimum Carpal/Tarsal Angle in Swing (º)	0.286	0.287
Maximum Carpal/Tarsal Angle in Swing (º)	0.002 *	0.002 *
Range Carpal/Tarsal Angle in Swing (º)	0.141	0.139
Minimum Elbow/Stifle Angle in Stance (º)	0.82	0.818
Maximum Elbow/Stifle Angle in Stance (º)	0.789	0.782
Range Elbow/Stifle Angle in Stance (º)	0.052	0.049 *
Minimum Elbow/Stifle Angle in Swing (º)	0.595	0.588
Maximum Elbow/Stifle Angle in Swing (º)	0.912	0.91
Range Elbow/Stifle Angle in Swing (º)	0.051	0.051